Surface complexation at mineral interfaces: Multisite and Charge Distribution approach

Tjisse Hiemstra

Thesis committee

Thesis supervisor
Prof. Dr. W.H. Van Riemsdijk
Professor of Soil Chemistry and Chemical Soil Quality
Wageningen University

Other members
Prof. Dr. M.A. Cohen Stuart, Wageningen University
Prof. Dr. R. Kretzschmar, Swiss Federal Institute of Technology, Zürich, Switzerland
Dr. M. L. Machesky, Illinois State Water Survey, Champaign, USA
Prof. Dr. S. Sjöberg, University of Umeå, Sweden

Surface complexation at mineral interfaces: Multisite and Charge Distribution approach

Tjisse Hiemstra

Thesis
submitted in fulfillment of the requirements for the degree of doctor
at Wageningen University
by the authority of the Rector Magnificus
Prof. dr. M.J. Kropff,
in the presence of the
Thesis Committee appointed by the Academic Board
to be defended in public
on Wednesday 13th October 2010
at 1.30 p.m. in the Aula.

Tjisse Hiemstra
Surface complexation at mineral interfaces: Multisite and Charge Distribution approach,
383 pages.

Thesis Wageningen University, Wageningen NL (2010)
With references, with summary in Dutch and English

ISBN 978-90-8585-717-4

Abstract

Ion adsorption is highly relevant in science, technology, and the environment. For many elements, the ion concentration is regulated by adsorption and desorption. In nature, three main classes of reactive materials are present, each with a specific characteristic in relation to ion binding. For organic matter, the main keyword is chemical heterogeneity, for clay minerals, it is permanent negative charge with corresponding cation exchange, and for metal (hydr)oxides, it is the dominance of electrostatics in ion binding.

This thesis describes a new framework for ion binding to metal (hydr)oxides that allows linking of the microscopic processes of ion binding to macroscopic adsorption phenomena. The novel framework is based on a structural approach of mineral surfaces as well as surface complexes, being described with respectively with the MUlti-SIte Complexation (MUSIC) model and the Charge Distribution (CD) approach.

In the MUSIC model, surface groups are distinguished based on their metal coordination that creates differences in charge. This leads to variation in affinity of the surface oxygens for protons. With the MUSIC model, the intrinsic proton affinity of the various types of groups can be derived, which is essential to calculate the overall surface charge of metal (hydr)oxides. For calculation of the particle charge, electrostatic theory is applied since accumulation of protons at the surface will create an electrostatic field that is experienced by the adsorbing protons themselves as well as other ions. The field will strongly affect the ion binding and therefore it is essential to account for this.

Ions form complexes at the surface and the structure of the complexes can be elucidated with in-situ spectroscopy and molecular modeling. At the scale of the interface, surface complexes will experience a gradient of repulsion and/or attraction by the electrostatic field. To account for this important phenomenon, a new approach, known as the CD model, has been developed as logical extension of the MUSIC model. The charge distribution is tightly linked to the microscopic structure of the surface complexes. The innovative CD model is able to calculate accurately the electrostatic energy involved in ion binding. This is essential since ion binding at mineral-solution interfaces is dominated by changes in the electrostatic field at variation of solution conditions such as pH, ionic strength, and the concentration of the ion involved as well as of all its competitors.

The new ion adsorption framework is able to describe the main macroscopic adsorption phenomena. The CD-MUSIC model has been tested successfully for a series of ions bound in competition to different mineral surfaces, in particular the various Fe and Al hydroxides that play an important role in the environment.

To apply the model in field samples, a new methodology has been developed to measure the equivalent reactive surface area of the natural oxide fraction. It reveals that the metal oxide fraction can be considered as a collection of nanoparticles that are covered by and/or embedded in a matrix of natural organic matter. To apply the new framework in soil, a practical solution has been suggested to account for the interaction of oxide particles with natural organic matter.

Content

Bestaan is een feit, leven een kunst

Chapter 0

Preface and Outline of the Thesis

Preface

On geological time scales, elements are part of global cycling. Such phenomena can be understood focusing on the underlying biogeochemical processes that act and are visible on a local scale. A strategy to elucidate biogeochemical processes in general can be comparing the behavior of elements in various natural systems, measuring and monitoring the relevant characteristics. The advantage of studying systems holistically is that one may grasp the integrated effect of a comprehensive set of natural processes being active at the field scale. The disadvantage is that natural systems are often highly variable. The overall effect is the result of a large number of interacting and counteracting processes. Such systems can be too complicated to unravel the fundamental processes that rule their behavior, even if the collected databases are very extensive (and expensive).

The study of individual factors may strongly contribute to a proper understanding of the overall behavior of elements in the natural environment and impact of changing environmental conditions. The latter is highly relevant if the objective is to control biogeochemical processes in a natural or technological setting, for instance optimization of chemical soil fertility, enhancing or reducing bioavailability of elements, prevent or stimulate ion mobility, and minimization of risks of pollution, *etcetera*. For such studies, one may isolate part of a system as is done with sampling. Chemical changes can be induced in the samples and responses can be measured. This is typically done in a laboratory if the aim is to limit the number of factors that will vary. Measured responses can still be difficult to understand if a large number of processes is contributing. For instance, an element may be bound or released by different constituents present in the sample, each having a different behavior. The overall effect can be the sum of the individual contributions, but often various constituents also interact with each other too, further complicating systems. To understand these mutual interactions, it can be opportune to study the fundamental laws of behavior in better-defined systems. Use of model systems often allows understanding and quantification of basic principles, and allows model development that can be applied as tool in field samples.

In nature, macroscopic behavior is based on the underlying microscopic processes. A "*Leitmotiv*" of the present research is that whatever the variability is in nature, the physical chemical processes are the invariant factor. The fundamental chemical interactions like chemical binding take place at the molecular level. The challenge is to link the microscopic reality to the behavior that we observe at the macroscopic scale. However, understanding and quantification of fundamental microscopic processes and properties require "up-scaling" if to be applied in a model handling macroscopic phenomena. To be successful, the main microscopic processes have to be integrated and the overall microscopic behavior is to be described by another approach suitable at that level. Preferentially, parameters of the macroscopic model are linked to properties of the lower scale.

Microscopic surface complexation phenomena are often difficult to apply practically. In soil- and geochemical applications, the challenge is to link adsorption phenomena to a corresponding concentration in solution. Ultimately, this aqueous concentration is often most vital for the fate of elements in nature. To link surface complexation data to solution

chemistry, a thermodynamic vehicle is needed. This thesis is about the development of such an essential tool.

The first chapter of this thesis will highlight the development of a framework for modeling ion adsorption. The framework incorporates major characteristics that are observed at the microscopic level. During the last twenty years, the possibilities to measure the behavior of components *in-situ* at the scale of the interface have increased substantially. The onset of the present framework was published more than 20 years ago. The development started with the notion that mineral surfaces are heterogeneous affecting the reactivity, and this is reflected in the name "MUlti Site Ion Complexation" (MUSIC) model. The keyword of the framework is "structure". Many aspects of structure can be understood and described applying the so-called bond valence concept, originating from Linus Pauling (PAULING, 1929). In the Pauling bond valence concept, charge and coordination of atoms are linked and this combination is very useful in the MUSIC model where reactive sites are defined based on metal coordination and corresponding charge.

The original MUSIC framework (HIEMSTRA et al., 1989a) using the Pauling bond valence has been improved by applying the more recently formulated bond valence concept of Brown (BROWN, 1978). The Brown bond-valence model gives an empirical but very powerful description of the relation between bond length and bond valence.

The MUSIC model focuses on the reactions with protons. It relates pH and pristine charge of surfaces. In-situ spectroscopy, applied to mineral surfaces, has shown a large variety of surface structures that form when ions and surface sites react. The notion of the relevance of the structure of surface complexes has led to further development of the ion adsorption framework. The resulting charge distribution (CD) model (HIEMSTRA and VAN RIEMSDIJK, 1996a) is a logical extension of the MUSIC model. In the CD model, the charge of a surface complex is distributed in the interface using the same concepts of a formal charge as used in the MUSIC model. The initial interpretations of the CD values were based on the Pauling bond valence. The charge distribution was linked to ligand distribution that could be observed with spectroscopy. Over time, advances in spectroscopy increasingly revealed more details of the structures of surface complexes, and for some elements, strong asymmetry in the coordination environment was observed. Interpretation of corresponding macroscopic adsorption data pointed to the same phenomena when the CD value was evaluated, showing the potential power of the framework. The asymmetry in the coordination environment is typically described with the Brown bond valence concept in which bond length is the central parameter. Small differences in bond length are difficult to grasp with current spectroscopic techniques. The bond length is a key characteristic of molecular structures that can be assessed with quantum chemical computations allowing "*ab initio*" optimization of geometries. Fortunately, a considerable and continuous progress has been made in the development of these tools. This development allows at present a reliable application of this computational technique for geometry optimization. With geometry optimization, basic electronic properties can actually be scaled to formal valences that can be incorporated in the CD-MUSIC framework (HIEMSTRA and VAN RIEMSDIJK, 1996a).

Application of this new approach to adsorption of uncharged solution species, suggested a larger interfacial charge distribution than expected and this may be due to dipole orientation

of water molecules at the interface in agreement with some spectroscopic evidence. To cope with this phenomenon, the CD model has been further development (HIEMSTRA and VAN RIEMSDIJK, 2006). Another recent development is the measurement of the structure of the water in the electrical double layer (EDL) near the surface. Water molecules are rather ordered in the compact part of the double layer. This suggests that the diffuse part of the EDL is located at a larger distance from the surface. It justifies adapting the electrostatic double layer model.

The above shows that the CD-MUSIC framework has been improved progressively leading to a firm and powerful tool that links surface speciation to solution chemistry via thermodynamic relationships that are based on well-defined processes observed with precision on the microscopic scale. In future, much more information will become available from studying microscopic phenomena related to surface complexation. The expectation is that the conceptual framework will correspondingly evolve.

Despite all the power of spectroscopists and computational chemists, it should be realized that ultimately understanding of the microscopic behavior is not an aim in itself, but merely an instrument. The challenge is to link this information to the macroscopic level. This requires a vehicle as the framework developed. Science and society may benefit from CD-MUSIC as instrument ☺ when it comes to application in technology and environment.

Outline of the thesis

This thesis will start in chapter 1 with an introductory overview, discussing and summarizing the major phenomena of the mineral-water interface in relation to the development of the CD-MUSIC framework (HIEMSTRA and VAN RIEMSDIJK, 2002). After this introduction, the MUSIC model will be discussed in detail in chapter 2 (HIEMSTRA et al., 1996b). The focus is on estimating the proton affinity constants. As mentioned above, the theory is centered on application of the Brown bond valence concept. Important in the concept is the role of H-bonding and this is an improvement of our earlier work (HIEMSTRA et al., 1989a) on the MUSIC model. The MUSIC model is applied in chapter 3, analyzing the proton charging behavior of $Al(OH)_3$ (gibbsite) and Al_2O_3 (HIEMSTRA et al., 1999b). Gibbsite can be found in nature, but the main reason to analyze its proton binding behavior is that it has very distinct crystal faces that differ in surface composition and chemical behavior. Therefore, it is a model hydroxide "*pur sang"*.

It has been mentioned that the CD model is a logical extension of the MUSIC framework and it will be presented and applied in chapter 4, using as example phosphate (PO_4^{3-}) as an oxyanion and goethite (α-FeOOH) as mineral. This combination is highly relevant, since goethite is the main Fe (hydr)oxide in soils and phosphate is a major nutrient for plants, whereas phosphorous is a minor element in the natural solution. A further important reason to analyze the adsorption behavior of phosphate was the availability of a unique data set collected for the first time with *in-situ* spectroscopy. Moreover, a consistent modeling of the most relevant related phenomena can be seen as a major scientific challenge.

Metal (hydr)oxides may also react with neutral species such silicic acid, $H_4SiO_4^o$, boric acid, $B(OH)_3^o$, arsenite, $As(OH)_3^o$, and others. Analysis of the adsorption behavior points to a

charge distribution that differs from what is expected from a Pauling bond valence analysis. The interfacial charge distribution is a combination of delicate changes in the coordination sphere of the species when bound, and in addition a possible change in orientation of the dipole of water molecules near the surface, induced by the electrostatic field upon ion adsorption. As will be described in chapter 5 (HIEMSTRA and VAN RIEMSDIJK, 2006), the changes in the coordination sphere can be assessed doing quantum chemical MO/DFT calculations for the hydrated complexes and a theory has been developed and parameterized that may account for the energy changes related to dipole orientation of adsorbed water. In chapter 6 (HIEMSTRA et al., 2007), this approach is applied to the adsorption of $H_4SiO_4^o$. Silicon is omnipresent in the natural solution and is the second element in the earth crust. This may be a further reason to study the adsorption of this element. The last chapter on the development of the CD-MUSIC framework (chapter 7) focuses on the change of the interfacial charge distribution due to electron transfer (HIEMSTRA and VAN RIEMSDIJK, 2007). Fe(II) may adsorb to Fe (hydr)oxide surfaces upon (bio)chemical reduction of natural systems. Depending on the pH, surface oxidation may occur with corresponding hydrolysis. As will be shown, surface oxidation with electron transfer occurs only when Fe(II) is adsorbed to Fe (hydr)oxides.

Surface complexation modeling is highly relevant in technological and natural environments to understand the chemical behavior of elements and to control them if required. The natural systems are typically multi-component systems and therefore are extremely complex. Series of mineral surfaces exist that may bind a variety of ions that all may interact with each other. With our work, a consistent and realistic surface complexation model has been developed that is able to describe interaction of ions in multi-component model systems as successfully has been tested in a number of cases. To apply surface complexation modeling to natural systems, there are still many obstacles. Two main challenges are a) to determine the reactive surface areas of the relevant mineral surfaces and b) to describe the interaction of mineral surfaces with the natural organic matter fraction. Both phenomena have been studied, as will be explained in respectively chapter 8 (HIEMSTRA et al., 2010a) and 9 (HIEMSTRA et al., 2010b) from the perspective of application to soils. It should be realized that it is a starting point that needs improvements and further testing in future research.

References

Brown I. D. (1978) Bond Valences -A Simple Structural Model for Inorganic Chemistry. *Chem. Soc. Rev.* 7, 359-376.

Hiemstra T., Antelo J., Rahnemaie R., and van Riemsdijk W. H. (2010a) Nanoparticles in natural systems I: The effective reactive surface area of the natural oxide fraction in field samples. *Geochim. Cosmoschim. Acta* 74(1), 41-58.

Hiemstra T., Antelo J., van Rotterdam A. M. D., and van Riemsdijk W. H. (2010b) Nanoparticles in natural systems II: The natural oxide fraction at interaction with natural organic matter and phosphate. *Geochim. Cosmoschim. Acta* 74(1), 59-69.

Hiemstra T., Barnett M. O., and Van Riemsdijk W. H. (2007) Interaction of Silicic Acid with Goethite. *J. Colloid Interf. Sci.* 310, 8-17.

Hiemstra T., Han Yong, and Van Riemsdijk W. H. (1999b) Interfacial Charging Phenomena of Aluminum (Hydr)oxides. *Langmuir* 15, 5942-5955.

Hiemstra T. and Van Riemsdijk W. H. (1996a) A surface Structural Approach to Ion Adsorption: The Charge Distribution (CD) Model. *J. Colloid Interf. Sci.* 179, 488-508.

Hiemstra T. and Van Riemsdijk W. H. (2002) On the Relationship between Surface Structure and Ion Complexation of Oxide-Solution Interfaces. In *Encyclopaedia of Surface and Colloid Science*, pp. 3773-3799. Marcel Dekker, Inc.

Hiemstra T. and Van Riemsdijk W. H. (2006) On the relationship between charge distribution, surface hydration and the structure of the interface of metal hydroxides. *J. Colloid Interf. Sci.* 301, 1-18.

Hiemstra T. and Van Riemsdijk W. H. (2007) Adsorption and surface oxidation of Fe(II) on metal (hydr)oxides. *Geochim. Cosmochim. Acta* 71(24), 5913-5933.

Hiemstra T., Van Riemsdijk W. H., and Bolt G. H. (1989a) Multisite Proton Adsorption Modeling at the Solid/Solution Interface of (Hydr)oxides: A New Approach. I. Model Description and Evaluation of Intrinsic Reaction Constants. *J. Colloid Interf. Sci.* 133, 91-104.

Hiemstra T., Venema P., and Van Riemsdijk W. H. (1996b) Intrinsic proton affinity of reactive surface groups of metal (hydr)oxides: The bond valence principle. *J. Colloid Interf. Sci.* 184, 680-692.

Pauling L. (1929) The Principles Determining the Structure of Complex Ionic Crystals. *J. Am. Chem. Soc.* 51, 1010-1026.

Chapter 1

On the Relationship between Surface Structure and Ion Complexation of Oxide-Solution Interfaces

Updated and extended, based on the invited publication of
Tjisse Hiemstra and Willem H. van Riemsdijk

in Encyclopaedia of Surface and Colloid Science, pp. 3773-3799.
Marcel Dekker, Inc. 2002

Introduction and historical note

It is said that Wolfgang Pauli (1900-1958) once wrote that if God made materials, surfaces were the work of the Devil. The complexity of surfaces is still provocative. Surfaces are important since no material exists without surfaces. It is the daily live experience of colloid, surface, and interface chemists. Fortunately, surfaces are the border between two phases, like the solid and solution phase, i.e. surfaces are an element of the interface. Part of the characteristics of surfaces originates from the underlying materials, but its behavior is also determined by the bordering phase, e.g. an aqueous solution. Therefore, interfaces can be studied from different perspectives, theoretically and experimentally using thermodynamics, colloid chemistry, crystallography, and mineralogy, inorganic and physical chemistry, spectroscopy and modeling as tools to analyze and understand the observed behaviors in terms of processes.

A historical note on the development of interface chemistry may start in the year 1895 with the discovery of an unknown kind of radiation, X-rays, by Wilhelm Conrad Röntgen. It was going to play an important role in inorganic and interface chemistry. In 1912, X-rays were used for the first time by Laurence Bragg to identify the structure of minerals. Atoms were proven to be ordered in regular patterns. In the following years, structure was found to be the key to understand materials. The rules that lead to a stable arrangement in crystals were formulated in an important paper of Linus Pauling in 1929 (PAULING, 1929). Almost a century after the Röntgen's discovery, X-rays play nowadays again an important role unraveling structure. In 1987, for the first time the surface structure of an adsorbed ion was measured (HAYES and LECKIE, 1987b). Like in the early years of Lawrence Bragg, also this knowledge of structure will be an important landmark in the understanding of the chemistry of interfaces.

One of the most eye-catching properties of colloids is the existence of surface charge, due to separation of charge, described as concept by Hermann Von Helmholtz in 1879 (HELMHOLTZ 1879), visualized Fig.1. The charge separation ($+\eta_0$-η_0) results in an electrostatic potential difference ψ_0 in Volt, which is a measure for the corresponding energy E in Joule per charge unit expressed in Coulomb (V = J / C).

The surface charge of colloids in suspension is balanced by counter ions in the aqueous phase. The combination is called a double layer. The counter ions are diffusely distributed with a decreasing concentration towards the solution. This double layer structure is experienced in a large number of properties studied by colloid chemists. In 1910 and 1913, Louis Georges Gouy (1910) and David Leonard Chapman (1913) developed separately from each other a theory that is known as the diffuse double layer (DDL) theory. It describes the diffuse distribution of charged ions as a function of distance from a planar surface. In Fig.2, the corresponding potential distance relationship is given.

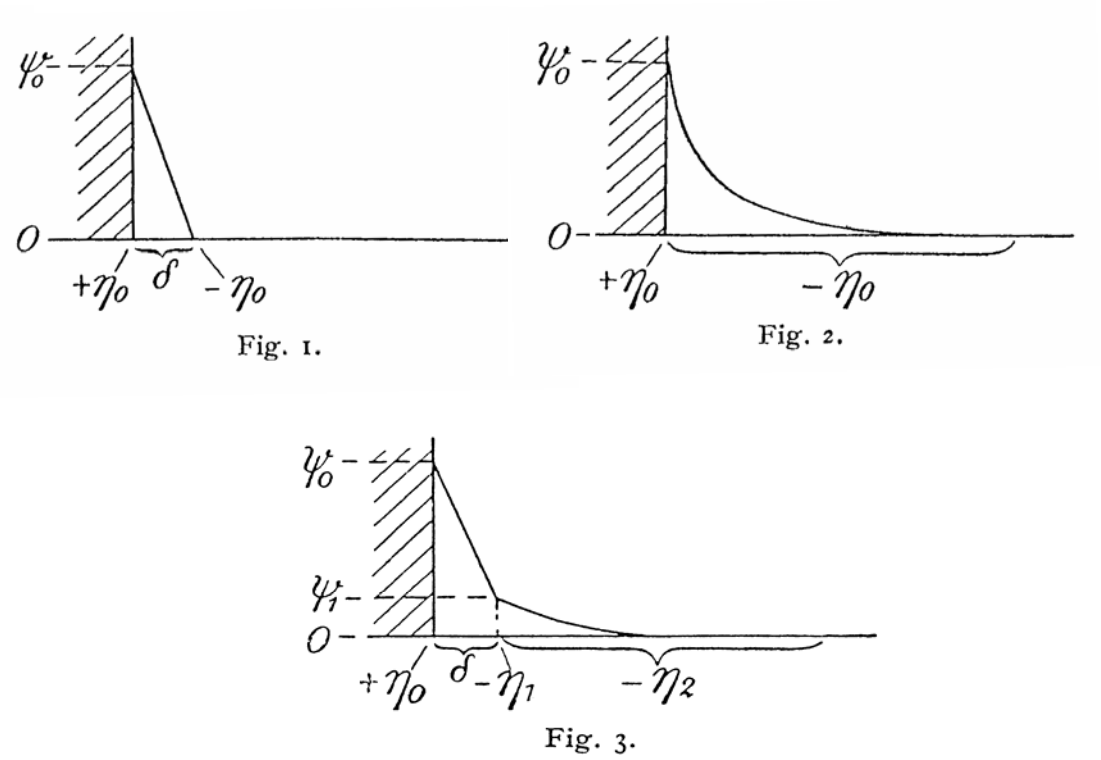

Fig.1-3. The schematic double layer structures published by Stern (1924), visualizing the basic concepts. Stern's Fig.1 gives the charging concept of Von Helmholtz (1879). Fig.2 gives the diffuse double layer of Gouy (1909) and Chapman (1913), and in Fig.3, the model of Stern himself (1924) is shown. In the figures, the potentials ψ given are as a function of distance. The location of the charge η is indicated at the horizontal axis, being in the surface η_0, in the Helmholtz plane -η_1, or in the diffuse double layer -η_2. Note η_0-η_1-η_2 = 0

Ten years after the formulation of the DDL concept, Otto Stern (1924) extended the double layer theory to explain the relation between the charge of a mercury electrode and the interface potential between mercury and an electrolyte solution. He concluded that the charge in the diffuse double layer was separated from the surface charge of the mercury electrode by an empty layer, nowadays known as the Stern layer (Fig.3). The physical explanation of the Stern layer was the notion that the counter ions have a finite size with corresponding minimum distance of approach to the surface, i.e. the structure of ions was involved. Stern recognized that at the scale of the compact part of the double layer, ions should not be considered as point charges. Stern also recognized that electrolyte ions might specifically adsorb at the Stern plane. This concept was later refined by David Grahame (1947). Adsorption of such electrolyte ions is nowadays called outer sphere complex formation (SPOSITO, 1984).

The primary charge of colloids may originate from two different sources. In the lattice of some minerals, ions with a higher valence can be replaced by ions with approximately the same size but with a lower valence. This is known as isomorphic substitution. The resulting

charge deficiency is compensated outside the primary structure. In contact with water, these ions may form a diffuse double layer. Since the charge deficit is located in the primary structure, the mineral has a permanent charge, which is independent of the conditions in solution.

The permanent charge concept contrasts with that of variable charge. If present, the surface charge depends on the chemical composition of the solution. A classical example is AgI(s), which has been used as a model colloid (LYKLEMA and OVERBEEK, 1961; OVERBEEK, 1952). Due to a better solubility of Ag^+ compared to I^- ions, a neutral AgI crystal will become negatively charged in contact with water. The particle charge can be diminished by the addition of extra Ag^+ ions, which may adsorb depending on the solution concentration. It suggests that the ion that determines the potential of the surface is the Ag^+ ion. At a certain Ag^+ concentration, there is no excess adsorption. From a thermodynamic point of view, the difference of adsorbed silver (Γ_{Ag}) and iodide (Γ_I) ions is zero (Γ_{Ag}-Γ_I = 0). If equal numbers of Ag^+ and I^- ions are adsorbed, the colloid becomes uncharged. At this solution condition, AgI(s) is in its point of zero charge (PZC). The structural details of the charging process of AgI(s) will be described later.

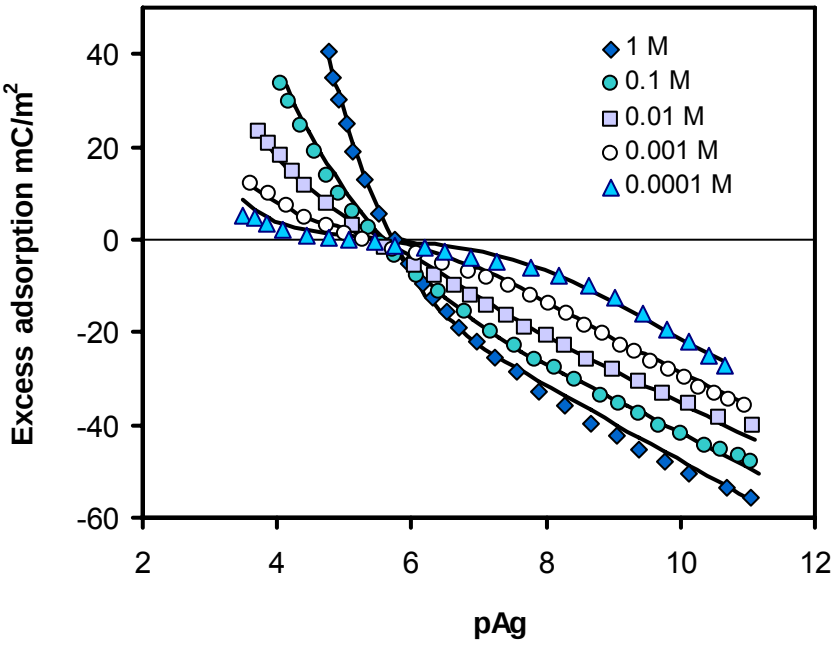

Fig.4. The excess adsorption, Γ_{Ag} -Γ_I , expressed in mC/m^2 as a function of the negative logarithm of the Ag^+ activity in solution (pAg) for AgI (s) colloids at different KNO_3 electrolyte concentrations (Bijsterbosch and Lyklema, 1978). The lines have been calculated with the CD model as discussed later in the text.

Metal oxides form a different group of variable charge minerals. Interest in these minerals started in the late 50 and early 60thies. Bolt (1957) measured for the first time the variable charge of silica and Parks and De Bruyn (1962) did it for iron oxides in 1962, later followed by Bérubé and De Bruyn (1968) for titanium oxide. These surfaces are amphoteric, being negatively, zero, or positively charged. The variation in charge at these surfaces was

related to the degree of proton adsorption, depending on the pH in solution. Variable charge has been interpreted classically with the Nernst equation (BLOK and DE BRUYN, 1970; LYKLEMA and OVERBEEK, 1961) without sites and mass law equations. Parks and De Bruyn (1962) and Parks (1965; 1967) introduced the concept of a neutral site (SOH^o) that may dissociate (SO^-) or associate (SOH_2^+) a proton. This formalism has been embraced for many years and the concept is known as the 2-p*K* model.

The first attempt to identify the imaginary site in terms of a physical structure was of Hingston et al. (1968), who proposed that for sesquioxides with octahedral metal coordination, the site is a combination of two surface groups, i.e. a ≡OH and a $\equiv OH_2$. Implicitly, they applied the so-called Pauling bond valence concept (PAULING, 1929) and attributed to each ligand an average charge of +1/2 valence unit (v.u.), leading to $(\equiv OH^{-0.5})_2]^{-1}$, $(\equiv OH^{-0.5})(\equiv OH_2^{+0.5})]^0$, and $(\equiv OH_2^{+0.5})_2]^{+1}$ for the surface species SO^{-1}, SOH^o, and SOH_2^{+1}. In 1982, Bolt and Van Riemsdijk (1982) abandoned the 2-p*K* concept of protonation as the major explanation for variable charge of sesquioxides. They proposed the use of a single step, i.e. $SOH^{-1/2} + H^+ \Leftrightarrow SOH_2^{+1/2}$.

Spectroscopy has played an important role in directing the development of theoretical concepts. In the early years, infrared (IR) spectroscopy had shown the existence of different types of surface groups. Surface groups were defined based on the number of metal ions coordinating with the surface oxygen ions using a crystallographic analysis as illustrated in the work around 1970 of Peri (1968), Jones and Hockey (1971), Yates (1975), and Rochester and Topham (1979). The importance of metal ion coordination on the reactivity of surface groups has become increasingly clear in the seventies by the work of Parfitt (PARFITT et al., 1975; PARFITT et al., 1977c; PARFITT et al., 1977a; PARFITT et al., 1977b; PARFITT and RUSSELL, 1977d; PARFITT et al., 1976), Russell (RUSSELL et al., 1974), and others. However, for a long time no attempts were made to include this information in a surface complexation model until 1989, when a surface structural framework was presented known as the Multi Site Complexation (MUSIC) model (HIEMSTRA et al., 1989b; HIEMSTRA et al., 1989a). Such a surface structural approach will become increasingly valuable due to the modern developments in spectroscopy, elucidating the relation between surface structures and binding of ions. Molecular orbital (MO) calculations and molecular dynamic (MD) simulations will also increasingly contribute to this in our modern era of fast-computing and software, elucidating the structural behavior of surfaces. In the MUSIC model, the charge of the individual surface oxygens is based on the number of coordinating metal ions. The bond valence concept is used as a charge bookkeeping tool.

Proton affinity of individual types of surface groups is essential in any multiple site surface complexation model. The first *a priori* calculated affinities for individual surface groups for various metal (hydr)oxides were published by Hiemstra et al. (1989a). The proton (H) affinity of the surface groups was related to the so-called Pauling bond valence charge of the coordinating metal ion (Me) of the solid and combined with an H-Me distance parameter, inspired by a similar electrostatic interpretation of the PZC of Parks (1967) and Yoon et al. (1979). However, the Pauling concept is only adequate for a symmetrical coordination environment of metal ions. In many minerals such as goethite, hematite, corundum, anatase

and rutile, the coordination sphere is asymmetric. In a next attempt to estimate the proton affinities (HIEMSTRA et al., 1996b), asymmetry in the coordination environment was introduced, using the bond valence-bond length relation as developed by Brown (1978) in 1978. In recent years, some attempts have been made to find the proton affinities by molecular modeling techniques (AQUINO et al., 2008; MACHESKY et al., 2008; RUSTAD et al., 1996b; RUSTAD et al., 1998; VLCEK et al., 2007). Such new estimates can be incorporated in the MUSIC framework (FELMY and RUSTAD, 1998).

Metal (hydr)oxide surfaces are widely studied because of the capability to interact with cation and anions. The chemical interaction of ions is strongly influenced by the electrostatic interaction between the surface and the adsorbing ions. From the late sixties on, a series of surface complexation models (SCM) have been used. These models comprise surface reactions in combination with some electrical double layer option founded in the classical Gouy-Chapman-Stern-Grahame approach (CHAPMAN, 1913; GOUY, 1910; GRAHAME, 1947; STERN, 1924). Known are the Constant Capacitance (CC) model (ATKINSON et al., 1967; GOLDBERG and SPOSITO, 1984a; KUMMERT and STUMM, 1980; SCHINDLER and KAMBER, 1968; SIGG and STUMM, 1981), the Diffuse Double Layer (DDL) model (DZOMBAK and MOREL, 1990; STUMM et al., 1970), the Basic Stern (BS) model (WESTALL and HOHL, 1980; BORKOVEC, 1997; CHRISTL and KRETZSCHMAR, 1999; FELMY and RUSTAD, 1998; HIEMSTRA et al., 1987; LÜTZENKIRCHEN, 1998; MACHESKY et al., 1998; SCHUDEL et al., 1997), the Triple Layer (TL) model, (DAVIS et al., 1978a; HAYES and LECKIE, 1987b; YATES et al., 1974), and the Variable Charge - Variable Potential (VC-VP) model (BOWDEN, 1973; BOWDEN et al., 1980; BOWDEN et al., 1977; BARROW and BOWDEN, 1987a; BARROW and BOWDEN, 1987b; BARROW et al., 1980). The use of surface complexation models (SCM) was enabled by the development of a systematic approach to solve chemical equilibria in an iterative manner with computers (MOREL and MORGAN, 1971). Westall (WESTALL and HOHL, 1980; WESTALL, 1979) has shown how surface complexation models can be introduced in the general procedure of solving chemical equilibria.

The above thermodynamic models differ in the formulations of adsorption reaction(s) and the calculated electrostatic contribution to the overall Gibbs free energy change. Over the years, it became clear that the same adsorption phenomena could be described with very different sets of surface species. From a thermodynamic point of view, it is relatively easy to describe the adsorption with surface complexation models, provided that one is allowed to choose freely the type and number of surface species and surface sites. It is even possible to describe ion adsorption phenomena thermodynamically correct without electrostatics using a large series of sites, which differ in chemical affinities (BORKOVEC et al., 1998; CERNÍK and BORKOVEC, 1996). The calculated surface speciation of most models is hypothetical and model dependent. Surface complexation models, which are thermodynamically correct while using hypothetical species, may have severe limitations. It is *a priori* not obvious and from a thermodynamic point of view not necessary that models, which correctly describe the pH- and concentration- dependent binding of one component in a simple system, will properly predict the ion interactions in multicomponent systems. One of the main reasons is that interaction of ions is very strongly determined by the electrostatic contributions to the Gibbs free energy change. This property should therefore be matched closely in a model.

The electrostatic interaction strongly depends on the location of the ion charge in the electrical double layer (EDL) profile. The importance of the location of an adsorbed ion became clear through the work of Fokkink et al. (1987). They showed that the location of the charge of an ion is a key factor in the co-adsorption or co-desorption of protons during ion adsorption. This fact is all the more important since two years before, in 1985, Perona and Leckie (1985) showed, on a thermodynamic basis, that the co-adsorption or release of protons is related to the pH dependency of adsorption. Combination of both findings leads to the conclusion that *the location of the ion charge in the electrostatic double layer profile and the pH dependency are tightly connected*. Most SCM locate innersphere complexes on a single electrostatic position, treating the ion as a point charge, although it has been argued that in principle the charge of a species, e.g. a $ZnOH^+$ ion, may be located on different positions, e.g. Zn^{2+} at one position and the OH^- at another (Davis and Leckie, 1978b). It is clear from the structure of innersphere complexes that only part of the adsorbing ion and the corresponding charge is incorporated in the surface, while the other part is at a larger distance from the surface ligands. Innersphere complexes of ions such as SeO_3^{2-} and SeO_4^{2-} are formed via ligand exchange, but their surface structure is very different (Fig.5). Rietra et al. (Rietra et al., 1999a) showed about ten years ago that this difference in structure is reflected by the co-adsorption of protons and corresponding pH dependency.

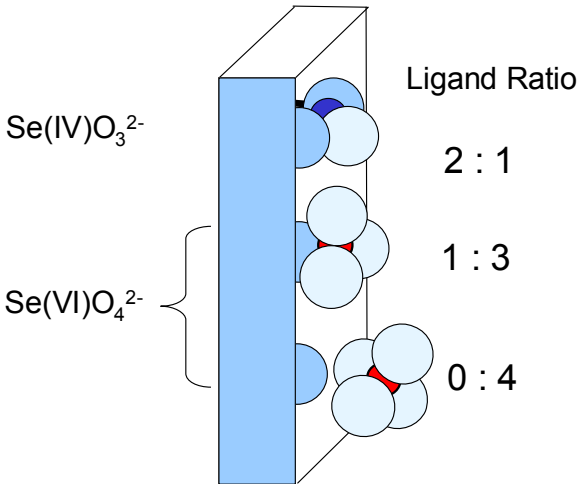

Fig.5. The ligand distribution over surface and solution for surface complexes. The bidentate innersphere complex of SeO_3^{2-} has two ligands common with the surface while SeO_4^{2-} may form a monodentate innersphere complex or an outersphere complex having one respectively or zero ligands common with the surface. The different ligand distribution leads to a different interfacial distribution of charge as implemented in the charge distribution (CD) model.

For a long time, the notion of ligand exchange, observed by spectroscopy, was considered as an obstacle in surface complexation modeling. Ion adsorption with ligand exchange was treated in a rather simplistic way, in the sense that the adsorbing ions were considered as a point charge, located in the surface. In a new model approach (HIEMSTRA and VAN RIEMSDIJK, 1996a), ligand exchange was rationalized with the introduction of the bond

valence concept and it resulted in a distribution of charge in the compact part of the interface. The charge of the adsorbed ions is distributed over the ligands, which in turn are distributed over the interfacial locations (Fig.5). The new approach is known as the charge distribution (CD) model. It can be considered as a logical extension of the MUSIC approach. The combination of the CD model and the MUSIC model integrates the knowledge of the structure of crystals and surfaces, the structure of surface complexes, and the structure of the double layer. Essential in the approach is the relation between electrostatics and structure. The paradigm forms a powerful framework for ion adsorption modeling and is essential if the aim is using physical realistic species as observed with modern in-situ spectroscopic methods and characterized by powerful gain-grounding computational techniques.

Modus operandi

In the next paragraphs, we will present a surface structural and mechanistic approach to ion adsorption modeling and will review main contributions described in literature. We will explain for various important minerals in detail the role of surface structure on surface protonation and surface charge development. The structure of surface complexes will be discussed in relation to electrostatics and we will emphasize how the structure of surface complexes is related to the pH dependency of adsorption. As will be explained, the same structure-charge-potential relationship is responsible for the pH dependent distribution of a component over mono- and bidentate complexes and the distribution over inner- and outersphere complexes. It also governs the competition and cooperative effects of different components. The charge, attributed to the surface, is highly relevant for the pH dependency of ion adsorption since at the surface the protons reside, while the charge located in the Stern plane at some distance from the surface is strongly ruling competitive interaction of ions and the shape of the adsorption isotherm. Both aspects are regulated by the interfacial charge distribution (CD) that is rooted in various aspects of structure.

As evidenced by different experimental approaches such as force measurements (ISRAELACHVILI and WENNERSTROM, 1996; PASHLEY and ISRAELACHVILI, 1984), X-ray reflectivity (CATALANO et al., 2006; FENTER and STURCHIO, 2004; TONEY et al., 1995), and Sum Frequency Spectroscopy (KATAOKA et al., 2004; OSTROVERKHOV et al., 2005; SHEN and OSTROVERKHOV, 2006; YEGANEH et al., 1999), water near the surface is increasingly ordered over a distance of about 0.7-0.9 nm, which is equivalent to about 2-3 layers of water molecules (HIEMSTRA and VAN RIEMSDIJK, 2006). Water and the major minerals of the earth crust (silicates oxides) can be considered as a stacking of oxygen ions, neutralized by small cations in between. A major difference is that free water has a low packing density (HIEMSTRA and VAN RIEMSDIJK, 2009a; HIEMSTRA et al., 2009b). In the interface, this changes.

Although a water molecule as a whole is neutral, the orientation of water may contribute to the interfacial charge distribution, since water molecules have a dipole that may orientate in an electrostatic field, contributing to its neutralization. As discussed, this effect can be in incorporated in the CD framework as shown recently (HIEMSTRA and VAN RIEMSDIJK, 2006).

Surfaces and sites

Minerals and solutions can be considered as three-dimensional networks of bonds. The interface is a discontinuity in the network, leading to the formation of surface groups. Surface groups of oxides may have lower metal ion coordination than oxygen ions in the mineral bulk. The charge of the surface oxygens is then less well neutralized, which can be compensated by the uptake of one or two protons. This may be written as:

$$\equiv O^{?} + 2H^{+}(aq) \Leftrightarrow \equiv OH^{?+1} + H^{+}(aq) \Leftrightarrow \equiv OH_2^{?+2} \qquad [1]$$

For minerals, counting the number of the various groups involved and their corresponding charge can establish the surface charge. Based on eq.[1], it is however not possible to do this *a priori*, since the oxygens are partly neutralized by one or more metal ions of the mineral, leading to a question mark in eq.[1]. The charge attribution can be calculated using the Pauling bond valence concept as a bookkeeping tool. The Pauling bond valence ν expresses the mean available charge per bond and is simply the charge *z* of the metal ion divided by the coordination number CN, i.e.

$$\nu = \frac{z}{CN} \qquad [2]$$

The lowest metal coordination number in oxides and hydroxides is two. Quartz as oxide and gibbsite as hydroxide are the most important representatives of such metal (hydr)oxides. In terms of metal coordination, only two types of surface groups are found for these minerals, i.e. singly and doubly coordinated surface groups. From this perspective, these minerals are relatively simple and are therefore discussed first.

Quartz and silica

In Fig.6, a two-dimensional representation of the quartz structure with linked SiO_4 tetrahedra is given. In the bulk, all oxygens are doubly coordinated. Each Si-O bond represents 1 valence unit (v.u.), as is found applying eq.[2] with $z = 4$ and $CN = 4$, resulting in $\nu = +1$ v.u. Two Si ions in the bulk neutralize the charge (-2 v.u) of the oxygen, as calculated with the bond valence sum rule, $\sum\nu - 2 = 0$. Doubly coordinated $\equiv Si_2O$ groups are also found at the surface, not only for quartz, but also at the 001 faces of phyllosilicates such as kaolinite, mica, and montmorillonite. It is extremely difficult for $\equiv Si_2O$ groups to accept a proton. The log*K* of the reaction $\equiv Si_2O^0 + H^+ \Leftrightarrow \equiv Si_2OH^+$ is estimated to be extremely low (HIEMSTRA et al., 1989a). It implies that this group can be considered as chemically inert with respect to proton binding.

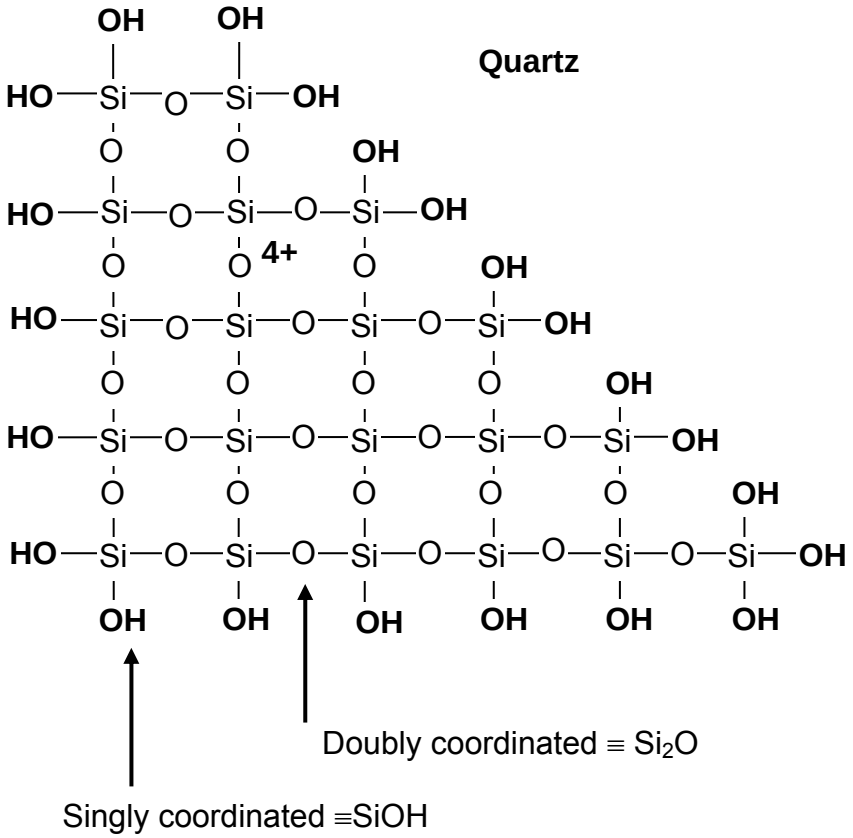

Fig.6. The schematic mineral and surface structure of quartz. The oxygen ions in the bulk are doubly coordinated. This group $\equiv Si_2O$ is also present at the surface. Singly coordinated surface groups result from absence of a coordinating Si. The missing charge can be compensated with binding of a proton.

Another type of surface group at the solution-water interface of quartz is the singly coordinated group that arises from the absence of one coordinating Si^{4+} ion. The negative charge, found by applying eq.[2] and adding the valence of the oxygen equals -1 v.u. (bond valence sum rule $\sum v-2 = +1-2 = -1$ v.u.). The charge can be compensated by the uptake of one proton, according to the reaction:

$$\equiv SiO^{-1} + H^{+}(aq) \Leftrightarrow \equiv SiOH^{0} \qquad \log K_1 \qquad [3]$$

The $\equiv SiOH^0$ group at the surface of quartz and silica is the only proton reactive group. For simplicity, no distinction is made between isolated and geminal groups in terms of proton affinity. The $\log K_1$ value can be found by modeling the charging curve. Modeling the data of Bolt (1957) for silica with the Basic Stern option yields a $\log K_1$ value of 7.5 (HIEMSTRA et al., 1989b). Schindler and Kamber (1968) found $\log K_1 = 6.8$ for amorphous silica. A mean value of $\log K_1 = 7.3 \pm 0.3$ was obtained for a series of SiO_2 materials published in literature (SAHAI and SVERJENSKY, 1997). With IR spectroscopy, a value of $\log K_1 = 7.2$ is found (HAIR and HERTL, 1970; MARSHALL et al., 1974). The intrinsic proton affinity of the surface reaction is about 2 $\log K$ units lower than the affinity (corrected for electrostatic energy) of the

comparable group in solution (log$K$ = 9.2). This has been attributed to the Born solvation energy (SVERJENSKY, 1994), to be discussed later. Several attempts have been made to predict the logK_1 value of $\equiv SiO^-$. A logK_1 of 7.7 is found with a bond valence approach (HIEMSTRA et al., 1996b). With molecular modeling, Rustad et al. (1998) found logK_1 = 8.5.

According to eq.[3], quartz and silica are neutral or negatively charged, which contrasts with electrophoresis showing positive particles at very low pH. The iso electric point (IEP) is about 2 (SPOSITO, 1984). A positive charge results from the formation of $\equiv SiOH_2^+$ according to:

$$\equiv SiOH^0 + H^+(aq) \Leftrightarrow \equiv SiOH_2^+ \qquad \log K_2 \qquad [4]$$

The predicted logK_2 value for this reaction is -3.9 (HIEMSTRA et al., 1996b). The logK_2 value can also be found combining the experimental logK_1 value of the first protonation step (logK_1 = 7.5) with the experimental PZC value (PZC = 2) since PZC = (logK_1 + logK_2) / 2, leading to a logK_2 of about -3.5. The agreement is very satisfactory. What we can learn from this analysis is that the *difference in logK value between the first and second step on one and the same surface group is very large*. A large ΔpK is supposed to be an intrinsic property of the surface groups on all oxides. As a result of the large difference, in general only one of both protonation steps can be observed in the experimental pH window (HIEMSTRA et al., 1989a).

Gibbsite α-Al(OH)$_3$

Doubly coordinated surface groups

As for quartz, the mineral structure is formed by double coordination of the oxygen to the metal ions. In case of gibbsite, in addition a proton is bound. The Al^{3+} ions are present in octahedra. The hexa-coordination leads to a mean bond valence of ν =+3/6 = 0.5 v.u. (eq.[2]). Two Al-O bonds are needed to neutralize the OH^- in the bulk. Doubly coordinated hydroxyls are also found on the crystal faces. The dominant 001 face of the flat hexagonal crystal (Fig.7) has, ignoring imperfections, only $\equiv Al_2OH^o$ groups (Fig.7). This group is uncharged but may associate or dissociate a proton:

$$\equiv Al_2O^{-1} + 2H^+(aq) \Leftrightarrow \equiv Al_2OH^0 + H^+(aq) \Leftrightarrow \equiv Al_2OH_2^+ \qquad [5]$$

By varying the contribution of the 001 face in synthetic gibbsite preparations, it has been shown (HIEMSTRA et al., 1999b) that the 001 face with these doubly coordinated groups remain uncharged ($\equiv Al_2OH^o$) over a wide experimental pH range between pH 4-10 (Fig.8). The titrations were reversible without hysteresis (HIEMSTRA et al., 1999b; HIEMSTRA et al., 1987) showing that equilibrium was approached for the process studied, i.e. protonation of singly coordinated surface groups. The experimental result suggests that the logK_1 of the first step (eq.[5]) must be high and that of the second step very low, i.e. a large ΔpK is required to lead to the dominance of $\equiv Al_2OH^o$ over a vast pH range. This behavior also follows from the

predicted log$K$ values of Hiemstra et al. (1996b) for the reaction of eq.[5] ($\log K_1 \approx 12$ and $\log K_2 \approx 0$).

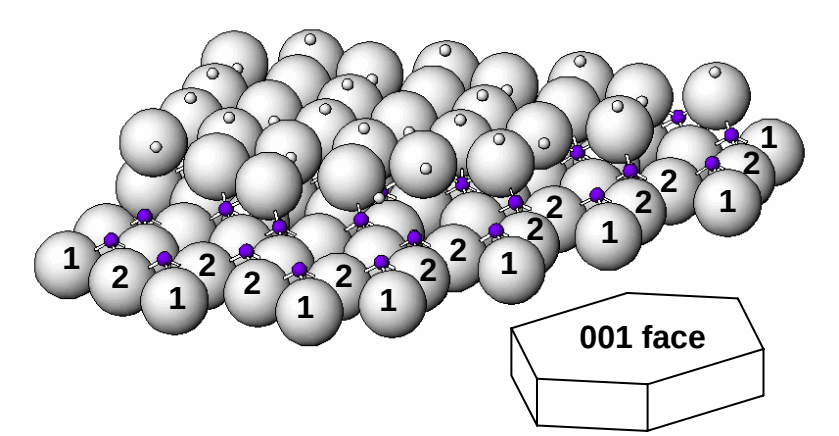

Fig.7. $Al(OH)_3$ layer of a hexagonal gibbsite crystal, in which half of the doubly coordinated OH ligands on top are removed to show the coordination with Al^{3+} ions. The coordination of the OH at the edges is indicated with a number, i.e. 1 for singly, and 2 for doubly coordinated groups. Only coordinated protons of the top layer of oxygen ions are shown.

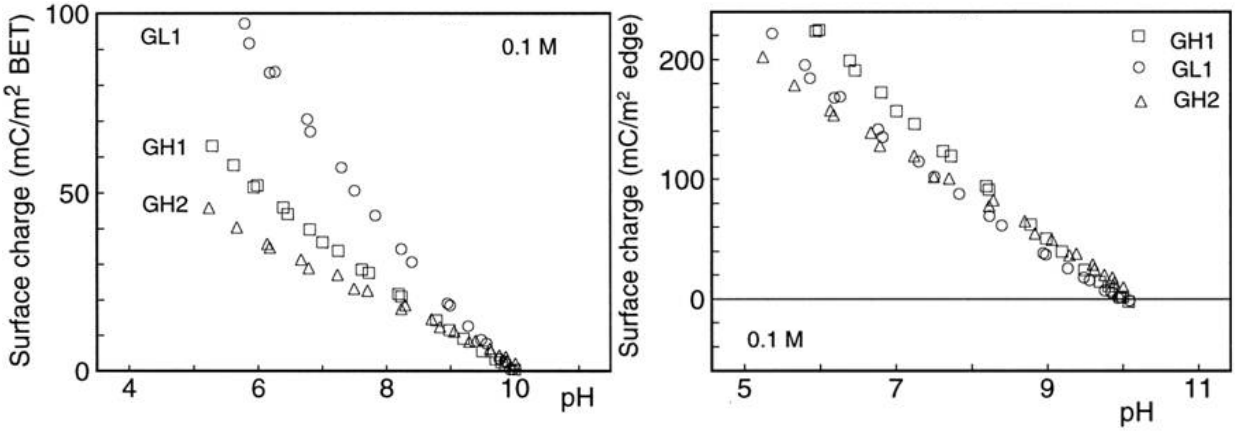

Fig.8 a) The charging of differently prepared hexagonal gibbsite crystals scaled on the total BET surface area and b) scaled on the edge face area, showing that reactivity of edge faces and the absence of a considerable contribution of the 001 faces (data taken form (Hiemstra et al., 1999b)). Note that the surface charge scaled at the BET surface area is unusually low for metal (hydr)oxides.

More recently, it has been suggested (ROSENQVIST et al., 2002) that gibbsite particles may carry much more charge than found in our experiments (HIEMSTRA et al., 1999b; HIEMSTRA et al., 1987). Rosenqvist et al. (2002) found for an aged sample a much stronger acid/base consumption when the titration was done very slowly. The larger acid-base consumption in slow titrations has been attributed to the slow kinetics of protonation of

surface groups, a phenomenon so far never observed for (hydr)oxides. In case of non-aged gibbsite, a different picture is found. The total proton adsorption is considerably less. Enhancement of the acid/base adsorption is found for this material below pH~5 and above pH~8 while in the intermediated pH range, the slope is practically equal to the slope found in our samples, even though the non-aged gibbsite of Rosenqvist et al. (2002) was titrated slowly.

In the modeling approach of Rosenqvist et al. (2002), the surface charge of the 001 face of aged gibbsite is only created by the formation of strong ion pairs, i.e. $\equiv Al_2OH_2^+$-Cl^- and $\equiv Al_2O^{-1}$-Na^+. Since $\equiv Al_2OH_2^{+1}$ and $\equiv Al_2O^{-1}$ are absent in the model *by definition*, no diffuse double layer (DDL) charge can develop on the 001 face. Experimentally, indeed a large quantity of Cl^- has been found in their dialyzed material (pH~4.6), i.e. ~3 μmol/m^2, which is in the order of the amount of H^+ expected from slow titrations. This contrasts with the work of Hingston et al. (1972) and Wendelbow (WENDELBOW, 1987). Wendelbow did not find a large amount of Cl^- in his experiments. He measured the ^{36}Cl and ^{22}Na counter and co-ion adsorption as a function of pH for a well-crystallized gibbsite. The equilibrium time in these experiments was about 18-20 hours (WENDELBOW, 1987). At pH 5, Wendelbow found about 0.25 μmol ^{36}Cl /m^2 BET for 0.001 M NaCl. As shown by Hiemstra et al. (HIEMSTRA et al., 1999b), this adsorbed amount could be very well understood assuming only charge development at the edge faces of the gibbsite crystals (8 m^2/g) and the behavior of his gibbsite preparation is quantitatively in agreement with the behavior of our own preparations that have been characterized using relatively short reaction times.

In either gibbsite model, no significant DDL will develop and this is supported (GAN and FRANKS, 2006) by atomic force measurements (AFM). Interpretation of the AFM data leads to a very small, but pH-dependent diffuse double layer potential (~ 0-10 mV) that develops in the pH range from pH 9 to pH 4 (Fig.9). The corresponding double layer charge is extremely low with a maximum of ~10^{-3} μmol/m^2 and this result is attributed to the presence of strong specific adsorption of Cl^-, neutralizing the $\equiv Al_2OH_2^+$ groups locally in the Stern layer (ROSENQVIST et al., 2002), forming $\equiv Al_2OH_2^+$-Cl^-. From the experiments described, one may conclude that no DDL is developed at the 001 face.

At the 001 face, there are different types of $\equiv Al_2OH^o$ surface groups. According to Bickmore et al. (BICKMORE et al., 2004), two of these types would have an extremely high affinity, i.e. $\log K_{H2a}$ = ~ 11 and $\log K_{H2b}$ = ~ 5, for the protonation reaction $\equiv Al_2OH^o + H^+ \Leftrightarrow \equiv Al_2OH_2^+$. The affinity of the other types of groups is very low. Using the proposed affinity constants, a calculation of the surface speciation shows that only protonation of the surface group with the highest affinity constant ($\log K_{H2a}$) is relevant for charging the surface. As pointed out by Hiemstra et al. (HIEMSTRA et al., 1989b), the reason is that the protonation of the surface group with a highest affinity creates a potential difference between surface and solution that will suppress the protonation of other groups with a lower proton affinity. It shows that the observed development of a double layer potential around pH~5- cannot be explained, as suggested by Gan and Franks (GAN and FRANKS, 2006), by the affinity constants derived in the model of Bickmore et al. (BICKMORE et al., 2004). We further note that Bickmore's proton affinity of the reactive $\equiv Al_2OH^o$ group ($\log K_{H2a}$) is very high

compared to their predicted proton affinities of singly coordinated $\equiv AlOH^{-1/2}$ surface groups, i.e. both being in the same order. Moreover, their $\log K_{H2a}$ for protonation of $\equiv Al_2OH^0$, is in the same order as the $\log K_{H1}$ for protonation of $\equiv Al_2O^{-1}$ in our model.

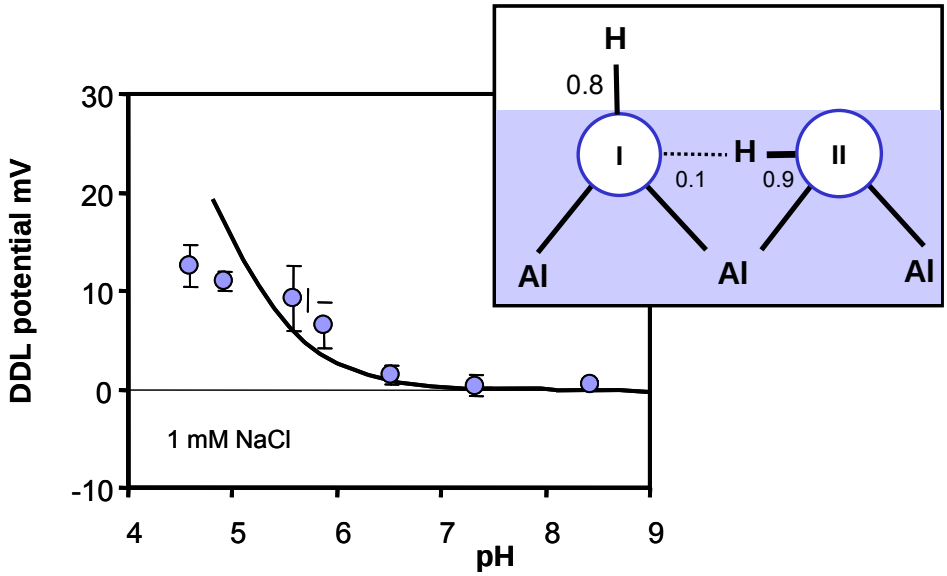

Fig.9. The diffuse double layer potential (DDL) measured with AFM on the 001 face of gibbsite (data points) as a function of pH in 0.001 M NaCl (Gan and Franks, 2006). The line has been calculated assuming affinity constants for successive protonation steps (eq.[5]) that are 2 units higher than predicted previously, i.e. $\log K_{H1}$ = 11.9 +2 = 13.9 and $\log K_{H2}$= 0 +2 = 2. Two types of doubly coordinated surface can be found at the 001 face. Site I is able to dissociate a proton and site II may adsorb one.

If we would like to explain the double layer potential data measured with AFM (Fig.9), a possibility is to increase the affinity constants for the protonation of $\equiv Al_2O^{-1}$ and $\equiv Al_2OH^o$, as predicted with the MUSIC model. An increase of the $\log K_H$ of both steps with 2 units (i.e. $\log K_1(\equiv Al_2O^{-1})$ = 11.9 + 2 = 13.9 and $\log K_2(\equiv Al_2OH^o)$ = 0 +2 = 2) is enough to create a DDL potential of ~15 mV at pH = 5 (Fig.9) and to keep the potential at zero at the highest pH. A value of $\log K_2(\equiv Al_2OH^o)$ = 2 has recently been suggested by Jodin et al. (JODIN et al., 2005) using our MUSIC approach.

Detailed analysis of the structure of gibbsite shows that there are 6 different types of $\equiv Al_2OH^o$ groups in the gibbsite lattice that can be divided into two main groups of $\equiv Al_2OH^o$ species. Half of the hydroxyls forms, within a single $Al(OH)_3$ sheet, H-bridges with another hydroxyl, and the other half forms out-of-plane H-bridges that link the single $Al(OH)_3$ sheets together. According to ATR-FTIR spectroscopy (JODIN et al., 2005), the charge distribution of the internal O-H···O differs from the charge distribution in aqueous solutions. In Fig.9, we have given a schematic picture of the two types of $\equiv Al_2OH^o$ groups at the 001 face according to Jodin et al. (JODIN et al., 2005). If the internal H-bridge is maintained, type II will be able to accept a second proton from solution whereas type I is able to release a proton. Assuming

relaxation of the Al-O bonds in the lattice to a bond valence of 0.5 v.u. and using the charge distribution of H^+ in the H-bond as given in Fig.9, the calculated MUSIC affinities are log-$K_1(\equiv Al_2O^{-1}) = +14$ and $\log K_2(\equiv Al_2OH^o) = +2$. These predictions fit with the above data. It is obvious that small changes in the assumption lead to quite large changes in the predictions, indicating that in general some precaution is recommended. Over time, better methods, e.g. based on molecular computations, will improve the estimates and these can be incorporated in the MUSIC framework for thermodynamic modeling.

Application of the above estimated affinity constants confirms that in the option with a slight shift of the log$K$, no significant charge (only 1 mC/m^2 at pH 5) is developed at the 001 face in the pH range used in Fig.9. The description of the potential is rather accurate, except for pH values below 5. A reason might be that in the AFM experiments SiO_2 spheres have been used that in principle may adsorbed Al^{3+} ions and this may change the charge and double layer potential of the tip, which in turn may affect the data analysis.

Finally, we note that one of the planar crystal faces of kaolinite closely resembles the structure of the 001 face of gibbsite, i.e. it consists of doubly coordinated surface groups only. For this mineral face, it is generally believed that it is uncharged, which is in line with our model for gibbsite.

Singly coordinated surface groups

At the edge faces of the hexagonal gibbsite crystals, singly coordinated groups (Fig.7) can be found (PARFITT et al., 1977b), (HIEMSTRA et al., 1987), (HIEMSTRA et al., 1999b). These groups lack the coordination of one Al^{3+} ion with corresponding neutralization. Therefore, the charge deficit will be +0.5 v.u. based on the bond valence sum applying the Pauling bond valence concept (Eq. [2]), i.e. $\sum v\text{-}2 = +0.5+1-2 = -0.5$ v.u. Therefore, the groups can be represented as $\equiv AlOH^{-0.5}$. In principle, this group may accept or donate a proton. The formal adsorption reactions can be written as:

$$\equiv AlO^{-3/2} + 2H^+(aq) \Leftrightarrow \equiv AlOH^{-1/2} + H^+(aq) \Leftrightarrow \equiv AlOH_2^{+1/2} \qquad [6]$$

The experiments (Fig.8) show that gibbsite is positively charged in the pH range 4-10, illustrating the dominance of $\equiv AlOH_2^{+0.5}$ over $\equiv AlOH^{-0.5}$. Since a large ΔpK exists between the first and second step on the same group, $\equiv AlO^{-3/2}$ will practically not exists. In contact with an aqueous solution, the large undersaturation of charge of any $\equiv AlO^{-3/2}$ immediately will lead to protonation of $\equiv AlO^{-3/2}$, forming $\equiv AlOH^{-1/2}$. This implies that the charge on gibbsite is actually determined by only one protonation step. For this reason, it is possible to find the log$K$ value experimentally from the surface charge curves. At zero charge, equal numbers of $\equiv AlOH^{-0.5}$ and $\equiv AlOH_2^{+0.5}$ are present. This leads to log$K$ = PZC (BOLT and VAN RIEMSDIJK, 1982). This value is approximately 10 ± 0.5 (HIEMSTRA et al., 1999b; HIEMSTRA et al., 1987) and equals the logK_2 value predicted with the bond valence approach (HIEMSTRA et al., 1996b).

Charge and potential

The above analysis shows that the proton reactivity of quartz as well as gibbsite is determined by essentially one type of surface group. Nevertheless, one observes experimentally that both surfaces react totally different in terms of charging behavior. The mathematical formalism of both one-step protonation reactions (S + H ⇔ SH) is equivalent. What differs is the charge attribution. This leads to a very different relationship between surface charge and surface potential, which is due to a very different ratio [SH]/[S] (mixing entropy) in the PZC. The different pH-charge-potential relationship results in a completely different shape of the charging curve.

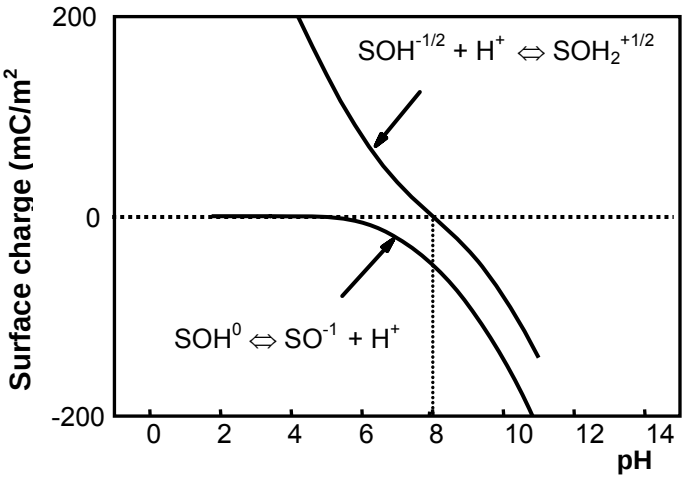

Fig.10. Comparison of the charging of two metal (hydr)oxides with one reactive type of surface group (N_s = 6 nm^{-2}), both having a single-step protonation with the same proton affinity (log$K$ = 8), but a different charge attribution (0/-1 and -0.5/+0.5), which is related to the mineral and surface structure (see text). The PZC of the surface with ≡SOH^0 groups is very low. Note the discrepancy between the log$K$ and PZC for this oxide.

In Fig.10, the above is illustrated with the calculation of two charging curves using the same log$K$, the same site density N_s, and the same Stern layer capacitance C, but a different charge attribution to the sites and corresponding transition. More generally, the shape of the experimental charging curves of iron, aluminum, and titanium oxides corresponds to the -0.5/+0.5 transition, that of quartz and silica but also latex and (natural) organic acids *etceteras* to the -1/0 transition. These different pH-potential relationships have been found experimentally (VAN HAL et al., 1996) using Ion-Sensitive Field-Effect Transistors (ISFET). Figure 11 illustrates this for SiO_2 and Al_2O_3. Around the PZC, SiO_2 reacts strongly non-Nernstian, in contrast to Al_2O_3, which reacts near-Nernstian.

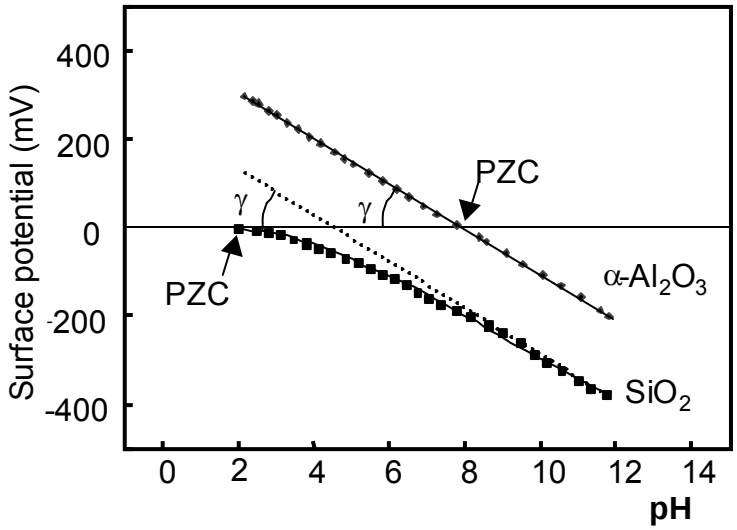

Fig.11. Comparison of the experimental surface potentials of a SiO_2 and Al_2O_3 ISFET. Data are taken from Van Hal et al. (1996). Silica reacts strongly non-Nernstian, in particular around the PZC. The Al_2O_3 reacts near-Nernstian and has a slope (γ) of approximately 55 mV/pH.

Proton affinity

Most metal oxides have a higher metal ion coordination number than quartz and gibbsite. In general, this will lead to a higher number of possible types of groups present at the surface. Due to accumulation of charge and resulting electrostatic interactions, the intrinsic proton affinity of the various surface groups cannot be derived experimentally for such metal (hydr)oxides from acid/base titrations.

As mentioned above, the first attempt to derive individual protonation constants (HIEMSTRA et al., 1989a) was based on an electrostatic interpretation of bond valence similar to the approach used by Yoon et al. to explain the PZC of metal oxides (YOON et al., 1979). In our model, the variable degree of metal coordination was shown to be a major factor in the proton affinity of different types of groups. However, the initial Pauling bond valence approach was not able to predict differences in proton affinity for surface groups with the same metal ion coordination. Later (HIEMSTRA et al., 1996b), this problem was solved by using actual bond valences based on the work of Brown (BROWN, 1977; BROWN, 1978; BROWN and ALTERMATT, 1985). The model has been extended to incorporate the effect of temperature on the proton affinity in the work of Machesky et al. (MACHESKY et al., 2001).

Brown bond valence

In the Pauling bond valence concept, the charge is equally distributed over the coordinating bonds. This is equivalent with an equal bond length. However, within one metal (hydr)oxide, bond lengths may differ considerably. Goethite (α-FeOOH) is a typical example. In this mineral, each oxygen ion is coordinated to three Fe^{3+} ions, saturating the oxygen

charge in combination with a contribution of an asymmetrical H bond, leading to a Fe_3OH-OFe_3 moiety (Fig.12).

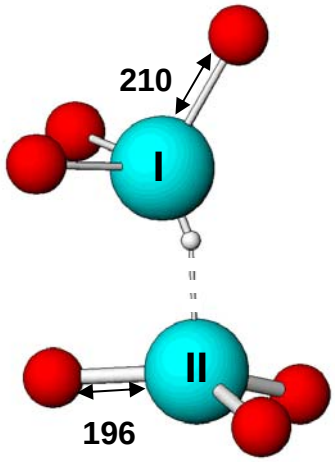

Fig.12 The schematic representation of O and OH in α-FeOOH (goethite) structure. The OH and O are both triply coordinated. The Fe-O_IH distance (in pm) is larger than the Fe-O_{II} distance, implying a lower charge attribution of the coordinating Fe ions to oxygen I than to II. This leads to a higher proton affinity of oxygen I (Actually, it is a hydroxyl!).

The proton is attached closer to oxygen I than II (Fig.12). It demonstrates the higher proton affinity of one oxygen ion (O_I) over the other (O_{II}), although both oxygens are triply coordinated. The proton attributes more charge to the short H-O_I bond than to the H···O_{II} bond. Therefore, the Fe ions coordinated to oxygen O_{II} of the non-protonated part (Fe_3O_{II}) have to contribute more to the neutralization of this oxygen whereas the Fe ions of the Fe_3O_IH part contribute less than expected based on the Pauling bond valence. The difference in neutralization finds its expression in the crystal structure by large Fe-O_I bond lengths in the Fe_3O_IH part (R = 210 pm) and smaller distances in the $O_{II}Fe_3$ part (R = 196 pm). It implies that bond valence, charge distribution, and bond length are related. The actual bond valence s can be calculated (BROWN, 2009; BROWN and ALTERMATT, 1985) with:

$$s = e^{-(R-R_o)/B} \qquad [7]$$

in which R_0 is an element specific reference length and B a constant (usually B = 37 pm).

Both types of oxygens of the mineral bulk of goethite can also be found at the surface (≡Fe_3O_IH and ≡Fe_3O_{II}). These surface groups differ in proton affinity and can be distinguished using the actual bond valence concept (HIEMSTRA et al., 1996b). The actual bond valence concept in the proton affinity modeling originates from Brown (BROWN, 1978), who calculated on this basis the neutralization of organic acids. The presence of H-bonds was ignored. Bleam (BLEAM, 1993) pointed to the importance of H bonds. In the actual bond valence approach, the charge neutralization is calculated using donating and accepting H bonds. According to Brown (BROWN, 1992), an unstressed H bond distributes its charge

asymmetrically with 0.8 v.u. for the donating O-H bond and 0.2 v.u. for the accepting O$^{\cdots}$H bond. This situation is found in water, which acts as thermodynamic reference for the proton affinity of aqueous species. Using the bond valence for H bonds in water, the charge saturation of surface groups was calculated (Σs_i-2). The calculated charge deviates from the bond valence sum rule, i.e. (Σs_i-2)≠0. *This calculated degree of charge saturation can be considered as the tendency to change H bonds and accept proton charge*. The value therefore will correlate with the proton affinity. This was shown for species in aqueous solutions. The calibrated relation log$K$ = -A (Σs_i-2) with A = 19.8, can be used to calculate the proton affinities of the individual surface groups. In this approach, it is important to know the number of accepting (n) and donating (m) H-bonds (HIEMSTRA and VAN RIEMSDIJK, 1996a).

As notified for quartz and silica, the proton affinity of a surface group can be lower than for the same group in solution. This may be due to differences in the dielectric medium (SVERJENSKY, 1994). According to Borkovec (BORKOVEC, 2001), the Born solvation term (expressed in log$K$ units) is approximately proportional with the inverse of the dielectric constant, according to $\propto \Lambda(1+2z)/\varepsilon$ units with Λ as proportionality factor and z as the valence of the reactant. Quartz and silica are known for their extremely low dielectric constant ($\varepsilon = 4$). As mentioned, the difference between the log$K$ for the protonation reaction $\equiv SiO^{-1} + H^+ \Leftrightarrow \equiv SiOH^0$ and $H_3SiO_4^{-1} + H^+ \Leftrightarrow H_4SiO_4^0$ is about 2, leading to a proportionality factor of $\Lambda \approx 8$, if we use $\varepsilon = 4$ for the adsorption phase. The Born solvation correction, i.e. $8\,(1+2z)/\varepsilon$ log$K$ units, can be calculated along the same lines for a mineral like goethite, FeOOH ($\varepsilon = 12$), and hematite, Fe_2O_3 ($\varepsilon = 25$), or rutile, TiO_2 ($\varepsilon = 120$), and casserite, SnO_2 ($\varepsilon = 9$). On these minerals, different groups with different values of z exist. The affinity correction for the protonation of the doubly coordinated $\equiv Fe_2O^-$ group (z = -1) will be for goethite and hematite respectively -0.7 and -0.3 log$K$ unit. The corrections are small and do not affect previous conclusions (HIEMSTRA et al., 1999b),(HIEMSTRA et al., 1996b),(HIEMSTRA and VAN RIEMSDIJK, 1999c) that uncharged $\equiv Fe_2OH^o$ will dominate in the normal pH range. The surface groups responsible for the charging reactions on Fe and Al (hydr) oxides are $\equiv FeOH^{-1/2}$ and $\equiv Fe_3O^{-1/2}$. Both have a valence z = -1/2. Therefore, $(1+2z) = 0$, no shift is expected for these groups (BORKOVEC, 2001). Rutile has a very high dielectric constant ($\varepsilon = 120$). In such case, the Born solvation term equals ≈ 0.0 and for isostructural SnO_2 the low dielectric constant ($\varepsilon = 9$) results in a correction of -0.3 and + 0.3 log$K$ units for respectively $\equiv SnOH^{-1/3}$ and $\equiv Sn_2O^{-2/3}$. Since both types of surface groups are present on the main crystal phases in equal amounts (MACHESKY et al., 2008), the opposite correction will have no effect of the PZC, being the average of both log$K$ values.

The above Born solvation corrections are relatively small, except for silica and quartz. The corrections have been ignored in the application of the (actual) bond valence concept for estimating logK_H. The above analysis suggests that this is not a major problem, since the corrections fall mostly within the uncertainty of predictions.

Before evaluating the implication of the calculated proton affinities of individual groups for goethite, hematite, and titanium oxide, we will discuss the use of the bond valence approach in relation to the concept of charge.

Concept of charge

Various concepts of charge are used in chemistry. Although the elementary charge of a single electron or atom is well defined, the charge in a collection of atoms in a solution or solid is less clear. In quantum chemistry, charge of atoms can be calculated from electron densities. Even at this level, arbitrary choices have to be made in the attribution of electron charge to individual atoms, yielding a certain formal charge. Quantum chemical calculation of the Mulliken charge of PO_4^z in the moiety $PO_4(H_2O)_{12}$ yields approximately z = -1, which is quite different from the formal charge (-3 v.u.) obtained from a classical valence analysis. It illustrates that formal charge depends on the definition.

Bond valence can be considered as a simple and adequate tool to define formal charges. The use depends on the application. With the Pauling bond valence concept, a formal charge can be attributed to ions in a mineral. This does not always lead to local neutrality. Charge on ions/ligands in minerals is generally absent if one applies the Brown bond valence concept (eq.[7]) in combination with the bond valence sum rule ($\sum s_j$-2). Applying the bond valence sum rule as concept to a solution will result in neutral ligands.

In surface complexation, formal charge is defined based on excess of adsorbed ions in the interface and corresponding valence charge. For instance, addition of an acid like HCl to an oxide suspension in the PZC will lead to a simultaneous adsorption of H^+ as well as Cl^-. Overall, the adsorption phase is and remains uncharged, but locally excess of charge can be defined in the interface. In a physical-chemical picture, the protons are bound at the surface oxygens and the chloride ions are present in a diffuse pattern close to the surface. Thermodynamically, electrostatic energy can be related to the concentration profile. Recent molecular dynamic (MD) simulations suggest that the sum valence rule is not obeyed for surface groups (MACHESKY et al., 2008), while it usually is in mineral lattices.

In surface complexation models, the formal proton charge is attributed to a defined location, a so-called electrostatic plane. The accumulated proton charge is smeared-out in that plane that results in a mean electrostatic field radiated by the surface of the plane. The mean field is gradually neutralized by the counter ions accumulated at the interface. If the aim is to calculate electrostatic energy, any bond valence sum rule is to be neglected deliberately. To relate the local proton excess to surface charge, one needs a charge bookkeeping tool for the reference state. The Pauling bond valence concept is very useful for this (HIEMSTRA et al., 1989a), but other choices can also be made (Hiemstra et al., 1996b) MACHESKY et al., 2008) (RIDLEY et al., 2009).

Surface speciation

Goethite (α-FeOOH)

Goethite has different crystal faces. Dominant is the 110 face (Fig.13). AFM also shows the presence of 100 faces in some preparations, which are found to be less stable than the 110 face (WEIDLER et al., 1999). At the top end of the crystals, 021 and 001 faces can be found

(WEIDLER et al., 1996). As shown in Fig.13, the dominant faces have 4 different types of surface groups, one singly-, one doubly-, and two types of triply- coordinated oxygen ions. *In situ* IR spectroscopy of Sun and Doner (SUN and DONER, 1996) in combination with data of Parfitt et al. (PARFITT et al., 1976), established the the presence of protonated surface groups, as is discussed in Hiemstra et al. (HIEMSTRA and VAN RIEMSDIJK, 2000), see Fig.13. The predicted log*K* values for the different proton reactive groups of the main crystal face (110 face) are given in Table 1. Site densities can be found in (BARRÓN and TORRENT, 1996).

We note that the 110, 021, and 001 can also be indexed as 101, 210, and 010 face.

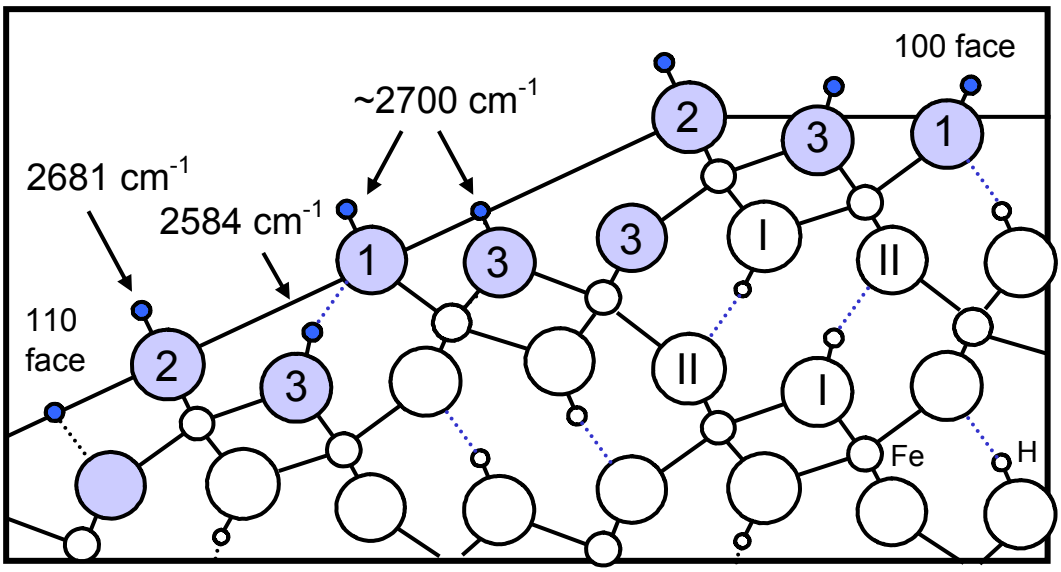

Fig.13 The schematic cross section of α-FeOOH, perpendicular on the c -axis, showing the 110 face (diagonal) and the 100 face (horizontal). The coordination numbers of the surface groups are indicated. The representative unit has one singly, one doubly, and three triply coordinated surface groups. The wave numbers of the stretching frequencies in D_2O are taken from Parfitt et al. (PARFITT et al., 1976) and Sun and Doner (SUN and DONER, 1996), as discussed in Hiemstra and van Riemsdijk (HIEMSTRA and VAN RIEMSDIJK, 2000). The roman numbers I and II refer to the oxygens given in Fig.12. We note that very recently (RUSTAD and BOILY), the lowest frequency has been attributed the triply coordinated O_IH group that interacts via H bonding with the singly coordinated surface groups. The singly coordinated surface group has a frequency close to 2700 cm^{-1}. Upon adsorption of F^-, AsO_4, or PO_4, by ligand exchange with the singly coordinated surface groups, the 2584 cm^{-1} band disappears, which is due to breaking the H-bridge with the singly coordinated surface ligand. It may imply that this band will also disappear if the $\equiv FeOH_2^{+1/2}$ group is formed (see discussion Fig.14).

Table 1. The surface groups of the goethite 110 face, the corresponding potential undersaturation of charge (Σs_i-2) and resulting proton affinity (log*K*). The index I and II indicates the type of oxygen of the lattice (Fig.12).

Species [a]	Σs_i-2	log*K* [b]	log*K* [c]
$\equiv FeO_IH^{-1/2}$ (-OH)	-0.39	+7.7	+12.1
$\equiv Fe_2O_{II}^{-1}$ (μ-O^-)	-0.60	+12.3	+9.5
$\equiv Fe_3O_I^{-1/2}$ (μ_3-O_I^-)	-0.60	+11.9	+10.0
$\equiv Fe_3O_{II}^{-1/2}$ (μ_3-O_{II}^-)	+0.20	+0.4	low

a) Between brackets, the alternative name for the species is given.
b) From (HIEMSTRA et al., 1996b)
c) Recently calculated with MO/DFT (AQUINO et al., 2008).

In Fig.14, the surface speciation is shown, calculated with the affinity constants given in Table 1. The variation of surface charge in Fig.14a is mainly due to the presence of two types of surface groups, i.e. $\equiv FeO_IH^{-1/2}$ and $\equiv Fe_3O_IH^{+1/2}$. This allows a simplification of using only these two sites, as hypothesized by Hiemstra and Van Riemsdijk (HIEMSTRA et al., 1996b). The charge of half the sites of $\equiv Fe_3O_IH^{+1/2}$ is compensated by the charge of $\equiv Fe_3O_{II}^{-1/2}$, leading to a reduced apparent site density of 3 nm^{-2} for triply coordinated surface groups. As shown in Fig.14a, the change in the speciation of singly coordinated groups dominates most strongly the overall change in surface charge. In the normal pH range (pH 4-10), the triply coordinated groups act as a permanent negative charge $\equiv Fe_3O_{II}^{-1/2}$, or positive charge $\equiv Fe_3O_IH^{+1/2}$. Both behave very similar like the oxygens in the bulk where O_I is protonated in contrast to O_{II} (Fig.12).

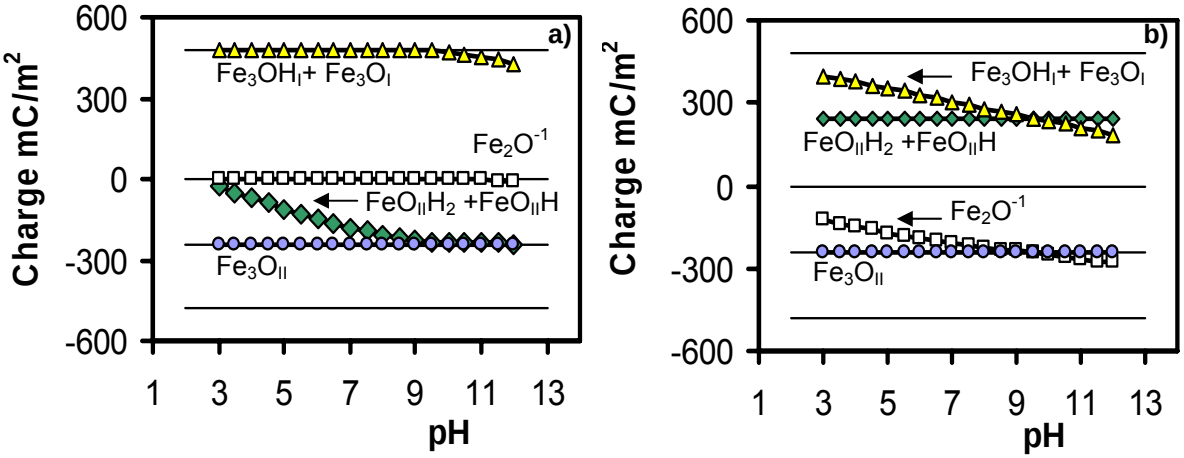

Fig.14 The calculated contribution of the various surface groups to the charge development at the 110 face as a function of pH for 0.1 M $NaNO_3$ using the protonation constants of (a) the MUSIC model (HIEMSTRA et al., 1996b) and (b) the MO/DFT calculated values (Aquino et al., 2008). The capacitances and ion pair formation constants ($\log K_c$ and $\log K_a$) are from Hiemstra and Van Riemsdijk (2006). The site density per group is 3 nm^{-2} The corresponding maximum charge contribution is given in thin horizontal lines. In Fig.14a), the singly coordinated surface group is $\equiv FeO_IH^{-1/2}$ at high pH and it is gradually protonated at lowering pH. This group is mainly responsible for the charge development. Both types of triply coordinated surface groups behave very similarly as in the bulk mineral, i.e. $\equiv Fe_3O_IH$ is mainly protonated and $\equiv Fe_3OII$ not. In Fig.14b, the singly coordinated groups are always protonated $\equiv FeO_{II}H_2^{+1/2}$, which strongly contrasts with the speciation in Fig.14a. This may be problematic in light of interpreting the IR spectrum, see text. The charge development on the 110 face is due to protonation of $\equiv Fe_3O_I^{-1/2}$ and $\equiv Fe_2O^{-1}$ when using the MO/DFT calculated log*K* values of Aquino et al. (Aquino et al., 2008). In the PZC, about half of the doubly coordinated surface groups is deprotonated, whereas no deprotonation occurs according to the MUSC model.

In a recent approach (Aquino et al., 2008), the protonation of aqueous Fe monomers as well as surface species was calculated with an ab-initio molecular orbital (MO) approach using density functional theory (DFT). Explicitly and implicitly, hydration was included. The proton affinity of the various monomeric Fe-hydroxyl species in solution was predicted and

compared to experimental data. This showed a deviation of $\Delta \log K_H \leq$ ~1-3 units, which is promising.

For surface groups, comparison of calculated affinity constants of individual surface groups with data is in general more problematic, because the protonation of the surface is the result of the interplay of various types of surface groups and is strongly masked by the electrostatic field. Generally, the predicted value of the PZC is used as a first test. In the particular case of TiO_2, *in-situ* FTIR data have been used as test. As shown later, good agreement with predictions from the MUSIC model (Hiemstra and Van Riemsdijk, 2002) are obtained for TiO_2.

For the 110 face of goethite, the estimated PZC is 9.8 when calculated from the predicted $\log K_H$ values of Aquino et al. (2008) using a full speciation model (Hiemstra et al., 1996b) with the appropriate site densities for the singly-, doubly-, and triply- coordinated surface groups. The predicted PZC value is the same as the PZC value predicted with the MUSIC model, but the individual $\log K_H$ constants are rather different (Table 1). Detailed analysis (Fig.14b) shows that the charging behavior according to $\log K$ values of Aquino et al. is mainly due to protonation of $\equiv Fe_3O_I^{-1/2}$ to $\equiv Fe_3O_IH^{+1/2}$ and of $\equiv Fe_2O_{II}^{-1}$ to $\equiv Fe_2O_{II}H^o$, while the other surface species are mainly present as $\equiv Fe_3O_{II}^{-1/2}$ and $\equiv FeO_{II}H_2^{+1/2}$. This picture strongly differs from Fig.14a, in particular with respect to the singly coordinated surface groups. Singly coordinated surface groups are mainly present as a hydroxyl (≡OH) according to the estimates of Hiemstra et al. (HIEMSTRA et al., 1996b), while it is mainly water ($\equiv OH_2$) as group when the $\log K$ values, based on the MO/DFT approach, are correct (AQUINO et al., 2008). Note that the differences in $\log K$ value (Table 1) for the reactive groups differ less than $\Delta \log K_H \leq$ ~2-4 units and this variation is in the range of the accuracy of the present MO/DFT approach. Despite the relatively slight differences in $\log K$ values, a significantly different speciation is predicted. It is a challenge to bring this difference to a test using spectroscopic and/or computational tools.

The goethite surface has two main O-H stretching bands, i.e. ~ 3660 cm^{-1} and 3490 cm^{-1} (BOILY and FELMY, 2008), comparable with the stretching found in D_2O (Fig.13) The highest frequency has contributions of various hydroxyls, as found very recently (RUSTAD and BOILY) by molecular orbital (MO) computations using density functional theory (DFT). The lowest frequency is due to a $\equiv Fe_3O_I$-H that interacts with the nearby singly coordinated surface group that neighbors it, i.e. $\equiv Fe_3$-O_I-H$\cdots\cdots$$O_{II}$-Fe≡ (see Fig.13). If the singly coordinated surface group reacts by ligand exchange with AsO_4 or PO_4, the bond is broken, due to oversaturation of oxygen valence of O_{II}. The proton of $\equiv Fe_3$-O_I-H is supposed to form an H bond with a water molecule in the Stern layer. According to this reasoning, one may expect the same in case of the formation of $\equiv FeO_{II}H_2^{1/2}$. If true, the lower frequency is problematic in the above-described speciation of Aquino et al. (AQUINO et al., 2008) where $\equiv FeO_{II}H_2^{+1/2}$ is fully dominant over the entire pH range, making the O-H $\cdots$O bond and corresponding frequency impossible. Sun and Donor (1996) have measured with ATR-FTIR the relevant part of the spectrum for the pD range 3-8.5 without the addition of a background electrolyte, showing the presence of a low frequency band in the entire pD range, i.e. the presence of $\equiv Fe_3$-O_I-D$\cdots\cdots$$O_{II}$-Fe≡. Although no variation in intensity could be noticed, the presence of a low frequency is

more in agreement with the surface speciation of Fig.14a, where $\equiv FeO_{II}H^{-1/2}$ is dominant in a considerable part of the pH range, in particular if no background electrolyte is present that will enhance protonation. At high pH, some information is available from recent FTIR data of dried goethite (BOILY and FELMY, 2008), showing that the intensity of the lower frequency band diminishes at increase of negative surface charge above the PZC, which might be explained by deprotonation of the triply coordinated $\equiv Fe_3\text{-}O_I\text{-}H$ species. In case of proton excess below the PZC, the band also disappears, which might be explained by the formation of $\equiv FeO_{II}H_2^{+1/2}$, breaking the H-bridge with the triply coordinated group below (Fig.13). In conclusion, the above analysis suggests that the proton affinity of singly coordinated surface groups ($\equiv FeO_{II}H$) is lower than that of the triply coordinated surface group ($\equiv Fe_3O_I$), i.e. $\log K_{FeOIIH} < \log K_{Fe3OI}$.

Another interesting point is the prediction of a large $\Delta \log K$ for two successive protonation steps with the MUSIC approach ($\Delta \log K \sim 12$). The recent MO/DFT calculations suggest $\Delta \log K \sim 15$ for $\equiv Fe_2O^{-1} \Leftrightarrow \equiv Fe_2OH^0 \Leftrightarrow \equiv Fe_2OH_2^{+1}$. However, $\Delta \log K \sim 3$ is found for $\equiv FeO^{-3/2} \Leftrightarrow \equiv FeOH^{-1/2} \Leftrightarrow \equiv FeOH_2^{+1/2}$. The latter $\Delta \log K$ is small and this can be questioned. Such small differences for individual ligands are not observed in solution chemistry.

Hematite (α-Fe_2O_3)

Hematite is another important iron (hydr)oxide mineral. Different synthetic preparations may lead to a large variation in reactivity, which is related to the relative presence of various types of faces in the preparations. The 001 face is rather unique, in the sense that only one type of surface groups may be present. In a classical lattice termination, it consists of only doubly coordinated surface groups. These are unable to react with oxyanions like PO_4 and SO_4 to form innersphere complexes, since oversaturation of charge would occur on the common ligand(s). The reason is the high Pauling bond valence of P (1.25 v.u.) and S (1.5 v.u.). Sugimoto and Wang (SUGIMOTO and WANG, 1998) have shown experimentally that the reactivity of hematites for SO_4 can indeed vary considerably. This variation can be related to the presence of the 001 face as shown in Fig.15 (HIEMSTRA and VAN RIEMSDIJK, 1999c).

The data suggests that the 001 face is quite inert with respect to the binding of SO_4. A similar suggestion has been made for the adsorption of PO_4. Colombo et al. (COLOMBO et al., 1994) studied the relation between the morphology of hematite and the PO_4 adsorption. The phosphate adsorption for some hematite preparations was considerably lower than for goethite, which has been attributed to the presence of the 001 face. The unique character of the 001 face of hematite has been confirmed recently with cryogenic-XPS (SHCHUKAREV et al., 2007), showing the formation of a $NaCl.2H_2O$ structure on the 001 face when the suspension is fast-frozen. This structure is not found for colloidal hematite that does not have a significant contribution of the 001 face.

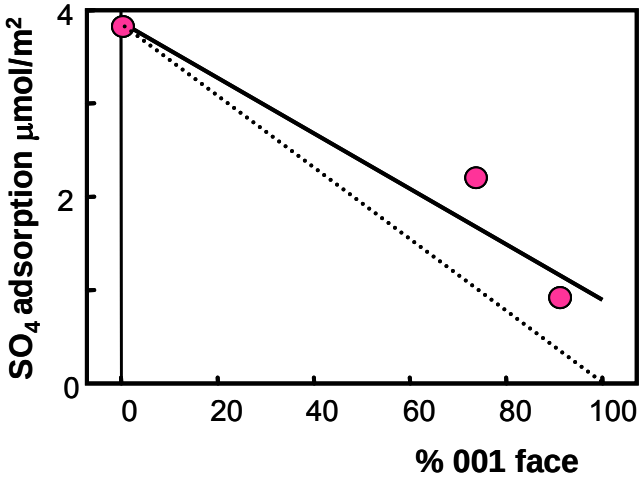

Fig.15 The adsorption of sulfate on hematite particles that have a different contribution of the 001 face. Data are from Sugimoto and Wang (SUGIMOTO and WANG, 1998). The dashed line is the expected relation in case of zero adsorption on the 001 face.

The Fe ions in the hematite structure are not symmetrically located in the octahedra due to electrostatic repulsion of neighboring Fe ions. This leads to two different Fe-O distances with corresponding bond valences 0.4 and 0.6 v.u. (HIEMSTRA et al., 1996b). At the 001 face, the doubly coordinated oxygen is partly neutralized by both types of bonds leading to an overall charge of -1 v.u. The uptake of a proton yields the $\equiv Fe_2OH^0$ group. The 001 face is comparable with the 001 face of gibbsite. Both surfaces are mainly uncharged in the normal pH range. The predicted values for the affinity constants (VENEMA et al., 1998) for the uptake of the first and second proton are $\log K_1 = 11.9$ and $\log K_1 = 0$ (as for gibbsite). The charging behavior of the 001 face is quite different from what is found for colloidal hematite, which reacts according to a multi-one pK (-0.5/+0.5) mechanism (SCHUDEL et al., 1997).

Eggleston and Jordan (EGGLESTON and JORDAN, 1998) have used an atomic force microscope to measure the double layer forces at the 001 face as a function of pH. At the tip of the microscope, a shard of a crushed hematite was placed. At high pH, a considerable force was developed. In the lower pH range, the forces were very low (Fig.16). The forces can be interpreted with the DLVO theory, using the above charging mechanism and corresponding log$K$ values (HIEMSTRA and VAN RIEMSDIJK, 1999c).

Adsorption studies using single-crystals with an exposed 001 face show that the 001 face is reactive in many cases (WAYCHUNAS et al., 2006). The reactivity can be explained by the presence of adsorbed Fe octahedra that grow the crystal. These octahedrons possess singly coordinated surface groups that are proton reactive and may form surface complexes with ions.

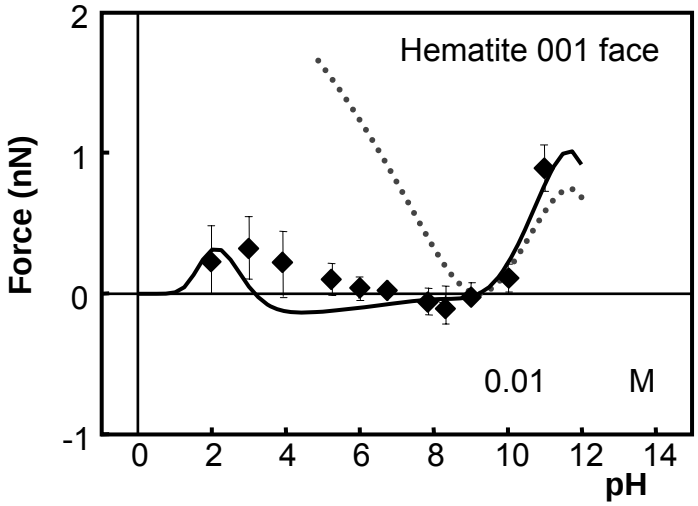

Fig.16 Force at contact between a hematite SFM tip and the 001 face of a cleaved hematite crystal. The data are of Eggleston and Jordan (EGGLESTON and JORDAN, 1998). The solid line is calculated using the predicted proton affinity constants for the doubly coordinated surface group on the 001 face. The dashed line would result if the 001 face would behave like colloidal hematite particles (see (HIEMSTRA and VAN RIEMSDIJK, 1999c).

Titanium oxides

The speciation of Ti oxides has been examined rather recently with *in-situ* IR spectroscopy. The results can be compared with what is calculated with the MUSIC model. Rutile and anatase are two main oxides of Ti oxide, which differ in the arrangement of Ti^{4+} filled octahedra. The Pauling bond valence is 2/3. Three Ti bonds saturate the oxygen charge in the bulk ($\Sigma\, s_j + V = 3 * 2/3 + -2 = 0$). At the surface, singly and doubly coordinated oxygen ions exist. The important charging reactions can be formulated as:

$$\equiv TiOH^{-1/3} + H^{+}(aq) \Leftrightarrow \equiv TiOH_2^{+2/3} \qquad [8]$$

and

$$\equiv Ti_2O^{-2/3} + H^{+}(aq) \Leftrightarrow \equiv Ti_2OH^{+1/3} \qquad [9]$$

The crystal structure of rutile and anatase is built from octahedra with two long (a) and four slightly shorter (b) Ti-O bonds. The surface composition is face-dependent and the corresponding proton affinity constants are given in Table 2.

Table 2. The undersaturation of surface oxygen charge (Σs_i-2) and resulting proton affinity (log$K$) for singly and doubly coordinated groups at the 001 face of anatase and 110 & 100 face of rutile respectively (Hiemstra et al.1996).

Species		Σs_i-2	log$K$
$\equiv TiO(b)H^{-1/3}$	Anatase 001	-0.37	+7.2
$\equiv Ti_2O(2a)^{-2/3}$	Anatase 001	-0.23	+4.7
$\equiv TiO(b)H^{-1/3}$	Rutile 110 &100	-0.38	+7.5
$\equiv Ti_2O(2a)^{-2/3}$	Rutile 110 & 100	-0.22	+4.4

The log$K$ values in Table 2 are typically calculated assuming no significant relaxation of the Ti-O bonds at the surface. In addition, an integer number (0, 1, or 2) of accepting (n) and donating (m) H bonds has been assumed in the model. For $\equiv TiOH^{-1/3}$, n = 1 and m = 1, and for $\equiv Ti_2O^{-2/3}$, n = 2 and m = 0. Recently, the surface relaxation (Ti-O bond length) has been quantified with MO/DFT and molecular dynamic MD approaches (MACHESKY et al., 2008). Machesky et al. (2008) also quantified the average number of the accepting (n) and donating (m) as well as the corresponding H$\cdots$O bond lengths. The latter are slightly shorter than assumed in the calculation of the log$K$ values of Table 2. Including these results in the classical MUSIC approach to estimate the affinity constants, leads to adjustment of the log$K$ values of log$K$($\equiv TiOH^{-1/3}$) = 5.9 ± 0.5 and log$K$($\equiv Ti_2O^{-2/3}$) = 4.9 ± 1.0. The given uncertainty represents the uncertainty in the Ti - O oxygen bond lengths (± 25 pm). The results show (when compared to the log$K$ values in Table 2) that in particular the log$K$ value of the singly coordinated $\equiv TiOH^{-1/3}$ has changed leading to a smaller Δlog$K$ between both groups. The lower log$K$ for $\equiv TiOH^{-1/3}$ is due to a larger H$\cdots$O bond contribution, equivalent with Δlog$K$~1.5. The thus-calculated values match slightly better with the PZC of 110 face of rutile (PZC = 5.4 ± 0.2).

Interestingly, this group of scientists (MACHESKY et al., 2008; VLCEK et al., 2007) has also studied recently the surface chemistry of SnO_2 (casserite). This mineral is isostructural with rutile, but has a lower PZC. It has been shown that the lower PZC results from a much larger H-bond interaction of water with the terminal surface oxygen ion ≡SnOH(H), which is equivalent with a higher charge neutralization (~0.1 v.u) and corresponding decrease of the proton affinity constant (~2 log$K$ units). For the bridging $\equiv Sn_2O(H)$, the differences with $\equiv Ti_2O(H)$ are small. Since for SnO_2, ≡SnOH(H) and $\equiv Sn_2O(H)$ are present in equal site densities, the lower log$K$ value (~2 units) for $\equiv SnOH^{-1/3}$ will result in a PZC that is about 1 unit lower, which agrees very well with the experimental value (VLCEK et al., 2007), i.e. PZC = 4.4.

Using the constants given in Table 2, the surface speciation has been calculated (Fig.17) for the 001 face of anatase. Two species are dominant (Fig.17a), i.e. $\equiv Ti_2O^{-2/3}$ (dashed line) and $\equiv TiOH_2^{+2/3}$ (full line). The speciation changes only slightly with pH compared with reactions in solution. This is due to the decelerating action of the electrostatic field. The calculated speciation can be compared with the results of *in-situ* IR spectroscopy CONNOR et al. (CONNOR et al., 1999a) measured the surface speciation for a titanium oxide film at a series of pH values in the range pH 2.3-10.7. The $\equiv TiOH_2^{+2/3}$ species is visible in the

in-situ IR spectrum with an OH stretching band at ≈ 3200 cm^{-1}, which can be removed (3150 cm^{-1} band) upon adsorption of phosphate (CONNOR and MCQUILLAN, 1999b). The band is present over the entire pH range, but growing with decreasing pH. It is maybe surprising (CONNOR et al., 1999a) that at high pH still dominance of coordinated water can be found, but this is due to the relatively high proton affinity constant of this species and the large negative surface potential strongly attracting H^+ ions. The IR-findings nicely fit qualitatively with the MUSIC calculations.

In Fig.17b, the speciation of $\equiv TiOH^{-1/3}$ and $\equiv Ti_2OH^{+1/3}$ is given. At very low pH, the surface concentration of $\equiv Ti_2OH^{+1/3}$ is important. The ≈ 3000 cm^{-1} band in combination with a 927 cm^{-1} band could be assigned to the doubly coordinated surface species and was present below pH 4.3, i.e. at pH 3.3 and pH 2.3 (Fig.17b). The surface concentration of $\equiv TiOH^{-1/3}$ increases with pH. The corresponding OH stretching band (≈ 3400 cm^{-1}) was found above pH 4.3 (pH 6.7 and higher), qualitatively in agreement with the MUSIC predictions.

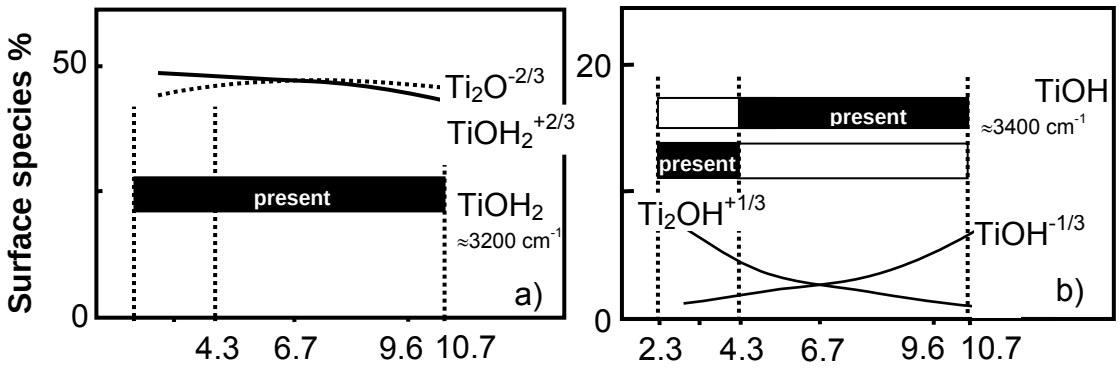

Fig.17a The calculated speciation of the dominant $\equiv TiOH_2^{+2/3}$ and $\equiv Ti_2O^{-2/3}$. The $\equiv TiOH_2^{+2/3}$ species is visible over the entire pH range in the *in-situ* IR spectra of Conner et al. (CONNOR et al., 1999a), who measured at pH 2.3, 3.3, 4.3, 6.7, 9.6, and 10.7. Fig.17b The presence of $\equiv Ti_2OH^{+1/3}$ and $\equiv TiOH^{-1/3}$. The $\equiv Ti_2OH^{+1/3}$ is found at low pH in agreement with the IR spectrum. The $\equiv TiOH^{-1/3}$ species is found at higher pH. The speciation is calculated for 0.01 M NaCl using the log*K* values of Table 2 and the ion pair formation constants of Bourikas et al. (BOURIKAS et al., 2001).

The calculated speciation with dominance of $\equiv TiOH_2^{+2/3}$ and $\equiv Ti_2O^{-2/3}$ can be understood starting in the PZC (pH ≈ 6). Without the action of electrostatics, the higher log*K* value of $\equiv TiOH^{-1/3}$ (Table 2) causes the dominance of $\equiv TiOH_2^{+2/3}$ over $\equiv TiOH^{-1/3}$ (eq.[8]) and the lower log*K* value of $\equiv Ti_2O^{-2/3}$ leads to dominance of $\equiv Ti_2O^{-2/3}$ over $\equiv Ti_2OH^{+1/3}$ (eq.[9]). It has been suggested that the situation is opposite for casserite, SnO_2, where $\log K(\equiv Sn_2O^{-2/3}) > \log K(\equiv SnOH^{-1/3})$ (MACHESKY et al., 2008; VLCEK et al., 2007). It implies that in that case $\equiv SnOH^{-1/3}$ and $\equiv Sn_2OH^{+1/3}$ are the dominant species oppositely of what is found for TiO_2 (Fig.17a). In principle, this observation can be brought to a test experimentally, but has not been done so far. Moreover, if a quantitative interpretation of the IR spectra is possible, the $\Delta \log K$ can be assessed.

Ion Adsorption

Interaction of cations and anions with metal (hydr)oxide surfaces is important in many fields of chemistry. Strong interactions are generally related to formation of innersphere complexes in which O or OH ligand(s) of the ion are shared with one or more metal ion(s) of the solid. Typical examples of ions that form innersphere complexes, as observed with spectroscopy, are SeO_3^{2-} (HAYES et al., 1987a), PO_4^{3-}, (TEJEDOR-TEJEDOR and ANDERSON, 1990), Cr^{3+} (CHARLET and MANCEAU, 1992), UO_2^{2+} (MANCEAU et al., 1992), (WAITE et al., 1994), NpO_2^{+} (COMBES et al., 1992), AsO_4^{3-} (WAYCHUNAS et al., 1993), Cd^{2+} (SPADINI et al., 1994), (RANDALL et al., 1999), (COLLINS et al., 1999b), Pb^{2+} (BARGAR et al., 1997a), (BARGAR et al., 1997b), (BARGAR et al., 1998), CrO_4^{2-} (FENDORF et al., 1997), $As(OH)_3^{o}$ (MANNING et al., 1998), Hg(II) (COLLINS et al., 1999a), Cu^{2+} (PARKMAN et al., 1999), Sr^{2+} (FENTER et al., 2000) and many others that have followed.

Another type of surface complexes is called outersphere complexes (SPOSITO, 1984). In these complexes, the primary ligands of the adsorbing ion are retained. Monovalent electrolyte ions like Na^{+}, K^{+}, Cl^{-}, and NO_3^{-} are typical examples, but also Ca^{2+} (RIETRA et al., 2001a), Sr^{2+} (AXE et al., 1998), SO_4^{2-}, SeO_4^{2-} (RIETRA et al., 2001b) and some groups of organic acids (FILIUS et al., 1997; FILIUS et al., 2000; FILIUS et al., 1999) may form these complexes under certain pH conditions.

Thermodynamic consistency

The ion-surface interactions are extremely influenced by electrostatic interactions (HIEMSTRA and VAN RIEMSDIJK, 1999a). Cations are generally adsorbed relatively weakly at low pH, since at these conditions adsorbed protons have created a non-favorable electrostatic potential. In contrast, adsorption of anions is promoted at these conditions. With increasing pH, the surface charge and its repulsive action on cation adsorption is reduced, yielding a higher cation adsorption. For anions the opposite occurs.

From a thermodynamic perspective, the pH dependency of ion adsorption can be related to co-ad(de)sorption of protons. Perona and Leckie (PERONA and LECKIE, 1985) have formulated the thermodynamic relation:

$$\left(\frac{\partial \Gamma_H}{\partial \Gamma_i}\right)_{pH} = \left(\frac{\partial \log a_i}{\partial pH}\right)_{\Gamma_i} \qquad [10]$$

The expression says that the change in H adsorption (Γ_H) due to adsorption of ion *i* at the surface (Γ_i) for a given pH is equal to the change of the negative logarithm of the ion activity a_i with pH at a given level of ion adsorption (Γ_i). The value of ($\partial\Gamma_H$ / $\partial\Gamma_i$) is negative for cations (co-desorption) and positively for anions (co-adsorption), i.e. their pH dependency is opposite.

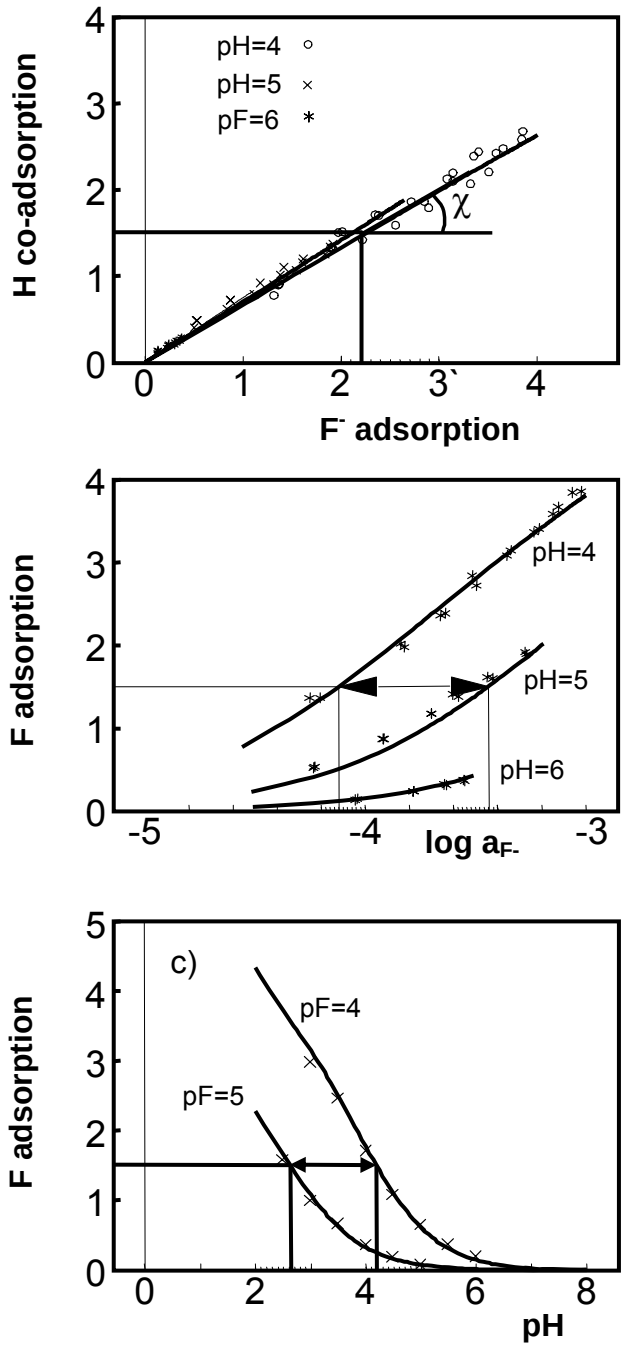

Fig.18. Fluoride adsorption behavior (μmol/m^2) on goethite in 0.1 M $NaNO_3$ (Hiemstra and Van Riemsdijk, 2000). Fig.18a The proton co-adsorption (μmol/m^2) for three pH values. Fig.18b Adsorption isotherms at constant pH. Fig.18c Adsorption-edge (μmol/m^2) at a constant activity (pF). The differential proton co-adsorption ratio $\partial\Gamma_H / \partial\Gamma_F = \chi$ in Fig.18a is about 0.68. According to the thermodynamic consistency (Eq.[10]) the value of χ leads at a given F^- loading to an equal differential change of the F^- activity with pH ($\partial \log a_F / \partial$pH). If $\partial\Gamma_H / \partial\Gamma_F$ is pH independent, $\Delta \log a_F / \Delta$pH in Fig.18b and $-\Delta$pF/ΔpH in Fig.18c, equals χ of Fig.18a.

The thermodynamic relation (eq.[10]) between the pH dependency of the adsorption and the co-adsorption relation is illustrated in Fig.18 for the adsorption of fluoride ions. The activity of F^- (a_F) can be measured experimentally using an ion selective electrode. In Fig.18a), the H co-adsorption is given as a function of the amount of F^- adsorbed. The slope of the lines in the figure represents the differential proton co-adsorption ratio $\partial\Gamma_H / \partial\Gamma_F$ or χ (left hand side of eq.[10]). In this specific case, the slope χ does not change strongly with the loading and is about 0.68 (at 1.5 μmol F^-/m^2, pH = 4). According to the thermodynamic consistency (eq.[10]), this value of χ will lead, at a given F^- loading, to a differential change of the F^- activity with pH ($\partial \log a_F / \partial pH$) of 0.68. If $\partial\Gamma_H / \partial\Gamma_F$ is pH independent, it equals $\Delta \log a_F / \Delta pH$, i.e. $\Delta pF/\Delta pH$ in Fig.18b ($\Delta pF \approx 1.5$ at $\Delta pH = 1$), and also in Fig.18c ($\Delta pH \approx 1.5$ at $\Delta pF = 1$). The analysis shows that the experimental pH dependency can be used to predict proton-ion stoichiometry χ and *vice versa* (GIRVIN et al., 1991).

In many cases, a considerable difference exists between the free activity of an ion and the total concentration in solution (C_t). The difference is most strongly for ions of which the speciation changes in solution due to hydrolysis or protonation. Examples are $Hg(OH)_m^{+2-m}$ and $H_nPO_4^{-3+n}$. The above expression (eq.[10]) can be written in a general form (RIETRA et al., 2000a) relating the overall pH dependency of ion adsorption ($\partial \log C_t / \partial pH$) to the proton coadsorption. The expression is:

$$\left(\frac{\partial \log C_t}{\partial pH}\right)_{\Gamma_i} = \left(\frac{\partial \Gamma_H}{\partial \Gamma_i} - n_H\right)_{pH} \equiv \left(\chi_H - n_H\right)_{pH} \qquad [11]$$

in which $\chi \equiv \partial\Gamma_H / \partial\Gamma_i$, the proton coadsorption relative to a chosen reference state of component *i*, and *n* is the change of the mean excess number of protons per ion *i*, defined as a proton excess relative to the same reference state of *i*. An important and often confusing point is the choice of the reference state from which the number of H is counted. Often unprotonated species, like Hg^{2+} and PO_4^{3-} are chosen as reference. In case of using PO_4 as reference, the mean excess number of protons (*n*) per PO_4 in solution can be calculated. At pH 9, the main phosphate species in solution is HPO_4^{2-}, yielding $n \approx 1.0$ if PO_4 is the chosen reference. The experimental co-adsorption χ at this pH is $\chi \approx 2.3$ (HIEMSTRA and VAN RIEMSDIJK, 1996a) if counted relative to PO_4^{3-} as reference species. Thermodynamically, we could also have chosen HPO_4^{2-} as reference. In that case, *n* would be zero since the mean number of protons per phosphate ion is zero if counted as an excess relative to HPO_4. Using also HPO_4 as reference for determining the co-adsorption (instead of PO_4) gives $\chi = 1.3$. So the individual values of *n* and χ decrease with the same number (an integer) if the reference state is changed. However, the difference, χ - *n*, remains the same and is independent of the choice of the reference, provided that the same reference species is chosen for χ and for *n*. Finally, note that negative values of *n* may occur if the species in solution have on average fewer protons than the chosen reference. This occurs in case one chooses a reference species

that is only dominantly present at low pH. Examples are HF and H_3PO_4 (deprotonation), and Hg^{2+} and Al^{3+} (hydrolysis).

Proton ion adsorption ratio χ

The thermodynamic consistency relationship of Eq. [11] shows that the overall change in adsorption with pH is a combination of a true surface property (expressed in χ) and a chemical property of the component in solution (expressed in n). It shows that if the solution speciation changes, this will affect adsorption. In the past, Hingston et al. (HINGSTON et al., 1967) has recognized this and formulated the concept of adsorption envelopes. The surface property χ can be assessed experimentally. Recently, Rietra et al. (RIETRA et al., 1999a) has proposed for the determination of χ the use of a proton-ion titration at high solid concentrations and constant pH. It is particularly useful for ions and pH conditions with a relatively strong adsorption. This method allows a direct measurement of χ from the back titration with H/OH upon addition of the ion, without analysis of the solution as long as almost all added ions adsorb.

The co-adsorption of protons can also be assessed indirectly with the classical acid/base titrations of systems in which a certain quantity of ion I is added, e.g. Lövgren et al. (LÖVGREN et al., 1990) and Gunneriusson et al. (GUNNERIUSSON and SJÖBERG, 1993), (GUNNERIUSSON et al., 1994). In this type of experiments, the co-ad(de)sorption of H is measured over a wide pH range in which the added ions are bound in a variable degree. From such data, the coadsorption can only be found using a model, if it can describe the curves correctly. From a thermodynamic point of view, the reactions in the model do not necessarily have to reflect the physical picture as for instance observed with spectroscopy. This leads to the conclusion that one cannot derive the nature of the adsorbing species by such an analysis, as has often been done in the past.

The proton co-adsorption ratio χ can be interpreted as a mean proton stoichiometry of the binding reaction. It is usually not an integer, which implies that the adsorption is non-stoichiometric. In a simple thermodynamic picture, the non-stoichiometry can be considered as a combination of formation reactions leading to series of surface species with different numbers of protons bound. However, series of surface species may be in conflict with what can be observed with spectroscopy. To approach physical reality, it should be realized that non-stoichiometry could be largely due to the electrostatic interaction of the adsorbing ion with protons located on other surface groups. This electrostatic interaction depends of the total charge of the adsorbed ion involved, but also on the location of this charge. The latter is related to structure of the surface complex (RIETRA et al., 1999a), to be shown below.

Proton co-adsorption and location of charge

In order to relate proton co-adsorption and pH dependency with the structure of surface complexes, we will start with a very simple picture of a moving test charge in an electrostatic field. When negative charge moves towards a positive metal oxide surface, the surface reacts with the adsorption of an increasing number of protons. The maximum interaction and corresponding number of co-adsorbed protons is attained when the negative test charge reaches the surface where the proton charge is located. If the surface reacts according to Nernst law, the number of protons adsorbed is equal to the valence of the test charge (FOKKINK et al., 1987), (VENEMA et al., 1996a). Therefore, the co-adsorption ratio χ depends on the location of an ion in the electrostatic field. It is very important to emphasize that in the limiting case of a Nernstian surface, the co-adsorption ratio χ becomes *independent* of the formulated reaction including the number of protons written in it, i.e. *independent* of the intrinsic stoichiometry of the reaction! This is also almost the case for Near-Nernstian surfaces, i.e. electrostatics are an important and often the most important explaining factor in the pH dependency of adsorption (apart from the behavior of the species in solution, eq.[11]).

Rietra et al. (RIETRA et al., 1999a) have measured the co-adsorption for a series of divalent ions (Fig.19) adsorbed on goethite at low pH. All these ions form innersphere complexes (HAYES et al., 1987a), (FENDORF et al., 1997), (HUG, 1997), (PEAK et al., 1999), (WIJNJA and SCHULTHESS, 2000). The explanation for the difference in co-adsorption is a different location of the ion charge in the interface of the Near-Nernstian metal (hydr)oxide. The mean distance of the ion charge from the surface follows the order $SeO_3^{2-} < CrO_4^{2-} < SO_4^{2-}$. This difference can be correlated with the difference in structure of the surface complex. The SeO_3^{2-} ion binds as a bidentate (Fig.19) and has only one non-coordinated ligand (Hayes et al. 1987). Recently, it has been shown that the proton co-adsorption behavior of carbonate is very similar to SeO_3^{2-}(HIEMSTRA et al., 2004), suggesting that CO_3^{2-} binds to the surface in a similar manner as SeO_3^{2-}, i.e. a bidentate complex.

At low pH, the dominant surface complex of SO_4^{2-} is a monodentate complex in which three of the four ligands are non-coordinated (HUG, 1997), (PEAK et al., 1999), (WIJNJA and SCHULTHESS, 2000). In addition, some SO_4 outersphere complexation may occur. In both cases, the charge of sulfate is on the average located at a larger distance from the surface than selenite, which has 2/3 of its ligands common with the surface. The chromate ion has an intermediate position. For this ion, bidentate complex formation has been reported (FENDORF et al., 1997). At high pH and low loading, monodentate chromate complexes can be found too, but bidentate species have the tendency to dominate at low pH, as will be explained later.

Experimentally, a different change of co-adsorption ratio χ with loading is observed for the three ions with a different complex structure ($\equiv \partial\Gamma_H / \partial\Gamma_{ion}$, slope of the lines in Fig.17). The ion (SO_4^{2-}) with the largest number of outer ligands (i.e. charge) has the highest change in χ with loading and has the most non-linear behavior. We will show that this is also an electrostatic effect. We will analyze two extreme situations of the location of the charge in a double layer, i.e. at the surface or at the head end of the DDL, resulting in the dashed lines in Fig.19.

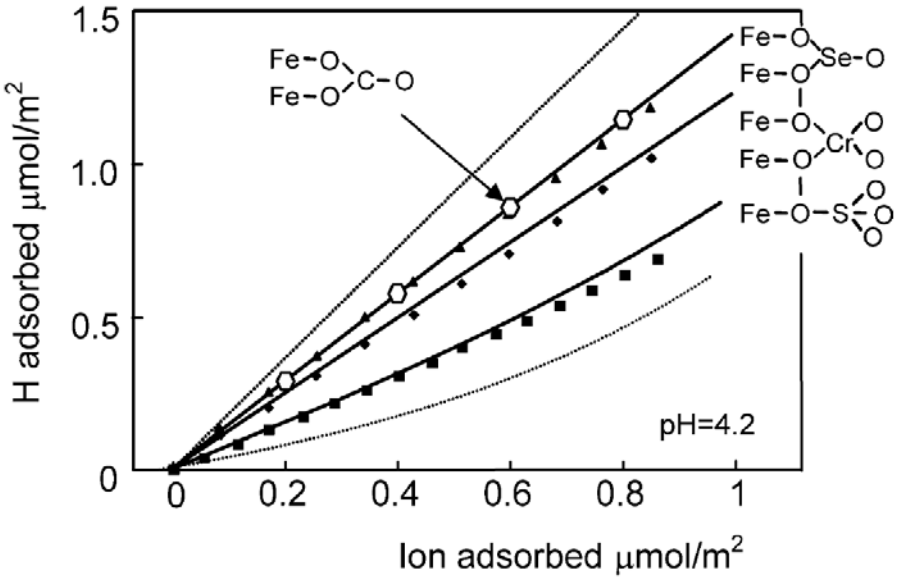

Fig.19. The co-adsorption of protons due to the binding of CO_3^{2-}, SeO_3^{2-}, CrO_4^{2-}, and SO_4^{2-} on goethite in 0.01 M $NaNO_3$ at pH = 4.2. The dashed lines indicate the expected co-adsorption in case all ion charge (-2) is present at the surface or in the 1-plane (BS approach), yielding a very high and a low co-adsorption respectively. The full lines have been calculated assuming a Pauling distribution of charge of the central ion over the coordinating ligands, leading to a surface charge attribution of respectively 67, 50, and 25 % of the anion charge (-2). Data are of Rietra et al. (RIETRA et al., 2000a), except for carbonate which are based on the excellent data set of Villalobos et al. (VILLALOBOS and LECKIE, 2000), see Hiemstra et al.(HIEMSTRA et al., 2004).

If all anion charge (-2 v.u.) is attributed to the surface and the surface would be perfectly Nernstian, exactly the same amount of charge is co-adsorbed as protons (2 H^+). Therefore, there is no change in surface charge σ_o and surface potential ψ_o and hence no variation in χ. In case of a near Nernstian behavior, approximately the same will occur (upper dashed line in Fig.19). However, if the ion charge is introduced in the non-Nernstian environment of the 1-plane, the charge (σ_1), and hence potential (ψ_1) of the 1-plane, will strongly change with loading. The changes in the 1-plane will affect the charge at the surface. The surface charge σ_o increases which can be rationalized with the electrostatic relation for an electrostatic capacitor:

$$\sigma_0 = C(\psi_0 - \psi_1) \qquad [12]$$

At a constant surface potential ψ_o, the surface charge σ_o will increase with a decreasing ψ_1 potential (eq.[12]) resulting from outersphere complexation. This increase in σ_o is in this picture equal to the number of protons co-adsorbed. The decrease of ψ_1 is non-linear with the net charge of the particle (σ_o + σ_1) which follows from the well-known DDL equation in combination with charge balance:

$$\sigma_0 + \sigma_1 = -\sigma_d = \pm \sqrt{2000\ \varepsilon_o \varepsilon_d RT\ \sum_i C_i (exp\frac{z_i F\Psi_d}{RT} - 1)} \qquad [13]$$

realizing that $\psi_1 = \psi_d$ in the Basic Stern model. The non-linearity results in a curve with a slope that is changing with loading (lower dashed line in Fig.19).

Summarizing, the pH dependency is determined by two factors, i.e. solution chemistry (n) and the co-adsorption or co-desorption of protons (χ). The latter is a true surface property. This property is very strongly determined by the electrostatic reaction due to introduction of charge in the electrostatic field around metal (hydr)oxide particles. This electrostatic concept is not very intuitive and scientists, who are not familiar with it, have the tendency to emphasis the role of the intrinsic stoichiometry of the reaction. However, only in rare cases, the intrinsic stoichiometry will play a role.

Interfacial Charge Distribution

In the previous paragraph, it was shown that the location of a charge and the co-adsorption of H are related and how this is linked to the structure of the innersphere complex. Because of the different electrostatic location of the ligands of specifically adsorbed ions, the charge is spatially distributed and can be modeled along the same lines previously used in the MUSIC model.

In the MUSIC approach, the charge of the surface oxygen can be calculated with the Pauling bond valence concept. The coordinating proton(s) and the metal ion(s) of the solid are present at different positions, but the charge is attributed to the surface oxygen (Fig.20). In case of the formation of an innersphere surface complex, part of the neutralization of the surface oxygen(s) stems from the central ion in the innersphere complex. The remaining charge of the central ion in the complex is used by the other coordinating oxygens. The latter oxygens are located at a different electrostatic position in the interface than the ligands of the complex common with the metal ions of the solid. So in this picture, the charge of the adsorbed ion is no longer considered as a point charge, but the location of charge is based on the structure of surface complex. The use of such concepts is important since it fits in the language of spectroscopists working at the microscopic level.

The charge distribution in the interface will depend on the charge of the ligands and the distribution of the ligands in the interface. The use of the Pauling bond valence (eq.[2]) implies that in case of SeO_3^{2-} ion adsorption (Fig.19), 2/3 of the total charge (z = -2) is to be attributed to the surface (z_0 = -1.33) and 1/3 to the 1-plane (z_1 = -0.67). In case of CrO_4^{2-} and SO_4^{2-} adsorption (Fig.19), the charge attribution to the 0- / 1-plane is -1.0/-1.0 and -0.5/-1.5 v.u. respectively. With this Pauling charge distribution, we have calculated the expected co-adsorption corresponding to the formation of the given surface complexes. As shown in Fig.19, the predicted co-adsorption values χ are quite close to the experimental values. Only a slight adjustment is needed to get an almost perfect description.

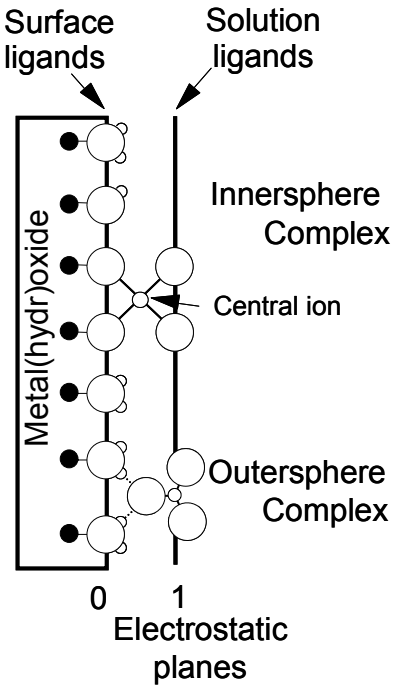

Fig.20. A schematic representation of a metal (hydr)oxide surface with protonated surface oxygens, innersphere complex formation and outersphere complex formation. The charge of protonated surface oxygens originates from the coordinating metal ion(s) of the solid and adsorbed proton(s). In case of an innersphere surface complex, also part of the charge of the central ion contributes to the neutralization of the (common) surface oxygen. The charge of the central ion in the innersphere complex is also partly used to contribute to the neutralization of the ligands that are solution oriented, as depicted. The mean location of the charge of the outersphere complexes is at the outer electrostatic plane. The layer between both electrostatic planes is called a Stern layer. A model combining one Stern layer is called a Basic Stern (BS) model. If extended with a second Stern layer, it may be called an Extended Stern (ES) layer model.

More factors may influence the interfacial charging behavior. Besides ligand distribution, also the charge distribution because of asymmetry in the coordination sphere will be important, as discussed later. In case of surface oxidation in combination with electron transfer, the CD is strongly affected, as found by analyzing the Fe(II) adsorption on a variety of minerals (HIEMSTRA and VAN RIEMSDIJK, 2007a). The electron transfer will lead to the adsorbed Fe^{3+} and as a result, this species will hydrolyze leading to adsorbed $Fe(III)(OH)_2^+$. Another factor that may influence the interfacial charge distribution is the orientation of water dipoles in the interface. Dipoles may react on a change in surface charge due to ion adsorption. This may lead to some local neutralization of surface charge with interfacial charge transfer towards the solvent (HIEMSTRA and VAN RIEMSDIJK, 2006), as discussed later.

Formation of outersphere surface complexes

The concept of outersphere adsorption of electrolyte ions has been used to relate surface charge and potential (GRAHAME, 1947; STERN, 1924). Experimentally, simultaneous adsorption of electrolyte cations and anions in the PZC has been found (SHIAO and MEYER, 1981; SMIT and HOLTEN, 1980; SPRYCHA, 1984; SPRYCHA, 1989b), which depends on the electrolyte concentration. The interaction is weak and has a large electrostatic contribution. The outersphere complexes have no common ligands with the metal ions of the solid (Fig.20) and remain at some minimum distance of approach. From an electrostatic point of view, these

complexes may be treated with less structural detail. They are often considered as a point charge, located at the head end of the diffuse double layer.

In the simplest model approach for ion adsorption, the same affinity is assumed for the outersphere complex formation of electrolyte cations and anions. However, it has been shown that surface charge varies with the type of electrolyte cations and anions (BOURIKAS et al., 2001; BREEUWSMA and LYKLEMA, 1973; KALLAY et al., 1994; SAHAI and SVERJENSKY, 1997; SPRYCHA, 1984), indicating differences in affinity. Rietra et al. (2000a) have measured the variation in electrolyte anion binding (Fig.21) for goethite. Almost no intrinsic affinity was found to exists for ClO_4^- ($\log K$ = -1.7). In case of Cl^-, the higher affinity was about ten times higher, $\log K$ = -0.5. Nitrate is in between with $\log K$ = -1. It has been shown experimentally (RIETRA et al., 2000a) that these differences have a considerable effect on weakly adsorbed ions like SO_4^{2-}. In addition, effects on the PO_4 adsorption could be observed.

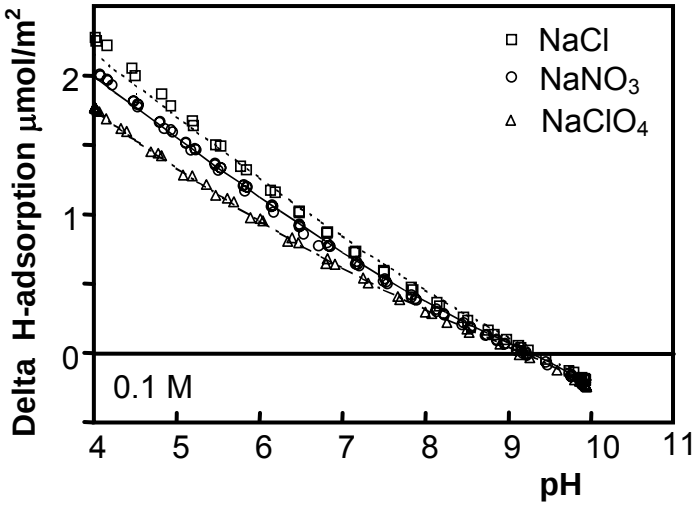

Fig.21. The adsorption of protons in NaCl and $NaClO_4$, measured relatively to the H binding in $NaNO_3$, using the PZC in $NaNO_3$ as reference (zero proton binding). Data are of Rietra et al. (RIETRA et al., 2000a).

For goethite with a high PZC, such an analysis has been done by measuring at various high concentrations, the acid-base behavior for a series of solutions containing different combinations of electrolyte cations and anions. In the experimental approach, it is important to scale the data of each type of salt not individually by using a common intersection point (CIP), but scaling them all relatively to the charge of a stock suspension (HIEMSTRA and VAN RIEMSDIJK, 2006; RAHNEMAIE et al., 2006). In this way, all data become consistent. For a given anion (Cl^-, or NO_3^-), the corresponding titration curves for Li^+, Na^+, K^+, and Cs^+ show a distinct difference. The simultaneous interpretation of all data points leads to a consistent set of parameters (HIEMSTRA and VAN RIEMSDIJK, 2006), given in Table 3.

Table 3. The allocation of charge (Δz) and the affinity constants of interaction ($\log K$) with goethite (FeOOH) if all electrolyte ions are placed at the 1-plane. The fitted capacitance for the first and second layer are respectively $C_1 = 0.93 \pm 0.01$ and $C_2 = 0.74 \pm 0.10$ F m^{-2}.

Ions*	Δz_0	Δz_1	Δz_2	$\log K$
Li^+	0	+1	0	+0.10 ± 0.02
Na^+	0	+1	0	- 0.60 ± 0.03
K^+	0	+1	0	- 1.61 ± 0.13
NO_3^-	0	-1	0	- 0.68 ± 0.03
Cl^-	0	-1	0	- 0.45 ± 0.03

* Cs^+ ions do not form significantly ions pairs on goethite

An interesting result of the analysis was that the data could only be described satisfactory using a double layer model with two Stern layers. The outersphere electrolyte ions are placed at a minimum distance of approach (plane 1 in Fig.20). Between this plane and the start of the diffusion double layer, the second Stern layer is situated. The reason might be ordering of water molecules in 2-3 layers near the surface. The physical-chemical interpretation is described later, see (HIEMSTRA and VAN RIEMSDIJK, 2006).

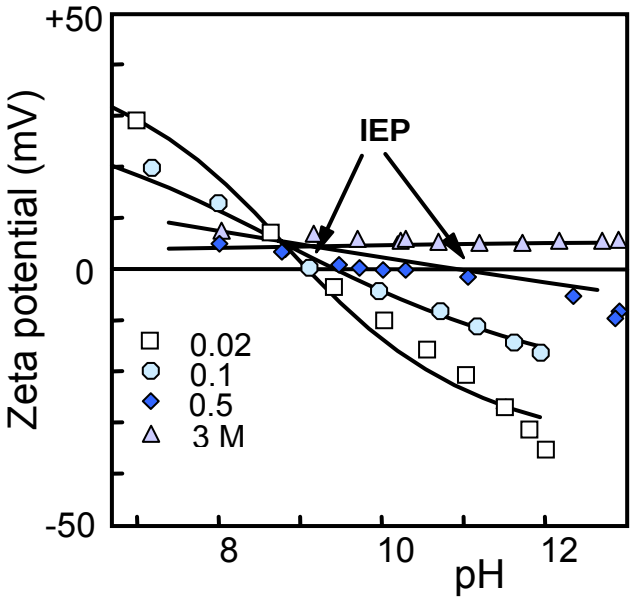

Fig.22. The shift of the IEP at increasing concentrations of electrolyte, measured with electro-acoustophoresis. Data are of (Rowlands et al., 1997). The lines have been calculated with the MUSIC model. The shift of the IEP is due to a larger affinity of the surface for electrolyte cations than anions. For details see Hiemstra et al. (Hiemstra et al., 1999b).

A higher intrinsic affinity of a cation than for an anion may result in an upward shift of the IEP (Hiemstra et al. 1999). Using novel electro-acoustophoresis, it has been shown experimentally (Rowell et al. 1999) that for instance gibbsite particles can become positively charged over the entire pH range even above pH = 12 (Fig.22). An upward shift of the IEP is not only found for gibbsite but also for rutile (KOSMULSKI, 1997) for a series of electrolytes.

As shown in the next section, TiO_2 has a stronger affinity for cations than anions, in particular at high ionic strength, explaining such behavior of the IEP.

Innersphere and outersphere complexation of electrolyte ions

Bourikas et al. (BOURIKAS et al., 2001) have carried out a systematic analysis of the charging behavior of rutile and anatase and determined the intrinsic affinity constants for a large series of electrolyte ions, assuming outersphere complexation only. They found that in general a stronger complexation for cations than anions. The variation in affinity of electrolyte anion and cations is relatively easily assessable for a material like rutile because it has a PZC value in the middle of the experimental pH window. Recently, the affinity of electrolyte cations has been described in more detail for rutile (RIDLEY et al., 2009). As discussed below, the electrolyte cations may form a combination of inner- and outersphere complexes, very well in agreement with spectroscopy and molecular dynamic simulations. For the electrolyte anions, only outersphere complexation is found.

Table 4. The allocation of charge (Δz_0, Δz_1) of electrolyte ions in the Basic Stern model, derived from the data of Ridley et al. (RIDLEY et al., 2009) for rutile (TiO_2), in comparison with the values expected assuming a Pauling distribution of charge in the various innersphere complexes formed using the coordination number given. Spectroscopy (FENTER et al., 2000; ZHANG et al., 2004; ZHANG et al., 2007) shows that ions usually form tetradentate surface complexes with adsorbed ions. For Na^+, and Ca^{2+} bidentate complexation has been suggested based on molecular dynamic MD simulations (PREDOTA et al., 2007). This is also assumed for Sr^{2+}. The fitted capacitance (BS model) is $C_1 = 0.64 \pm 0.01$ F/m^2.

Ions	Δz_0*[a)]	Δz_1*[a)]	CN	Δz_0*[b)]	Δz_1*[b)]
Na^+-bi*[c)]	0.39 ± 0.02	0.61	6	0.33	0.67
Na^+-tet*[c)]	0.77 ± 0.09	0.23	6	0.67	0.33
K^+-tet*[c)]	0.49 ± 0.01	0.51	8	0.50	0.50
Rb^+-tet*[c)]	0.47 ± 0.01	0.53	8	0.50	0.50
Ca^{2+}-bi	0.90 ± 0.08	1.10	6	0.67	1.33
Ca^{2+}-tet	1.23 ± 0.02	0.77	6	1.33	0.67
Sr^{2+}-bi	0.65 ± 0.02	1.35	6-8	0.57 ± 0.1	1.43
Sr^{2+}-tet	1.18 ± 0.05	0.82	6-8	1.14 ± 0.1	0.86

*[a)] From data analysis
*[b)] Calculated Pauling distribution using the CN value given
*[c)] For Na^+, no outersphere complexation revealed, in contrast to K^+ and Rb^+ using $\Delta z_0 = 0$ and $\Delta z_1 = +1$

Large cations like Rb^+ may form innersphere complexes, as follows for rutile from spectroscopic work (FENTER et al., 2000; ZHANG et al., 2004; ZHANG et al., 2007). Recently, a high-quality set of titration curves of TiO_2 has been analyzed, allowing innersphere as well as outersphere complex formation of electrolyte ions (RIDLEY et al., 2009). The CD-MUSIC model has been applied, in which the charge of electrolyte ions is placed at the 1-plane and additionally, the electrolyte ions were allowed to form an innersphere complex having a charge distribution (CD). The analysis indeed reveals the presence of innersphere complex formation for electrolyte cations that typically occurs at high pH and high electrolyte concentrations, as expected. A second important result of the analysis was the interpretation of the fitted values of the CD (Table 4). The fitted CD values of the various inner-sphere

complexes of the mono- and divalent ions can be linked to the microscopic structure of the surface complexes found by spectroscopy. For instance, Rb^+ ion forms a tetradentate complex (ZHANG et al., 2007). In case of a coordination number of 8, half of the ligands is common with the surface. Applying the Pauling bond valence concept, one expects a set of CD values of $\Delta z_0 = +0.5$ and $z_1 = +0.5$ v.u. and this CD is also found by fitting (Table 4).

For the Na^+ ion, the CD value can only be well understood allowing the presence of a bidentate as well as a tetradentate inner-sphere complexation in the data analysis. These surface complexes have also been suggested in a recent MD study (PREDOTA et al., 2007). The fitted CD values are in agreement with the Pauling distribution. Moreover, the interpretation of the CD model suggests similar amounts of bidentate and tetradentate Na^+ innersphere complexes at the conditions used in the MD simulations, which is (semi-) quantitatively in agreement with the MD results. Since the above suggests that the Pauling bondvalence can be used to estimate the CD for the electrolyte ions, the number of adjustable parameters can be reduced by imposing a Pauling distribution (RIDLEY et al., 2009).

The parameterized CD model can be used to predict the surface loading with Rb^+ in the tetradentate configuration for the condition used in spectroscopic experiment (ZHANG et al., 2007). With *in-situ* spectroscopy, a Rb^+ surface loading of 3.5 ± 1 μmol/m^2 was found at pH = 12 in 1 M RbCl solution. With the CD model, only parameterized with titration data in the pH range 3-10 (I = 0.03-0.3 M), the predicted loading is 3.0 μmol/m^2. The agreement is excellent.

In the work of Bourikas, (BOURIKAS et al., 2001), it was noticed that two types of TiO_2 materials could be distinguished, i.e. materials with a low and with a high proton loading. Without allowing innersphere complexation, the high loading leads to a higher capacitance value for the Stern layer than usually is found for metal oxides. With the above model, allowing innersphere complexation, the difference in charging might be understood. The high charging is for surfaces having innersphere complexation of electrolyte ions and the capacitance value is in a range that can be expected. The TiO_2 materials with a low charging, innersphere complexation might be less, for instance due to less well-organized surfaces not allowing the formation of these complexes that require the specific tetradentate configuration.

In conclusion, this recent work (RIDLEY et al., 2009) is a large step forward giving strong evidence for the tight relationship between the macroscopic phenomena, interpreted with the CD model, and the microscopic reality as found experimentally, or found with modern chemical computational approaches.

Partitioning of inner- and outersphere surface complexes

Recent IR and Raman spectroscopy have shown that selenate SeO_4^{2-} and sulfate SO_4^{2-} ions may form inner- and outer-sphere complexes (PEAK et al., 1999), (WIJNJA and SCHULTHESS, 2000). Outersphere complex formation occurs at high pH, while at low pH these anions are mainly bound as a monodentate innersphere complex. The different pH

dependency of outer- and inner-sphere complexes is illustrated in Fig.23, using the parameter values of Rietra et al. (RIETRA et al., 2001; RIETRA et al., 2001a).

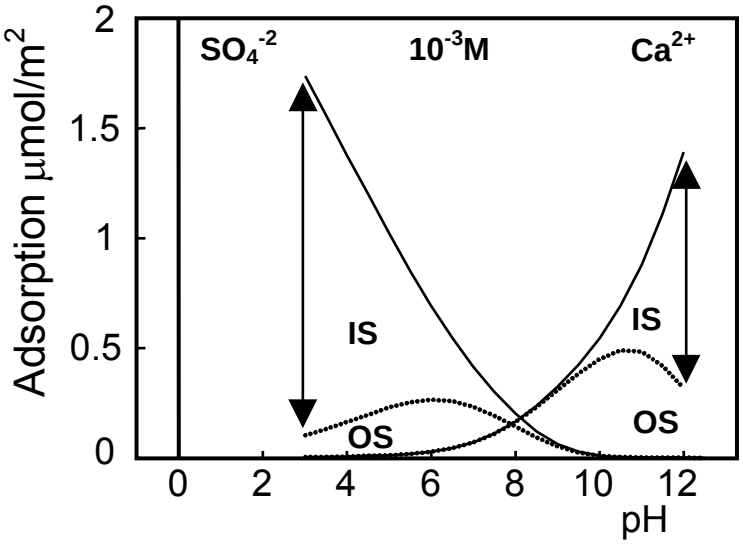

Fig.23. The adsorption in a SO_4^{2-} -goethite and a Ca^{2+}- goethite system at an ion concentration of 0.001 M in 0.1 M $NaNO_3$ (full line). The contribution of outersphere complexes (os) is given as dotted line. The difference between both lines gives the contribution of innersphere (is) complexes. Parameters are taken from Rietra et al. (RIETRA et al., 2001; RIETRA et al., 2001a).

The pH dependent partitioning of an ion over outer- and innersphere complexes is due to the difference in structure of both complexes, resulting in a different location of the charge in the electrostatic field and a different pH dependency. The outersphere complexes of SO_4^{2-} (but also SeO_4^{2-}) will attribute less negative charge to the surface than the innersphere complexes, which leads to less co-adsorption of protons and to a smaller pH dependency than the innersphere complex. Spectroscopy shows that at high pH the outersphere complex dominates. The innersphere species may also be present, but at a lower adsorption density. With lowering the pH, the adsorption density of the outersphere complex will increase, but the innersphere complex will increase stronger, since it has a larger pH dependency. The innersphere complexes will thus start to dominate at some point (Fig.23) and will further increase its relative presence due to mainly electrostatic competition between the inner- and outer-sphere complexes.

For cations, an opposite pH dependent partitioning over inner- and outersphere complexes exists. Innersphere complexes of Sr^{2+} are found at relatively high pH (COLLINS et al., 1998), (FENTER et al., 2000) and outersphere complexes are found at lower pH values (AXE et al., 1998), (SAHAI et al., 2000). Based on modeling, the same can be concluded for Ca^{2+} (RIETRA et al., 2001a). We know for cations that the co-adsorption of protons is negative. Therefore, the pH dependency of adsorption is opposite to that of anions. In case of a combination of outer and innersphere complex, the complex with the largest charge attribution to the surface (innersphere) will have the highest proton co-desorption and pH

dependency. This implies that ultimately the innersphere complex will win at sufficiently high pH (Fig.23).

Mono- and bidentate innersphere surface complexation

The above principle of a different speciation of a particular ion as a function of pH, due to a difference in structure of the surface complexes, can also be applied to the partitioning of an ion over bidentate and monodentate complexes. It has been shown (TEJEDOR-TEJEDOR and ANDERSON, 1990) that monodentate $\equiv FeOPO_3$ dominates at high pH and low loading. The pH effect is explained similar as for the partitioning of an ion over outersphere and innersphere complexes. As pointed out above, the increase of loading changes the charge and in particular the potential at the location of the outer ligands (1-plane). This has also been discussed previously (HIEMSTRA and VAN RIEMSDIJK, 1999a), (HIEMSTRA and VAN RIEMSDIJK, 1996a).

Bourikas et al. (BOURIKAS et al., 2000) have studied for anatase the proton/molybdate co-adsorption ratio as a function of pH. In case of the assumption of one adsorbed species, the calculated charge distribution increased at low pH. It indicates that the mean distance between molybdate and the protons at the surface decreases, which leads to an increase of interaction between both components, i.e. a higher proton co-adsorption. This observation can be interpreted in terms of structure. The bidentate complexes have on average a smaller charge distance from the surface (Fig.19). The dominance of bidentate over monodentate complexes at low pH was recently also demonstrated with the CD-MUSIC model for CrO_4 (WEERASOORIYA and TOBSCHALL, 2000).

Hayes et al. (HAYES et al., 1987a), (HAYES et al., 1988) were the first who tried to relate ion adsorption and the structure of surface complexes, using spectroscopy. This was done for Se. A bidentate innersphere complex was found for selenite, SeO_3. However, this complex could not be used in their modeling, since its use would lead to a too high pH dependency. Hiemstra and van Riemsdijk (HIEMSTRA and VAN RIEMSDIJK, 1999a) have analyzed the reason for this failure and showed that this was due to the use of the 2-p*K* model. Actually, the adsorption of SeO_3 on goethite is an extremely valuable example illustrating the tight relationship between pH dependency of ion adsorption, its surface structure, and the MUSIC model.

In case of the homogeneous 2-p*K* model, the surface groups in the PZC can be represented by SOH^0. The intrinsic reaction is:

$$2\ SOH^0 + 2H^+(aq) + SeO_3^{2-}(aq) \Leftrightarrow (SO)_2SeO^0 + 2H_2O(l) \qquad [14]$$

According to reaction eq.[14], no change in surface charge occurs if all charge is attributed to the surface as a point charge (classical treatment of innersphere complex formation). At an uncharged surface, electrostatics will not influence the behavior and the intrinsic stoichiometry of the reaction is equal to the proton co-adsorption ratio, i.e. $\chi = 2$ if SeO_3 is added. This is not found experimentally. A value of $\chi = 2$ will lead to a too high pH dependency (eq.[11]). Moreover, other experiments (Fig.24) show a large change of the IEP

when selenite is adsorbed (HANSMANN and ANDERSON, 1985) (SU and SUAREZ, 2000), which does not follow from the above reaction. To cope with these problems, Hayes et al. (HAYES et al., 1988) have used a monodentate SeO_3 adsorption reaction in the modeling. However, this is not satisfactory if the aim is to relate spectroscopy, structure, and ion adsorption modeling.

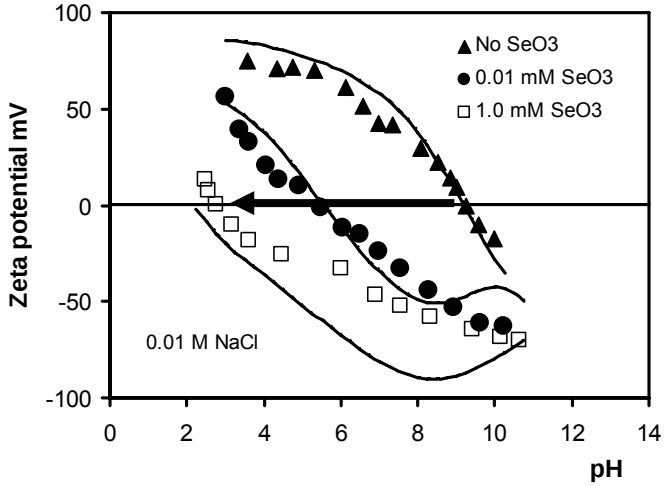

Fig.24. The decrease of the IEP (arrow) with increasing adsorption of selenite on goethite which introduces negative charge in the interface of goethite according to the MUSIC model (eq.[15]). The downward shift of the IEP cannot be explained if the 2p*K* model is used (eq.[14]). Data are from Su and Suarez (SU and SUAREZ, 2000). Lines have been calculated with the CD model (HIEMSTRA and VAN RIEMSDIJK, 2007b).

The above situation changes with the use of the MUSIC model. The surface composition in the PZC can be represented in this case by equal numbers of $SOH^{-1/2}$ and $SOH_2^{+1/2}$, yielding for a bidentate reaction:

$$SOH^{-1/2} + SOH_2^{+1/2} + 1H^+(aq) + SeO_3^{2-}(aq) \Leftrightarrow (SO)_2SeO^{-1} + 2H_2O(l) \qquad [15]$$

Without the influence of electrostatics, the value of χ will be 1. Due to the increase of negative charge of the surface as a result of selenite adsorption, additional protons are adsorbed, i.e. χ will be higher. The correct pH dependency can be modeled with this approach and the shift of the IEP with the selenite loading is explained (Fig.24).

As pointed out above, the charge distribution (CD) of surface complexes in the interface is related to the charge of the central ion and the charge and number of coordinating ligands. However, bond length may also play an important role, as will be discussed after discussing factors determining the shape of ion adsorption isotherms.

Shape of the ion adsorption isotherm

As illustrated above, the electrostatic behavior is important in regulating the competition of different types of ions. In pseudo-monocomponent systems with only one type of ion, e.g. Cd^{2+}, these processes also occur. Actually, with increasing adsorption, ions of the same type will increasingly experience the electrostatic competition of the ions that have

already been adsorbed. This changes the shape of the adsorption isotherm. If at a given pH, Cd^{2+} is adsorbed as an innersphere complex with charge distribution, charge will accumulate and affect the electrostatic potential. The potential of the surface is usually mainly regulated by the adsorbed protons in the surface. If the pH is constant, the potential is hardly affected and the corresponding adsorption energy contribution remains constant. This is very different for the 1-plane. Without Cd^{2+} adsorption, a certain potential exits but this electrostatic potential can be easily changed due to the absence of buffering of charge, compared to the surface by the protons. The increasing loading will make the potential of the 1-plane more positive and this will change the electrostatics. This contribution depends on the amount of the Cd^{2+} charge that resides in that plane,

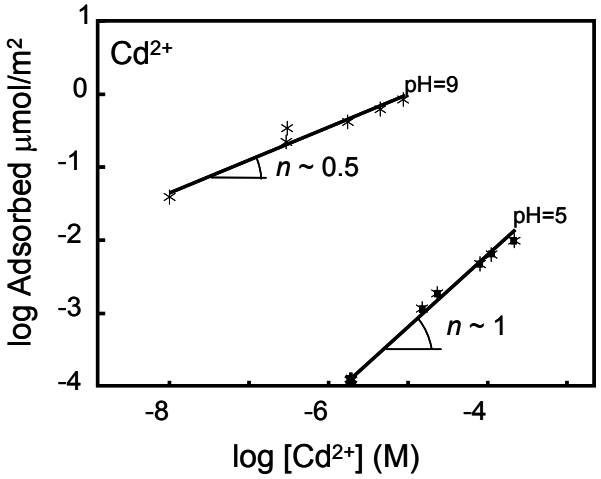

Fig.25. The adsorption isotherm of Cd^{2+} on goethite in 0.1 M $NaNO_3$ for two pH values, given in a double logarithmic plot. Data of Venema et al. (VENEMA et al., 1996b). At low pH, the slope of the isotherm n is $n \sim 1$, which is equivalent with a linear adsorption isotherm on the linear scale. The reason is the low Cd^{2+} loading. The electrostatic interaction contribution is nearly constant, not affecting the overall Gibbs free energy of adsorption. At increase of the pH, the positive and repulsive potential of the surface (ψ_0) is reduced and therefore, the adsorption increases strongly. The change of the electrostatic contribution ($-\Delta z_0 F\psi_0$) with pH will depend on the amount of charge of Cd^{2+} (Δz_0) that is attributed to the surface. At constant pH, the contribution $-\Delta z_0 F\psi_0$ is constant. However, the energy contribution of 1 - plane ($-\Delta z_1 F\psi_1$) will change at higher loading, suppressing the adsorption since the potential is repulsive. The lower slope ($n \sim 0.5$) is equivalent with a bending adsorption isotherm at the linear scale. The bending at the given loading is hardly affected by site saturation effects, which will occur above ~ 0.5 umol/m^2.

Bond length and charge distribution

The charge distribution in surface complexes of oxyanions like PO_4^{3-}, SeO_3^{2-}, and SO_4^{2-} can often be approximated using as a first approach the Pauling bond valence concept (HIEMSTRA and VAN RIEMSDIJK, 1996a), (HIEMSTRA and VAN RIEMSDIJK, 1999a). It also applies to the Cd surface complex on goethite $\equiv(FeOH)_2Cd(OH_2)_4$ (VENEMA et al., 1996b). However, for many important ions, the coordination environment is highly asymmetrical. The uranyl UO_2^{2+} ion is an excellent example (HIEMSTRA et al., 2009b) in which the axial U-O

bonds are much shorter than the equatorial U-OH_2 bonds (DENT et al., 1992), (CHISHOLM-BRAUSE et al., 1994), (CHISHOLM-BRAUSE et al., 1994), (WAITE et al., 1994). As a result, a larger part of the charge of the central U^{6+} is used for charge neutralization of the axial oxygens, and this results in a very low proton affinity, i.e. these ligands are only present as oxygen. The equatorial oxygen ions have a longer U-O bond and the neutralization by U^{6+} is insufficient leading to ligands binding one (OH) or two protons (OH_2).

Very strong asymmetry has also been revealed by EXAFS measurements for the Hg innersphere complex at the surface of goethite (COLLINS et al., 1999a). The detected distance of Hg with the surface oxygens of $\equiv(FeO)_2Hg(OH_2)_n$ is very short in contrast to the Hg-O distance with coordinating water molecules (Fig.26a).

The large asymmetry in the coordination environment of Hg(II) adsorbed at the surface is reflected in the charge distribution coefficients that can be found when we described the Hg adsorption of Barrow and Cox (BARROW and COX, 1992; GUNNERIUSSON and SJÖBERG, 1993) with the CD model. According to the CD model, the majority of the Hg^{2+} charge ($z_0 \approx 1.7$) is attributed to the surface, which fits well with the measured details of the Hg surface complex structure, revealing the very tight bonds with the surface oxygens.

Distortion and hydrolysis of surface complexes

On goethite, mercury ions react with two singly coordinated surface hydroxyls (COLLINS et al., 1999a). Quantum chemical calculations for the Hg surface complex (COLLINS et al., 1999a) have shown that the common ligands of the surface complex are oxygens, i.e. the proton is removed from the surface hydroxyl. In this respect, mercury can be considered as an exception, since most other heavy metal ions that react with singly coordinated ≡FeOH have one or two hydroxyls as common ligand with the surface. The removal of the proton from the common ligand in the Hg complex is due to the short Hg-O bond, which contributes sufficient charge (eq.[7]) to neutralize the common oxygen in combination with the metal ion of the solid. Due to the large charge attribution, hardly any charge is left for the other ligands. It implies a very low bond valence and long Hg-OH_2 distances (Fig.26a). This bond valence for the coordinated water is even smaller than in aqueous $Hg^{2+}(OH_2)_6$, i.e. the interaction of Hg with protons on the water ligands is less. Therefore, the outer ligands of the surface complex can persist as water molecules without hydrolysis. So, such a distortion in surface complexes due to adsorption will lead to a relative suppression of the hydrolysis of OH_2 ligands if compared with the relevant complex in solution, i.e. distortion and hydrolysis of the outer ligands are related. Experimentally, it is not an easy task to pinpoint any hydrolysis of adsorbed complexes from adsorption measurements, since hydrolysis is also strongly determined by electrostatic effects. However, we have been able to develop a consistent combination of modeling, spectroscopy and bond valence analysis for the determination of the hydroxylation of adsorbed cations. The results will be illustrated for Pb, Cu and Cd adsorption (Fig.26 b,c,d).

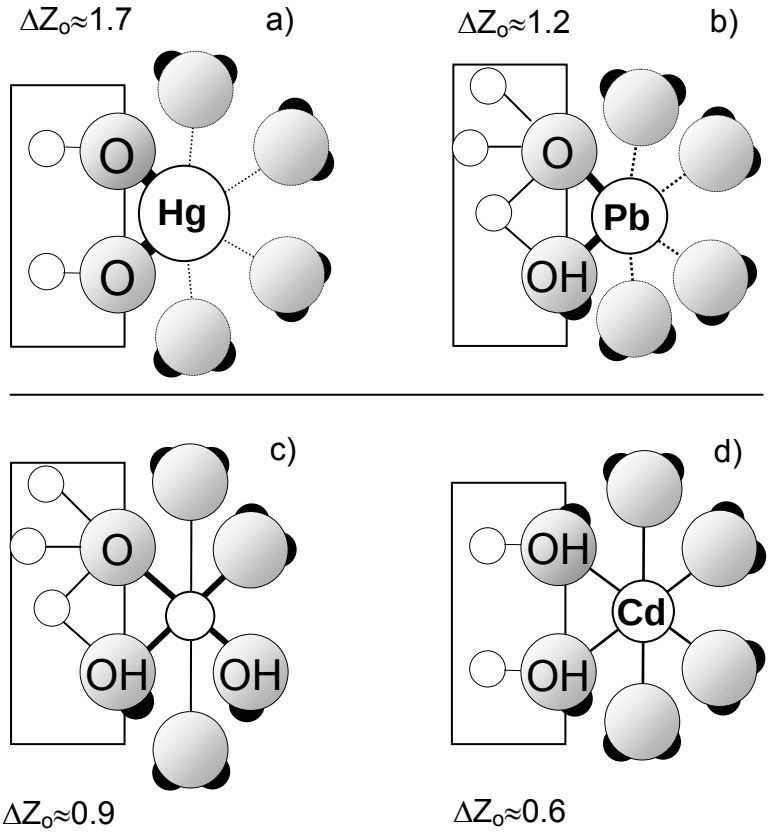

Fig.26. The surface complexes of Hg, Pb, Cu, and Cd on goethite. The Hg ion is highly distorted in the coordination environment. It attributes so much charge to the surface ligands that no proton can be retained on the common ligand. The asymmetry prevents hydrolysis of the loosely bound water molecules due to reduction of charge attribution to the ligands. Asymmetry is less strong in the Pb surface structure. The common ligand of the singly Fe coordinated group can remain a hydroxyl. The asymmetry causes longer Pb-OH_2 bonds, which suppress hydrolysis of those ligands. The distortion of Cu is symmetrical. This leads to a relatively high charge attribution to both surface and solution ligands of the equatorial plane. This enables hydroxylation of the solution-oriented ligands, which is strongly stimulated by the repulsive charge of the surface on the H. The attribution to the surface ligands is not high enough to cause deprotonation of the OH ligand of the singly coordinated group. The cadmium (Cd) environment is symmetrical. The bond valence to each ligand is relatively low, preventing hydrolysis in the major pH range.

On goethite lead ions are bound to singly and triply coordinated groups, as shown in Fig.26b (OSTERGREN et al., 1999b). The Pb surface complex has characteristics in common with that of adsorbed mercury. The Pb ion is also distorted in the coordination environment (OSTERGREN et al., 1999b). The distortion is not that strong as in the mercury surface complex. Therefore, the Pb is unable to remove the proton from the singly coordinated FeOH in the pH range of the experiments (≈ pH <7). A bond valence analysis has shown that the

common ligands are almost fully neutralized (BARGAR et al., 1997a), (BARGAR et al., 1997b). On the other hand, the distortion is sufficiently large to lead to relatively large Pb-OH_2 distances (Fig.26b), which suppresses the tendency to hydrolyze. The CD-modeling of Pb adsorption data (HAYES and LECKIE, 1987b), (KOONER, 1993), (GUNNERIUSSON et al., 1994) shows that a relatively high proportion of the charge is directed to the surface ($z_0 \approx 1.2$) and that no $\equiv Fe_2(OH)_2PbOH$ complex is formed below pH 7. The fitted charge distribution coefficient is equivalent with a charge attribution of approximately 0.6 v.u. per Pb-OH bond. This leads to an almost complete saturation of the common surface ligands, similar as what has been concluded from the bond valence analysis of the structure of the surface complex (BARGAR et al., 1997b).

On goethite, the copper ion is bound at the edge of Fe octahedra of the solid (PARKMAN et al., 1999), interacting with a singly and a triply Fe coordinated group. The surface and solution complex of Cu are Jan Teller distorted (PARKMAN et al., 1999). In both complexes, the axial Cu-O distance is larger than the four equatorial Cu-O bonds. Two of the equatorial bonds are with the surface hydroxyls (Fig.26c). The Cu ion is bound at the edge of Fe octahedra (PARKMAN et al., 1999). The CD-modeling of the very large set of Cu-adsorption data of Robertson et al. (ROBERTSON and LECKIE, 1998) shows that the hydrolyzed surface complex of Cu, i.e. $\equiv(Fe_3OFeOH)CuOH$, becomes dominant in the pH range above pH 4. In solution, hydrolysis occurs above pH ≈ 6. The difference is mainly due to the strong repulsion of H in the positive electrostatic field present at pH = 4. The intrinsic constant for hydrolysis in solution and on the surface is not very different. The action of the electrostatic field can be seen as cooperative hydrolysis.

At a high Cd loading, the main Cd complex on goethite is a bidentate complex, interacting with singly coordinated surface groups (SPADINI et al., 1994), (RANDALL et al., 1999). Boily (BOILY, 1999) has measured the Cd adsorption for these high loading conditions. Modeling in combination with the data of Venema et al. (VENEMA et al., 1996b) leads to a charge attribution coefficient of $z_0 \approx 0.7$. This value corresponds to an almost symmetrical distribution of charge over six ligands, as is also found in solution. In solution, cadmium ions are mainly present as Cd^{2+}, i.e. non-hydroxylated ($pK_1 = 10$). At the surface, this is also found, i.e. the dominant Cd surface complex is not hydroxylated (below pH = 8). It can be noted that both Cu and Cd have a similar hydrolysis behavior comparing surface and solution. For Hg, this is certainly not the case and due to the distortion upon adsorption.

Cooperative Protonation of surface complexes

IR spectroscopy has shown (TEJEDOR-TEJEDOR and ANDERSON, 1990) that adsorbed phosphate ions are mainly unprotonated, if the surface is still positively charged, i.e. at a low loading with negatively charged PO_4^{3-} ions. The $\equiv(FeO)_2PO_2^{2-}$ species becomes protonated at high loading when the positive particle charge is not longer repulsive enough on the H^+, as is illustrated in Fig.27 (HIEMSTRA and VAN RIEMSDIJK, 1996a).

More recently, the IR spectra of adsorbed phosphate have been simulated with MO/DFT computations (KWON and KUBICKI, 2004) and have been compared with experimental data.

The authors suggest the formation of bidentate complexes only. At low pH, the $\equiv(FeO)_2PO_2^{-2}$ will become doubly protonated $\equiv(FeO)_2P(OH)_2^0$. In a later work (LI et al.), using ^{31}P-NMR spectroscopy for boehmite, γ-AlOOH, the presence of two types of complexes was suggested. Besides a non-protonated bidentate complex $\equiv(AlO)_2PO_2^{-2}$, the presence of a singly protonated bidentate surface complex $\equiv(AlO)_2POOH^{-1}$ was claimed.

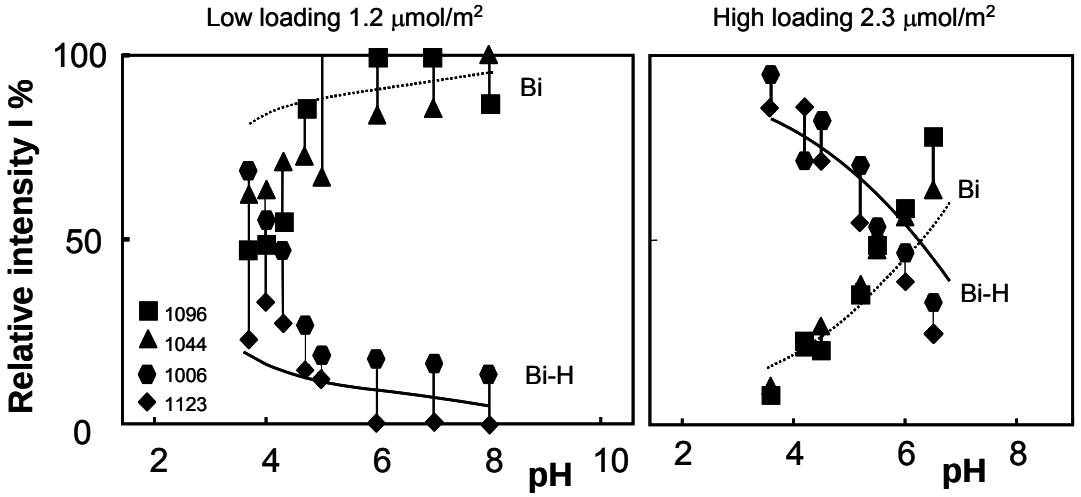

Fig.27.The increase of the relative IR intensity of the protonated bidentate $\equiv(FeO)_2POOH$ (Bi-H) and corresponding decrease of the non protonated $\equiv((FeO)_2PO_2$ (Bi) bands with the increase of the P-loading. Data are of Tejedor-Tejedor and Anderson (TEJEDOR-TEJEDOR and ANDERSON, 1990). The lines have been calculated using the CD model (HIEMSTRA and VAN RIEMSDIJK, 1996a).

The interpretation of only bidentate complex formation contrasts with the interpretation of Persson (PERSSON et al., 1995) suggesting the formation of monodentate complexes. Recently, monodentate complex formation has also been suggested for arsenate (LORING et al., 2009), an analogue of phosphate in many aspects. It has been claimed (LINDEGREN and PERSSON, 2010) that similarly, phosphate will form singly coordinated surface species (monodentate) that are singly ($\equiv FeOPO_2OH^{-1.5}$) or doubly ($\equiv FeOPO(OH)_2^{-0.5}$) protonated.

The surface speciation of phosphate (Fig.27) has been reanalyzed by Rahnemaie et al. (RAHNEMAIE et al., 2007) using the CD model. In the new approach, the CD values have been fitted and have been predicted using the MO/DFT optimized geometry of hydrated phosphate Fe structures. Analysis of the macroscopic data with the CD model suggests the dominant presence of a non-protonated bidentate complex, as found previously $\equiv(FeO)_2PO_2^{-2}$. However, at low pH, the fitted CD value is consistent with the formation of a singly protonated PO_4 surface species, i.e. $\equiv FeOPO_2OH^{-1.5}$. Most data could be described well with the new approach, with the exception of the shift of the IEP with loading, as measured by Tejedor-Tejedor and Anderson (TEJEDOR-TEJEDOR and ANDERSON, 1990).

Protonation of ligands can be enhanced by the presence of other negatively charged ions. For instance in case of the adsorption of SeO_3, protonation of the selenite species occurs if PO_4^{3-} ions are added to the system (Fig.28). The surface complex can be formed because PO_4 has decreased the particle charge sufficiently. Recently, the adsorption of SeO_3^{2-} and its

competition with phosphate have been reanalyzed with the CD model (HIEMSTRA and VAN RIEMSDIJK, 2007b) using a set of CD coefficients that have been calculated with a bond valence analysis using the MO/DFT optimized geometry of hydrated selenite Fe structures. The dominant species is ≡ $(FeO)_2SeO^-$, as found previously, but at low pH, the data are better described using a protonated monodentate complex ≡FeOSeOOH. The formation of the monodentate complex only occurs at high concentration and very low pH (pH<4) and in a speudo-monocomponent system, the contribution is 20% or less, and may not have been detected for this reason by EXAFS (HAYES et al., 1987a). In the new interpretation, the contribution of the protonated species in PO_4-SeO_3 systems is less strong than previously (Fig.28) found.

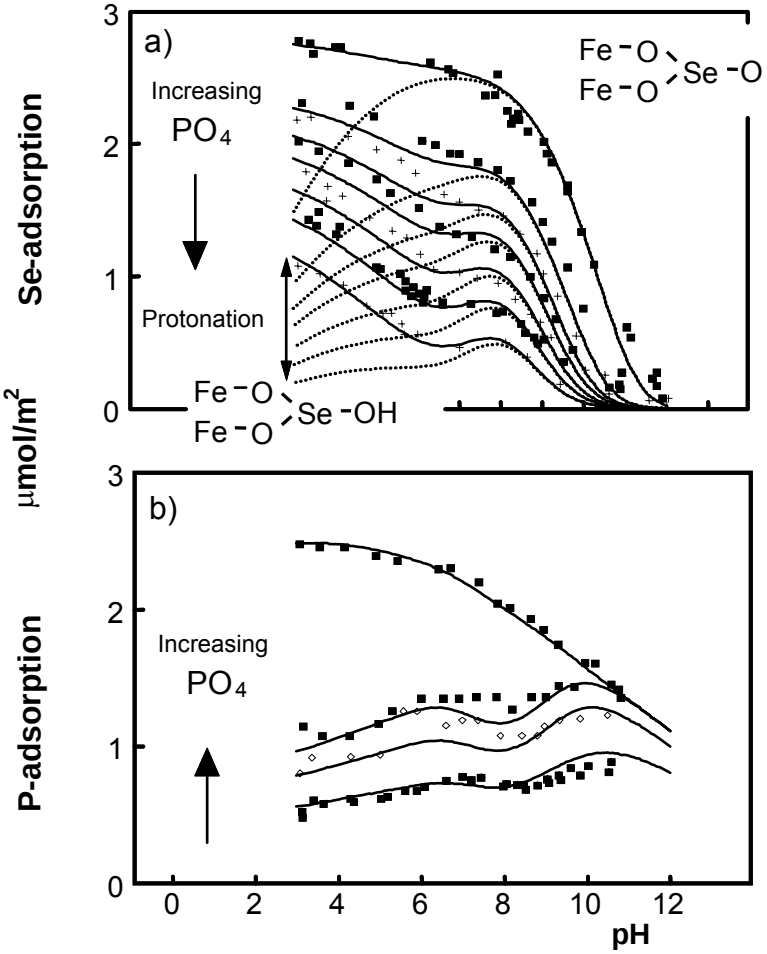

Fig.28. The competition between selenite and phosphate ions on goethite. Adsorption of SeO_3^{2-} at increasing concentrations of PO_4^{3-} (a) and the corresponding binding of PO_4^{3-} (b). Data are of Hingston et al. (HINGSTON et al., 1971). Lines have been calculated with the CD model (HIEMSTRA and VAN RIEMSDIJK, 1996a), (HIEMSTRA and VAN RIEMSDIJK, 1999a). The difference between the dotted lines and the full lines in a) is the contribution of the protonated ≡$(FeO)_2SeOH$. This species is only present at a high loading of anions, which reduce the repulsive potential for protons. In a later interpretation, the protonation has been attributed to formation of ≡FeOSeOOH (HIEMSTRA and VAN RIEMSDIJK, 2007b) (not shown).

The adsorption of protons may influence the proton co-adsorption ratio χ depending on where the proton is located (HIEMSTRA et al., 2004). If the proton would adsorb at the surface ligands, no effect is to be expected if the surface reacts purely Nernstian. The introduction of the extra proton charge would lead to an equal decrease in charge due to desorption of a proton from other surface groups. Almost the same happens on a near-Nernstian surface. If χ is not affected, the pH dependency will not change if n remains constant (eq.[11]). However, the proton of the phosphate species is located at the outer ligands. At this electrostatic position, the interaction of the proton with the surface and its protons is less strong, leading to an increase of the co-adsorption ratio χ and a higher pH dependency.

AgI, a long-standing issue

Ag halogen minerals (AgI, AgBr, AgCl) are used as model colloids. The solubility of AgI(s) is lowest ($\log K_{AgI} = -16.1 < \log K_{AgBr} = -12.3 < \log K_{AgCl} = -9.8$). The colloidal behavior of AgI(s) has been studied for many years, starting at the beginning of the previous century (OVERBEEK, 1952). A classical overview of the surface and colloid chemical properties has been given by Bijsterbosch and Lyklema (BIJSTERBOSCH and LYKLEMA, 1978). The model colloid has been considered from the Thermodynamic point of view. It is also possible to give it a structural basis and analyze the classical data with the CD model. As far as we are aware, the data have not been modeled in a successful manner so far.

Interfacial charge distribution modeling

It is not obvious where the interfacial charge is located. Therefore, the CD model was used and the charge of the constituting ions was allowed to be distributed in the compact part of the interface, i.e. the inner Stern layer. Additionally, electrolyte ions were allowed to adsorb as ion pair in the 1-plane. Since the head end of the DDL not necessarily may coincide with the inner Helmholtz plane, a second Stern layer was allowed and the capacitance of both Stern layers was fitted.

Modeling of the excess adsorption (Γ_{Ag}-Γ_{I}) data of Fig.4 shows that negative charge is created in the surface and positive charge in the 1-plane. If formation of negative charge is interpreted as I^- adsorption, and the positive charge as the adsorption of Ag^+ ions, it is, -without a precise surface structural picture-, difficult to understand why the smaller Ag^+ ($r \sim 66$ pm) would be at a larger distance from the surface than the larger I^- ($r \sim 216$ pm) ion.

Surface structure

At room temperature, AgI(s) can be present in two polymorphs, i.e. a structure with a cubic (γ-AgI) or a hexagonal (β-AgI) packing (SUGIMOTO and SHIBA, 1999a). Cubic γ-AgI(s) can be found in nature as miersite. The hexagonal β-AgI mineral is known as iodargyrite. Both crystal structures differ from chlorargyrite AgCl(s) and bromargyrite AgBr(s), that have

a structure similar to NaCl(s) with a coordination number of CN = 6, while CN = 4 in AgI(s), see Table 5.

Iodargyrite will develop hexagonal crystals (Fig.29a) with two main faces, the 100 face and its equivalents at the edges, and the 100/00-1 face at the planar side. The mineral shape of cubic miersite can be a tetrahedron with the 111 face and its equivalents (Fig.29b), or it may develop additionally the 110 face resulting in a dodecahedron (Fig.29 c).

Table 5 Overview of structural properties of Ag halogens.

Component	β-AgI	γ-AgI	AgBr	AgCl
mineral name	iodargyrite	miersite	bromargyrite	chlorargyrite
ion arrangement	hexagonal	cubic	fcc	fcc
structure as	würtzite ZnS	sphalerite ZnS zinc blende ZnS	halite NaCl	halite NaCl
CN	4	4	6	6
lattice parameters	a = 0.495 nm c = 0.752 nm	a = 0.650 nm	a = 0.577 nm	a = 0.555 nm
crystal faces	100 edge , 001 planar,	111, 110	100, 111	100, 111
crystal shape	prisms rods	tetrahedra dodecahedrons	cubes	cubes

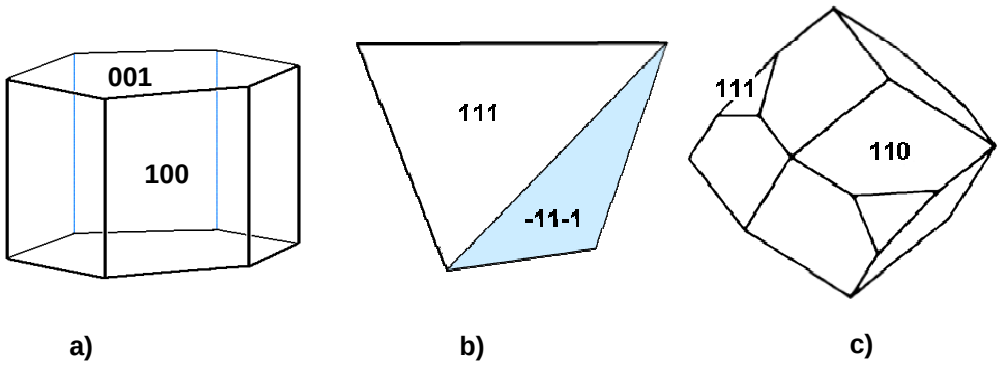

Fig.29a Morphology of iodargyrite (β-AgI), a hexagonal prism (a) with 100 faces at the edge and 001/00-1 faces at the planar side. Fig.29b,c The morphology of miersite (γ-AgI) with b) a tetrahedron terminated by the 111 face and its equivalents and c) a dodecahedron with 110 and 111 faces.

Kolkmeijer and van Hengel (KOLKMEIJER and VAN HENGEL, 1934) found that silver iodide will precipitate from solution in the cubic form (γ-AgI) if Ag^+ ions are in excess, and in hexagonal form (β-AgI) if I^- ions are in excess. The latter condition is typical for preparing an AgI sol (BIJSTERBOSCH and LYKLEMA, 1978), suggesting the presence of iodargyrite. However, miersite will coexist, although this mineral is probably metastable with respect to iodargyrite (BURLEY, 1963). Twinning of both minerals is possible due to the similar surface structure of the planar face of iodargyrite and the 111 face of miersite.

Iodargyrite

Hexagonal crystals of iodargyrite, β-AgI(s), have two types of faces, the planar 001/00-1 face and at the edges the 100 face and its equivalents. In case of similar particle dimensions in the main directions, the edge faces are dominant. Simplifying to a cylinder with equal height and diameter, the fraction of edge faces (100 face) is 2/3. The same is found if one simplifies to a cube.

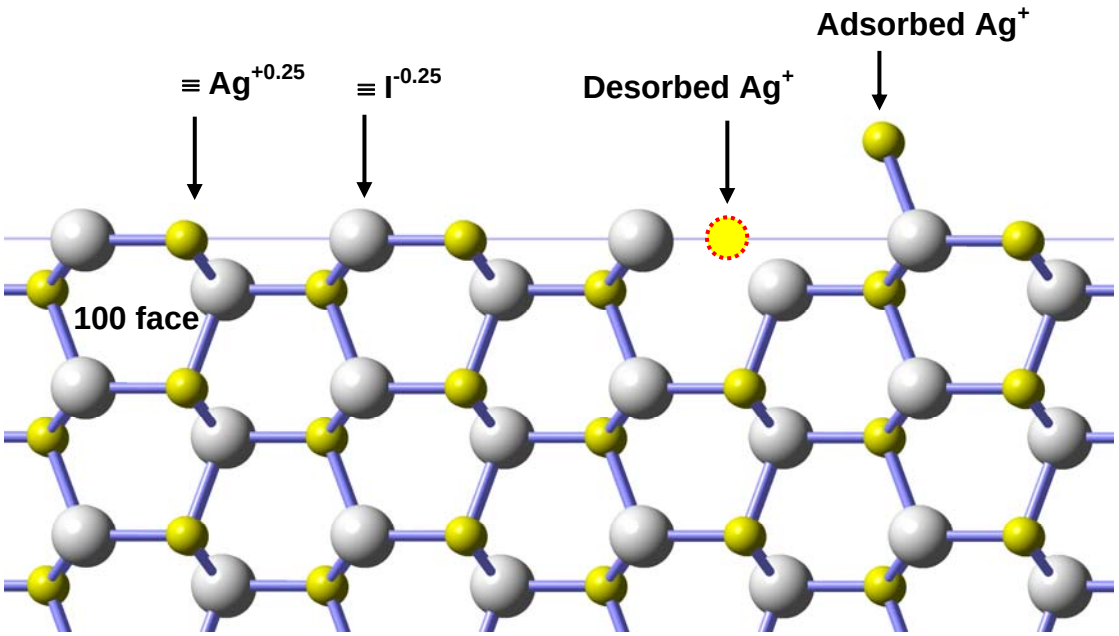

Fig.30. The mineral structure of iodargyrite, β-AgI(s) with internally rows of tetra-coordinated Ag^+ (small spheres) and I^- (large spheres) ions. The Pauling bond valence is 0.25 v.u. The termination at the edge face (100) yields triply coordinated surface groups, i.e. the ions lack one bond, resulting in $\equiv Ag^{-+0.25}$ and $\equiv I^{-0.25}$ sites (N_s = 2.9 nm^{-2} each). Note that one bond is not visible in this projection. Charging the mineral positively occurs by adsorption of Ag^+. These Ag^+ ions are located above the 100 face, as indicated. Negative charge can be created by desorption of Ag^+ ions, which are removed from the 100 face as suggested from the interpretation of the charging data (BIJSTERBOSCH and LYKLEMA, 1978) with the CD model. The 110 face of miersite has the same type of structure as the edge (100) face of iodargyrite, but has a higher site density (N_s = 3.4 nm^{-2}).

Edge faces

In Fig.30, the mineral and surface structure of the 100 edge face of iodargyrite β-AgI(s) is given. In the interior, the ions are four-fold coordinated, which results in a Pauling bond valence of 0.25 v.u. At the surface, Ag^+ and I^- ions are present with a lower coordination. For this crystal face, the groups are triply coordinated, which results in $\equiv Ag^{+0.25}$ and $\equiv I^{-0.25}$. Both groups are present in equal amounts and the surface is neutral. The mineral face can be positively charged by adsorbing Ag^+ ions. The coordination of the Ag^+ is with the $\equiv I^{-0.25}$ group and the Ag^+ will protrude from the surface.

When the Ag^+ concentration in solution is lower than the value in the PZC, the surface will be negatively charged. In principle, negative charge can be created at the 100 face by the adsorption of I^- that has to protrude from the surface. Another possibility is to desorb Ag^+ ions from the surface. In that case, negative charge is created in the surface while in case of

adsorption, the charge will approximately be at the same position where the Ag^+ ions reside without a significant charge separation.

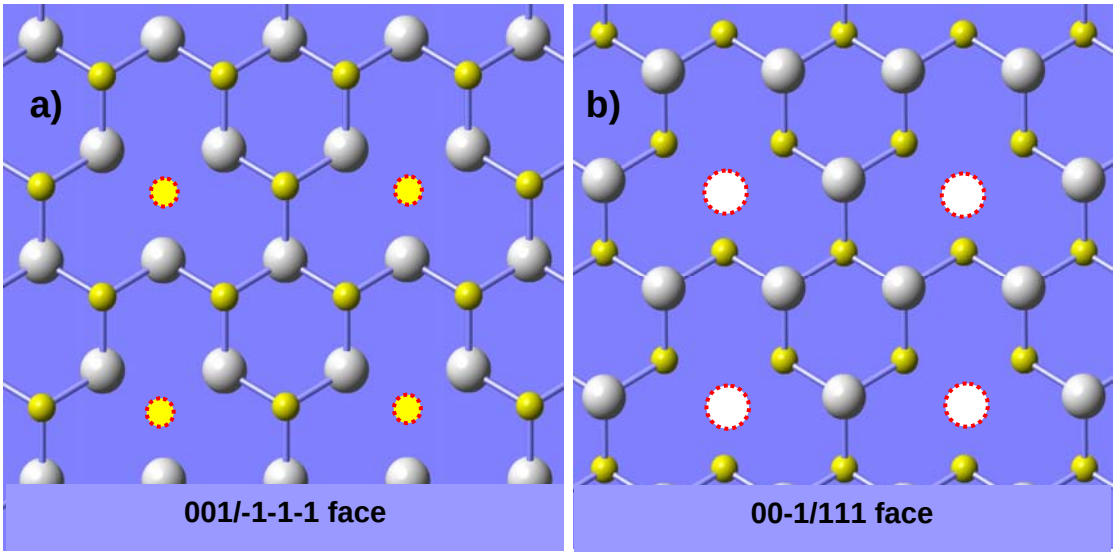

Fig.31. The surface structure of the neutral 001 (31a) and 00-1 face (31b) of iodargyrite. Both faces have triply coordinated surface sites only. The small spheres are Ag^+ that lay on top at the 100 face. The large spheres represent I^-, which lay on top at the 00-1 face. Part of the sites are subsurface, created by desorption of ions (dotted spheres), being Ag^+ in Fig.31a and I^- in Fig.31b. The densities of the $\equiv Ag^{+0.25}$ and $\equiv I^{-0.25}$ groups at the neutral surface are 4.1 nm^{-2}. The surface structure of the 111 / -1-1-1 faces of miersite is identical to the structure of respectively the 00-1 / 001 faces of iodargyrite.

Planar faces

In contrast to the 100 face, formation of the 001/00-1 face by cutting the crystal does not lead to the same composition on either surface due to asymmetry in the structure. We consider the configuration resulting from the termination of a crystal by groups that have the highest coordination as most stable and these structures are discussed.

The 001 face can be terminated with triply coordinated Ag^+ ions only. The I^- ions are located deeper in the crystal and are fourfold coordinated. The created crystal face has only $\equiv Ag^{+0.25}$ as surface group. However, this termination results in a positively charged surface. The positive charge can be neutralized by adsorbing I^- that will have a low coordination. However, another possibility is to create negative charge by desorption of Ag^+, leading to three triply coordinated $\equiv I^{-0.25}$ ions in the sub-surface per Ag^+ desorbed, as given in Fig.31a. We note that one of the bonds in the picture is behind the I^- ions and therefore not visible. The composition in Fig.31a represents a neutral surface and note that it has only triply coordinated surface groups, similar as on the 100 face in Fig.30.

The structure of the mirrored 00-1 face has similarities with the 001 face, but at this face, triply coordinated $\equiv I^{-0.25}$ sites are present when terminated. To make this surface neutral, I^- ions can desorb yielding a composition as sketched in Fig.31b for a neutral surface. Another

way to neutralize the $\equiv I^{-0.25}$ surface groups is adsorption of Ag^+. A loading of 25 % is required to make the particles neutral. The adsorption of the Ag^+ will take place outside the surface.

Miersite

Miersite is another polymorph of AgI, also known as γ-AgI (Table 5). Both minerals are often present in a mixture. Miersite has a cubic structure comparable with sphalerite (ZnS). The mineral shape is given in (Fig.29b,c). Sphalerite tetrahedra may form + and - crystals with faces having a different composition (KOMATSU and SUNAGAWA, 1965; WANG et al., 2000). The + and - form may twin on the 111/ -1-1-1 face that may lead to pseudo-octahedrons. The positive (+) form of ZnS has 111 faces that terminate with S^{2-} ions. The + form is formed in basic solutions with dominance of S^{2-} (WANG et al., 2000). Miersite may also form + and - crystals. In the next discussion, we will define the AgI crystal using the parameters of Hull and Keen (HULL and KEEN, 1999), leading to 111 faces terminated by I^{-1} ions (+ form) and to the -1-1-1 faces terminated by Ag^+ ions (- form). Note that in literature often no distinction is made with respect to the + and - form. One simply refers to the 111 face as done in Fig.29b.

With the chosen definition, the 111 face will have $\equiv I^{-0.25}$ on top. The 111 face of miersite has the same structure as the 00-1 face of iodargyrite, β-AgI(s) given in Fig. 31b. The -1-1-1 face with $\equiv Ag^{+0.25}$ on top is identical with the 001 face of iodargyrite, β-AgI(s) given in Fig. 31a. Interestingly, the fully loaded 111/-1-1-1 face of miersite can perfectly match with the fully loaded 001/00-1 face of iodargyrite β-AgI. Both faces have the same site density and structure, enabling twinning of miersite and iodargyrite as observed for large crystals. The 110 face of miersite (Fig.29c) has the same type of structure as found for the 100 edge face of iodargyrite (Fig.30). A difference is the site density, which is slightly higher, $N_s = 3.4$ nm^{-2}.

The above-sketched structures can be linked to the results of the CD modeling showing that charging of the AgI(s) is accompanied with creation of positive charge at some distance above the surface and by negative charge in the surface. Qualitatively, the latter can be explained by adsorption of I^- ions at the structure of Fig.31b or desorption of Ag^+ from the structure of Fig.31a. Positive charge at some distance from the surface can be created by adsorption of Ag^+ at all faces that have $\equiv I^{-0.25}$ on top, but not on a face with $\equiv Ag^{+0.25}$ on top as in Fig.31a. An overview of the reactivity is given in Table 6.

Table 6 Overview crystal faces and the surfaces

Mineral	face	location	Reference Site(s) *[b)]	N_s (nm^{-2}) *[b)]
Iodargyrite β-AgI	100	edges	$\equiv Ag^{+0.25}$ and $\equiv I^{-0.25}$	2.90
	001	planar	$\equiv I^{-0.25}$	2.74
	00-1	planar	$\equiv Ag^{+0.25}$	2.74
Miersite γ-AgI	110	dodecahedrons	$\equiv Ag^{+0.25}$ and $\equiv I^{-0.25}$	3.37
	111/-1-1-1*[a)]	+/- tetrahedrons	$\equiv I^{-0.25}$/ $\equiv Ag^{+0.25}$	2.74

*[a)] The type of surface group depends on crystal development in + or - crystals.
*[b)] At the non-depleted crystal faces

CD-MUSIC Modeling

After the above analysis of the surface structure, the final modeling can be done. As follows from table 6, two types of reactive sites are found, i.e. $\equiv Ag^{+0.25}$ and $\equiv I^{-0.25}$. For defining in the model the sites and the site densities, we will use the non-depleted surface as reference, i.e. for miersite, the 111 face with only $\equiv I^{-0.25}$ or the -1-1-1 face with only $\equiv Ag^{+0.25}$, and the 110 face with both in equal numbers.

Reactions

The 100 face of iodargyrite, β-AgI(s) and the 110 face of miersite, γ-AgI, are terminated by triply coordinated Ag^+ as well as I^- groups (fig.30) forming respectively the $\equiv Ag^{+0.25}$ and $\equiv I^{-0.25}$ site. The sites may release or accept Ag^+ respectively. In principle, the $\equiv Ag^{+0.25}$ site may also bind an I^- ion which has been allowed in the modeling. The charge is allocated to the 1-plane. This leads to:

$$\equiv Ag^{+0.25} \Leftrightarrow \equiv^{-0.75} + Ag^{+}(aq) \qquad K_{dAg} \qquad [16]$$

$$\equiv Ag^{+0.25} + I^{-}(aq) \Leftrightarrow \equiv Ag^{+-0.25}\text{-}I^{-} \qquad K_{aI} \qquad [17]$$

$$\equiv I^{-0.25} + Ag^{+}(aq) \Leftrightarrow \equiv I^{-0.25}\text{-}Ag^{+1} \qquad K_{aAg} \qquad [18]$$

To account for interaction with electrolyte ions, we may define

$$\equiv Ag^{+0.25} + NO_3^-(aq) \Leftrightarrow \equiv Ag^{+0.25}\cdots NO_3^- \qquad K_{NO3} \qquad [19]$$

$$\equiv I^{-0.25} + K^{+}(aq) \Leftrightarrow \equiv I^{-0.25}\cdots K^{+} \qquad K_{K} \qquad [20]$$

In a first approach, both ions will be located in the inner Helmholtz plane.

Without depletion, the planar 001/00-1 faces of iodargyrite, β-AgI(s), and the -1-1-1/111 face of miersite, γ-AgI, are terminated by respectively the triply-coordinated Ag^+, only forming the $\equiv Ag^{+0.25}$ site and by the triply coordinated I^-, only forming the $\equiv I^{-0.25}$ site. In the latter case, the desorption of I^- and the corresponding ion pair formation can be described with

$$\equiv I^{-0.25} \Leftrightarrow \equiv^{+0.75} + I^{-}(aq) \qquad K_{dI} \qquad [21]$$

$$\equiv I^{-0.25} + NO_3^-(aq) \Leftrightarrow \equiv I^{+0.75}\cdots NO_3^- + I^{-}(aq) \qquad K_{dINO3} \qquad [22]$$

The other reactions are defined in eqs.[18] and [20].

Results

Unfortunately, the face distribution in an AgI sol is unknown, complicating a detailed analysis. We have analyzed the charging behavior of AgI(s) representing in the modeling the surface by only one plane, that may be 100 of β-AgI(s) and 110 face of γ-AgI (option A), or it is the 00-1 of β-AgI(s) and 111 face of γ-AgI (option B).

The site density of the edge (100) face of iodargyrite, β-AgI(s) differs from the site density of the 110 face of miersite (Figs. 30 and 31) (Table 6). In the modeling (option A), the mean value (N_s = 3.1 nm^{-2}) has been used for $\equiv Ag^{+0.25}$ and for $\equiv I^{-0.25}$. With these faces, the data of Bijsterbosch and Lyklema (BIJSTERBOSCH and LYKLEMA, 1978) can be described very well (R^2 = 0.997). A good description with the same quality (R^2 = 0.997) is also found (option B) when using the 111 face miersite as well as the 00-1 face of iodargyrite. Both fully loaded faces have only the $\equiv I^{-0.25}$ on top with the same site density, N_s = 2.74 nm^{-2}.

Using the other faces, i.e. 001 of β-AgI(s) and -1-1-1 γ-AgI(s) having only $\equiv Ag^{+0.25}$ on top, no proper description can be found within the present approach. It is possible that these faces are less or not important in the AgI sol prepared. For miersite, this suggestion can be in line with the results found for sphalerite (ZnS), showing that the positive (+) tetrahedron with S^{2-} termination is formed in basic solutions with excess S^{2-} (aq) (WANG et al., 2000). In the AgI sol preparation, I^- (aq) is also present in excess and this may suggest the formation of + crystals with the 111 face, terminated by $\equiv I^{-0.25}$. This 111 face is also able to twin with the 001 face β-AgI(s), iodargyrite. Such a twinning will diminish the presence of 001 faces of β-AgI(s).

It is concluded that charging of AgI sols can be due to a) adsorption and desorption of Ag^+ ions at the edge faces of iodargyrite and the 110 faces of miersite and/or b) adsorption Ag^+ and desorption of I^- at the 00-1 face of iodargyrite site and the 111 face of miersite.

The fitting parameters corresponding to both charging mechanisms have been given in Table 7. In option A, I^- adsorption as monodentate complex was allowed but no binding of I^- to $\equiv Ag^{+0.25}$ was found. This may suggest that the affinity of I^- for $\equiv Ag^{+0.25}$ is low which is in line with a recent MD simulation for the AgCl(s)/0.05 M KCl solution interface (Zarzycki and Rosso, 2010). Zarzycki and Rosso found no chloride-innersphere complexation with the AgCl surface despite the high concentration of Cl^- ions in solution. The absence of complexation of I^- ion with $\equiv Ag^{+0.25}$ in our modeling (eq.[17]) suggests that the stability of triply coordinated $\equiv Ag^{+0.25}$ is sufficiently high in the interface and no coordination with I^- is required.

In contrast to I^-, Ag^+ may adsorb as innersphere complex protruding from the surface (eq.[18]). Ag^+ binds to the triply coordinated surface groups ($\equiv I^{-0.25}$). In both model options (Table 7), the affinity constant derived is rather similar, i.e. log$K$ = 4.1. This is also the case of the binding constant of K^+ (log$K$ = -2.1 ± 0.1).

Ag^+ may also bind to three triply coordinated I ($\equiv^{-0.75}$) in the subsurface (Fig.30,31a), forming $\equiv Ag^{+0.25}$. The corresponding affinity can be estimated from the inverse of reaction [16] and is log$K$~5 (Table 7 option A). The value can be compared with the affinity of I^- to bind to three triply coordinated Ag^+ ions ($\equiv^{+0.75}$) in the solid (eq.[21]), forming $\equiv I^{-0.25}$ (Fig31b). By analogy, writing the corresponding reaction (eq.[21]) inverse, a much higher affinity is found (log$K$~13) when the data are interpreted according to option B. Comparing

both affinity constants suggests that surfaces are easier depleted by Ag^+ than by I^-. This agrees with the observation that the PZC of AgI is about 5.5, which is about 2.5 units higher than expected based on the solubility product of AgI ($1/2 \log K_{so} \approx 8$) at equal affinity. This also supports that in an AgI sol the + form of miersite (111 face terminated by I^- ions) is more likely than the (-) form (-1-1-1- face terminated by Ag^+ ions).

Table 7
Option A. Reactivity of the 100 face of iodargyrite and the 110 face of miersite
The charge distribution coefficients and formation constants for surface species at the AgI solid solution interface. The capacitance of the inner and outer Stern Layer is respectively $C_1 = 0.16 \pm 0.01$ and $C_2 = 0.47 \pm 0.03$ F/m^2. The site densities of $\equiv I^{-0.25}$ and $^-\equiv Ag^{+0.25}$ are each 3.1 nm^{-2}. $R^2 = 0.998$ $n = 125$ data points.

Species	equation	Δz_0	Δz_1	Δz_2	log$K$
$\equiv^{-0.75}$	[16]	-1	0	0	-4.87 ± 0.15
$\equiv Ag\text{-}I^-$	[17]	0	-1	0	<< *)
$\equiv I - Ag^+$	[18]	0	+1	0	+4.02 ± 0.04
$\equiv Ag^{\cdots\cdots}NO_3^-$	[19]	0	-1	0	-1.02 ± 0.05
$\equiv I^{\cdots\cdots}K^+$	[20]	0	+1	0	-2.16 ± 0.12

*) The affinity is too low to be revealed by the model.

Option B Reactivity of the 00-1 face of iodargyrite and the 111 face of miersite.
The charge distribution coefficients and formation constants for surface species at the AgI solid solution interface. The capacitance of the inner and outer Stern Layer is respectively $C_1 = 0.15 \pm 0.01$ and $C_2 = 0.42 \pm 0.04$ F/m^2. The site density of $\equiv I^{-0.25}$ is 2.74 nm^{-2}. $R^2 = 0.997$ $n = 125$ data points.

Species	equation	Δz_0	Δz_1	Δz_2	log$K$
$\equiv^{+0.75}$	[21]	1	0	0	-13.29 ± 0.16
$\equiv I - Ag^+$	[18]	0	+1	0	+4.09 ± 0.05
$\equiv^{+0.75\cdots\cdots}NO_3^-$	[22]	1	-1	0	-13.52 ± 0.19
$\equiv I^{\cdots\cdots}K^+$	[20]	0	+1	0	-1.97 ± 0.12

Charge Distribution

In the above analysis, a simple approach was followed in which the charge of the adsorbed Ag^+ in the complex ≡I-Ag, has been fully attributed to the electrostatic plane where also the K^+ ions reside. This may be a good choice since it has been shown by MD simulation that the K^+ ion also binds as an innersphere complex (Zarzycki and Rosso, 2010). For NO_3^-, the mechanism is unknown, but in our approach, the NO_3^- ion has been located at the same plane. However, in the CD model for ion adsorption to oxides, the charge of innersphere complexes is distributed between surface and solution. Can this also be done in this case?

In solution, solvated silver ions are coordinated to 4 water molecules (CN = 4). The structure has two short (231 pm) and two significantly longer Ag-O bonds (248 pm), equivalent with a bond valence of 0.3 and 0.2 v.u. (PERSSON and NILSSON, 2006). For Ag^+, coordinated to $\equiv I^{-0.25}$, the charge distribution has been estimated by calculating the geometry of the surface complex with MO/DFT with a variety of models (B3lyp, Blyp, EDF1). To mimic the surface, a structure with IAg_4I_3 moiety has been defined having a geometry as in AgI(s). One of the Ag^+ ions was hydrated with three water molecules (Fig.32) and this coordination sphere was allowed to relax, together with the Ag-I bonds of the I^- tetrahedron. The position of the other 3 Ag^+ and 3 I^- was fixed. The modeling (B3lyp/6-31+G**) shows

that the Ag-I bond length in Ag^+ sphere with three H_2O and one I^- growths from the initial value of d = 282 pm in the solid to d = 304 pm in the complex and the other three Ag-I bonds in the lower part shorten to d = 273 pm. The bond length for Ag-OH_2 is d = 239 pm. Applying the bond valence distance relationship (eq.[7]) to the structures, the mean ionic bond valence distribution is Δn_0 = +0.12 ± 0.00 and Δn_1 = +0.88 v.u. and including a possible dipole correction (HIEMSTRA and VAN RIEMSDIJK, 2006), the CD values are about Δz_0 = +0.14 and Δz_1 = +0.84 v.u. This suggests that only a small fraction of the Ag^+ charge is to be attributed to the surface. For K^+, the interfacial CD has been estimated assuming a Pauling bond valence distribution. The coordination of K^+ is in the range CN = 8-12, leading to a small charge attribution of Δz_0 = 0.12 ± 0.02 and Δz_1 = 0.88 ± 0.02 v.u. The CD numbers for K^+ and Ag^+ are very similar.

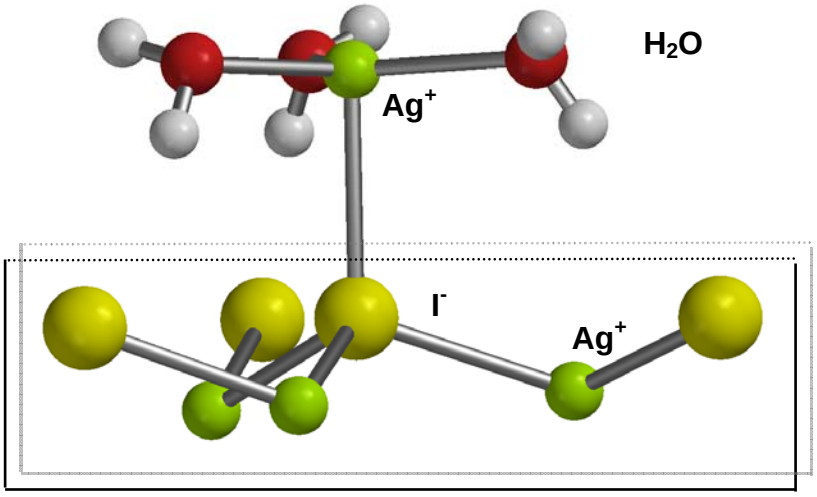

Fig.32. MO/DFT (B3lyp//6-31+G**) optimized structure with a hydrated Ag^+ ion on top, attached to a triply coordinated ≡ $I^{-0.25}$ as part of a surface structure of Ag and I with d-Ag-I = 282 pm and d(I-I) = 459 pm. The coordination sphere of the Ag^+ ion on top with three H_2O and one ≡ $I^{-0.25}$ and the AgI-bonds of the fourfold coordinated I^- ion were allowed to relax in the geometry optimization. The corresponding Ag-I bond (d = 304 pm) is significantly larger than in the AgI structure suggesting a low bond valence. Most charge of the Ag^+ is for the Ag-OH_2 bonds.

As an exercise, we implemented the above CD values in the model. With this choice, a slightly better fit of the data is obtained for option A using the same number of adjustable parameters. It shows that in principle the full CD model can be applied. For option B, the fit was not improved but was slightly less, unless we allow the NO_3^- ion to distribute its charge too, leading, for this ion, to Δz_0 = -0.42 ± 0.08 and Δz_1 = -0.58 ± 0.08 v.u. This distribution may point to some innersphere complexation. This is supported by the high log$K$ value for the NO_3^- adsorption, i.e. log$K$ = +0.2 ± 0.2. The fitted capacitance values are C_1 = 0.125 ± 0.005, C_2 = 0.51 ± 0.05 F/m^2 (Option A), and C_1 = 0.115 ± 0.003, C_2 = 0.43 ± 0.04 F/m^2 (Option B). In both model options, the capacitance of the outer Stern layer is within the error equal to the value found for goethite (HIEMSTRA and VAN RIEMSDIJK, 2006). From the exercise, we conclude that in principle the charging data of AgI(s) can be described with the CD approach.

AgCl(s) and AgBr(s)

The mineral structure of AgCl(s) and AgBr(s) differs from AgI (Table 5). The coordination number is larger (CN = 6) because the relative size of the halide ligand is smaller. The coordination number in these minerals is 6 leading to a bond valence of 0.167 v.u. Termination on the 100 faces of both minerals gives surface groups with a coordination of 5 and the groups can be defined as $\equiv Ag^{+0.167}$ and $\equiv I^{-0.167}$. Both groups are present in equal amounts and the surface is neutral. Model results of Sugimoto and Shiba (SUGIMOTO and SHIBA, 1999b) suggest for all silver halides (AgCl, AgBr, and AgI) asymmetry for the charging curve similar as in Fig.4. To our knowledge, no direct experimental charging data for colloidal AgCl(s) or AgBr(s) are available that allows to reveal by analogy the above-defined charging mechanisms. However, some important information comes from recent MD simulations showing that the Cl^- ion will not bind to $\equiv Ag^{+0.167}$ in the surface (Zarzycki and Rosso, 2010), despite the presence of a high Cl^- concentration. In the MD simulation, a stoichiometric AgCl crystal (2.5x2.5x2.5 nm with 100 faces) was built in contact with a 0.05 M KCl solution (1 KCl and 1046 H_2O molecules). The 0.05 M chloride concentration is far above the PZC of AgCl (PZC~ 5.2) and therefore the surface should be negatively charged. If the Cl^- ion in the simulation box on average would only bind at the surface, the corresponding charge would be -25 mC/m^2, which is a reasonable number (Fig.4). However, the MD simulation shows that Cl^- does not adsorb as an innersphere complex and no negative charge is created. The MD simulation can be understood if formation of negative charge on the AgCl 100 face at a high Cl^- concentration is due to desorption of Ag^+, i.e. the same charging mechanism for AgCl(s) as suggested in option A for AgI(s). Formation of negative charge by this mechanism starting with a neutral AgCl-box is not easily simulated with MD, since it requires the release of one Ag^+ that cannot be present in a small solution box because it would create a very high Ag^+ concentration, while the equilibrium concentration above the PZC needs to be $<< 10^{-5}$ M.

Chlorargyrite and bromargyrite (SUGIMOTO and SHIBA, 1999b) may also develop the 111 faces that can be terminated by triply coordinated $\equiv Ag^{+0.5}$ or $\equiv Cl/Br^{-0.5}$. To create a neutral surface, half of the ions in either case has to be removed, which leads in both cases to the same 1:1 mixture of triply coordinated groups ($\equiv Ag^{+0.5}$ or $\equiv Cl/Br^{-0.5}$). Excess ad/desorption of Ag^+ and Cl/Br^- ions by the triply coordinated surface groups will create surface charge.

Nernst law

Nernst law is not obeyed by any mineral surface that has a limited number of sites creating charge. This is due to a surface mixing entropy (BOLT and VAN RIEMSDIJK, 1982) expressed in the factor θ / (1-θ) in case of a single adsorption reaction, where θ is the fractional occupation of the site. The factor $\theta/(1-\theta)$ expresses the ratio between occupied and empty sites. Nernst law is only applicable to systems where charge is dislocated as it is in metal-electrodes. The relative deviation from Nernst law can be expressed in a factor α (PREOCANIN et al., 2009). The Nernstian slope is 59.13 mV per decade at 25 ^oC. According to

our model, the deviation from Nernst law is condition dependent. Since it is very difficult to measure subtle differences as a function of loading, the mean slope has been evaluated as done in literature (PREOCANIN et al., 2010). The AgI(s) sol behaves as near-Nernstian. Depending on the model option, the deviation is between 2-8 %. A larger deviation is due to a larger entropy term. The mean deviation from Nernst law, expressed in the factor α depends on the electrolyte level (Fig.32). In the modeling, deviation from Nernst law increases with ionic strength. For single crystal electrodes of AgBr(s) (PREOCANIN et al., 2010) or AgCl(s) (KALLAY et al., 2008; PREOCANIN et al., 2009), the opposite trend has been found. For the single crystal electrode, the measured deviation from Nernst law is relatively strong and for AgCl, it deviates significantly from the calculated behavior of an AgI sol. The latter behavior is near-Nernstian as is also found for classical AgCl electrodes with micro AgCl crystals (KALLAY et al., 2008).

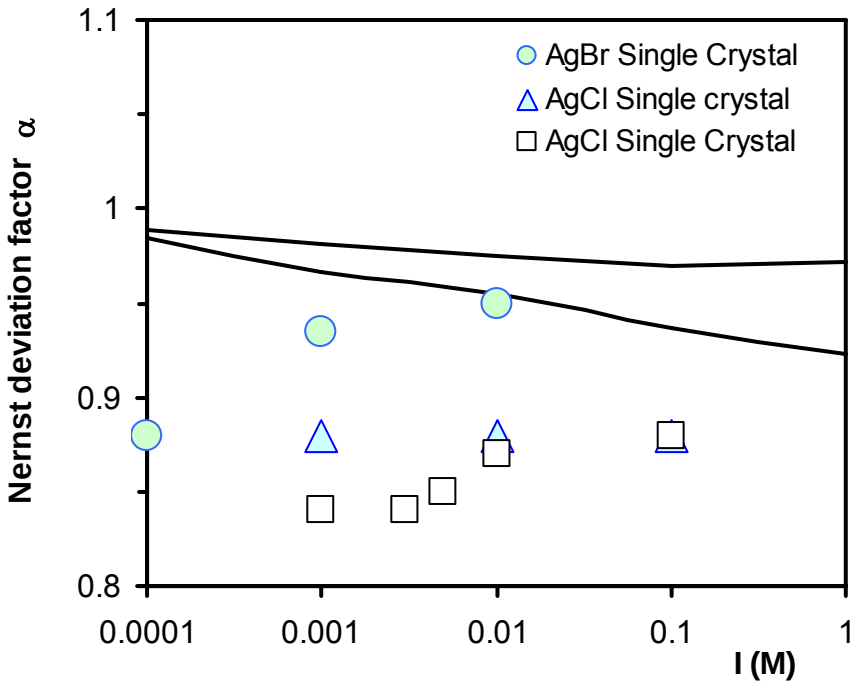

Fig.32. The mean fractional deviation from Nernst law (full lines) calculated for AgI(s) (Table 7 option B upper line, option A lower line) as a function of the ionic strength in comparison with very recent experimental data collected for single crystal electrodes of AgBr(s) (PREOCANIN et al., 2010) and AgCl(s) (KALLAY et al., 2008) (KALLAY et al., 2008; PREOCANIN et al., 2009). Classical electrodes with micro-crystallites behave more near-Nernstian (KALLAY et al., 2008).

Capacitance

The capacitance values that have been derived show an interesting feature. The inner capacitance is very low. The low number points to a low dielectric constant in the compact part of the EDL. This might be due to the strong orientation of the water molecules as suggested previously in our original paper on the interpretation of the capacitance of AgI (HIEMSTRA and VAN RIEMSDIJK, 1991). This molecular picture has recently been confirmed

by MD simulations (ZARZYCKI and ROSSO 2010). The water molecules at the surface form the primary hydration water on which the dipole is oriented. The capacitance C of a capacitor is related to distance d according to

$$C = \frac{\varepsilon_r \varepsilon_0}{d} \qquad [23]$$

in which the relative and absolute dielectric constant are represented by ε_r and ε_0 ($8.85\ 10^{-12}$ $CV^{-1}m^{-1}$). According to our structural model for AgI (Fig.30), the distance d between the surface and 1-plane is $d \sim 0.4$ nm. In combination with the fitted capacitance value ($C_1 = 0.11$-0.16 F/m^2), the relative dielectric constant is $\varepsilon_r \sim 6$, which is a typical number at saturation (HIEMSTRA and VAN RIEMSDIJK, 1991). We note that AgI(s) has a similar ε_r value ($\varepsilon_r = 7$).

The relative dielectric constant can be compared with the value that is found for the compact part of the double layer of well-crystallized goethite and other minerals. The inner Stern layer capacitance of goethite and gibbsite is about 0.9-1.0 F/m^2. If the average size of the counter ions (e.g. $d = 0.35$ nm) is a measure for the minimum distance of approach, the equivalent relative dielectric constant is $\varepsilon_r \approx 40$ (HIEMSTRA and VAN RIEMSDIJK, 2006). For rutile (TiO_2), the capacitance of $C = 0.64$ F/m^2 is equivalent with $\varepsilon_r \approx 30$. The first number, is about half between the dielectric constant of free water ($\varepsilon_r = 78$) and the solid (for goethite $\varepsilon_r = 11$), but the latter value for rutile is not (for rutile $\varepsilon_r = 120$). Rutile as well as water has a high dielectric constant. Nevertheless, the mean ε_r may be lower. This indicates that not necessarily the interfacial dielectric constant is a property that follows from the solid. We note that in modeling, the permittivity is generally considered as a constant. However, in a homogeneous continuum, the dielectric constant may depend on the field strength. A potential fall of 0, 100, or 200 mV over the Stern layer will lead to respectively $\varepsilon_r = 78$, $\varepsilon_r \approx 40$ and $\varepsilon_r \approx 20$ (HIEMSTRA and VAN RIEMSDIJK, 2006). However, also note that the actual situation in the Stern layer can be more complicated since surfaces are crowded by hydrated ions.

Another interesting observation is the capacitance of the second Stern layer. The fitted numbers $C_2 = 0.45 \pm 0.03$ F/m^2 or 0.47 ± 0.04 F/m^2 are slightly lower than the capacitance value ($C = 0.74 \pm 0.10$ F/m^2) recently found for goethite when analyzing in a consistent manner the charging behavior measured extensively for a large series of electrolytes (RAHNEMAIE et al., 2006). If the head end of the DDL differs from the minimum distance of approach of electrolyte ions by a layer thickness of 3 water molecules, e.g. $d \sim 0.75$ nm as discussed in the next section, the dielectric constant is about $\varepsilon_r \sim 40$, obviously lower than in pure water, pointing to water structuring.

Surface hydration and Charge Distribution

From the perspective of volume, the major constituent of oxides, silicates, and water is the oxygen ion, accounting for almost 90 % of the occupied space. The oxygens are neutralized by cations. For water, these cations are hydrogen ions that form long and rather linear

hydrogen bridges and this leads to an open network of oxygens (Fig.34) allowing dissolved ions to occupy the large amounts of space in between without a significant change in volume. The molar oxygen volume of pure water is ~18 cm^3/mol and in ice, it is ~20 cm^3/mol. This is higher than the mean molar volume in minerals, i.e. 11 cm^3/mol (HIEMSTRA and VAN RIEMSDIJK, 2009a). The molar volume of ice can be reduced to that of minerals when it is pressurized, filling all space (HIEMSTRA and VAN RIEMSDIJK, 2009a). Then, the mass density may double.

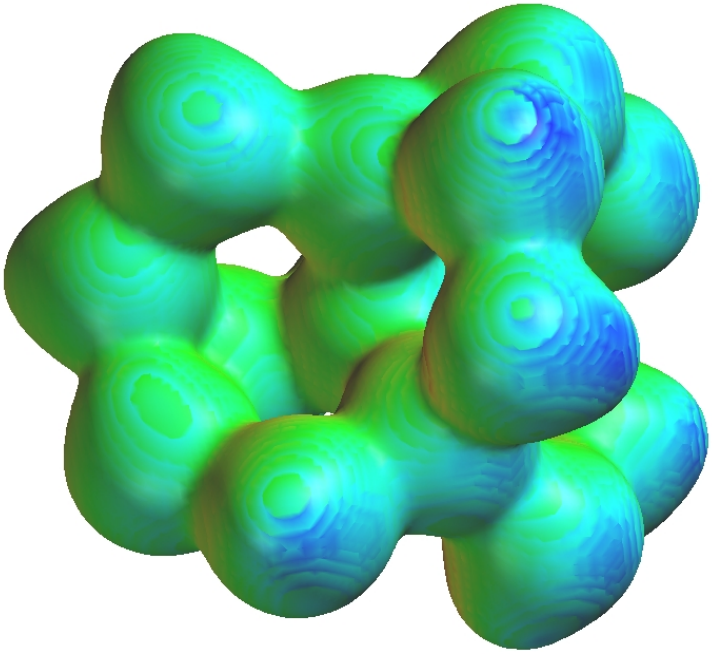

Fig.34. The open water network of 17 H_2O derived by molecular orbital computations (MO/HF 6-31G**)

Water molecules in contact with a surface are lined-up. This may increase the mass density. Structuring of water in the interface has been demonstrated nicely in a classical experiment of Pashley and Israelachvili (PASHLEY and ISRAELACHVILI, 1984), measuring the force-distance relationship for two mica plates that are pressed together. At large distances, the force gradually increases (Fig.35) as is expected for an overlapping diffuse double layer. Once the plates are at a small distance, the force starts to oscillate which is due to the increased ordering of the water molecules and counter ions in the neighborhood of the surface, acting as a hard wall. The repetitive oscillation has a wavelength (~0.25 nm) that is about the size of a water molecule. The data (Fig.35) can be interpreted as a layer of two water molecules at each mica sheet that are strongly ordered. The third layer has less ordering and forms the transition to the diffuse distribution of the DDL. Note that two surfaces are involved, which will double the number of layers in Fig.35.

The presence of water ordering at oxide surfaces has been measured with spectroscopy (CATALANO et al., 2006; FENTER and STURCHIO, 2004; TONEY et al., 1995) and these works also point to the presence two to three water layers that are more ordered than water of the bulk.

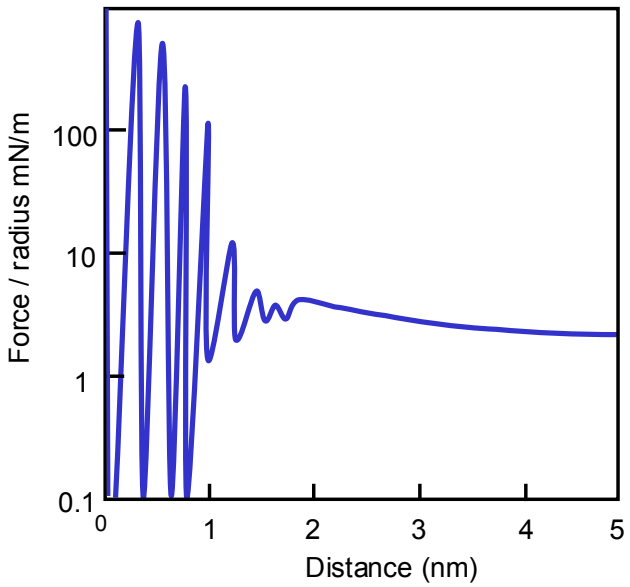

Fig.35. The force as a function of distance needed to press to flat two mica plates together. At large distance, the force gradually increases as predicted by the diffuse double layer theory. At short plate distances of about 1.2-1.6 nm, the force oscillates with a distance frequency of about 0.25 nm, close to the diameter of one water molecule. About 2-3 layers of water molecules in the EDL at each plate side are structured. Data from Pashley and Israelachvili (1984).

As mentioned above, the interfacial charge distribution can be partly the result of orientation of water dipoles in the interface, particularly in the Stern layer (HIEMSTRA and VAN RIEMSDIJK, 2006). Orientation of dipoles on the change of the electrostatic field leads to interfacial charge transfer (Fig.36). The charge near the surface is locally slightly neutralized by the dipole charge.

The mean charge transfer is rather limited and therefore will only play a distinct noticeable role if the adsorbed species has no or almost no charge. A typical example is the adsorption of $H_4SiO_4^0$ (HIEMSTRA et al., 2007) and $As(OH)_3^0$ (STACHOWICZ et al., 2006). In these complexes, the charge distribution is rather symmetrical in the coordination sphere leading to only small changes in the Δz_0 and Δz_1, whereas the data suggest larger effects. The adsorption and proton coadsorption can be better understood if we account for effect of orientation of interfacial water because of a change of the surface charge. For both ions these effect are about 0.1 v.u. (HIEMSTRA and VAN RIEMSDIJK, 2006).

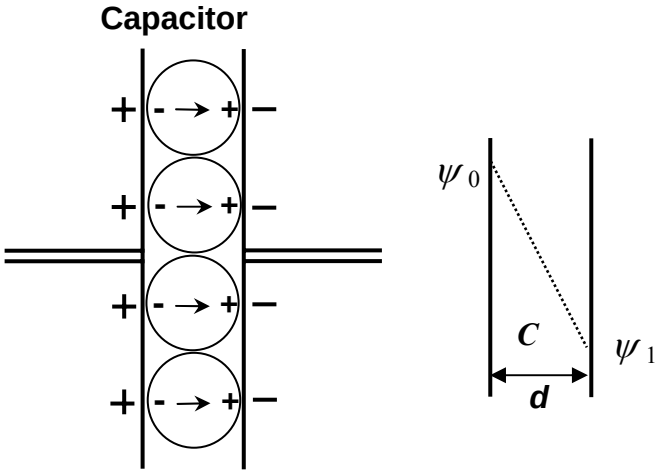

Fig.36. The orientation of water molecules in a charged capacitor with capacitance *C* representing the Stern layer. Because of charging, a potential difference ψ_o- ψ_1 is created over a distance *d* in which water may orientate. This is leads of redistribution of charge Δq. The corresponding energy is $-\Delta q\,\psi_0 /RT + \Delta q\,\psi_1/RT$ (Hiemstra and Van Riemsdijk, 2006).

Sverjensky and Fukushi (SVERJENSKY and FUKUSHI, 2006) have recently also suggested dipole orientation. They described the arsenite adsorption with the ligand exchange reaction given as

$$2\,SOH^0 + 2\,H^+(aq) + AsO_2OH^{2-}(aq) \Leftrightarrow S_2^{2+}....AsO_2OH^{2-} + 2\,H_2O(l) \qquad [24]$$

in which the charge of the protons is located in the 0-plane ($^{2+}$) and the charge of the divalent arsenite anion in the β-plane ($^{2-}$). This plane is also used to accommodate outersphere complexes. The created ionic charge distribution is huge for the inner sphere complex i.e. n_0 = +2 and n_1 = -2 v.u. compared to our approach, i.e. n_0 = +0.19 and n_1 = -0.19 v.u. To be able to describe the data, Sverjensky and Fukushi (SVERJENSKY and FUKUSHI, 2006) suggest to correct the charge distribution by a supposed very large shift of charge (i.e. 2 v.u., which implies a complete neutralization of the charge of 2 protons by the dipoles of water!). This large shift is motivated as a result of a change in dipole energy due to release of 2 H_2O molecules from the surface plane. This leads to $\Delta z_0 = 0$ and $\Delta z_1 = 0$ v.u., that is used in the model.

In Sverjensky's model, the dipole energy of the water molecules that coordinate to the Fe ions in the surface (i.e. surface groups SOH_2) is a variable quantity that depends on the potential change in the Stern layer region where the coordinated H_2O of the group does not at all reside. Moreover, the large energy correction suggests that the water molecules are able to orientate strongly depending on the pH- and concentration- dependent strength of the mean field. However, this is very unlikely since the coordinated water has a fixed orientation in the very strong local field of the Fe^{3+} ion. If the water molecules are released, this energy is released and since this is a constant contribution, independent of the field in the Stern layer. It

will be a constant part of the intrinsic constant. In our model, the (small) dipole energy contribution comes from water molecules present in the Stern layer, not from coordinated / fixed water.

Epilogue

We have seen that ion adsorption behavior in a metal (hydr)oxide system is determined by true surface properties in combination with the solution chemistry, as demonstrated in the concept of thermodynamic consistency (Eq.[11]). The surface properties are strongly influenced by the electrostatic field. The location of charge of the surface complex in this field is a crucial factor. Surface complexes are differently located in this field depending on the structure. We showed how this *structure-charge-potential* relationship regulates the partitioning of an ion over inner- and outersphere complexes and over mono- and bidentate complexes as a function of pH. It also strongly influences hydrolysis and protonation (cooperative hydrolysis and protonation). Changes in the electrostatic potential are large in the compact part of the double layer and the location of the charge becomes delicate. Small differences in location have a large impact. Therefore, ions cannot be treated anymore as point charges at a single electrostatic location, since they are on the scale of the interface spatially distributed. The bond valence approach is a powerful tool to distribute the charge based on the structure, observed experimentally by spectroscopy. This concept is incorporated in the CD model and it is a logical extension of the MUSIC model. The combination is a powerful surface structural framework for ion adsorption modeling. Surface structural approaches will become increasingly valuable due to the modern developments in spectroscopy, elucidating in a progressive degree of detail the structures of surface complexes. Computational chemistry is a growing field that increasingly enables quantification and verification of the microscopic processes.

Commonly-used surface complexation models are generally also able to describe adsorption data well if species and sites can be freely chosen. 66
70
This is inherent to the thermodynamic foundations of most adsorption models. A first choice in fitting these commonly used models is the location of the ion point charge, accounting in a simple manner for inner- *or* outersphere complexation. Furthermore, the number of protons in the surface species is chosen differently. Such protonated or hydrolyzed species are chosen to regulate the pH dependency in combination with a sub-Nernstian behavior of the surface potential, partly created by choosing a ΔpK for the protonation of the surface groups. If necessary, charge is distributed by choosing combinations of inner- *and* outersphere complexes, which are located at different electrostatic planes. The achieved correct description remains unsatisfactory. The SCMs, that described correctly the pH dependent binding of one component in simple systems, will not predict *a priori* properly the ion interactions in multicomponent systems. The foremost reason is that the interaction is mainly of an electrostatic nature and models differ strongly in the way this is handled.

To make progress, models should be constrained. One of the possibilities is the introduction of surface chemistry based on crystallography, yielding physically realistic values for the type and number of sites. Furthermore, models should ideally be tested on an surface speciation, experimentally obtained, identified in-situ, in a quantitative manner, over a range of conditions. One of the first studies that dealt with the latter objective was of Tejedor-Tejedor & Anderson (TEJEDOR-TEJEDOR and ANDERSON, 1990). The CD-MUSIC model was able to describe the quantitatively measured partitioning over the different surface species as a function of pH and loading and was able to describe corresponding macroscopic adsorption phenomena. In the approach, also the types and the numbers of surface sites were constraint to physically realistic values. Another impressive example is the work done for TiO_2 as demonstrated by Machesky et al. (MACHESKY et al., 2008). These results illustrate the great value of a surface structural approach based on spectroscopy.

Another important development comes from molecular orbital (MO) calculations and molecular dynamic (MD) simulations. The latter integrates the action of many molecules in a dynamic fashion and is an ideal candidate to elucidate the behavior of ions in the interface, the binding at the surface as well as behavior in the EDL. Expected is that with the development of fast-computing and software this technique may increasingly contribute. Ridley et al. (RIDLEY et al., 2009) have shown that combining information of MD simulations and CD modeling can amplify our understanding of interfacial behavior of ions.

Hydrolysis and protonation of surface complexes are important factors in regulating the adsorption and competition of ions. This aspect is still underexposed in the spectroscopic approaches and should receive more attention. To cope with a potential hydrolysis of cations, we have developed the approach that accounts for variation in bond length that is linked to charge distribution and that describes the pH dependency part of adsorption that is not directly related to hydrolysis or protonation. In the procedure, a bond valence analysis is used to combine consistently the results of CD-modeling with the experimental geometry of surface complexes. The model may evaluate hydroxylation of adsorbed cations. For verification, new spectroscopic data are needed focusing on the protons present on the ligands.

It is obvious that spectroscopy regularly results in opposing microscopic models. Combining, comparing, and confronting such results with macroscopic observations and vice versa will improve our understanding of interface chemistry as illustrated recently for UO_2^{2+}-CO_3^{2-} ferrihydrite systems (ROSSBERG et al., 2009), (HIEMSTRA and VAN RIEMSDIJK, 2009a; HIEMSTRA et al., 2009b). The CD and MUSIC framework is a logical vehicle for that and can be applied in science, in technology, as well as in the environment.

References

Aquino A. J. A., Tunega D., Haberhauer G., Gerzabek M. H., and Lischka H. (2008) Acid-base properties of a goethite surface model: A theoretical view. Geochim. Cosmoschim. Acta 72(15), 3587-3602.

Atkinson R. J., Posner A. M., and J.P. Q. (1967) Adsorption of potential-determining ions at the ferric oxide-aqueous interface. J. Phys. Chem. 71, 550-558.

Axe L., Bunker G. B., Anderson P. R., and Tyson T. A. (1998) An XAFS Analysis of Strontium at the Hydrous Ferric Oxide Surface. J. Colloid Interf. Sci. 199, 44-52.

Bargar J. R., Brown G. E., Jr., and Parks G. A. (1997a) Surface Complexation of Pb(II) at Oxide-Water Interfaces: I XAFS and Bond-valence Determination of Mono- and Polynuclear Pb(II) Sorption Products on Aluminum Oxides. Geochim. Cosmochim. Acta 61, 2617-2637.

Bargar J. R., Brown G. E., Jr., and Parks G. A. (1997b) Surface Complexation of Pb(II) at Oxide-Water interfaces: II XAFS and Bond-valence Determination of Mononuclear Pb(II) Sorption Products and Surface Functional Groups on Iron Oxides. Geochim. Cosmochim. Acta 61, 2639-2652.

Bargar J. R., Brown G. E., Jr., and Parks G. A. (1998) Surface Complexation of Pb(II) at Oxide-Water Interfaces: III XAFS Determination of Pb(II) and Pb(II)-chloro Adsorption Complexes on Goethite and Alumina. Geochim. Cosmochim. Acta 62, 193-207.

Barrón V. and Torrent J. (1996) Surface Hydroxyl Configuration of Various Crystal Faces of Hematite and Goethite. J. Colloid Interf. Sci. 177, 407-410.

Barrow N. J. and Bowden J. W. (1987a) A comparison of Models for Describing the Adsorption of Anions on a Variable Charge Mineral Surface. J. Colloid Interf. Sci. 119, 236-250.

Barrow N. J. and Bowden J. W. (1987b) Reactions with Variable-Charge Soils. Martinus Nijhof Publishers.

Barrow N. J., Bowden J. W., Posner A. M., and Quirk J. P. (1980) An Objective Method for Fitting Models of Ion Adsorption on Variable Charge Surfaces. Aust. J. Soil Res. 18, 395-404.

Barrow N. J. and Cox V. C. (1992) The Effects of pH and Chloride Concentration on Mercury Sorption. I By Goethite. J. Soil Sci. 43, 437-450.

Bérubé Y. G. and De Bruyn P. L. (1968) Adsorption at the Rutile-Solution Interface. II Model of the Electrochemical Double Layer. J. Colloid Interf. Sci. 28, 92-105.

Bickmore B. R., Tadanier C. J., Rosso K. M., Monn W. D., and Eggett D. L. (2004) Bond-Valence methods for pK(a) prediction: critical reanalysis and a new approach. Geochim. Cosmochim. Acta 68(9), 2025-2042.

Bijsterbosch B. H. and Lyklema J. (1978) Interfacial Electrochemistry of Silver-Iodide. Advances in Colloid and Interface Science 9(3), 147-251.

Bleam W. F. (1993) On Modeling Proton Affinity at the Oxide/Water Interface. J. Colloid Interf. Sci. 159, 312-318.

Blok L. and De Bruyn P. L. (1970) The Ionic Double Layer at the ZnO/ Solution Interface. II Composition Model of the Surface. J. Colloid Interf. Sci. 32, 527-532.

Boily J.-F. (1999) The Surface Complexation of Ions at the Goethite (a-FeOOH)/ Water Interface: a Multisite Complexation Approach, Umeå University.

Boily J. F. and Felmy A. R. (2008) On the protonation of oxo- and hydroxo-groups of the goethite (alpha-FeOOH) surface: A FTIR spectroscopic investigation of surface O-H stretching vibrations. Geochim. Cosmoschim. Acta 72(14), 3338-3357.

Bolt G. H. (1957) Determination of the Charge Density of Silica Sols. J. Phys. Chem. 61, 1166-1169. ibid. 62: 1608.

Bolt G. H. and Van Riemsdijk W. H. (1982) Ion Adsorption on Inorganic Variable Charge Constituents. In Soil Chemistry, Vol. Vol. B (ed. G. H. Bolt), pp. 459-504. Elsevier.

Borkovec M. (1997) Origin of 1-pK and 2-pK Models for Ionizable Water-Solid interfaces. Langmuir 13, 2608-2613.

Borkovec M. (2001) Ionizable Interfaces. In Surface and Colloid Science, Vol. 16 (ed. E. Matijevic), pp. 2608-2613. Plenum Press.

Borkovec M., Rusch U., and Westall J. C. (1998) Modeling of Competitive Ion Binding to Heterogeneous Materials with Affinity Distributions. In Adsorption of Metals by Geomedia. Variables, Mechanisms and Model Applications (ed. E. A. Jenne), pp. 467-482. Academic Press.

Bourikas K., Hiemstra T., and Van Riemsdijk W. H. (2000) Adsorption of Molybdate Monomers and Polymers on Titania with a Multisite approach. J. Phys. Chem. 105(12), 2393-2403.

Bourikas K., Hiemstra T., and Van Riemsdijk W. H. (2001) Ion Pair Formation and Primary Charging behaviour of Titanium Oxide (Anatase and Rutile). Langmuir 17(3), 749-756.

Bowden J. W. (1973) Models for Ion Adsorption on Mineral Surfaces. PhD, University of West Australia.

Bowden J. W., Nagarajah S., Barrow N. J., Posner A. M., and Quirk P. J. (1980) Describing the adsorption of phosphate, citrate and selenite on a variable-charge mineral surface. Aust. J. Soil Res. 18, 49-60.

Bowden J. W., Posner A. M., and Quirk P. J. (1977) Ionic Adsorption on Variable Charge Mineral Surfaces: Theoretical-Charge Development and Titration Curves. Aust. J. Soil Res. 15, 121-136.

Breeuwsma A. and Lyklema J. (1973) Physical and chemical adsorption of ions in the electrical double layer. J. Colloid Interf. Sci. 43, 437-448.

Brown I. D. (1977) Predicting Bond Lengths in Inorganic Crystals. Acta Cryst. B33, 1305-1310.

Brown I. D. (1978) Bond Valences -A Simple Structural Model for Inorganic Chemistry. Chem. Soc. Rev. 7, 359-376.

Brown I. D. (1992) Chemical and Steric Constraints in Inorganic Solids. Acta Cryst. B48, 553-572.

Brown I. D. (2009) Recent Developments in the Methods and Applications of the Bond Valence Model. Chem. Rev. 109(12), 6858-6919.

Brown I. D. and Altermatt D. (1985) Bond-Valence Parameters Obtained from a Systematic Analysis of the Inorganic Crystal Structure Database. Acta Cryst. B41, 244-247.

Burley G. (1963) Polymorphism of Silver Iodide. Am. Mineral. 48(11-2), 1266-&.

Catalano J. G., Park C., Zhang Z., and Fenter P. (2006) Termination and water adsorption at the alpha-Al_2O_3 (012) - Aqueous solution interface. Langmuir 22(10), 4668-4673.

Cerník M. and Borkovec M. (1996) Affinity Distribution of Competitive Ion Binding to Heterogeneous Materials. Langmuir 12, 6127-6137.

Chapman D. L. (1913) A contribution to the theory of electrocapillarity. Philos. Mag. 6(25), 475-481.

Charlet L. and Manceau A. A. (1992) X-Ray absorption spectroscopic study of the sorption of Cr(III) at the oxide-water interface. J. Colloid Interf. Sci. 148, 443-458.

Chisholm-Brause C., Conradson S. D., Buscher C. T., Eller P. G., and Morris A. (1994) Speciation of uranyl sorbed at multiple binding sites on montmorillonite. Geochim. Cosmochim. Acta 58, 3625-3631.

Christl I. and Kretzschmar R. (1999) Competitive sorption of copper and lead at the oxide-water interface: Implications for surface site density. Geochim. Cosmoschim. Acta 63(19-20), 2929-2938.

Collins C. R., Ragnarsdottir K. V., and Sherman D. M. (1999b) Effect of Inorganic and Organic Ligands on the Mechanism of Cadmium Sorption to Goethite. Geochim. Cosmochim. Acta 63, 2989-3002.

Collins C. R., Sherman D. M., and Ragnarsdottir K. V. (1998) The Adsorption Mechanism of Sr^{2+} on the Surface of Goethite. Radiochim. Acta 81, 201-206.

Collins C. R., Sherman D. M., and Ragnarsdottir K. V. (1999a) Surface Complexation of Hg^{2+} on Goethite: Mechanism from EXAFS Spectroscopy and Density Functional Calculations. J. Colloid Interf. Sci. 219, 345-350.

Colombo C., Barrón V., and Torrent J. (1994) Phosphate adsorption and desorption in relation to morphology and crystal properties of synthetic hematites. Geochim. Cosmochim. Acta 58, 1261-1269.

Combes J. M., Chrisholm-Brause C. J., Brown G. E., Jr., Parks G. A., Conradson S. D., Eller P. G., Triay I. R., Hobart D. E., and Meijer A. (1992) EXAFS Spectroscopic Study of Neptunium(V) Sorption at the a-FeOOH / Water Interface. Environ. Sci. Technol. 26, 376-382.

Connor P. A., Dobson K. D., and McQuillan A. J. (1999a) Infrared Spectroscopy of the TiO_2/Aqueous Solution Interface. Langmuir 15, 2402-2408.

Connor P. A. and McQuillan A. J. (1999b) Phosphate Adsorption onto TiO_2 from Aqueous Solutions: An in Situ Internal Reflection Infrared Spectroscopic Study. Langmuir 15, 2916-2921.

Davis J. A., James R., and Leckie J. O. (1978a) Surface Ionization and Complexation at the Oxide/Water Interface. I Computation of Electrical Double Layer Properties in Simple Electrolytes. J. Colloid Interf. Sci. 63, 480-499.

Davis J. A. and Leckie J. O. (1978b) Surface ionization and complexation at the oxide/water interface. II Surface properties of amorphous iron oxyhydroxide and adsorption of metal ions. J. Colloid Interf. Sci. 67, 90-105.

Dent A. J., Ramsay J. D. F., and Swanton S. W. (1992) An EXAFS Study Uranyl Ion in Solution and Sorbed onto Silica and Montmorillonite Clay Colloids. J. Colloid Interf. Sci. 150, 45-60.

Dzombak D. A. and Morel F. M. M. (1990) Surface Complexation Modeling: Hydrous Ferric Oxide. John Wiley & Sons: New York, 393.

Eggleston C. M. and Jordan G. (1998) A New Approach to pH and Point of Zero Charge Measurement: Crystal-face Specificity by Scanning Force Microscopy (SFM). Geochim. Cosmochim. Acta 62(11), 1919-1923.

Felmy A. R. and Rustad J. R. (1998) Molecular Statics Calculations of Proton Binding to Goethite Surfaces: Thermodynamic Modeling of Surface Charging and Protonation of Goethite in Aqueous Solution. Geochim. Cosmochim. Acta 62, 25-31.

Fendorf S., Eick M. J., Grossl P., and Sparks D. L. (1997) Arsenate and Chromate retention mechanism on goethite. 1 Surface structure. Environ. Sci. Technol. 31, 315-320.

Fenter P., Cheng L., Rihs S., Machesky M., Bedzyk M. J., and Sturchio N. C. (2000) Electrical Double-Layer Structure at the Rutile-Water Interface as Observed in Situ with Small-Period X-ray Standing Waves. J. Colloid Interf. Sci. 225, 154-165.

Fenter P. and Sturchio N. C. (2004) Mineral-water interfacial structures revealed by synchrotron X-ray scattering. Progress Surf. Sci. 77, 171-258.

Filius J. D., Hiemstra T., and Van Riemsdijk W. H. (1997) Adsorption of small weak organic acids on goethite: Modeling of mechanisms. J. Colloid Interf. Sci. 195(2), 368-380.

Filius J. D., Hiemstra T., and Van Riemsdijk W. H. (2000) Adsorption of Fulvic Acid on Goethite. Geochim. Cosmochim. Acta 64(1), 51-60.

Filius J. D., Meeussen J. C. L., and van Riemsdijk W. H. (1999) Transport of malonate in a goethite-silica sand system. Colloid Surface A 151(1-2), 245-253.

Fokkink L. G. J., De Keizer A., and Lyklema J. (1987) Specific Ion Adsorption on Oxides: Surface Charge Adjustment and Proton Stoichiometry. J. Colloid Interf. Sci. 118, 454-462.

Gan Y. and Franks G. V. (2006) Charging behavior of the Gibbsite basal (001) surface in NaCl solution investigated by AFM colloidal probe technique. Langmuir 22(14), 6087-6092.

Girvin D. C., Ames L. L., Schwab A. P., and McGarrah J. E. (1991) Neptunium adsorption on synthetic amorphous iron oxyhydroxide. J. Colloid Interf. Sci. 141, 67-78.

Goldberg S. and Sposito G. (1984a) A chemical model of phosphate adsorption by soils I. Reference oxide materials. Soil Sci. Soc. Am. J. 48, 772-778.

Gouy G. (1910) Sur la Constitution de la charge électrique à la surface d'un électrolyte. J. Phys. 9, 457-468.

Grahame D. C. (1947) The Electrical Double Layer and the Theory of Electrocapillarity. Chem. Rev. 41, 441-501.

Gunneriusson L., Lövgren L., and Sjöberg S. (1994) Complexation of Pb(II) at the goethite (a-FeOOH) / Water interface: The influence of chloride. Geochim. Cosmochim. Acta 58, 4973-4983.

Gunneriusson L. and Sjöberg S. (1993) Surface Complexation in the H^+ - Goethite (a-FeOOH)-Hg(II)-Chloride System. J. Colloid Interf. Sci. 156, 121-128.

Hair M. L. and Hertl W. (1970) Acidity of Surface Hydroxyl Groups. J. Phys. Chem. 74(1), 91-94.

Hansmann D. D. and Anderson M. A. (1985) Using Electrophoresis in Modeling Sulfate, Selenite, and Phosphate Adsorption onto Goethite. Environ. Sci. Technol. 19(6), 544-551.

Hayes K. F. and Leckie J. O. (1987b) Modeling Ionic Strength Effects on Cation Adsorption at Hydrous Oxide/Solution Interfaces. J. Colloid Interf. Sci. 115, 564-572.

Hayes K. F., Papelis C., and Leckie J. O. (1988) Modeling Ionic Strength Effects on Anion Adsorption at Hydrous Oxide/Solution Interfaces. J. Colloid Interf. Sci. 125, 717-726.

Hayes K. F., Roe A. L., Brown G. E., Jr., Hodgson K., Leckie J. O., and Parks G. A. (1987a) In-situ X-ray absorption study of surface complexes: Selenium oxyanions on a-FeOOH. Science 238, 783-785.

Helmholtz H. (1879) Studien über electrische Grenzschichten. Ann. Physik. Chem. 7, 337-382.

Hiemstra T., Barnett M. O., and Van Riemsdijk W. H. (2007) Interaction of Silicic Acid with Goethite. J. Colloid Interf. Sci. 310, 8-17.

Hiemstra T., De Wit J. C. M., and Van Riemsdijk W. H. (1989b) Multisite proton adsorption modeling at the solid/solution interface of (hydr)oxides: A new approach. II. Application to various important (hydr)oxides. J. Colloid Interf. Sci. 133, 105-117.

Hiemstra T., Han Yong, and Van Riemsdijk W. H. (1999b) Interfacial Charging Phenomena of Aluminum (Hydr)oxides. Langmuir 15, 5942-5955.

Hiemstra T., Rahnemaie R., and Van Riemsdijk W. H. (2004) Surface Complexation of Carbonate on Goethite: IR spectroscopy, Structure and Charge Distribution. J. Colloid Interf. Sci. 278, 282-290.

Hiemstra T. and Van Riemsdijk W. H. (1991) Physical chemical interpretation of primary charging behaviour of metal (hydr)oxides. Colloids Surfaces 59, 7-25.

Hiemstra T. and Van Riemsdijk W. H. (1996a) A surface Structural Approach to Ion Adsorption: The Charge Distribution (CD) Model. J. Colloid Interf. Sci. 179, 488-508.

Hiemstra T. and Van Riemsdijk W. H. (1999a) Surface structural ion adsorption modeling of competitive binding of oxyanions by metal (hydr)oxides. J. Colloid Interf. Sci. 210, 182-193.

Hiemstra T. and Van Riemsdijk W. H. (1999c) Effect of Different Crystal Faces on the Experimental Interaction Force and Aggregation of Hematite. Langmuir 15(23), 8045-8051.

Hiemstra T. and Van Riemsdijk W. H. (2000) Fluoride adsorption on goethite in relation to different types of surface sites. J. Colloid Interf. Sci. 225(1), 94-104.

Hiemstra T. and Van Riemsdijk W. H. (2002) On the Relationship between Surface Structure and Ion Complexation of Oxide-Solution Interfaces. In Encyclopaedia of Surface and Colloid Science, pp. 3773-3799. Marcel Dekker, Inc.

Hiemstra T. and Van Riemsdijk W. H. (2006) On the relationship between charge distribution, surface hydration and the structure of the interface of metal hydroxides. J. Colloid Interf. Sci. 301, 1-18.

Hiemstra T. and Van Riemsdijk W. H. (2007a) Adsorption and surface oxidation of Fe(II) on metal (hydr)oxides. Geochim. Cosmochim. Acta 71(24), 5913-5933.

Hiemstra T. and Van Riemsdijk W. H. (2007b) Surface complexation of selenite on goethite: MO/DFT geometry and charge distribution. Croatica Chemica Acta 80(3-4), 313-324.

Hiemstra T. and Van Riemsdijk W. H. (2009a) A Surface Structural Model for Ferrihydrite I: Sites related to Primary charge, Molar Mass, and Mass Density. Geochim. Cosmochim. Acta 73, 4423-4436.

Hiemstra T., Van Riemsdijk W. H., and Bolt G. H. (1989a) Multisite Proton Adsorption Modeling at the Solid/Solution Interface of (Hydr)oxides: A New Approach. I. Model Description and Evaluation of Intrinsic Reaction Constants. J. Colloid Interf. Sci. 133, 91-104.

Hiemstra T., Van Riemsdijk W. H., and Bruggenwert M. G. M. (1987) Proton adsorption mechanism at the Gibbsite and aluminum oxide solid/solution interface. Neth. J. Agric. Sci. 35, 281-293.

Hiemstra T., Van Riemsdijk W. H., Rossberg A., and Ulrich K. U. (2009b) A Surface Structural Model for Ferrihydrite II: Adsorption of Uranyl and Carbonate. Geochim. Cosmochim. Acta 73(4437-4451).

Hiemstra T., Venema P., and Van Riemsdijk W. H. (1996b) Intrinsic proton affinity of reactive surface groups of metal (hydr)oxides: The bond valence principle. J. Colloid Interf. Sci. 184, 680-692.

Hingston F. J., Atkinson R. J., Posner A. M., and Quirk J. P. (1967) Specific adsorption of anions. Nature 215, 1459-1461.

Hingston F. J., Posner A. M., and Quirk J. P. (1968) Adsorption of Selenite by Goethite. In Symposium on adsorption from aqueous solution Advances in Chemical Series, Vol. 70, pp. 82-90.

Hingston F. J., Posner A. M., and Quirk J. P. (1971) Competitive Adsorption of Negatively Charged Ligands on Oxides Surfaces. Diss. Faraday Soc. 52, 334-342.

Hingston F. J., Posner A. M., and Quirk J. P. (1972) Anion adsorption by goethite and gibbsite. I. The role of the proton in determining adsorption envelopes. *J. Soil Sci.* 23, 177-192.

Hug S. J. (1997) In situ Fourier Transform Infrared Measurements of sulfate Adsorption on hematite in aqueous solutions. J. Colloid Interf. Sci. 188, 415-422.

Hull S. and Keen D. A. (1999) Pressure-induced phase transitions in AgCl, AgBr, and AgI. Physical Review B 59(2), 750-761.

Israelachvili J. N. and Wennerstrom H. (1996) Role of hydration and water structure in biological and colloidal interactions. Nature 379(6562), 219-225.

Jodin M. C., Gaboriaud F., and Humbert B. (2005) Limitations of potentiometric studies to determine the surface charge of gibbsite gamma-Al(OH)(3) particles. J. Colloid Interf. Sci. 287(2), 581-591.

Jones P. and Hockey J. A. (1971) Infra-red Studies of Rutile Surfaces II. Hydroxylation, hydration and Structure of Rutile Surfaces. Trans. Faraday Soc. 67, 2679-2685.

Kallay N., Colic M., Fuerstenau D. W., Jang H. M., and Matijevic E. (1994) Lyotropic effect in surface charge, electrokinetics and coagulation of a rutile suspension. Colloid Polym. Sci. 272, 554-561.

Kallay N., Preocanin T., and Supljika H. (2008) Measurement of surface potential at silver chloride aqueous interface with single-crystal AgCl electrode. J. Colloid Interf. Sci. 327(2), 384-387.

Kataoka S., Gurau M. C., Albertorio F., Holden M. A., Lim S. M., Yang R. D., and Cremer P. S. (2004) Investigation of water structure at the TiO2/aqueous interface. Langmuir 20(5), 1662-1666.

Kolkmeijer N. H. and Van Hengel J. W. A. (1934) Über das regulare und das hexagonale Silberjodid. Zeit. Krist. 88, 317-322.

Komatsu H. and Sunagawa I. (1965) Surface Structures of Sphalerite Crystals. Am. Mineral. 50(7-8), 1046-&.

Kooner Z. S. (1993) Comparative study of adsorption behavior of copper, lead, and zinc onto goethite in aqueous systems. Environ. Geol. 21, 242-250.

Kosmulski M. (1997) Attempt to determine pristine points of zero charge of Nb_2O_5, Ta_2O_5, and HfO_2. Langmuir 13(23), 6315-6320.

Kummert R. and Stumm W. (1980) The surface Complexation of Organic Acids on Hydrous g-Al_2O_3. J. Colloid Interf. Sci. 75, 373-385.

Kwon K. D. and Kubicki J. D. (2004) Molecular orbital theory study on surface complex structures of phosphates to iron hydroxides: Calculation of vibrational frequencies and adsorption energies Langmuir 20(1), 9249-9254.

Li W., Feng J., Kwon K. D., Kubicki J. D., and Phillips B. L. (2010) Surface Speciation of Phosphate on Boehmite (gamma-AlOOH) Determined from NMR Spectroscopy. Langmuir 26(7), 4753-4761.

Lindegren M. and Persson P. (2010) Competitive adsorption involving phosphate and benzenecarboxylic acids on goethite-Effects of molecular structures. J. Colloid Interf. Sci. 343(1), 263-270.

Loring J. S., Sandstrom M. H., Noren K., and Persson P. (2009) Rethinking Arsenate Coordination at the Surface of Goethite. Chemistry-a European Journal 15(20), 5063-5072.

Lövgren L., Sjöberg S., and Schindler P. W. (1990) Acid/base reactions and aluminium (III) complexation at the surface of goethite. Geochim. Cosmochim. Acta 54, 1301-1306.

Lützenkirchen J. (1998) Comparison of 1-pK and 2-pK versions of surface complexation theory by the goodness of fit in describing surface charge data of (hydr)oxides. Environ. Sci. Technol. 32, 3149-3154.

Lyklema J. and Overbeek J. T. G. (1961) On the Interpretation of Electrokinetic Potentials. J. Colloid Interf. Sci. 16, 595.

Machesky M. L., Predota M., Wesolowski D. J., Vlcek L., Cummings P. T., Rosenqvist J., Ridley M. K., Kubicki J. D., Bandura A. V., Kumar N., and Sofo J. O. (2008) Surface Protonation at the Rutile (110) Interface: Explicit Incorporation of Solvation Structure within the Refined MUSIC Model Framework. Langmuir 24(21), 12331-12339.

Machesky M. L., Wesolowski D. J., Palmer D. A., and Ichiro-Hayashi K. (1998) Potentiometric Titrations of Rutile Suspensions to 250 ^{o}C. J. Colloid Interf. Sci. 200, 298-309.

Machesky M. L., Wesolowski D. J., Palmer D. A., and Ridley M. K. (2001) On the temperature dependence of intrinsic surface protonation equilibrium constants: An extension of the revised MUSIC model. J. Colloid Interf. Sci. 239(2), 314-327.

Manceau A., Charlet L., Boisset M. C., Didier B., and Spadini L. (1992) Sorption and speciation of heavy metals on hydrous Fe and Mn oxides. From microscopic to macroscopic. Appl. Clay Sci. 7, 201-223.

Manning B. A., Fendorf S. E., and Goldberg S. (1998) Surface Structure and Stability of Arsenic (III) on Goethite: Spectroscopic Evidence for Innersphere Complexes. Environ. Sci. Technol. 32, 2383-2388.

Marshall K., Ridgewell G. L., Rochester C. H., and Simpson J. (1974) The acidity of surface silanol group on silica. Chemistry and Industry 19, 775-776.

Morel F. M. M. and Morgan J. J. (1971) A Numerical Method for Computing Equilibria in Aqueous Chemical Systems. Environ. Sci. Technol. 6, 58-67.

Ostergren J. D., Bargar J. R., Brown G. E., Jr., and Parks G. A. (1999b) Combined EXAFS and FTIR investigation of sulfate and carbonate effects on Pb(II)sorption to goethite (a-FeOOH). J. Synchotron Rad. 6, 645-647.

Ostroverkhov V., Waychunas G. A., and Shen Y. R. (2005) New information on water interfacial structure revealed by phase-sensitive surface spectroscopy. Physical Review Letters 94(4).

Overbeek J. T. G. (1952) Electrochemistry of the Double Layer. In Colloid Science I (ed. H. R. Kruyt), pp. 115-190. Elsevier.

Parfitt R. L., Atkinson R. J., and Smart R. S. C. (1975) The Mechanism of Phosphate Fixation by Iron Oxides. Soil Sci. Soc. Am. Proc. 39, 837-841.

Parfitt R. L., Fraser A. R., and Farmer V. C. (1977c) Adsorption on Hydrous Oxides. III Fulvic Acid and Humic Acid on Goethite, Gibbsite and Imogolite. J. Soil Sci. 28, 289-296.

Parfitt R. L., Fraser A. R., Russell J. D., and Farmer V. C. (1977a) Adsorption on Hydrous Oxides. I. Oxalate, Benzoate on Goethite. J. Soil Sci. 28, 29-39.

Parfitt R. L., Fraser A. R., Russell J. D., and Farmer V. C. (1977b) Adsorption on Hydrous Oxides. II. Oxalate, Benzoate and Phosphate on Gibbsite. J. Soil Sci. 28, 40-47.

Parfitt R. L. and Russell J. D. (1977d) Adsorption on Hydrous Oxides. IV. Mechanisms of Adsorption of Various Ions on Goethite. J. Soil Sci. 28, 297-305.

Parfitt R. L., Russell J. D., and Farmer V. C. (1976) Confirmation of the Structures of Goethite (a-FeOOH) and Phosphated Goethite by Infrared Spectroscopy. J. Chem. Soc. Faraday Trans. I 72, 1082-1087.

Parkman R. H., Charnock J. M., Bryan N. D., and Vaughan D. J. (1999) Reactions of copper and cadmium ions in aqueous solution with goethite, lepidocrocite, mackinawite, and pyrite. Amer. Min. 84, 407-419.

Parks G. A. (1965) The isoelectric points of solid oxides, solid hydroxides, and aqueous hydroxo complex systems. Chem. Rev. 65, 177-198.

Parks G. A. (1967) Aqueous Surface Chemistry of Oxides and Complex Oxide Minerals. Isoelectric Point and Zero Point of Charge. In Equilibrium Concepts in Natural Water Systems, Vol. 67 (ed. R. F. Gould). American Chemical Society.

Parks G. A. and De Bruyn P. L. (1962) The Zero Point of Charge of Oxides. J. Phys. Chem. 66, 967-973.

Pashley R. M. and Israelachvili J. N. (1984) Molecular layering of water in thin films between mica surfaces and its relation to hydration forces. J. Colloid Interf. Sci. 101(2), 511-523.

Pauling L. (1929) The Principles Determining the Structure of Complex Ionic Crystals. J. Am. Chem. Soc. 51, 1010-1026.

Peak D., Ford R. G., and Sparks D. L. (1999) An in-Situ ATR-FTIR Investigation of Sulfate Bonding Mechanisms on Goethite. J. Colloid Interf. Sci. 218, 289-299.

Peri J. B. and Hensley S. L., Jr. (1968) The Surface Structure of Silica Gel. J. Phys. Chem. 72(8), 2926-2933.

Perona M. J. and Leckie J. O. (1985) Proton Stoichiometry for the Adsorption of Cations on Oxide Surfaces. J. Colloid Interf. Sci. 106, 65-69.

Persson I. and Nilsson K. B. (2006) Coordination chemistry of the solvated silver(I) ion in the oxygen donor solvents water, dimethyl sulfoxide, and N,N '-dimethylpropyleneurea. Inorg. Chem. 45(18), 7428-7434.

Persson P., Nilsson N., and Sjöberg S. (1995) Structure and bonding of orthophosphate ions at the iron oxide-aqueous interface. J. Colloid Interf. Sci. 177, 263-275.

Predota M., Cummings P. T., and Wesolowski D. J. (2007) Electric double layer at the rutile (110) surface. 3. Inhomogeneous viscosity and diffusivity measurement by computer simulations. J. Phys. Chem. C 111(7), 3071-3079.

Preocanin T., Supljika F., and Kallay N. (2009) Evaluation of interfacial equilibrium constants from surface potential data: Silver chloride aqueous interface. J. Colloid Interf. Sci. 337(2), 501-507.

Preocanin T., Supljika F., and Kallay N. (2010) Charging of silver bromide aqueous interface: Evaluation of interfacial equilibrium constants from surface potential data. J. Colloid Interf. Sci. 346(1), 222-225.

Rahnemaie R., Hiemstra T., and Van Riemsdijk W. H. (2006) A new structural approach for outersphere complexation, tracing the location of electrolyte ions. J. Colloid Interf. Sci. 293, 312-321.

Rahnemaie R., Hiemstra T., and Van Riemsdijk W. H. (2007) Geometry, Charge Distribution and Surface Speciation of Phosphate on Goethite. Langmuir 23, 3680-3689.

Randall S. R., Sherman D. M., and Ragnarsdottir K. V. (1999) The mechanism of cadmium surface complexation on iron oxyhydroxide minerals. Geochim. Cosmochim. Acta 63, 2971-2987.

Ridley M. K., Hiemstra T., van Riemsdijk W. H., and Machesky M. L. (2009) Inner-sphere complexation of cations at the rutile-water interface: A concise surface structural interpretation with the CD and MUSIC model. Geochim. Cosmoschim. Acta 73(7), 1841-1856.

Rietra R. P. J. J., Hiemstra T., and Van Riemsdijk W. H. (1999a) The Relationship between Molecular Structure and Ion Adsorption on Variable Charge Minerals. Geochim. Cosmochim. Acta 63(19/20), 3009-3015.

Rietra R. P. J. J., Hiemstra T., and Van Riemsdijk W. H. (2000a) Electrolyte Anion Affinity and its Effect on Oxyanion Adsorption on Goethite. J. Colloid Interf. Sci. 229, 199-206.

Rietra R. P. J. J., Hiemstra T., and van Riemsdijk W. H. (2001) Comparison of selenate and sulfate adsorption on goethite. J. Colloid Interf. Sci. 240(2), 384-390.

Rietra R. P. J. J., Hiemstra T., and Van Riemsdijk W. H. (2001a) Interaction of Calcium and Phosphate Adsorption on Goethite. Environ. Sci. Technol. 35, 3369-3374.

Rietra R. P. J. J., Hiemstra T., and Van Riemsdijk W. H. (2001b) Comparison of Selenate and Sulfate Adsorption on Goethite. J. Colloid Interf. Sci. 240, 384-390.

Robertson A. P. and Leckie J. O. (1998) Acid/Base, Copper binding, and Cu^{2+}/H^{+} Exchange Properties of Goethite, an Experimental and Modeling Study. Environ. Sci. Technol. 32, 2519-2530.

Rochester C. H. and Topham S. A. (1979) Infrared Study of Surface Hydroxyl on Goethite. J. Chem. Soc. Faraday. Trans. I 75, 591-602.

Rosenqvist J., Persson P., and Sjoberg S. (2002) Protonation and charging of nanosized gibbsite (alpha-Al(OH)(3)) particles in aqueous suspension. Langmuir 18(12), 4598-4604.

Rossberg A., Ulrich K. U., Weiss S., Tsushima S., Hiemstra T., and Scheinost A. C. (2009) Identification of uranyl surface complexes on ferrihydrite: Advanced EXAFS data analysis and CD-MUSIC modelling. Environ. Sci. Technol. 43(5), 1400-1406.

Rowlands W. N., O'Brien W. R., Hunter R. J., and Patrick V. (1997) Surface Properties of Aluminum Hydroxide at High Salt Concentration. J. Colloid Interf. Sci. 188, 325-335.

Russell J. D., Parfitt R. L., Fraser A. R., and Farmer V. C. (1974) Surface structures of gibbsite, goethite, and phosphated goethite. Nature 248, 220-221.

Rustad J. R. and Boily J. F. Density functional calculation of the infrared spectrum of surface hydroxyl groups on goethite (alpha-FeOOH). Am. Mineral. 95(2-3), 414-417.

Rustad J. R., Felmy A. R., and Hay B. P. (1996b) Molecular Statics Calculations of Proton Binding to Goethite Surfaces: A New Approach to Estimation of Stability Constants for Multisite Surface Complexation Models. Geochim. Cosmochim. Acta 60, 1563-1576.

Rustad J. R., Wasserman E., Felmy A. R., and Wilke C. (1998) Molecular Dynamics Study of Proton Binding to Silica Surfaces. J. Colloid Interf. Sci. 198, 119-129.

Sahai N., Carroll S. A., Roberts S., and O'-Day P. A. (2000) X-ray Absorption Spectroscopy of Strontium(II) Coordination - II. Sorption and Precipitation at Kaolinite, Amorphous Silica, and Goethite Surfaces. J. Colloid Interf. Sci. 222(2), 198-212.

Sahai N. and Sverjensky D. A. (1997) Evaluation of Internally Consistent Parameters for the Triple-layer Model by the Systematic Analysis of Oxide Surface Titration Data. Geochim. Cosmochim. Acta 61, 2801-2826.

Schindler P. W. and Kamber H. R. (1968) Die Acidität von Silanolgruppen. Helv. Chim. Acta 15, 1781-1786.

Schudel M., Behrens S. H., Holthoff H., Kretzschmar R., and Borkovec M. (1997) Absolute Aggregation Rate Constants of Hematite Particles in Aqueous Suspensions: A Comparison of Two Different Surface Morphologies. J. Colloid Interf. Sci. 196, 241-253.

Shchukarev A., Boily J. F., and Felmy A. R. (2007) XPS of fast-frozen hematite colloids in NaCl aqueous solutions: I. Evidence for the formation of multiple layers of hydrated sodium and chloride ions induced by the {001} basal plane. J. Phys. Chem. C 111(49), 18307-18316.

Shen Y. R. and Ostroverkhov V. (2006) Sum-frequency vibrational spectroscopy on water interfaces: Polar orientation of water molecules at interfaces. Chem. Rev. 106(4), 1140-1154.

Shiao S.-Y. and Meyer R. E. (1981) Adsorption of Inorganic Ions on Alumina from Salts Solutions: Correlations of Distribution Coefficients with Uptake of Salt. J. Inorg. Nucl. Chemistry 43(12), 3301-3307.

Sigg L. and Stumm W. (1981) The interaction of anions and weak acids with the hydrous goethite (a-FeOOH) surface. Colloids Surfaces 2, 101-117.

Smit W. and Holten C. L. M. (1980) Zeta potential and radiotracer adsorption measurements on EFG a-Al_2O_3 single crystal in NaBr solution. J. Colloid Interf. Sci. 78, 1-14.

Spadini L., Manceau A., Schindler P. W., and Charlet L. (1994) Structure and Stability of Cd^{2+} Surface Complexes on Ferric Oxides. 1 Results from EXAFS spectroscopy. J. Colloid Interf. Sci. 168, 73-86.

Sposito G. (1984) The Surface Chemistry of Soils. Oxford University Press.

Sprycha R. (1984) Surface Charge and Adsorption of Background Electrolyte Ions at Anatase/Electrolyte Interface. J. Colloid Interf. Sci. 102(1), 173-185.

Sprycha R. (1989b) Electrical Double Layer at Alumina/electrolyte Interface II. Adsorption of Supporting Electrolyte Ions. J. Colloid Interf. Sci. 127, 12-25.

Stachowicz M., Hiemstra T., and Van Riemsdijk W. H. (2006) Surface speciation of As(III) and As(V) adsorption in relation to charge distribution. J. Colloid Interf. Sci. 302, 62-75.

Stern O. (1924) Zur theory der electrolytischen doppelschicht. Zeit fur Electrochemie 30, 508-516.

Stumm W., Huang C. P., and Jenkins S. R. (1970) Specific chemical interaction affecting the stability of dispersed systems. Croat. Chem. Acta 42, 223-245.

Su C. M. and Suarez D. L. (2000) Selenate and selenite sorption on iron oxides: An infrared and electrophoretic study. Soil Sci. Soc. Am. J. 64(1), 101-111.

Sugimoto T. and Shiba F. (1999a) A new approach to interfacial energy. 3. Formulation of the absolute value of the solid-liquid interfacial energy and experimental collation to silver halide systems. J. Phys. Chem. B 103(18), 3607-3615.

Sugimoto T. and Shiba F. (1999b) A new approach to interfacial energy. 4. Effects of adsorption of halide ions and gelatin on solid-liquid interfacial energies of silver halides. J. Phys. Chem. B 103(18), 3616-3625.

Sugimoto T. and Wang Y. (1998) Mechanism of the Shape and Structure Control of Monodispersed a-Fe_2O_3 Particles by Sulfate Ions. J. Colloid Interf. Sci. 207, 137-149.

Sun X. and Doner H. (1996) An Investigation of Arsenate and Arsenite Bonding Structures on Goethite by FTIR. Soil Sci. 161, 865-872.

Sverjensky D. A. (1994) Zero-Point-of-Charge Prediction from Crystal Chemistry and Solvation Theory. Geochim. Cosmochim. Acta 58, 3123-3129.

Sverjensky D. A. and Fukushi K. (2006) Anion adsorption on oxide surfaces: Intrusion of the water dipole in modeling the electrostatics of ligand exchange. Environ. Sci. Technol. 40(1), 263-271.

Tejedor-Tejedor M. I. and Anderson M. A. (1990) Protonation of Phosphate on the Surface of Goethite as Studied by CIR-FTIR and Electrophoretic Mobility. Langmuir 6, 602-611.

Toney M. F., Howard J. N., Richer J., Borges G. L., Gordon J. G., Melroy O. R., Wiesler D. G., Yee D., and Sorensen L. B. (1995) Distribution of water molecules at Ag(111)/electrolyte interface as studied with surface X-ray scattering Surf. Sci. 335 (1-3), 326-332

Van Hal R. E. G., Eijkel J. C. T., and Bergveld P. (1996) A general model to describe the electrostatic potential at the electrolyte oxide interfaces. Adv. Colloid and Interface Science 69, 31-62.

Venema P., Hiemstra T., and Van Riemsdijk W. H. (1996a) Comparison of different site binding models for cation sorption: Description of pH dependency, salt dependency, and cation-proton exchange. J. Colloid Interf. Sci. 181, 45-59.

Venema P., Hiemstra T., and Van Riemsdijk W. H. (1996b) Multisite Adsorption of Cadmium on goethite. J. Colloid Interf. Sci. 183, 515-527.

Venema P., Hiemstra T., and Van Riemsdijk W. H. (1998) Intrinsic Proton Affinity of Reactive Surface Groups of Metal (Hydr)oxides: Application to Iron (Hydr) oxides. J. Colloid Interf. Sci. 198, 282-295.

Villalobos M. and Leckie J. O. (2000) Carbonate Adsorption on Goethite under closed and open CO_2 systems. Geochim. Cosmochim. Acta 64(22), 3787-3802.

Vlcek L., Zhang Z., Machesky M. L., Fenter P., Rosenqvist J., Wesolowski D. J., Anovitz L. M., Predota M., and Cummings P. T. (2007) Electric double layer at metal oxide surfaces: Static properties of the cassiterite - Water interface. Langmuir 23(9), 4925-4937.

Waite T. D., Davis J. A., Payne T. E., Waychunas G. A., and Xu N. (1994) Uranium(VI) adsorption to Ferrihydrite: Application of a surface complexation model. Geochim. Cosmochim. Acta 58, 5465-5478.

Wang B. G., Shi E. W., and Zhong W. Z. (2000) On the morphological changes and twinning of ZnS (sphalerite) crystallites under hydrothermal conditions. Crystal Research and Technology 35(3), 279-289.

Waychunas G., Trainor T., Eng P., Catalano J., Brown G., Davis J., Rogers J., and Bargar J. (2006) Surface complexation studied via combined grazing-incidence EXAFS and surface diffraction: arsenate on hematite (0001) and (10-12) (vol 386, pg 2255, 2006). Anal. Bioanal. Chem. 386(7-8), 2255-2255.

Waychunas G. A., Rea B. A., Fuller C. C., and Davids J. A. (1993) Surface chemistry of ferrihydrite. 1. EXAFS studies of the geometry of coprecipitated and adsorbed arsenate. Geochim. Cosmochim. Acta 57, 2251-2269.

Weerasooriya R. and Tobschall H. J. (2000) Mechanistic modeling of chromate adsorption onto goethite. Colloids Surfaces 162, 167-175.

Weidler P. G., Hug S. J., Wetche T. P., and Hiemstra T. (1999) Determination of Growth Rates of 100 and 110 faces of Synthetic Goethite by Scanning Force Microscopy. Geochim. Cosmochim. Acta 62, 3407-3412.

Weidler P. G., Schwinn T., and Gaub H. E. (1996) Vicinal faces on synthetic goethite observed by atomic force microscopy. Clays Clay Minerals 44, 437-442.

Wendelbow R. (1987) Sulfate ion interaction with clays, University of Oslo, 1987.

Westall J. and Hohl H. (1980) A Comparison of Electrostatic Models for the Oxide/solution Interface. Adv. Colloid Interf. Sci. 12, 265-294.

Westall J. C. (1979) MICROQL, Computation of Adsorption Equilibria in BASIC.

Wijnja H. and Schulthess C. P. (2000) Vibrational Spectroscopy Study of Selenate and Sulfate Adsorption Mechanisms on the Fe and Al (hydr)oxide surfaces. J. Colloid Interf. Sci. 229(1), 286-297.

Yates D. E., Levine S., and Healy T. W. (1974) Site-binding Model of the Electrical Double Layer at the Oxide/Water Interface. J. Chem. Soc. Faraday Trans. I 70, 1807-1818.

Yates D. E. m. (1975) The Structure of the Oxide/Aqueous Electrolyte Interface. Ph.D. thesis, University of Melbourne.

Yeganeh M. S., Dougal S. M., and Pink H. S. (1999) Vibrational spectroscopy of water at liquid / solid interfaces: Crossing the isoelectric point of a solid surface Phys. Rev. Letters 83(6), 1179-1182

Yoon R. H., Salman T., and Donnay G. (1979) Predicting Points of Zero Charge of Oxides and Hydroxides. J. Colloid Interf. Sci. 70, 483-493.

Zarzycki P. and Rosso K. M. (2010) Molecular Dynamics Simulation of the AgCl/Electrolyte Interfacial Capacity. J. Phys. Chem. C 114(21), 10019-10026.

Zhang Z., Fenter P., Cheng L., Sturchio N. C., Bedzyk M. J., Predota M., Bandura A., Kubicki J. D., Lvov S. N., Cummings P. T., Chialvo A. A., Ridley M. K., Benezeth P., Anovitz L., Palmer D. A., Machesky M., and Wesolowski D. J. (2004) Ion adsorption at the rutile-water interface: linking molecular and macroscopic properties. Langmuir 20(12), 4954-4969.

Zhang Z., Fenter P., Sturchio N. C., Bedzyk M. J., Machesky M. L., and Wesolowski D. J. (2007) Structure of rutile TiO_2 (110) in water and 1 molal Rb^+ at pH 12: Inter-relationship among surface charge, interfacial hydration structure, and substrate structural displacements. Surf. Sci. 601(4), 1129-1143.

Chapter 2

Intrinsic Proton Affinity of Reactive Surface Groups of Metal (hydr)oxides

Tjisse Hiemstra, Peter Venema, and Willem H. Van Riemsdijk

Published in Journal of Colloid and Interface Science
Volume 184, Issue 2, Pages 680-692, December 25, 1996

Abstract

The proton affinity of individual surface groups has been calculated with a redefined version of the multi site complexation (MUSIC) model. In the new approach, the proton affinity of an oxygen ion originates from the undersaturation of the oxygen valence. The factors valence and coordination number, which are the basis of Pauling's definition of bond valence, in combination with the number of coordinating (Me and H) ions, are dominant in determining the proton affinity. The neutralization of an oxygen ion by Me ion(s) is calculated on the basis of the *actual* bond valence, which accounts for structural details, resulting from an asymmetrical distribution of charge in the coordination environment. An important role in the new version of the MUSIC model is given to the H bonds. The model shows that the proton affinity is determined not only by the number of donating H bonds but also by the number of accepting H bonds. The proton affinity of surface groups and at of solution complexes can be understood in one theoretical framework, based on a different number of donating and accepting H bonds. The MUSIC model predicts the variation in proton affinity constants for surface groups in particular those with the same number of coordinating Me ions but with a different structural position. The model is able to predict based on the proton affinity of the individual groups the correct PZC of Me hydroxides, oxo-hydroxides, and oxides, and explains previous exceptions. The model can also be applied in general to other minerals

Introduction

Metal (hydr)oxides play an important role in many fields of chemistry. The interfacial chemistry is of practical and theoretical importance. The proton affinity of surface groups is of special interest because acidity and basicity is of direct concern in many chemical processes like catalysis and it determines the pristine charging and with it the binding behavior of important chemical elements. The Point of Zero Charge (PZC) has been considered as a basic characteristic of metal (hydr)oxides and various attempts have been made (Parks 1965&1967, Yoon et al.1978, Sverjensky 1994) to relate this overall chemical feature to the general characteristics of the metal (hydr)oxide, treating the interface as chemically homogeneous. The surfaces of metal (hydr)oxides are however generally heterogeneous, i.e. several types of metal (hydr)oxides groups are present, and the PZC is only the resultant of a combined action of several types of surface groups. It implies that in general from the PZC value no direct information can be found about the proton affinity of individual types of surface groups. In addition, the charging curve as a whole will not give this important information a priori, in particular because it is very strongly influenced by the electrostatic field of the double layer, masking the individual contributions. With the development of the MUlti SIte Complexation model (MUSIC) a first attempt has been made to estimate the proton affinity for individual types of surface groups (Hiemstra et al.1989), resulting in a predicted PZC value once the chemical composition of the interface is known. In the MUSIC model, the proton affinity of the individual groups was calculated based on the Pauling bond valence (Pauling 1929) in which the charge of the central ion is equally distributed over its surrounding ligands. The MUSIC model predicts that one of the main differences in intrinsic proton affinity of surface groups is due to the number of metal ions coordinating to the surface oxygens. Another important prediction of the MUSIC model is that the difference in affinity between the first and second proton that binds to the same type of surface oxygen is very large, about 14 log$K$ units. The MUSIC model was calibrated using the oxo and hydroxo protonation reactions in solution. The MUSIC model has improved the understanding of the difference in charging behavior of metal (hydr)oxides and various authors claim to have been successful in the application of the model (Hiemstra et al.1989b, Nabavi et al.1993, Contescu et al.1994, Giacomelli et al.1995). Recently the MUSIC model has been extended applying the Pauling concept of Charge Distribution (CD) to the formation of surface complexes with cations and anions (Hiemstra and Van Riemsdijk 1996, Venema et al.1996) and is referred to as the CD-MUSIC model.

The MUSIC model for prediction of the proton affinity has been applied to an important metal oxohydroxide, namely α-FeOOH (goethite). Early electron microscopy work on goethite (Cornell et al.1974) suggested the presence of the 100, 010, and 001 crystal faces, which we have used in our previous applications of the MUSIC model (Hiemstra et al.1989b, Hiemstra and Van Riemsdijk 1991). However gradually, it has become clear that the main crystal plane of goethite is the 110 face (Schwertmann and Cornell 1991). This face is dominated by triply coordinated surface $\equiv Fe_3O(H)$ groups (Barrón and Torrent 1996, Hiemstra and Van Riemsdijk 1996), which implies that the proton affinity of these predominant groups will strongly determine the value of the PZC. The PZC of goethite is high

(9 ± 0.5) indicating that one expects a high value for the log$K$ of the protonation reaction of triply coordinated surface oxygens. This contrasts with the low log$K$ value for $\equiv Fe_3O$ groups, predicted by the MUSIC model. For this discrepancy, a first qualitative explanation has been formulated (Hiemstra and Van Riemsdijk 1996) which is based on structural details of the solid.

The crystal structure of goethite is characterized by Fe^{3+} ions in hexa-coordination with O and OH. Each O or OH coordinates with three Fe^{3+} ions. In the bulk of the FeOOH mineral two types of triply coordinated oxygen groups are found, one protonated ($\equiv Fe_3OH$) and one non-protonated ($\equiv Fe_3O$) group. The protonated $\equiv Fe_3OH$ group forms a hydrogen bond with the non-protonated one ($\equiv Fe_3O$). It suggests that a proton-oxygen bond of the $\equiv Fe_3OH^{1/2+}$ group is stronger than a proton-oxygen bond with the non-protonated $\equiv Fe_3O^{1/2-}$ group in the solid. It has been hypothesized that the difference in the proton-oxygen bond strength in the solid will also lead to different proton affinities in the interface (Hiemstra and Van Riemsdijk 1996). This illustrates that there can be different types of triply coordinated oxygens in the interface with different proton affinities. The first version of the MUSIC model does not consider these differences.

The presence of a strong difference in proton affinity of triply coordinated groups is also supported by results of ion adsorption modeling with the previous mentioned CD-MUSIC approach. In the modeling, we could only describe simultaneously a full range of adsorption phenomena, i.e. primary charging, concentration, pH and salt dependency, shift in zeta potentials and iso electric points (IEP), and ion/proton exchange ratios, *in-situ* IR spectroscopy data), within one concept if a large difference in proton affinity for the different types of $\equiv Fe_3O$ groups exists on the 110 face of goethite. For details, we refer to Hiemstra and Van Riemsdijk (1996).

The MUSIC model has also been applied to the charging behavior of silica. The shape of the charging curves is quite different from that of many other oxides. Similar observations have been made with respect to the experimentally measured pH dependent surface potential, where silica behaves quite non-Nernstian in contrast to other metal (hydr)oxides, which may react near-Nernstian (Bousse et al.1983,1987, VanHal 1995). All these observations can be understood within one theoretical framework, the MUSIC model, based on the difference in charge attribution of metal ions to surface groups (Hiemstra et al.1989a&b). Evaluation of the charging behavior of silica however also showed that the MUSIC model was unable to predict the correct value for the proton affinity constant (Hiemstra et al.1989b).

In the present paper, we will describe a refined version of the MUSIC model, which copes with the above discrepancies and predicts the variation in proton affinity constants of surface groups, in particular the variation for surface groups, which have the same number of coordinating Me ions, but different structural positions.

Pauling bond valence

The charge of ions in the solid of Me (hydr)oxides is internally fully compensated. The principle of electroneutrality implies that the charge of a cation is compensated by the charge of the surrounding oxygens and vice versa. For neutralization, the charge is distributed over

the surrounding ligands, which can be expressed per bond, leading to the concept of a bond valence ν as introduced by Pauling (Pauling 1929). The bond valence defined as the charge *z* of a cation divided by its coordination number CN, i.e. the mean charge per bond:

$$\nu \equiv \frac{z}{\mathrm{CN}} \qquad [1]$$

In the MUSIC model, we applied the bond valence concept to hydroxylated surfaces, assuming a symmetrical distribution of charge in metal (hydr)oxides. The bond valence expresses the effective repulsive force between the Me centre and protons present on the surrounding ligands. The interaction depends not only on the valence of the Me ion, but also on the number of surrounding oxygens able to screen the charge of the Me centre. The total amount of effective charge available for Me-H interaction will determine the proton affinity. This implies that the number of Me cations coordinating to the oxygen is important for the proton affinity of a surface group. In addition, the affinity is also strongly determined by the number of protons present at the surface ligand. The affinity of an oxo group is considerably larger than the affinity of the corresponding hydroxo group, because of the presence of a H-H interaction at the latter one.

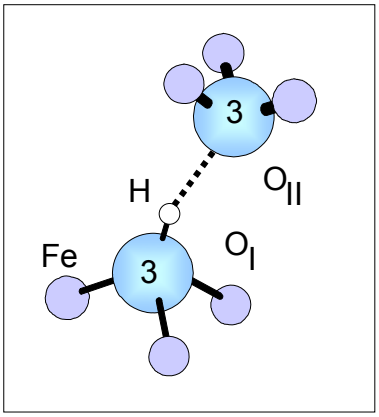

Fig.1 The schematic basic structural unit of goethite, comprising two types of oxygens O_I and O_{II}, both being triply coordinated to Fe. In the oxygens, the coordination number 3 is indicated. Between both types of oxygens an H-bond exists, which distributes its charge asymmetrically. The oxygen ion with the largest H contribution in the neutralization, receives from the coordinating Fe ions a smaller charge contribution for the neutralization. This leads to a larger FeO distance (R = 209-210 pm) in the $\equiv Fe_3OH$ configuration. The opposite holds for the $\equiv Fe_3O$ groups (R = 195-196 pm).

Actual bond valence

For the prediction of the log*K* in the first version of the MUSIC model, it was assumed that the charge is equally distributed over the ligands, according to Pauling's definition (eq.[1]). This is equivalent with assuming equal distances between the central metal (Me) ion and the surrounding oxygens (Brown 1978). However, within one mineral the Me-O distances may be quite different, like for instance in goethite (α-FeOOH). As mentioned, in this mineral the

oxygen charge is neutralized by three Fe^{3+} ions and in addition by a contribution of an asymmetric H bond, leading to a Fe_3OH--OFe_3 configuration (Fig.1).

The asymmetric contribution of H in the neutralization implies that the coordinating Fe ions in the Fe_3O part have to contribute more to the neutralization of the oxygen whereas the Fe ions in the Fe_3OH part contribute less than is expected based on the Pauling bond valences. This difference in neutralization finds its expression in the crystal lattice in different FeO distances for both units. It illustrates that charge distribution and neutralization are related to Me-O lengths, i.e. the actual bond valence is different from the Pauling bond valence based on equal charge distribution. Different distances can also be found in the oxides without hydrogen bonds in the structure, for instance in the isostructural minerals hematite (α-Fe_2O_3) and corundum (α-Al_2O_3). In this structure, close packed oxygen layers are bound together by Me^{3+} ions, filling two out of three octahedral positions in the lattice (Fig.2). Due to electrostatic Me-Me repulsion, the Me ions are displaced in the octahedrons towards the empty octahedral positions, resulting in an asymmetry within the octahedron and in different Me-O distances (Newham and DeHaan 1962, Schwertmann 1989). A bond with a smaller Me-O distance will contribute more to the neutralization of charge than a bond with a large Me-O distance. Smaller distances in an octahedron lead to higher charge attributions, i.e. higher actual bond valences than conform to Pauling's bond valence rule.

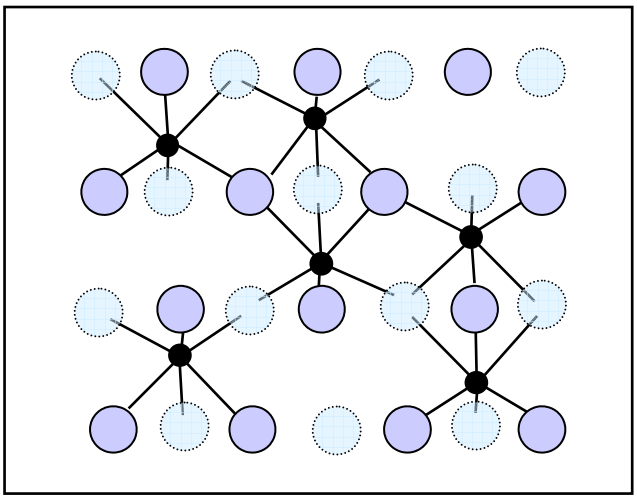

Fig.2 The schematic bulk structure of hematite and corundum, comprising closed packed layers of oxygens (open circles) in which two out of three octahedral positions are filled with Me ions (filled circles). The oxygens are below (dashed line) or above (full line) the plane of the Me ions. Electrostatic repulsion between the Me ions leads to an asymmetric position of the Me ion an octahedron, i.e. a different length and a different actual bond valence.

The actual bond valence (s), based on differences in Me-O distances, can be interpreted as correction on the Pauling bond valence ν and can be correlated with the Me-O distance (R) for instance according to $s = \nu\,(R/R^*)^{-n}$ (Brown and Shannon, 1973) in which n is a coefficient and R* is a distance parameter, giving the Pauling bond valence ν if R = R*. In

practice, one has used slightly different expressions such as $s = (R/R_1)^{-N}$ (Brown and Wu, 1976) where N and R_1 are element specific constants. More recently the expression:

$$s \equiv e^{-(R-R_0)/b} \qquad [2]$$

has been proposed (Brown and Altermatt 1985) in which R_o is an element specific distance and b a constant (b = 37 pm). The value of R_o has been obtained by analysis of the bond valence structure of many crystals, such that the sum of the actual bond valences Σs_j around an oxygen ion, based on the known distances R, is equal to the valence V of the oxygen. This model is astonishingly powerful, and can even be used to predict mineral structures with corresponding distances accurately (Brown 1978, O'Keeffe, 1989). Equation [2] will be used in this paper.

Proton affinity

Pauling (1929) has pointed out that the basic rules determining the structure of ionic minerals result from electrostatic considerations in which valence and distance play a role. On this basis Yoon et al. (1979) combined the Pauling bond valence concept (ν) with Coulomb's law in order to evaluate PZC values of metal (hydr)oxides, improving the earlier Coulombic approach of Parks (1965,1967), who used the valence z of the metal ion as parameter. In both PZC models a distance parameter L was introduced, as an expression of Coulomb's law.

With the introduction of the MUSIC model (Hiemstra et al.1989a), a first attempt was made to predict the proton affinity of individual surface groups, differing in the number n of coordinating Me ions. It was also the first attempt to predict the affinity of the first and second proton that binds to the same reactive group. In this model, we applied the Pauling bond valence concept and related the proton affinity to the parameter $n\ \nu / L$. As illustrated above and pointed out by Bleam (1993), distance dependency is already present in the actual bond valence s and the use of L in these proton affinity models therefore may be excessive.

The use of the actual bond valences s in proton affinity modeling originates from Brown (1978), who calculated on this basis the neutralization of oxygen charge and applied this concept to organic bases. Later the bond valence concept of Brown was applied to the protonation of oxo and hydroxo solution complexes by Bleam (1993). He calculated the neutralization of the charge ($\Sigma\ s_j$) on the basis of the Pauling bond valence ν of the Me ion and the number of bound protons.

In the MUSIC model, the proton affinity was evaluated based on a hypothetical unit charge binding to the surface oxygen. It has the advantage that proton affinity, surface protonation and surface charge can easily be combined in one framework. However, it has been pointed out that the actual proton charge, positioned at the ligand, is less than 1 because of the formation of H bonds (Bleam 1993). The charge distribution in a hydrogen bond expressed in the bond valence of donating (O-H) or an accepting ($O^{\cdots}H$) H bond, can be related to the O-O distance d (Brown and Altermatt 1985), as given in Fig.3.

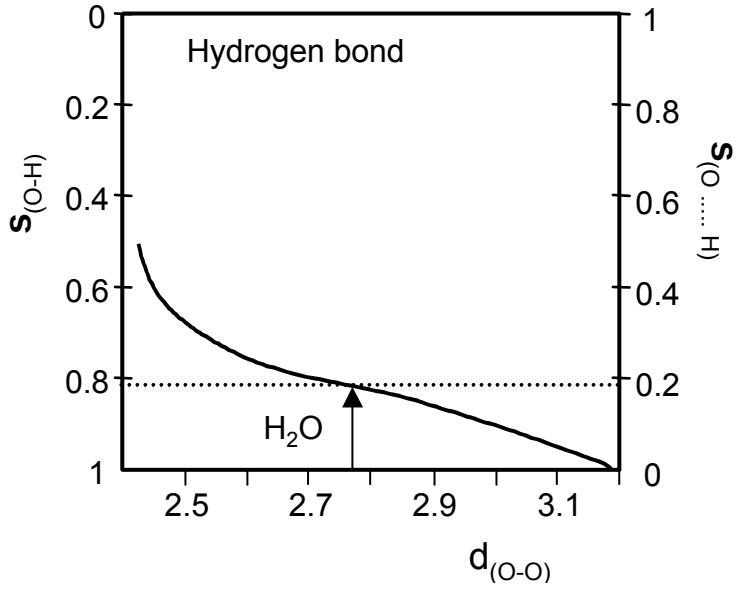

Fig.3 Bond valences *s* of the proton donating H-O bond and the proton accepting bond H...O as a function of the O-O distance d, using the data of Brown and Altermatt (1985). Based on the mean distance of O-O in water (276 pm), the bond valence of the donating and of the accepting H bond will be about 0.81 valence unit and 0.19 valence unit respectively.

The donating H bond valence in water is about 0.8 valence unit (v.u.) and this value was used by Bleam (Bleam 1993). This value is far too large to explain the difference in proton affinity of oxo and hydroxo solution complexes based on the approach of Bleam (Bleam 1993). In can be shown that the correct H-H interaction can only be explained with his application of the bond valence model assuming an unusually low apparent charge of about 0.6 unit valences for a proton ($s_{O\text{-}H}$).

Based on the Pauling bond valence sum rule, it can be shown that in stable ionic structures the undersaturation of the oxygen valence is less than about 0.05 valence units (Brown 1977,1978). An apparently higher value in the mineral lattice is usually due to unaccounted protons and H bonds. It has been presumed (Bleam 1993) that such a high degree of neutralization also prevails for surface oxygens. It should, however, be remembered that in mineral interfaces high electrostatic potentials (Lyklema and Overbeek 1961, Bousse et al.1983, VanHal 1995) and proton adsorptions (Bolt 1957, Parks and DeBruyn 1962, Atkinson et al.1967, Bérubé and DeBruyn 1968, Schindler and Kamper 1968, Stumm et al.1970) are measured, which can only be explained by accumulation of charge and therefore by valences considerably different from near zero for surface groups.

Based on the above considerations, the MUSIC model is redefined.

MUSIC model

Our approach starts with the bond valence sum rule, which states that the valence V of an oxygen ion in a mineral structure is neutralized by the bonds, each contributing to the sum of the actual bond valences, yielding:

$$V = -\Sigma s_j \qquad [3]$$

In the bond valence model of Brown (1978), the proton affinity has been related to what he calls the available valence, which can be defined as the undersaturation of the oxygen valence, i.e. the difference between valence V of the oxygen and the neutralization by coordinating cations: $V + \Sigma s_j$. This concept will be the basis of our new approach and can be applied to ligands of dissolved charged solution complexes and also to charged oxygens present in the interface of metal (hydr)oxides. The major problem in the application of the Brown bond valence model is the contribution of charge by the hydrogen bonds. For solution complexes, Brown (1978) has suggested that an oxygen ligand will accept three hydrogen bonds, while an OH ligand accepts one and donates one hydrogen bond, and an OH_2 ligand will only donate two hydrogen bonds. In his calculation of the available valence, however, he omitted the presence of oxygen-proton bond acceptors (O ····· H). This was followed by Bleam (1993) who only used donating H bonds on ligands. In the present approach, we will develop a concept for donating and accepting H bonds. In this concept, the structural environment of oxygens present in solution complexes may differ from the situation of a surface oxygen ion in the interface.

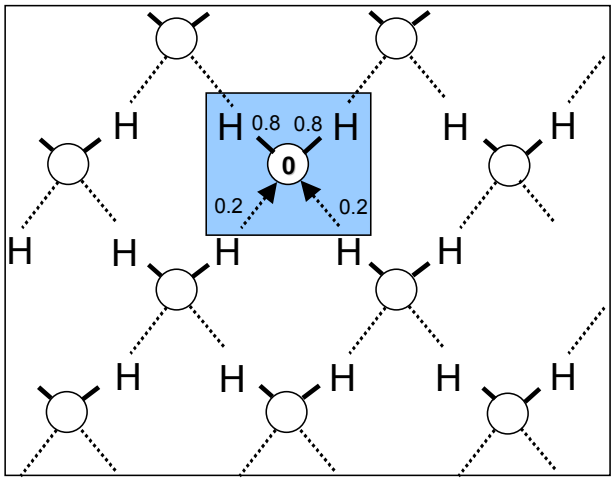

Fig.4 The schematic structural arrangement of water molecules in an aqueous solution with H bonding, transferring part of the proton charge from one to another oxygen ion. In a hydrogen bond between water molecules, about 0.2 v.u. are transferred. The H bond is formed between the H occupied orbital and an empty one. Both H occupied orbitals transfers each 0.2 v.u., but both other unoccupied orbitals of the same water molecule receive each 0.2 v.u. The water molecule as a whole remains uncharged.

The neutralization by protons can be most clearly analyzed focusing on a water molecule in an aqueous solution, as depicted in Fig.4. The oxygen ions have four sp^3 orbitals in a tetrahedral configuration.

Two of the four orbitals of O of the water molecule are occupied by protons. Both others are unoccupied. Hydrogen bond formation occurs between H occupied and unoccupied orbitals. About 0.2 v.u. charge is transferred in such a hydrogen bond (Fig.3). We may apply this model approach to the neutralization of the O in oxo and hydroxo solution complexes.

The actual bond valences in solution complexes are unknown. In the present approach we will use the simplification that on the average the charge of the central ion (Me) is distributed equally over the ligands, i.e. we apply the Pauling bond valence to the Me-O bond as we did before (Hiemstra et al. 1989a). The neutralization of the oxygen charge can be calculated from the contributions s by the Me ion ($s_{Me} = \nu \equiv z$ /CN), the H occupied (m) and the unoccupied (n) orbital(s), according to:

$$V \neq -\Sigma s_j = -\{s_{Me} + m\, s_H + n(1 - s_H)\} \qquad [4]$$

in which s_H is the bond valence of the H donating bond and (1-s_H) the bond valence of the accepting one. In our approach, the charge of the surface oxygens and the charge of oxygen ligands of solution complexes (V) is *a priori* not fully neutralized, i.e. $V \neq \Sigma\, s_{Me}$. In an oxocomplex one orbital is occupied by a Me ion and three empty orbitals are able to form hydrogen bonds i.e. $m = 0$, $n = 3$ and in a hydroxo complex one donating and two accepting hydrogen bonds are present, i.e. $m = 1$, $n = 2$. Note that in both cases for solution complexes the sum m+n equals 3.

The intrinsic proton affinity constant, log$K$, can be related to the undersaturation of the oxygen valence of the reactant, which is defined as - ($\Sigma s_j + V$). In solution chemistry, the intrinsic proton affinity of complexes is formulated with the Brönsted proton donor and acceptor concept in which the proton affinity of the donating reaction is defined relatively to the protonation reaction of water. The protonation reaction of water $H^+ + H_2O \Leftrightarrow H_3O^+$ has by definition an intrinsic log$K$ value of log$K \equiv 0$ ($K \equiv 1$), and the undersaturation valence of the oxygen of the reactant (water) is zero, i.e. ($\Sigma s_j + V$) = 0 (Fig.4). It implies that the relation between log$K$ and the actual oxygen charge, ($\Sigma s_j + V$), is of the kind:

$$\log K = -A\ (\Sigma s_j + V) \qquad [5]$$

in which A is a constant.

We have tested the relation of eq.[5], as given in Fig.5. The value of A equals +19.8. The best fit in our approach was achieved if we choose for a donor H bond the valence s_H of 0.80 v.u., close to the value for water (Fig.3). According to the analysis of Brown and Altermatt (1985), we know that this value is not too strongly influenced over a relatively broad range of O-O distances in minerals (Fig.3), justifying the use of one value throughout. Calculation shows that if the O-O distance varies with 0.01 nm (10 pm) around the mean value in water, the value of the actual oxygen charge ($\Sigma s_j + V$) changes with only about 0.03 v.u., equivalent with about 0.5 log$K$ unit. As shown in Fig.5, some deviation from the line exists, which may be due to the oversimplification of the use of the Pauling bond valence.

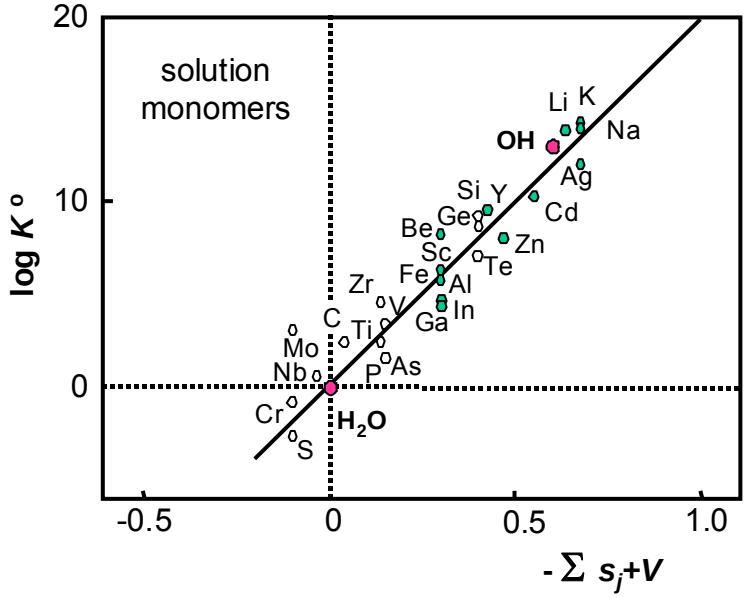

Fig.5 The intrinsic logK_{intr} values for the protonation of hydroxo and oxo complexes versus the undersaturation of charge on the oxygen ligand -Σs_j+V. The solid squares indicate the logK_{intr} values of the proton adsorption reaction of neutral hydroxo complexes, having a central cation with an electron configuration of rare gases. The corresponding open squares indicate the intrinsic logK_{intr} for the protonation of negatively charged oxo complexes with a similar electron configuration. The logK_{intr} of negatively charge oxo complexes has been corrected for the electrostatic work related to the discharging of the negative ion by the proton. The logK_{intr} for the protonation of hydroxo and oxo complexes of cations with 10-d electrons are indicated with solid and open diamonds respectively. The logK_{intr} values were taken from Baes and Mesmer (1976). For C(arbon) the true intrinsic log$K$ for the reaction $H_2CO_3 \Leftrightarrow H^+ + HCO_3^-$ of log$K$ = 3.8 was used (Stumm and Morgan 1981).

An important point is the value of the undersaturation of the oxygen charge. In minerals this value is nearly zero (eq.[3]). In our approach much larger values are allowed in ion complexes, and in this respect we differ from the bond valence concept as applied to charged ions by Brown (Brown 1978), where all ligands and the whole ion species are assumed to be uncharged, leading to large variations in the bond valence of protons and ions.

Interfaces

The above-sketched approach can be applied to reactive groups in interfaces. In our previous approach (Hiemstra et al.1989a) we found that surface groups in general had a higher proton affinity than the corresponding groups in solution (about 4 log$K$ units) with silica as an exception. The difference has been interpreted as due to "a different arrangement of -OH(H) species and solute molecules in a flat surface structure compared with the spatial arrangement for the monomer" (Hiemstra et al.1989a). In the redefined model, it can be quantified based on a difference in the number of H bonds between surface oxygens and water in the interface compared to the situation in solution. In solution monomers we have used three H bonds (m + n = 3). However, it may be assumed for steric reasons that singly coordinated groups at

surfaces often will interact with solute molecules with only two donating or accepting hydrogen bonds, i.e. $m + n = 2$. For triply coordinated surface groups only one orbital is available for proton interaction, i.e. $m + n = 1$. In case of a doubly coordinated surface group, one may find one or two orbitals interacting with water ($m + n = 1$ or 2).

It is of interest to notice that surface groups with one donating and one accepting H bond are in the model approach insensitive for a variation in the hydrogen bond valence, because the individual contributions cancel in the sum of both bonds, i.e. $s_H+(1-s_H) = 1$. In our new approach, we do not account for effects of surface relaxation. At present, we assume that the relaxation, changing distances in the structure, does not lead to an important redistribution of charge. It should be kept in mind that the Me ions coordinating with surface groups, still have to neutralize simultaneously also oxygens deeper in the structure, which implies that the bond valence of these oxygen bonds cannot change, even if distances increase in the coordination environment as a whole. Only redistribution of charge over surface groups via common Me ions is likely, if distances are unequally changed.

The new approach in the MUSIC model will be applied, as we did before (Hiemstra et al.1989b), to various oxides: $Al(OH)_3$, TiO_2, FeOOH, and SiO_2.

Gibbsite

Minerals with well-defined simple surfaces with one type of reactive group may allow us to determine unequivocally the experimental proton affinity constant. The mineral gibbsite can be a good candidate. The hexagonal mineral particles have two types of crystal faces, a dominant planar 001 face and edge faces parallel to the c-axis (Bragg and Claringbull 1965). The planar 001 face has only doubly coordinated surface groups $\equiv Al_2OH$. It has been pointed out that these doubly coordinated $\equiv Al_2OH$ groups are not proton reactive in the normal pH range (pH = 4-10) (Hiemstra et al. 1987, 1989b). This has been recently reconfirmed by comparing well-crystallized gibbsite preparations with a large variation in edge/planar face ratios, where the charging is directly related to the availability of the edge surface area and not to the total surface area (Hiemstra et al.1996). The reaction responsible for the charging is due to protonation of the singly coordinated hydroxyl surface groups:

$$\equiv AlOH^{(s-1)+} + H^+(aq) \Leftrightarrow \equiv AlOH_2^{(s)+} \qquad [6]$$

In view of our new approach the proton affinity in reaction [6] will be determined by the value of the actual bond valence *s*. Based on the detailed structure of $Al(OH)_3$ (Saalfeld and Wedde 1973), we know that the Al-OH distances R may vary quite significantly, which will lead, according to eq.[2], to a large variation in the bond valence *s* and therefore in log*K* (eq.[5]). Fortunately, this will not hinder a simplified evaluation, because one can show that, if for gibbsite all edge faces contribute equally to the charging behavior, the mean value of the actual bond valence *s* is equal to the Pauling bond valence ν which has a value of ν = 0.5, the value used for solution monomers (Fig.5). It implies that the experimental mean log*K* value found for the surface protonation (eq.[6]) is valid for a mean actual bond valence $s = 0.5$. Experiments show that the log*K* of the $\equiv Al\text{-}OH^{1/2-}$ protonation reaction equals 10 ± 0.5

(Hingston et al. 1972, Kavanagh et al.1975, Hiemstra et al.1987, 1996). As pointed out above this value differs from the corresponding log*K* value of the protonation of the monomer in solution ($\Delta \log K \sim 4$) because $m + n = 2$. Application of our redefined MUSIC model predicts for protonation of singly coordinated surface groups a mean log*K* of 9.9 (see Fig.8 later). It should be noticed that in our previous approach, gibbsite was used to calibrate the log*K* of surface reactions while here it is derived based on a different number of hydrogen bridges.

Rutile and anatase (TiO_2)

The basic unit of two TiO_2 polymorphs is a Ti^{4+} filled oxygen octahedron (CN = 6), linked together by two (rutile) or four (anatase) common edges (Pauling 1929), having only relatively small differences in Ti-O distances. The oxygen in the solid is triply coordinated ($\equiv Ti_3O^o$), receiving from each Ti a Pauling bond valence of +2/3. Based on the number of coordinating Ti^{4+} ions to surface oxygens, the mineral surfaces of TiO_2 may have in principle three different surface groups, namely singly, doubly, and triply coordinated surface groups. The surface groups with a lower coordination of Ti^{4+} than the oxygens in the solid may compensate the missing charge by the uptake of one ($\equiv Ti_2O(H)$) or two protons ($\equiv TiOH(H)$).

There are small differences in distances in the TiO_6 octahedron of rutile and anatase. The triply coordinated oxygens in rutile as well as anatase are bound by two short and one slightly longer Ti-O bonds as indicated in Table 1, which leads to different bond valences s_{Me}.

Table 1 Me-O distances (Cromer and Herrington 1955) and related bond valences (s_{Me}) in two polymorphs of TiO_2, rutile and anatase. Both structures are characterized by two (n bond = 2) short distances (a) and one slightly longer TiO distance (b). In order to calculate the bond valence s the R_o parameter of eq.[2] has to be slightly adjusted (R_0 = 180.8 and 179.5 pm for respectively rutile and anatase) in order to fulfill the sum valence rule for local neutralization in the structure $\Sigma s_j = -V = 2$ (eq.[3]).

	Rutile			Anatase		
Group	n_{Bond}	Distance (pm)	s_{Me}	n_{Bond}	Distance (pm)	s_{Me}
≡TiO(a)	2	194.6	0.69	2	193.7	0.68
≡TiO(b)	1	198.4	0.62	1	196.4	0.63

Based on the Ti-O distances two types of singly coordinated $\equiv TiOH^{s-1}$ surface groups can be distinguished in the interface, indicated as ≡TiO(a) and ≡TiO(b) in Table 2 & 3. Also two types of doubly coordinated $\equiv Ti_2O$ can be found, having a combination of a short (a) and a long (b) Ti-O distance (ab) or two short (a) distances (2a). The above-defined MUSIC model can be applied, taking into account the actual bond valence *s*. The singly coordinated surface groups are assumed to have two solution oriented orbitals able to become part of an H bond, i.e. $m + n = 2$. The same is assumed for the doubly coordinated surface groups. The calculated affinity of the different types of surface groups on the faces of rutile and anatase are given in Table 2 and 3 respectively.

Table 2 and 3. The affinity constants for rutile (Table 2) and anatase (Table 3) predicted with the MUSIC model for two types of singly coordinated ≡TiO (a and b) and two types of doubly coordinated $\equiv Ti_2O$ groups (2a and ab), taking into account effects of redistribution of charge in the coordination sphere of Ti (actual bond valence *s*). The log*K* values referring to the expected actual proton transfer reaction in the normal pH range (pH = 2-12) are written italic. The same is done for the actual oxygen charge of the corresponding reactant (Σs_j+V). Note that the site density for rutile differs with a factor two from earlier reported values (Hiemstra et al. 1989b).

Table 2 Rutile

Group	N_s (nm^{-2})	logK_{oxo}	log$K_{hydroxo}$	Charge $\Sigma s_j + V$ (oxo)	Charge $\Sigma s_j + V$ (hydroxo)	Crystal face index
≡TiO(a)	8.0	18.0	*+6.1*	-0.91	*-0.31*	101
≡TiO(a)	5.2 and 7.4	19.4	*+7.5*	-0.98	*-0.38*	110 and 100
$\equiv Ti_2O$(ab)	8.0	*+5.8*	-6.1	*-0.29*	+0.31	101
$\equiv Ti_2O$(2a)	5.2 and 7.4	*+4.4*	-7.5	*-0.22*	+0.38	110 and 100
$\equiv Ti_3O$(a)	-	*-4.0*	-	*+0.20*	-	110

Table 3 Anatase

Group	N_s (nm^{-2})	logK_{oxo}	log$K_{hydroxo}$	Charge $\Sigma s_j + V$ (oxo)	Charge $\Sigma s_j + V$ (hydroxo)	Crystal face index
≡TiO(a)	5.6 and 5.2	18.2	*+6.3*	-0.92	*-0.32*	010 and 011
≡TiO(a)	7.0	19.1	*+7.2*	-0.97	*-0.37*	001
$\equiv Ti_2O$(ab)	5.6 and 5.2	*+5.6*	-6.3	*-0.28*	+0.32	010 and 011
$\equiv Ti_2O$(2a)	7.0	*+4.7*	-7.2	*-0.23*	+0.37	001
$\equiv Ti_3O$(a)	-	*-4.0*	-	+0.20	-	All

With the predicted values, it must be possible to estimate the PZC of rutile and anatase. The 110 and 100 faces of rutile are considered as dominant ones (Jones and Hockey 1971). On these surfaces, the singly and doubly coordinated surface groups are present in a 1:1 ratio. The expected PZC value can be calculated on the basis of the log*K* values for the groups present, taking the mean of the log*K* of both groups (log*K* = 7.5 and 4.4), which leads to PZC = 5.9 (Fig.8). The 1:1 ratio is also found at the 101 face (Table 2). This face has the same PZC value. The PZC value is in accordance with reported PZC values for rutile of 5.8 ± 0.2 (Bérubé and DeBruyn 1968, Yates 1975, Fokkink et al.1989, Spanos et al.1995, Giacomelli et al.1995). Although the Ti-O distances in anatase are slightly different from those of rutile, the calculated PZC for the faces mentioned (Table 3) is the same and in accordance with reported values (Bérubé and DeBruyn 1968, Sprycha 1984, Spanos et al.1995). It is possible to explain a slightly higher or lower PZC value assuming a larger proportion of respectively singly or doubly coordinated surface groups in the Ti oxide interface. Very recently the bond valence concept have been applied in combination with our original MUSIC approach, leading to partly similar results (Contescu et al.1996)

Goethite (α-FeOOH)

The basic groups in the mineral structure of goethite have been discussed above. Monodomainic goethite crystals have predominantly 110 faces with 4 different types of surface groups. For the formation of a singly coordinated surface group two common Fe ions are removed, which may lead to a repulsive interaction of the former Fe oriented oxygen

orbitals. This can be minimized in general if a singly coordinated oxygen ion rotates around the Me-O bond. In goethite, this is probably only possible in the absence of an H bond between the surface oxygen and a ≡Fe_3OH group present more backwards in the structure. It implies that the H bond of the ≡Fe_3OH is reoriented to a water molecule in the interface (Fig.6).

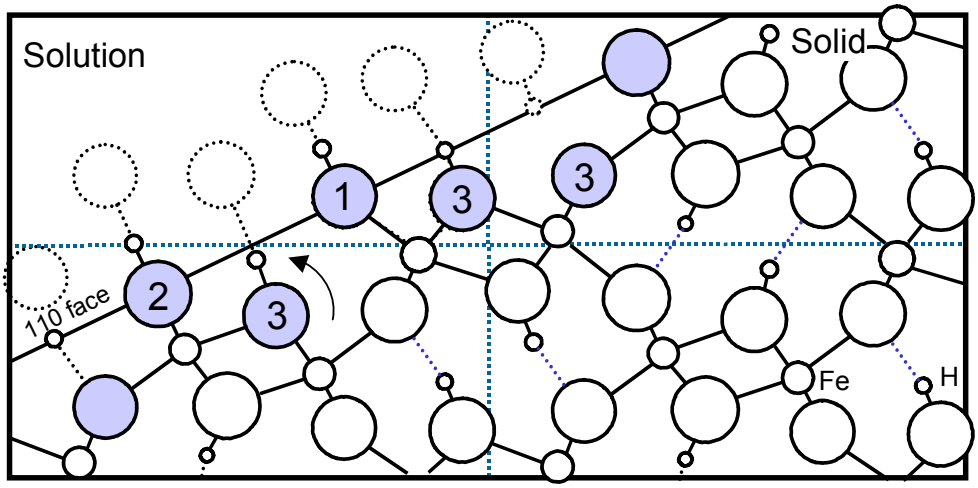

Fig.6 A schematic representation of the cross-section of goethite perpendicular to the c-axis showing the surface structure of the 110 face. In the solid, the oxygens (large circles) are triply coordinated with Fe^{3+} (only two Fe-O bonds are shown). The bold circles indicate a raised position in the lattice. Half of the oxygens have a proton attached (OH). At the interface, a lower coordination number (CN) is found. The CN is indicated by the numbers 1, 2, or 3, which identify the singly, doubly, or triply coordinated oxygens, respectively. The singly coordinated surface groups are assumed to have rotated to avoid overlapping orbitals, breaking the hydrogen bond with the backwards laying triply coordinated ≡Fe_3OH, which orients its H bond to a water molecule in the interface. The arrow indicates the reorientation of the H bond of ≡Fe_3OH towards H_2O in solution (dashed circles).

Based on the situation sketched, the log*K* values can be calculated. In Table 4, we present the predicted protonation constants. As indicated in Table 4, the log*K* for the protonation of doubly coordinated oxo groups is high, leading to ≡Fe_2OH groups, which will not react with an additional proton in the normal pH range, i.e. the groups can be considered as inert. The protonation constant of the ≡Fe_3O_{II} groups is predicted to be very low. It implies that this group will remain unprotonated as suggested previously (Hiemstra & Van Riemsdijk 1996). As will be discussed later, calculation shows that the PZC of the 110 face with the given groups equals about 9.5 (Fig.8). This value is in the range of PZC values reported for most well crystallized goethites, being PZC = 9-9.6 (Evans et al.1979, Bloesch et al.1987, Jung et al. 1987, Zeltner and Anderson 1988, Hiemstra et al.1989b, Tejedor-Tejedor and Anderson 1990, Johnson 1990, Hiemstra and Van Riemsdijk 1991,1996, Venema et al.1996). A lower PZC value could be achieved if the 021 faces at the end of the goethite needles have a lower PZC. This is discussed in Venema et al. (1998).

Table 4. The predicted intrinsic proton affinity constants ($\log K_{intr}$) for the 4 types of surface groups present at the 110 face using the goethite structure with lattice parameters of Hazeman et al.(1991). The $\log K$ values of the protonation reactions determining pH dependent charge are written in italic.

Group	N_s (nm^{-2})	$\log K$ (oxo)	$\log K$ (hydroxo)	Σs_{Me}	$m + n$
$\equiv Fe_1O_{II}$	3.0	+19.6	*+7.7*	0.61	2
$\equiv Fe_2O_{II}$	3.9	+12.3	+0.4	0.59+0.59	1*
$\equiv Fe_3O_I$	6.0	*+11.7*	-	0.40+0.40+0.40	1
$\equiv Fe_2O_{II}$	3.0	+0.2	-	0.60+0.60+0.60	1

Silica SiO_2

The charging curves of silica are quite different from what is usually found for Me (hydr)oxides. One aspect concerns the slopes of the charging curves in the PZC, which are extremely low. It can be understood based on the MUSIC approach as due to the specific bond valence in silica (Hiemstra et al. 1989a). In the PZC all reactive surface groups are protonated ($\theta = 1$) and uncharged ($\equiv SiOH^o$) while for many Me (hydr)oxides like gibbsite, goethite and Ti oxides in the PZC only part of the individual reactive groups have reacted with a proton ($\theta \neq 1$) and the surface groups remain charged. For details, we refer to Hiemstra et al. (1989a).

It has been suggested (Peri and Hensley, 1968) that the 100 face of cristobalite is a good starting model for understanding the surface structure of silica. At this face, singly coordinated surface groups are present in isolated pairs (Fig.7a). The $\equiv SiOH^o$ groups protrude from the surface. Also in other surface configurations, like the 0001 face of tridymite (Fig.7b), $\equiv SiOH^o$ groups protrude from the surface (Yates 1975). This typical type of surface structure is responsible for the relatively high charging of silicas, which is expressed in the high electrostatic capacitance C where C = 3-4 F/m^2 (Hiemstra et al.1989b, Hiemstra & Van Riemsdijk 1991), resulting from a relatively small separation of surface and counter charge (Fig.7c). The surface layer is penetrable for water molecules and this suggests that the possibilities for the formation of H bonds between the singly coordinated surface groups and water is larger than what is usually found on close-packed surface structures, i.e. the number of $m + n = 3$ instead of 2. Using this approach the calculated $\log K_{1,1}$ value for the singly coordinated surface groups is 7.9, being quite close to the value of 7.5 used in describing the charge of fully hydrated non porous silica (Hiemstra et al.1989b). We have assumed in this calculation an actual bond valence s_{Si} of 1. The predicted $\log K_{1,2}$ value for the protonation of $\equiv SiOH^o$ is -4.0 Combination of both $\log K$ values gives the prediction of the PZC (Fig.8), being about PZC = 1.9 very close to values reported for silica and quartz PZC = 2 ± 0.3 (Iler 1979, Sposito 1984).

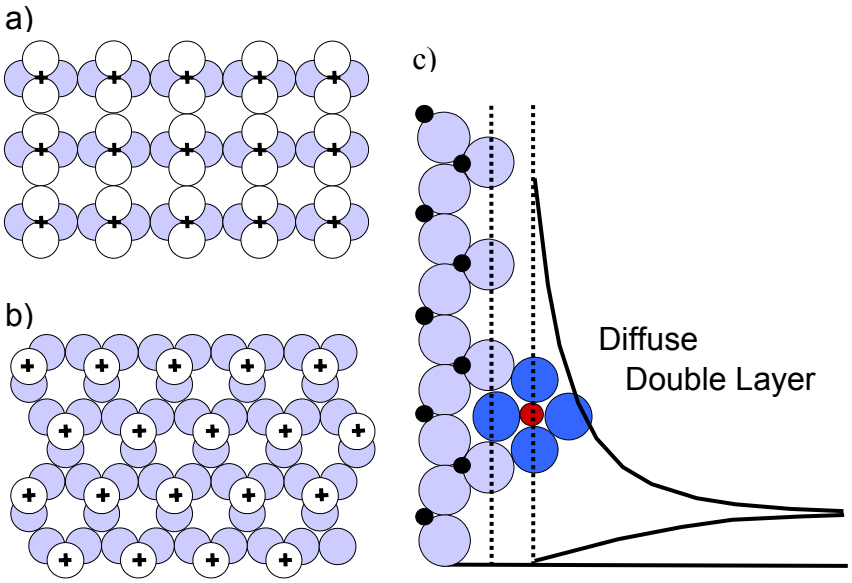

Fig.7a The schematic representation of the 100 face of cristobalite being a good starting model for understanding the surface structure of amorphous silica. The surface groups are present in isolated pairs, protruding the surface, creating a penetrable surface. The oxygens indicated with open circles protrude from the surface. A similar situation is found at the 0001 face of trydimite (Fig.7b). The Si ions, indicated as a cross, are present sandwiched between the oxygen layers. In Fig.7c, a schematic cross section of the interface is depicted, comprising groups protruded from the surface, and a double layer.

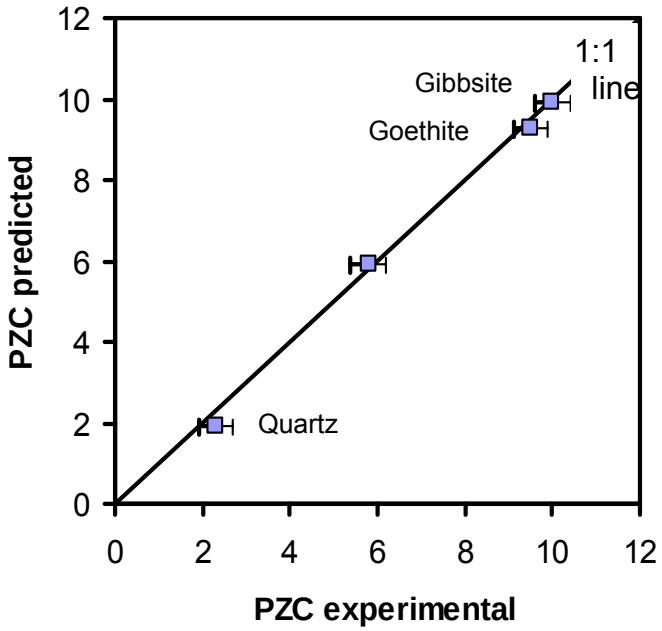

Fig.8 Experimental PZC values for various (metal) hydroxides in relation with the calculated PZC values. The values are based on predicted individual proton affinity constants of the various types of surface groups in the interface.

Modeling surface charge

The new MUSIC approach in terms of surface charge modeling needs some discussion. In the previous MUSIC model, the proton was in all aspects treated as a unit charge, which has the advantage that per definition all proton charge present, is attributed to the surface. However in case of the presence of hydrogen bonds, it is possible that some charge is leaking to adjacent adsorbed water, i.e. transfer of charge may occur. In principle, it is possible to take these details into account, but considerable detailed information at the atomic scale about the positioning and charge distribution of the ions in the interface is needed in relation to the hypothetical electrostatic planes. In the present study, we will simplify the approach assuming one electrostatic plane for the various types of surface groups to which all proton charge is attributed. It implies the use of a Basic Stern (BS) approach for charging curves, as we did before (Hiemstra et al.1989b), where the proton charge is attributed to 0-plane and where the counter- and co-ions are present in the 1 plane (ion pairs) or in the diffuse double layer. This approach has the advantage that the definition of surface charge (0-plane) remains equivalent with H adsorption, measured with acid/base titration, in contrast to the case of transfer of proton charge from one electrostatic plane to another.

In the modeling, the surface charge results from the presence of oxygens and protons and in addition coordinating Me ions contribute charge. A logical suggestion in view of the new approach is the use of the actual bond valence s as written in for instance eq.[6]. However, for the proper bookkeeping of charges at a surface (illustrated in Table 5 for the goethite interface) all reactions can also be written in terms of the Pauling bond valence, yielding the same results in terms of bookkeeping of charge. This can be understood realizing that the actual bond valence can be interpreted as the result of only a relative redistribution of charge within the structure, not affecting the overall charge.

Table 5. The bookkeeping of charge for the surface groups at the 110 interface of goethite on the basis of the actual bond valence s and the Pauling bond valence ν, attributing in both cases all proton charge to the surface group. Note that in case of the use of the actual bond valences the charge of surface species is often lower than what is found in the Pauling bond valence approach.

Group	Charge $\Sigma s_i + V$	Charge $n\,\nu + z_{O(H)}$
$\equiv Fe_1O_{II}H$	-0.39	-0.5
$\equiv Fe_2O_{II}H$	+0.18	0
$\equiv Fe_3O_IH$	+0.21	+0.5
$\equiv Fe_3O_IH$	+0.21	+0.5
$\equiv Fe_3O_{II}$	-0.21	-0.5
Sum	0	0

The advantage of the use of the Pauling bond valence for the calculation of the surface charge is that the formulation of the species and reactions are independent from the actual bond valence, which may include some uncertainty due to uncertainties in distances in crystal structures. Furthermore, the notation of the species is simpler and with the use of the Pauling bond valence for bookkeeping of charge, we keep the connection with our previous work in

terms of the MUSIC model and CD-MUSIC model. Another advantage is that for a proper bookkeeping some inert species types can be omitted. For instance, based on the log*K* values predicted for a doubly coordinated $\equiv Fe_2OH$ surface group, it will be shown later that in the pH range pH 2-12 this group will be not protonated nor deprotonated. Based on this phenomenon, the group can be considered as inert. In case of the use of Pauling bond valences ν for surface groups, the charge of the group $\equiv Fe_2OH$ is zero (Table 5), i.e. it is written as $\equiv Fe_2OH^{o}$ and it therefore does not have to be used in the calculation scheme. However, if the actual bond valence *s* of this group is used, the group is not uncharged, i.e. it is written as $\equiv Fe_2OH^{0.18}$ and it is necessary to account for that in a proper calculation of the surface charge.

In conclusion, we will use the actual bond valence and the H bonds to predict the log*K* values of the individual surface groups, and we will use at present the Pauling bond valence for a proper bookkeeping of charges in the interface, attributing all proton charge to the electrostatic surface plane.

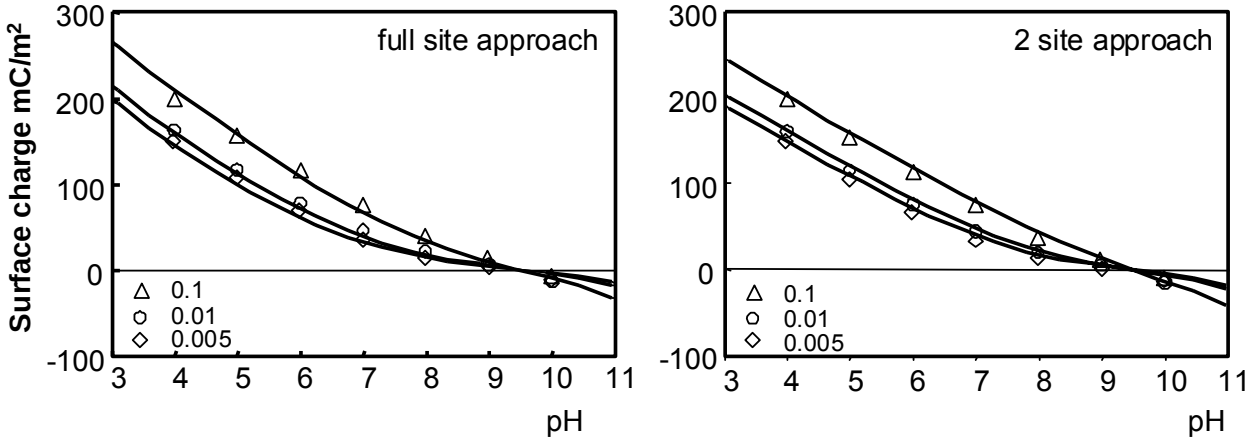

Fig.9a The calculated surface charge at the 110 face of goethite versus pH at three different electrolyte concentrations taking into account all surface groups with the appropriate predicted proton affinity constants of Table 4 and using cation and anion pair formation constants ($\log K_c = \log K_a = -1$) and $C = 1.35$ F/m^2. In Fig.9b the calculated surface charge is given for the simplified case (Hiemstra and Van Riemsdijk 1996) of the presence of two proton reactive surface groups with an equal proton affinity $\log K_{FeOH} = \log K_{Fe3O} = 9.5$ and $\log K_c = \log K_a = -1$ with $C = 0.9$ F/m^2. The data points indicate the experimental charge of goethite (Data Hiemstra and Van Riemsdijk 1996).

In a recent previous approach of the charging of the interface of goethite (Hiemstra and Van Riemsdijk 1996), the interfacial behavior in terms of proton adsorption and charging has been simplified to the use of two proton reactive groups ($\equiv FeOH^{-0.5}$ and $\equiv Fe_3O^{-0.5}$). It is of interest to analyze the charging behavior of goethite in view of the new approach and compare the calculated surface speciation with the simplified approach with 2 surface groups (Hiemstra and Van Riemsdijk 1996). In Fig.9, the calculated charge of the 110 face is given together with the experimental surface charge of goethite (data Hiemstra and Van Riemsdijk (1996)). The curves of Fig.9a have been calculated using a BS approach with a Stern layer capacitance of 1.35 F/m^2. The ion pair formation constants are set equal to the value

previously used ($\log K_c = \log K_a = -1$) (Hiemstra and Van Riemsdijk 1996). Description of the data with a simplified approach with 2 surface groups (Fig.9b) yields a lower value for the capacitance of the Stern layer ($C = 0.9$ F/m^2).

The speciation of the surface groups corresponding to the full site approach (Fig.9a) is given in Fig.10. As shown in the figure, the variation in surface charge is mainly due to variation in the speciation of two groups. This is in accord with the hypothesis of Hiemstra and Van Riemsdijk (1996) in which the proton reactive groups are singly coordinated surface groups and triply coordinated surface groups of type I. In case of the full-site approach, the contribution of both species to the change in surface charge is strongly pH dependent. At low pH (pH<PZC) it is determined by the changes in speciation of the singly coordinated surface group, while at high pH the charge is due to deprotonation of the $\equiv Fe_3O_IH$ group (Fig.10). It is of interest to note that in the standard pH range (pH = 4-10), the triply coordinated surface groups mainly act as a permanent negative charge ($\equiv Fe_3O_{II}$), or permanent positive charge ($\equiv Fe_3O_IH$).

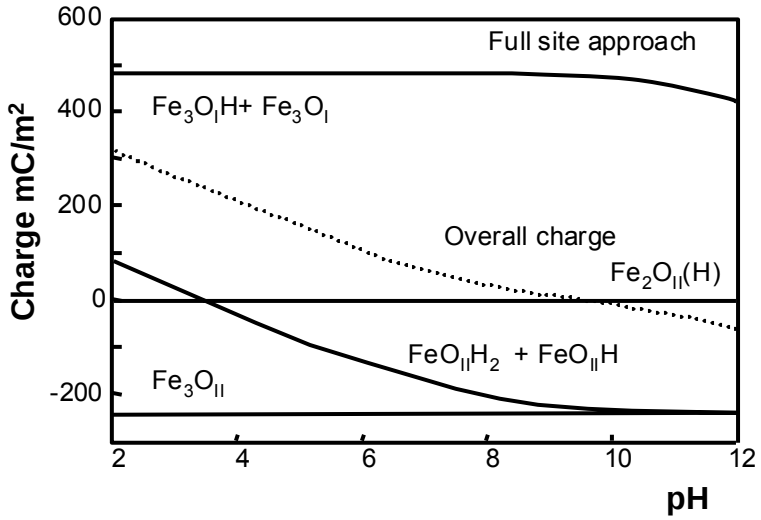

Fig.10 The calculated contribution of the various surfaces groups to the charge development as a function of pH in 0.1 M $NaNO_3$ for a full site approach. The site density of each site is $N_s = 3$ nm^{-2}. In all cases symmetrical ion pair formation is assumed ($\log K_c = \log K_a = -1$). The capacitance is 1.35 F/m^2. The overall charge is indicating by the dotted line.

The above given speciation can be compared with the speciation in the case of the simplified 2 site approach (Fig.11a). As shown, the speciation is now fully different. Both sites in the simplified approach contribute equally in the change of surface charge. This is mainly caused by the choice of one $\log K_H$ value for both groups, which was the result of the lack of information about the precise $\log K$ for both reactions. Based on the predicted difference in $\log K$, it is possible to simulate in a two-site approach the effect of a pH dependent contribution as found in the full site approach. This is indicated in Fig.11b, using the predicted values of $\log K_{FeOH} = 7.7$ and $\log K_{Fe3O} = 11.7$. In this case, the speciation of the proton reactive groups is nearly identical with the full site approach.

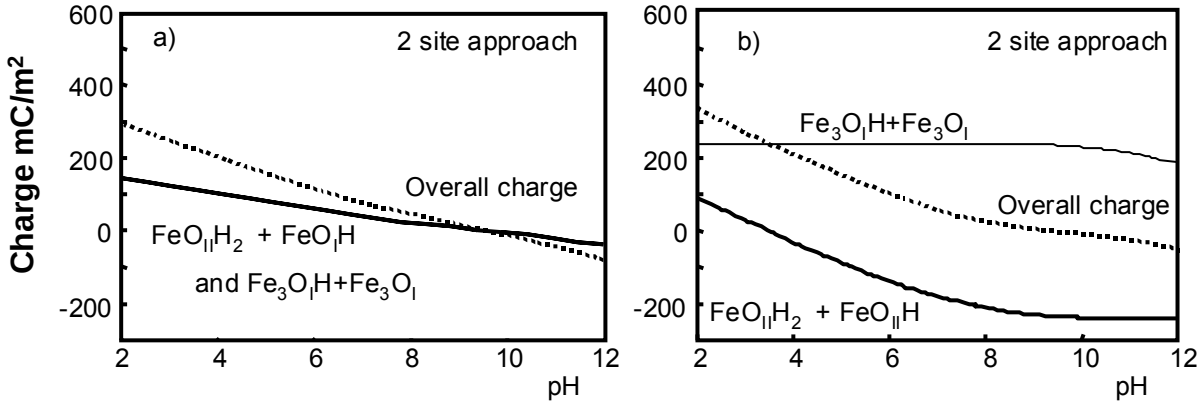

Fig.11. The calculated contribution of the various surfaces groups to the charge development as a function of pH in 0.1 M $NaNO_3$ for a simplified 2 site approach with one proton affinity constant $\log K_{FeOH} = \log K_{Fe3O} = 9.5$, as used by Hiemstra and Van Riemsdijk (1996), and a 2 sites approach using the predicted constants for $\log K_{FeOH} = 7.7$ and $\log K_{Fe3O} = 11.7$. The site density of each site is $N_s = 3$ nm$^{-2.}$ In all cases symmetrical ion pair formation is assumed ($\log K_c = \log K_a = -1$). The capacitances are respectively 0.9 F/m^2 and 1.5 F/m^2. The overall charge is indicating by the dotted lines in both figures.

It should be noticed that the difference in $\log K$ ($\Delta \log K = 0$ or 4) for the reactive groups (Fig.11a,b) is the main reason for apparent difference in the electrostatic capacitance C, needed to describe the same experimental data. A difference in $\Delta \log K$ between two single protonation reactions might also be part of the explanation for the quite different charging behavior observed for different Ti oxide preparations. Hiemstra and Van Riemsdijk (1991) reported that the experimental capacitance (slope charging curve) of the rutile preparation of Yates (1975) is considerably lower than those of the preparations of Bérubé and DeBruyn (1968) and Fokkink et al. (1989). Similar observations can be made for the anatase preparations of Bérubé and DeBruyn (1968) and Sprycha (1984) and that of Foissy et al.(1982). Recently, Spanos et al.(1995) have interpreted the difference in charging behavior of a rutile and an anatase in terms of a difference in the $\Delta \log K$ for the classical 2 step protonation reaction assuming one type of surface group. In view of the above approach, part of the difference in behavior may be due to the presence of different crystal faces in the preparations. The 101 face of rutile and the 010+011 face of anatase are typical examples of a surface with a very small difference in $\log K$ between two surface groups, while the 100+110 face of rutile and the 001 face of anatase have a large difference ($\Delta \log K \approx 3$) in proton affinity of the singly and doubly coordinated surface group (Table 2 & 3). This leads to a quite different surface speciation, similar as illustrated in Fig.10 and Fig.11b, and a different surface charge in case of the same electrostatic capacitance for the compact part of the double layer.

Table 6. The actual charge of the important (Fig.10) surface oxygen species at the 110 face of goethite, calculated using actual bond valence contributions s_{Me}, s_H, and (1-s_H) (eq.[4]), assuming charge transfer by hydrogen bonds. The sum of the charge of the surface oxygen and the charge transferred is attributed to the electrostatic surface plane given in the third column (see also Table 5). The actual charge of most surface oxygens is quite close to zero except the values of the proton reactive singly coordinated group, changing from ≡FeOH to ≡$FeOH_2$ with a corresponding change of surface charge.

Group	Actual oxygen Charge	Charge Transferred	Charge Sum
≡ $Fe_1O_{II}H$	-0.39	+0.00	-0.39
≡ $Fe_1O_{II}H_2$	+0.21	+0.40	+0.61
≡ $Fe_2O_{II}H$	-0.02	+0.20	+0.18
≡ Fe_3O_IH	+0.01	+0.20	+0.21
≡ Fe_3O_I	-0.59	-0.20	-0.79
≡ Fe_3O_{II}	-0.01	-0.20	-0.21

Finally, we want discuss the actual charge of surface oxygens present in the interface. Therefore, let's return to the speciation of the 110 face of goethite (Fig.10). In Table 6, the dominant surface species present in the pH range pH = 4-10 are given. For the surface oxygen of the given species, we have calculated the actual charge, the amount of charge transferred by H bonds and the overall charge (sum) attributed to the electrostatic surface plane (0-plane). The latter ones are equal to the values given in Table 5. Looking to the actual charge of the dominant species, one finds that most of the species are nearly uncharged. The increase of the surface charge below the PZC value (Fig.10) is mainly due to protonation of the surface group with the largest undersaturation of the oxygen, the singly coordinated surface group. In the reaction ≡$FeO_{II}H$ + H^+ ⇔ ≡$FeO_{II}H_2$ the charge of the reactant changes with 0.6 v.u., as a result of the change of an accepting H bond (1-s_H) into a proton donating H bond (s_H). The charge resulting from charge transfer in the H bond changes from 0.0 to +0.4 v.u. The sum of both changes is equal to the unit proton charge. At high pH the development of negative surface charge is mainly due to deprotonation of the nearly uncharged ≡Fe_3O_IH (+0.01 v.u), leading to ≡Fe_3O_I with an actual charge of -0.59 v.u. on the surface oxygen. The charge resulting from charge transfer by the H bond changes from +0.20 v.u. into -0.20 v.u.

Low actual oxygen charges of surface species are also found for Ti oxides (Table 2 and 3). For silica also such an observation can be made, where the overall charge of the SiO species is only -0.4 v.u. using the actual bond valence s (s_{Me} = 1) and three accepting hydrogen bonds (1-s_H = 0.2), whereas the use of the Pauling bond valence ν leads to a charge of -1 v.u. It illustrates that the present MUSIC model not fully but partly realizes Bleam's suggestion of a low undersaturation of charge of surface oxygens (Bleam 1993).

Conclusions

Based on the above presented refined MUSIC model several conclusions can be drawn:

- The proton affinity of oxygens originates from the degree of undersaturation of the valence.
- The saturation of oxygen valence is determined by the number of coordinating Me ions and the number of proton donating and also accepting H bonds.
- The charge attribution of the Me ions can be found from the Pauling bond valence ($\nu = z_{Me}/CN$) in case of a symmetrical distribution of charge in the coordination environment or from the actual bond valence s (Brown 1978), being related to the actual difference in the MeO distances in the coordination environment (asymmetric distribution).
- The charge attribution of protons results from H bridge formation. The charge attribution depends on the number of donating (m) and accepting H bonds (n). In monomeric oxo and hydroxo solution complexes the total number of donating and accepting H bonds equals 3 ($m + n = 3$).
- The number of donating (m) and accepting H bonds (n) in surface groups depends on the number of coordinating Me ions and the surface structure. The sum of donating and accepting H bonds $m + n$ is generally 2 (or 3) for singly (Me) coordinated surface oxygens, 1 or 2 for doubly coordinated oxygens and 1 for triply coordinated ones.
- The charge distribution in a hydrogen bond of solution complexes and of hydrated interfaces is relatively close to the value of 0.8 and 0.2 v.u. for respectively a donating and an accepting H bond.
- The actual charge of the surface groups in the pH range pH = 2-12 is often less than 0.5 v.u.
- The different behavior of silica in terms of proton affinity is due to the open surface structure with protruded reactive $\equiv SiOH^o$ groups, which may lead to a larger number of H bonds ($m + n = 3$ in stead of 2 as found for a close packed surface).
- The presence of a proton-accepting bond decreases the proton affinity with about 4 log$K$ units.
- The MUSIC model predicts based on the individual proton affinity constants the correct PZC of Me hydroxides, oxohydroxides, and oxides, like gibbsite, goethite, rutile, anatase, silica, and quartz.
- Bookkeeping of surface charge based on Pauling bond valences ν for Me ions is equivalent with a bookkeeping using actual bond valences of Me ions (s_{Me}).

References

1 Parks, G.A., Chem. Rev. 65, 177 (1965).
2 Parks, G.A., Adv.Chem.Ser. 67, 121 (1967).
3 Yoon, R.H., Salman,T. and Donnay,G., J.Colloid Interface Sci. 70, 483 (1979).
4 Sverjensky, D.A.,Geochim Cosmochin Acta 58, 3123 (1994)
5 Hiemstra, T., Van Riemsdijk, W.H., and Bolt, G.H., J. Colloid Interface Sci. 133, 91 (1989).
6 Pauling, L., J.Am.Chem.Soc. 51, 1010 (1929).
7 Hiemstra, T., De Wit, J.C.M., and Van Riemsdijk, W.H., J. Colloid Interface Sci. 133, 105 (1989).
8 Nabavi, M., Spalla, O. and B. Cabane, J. Colloid Interface Sci. 160, 459 (1993).
9 Contescu, C., Contescu, C., and J.A. Schwarz, J. Phys. Chem. 98, 4327 (1994).
10 Giacomelli, C.E., Avena, M.J., and De Pauli, C.P., Langmuir 11, 3483 (1995).
11 Hiemstra, T., and Van Riemsdijk, W.H., J. Colloid Interface Sci. 179, 488 (1996).
12 Venema P., Hiemstra T., and Van Riemsdijk W. H. (1996b) J. Colloid Interf. Sci. 183, 515-527.
13 Cornell, R.M., Posner, A.M., and Quirk, P.J., J. Inorg. Nucl.Chem. 36, 1937 (1974).
14 Hiemstra, T., and W.H. Van Riemsdijk, Colloid Surf. 59, 7 (1991).
15 Schwertmann, U., and Cornell, R.M., "Iron Oxides in the Laboratory. Preparation and Characterization", Chap.5, VCH verlag, Weinheim, Germany, 1991.
16 Barrón, V., J. Torrent, J.Colloid Interf. Sci. 177, 407 (1996).
17 Bousse, L., De Rooij, N.F., and P. Bergveld, Surf. Sci. 135, 479 (1983).
18 Bousse, L., Mostarshed, S., Van Der Schoot,B., De Rooij, N.F., Gimmel, P., and W. Gopel, J.Colloid Interface Sci. 147, 1991.
19 Van Hal, R.E.G., Thesis, University Twente, Enschede, The Netherlands (1995)
20 Brown, I.D., Chem. Soc. Rev. 7, 359 (1978).
21 Newham, R.E., and De Haan, Y.M., Z. Kristall. B117, 235 (1962).
22 Schwertmann, U., in "Minerals in Soil Environment", Dixon and Weed (eds), chap.5, SSSA Madison (1989)
23 Brown, I.D., and Shannon, R.D., Acta Cryst. A32, 266 (1973).
24 Brown, I.D., and Wu, K.K., Acta Cryst. B32, 1957 (1976).
25 Brown, I.D., and Altermatt, K.K., Acta Cryst. B41, 244 (1976).
26 Brown, I.D., in Structure and bonding in Crystals, M.O'Keeffe and A. Navrotsky (eds), Vol.2, New York, Academic Press 1981.
27 O'Keeffe, M., Struct. Bonding 71, 162 (1989)
28 Bleam, W.F., J.Colloid Interf. Sci. 159, 312 (1993).
29 Cromer, D.T., and K. Herrington, J.Am.Chem.Soc. 77, 4708 (1955).
30 J. Lyklema, and J.Th.G. Overbeek, J.Colloid Interface Sci. 16, 595 (1961)
31 Bolt, G.H., J.Phys.Chem. 61, 1166 (1957).
32 Parks, G.A., and P.L. DeBruyn, J.Phys. Chem. 66, 967 (1962)
33 Atkinson, R.J., Posner, A.M., and J.P. Quirk, J. Phys.Chem. 71, 550 (1967).
34 Bérubé Y.G., and P.L. DeBruyn, J.Colloid Interf. Sci. 27, 305 (1968)

35 P. Schindler and H.R. Kamper, Helv. Chim. Acta 51, 1781 (1968)
36 W. Stumm, C.P. Huang and S.R. Jenkins, Croat. Chem. Acta, 42 223 (1970)
37 Baes, C.F., Mesmer, R.E., Hydrolysis of Cations, John Wiley & Sons, New York, 1976.
38 Stumm, W. and J.J. Morgan, Aquatic Chemistry, Chap 3, John Wiley & Sons, New York, 1981.
39 Bragg, L., and Claringbull, G.F.,in "The Crystalline State" (L. Bragg, Ed.) Vol.IV, Bell and Sons, London. 1965
40 Hiemstra, T., Van Riemsdijk, W.H., and Bruggenwert, M.G.M., Neth.J.Agric.Sci. 35, 281 (1987).
41 Hiemstra T., Han Yong, and Van Riemsdijk W. H. Langmuir 15, (1999b) 5942
42 Saalfeld, H., and M. Wedde, Z. Kristall. 139, 129 (1974)
43 Hingston, F.J., Posner, A.M., & Quirk, P.J., J. Soil Sci. 23, 177 (1972)
44 Kavanagh, B.V., Posner, A.M., and Quirk, P.J., Disc. Farad. Soc., 59, 242 (1975)
45 Jones, P., and Hockey, J.A., Trans. Faraday Soc. 67, 2679 (1971).
46 Yates, D.E., The structure of the oxide/aqueous electrolyte interface. Ph.D. thesis, University of Melbourne, Melbourne, 1975.
47 Fokkink, L.G.J., De Keizer, A., and J. Lyklema, J.Colloid Interf.Sci. 127, 116 (1989).
48 Spanos, N., Georgiadou, I. and A. Lycourghiotis, J.Colloid Interf.Sci. 172, 374 (1995).
49 Sprycha, R., J Colloid Interf. Sci., 102, 173 (1984)
50 Contescu, C., Popa, V.T. and J.A. Schwarz, J Colloid Interf. Sci., 180, 149 (1996)
51 Hazeman, J.L., Brerar, J.F., and A .Manceau, J. Mat. Sci. Forum 79, 821 (1991)
52 Evans, T.D., Leal, J.R. and Arnold, P.W., J. Electroanal. Chem 105, 161 (1979).
53 Bloesch, P.M., Bell, L.C., and Hughes, J.D., Aust.J.Res. 25, 377 (1987).
54 Jung, R.F., James, R.O., and Healy, T.W., J.Colloid Interface Sci. 118, 463 (1987).
55 Zeltner, W.A., and Anderson, M.A., Langmuir 4, 469 (1988).
56 Johnson, B.B., Environ. Sci. Technol. 24, 112 (1990).
57 Tejedor-Tejedor, M.I., and Anderson, M.A., Langmuir 6, 602 (1990).
58 Venema P., Hiemstra T., and Van Riemsdijk W. H. (1998) . J. Colloid Interf. Sci. 198, 282-295
59 Peri, J.B., and Hensley, A.L., J.Phys.Chem. 72, 2926 (1968).
60 Iler, R.K., "The Chemistry of Silica". Wiley, New York, 1979
61 Sposito, G., "The Surface Chemistry of Soils". Oxford Univ. Press, New York, 1984.
62 Foissy, A.M., Pandou, A., Lamarche J.M., and N. Jaffizic-Renault, Colloids Surf. 5, 363 (1982)

Chapter 3

The Interfacial Charging Phenomena of Al (hydr)oxides

Hiemstra Tjisse, Han Yong, and Willem H. Van Riemsdijk

Published in Langmuir
Volume 15, Issue 18, Pages 5942-5955, August 31, 1999

Abstract

The interfacial charging of $Al(OH)_3$ (gibbsite and bayerite) and Al_2O_3 has been studied. For $Al(OH)_3$ it can be shown that the very strong variation in charging behavior for different preparations is related to the relative presence of differently reacting crystal planes. The edge faces of the hexagonal gibbsite crystals are proton reactive over the whole pH range in contrast to the 001 plane, which is mainly uncharged below pH = 10. On this crystal face, only doubly coordinated surface groups are found, in contrast to the edges, which also have singly coordinated surface groups. The results are fully in agreement with the predictions of the MUlti SIte Complexation (MUSIC) model. The proton adsorption, electrolyte ion adsorption and shift of the IEP of gibbsite and Al oxide have been modeled simultaneously. For gibbsite, the ion pair formation of Na is larger than that of Cl, as is evidenced by modeling the experimentally observed upward shift of the IEP and charge reversal at high electrolyte concentrations (Rowlands et al.1997). All these experimental results can be modeled with the MUSIC model, including the experimental surface potential of Al oxide (ISFET).

Introduction

Interfacial chemistry of Al hydroxides is important because of the role of Al hydroxides in the environment and because of its use in industrial processes. One of the basic properties of Al hydroxides is the protonation of surface groups resulting in the development of surface charge (σ_0). The charging behavior has been studied by various techniques like counter- and co-ion adsorption (Hingston et al. 1972, Ferris & Jepson 1975, Mashali 1976, Wendelbow 1987) or by H/OH titration (Kavanagh et al. 1975, Pulver et al. 1984, Hiemstra et al. 1987, 1989b). Compilation of the experimental data of Al hydroxides given in literature indicates the existence of very large differences in charging properties. The experimental capacitance (slope of the σ_0-pH curves) of the various Al hydroxides is found to vary extremely as shown in Fig.1. It should be noticed (Fig.1) that even within one type of mineral (gibbsite) a large difference in proton adsorption can be found.

Interfacial chemistry of Al hydroxide is especially interesting because some Al (hydr)oxides, like bayerite (γ-$Al(OH)_3$), gibbsite (α-$Al(OH)_3$) and boehmite (γ-AlOOH), may clearly develop crystal planes which differ in chemical surface composition. If the chemical composition of reactive surfaces (number and type of surface groups) is different, it may lead to a difference in charging. In order to explain experimental information, it has been hypothesized that adsorption in the interface of gibbsite only takes place at surfaces with singly coordinated surface groups (Parfitt et al. 1977, Van Riemsdijk and Lyklema 1980, Hiemstra et al. 1987). In literature, generally the relative presence and the type of crystal faces is not analyzed, prohibiting direct experimental evidence for the above given explanation. In this contribution, we will analyze experimentally the differences in proton adsorption of $Al(OH)_3$, in particular several gibbsite preparations, compare them with bayerite and try to relate the charging behavior to the crystallographic properties of the materials. Therefore, we will synthesize various types of gibbsite crystals, differing in morphology, which leads to variation in the contribution of crystal faces.

In the analysis, we will use the MUlti SIte Complexation (MUSIC) model (Hiemstra et al.1989a, 1996), which allows estimation of the proton affinity of various types of surface groups.

In the second part of the paper, the modeling of the primary charging phenomena (proton and electrolyte ion adsorption) will be discussed. We will explore the possibility to integrate this information with recent data on the electrokinetics of gibbsite (Rowlands et al.1997). These data comprise zeta potentials for gibbsite at very high electrolyte levels using acousto-electrophoresis. High concentrations of electrolyte lead to an upward shift of the iso electric point (IEP) and gibbsite becomes positively charged in concentrated solutions even at very high pH values. We will elaborate a concept, which enables description of this electrokinetic behavior.

The outcome of our evaluation of the charging behavior of Al hydroxides can be used to improve the understanding of charging behavior of Al oxides. We therefore will evaluate the extensive data sets of Sprycha (1989a, 1989b) on γ-Al_2O_3, comprising titration data, electrolyte ion adsorption data, and zeta potentials. In addition, experimental information of the direct measurement of the surface potential will be incorporated (Bousse et al.1983).

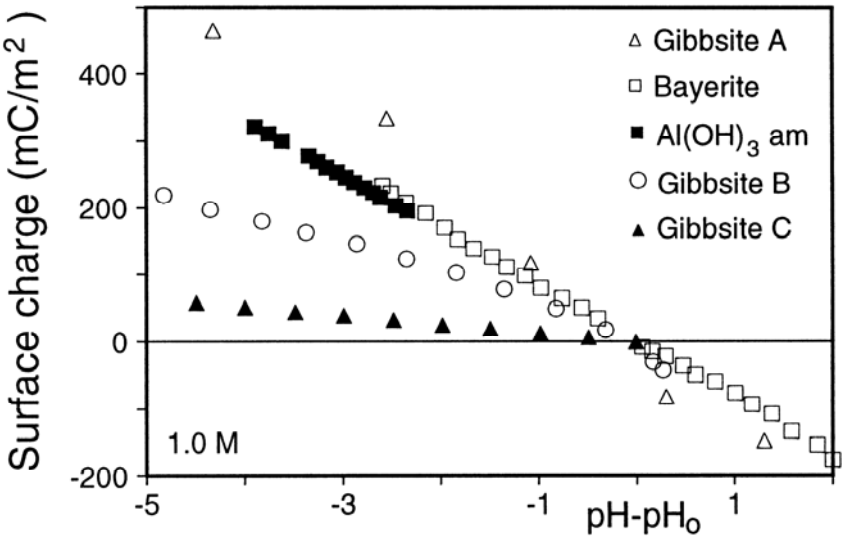

Fig.1 The large variation in surface charge of various Al hydroxides (X ray amorphous, gibbsite and bayerite) as a function of pH at the 1 M electrolyte level. Literature data of gibbsite A (Mashali 1976), bayerite (Pulver et al.1984), freshly prepared amorphous $Al(OH)_3$ (Kinniburgh 1975, assuming A = 690 m^2/g and a PZC of 9.4 from Anderson and Malotky, 1979), gibbsite B (Kavanagh et al.1974) and Gibbsite C (Hiemstra et al.1987, extrapolated from the 0.5 to 1 M salt level using given model parameter values).

Crystal structure and morphology

For crystalline Al hydroxides, three known polymorphs exist, called gibbsite, bayerite and nordstrandite (Hsu 1989). The various Al hydroxides polymorphs are composed of the same basic structural unit of Al ions in hexa-coordination with OH groups. The basic structural unit consists of two layers of close packed OH ions (Fig.2: row A and B) with Al ions sandwiched between them. The polymorphs differ in the relative stacking of the unit layer. In gibbsite, the hydroxyls in one unit reside directly on top of the hydroxyl of the next layer. In bayerite, the OH ions in one unit are positioned in depressions between the OH ions of the other unit, i.e. they are closer packed yielding a slightly larger bulk density.

The two polymorphs of this study, gibbsite and bayerite, differ in their crystal morphology. Gibbsite crystals are well developed in the *x* and *y* directions, but limited in the *z* direction. This results in thin flat hexagonal crystals (Fig.2). During preparation, the thickness of the crystals can be influenced by the temperature in the dialyses step of the preparation process (Gastuche and Herbillon 1962). The bayerite crystals are, in contrast to gibbsite, very strongly developed in the *z* direction. They often appear as prisms or rods in electron microscopic observations.

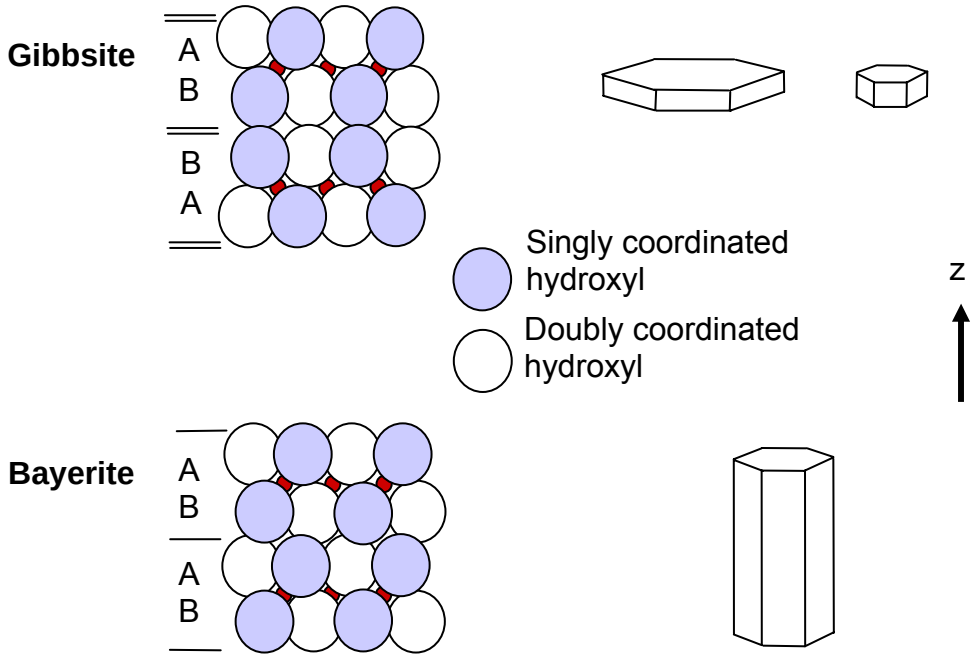

Fig.2 Schematic presentation of the structural arrangement of surface groups at the edge faces of gibbsite and bayerite. Both polymorphs are composed of the same type of basic structural unit layer, having Al ions sandwiched between two OH planes (A,B). The unit layers are differently stacked. The large shadowed circles represent the singly coordinated OH(H) surface groups. The large open circles represent the doubly coordinated OH groups. These groups are positioned more backwards. The Al ions are indicated with small black spheres present at different positions on the background. At the right hand side the morphology of both minerals is given. The bayerite crystals are much stronger developed in the *z* direction than gibbsite crystals.

The crystal structure of Al hydroxide can be analyzed applying the well-known Pauling rules (Pauling 1929, Sposito 1984). In the structure, Al ions are in hexa-coordination with hydroxyls. The trivalent Al^{3+} ions distribute their charge over the six surrounding oxygen ions of the octahedron, neutralizing on the average half a unit charge per Al-OH. An oxygen ion in the structure is bound by two Al^{3+} ions, each contributing on the average half a unit charge. The remaining negative charge of the oxygen (-1) is neutralized by the presence of a H^+ ion. The OH ions in the planar face of ideal bayerite and gibbsite crystals (001 face) are all doubly coordinated, like in the interior of the crystal and those doubly coordinated OH groups are therefore fully neutralized.

At the edges, the situation is different. The hexagonal morphology could be in case of an ideal hexagonal arrangement of Al ions, the result of the presence of two different types of crystal faces, namely the 010 face and its equivalents (Fig.3 of Hiemstra et al.1987) or the 100 face and its equivalents (Fig.4 Parfitt et al.1977, and Fig.2 this study). Own TEM observations of gibbsite crystals in combination with electron diffraction showed the latter

one to be present: the 100 face and its equivalents. However, also twinned crystals were observed with common edges, indicating that both faces can be found.

As demonstrated in Fig.2, equal numbers of singly and doubly coordinated OH ions are present at the 100 edge face. Based on the known crystal parameters of gibbsite, the site density N_s of each type of surface groups at the edges can be calculated and equals 8.15 nm^{-2}. The site density of the surface groups at the planar 001 face of gibbsite, having only doubly coordinated $\equiv Al_2OH$ surface groups, equals 13.8 nm^{-2}. The site density N_s of the bayerite edge equals for each type of surface group 8.35 nm^{-2}.

Proton adsorption

As described above, the oxygen of a singly coordinated ≡AlOH surface group is not fully neutralized. The oxygen receives on the average half a unit charge from the trivalent Al and one unit charge is neutralized by the presence of a proton. The mean remaining negative charge of the ≡AlOH group therefore equals -1/2. The negative charge can be neutralized by the adsorption of a proton, leading to the presence of the $\equiv AlOH_2$ groups with a mean charge of +1/2. The equilibrium reaction between both species can be described according:

$$\equiv AlOH^{-1/2} + H^{+}(aq) \Leftrightarrow \equiv AlOH_2^{+1/2} \qquad [1]$$

in which $K_{1,2}$ is the intrinsic proton association constant. For the ≡AlOH(H) groups present at the edges of gibbsite, the experimental log$K_{1,2}$ of this reaction is close to 10 (Hiemstra et al.1987). For bayerite, no reliable estimate is yet available in literature, but will be determined in this study.

As follows from reaction [1], a crystal face with only singly coordinated surface groups will be neutral if equal numbers of negative and positive surface groups are present. The pH at which the surface will not be charged is called the PZC. At other pH values surface charge will develop. The surface charge (σ_0) can be calculated from a proper bookkeeping of the number of surface species present in the interface (mol/m^2) and their corresponding charge. The relation between the pH and σ_0 can be found by extending the above described site binding approach with an electrostatic model. In case of the absence of inner sphere complex formation, one may use the so-called Basic Stern (BS) approach (Westall and Hohl 1980). The BS model is a simple but physically realistic double layer model (Hiemstra & Van Riemsdijk 1991), comprising an electrostatic surface plane and a diffuse double layer, separated by an empty Stern layer. The mathematical description can be found elsewhere (Westall and Hohl 1980, Hiemstra et al.1987,1989a, Hiemstra and Van Riemsdijk 1996).

According to the refined MUSIC model (Hiemstra et al.1996), the log$K$ value for the proton association reaction of a surface group depends on the degree of the undersaturation of the oxygen charge. The proton affinity of the singly coordinated oxo species ($AlO^{-3/2}$) is predicted to be extremely higher (about 12 log$K$ units) than the log$K$ of the protonation of hydroxo $\equiv AlOH^{-1/2}$ species. It implies that singly coordinated surface groups will only be

present as $\equiv AlOH^{-1/2}$ and $\equiv AlOH_2^{+1/2}$ groups. The neutralization of the oxygen charge depends on the charge distribution of the Al ions in the interface. Using an average bond valence of 0.5 valence units (v.u.) in combination with the refined MUSIC model (Hiemstra et al.1996) leads to a predicted log*K* value for the second protonation step of singly coordinated surface group (eq.[1]) which is 9.9.

At the crystal faces of $Al(OH)_3$, one may find the doubly coordinated $\equiv Al_2OH^0$ groups. The non-charged doubly coordinated $\equiv Al_2OH^o$ groups can only be protonated at very low pH values, since the oxygen charge is adequately neutralized. At very high pH values, doubly coordinated OH ions will dissociate a proton, forming an oxo surface species ($\equiv Al_2O^{-1}$). The proton association reactions can be formulated as:

$$\equiv Al_2O^{-1} + H^+(aq) \Leftrightarrow \equiv Al_2OH^0 \qquad K_{2,1} \qquad [2]$$

and:

$$\equiv Al_2OH^0 + H^+(aq) \Leftrightarrow \equiv Al_2OH_2^+ \qquad K_{2,2} \qquad [3]$$

For gibbsite, the log*K* values for both reactions can be estimated with the refined MUSIC model. The predicted log*K* values are respectively: $\log K_{2,1} = 11.9$ and $\log K_{2,2} = 0$ if a bond valence of 0.5 v.u. is used (Hiemstra et al.1996).

Experimental

Synthetic gibbsite was prepared using the method described by Gastuche & Herbillon (1962). In this procedure, first an amorphous Al hydroxide suspension is produced, followed by a dialysis at a certain temperature. The amorphous Al hydroxide suspensions were obtained by titrating 2 liter of an aluminum nitrate solution (1M) with a 4M NaOH in a plastic vessel to a pH 4.5 under a nitrogen gas atmosphere to eliminate CO_2. The titrant was added at a constant rate of about 10 mL/min. All chemicals were of an analytical reagent grade and fresh double-distilled water was used.

In this study, several gibbsite suspensions were synthesized. The temperature of dialysis influences the crystal dimensions of the gibbsite particles (Gastuche & Herbillon,1962). Two different temperatures of dialysis were chosen. Two amorphous Al hydroxide suspensions were dialyzed against double-distilled water at 70 ^oC for 4 weeks with daily refreshing the solution, resulting in gibbsite GH1 and GH2 and one gibbsite suspension was prepared by dialyses of the amorphous hydroxide suspension against double-distilled water at 4 ^oC for 8 weeks with daily refreshing the solution, yielding GL1. After preparation of this gibbsite, the sample was in addition subsequently dialyzed another 2 months at 70 ^oC in order to increase the crystallinity. In addition, a fourth gibbsite sample G♦ has been prepared, also at low temperature. This non-aged sample was used in titration experiments without a further

dialysis at high temperature. Later this suspension has been aged shortly at 70 ^{o}C during approximately 2-3 weeks and again titrated.

Bayerite was obtained by titrating 2-liter alkaline aluminum nitrate solution (0.1 M) with an OH/Al ratio of 6, with HNO_3 to a pH 8 at 70 ^{o}C in a plastic vessel under nitrogen gas atmosphere. The titrant was added with a speed of 1.7 mL/min. The resulting precipitate was left in the mother liquid overnight at room temperature and was then washed with double-distilled water to remove as much as possible alkali ions and anions. From this suspension, the fraction smaller than approximately 1 μm was used in the experiments.

The synthetic gibbsite and bayerite preparations were used to perform titration experiments in the pH range between pH5 and pH10 at two different electrolyte levels, 0.005 and 0.1M $NaNO_3$, at a constant temperature of 20 ^{o}C and under nitrogen gas atmosphere. A volume of 50 mL of the sample suspension was pipetted together with 1 mL 0.25 M $NaNO_3$ electrolyte into a 100 mL plastic vessel. In order to prevent contamination of the suspension with CO_2, purified moist N_2 gas was led over the suspension in the closed vessel (Hiemstra et al.1989b). First the sample stood overnight at a pH of about 6-7 to eliminate dissolved and adsorbed (bi)carbonates. For each electrolyte level a forward and a backward titration with respectively base and acid was performed. These titrants had the same sodium concentrations as the concentration levels of $NaNO_3$ in the suspension in order to keep the electrolyte concentrations constant. The change in electrolyte level was carried out at low pH by pipetting the appropriate amount of a 1M $NaNO_3$ solution. Acid and base were added with a Metrohm 655 dosismat. The pH was measured with a combined glass electrode after stabilization of the pH (in case of gibbsite 2 min, in case of bayerite 10 min).

Air-dried samples of the prepared Al hydroxides have been characterized by TEM, X-ray diffraction of a random oriented powder and a BET N_2 gas adsorption analysis (outgassing at 105 ^{o}C for 24 hours). The specific total and edge surface area of gibbsite were measured from electron micrographs samples shadowed at an angle of 20 degree.

All calculations were done using a computer algorithm (ECOSAT) based on the principles of Westall and Hohl (1980). The activity coefficients are calculated using the extended Davies equation. The ion speciation table needed to do the calculation with surface components with broken charges is given in the appendix. See also Hiemstra & Van Riemsdijk (1996).

Results and Discussion

Sample characterization

The X ray diffraction analysis showed that in the gibbsite samples no other minerals were detectable. Precipitation of Al hydroxide from an aluminate solution at high pH resulted in a bayerite preparation, which was almost pure. It contained traces of probably pseudoboehmite, which can easily be formed when this preparation method is used (Van Straten & De Bruyn 1984).

The surface area has been measured with N_2 gas adsorption. Analysis of the gas adsorption data yields a BET surface area A_{BET} for the different preparations (Table I). The gibbsite samples did not show important porosity. The bayerite sample was however macroporous.

An estimate of the surface area A_{EM} was also made using Electron Microscopic (EM) observations (Table I). Electron microscope observations of the gibbsite samples showed the characteristic hexagonal morphology (Hiemstra et al.1987). The particles in the bayerite preparation were large and appeared as rods, similar as found by Van Straten and De Bruyn (1984). The particles seemed multidomainic, which is probably a reason for the observed porosity. The width to length ratio of the bayerite crystals was about 0.1. From electron micrographs of shadowed gibbsite specimens, the dimensions of individual crystals have been determined, which can be used to calculate the surface area. The data for the EM surface area A_{EM} are given in Table I.

Table I The experimental edge surface area (A_{Edge}) of synthetic gibbsite and the total surface area determined by gas adsorption (A_{BET}) or electron microscopy (A_{EM}) of gibbsite and bayerite. The well-crystallized gibbsite (G) preparations made at high (H) or low (L) temperature are named GH1 & GH2 and GL1 respectively. The gibbsite prepared at low temperature without aging is named G♦. In addition literature data of samples are given: G-Kavanagh (Kavanagh et al.1975), G-Hiemstra (Hiemstra et al.1987), G-Wendelbow (Wendelbow 1987) and G-Parfitt (Parfitt et al.1977) together with the unpublished data of A_{EM} of the preparation of Hiemstra et al.1987.

Sample	A_{BET} m^2/g	A_{EM} m^2/g	A_{edge} m^2/g	% Edge Area (m^2/m^2BET)
GH1	18.0	27.6	4.2	23
GH2	40.3	86.7	9.2	23
GL1	40.8	51.2	20.3	50
G♦	42.1	78.6	7.3	17
B	13.1			91[*a]
G-Kavanagh	48	68*[b]	10[*b]	22
G-Hiemstra	19.8	30.2	3.4	17
G-Parfitt	45	109	9	20
G-Wendelbow	40		8	20

[*a] Estimated on the basis of the length to width ratio of the particles

*b Calculated from the reported mean crystal dimensions: d = 180 nm, h = 15 nm

One of the first interesting observations which can be made (Table I), is the difference in total surface area determined from the BET analysis and the EM observations. The latter one is in most cases considerably larger. A lower A_{BET} can be due to the presence of 001 face-to-face contacts, resulting from drying the specimens before the gas adsorption measurements as was suggested by Parfitt et al. (1977). Lower values for A_{BET} are also often observed for layer silicates like kaolinite and montmorillonite (Greenland & Hayes 1978, Sposito 1984). An additional explanation of the lower A_{BET} might be a 001 face-to-face contact because of growth phenomena, for we observed with EM that in some gibbsite preparations it was difficult to get individual single crystals. If real face-to-face contact in solution is present, the

best estimate of the total external surface is A_{BET}. In the calculations, A_{BET} is used as an estimate of the external surface area in order to conform to common practice.

Reversibility of the charging behavior

From the experimental titration data, the charging curves can be calculated correcting the total added amount of acid/base for the calculated acid/base consumption of the electrolyte solution. An example of the σ_0 -pH curves of one of the gibbsite samples and of the bayerite preparation is given in Fig.3 and Fig.4 respectively.

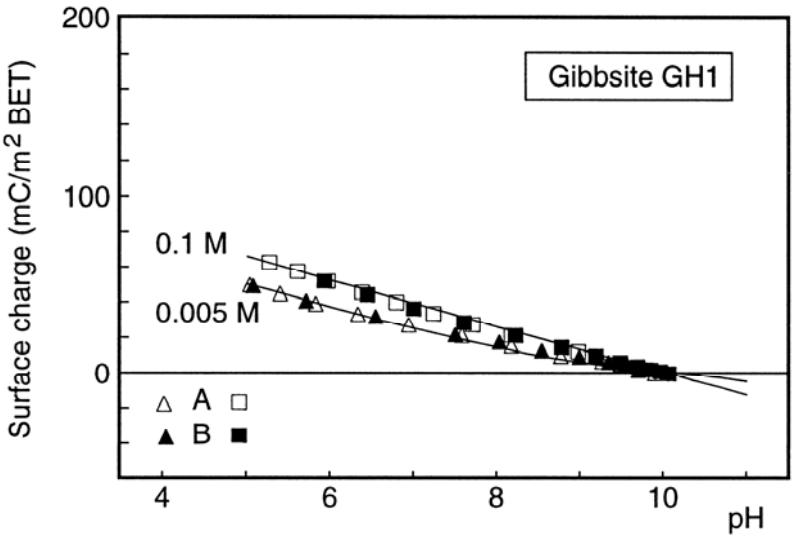

Fig.3 Charging behavior of gibbsite (GH1) in 0.005 and 0.1 M $NaNO_3$. The reversibility of titration was checked by comparing the charging in case of acid addition (A) with that of base additions (B). The model lines have been calculated assuming charging of edges using the parameter values given in Table II.

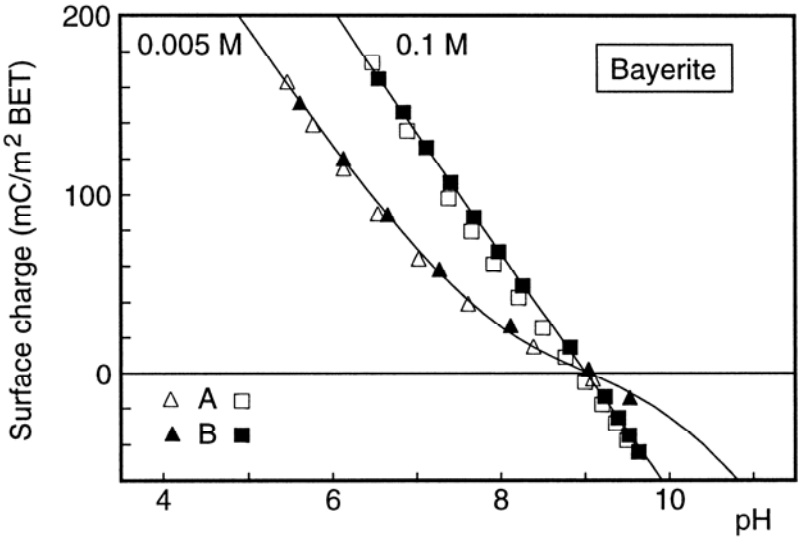

Fig.4 Charging of bayerite as a function of pH in 0.005 and 0.1 M $NaNO_3$. The reversibility of titration was checked by comparing the charging in case of acid addition (A) with that of base additions (B) The model lines

have been calculated assuming charging of the whole BET surface area, using the parameter values given in Table II.

The reversibility of the titration behavior was experimentally checked by titration of the sample at the lowest salt level subsequently with acid/base/acid, followed by a base/acid (B/A) cycle at the higher salt level. The reversibility of the gibbsite samples in fast titrations (2 min. per step) was good. However, titration of the bayerite preparation showed hysteresis if the titration was carried out with only two minutes per step. This hysteresis disappeared if the titration procedure was carried out with larger equilibrium times (10 min. per step) between the appropriate additions (Fig.4). The explanation is probably the presence of sites that have no direct access to the solution as found in pores. The observed macro-porosity of the bayerite sample supports this.

σ_o -pH of gibbsite

The proton affinity constants predicted by the refined MUSIC model, lead to a PZC for the edge faces of 9.9. All our gibbsite preparations showed a nearly similar Point of Zero Charge (PZC), which was close to 10. Similar high PZC values for gibbsite samples have been reported in literature (Kavanagh et al.1975, Hiemstra et al.1987, Wendelbow 1987). Kavanagh et al. (1975) reported a PZC value of 9.8 and an IEP value of 10. One may conclude that the PZC / IEP of gibbsite can be considered as rather well established. Our experimental charging curves of the various gibbsite preparations are presented in Fig.5. Assuming as a first step that the whole surface area is reactive, the surface charge is expressed per unit BET surface area, which is common practice.

The experimental capacitances ($\partial\sigma_0/\partial$pH, i.e. the slope of the curves) are low compared with most other oxides like iron (hydr)oxides and titanium oxides. Moreover, the curves of gibbsite show very strong differences in the experimental capacitances (Fig.5). Both phenomena indicate that probably part of the BET surface area is not reactive in the pH range under consideration. If it is assumed that the edge faces of gibbsite are the only reactive ones, the H adsorption should be expressed per unit edge area, as done in Fig.6. In this case, most of the variation disappeared within the experimental error. This plot also results in a much higher charging per unit area of surface, which is much more in agreement with the charging of many other metal (hydr)oxides.

The gibbsite samples have been prepared at different temperatures (dialysis at 5 and 70 ^{o}C). The sample GL1, prepared with dialysis at 5 ^{o}C, has been aged after the preparation for more than two months at 70 ^{o}C before the proton adsorption was determined. Later, we have prepared in addition another gibbsite (G♦) at low temperature without this aging step at high temperature. This sample had a relatively high proton adsorption capacity as shown in Fig.7. If one expresses the charge per unit edge surface area (A_{edge} = 7.3 m^2/g), the charging is higher (Fig.7a, right scale) than that of the other three gibbsite samples (Fig.6) and very much above the values to be expected in general for metal (hydr)oxides.

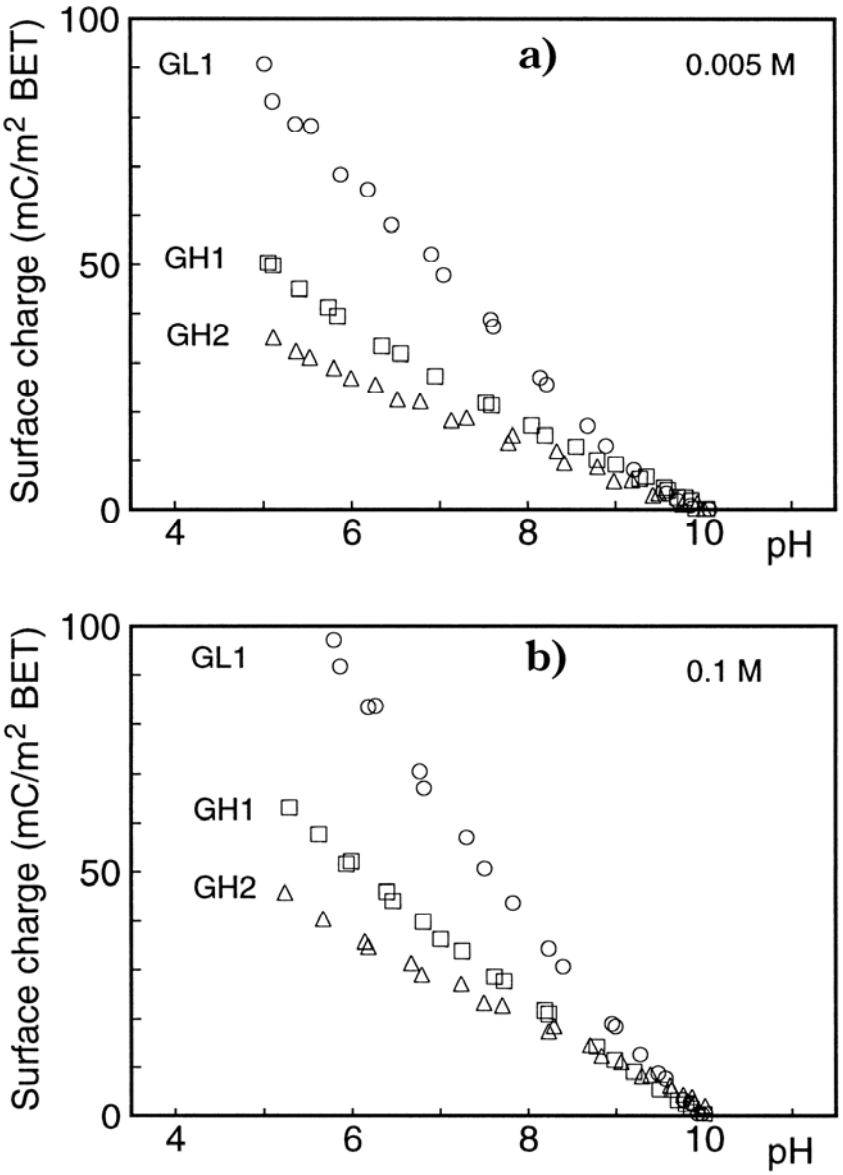

Fig.5 Charging behavior of three gibbsite preparations (GL1, GH1 and GH2) in 0.005 $NaNO_3$ (Fig. 5a) and in 0.1 $NaNO_3$ (Fig. 5b). The proton reactivity is expressed based on the overall surface area measured with BET gas adsorption.

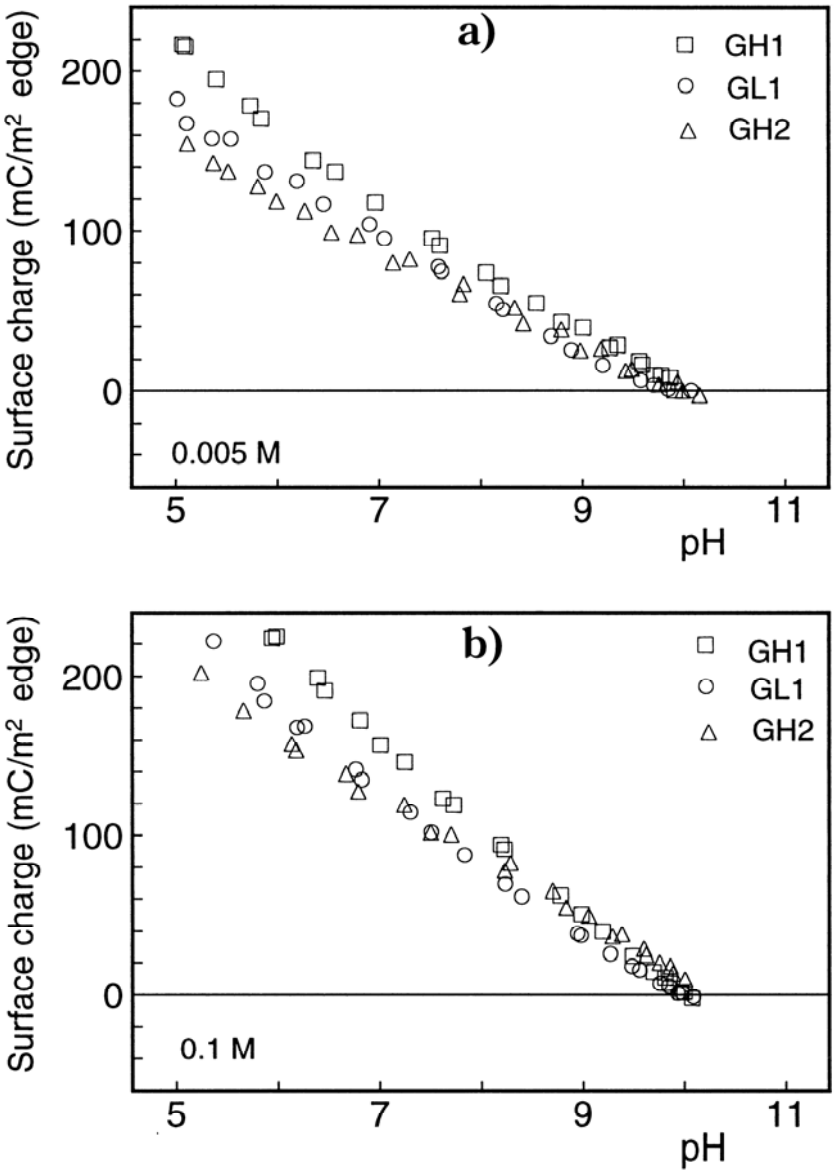

Fig.6 Charging behavior of three gibbsite preparations (GL1, GH1, and GH2) in 0.005 $NaNO_3$ (Fig. 6a) and in 0.1 $NaNO_3$ (Fig. 6b). The proton reactivity is in this case expressed based on the edge surface area of the gibbsite crystal, which is expected to be proton reactive.

The apparently very high edge face protonation (Fig.7a, right scale) indicates that the adsorption of H in this sample is probably not restricted to the edge faces alone. Some reactive sites may be present at the planar side of the crystals. Presumably, part of these sites is present at defects in the structure or present at very small steps. This suggestion is supported by the observation that during a short aging time (2-3 weeks at 70 ^{o}C), the pH of the G♦ suspension decreased from pH = 6.5 to about pH = 4. The proton release can be understood as the production of $\equiv Al_2OH^{o}$ groups on account of $\equiv AlOH_2^{1/2+}$ groups, according to the reaction: $2 \equiv AlOH_2^{1/2+} \Leftrightarrow \equiv Al_2OH^{o} + H_3O^{+}$. After this short aging process of the G♦ suspension, indeed a decrease in reactivity was observed (Fig.7b), due to a decrease in reactive sites. It is noticed that the charge is still higher than that of the three well-crystallized samples of Fig.5&6, which can be due to the relatively short aging period of the G♦ sample.

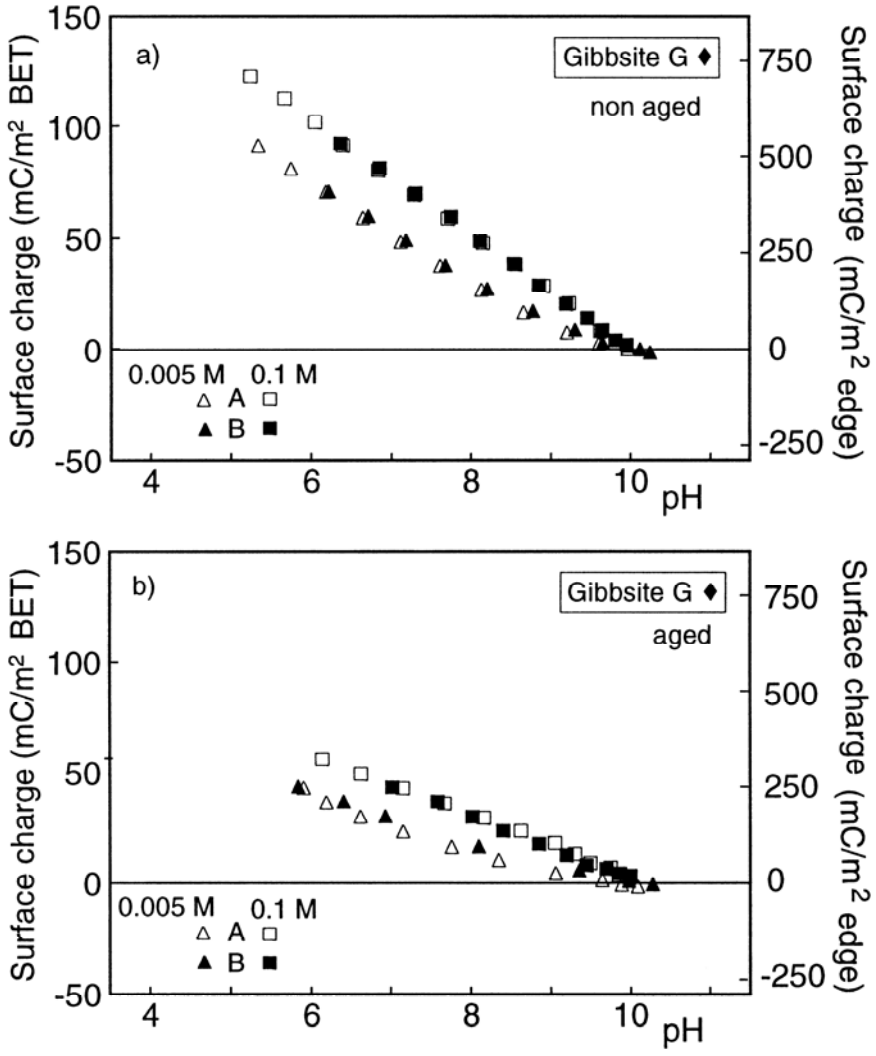

Fig.7. The charging behavior of the gibbsite sample G♦, prepared at low temperature (4^{o}C), before (7a) and after (7b) a short aging time (2-3 weeks) at high temperature (70 ^{o}C). The charging can be expressed per unit BET surface area (left axis) or per unit edge area (right axis). In 7a the behavior expected based on charging of edges, indicates a too large reactivity, which is explained assuming additional charging at the 001 side. The charging behavior decreases (7b) after aging due to increased crystallinity of the sample, decreasing the proton reactivity at the basal 001 face.

High charging of gibbsite samples has also been reported in literature. The gibbsite preparation of Mashali (Greenland and Mott 1978), given in Fig.1, is a typical example. The calculated charging of this sample is based on the measured adsorption of CsCl. Kavanagh et al. (1975) published titration curves for a synthetically prepared gibbsite. Based on the reported mean dimensions of the hexagonal crystals, we estimated the relative contribution of the edge area at about 20% (Table I), which allows calculation of the charge per unit edge area. In Fig.8, the surface charge data are presented, expressed per unit BET surface area as well as per unit edge area. The surface charge expressed per edge area is so high (right scale) that it is certain that their gibbsite preparation is reactive over almost the whole surface area, including the 001 sides of the crystal (defects/steps).

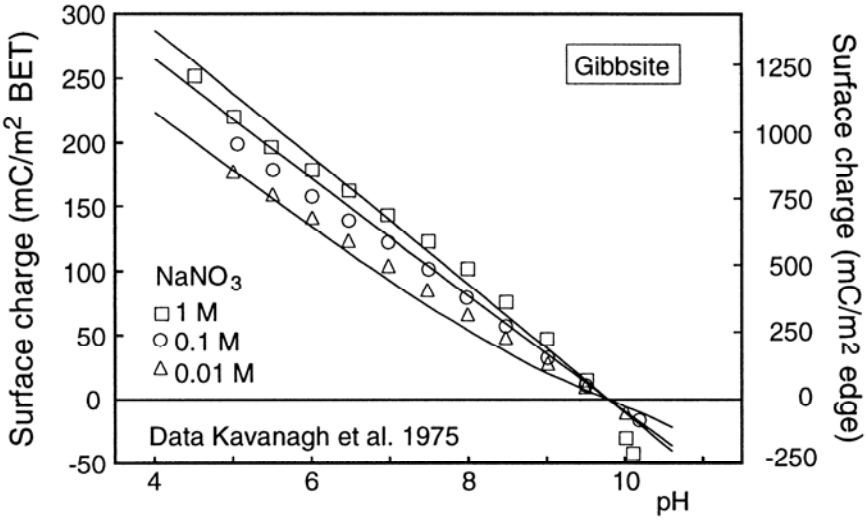

Fig.8. Charging behavior of a gibbsite. The charging is higher than the charging of the gibbsite preparations given in Fig.5. It is too high in comparison with what can be expected based on charging of edges alone, indicating reactivity at the basal 001 face. The lines have been calculated using the parameter values given in Table II. The site density of the singly coordinated groups is set 4 nm^{-2}, a value which represents the mean of the density of these groups at the edge (8 nm^{-2}) and the 001 face (0 nm^{-2}).

Bayerite

Bayerite adsorbs generally much more protons than gibbsite as is illustrated by comparing Fig.3 and 4 (see also Fig.1). This behavior can be understood if one realizes that nearly all surface area of the bayerite preparation has a composition comparable with the edge faces of gibbsite, i.e. it has singly coordinated ≡AlOH(H) groups. It implies that the charging of bayerite will be similar to the charging of the edges of gibbsite. The PZC value of bayerite is slightly lower than the PZC of our gibbsite samples and equals 9.1. To compare the surface charge of bayerite with that of the edges of gibbsite samples, it is plotted as a function of pH-

PZC in Fig.9. Based on this figure, it is concluded that the assumption of only edge charging of well-crystallized gibbsite samples is in accord with the assumption of charging of the whole bayerite surface, because the charging curves are very similar with the gibbsite data expressed per edge area.

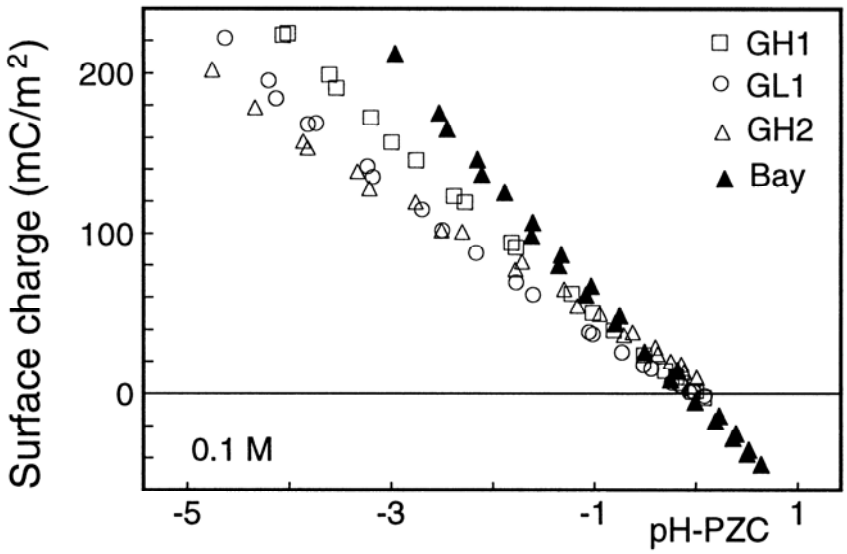

Fig.9. The charging behavior of bayerite in 0.1 M $NaNO_3$ (expressed per m^2 BET) in comparison with the gibbsite data expressed per m^2 edge face area.

Modeling gibbsite and bayerite data

Sites

Several approaches can be followed in modeling the σ_0-pH data. It could be assumed that all surface groups, irrespective of their coordination with metal ions of the solid contribute to the surface charge. The approach leads to a very good description of the charging phenomena of gibbsite (Hiemstra et al.1987). However the fitted value of the Stern layer capacitance, C = 0.25 F/m^2 (Basic Stern double layer approach), is very low compared with the values found for other Al (hydr)oxides. It does not lead to a unifying concept for the description of the charging of the Al (hydr)oxides in general and moreover, such a low value of the capacitance is difficult to understand in terms of the physico-chemical double layer interpretation presented by Hiemstra and Van Riemsdijk (1991).

Another more realistic approach could be to give credit to the crystallographic information, i.e. the presence of two types of crystal faces with a different chemical composition. The above relation between the edge area of gibbsite and the proton adsorption indicates that in well-crystallized gibbsite, the 001 face probably does not contribute

significantly to the total surface charge in the pH range under consideration. These findings are in agreement with the calculated MUSIC model estimations, which showed that the planar 001 face would only be considerably reactive for pH values above 10. In the range pH 4-10 the charge development is mainly determined by the presence of singly coordinated surface groups at the edge faces. The doubly coordinated surface groups at the edge faces (Fig.2) are even not reactive in the pH range above pH 10 (Hiemstra et al.1989b).

Based on the above given considerations, we conclude that a sufficiently accurate description of the surface charge can be done using only the protonation of the singly coordinated surface groups (eq.[1]).

Ion pair formation

An interesting phenomenon for all Al hydroxides and Al oxides too is the low salt dependency of the charging curves in comparison with other Me hydroxides. The description of the salt dependency of the σ_0 -pH curves of gibbsite, assuming that the charge is present at the edge faces, is only possible if ion pair formation of surface groups with electrolyte ions is taken into account. The idea of ion pair formation has already been suggested by Yates (Yates 1973, 1974) and was later applied by Davis et al.(1978). For Al oxide, the presence of weakly adsorbed electrolyte ions is supported experimentally (Shiao and Meyer 1981, Sprycha 1983, 1989b). Because of the presence of ion pair formation simultaneous adsorption of cations and anions can be expected in the PZC. For gibbsite, simultaneous adsorption of cations and anions has also been reported (Mashali / Greenland & Hayes (1976/1978), Hingston et al. (1972) and Wendelbow (1987)).

The ion pair formation reactions can be defined as:

$$\equiv \mathrm{AlOH}^{-1/2} + \mathrm{C}^{z+}(\mathrm{aq}) \Leftrightarrow \equiv \mathrm{AlOH}^{-1/2}\text{-}\mathrm{C}^{z+} \qquad K_{\mathrm{c}} \qquad [4]$$

and

$$\equiv \mathrm{AlOH}_2^{+1/2} + \mathrm{A}^{z-}(\mathrm{aq}) \Leftrightarrow \equiv \mathrm{AlOH}_2^{+1/2}\text{-}\mathrm{A}^{z-} \qquad K_{\mathrm{a}} \qquad [5]$$

In the Basic Stern double layer approach, the charge of the weakly adsorbed electrolyte ion of the ion pair is situated in an electrostatic adsorption plane at the solution side of the Stern layer. The distance of slightly more than approximately 1 water molecule (Hiemstra and Van Riemsdijk 1991) separates the weakly bound ions from the surface. Variation in charging of metal (hydr)oxides in different simple background electrolyte ions is usually relatively small. Based on modeling of charging data sets for Al_2O_3, it has been suggested (Lützenkirchen et al.1995) to use equal values for the ion pair formation constant of cations and anions, since no accurate significant difference could be determined by modeling. This is especially true for Me (hydr)oxides with a very high PZC, where most of the data are present at the acid side of the PZC. Following this suggestion, we simplified, as a first approach, the data treatment by presuming symmetrical ion pair formation, i.e. $\log K_{\mathrm{c}} = \log K_{\mathrm{a}}$.

The data for the 0.005 and 0.1 M $NaNO_3$ level were fitted simultaneously for each gibbsite and bayerite sample. The parameter values for the best fit are presented in Table II, together with the standard deviation σ*. The parameter values for data presented in literature have also been given.

All three gibbsite preparations of Fig.5 have the same ion pair formation constant (log$K$ = +0.1), which is large compared with pair formation constants found by a similar approach for hematite Fe_2O_3 (log$K$ = -0.3) (Schudel et al. 1997), silica SiO_2 (log$K$<-1.5) (Hiemstra et al.1989b), goethite FeOOH log$K$ = -1 (Hiemstra and Van Riemsdijk 1996), rutile TiO_2 (log$K$ = -0.6) (Hiemstra & Van Riemsdijk 1991). The best fit for bayerite gives ion pair formation constants slightly lower that those of gibbsite, although the data could be described also very well with the ion pair formation constant of gibbsite. In the bayerite modeling, two options can be followed. One could assume that the 001 face of the bayerite crystals is perfectly crystallized and therefore not reactive because of the presence of only inert $\equiv Al_2OH^o$ groups. It also can be assumed that the whole surface area is reactive (as in Fig.9), which leads to a slightly lower capacitance value (Table II).

Table II
The fitted parameter values for the description of the experimental σ_0-pH data sets of well-crystallized gibbsite and bayerite: Stern Layer capacitance C and the ion pair formation constant logK_i, assuming symmetrical ion pair formation. The value σ* is the standard deviation, expressed in mC/m^2. In addition some fitted parameter sets derived from literature data of gibbsite samples are given: G-Kavanagh (Kavanagh al.1975), G-Hiemstra (Hiemstra et al.1987), G-Wendelbow (Wendelbow 1987).

Sample	C F/m^2	logK_i	σ* (mC/m^2)
GH1[*a]	1.17	0.1	14
GH2[*a]	0.83	0.1	19
GL1[*a]	0.91	0.1	20
G-Kavanagh[*b]	0.9	0.1[*c]	-
G-Wendelbow[*a]	0.9	0.1[*c]	-
G-Hiemstra[*a]	1.40	0.1	-
B[*b]	1.62	-0.1	12
B[*b]	1.47	0.1[*c]	12
B[*a]	1.65	0.1[*c]	12

[*a] Assuming that only the edge faces are reactive.
[*b] Assuming that the whole BET surface area is reactive.
[*c] This value was not fitted but fixed.

Capacitance

As follows from Table II, the fitted value of the Stern layer capacitance C of the three well-crystallized gibbsite preparations (Fig.5) varied, reflecting the experimental variation in slope, which remained after scaling based on the surface charge per unit edge area. We assume that the variation is mainly due to the difficulties of determining accurately the edge surface area from shadowed particles, particularly because of the use of a small angle of shadowing (20 degree) and due to the presence of particle overlay, reducing the possibility of choosing in an aselective manner the crystals in the EM observation. The assumption of an

uncertainty of 10% in the edge area already explains a large part of the variation (Fig. 6). A second reason for variation in the Stern layer capacitance is related to the potential reactivity at the 001 side of the crystal, resulting from the presence of defects and small steps. The contribution of these imperfections will increase the apparent capacitance value. In case of such a contribution, the lowest capacitance values are probably closest to the actual value. In conclusion we estimate the actual capacitance for a well-crystallized gibbsite surface to be 0.9 ± 0.1 F/m^2. This value is the same as the value of well-crystallized goethite (Hiemstra & Van Riemsdijk, 1996). It is of interest to note that both minerals mentioned have the same capacitance but a quite different log$K$ value for the ion pair formation. The value of the capacitance C can be interpreted in terms of a mean relative dielectric constant ε_r for the Stern layer, using the expression:

$$C = \varepsilon_r \varepsilon_o / d \qquad [6]$$

in which ε_r and ε_o are the relative and absolute dielectric constant and d the distance between the electrostatic planes. The calculated value of ε_r is 40 if we assume a Stern layer thickness of 0.4 nm (≈ radius of a hydrated ion) in eq.[6]. This value is somewhere between that of the solid phase (ε_r = 10) and that of water in the DDL (ε_r = 78).

The capacitance of the double layer of our bayerite preparation is considerably higher than that of gibbsite and equals C = 1.5 ± 0.1 F/m^2 (Table II). This indicates a difference in double layer properties. For goethite, it has been suggested that a higher capacitance is found for mineral preparations with a less well-developed regular structure, characterized by multi domains, defects, and porosity (Hiemstra et al. 1989b). Surface roughness will decrease the mean distance of minimum approach of hydrated counter ions, i.e. the capacitance increases (Hiemstra and Van Riemsdijk 1991). It is also possible that ions partly penetrate the surface structure, to be discussed later. Our bayerite preparation was porous and had rough surfaces, which may explain the higher experimental capacitance.

Zeta potentials

Very recently, zeta potentials have been measured for gibbsite using a novel electro-acousto technique (Rowlands et al. 1997), which allows the measurement of electrokinetic phenomena at very high electrolyte levels. The results (Fig.10) show a shift of the IEP (pH at zero potential) to higher pH values, which is here an indication of the stronger interaction of the electrolyte cation compared to the electrolyte anion. The asymmetrical ion pair formation contrasts with our previous assumption used in the evaluation (Table II). At the highest salt concentration (Fig.10), the gibbsite becomes positively charged over the entire broad range of pH values. It is interesting to notice that the shift of the IEP and the charge reversal at increasing electrolyte ion concentration is a general phenomenon for metal (hydr)oxides since it has also been observed for other oxides, like anatase and zirconium (Kosmulski and Rosenholm, 1996). Kosmulski and Rosenholm (1996) suggested that this effect might be independent of the type of oxide and can be related to the structure making and structure breaking properties of electrolyte ions. For anatase the increasing effect of series of ions (Cs <

K < Na < Li and Cl < NO_3 < ClO_4 < Br < I) can also be correlate to literature data of direct measurements of the extent of ion adsorption on anatase (Sprycha, 1984).

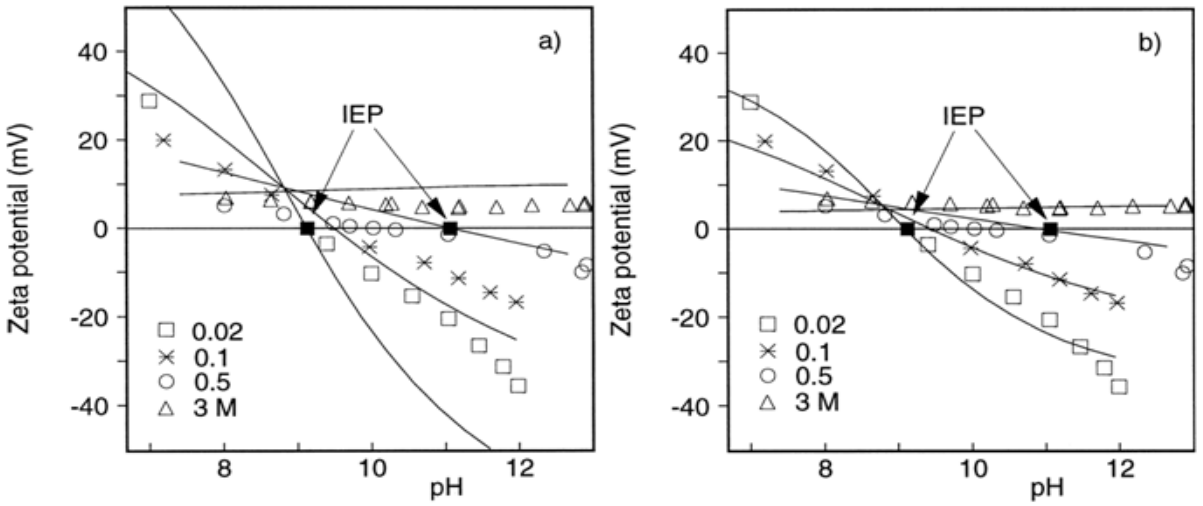

Fig.10. Experimental IEP values (black squares) of gibbsite in 0.02 M (IEP = 9.1), 0.1 M (IEP = 9.1) and 0.5 M NaCl (IEP = 11). These IEP values have been derived by Rowlands et al. (1997) based on a detailed analysis of the zeta potentials. Charge reversal is observed at high pH for c > 0.5 M NaCl, indicating a higher affinity of Na^+ for the gibbsite surface relative to Cl^- ion. The lines in 10 a) are based on the BS approach, locating the plane of shear at the head end of the DDL. In Figure 10 b), the plane of shear is set at respectively 1.2, 0.5, 0.2 and 0.1 nm from the head end of the DDL. The other parameter values are $\log K_{1,2} = 9.0$, $\log K_{Na} = 0.2$ and $\log K_{Cl} = -0.2$ (i.e. asymmetrical ion pair formation, see text). The capacitance C is set to 0.9 F/m^2 (see discussion above). For this gibbsite we assumed that the whole surface area can be considered as reactive, as in the case of the gibbsite of Kavanagh (Fig.8), having an apparent site density of 4 nm^{-2}.

The difference in affinity of electrolyte cations and anions can be interpreted in terms of different values for the change in Gibbs free energy of the formation reaction. This difference may arise from a difference in the intrinsic affinity ($\Delta G_{intr} \propto \Delta \log K_{intr}$), the electrostatic contribution (ΔG_{elec}), or the ion interaction in solution (individual activity coefficients). Kosmulski and Rosenholm (1996) have suggested the latter possibility. A difference in the intrinsic affinity can be used within the BS approach. The option of a different electrostatic contribution leads to the use of a three plane electrostatic model. Modeling shows that the Na ions should then be located at a larger distance. It implies that, in case of a negative surface, the Cl ions will encounter a larger repulsive force, favoring the relative adsorption of Na. A capacitance value of approximately 5 F/m^2 for the Stern layer present between the Na and Cl ions is enough to achieve the intended effect. This capacitance value is equivalent with a distance of approximately half a water molecule (Hiemstra and Van Riemsdijk 1996). The use of a model with different electrostatic planes for the electrolyte cations and anions has been suggested previously by Bousse et al. (1983), Charms and Piasecki (1996) and recently by Machesky et al.(1998). It is interesting to notice that in all these models the cation is placed

closer to the surface than the electrolyte anion in contrast to the model given here. The zeta potentials calculated by Charmas and Piasecki (1996) for anatase (extended 2p*K*-TL model) are in conflict with the experimental results of Kosmulski and Rosenholm (1996), since the calculated IEP shifts downward with an increasing ionic strength. A similar trend is predicted by Machesky et al. (1998), who used a 1p*K* model with electrolyte ions at different positions. The description of the shift of the IEP can easily be improved if the anion is placed at the smaller distance of approach than the cation, as suggested above.

From the three above options to account for the difference in affinity, we will use in this paper, for reasons of simplicity, the BS model in combination with a different intrinsic affinity.

Before discussing the modeling of the electromobility data of Fig.10, it should be noticed that zeta potential data in general are accompanied by a large uncertainty because of the theoretical complexity of the transformation of the experimental electromobility data to zeta potentials for non-ideal particle suspensions. The IEP, resulting from mobility data, can be considered as the most reliable experimental result (Davis and Kent, 1990) from electrokinetic measurements.

With the assumption of a difference in affinity of the electrolyte ions we are able to describe the increase of the IEP with an increase of the ionic strength (Fig.10). The description of the zeta potentials values is less straightforward. The potential at the head end of the diffuse double has been claimed to be equivalent with the zeta potential. Recently, it has been shown for spherical hematite particles (Schudel et al. 1997) that it is possible to model the zeta potential and the primary charging behavior within the BS framework. However, in other cases, the calculated double layer potentials based on the BS approach are far too high to explain published zeta potentials, especially data at low ionic strength. It questions either the reliability of these data or the physico-chemical interpretation of the interface. In a model approach, a drop of the potential can be achieved in two ways. One option used in the past is the introduction of a second charge free Stern layer between the head end of the DDL and the position of closest approach of hydrated ions. In the triple layer model, the outer Stern capacitance is set at 0.2 F/m^2. Introduction of this value in eq.[6] and the value for the dielectric constant of water (Hiemstra and Van Riemsdijk 1991) leads to a calculated thickness of the charge free layer of 3 nm, i.e. the neutralization of surface charge by the diffuse double layer starts at a distance of approximately ten water molecules from the primary Stern layer. The presence of such a large charge free layer can be considered as physically not very realistic. Another possibility to achieve a lower potential is to presume that the electrokinetic plane of shear is not at the head end of the diffuse double layer but at a larger distance from the surface. Healy and White (1978), who used a constant distance for the plane of shear (2 nm), have applied this approach. Dzomback and Morel (1990) suggested the use of a variable location of the plane of shear in the diffuse double layer, depending on the ionic strength.

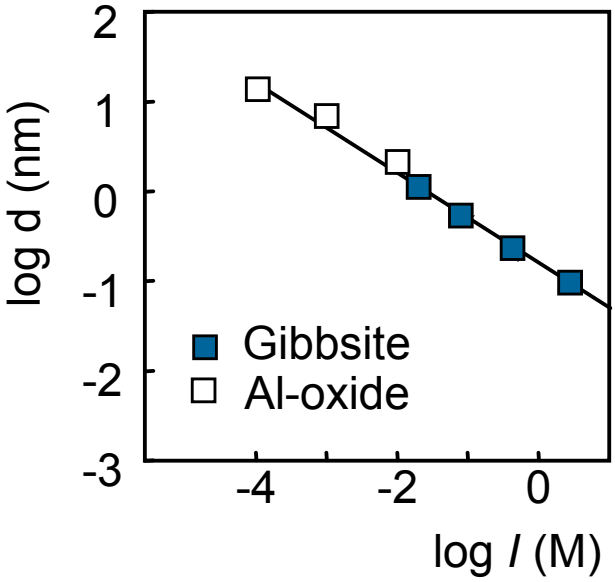

Fig.11. Empirical relation between the ionic strength and the apparent location of the plane of shear found for gibbsite (Fig.10) and an aluminum oxide (Fig.16). The location is expressed as the distance *d* from the head end of the DDL.

We have quantified the location of the plane of shear in the gibbsite interface in order to describe accurately the electrokinetic data. We found that the empirical distance between the plane of shear and the head end of the DDL is proportional with the root of the ionic strength of the equilibrium solution, i.e. it is proportional with the reciprocal Debye length $1/\kappa$ (see Fig.11). The empirical distance between the plane of shear and the head end of the double layer was found to be equal to $(2\kappa)^{-1}$ for gibbsite.

Electrolyte ion adsorption

The assumption of ion pair formation leads to the adsorption of electrolyte ions not only in the diffuse double layer as counter ion, but also in the adsorption plane at the solution side of the Stern layer. One data set with respect to electrolyte counter and co-ion adsorption has been presented in literature for a gibbsite with known crystal dimensions (Wendelbow 1987). This data set will be analyzed here. The gibbsite was prepared with the same procedure as used in this study (Gastuche and Herbillon 1962). The data are presented in Fig.12.

We were able to model the data set, using the same capacitance (C = 0.9 F/m^2) and the same set ion pair formation constants as used for the description of the zeta potentials in Fig.10 (asymmetrical ion pair formation). Using only the edge area as being reactive leads to a good description of the Cl adsorption which is mainly present at pH <10 (solid line in Fig 12). However, with this assumption we underestimate the Na adsorption at high pH. In case we account for the reactivity of the 001 face, additional Na is adsorbed since the 001 face becomes negatively charged at high pH. The use of the predicted protonation constant for the

reactive doubly coordinated surface group of the 001 face ($\log K_{2,1}$ = 11.9) and the experimental crystal face surface areas (Table II), leads to the results given in Fig.12. The calculations show that the simultaneous presence of cation and anion adsorption (Fig.12) is *a priori* not a prove of the ion pair formation concept, if oxide minerals have different crystal faces, which each react independently.

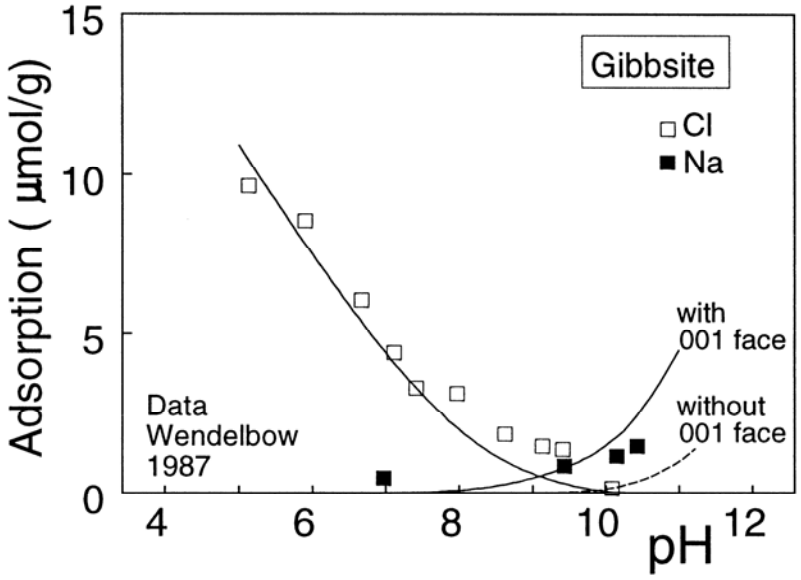

Fig.12. Adsorption of Na and Cl by gibbsite (µmol/g), in a 0.001 M NaCl solution. Note that in the PZC Na and Cl ions are present simultaneously. The solid lines are model calculations, assuming reactivity on the edge and the 001 face. Excluding reactivity of the 001 face, which adsorbs Na at high pH, leads to the dashed line for Na. The Cl adsorption remains unaffected by existence of the 001 face. Parameter values used for the edge face: $\log K_{1,2}$ = 10, $\log K_{Cl}$ = -0.2, $\log K_{Na}$ = 0.2, C = 0.9 F/m^2, N_s = 8.15 s/nm^2, A = 8 m^2/g and for the 001 face: $\log K_{2,1}$ = 11.9, $\log K_{Na}$ = 0.2, C = 0.9 F/m^2, N_s = 13.8 s/nm^2, A = 32 m^2/g.

Al oxide

We will analyze the Al oxide charging behavior using the unique extensive data set of Sprycha (1989a,b), which comprises not only proton titration data but also measurements of the electrolyte ion adsorption and the zeta potential. The data are combined with direct experimental information (Bousse et al. 1983) on the surface potential of an Al-oxide Ion-Sensitive Field Effect Transistor (ISFET). The data sets on Al oxide in combination with the above presented evaluation of the surface chemistry of gibbsite, allow an adequate analysis of the interfacial chemistry of these materials.

The chemical surface composition of Al oxides is uncertain and several crystal structures are known. In the bulk structure of corundum (α-Al_2O_3), the Al ions are hexa-coordinated and the coordination of oxygen is 4. At the surface, also oxygens with a lower coordination can be found, ranging from singly to triply coordinated surface groups. At the 110 face for instance equal numbers of singly ≡AlOH, doubly ≡Al_2OH and triply ≡Al_3O coordinated surface sites are present. In other polymorphic Al-oxides, like γ-Al_2O_3, the

situation is even more complicated because the Al ion is not only present in hexa coordination (VI) but also in tetrahedral coordination of Al (IV) (Tsyganenko and Mardilovich, 1996). The refined MUSIC model (Hiemstra et al.1996) predicts a lower proton affinity for the reactive groups $\equiv Al(IV)OH^{-1/4}$ (log$K$ = 5), $\equiv Al(IV)Al(VI)O^{-3/4}$ (log$K$ = 7) and $\equiv Al(VI)_3O^{-1/2}$ (log$K$ = 6) in case of a Pauling bond valence of 0.5 v.u. The presence of these groups can be a reason for a lower PZC for some Al oxides. The PZC of the Al oxide of Sprycha (1989) and Bousse et al. (1983) was 8.

The values of the estimated affinities of the mentioned acidic groups are uncertain and the surface composition is unknown. In the modeling, the acidic groups are represented by an equivalent site ($SO^{-1/2}$). The protonation can be written as:

$$\equiv SO^{-1/2} + H^{+}(aq) \Leftrightarrow \equiv SOH^{+1/2} \quad K_{eq} \qquad [7]$$

The site density of the acid surface site is set for simplicity equal to that of the singly coordinated surface groups.

We will start the evaluation of the charging phenomena of Al oxide with the surface potential. The determination of the surface potential using an ISFET showed that Al-oxide has a near Nernstian surface potential with a mean slope of about 55 mV (Fig.13). The change of the surface potential is most affected by the difference in proton affinity of the sites expressed as a ΔpK. In case of equal site densities for both types of sites, the ΔpK is found to be approximately 2.0. In combination with the PZC value of 8.0, it leads to an affinity constant for the singly coordinated ≡AlOH of log$K_{1,2}$ = 9.0 and for the acid site of logK_{eq} = 7.0.

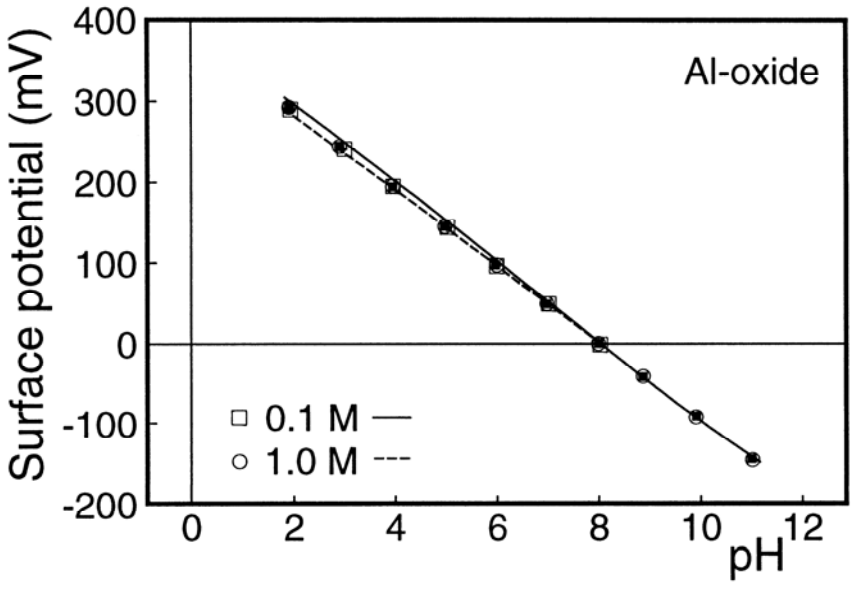

Fig.13 The experimental surface potential of Al oxide present on an ISFET (Data of Bousse et al. 1983) in 0.1 and 1.0 M NaCl. The lines have been calculated using the reactions and parameter values given in the appendix.

The combination of the proton affinity constants with the ion pair formation constants and capacitance derived for the gibbsite data (Fig.10 & 12), can be applied to the description of the proton titration data. The results are presented in Fig.14a as dashed lines. The predictions are good for the lowest two salt levels, but considerably off for the highest two electrolyte concentrations. The experimental data at high salt level are strongly asymmetrical around the PZC in contrast to the calculated proton adsorption curves. We have explored the possibilities of describing this phenomenon. We are only able to come to a consistent description of the whole data set (charging data, ion adsorption, zeta potentials, surface potentials) if we assume that some electrolyte ions (partly) penetrate the surface layer. This assumption implies the presence of porosity and surface roughness. For this Al oxide, porosity is likely since a considerable discrepancy exists between the surface area based on the particle size of 0.5-1.0 μm (A = 1-3 m^2/g) and the BET surface area of 154 m^2/g (Sprycha 1989a). To do the modeling, we assume that part of the sites (≡AlOH and ≡SO) is located sub surface (25%).

In the modeling, we used the recently developed Charge Distribution approach (CD model), in which three electrostatic planes are present. In this model, the proton charge is attributed to the surface (0-) plane, the adsorbed ion pairs are located in the 2-plane and the charge of inner sphere complexes (if present) is distributed over the 0- and 1- plane. The capacitance C_2 of the outer Stern layer is 5 F/m^2 (Hiemstra and Van Riemsdijk 1996). It implies that the inner Stern layer capacitance C_1 equals 1.0 F/m^2 if the total capacitance C is 0.9 F/m^2 ($1/C = 1/C_1+1/C_2$). In the appendix, one may find the detailed table of species, which forms the basis of the surfaces charge calculations in case of broken charges.

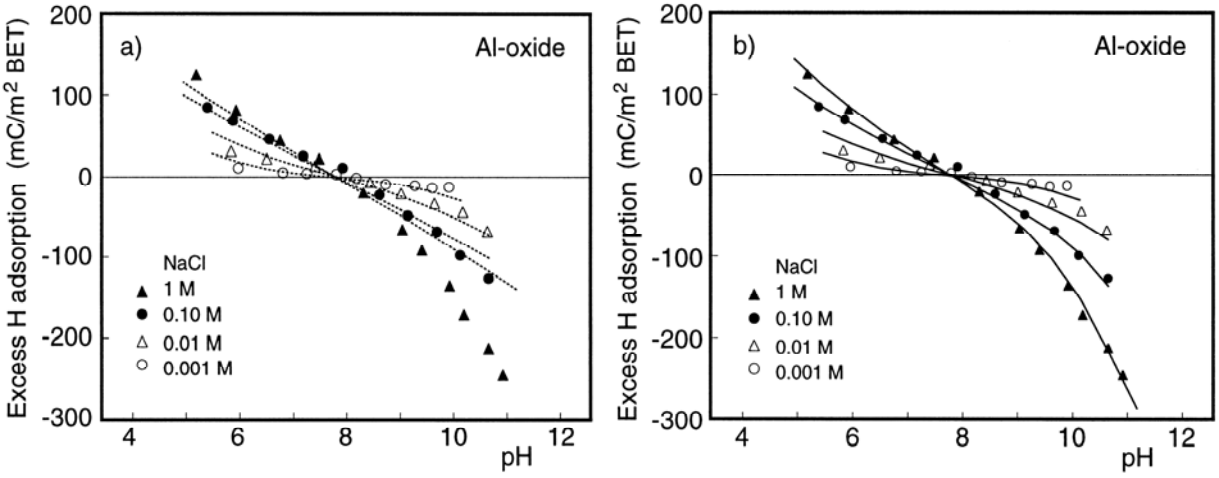

Fig.14 Proton binding on Al oxide in NaCl as a function of pH, showing a strong asymmetric behavior. The asymmetry is modeled assuming penetration of electrolyte ions into the surface (solid line in b). The dashed line (a) indicates the modeling without penetration of electrolyte ions, see text. The reactions are given in the Appendix.

In the present case of sub surface sites, the charge of the Na ion adsorbed on these sites has been fully attributed to the surface plane. The charge of the Cl is partly (50%) attributed to the surface and partly (50%) to the 1 -plane. This difference between Na and Cl on internal sites is maybe related to differences in ion size. The charge of the electrolyte ions bound on the other sites is treated in the normal way by locating it in the 2-plane. Using this approach in combination with the constraints imposed by the other data, we are able to describe the asymmetry in the titration curves (solid lines in Fig.14b) in contrast to the situation without this site (dashed lines in Fig.14a). It should be noticed that the data in Fig.14 are proton adsorption curves. Normally the H adsorption data are transformed into surface charge σ_0, assuming that the charge in the 0-plane only arises from the H adsorption. In case of a contribution of charge of Na and partly of the Cl ion, this cannot be done. So, the curves of Fig.14 are actually excess proton adsorption curves expressed in mC/m^2.

For the same Al oxide, also Na and Cl adsorption data are available. The data in Fig.15 refer to the Na en Cl adsorption within the plane of shear, which is slightly different from the total adsorption (Sprycha 1983). The description of the Na and Cl ion adsorption data is relatively sensitive to the chosen value for the total site density N_s, in combination with the affinity constants. In the PZC, the ion adsorption is independent of the electrostatics. A good description is found with a site density of N_s = 2.5 nm^{-2} for each normal surface site. The affinity constant for the Na and Cl ions corresponding to these sites is taken equal to the values found for gibbsite. The site densities of the singly and multiple coordinated SO sites, identified as sub surface sites, are each N_s = 0.8 nm^{-2}. The affinity constant for the ion pair formation with these sites is considerably lower and the ions pairs can be classified as very weakly bonded: $\log K_{Na} = \log K_{Cl}$ = -1.5. The model is in good agreement with all the experimental observations (Fig.12-15).

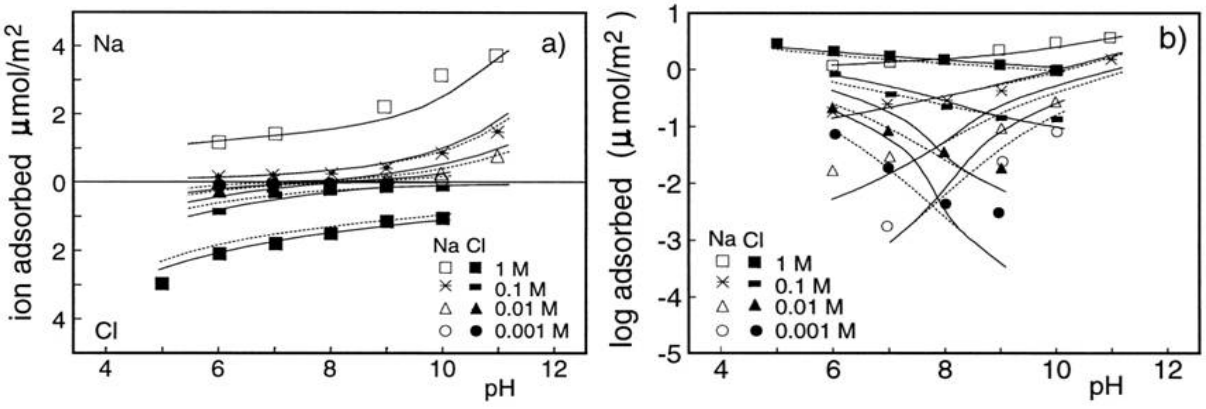

Fig.15 Adsorption of Na and Cl by Al oxide (µmol/m^2BET) on a linear (a) and logarithmic (b) scale for NaCl concentrations of 10^{-3} - 1 M. Note that in the PZC Na and Cl ions are present simultaneously. The lines are model calculations using the same data set as Fig.13, 14 and 16. Solid lines: total amount adsorbed. Dashed lines: adsorbed amount of ion pairs.

In summary, in the above modeling process we have distinguished two sites to account for the sub Nernstian behavior (Fig.12). Part of these sites (25%) have been identified as sub

surface sites, allowing electrolyte ion penetration in order to describe the asymmetry of the H adsorption at high electrolyte levels (Fig.13). Finally, the site densities have been established using ion adsorption data (Fig.14).

With the given parameter set, we are unable to describe the zeta potentials using the head end of the DDL as location of the plane of shear, since the reported values of this Al oxide (Fig.16) are far too low in comparison to our calculated values. Recently much higher values for the zeta potentials (factor 2 at 10^{-2} M) have been reported for Al_2O_3 (Johnson et al. 1998) which are in line with our predictions. This may question the validity of the zeta potential data. For an empirical description of the data of Fig.16, the location of the plane of shear has to be set in these cases much further away from the head end of the DDL. The derived distances are respectively 14, 7.0, and 2.5 nm. Analysis of the zeta potential data of Wiese and Healy (1975) leads to similar results. The distances are plotted in Fig.10 and follow the tendency as the data for gibbsite, i.e. the empirical distance increases with decreasing ionic strength.

Sprycha (1989a,b) has analyzed his data using a 2p*K*-TL type of approach. The TL approach has claimed to be able to describe simultaneously the surface charge and zeta potentials. However, Sprycha concluded that the analysis of his extensive data set, comprising surface charge, electrolyte adsorption and zeta potentials, indicates that in the TL approach the capacitance C_2 of the layer between the adsorbed electrolyte ions and the plane of shear must be taken to vary with the electrolyte ion concentration. If this variation in capacitance is interpreted in terms of distance (eq.[6]), his analysis is pointing to our approach of a variable thickness of the diffuse double layer part within the plane of shear.

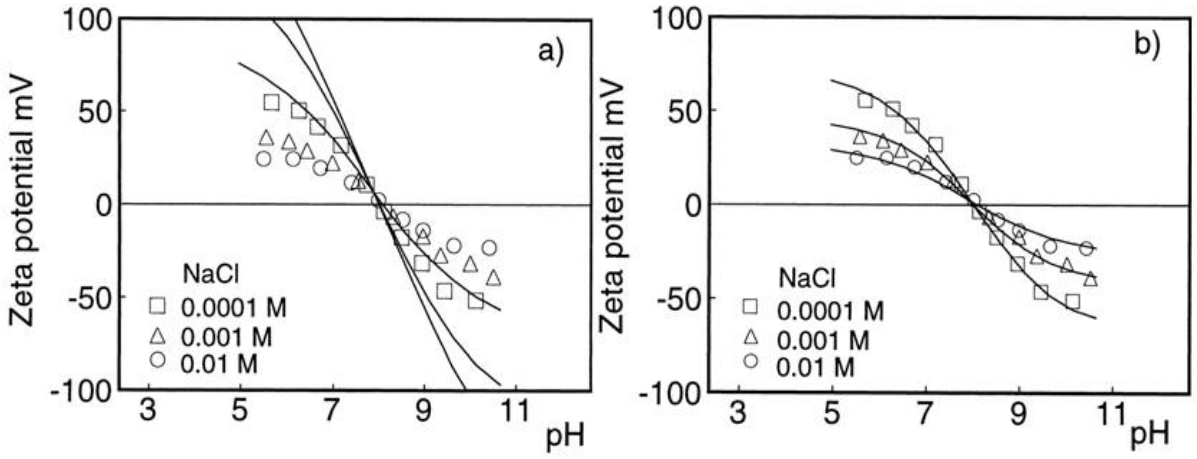

Fig.16. Zeta potential of Al oxide in solution of 10^{-4}, 10^{-3}, and 10^{-2} M $NaNO_3$. The lines are model calculations using the same parameter set as Fig. 13-15 and the fitted positions of the plane of shear. In part (a) the plane of shear is at the head end of the DDL and in part b, it is 14, 7.0, and 2.5 nm from the head end of the DDL.

Other minerals

One of the interesting conclusions we have drawn in the above given analysis is the absence of proton reactivity on the 001 surface of an Al hydroxide structure, which can be related to the presence of only doubly coordinated surface groups. Similar types of crystal planes are also found at boehmite (γ-AlOOH). This mineral has a lath type of crystal morphology with a 010 face, which has doubly coordinated surface groups (and inert fourfold bound oxygens). It is predicted that this mineral will not develop a high overall surface charge if it is well crystallized. This mineral will have a limited reactivity, because the face not only remains uncharged, it also does not adsorb ions like for instance PO_4 via a ligand exchange reaction as shown by Lewis and Farmer (1986). The limited reactivity also follows from a study in which the adsorption of benzoic acid on corundum (α-Al_2O_3) and boehmite (γ-AlOOH) were compared (Madsen and Blokhus 1994).

The presence of an inert crystal plane with only doubly coordinated $\equiv Al_2OH^o$ surface groups is also found on the clay mineral kaolinite ($Al_2Si_2O_5(OH)_4$). Well crystallized kaolinite will only be charged by proton ad-or(de)sorption on the edges of the mineral. It has been shown (Ferris and Jepson 1975) that Na adsorption increases strongly above pH 10, which can be explained from the deprotonation of doubly coordinated $\equiv Al_2OH^o$ of the 001 face. In the pH range below about pH 10, the 001 face remains uncharged. For this mineral, it has also been suggested that anion adsorption such as PO_4 adsorption is restricted to only the edge surfaces (Muljadi et al. 1966).

Conclusions

The above presented results can be summarized in the following conclusions:

- Gibbsite preparations show a very large difference in experimental charging. The strong difference in proton reactivity is related to the difference of the relative presence of crystal phases, which react differently. The edge faces of well-crystallized gibbsite are proton reactive in the pH range 4-10, in contrast to the planar 001 face, which is not reactive in this pH range. On gibbsite, singly coordinated surface groups are responsible for the charging behavior in the range 4-10. Doubly coordinated surface groups on the 001 face become only negatively charged at pH value of 10 and higher. Less well-crystallized gibbsite preparations may exhibit a higher protonation than is expected based on edge protonation alone and this may be due to defects and steps on the planar 001 side of the crystal.
- The PZC of gibbsite and the logarithm of the protonation constant of singly coordinated surface ≡AlOH groups are in agreement with the refined MUSIC predictions. The electrostatic inner layer capacitance of well-crystallized gibbsite edge surfaces is 0.9 ± 0.1 F/m^2 (Basic Stern approach) and is equal to that of well-crystallized goethite interfaces.
- The interfacial properties of Al (hydr)oxides can only be well understood using the ion pair formation concept. Ion pair formation differs for cations and anions (asymmetry)

and can be modeled using a different intrinsic affinity constant or a different electrostatic position. If the latter factor dominates, the simple electrolyte anions are located closer to the surface than electrolyte cations.

- Asymmetry in charging curves may result from electrolyte ions, which penetrate the surface differently. Asymmetry in charging curves may also result from the presence of differently reacting crystal planes, like the edge faces of gibbsite (positively or negatively charged over a very large pH range) and the planar 001 face which is uncharged below pH 10 and contributes only to the overall (negative) charged above pH 10.
- Reported zeta potentials are often too low to be only in line with the other experimental surface properties (proton adsorption, electrolyte ion adsorption, surface potentials) within a BS concept. Such data can be described if the plane of shear is not set at the head end of the DDL, but located in the DDL at some distance from the Stern layer.
- The surface potential of Al_2O_3 measured with an ISFET can be explained if heterogeneity of the surface is considered.

Acknowledgements

Mr.Th.A. Vens is gratefully acknowledged for assistance during the experimental work. Thanks are also due to Mr. A.J. Korteweg (Laboratory of Physical and Colloid Chemistry) and the Department of Chemistry, RU Utrecht for the BET analysis. We also thank Mr. J.D.J. Van Doesburg (Laboratory of Soil Science & Geology) for the x-ray diffraction analysis. Mr. Ehlerie is gratefully acknowledged for his contribution in the characterization of the gibbsite and bayerite using TEM.

References

1 Hingston, F.J., Posner, A.M., and Quirk, P.J., *J. Soil Sci*. 23, *177* .1972

2 Ferris, A.P., and Jepson, W.B., *J. Colloid Interf. Sci.,* 51, *245* (1975)

3 Mashali, A.M. in: Greenland, D.J., and Mott, C.J.B., in "The chemistry of soil constituents" (Greenland, D.J., and Hayes, M.H.B. eds.) Wiley, New York, 1978.

4 Wendelbow, R., PhD Thesis, University of Oslo, 1987

5 Kavanagh, B.V. , Posner, A.M., and Quirk, P.J., *Disc. Farad. Soc.,* 59, *242* (1975)

6 Pulver, K., Schindler, P.W., Westall, J.C., and Grauer, R., *J. Colloid Interface Sci.* 101, *554* (1984)

7 Hiemstra, T., Van Riemsdijk, W.H., and Bruggenwert, M.G.M., *Neth. J. Agric. Sci*. 35, *281* (1987)

8 Hiemstra, T., De Wit, J.C.M., and Van Riemsdijk, W.H*., J. Colloid Interface Sci*. 133, *105* (1989).

9 Parfitt, R.L., Fraser, A.R., Russell, J.D., and Farmer, V.C., *J. Soil Sci.* 28, 40 (1977)

10 Van Riemsdijk, W.H., and Lyklema, J*., Colloids Surf.* 1,*33* (1980).

11 Hiemstra, T., Van Riemsdijk,W.H., and Bolt,G.H.,. *J. Colloid Interface Sci.* 133, *91* (1989).

12 Hiemstra, T., Venema,P., Van Riemsdijk, W.H., *J. Colloid Interface Sci*., 184, *680* 1996

13 Kinniburgh, D.G., PhD Thesis, University of Wisconsin, Madison, USA. (1994)

14 Anderson, M.A., and Malotky, D.T., *J. Colloid Interface Sci.* 72, *413* (1979)

15 Hiemstra, T., and Van Riemsdijk, W.H., *Colloid Surf*. 59, *7* (1991).

16 Hiemstra, T., and Van Riemsdijk, W.H., *J. Colloid Interface Sci.* 179, *488* (1996).

17 Sprycha, R., *J. Colloid Interf. Sci*., 127, 1 (1989a)

18 Sprycha, R., *J. Colloid Interf. Sci.,* 127, *12* (1989b)

19 Sprycha, R., *J. Colloid Interf. Sci*., 96, *551* (1983)

20 Bousse, L., De Rooij, N.F., and Bergveld, P., *Surf. Sci*. 135, *479* (1983).

21 Van Hal, R.E.G., PhD Thesis, University Twente, Enschede, The Netherlands (1995)

22 Hsu, Pa Ho, in "Minerals in Soil Environments" (Dixson,J.W., and Weed, S.B. eds.) SSSA Book series:1, second ed., Madison, USA, 1989.

23 Van Riemsdijk, W.H., Bolt, G.H., Koopal, K.L., and Blaakmeer, J., J. *Colloid Interface Sci.* 109, *219* (1986)

24 Gastuche, M.C., and Herbillon, A., *Bull. Soc. Chim. France* 1, *14*

25 Pauling, L., The principles determining the structure of complex ionic crystals. *J.Am.Chem.Soc*. 51, *1010* (1929)

26 Sposito, G., "The surface chemistry of soils". Oxford Univ.Press, New York, 1984.

27 Westall, J. and Hohl, H., *Adv.Colloid Interf.Sci*., 12, *265* (1980)

28 Hiemstra, T., and Van Riemsdijk, W.H., *Colloids and Surf.,* 59,*7* (1991)

29 Van Straten, H.A., and De Bruyn, P.L., *J.Colloid Interface Sci.* 102, *260,* (1984)

30 Greenland, D.J., and Mott, C.J.B., in "The chemistry of soil constituents" (Greenland, D.J., and Hayes, M.H.B. eds.) Wiley, New York, 1978.

31 Yates, D.E., Levine, S., and Healy, T.W., *Chem. Soc. Faraday Trans.I, 70,1807* (1974)

32 Yates, D.E., The structure of the oxide/aqueous electrolyte interface Ph.D.thesis, University of Melbourne, Melbourne, 1975.

33 Davis, J.A., James, R.O., and J.O. Leckie., *J. Colloid Interface Sci*. 63, *480* (1978)

34 Shiao, S.-Y., and Meyer, R.E., *J.Inorg.Nucl.Chem*. 43, *3301* (1981)

35 Lützenkirchen, J., Magnico, P., and Behra, P., *J. Colloid Interface Sci*. 170, *326* (1995)

36 Rowlands, W.N., O'Brien, R.W., Hunter, R.J., and Patrick, V., *J. Colloid Interface Sci*. *188*, *325* (1997).

37 Davis, J.A., and Kent, D.B., in "Mineral-Water Interface Geochemistry" Reviews in Mineralogy (Hochella M.F., and White, A.F., Eds.), Vol.23, p.177., Miner.Soc.Am., Wasinghton D.C., 1990.

38 Dzombak, D.A., and Morel, F.M.M., "Surface complexation modeling: Hydrous Ferric Oxide", John Wiley, New York, 1990.

39 Schudel, M., Behrens, H., Holthoff, H., Kretzschmar, R., and Borkovec, M., *J. Colloid Interface Sci*. 196, *241* (1997)

40 Kosmulski, M., and Rosenholm, J.B., *J. Phys. Chem.* 100, *11681* (1996)

41 Charmas, R., and Piasecki, W., *Langmuir* 12, *5458* (1996).

42 Machesky, M.L., Wesolowski, D.J., Palmer, D.A., and Ichiro-Hayashi, K., J. *Colloid Interf. Sci.* 200*, 298* (1998)

43 Johnson, B., Rusell, A.S., and Scales, P.J., *Colloids Surf. A* 141, *119* (1998).

44 Sprycha, R., *J. Colloid Interf. Sci.,* 102, *173* (1984)

45 Healy, T.W., White, L.R., *Adv. Colloid Interface Sci*. 9, *303* (1978)

46 Tsyganenko, A.A., and Mardilovich, P.P., *J. Chem. Soc. Faraday Trans*. 92, *4843* (1996)

47 Wiese, G.R., and Healy, T.W., *J. Colloid Interface Sci*. 51, *427 (*1975)

48 Madsen, L., and Blokhus, A.M., *J. Colloid Interface Sci*. 166, 259 (1994)

49 Lewis, D.G., and Farmer, V.C., *Clay Minerals* 21, *93* (1986)

50 Muljadi, D., Posner, A.M., and Quirk, P.J., *J.Soil Sci*. 17, *230* (1966)

Appendix

Gibbsite

The relations for the calculation of the primary charging of the gibbsite can be defined in a table of species. The formation reactions of the single site one-p*K* approach are described in the text. The table refers to the BS model.

Components Species (mol/L)	$e^{-F\psi o/RT}$	$e^{-F\psi 1/RT}$	≡AlOH	H	C	A	log*K*
$\equiv AlOH^{-1/2}$	0	0	1	0	0	0	0
$\equiv AlOH_2^{+1/2}$	1	0	1	1	0	0	$\log K_{1,2}$
$\equiv AlOH^{-1/2}$ -C^+	0	1	1	0	1	0	$\log K_C$
$\equiv AlOH_2^{+1/2}$ -A^-	1	-1	1	1	0	1	$\log K_A+\log K_{1,2}$
Sum	Σ_1	Σ_2	Σ_3	Σ_4	Σ_5	Σ_6	

$$\Sigma_1 = \rho A / F\ (\sigma_0 - zFN_s) \quad [A\text{-}1]$$

$$\Sigma_2 = \rho A / F\ \sigma_1 \quad [A\text{-}2]$$

$$\Sigma_3 = \rho A N_s \quad [A\text{-}3]$$

$$\Sigma_4 = H(t)\text{-}OH(t) \quad [A\text{-}4]$$

$$\Sigma_5 = C(t) \quad [A\text{-}5]$$

$$\Sigma_6 = A(t) \quad [A\text{-}6]$$

$$\sigma_0 = C\ (\psi_o\text{-}\psi_1) \quad [A\text{-}1a]$$

$$\sigma_1 = C\ (\psi_1\text{-}\psi_0) \pm 1/2\ \sqrt{(8000\ \varepsilon_r \varepsilon_o RT)}\ \sqrt{(\Sigma\ C_i\ \{e^{-zi\ F\psi 1\ /\ RT)}\text{-}1\})} \quad [A\text{-}1b]$$

In the above table, $\log K_{1,2}$ is the intrinsic protonation constant for singly coordinated surface groups. The $\log K_C$ and $\log K_A$ are respectively the pair formation constants of the electrolyte cations C^+ and anions A^-. Note that all log*K* values are based on intrinsic constants, adjusted for activity corrections in the case of $I \neq 0$. The activity coefficients were calculated using the Davies equation as defined in Hiemstra and Van Riemsdijk (1996).

The parameters in the summation terms are: ρ the solid solution ratio in kg L^{-1}, *A* the specific surface area in $m^2\ kg^{-1}$, F the Faraday constant (C mol^{-1}), σ_o and σ_1 the charge (C m^{-2}) in respectively the 0- and 1- plane, *z* the charge of the surface reference group, i.e. ≡AlOH (*z* = -0.5). The parameter N_s (in mol m^{-2}) represents the site density. The ψ_0 and ψ_1 are the electrostatic potential (V) of respectively the 0- and 1-plane, *C* the capacitance of the layer between the 0- and 1-plane, ε_o the absolute dielectric constant (C V^{-1} m^{-2}), ε_r the relative dielectric constant, R the gas constant (J $mol^{-1}K^{-1}$), T the absolute temperature (K), C and A the concentrations of the dissolved electrolyte solution species with charge z_i.

Al-oxide

The primary charging of the Al oxide leads to a slightly more complicated table of species, due to the presence of singly (≡AlOH) and multiple (≡SO) coordinated sites. In addition, subsurface location of part of these sites is assumed (b-sites). Since Cl ions, which associate with these b-sites, do not fully penetrate the surface, part of the charge is placed in a separated plane between the surface and the head end of the DDL layer. This leads to the CD approach with an electrostatic three-plane model (Hiemstra and Van Riemsdijk 1996).

The parameters in the summation terms, σ_0, σ_1, and σ_2 (of the table below) refer to the charge in respectively the 0-, 1-, and 2- plane. The charge of the surface reference groups ≡AlOH and SO is $z_1 = z_2 = -0.5$. The value $N_{s,j}$ (in mol m^{-2}) represents the site densities of the normal surface sites ≡aAlOH and ≡aSO ($N_{s,a} = 2.5$ $nm^{-2} = 4.17$ μmol m^{-2}) and the sub surface sites ≡bAlOH and ≡bSO ($N_{s,b} = 0.8$ $nm^{-2} = 1.33$ μmol m^{-2}). The ψ_0, ψ_1, and ψ_2 are the electrostatic potential (V) of respectively the 0-, 1-, and 2- plane, C_1 the capacitance of the layer between the 0- and 1- plane, and C_2 the capacitance of the layer between the 1- and 2-plane. In the modeling of the Al-oxide data (Figs.13-16), we used $\log K_{H1} = 9.0$ and $\log K_{H2} = 7.0$, $\log K_{C1} = +0.2$ and $\log K_{A1} = -0.2$ (as for gibbsite), $\log K_{C2} = -1.5$ and $\log K_{A2} = -1.5$, $C_1 = 1.0$ F/m^2 and $C_2 = 5.0$ F/m^2.

Table

Components Species (mol/L)	$e^{-F\psi o/RT}$	$e^{-F\psi 1/RT}$	$e^{-F\psi 2/RT}$	≡aAlOH	≡aSOH	≡bAlOH	≡bSOH	H	C	A	log*K*
$\equiv aAlOH^{-1/2}$	0	0	0	1	0	0	0	0	0	0	0
$\equiv aAlOH_2^{+1/2}$	1	0	0	1	0	0	0	1	0	0	$\log K_{H1}$
$\equiv aAlOH^{-1/2}$ -C^+	0	0	1	1	0	0	0	0	1	0	$\log K_{C1}$
$\equiv aAlOH_2^{+1/2}$ -A^-	1	0	-1	1	0	0	0	1	0	1	$\log K_{A1}+\log K_{H1}$
$\equiv aSOH^{-1/2}$	0	0	0	0	1	0	0	0	0	0	0
$\equiv aSOH_2^{+1/2}$	1	0	0	0	1	0	0	1	0	0	$\log K_{H2}$
$\equiv aSOH^{-1/2}$ -C^+	0	0	1	0	1	0	0	0	1	0	$\log K_{C1}$
$\equiv aSOH_2^{+1/2}$ -A^-	1	0	-1	0	1	0	0	1	0	1	$\log K_{A1}+\log K_{H2}$
$\equiv bAlOH^{-1/2}$	0	0	0	0	0	1	0	0	0	0	0
$\equiv bAlOH_2^{+1/2}$	1	0	0	0	0	1	0	1	0	0	$\log K_{H1}$
$\equiv bAlOH^{-1/2}$ -C^+	0	0	1	0	0	1	0	0	1	0	$\log K_{C2}$
$\equiv bAlOH_2^{+1/2}$ -A^-	1	0	-1	0	0	1	0	1	0	1	$\log K_{A2}+\log K_{H1}$
$\equiv bSOH^{-1/2}$	0	0	0	0	0	0	1	0	0	0	0
$\equiv bSOH_2^{+1/2}$	1	0	0	0	0	0	1	1	0	0	$\log K_{H2}$
$\equiv bSOH^{-1/2}$ -C^+	1	0	0	0	0	0	1	0	1	0	$\log K_{C2}$
$\equiv bSOH_2^{+1/2}$ -A^-	0.5	-0.5	0	0	0	0	1	1	0	1	$\log K_{A2}+\log K_{H2}$
Sum	Σ_1	Σ_2	Σ_3	Σ_4	Σ_5	Σ_6	Σ_7	Σ_8	Σ_9	Σ_{10}	

$$\Sigma_1 = \rho A / F\ (\sigma_0 - zFN_s) \quad \text{[A-1]}$$

$$\Sigma_2 = \rho A / F\ \sigma_1 \quad \text{[A-2]}$$

$$\Sigma_3 = \rho A / F\ \sigma_2 \quad \text{[A-3]}$$

$$\Sigma_4 = \rho A N_{s,a} \quad \text{[A-4]}$$

$$\Sigma_5 = \rho A N_{s,a} \quad \text{[A-5]}$$

$$\Sigma_6 = \rho A N_{s,b} \quad \text{[A-6]}$$

$$\Sigma_7 = \rho A N_{s,b} \quad \text{[A-7]}$$

$$\Sigma_8 = H(t)\text{-}OH(t) \quad \text{[A-8]}$$

$$\Sigma_9 = C(t) \quad \text{[A-9]}$$

$$\Sigma_{10} = A(t) \quad \text{[A-10]}$$

$$\sigma_0 = C_1(\psi_o\text{-}\psi_1) \quad \text{[A-1a]}$$

$$\sigma_1 = C_2\ (\psi_1\text{-}\psi_2) - C_1\ (\psi_o\text{-}\psi_1) \quad \text{[A-2a]}$$

$$\sigma_2 = C\ (\psi_2\text{-}\psi_1) \pm 1/2\ \sqrt{(8000\ \varepsilon_r\ \varepsilon_o\ RT)}\ \sqrt{(\Sigma\ C_i\ \{e^{-zi\ F\psi 2\ /\ RT}\text{-}1\})} \quad \text{[A-3a]}$$

Chapter 4

A Surface Structural Approach to Ion Adsorption: The Charge Distribution (CD) model

Tjisse Hiemstra and Willem H. Van Riemsdijk

Published in Journal of Colloid and Interface Science
Volume 179, Issue 2, Pages 488-508, May 10, 1996

Abstract

An ion adsorption model for metal hydroxides has been developed which deals with the observation that in the case of inner sphere complex formation only part of the surface complex is incorporated into the surface by a ligand exchange reaction while the other part is located in the Stern layer. The charge distribution (CD) concept of Pauling, used previously in the multi site complexation (MUSIC) model approach, is extended to account for adsorbed surface complexes. In the new model, surface complexes are not treated as *point* charges, but are considered as having a *spatial* distribution of charge in the interfacial region. The new CD model can describe within a *single* conceptual framework *all* important experimental adsorption phenomena, taking into account the chemical composition of the crystal surface. The CD model has been applied to one of the most difficult and challenging ion adsorption phenomena, i.e., PO_4 adsorption on goethite, and successfully describes simultaneously the basic charging behavior of goethite, the concentration, pH, and salt dependency of adsorption, the shifts in the zeta potentials and isoelectric point (IEP), and the OH/P exchange ratio. This is all achieved within the constraint that the experimental surface speciation found from *in situ* IR spectroscopy is also described satisfactorily.

Introduction

Cation and anion adsorption at the solid/solution interface of metal (hydr)oxides plays an important role in several fields of chemistry, including colloid and interface chemistry, soil chemistry and geochemistry, aquatic chemistry, environmental chemistry, catalysis and chemical engineering. A large number of models, describing adsorption, is available (1-8). These differ in the formulation of the surface reactions and/or in the description of the electrostatic double layer. Further progress in the unification and development of models is desirable.

Various adsorption phenomena can be studied experimentally. Adsorption has frequently been studied as a function of pH, and data are either presented as adsorption isotherms or as so-called 'adsorption edges'. Such primary data are often fitted to an adsorption model. Given a limited data set, many models can often describe such data reasonably well. However, the underlying physical chemical nature of these adsorption models can be very different and additional information may help to discriminate between the various options. For instance, measurement of the electrolyte dependency of ion adsorption or the simultaneous release or uptake of protons may be informative since the experimental proton balance can be related to the change in particle charge. This type of information can be extended with measurements of the shift in electromobility and the resulting shift of the Iso Electric Point (IEP) following ion adsorption. The study of competition and synergistic adsorption of ions may also yield valuable additional information. Unfortunately, such extended data sets for one particular ion and for one surface are not available. This limits the possibility of discriminating between the various models. At present, model development can only be achieved by a critical combination of data sets from various authors covering a broad range of adsorption phenomena.

An important aid to the process of model development is the availability of detailed molecular information about the ion adsorption mechanism resulting from powerful new in situ spectroscopic techniques. It has been known for quite sometime that ions, such as phosphate, may be adsorbed by ligand exchange (9-12). However, only recently quantitative data have become available for the surface speciation. For example, in situ Cylindrical Internal Reflection - Fourier Transformed InfraRed spectroscopy (CIR-FTIR) has shown that the binuclear bidentate $\equiv(FeO)_2PO_2$ surface complex is the dominant adsorbed phosphate species at neutral pH values, and that one of the solution oriented ligands of this complex may be protonated at low pH (13). These measurements have also shown that the ratio of protonated/non-protonated PO_4 surface complexes is dependent on the phosphate concentration. This detailed quantitative information will be used in the present paper.

The ligand exchange process can be considered as an obstacle in model development (14). It has usually been treated in a rather simplistic way, in the sense that the adsorbing ions have been treated as point charges. In the case of oxyanion adsorption, for example, only part of the adsorbing molecule is incorporated into the surface. This changes an OH(H) surface ligand into an oxygen O. It is clear from the structure of the interface that only part of the adsorbed molecule is incorporated into the surface structure while the other part is present in

the so-called Stern layer. Here we extend the Charge Distribution (CD) approach of our earlier MUSIC model (15,16) by including adsorbed surface complexes.

Additional useful information for model development may also be available from the solid side of the interface. The adsorption of ions is dependent on the crystal surface structure (17-22), which is related to the surface chemical composition. Several types of groups may be present at the surfaces and these may differ in their coordination with the metal (Me) ions of the solid bulk mineral. This implies that model parameters related to the surface composition (type and number of surfaces groups) will be determined by the crystal planes present. Therefore, the relevant model parameters should not be a priori available as free fitting parameters, but should be constrained by the physical-chemical reality.

Based on the above considerations, we present a new model, which can incorporate surface structural information. It treats both cation and anion adsorption in the same way and is based on the Pauling concept of Charge Distribution of ions over the coordinating ligands (23). It will therefore be referred to as the CD model. Phosphate adsorption on goethite has been chosen for testing and validating the CD model because it has been widely studied (9,11,13,19,24-28), shows a complex adsorption behavior, and important new spectroscopic data for the phosphate surface complex has recently become available (13).

Interface: between solid and solution

Classically a description of ion adsorption is based on well-known ideas of the solution side of the interface. The principle concept is based on the treatment of ions as point charges. For instance, the overall charge (z = -3) of an oxyanion such as PO_4^{3-}, made up from a P^{5+} ion and four surrounding O^{2-} ions, can be thought to be centered at one point. The classical Gouy-Chapman treatment of the diffuse double layer (3,29) is a typical example of the use of this concept. On the solid side of the interface, the concept of charge distribution introduced by Pauling in 1929 (23) is used. The MUSIC model (15) applies this concept to charged interfaces. Our new CD model combines both of these concepts. Inner sphere complex formation, responsible for most specific ion adsorption phenomena, will be described using this concept of charge distribution. Ion pair formation, being more solution-side oriented, will be described in terms of point charges.

Protonation and Surface Charge

Hydroxide and oxide interfaces are characterized by oxygens bound together by metal (Me) ions present in the bulk of the solid. The oxygens at the interface of (hydr) oxides may *in principle* bind protons in two consecutive steps, forming OH and OH_2 ligands, respectively. This may be written as:

$$O^{-2} + 2H^{+} \Leftrightarrow OH^{-1} + H^{+} \Leftrightarrow OH_2^0 \qquad [1]$$

Equation [1] shows that the surface may contain O^{-2}, OH^{-1}, and OH_2^0. In variable charge models, the overall charge at the surface (σ_0) is a basic property, which can be established by

counting the number of the various types of groups and their corresponding charge that are present at the interface. On the basis of Eq.[1], it is not possible to do this a priori because the surface oxygen is not only partially neutralized by protons, but is also partially neutralized by the Me ion(s) in the mineral structure. Therefore, the total charge of the surface group depends on the degree of neutralization coming from the Me ion(s) in the solid. The question that now arises is: "How much charge from the Me ion(s) in the solid should be attributed to the O^{2-}, OH^{-1}, and OH_2^o present at the interface?" The answer depends on how the charge of O^{2-} and OH^{1-} in the solid is neutralized, as discussed below.

Charge Distribution

Ionic crystals can be visualized as structures in which the interior ions are surrounded by neighbors of opposite sign. In stable oxide structures, the principle of electroneutrality implies that the charge of a cation is compensated by the charge of the surrounding oxygens. Therefore, the neutralization of the positive charge can be considered as being distributed over all the oxygens that coordinate to the cation. In turn, the charge of an oxygen ion is compensated by several cations and is therefore only partially neutralized by a single cation. If the degree of neutralization of charge is expressed per bond, the neutralization of the anionic charge will be equal to the sum of the coordinated cationic charges reaching the anion. This concept was introduced by Pauling (23) and is known as one of the Pauling rules (30). The symmetric distribution of charge over the surrounding bonds leads to the definition of a formal bond valence (v) as the charge (z) of a cation divided by its coordination number (CN):

$$\nu \equiv \frac{z}{\mathrm{CN}} \qquad [2]$$

Application of the CD concept leads to the definition of surface groups and their corresponding charge. For example, in the crystal structure of goethite, the Fe^{3+} ions (z = +3) are surrounded by 6 O(H) ligands (CN = 6). Applying Eq.[2], the charge per bond ν, attributed to one ligand will be ν = 1/2. At the surface of a mineral, the oxygens can be coordinated to 1, 2, or even 3 Fe^{3+} ions in the bulk, leading to singly, doubly, and triply coordinated groups, respectively. Applying the charge attribution concept to the surface oxygens presented in Eq.[1] leads for singly coordinated oxygens to the following surface species:

$$\equiv \mathrm{Fe\text{-}O}^{-3/2} + 2\mathrm{H}^+ \Leftrightarrow \equiv \mathrm{Fe\text{-}OH}^{-1/2} + \mathrm{H}^+ \Leftrightarrow \equiv \mathrm{Fe-OH_2}^{+1/2} \qquad [3]$$

The classical 2-pK models assume a priori an attribution of 1 unit charge per bond, leading to FeO^-, $FeOH^o$, and $FeOH_2^{+2}$ surface species.

Double layer structure

As described above, surface oxygens are neutralized by both Me ions belonging to the solid and a variable number of adsorbed protons. Depending on the solution pH, an excess or a deficiency of protons may be present at the interface, which leads to a positively or negatively charged surface, respectively. This surface charge, σ_0 (Fig.1), is compensated by electrolyte ions in a double layer, normally assumed to be a Diffuse Double Layer (DDL). The formulations of the diffuse and the compact part of the double layer are given in the Appendix. The concentration of the counter ions increases towards the surface (Fig.1). The co-ion concentration follows the opposite trend. The ions present in the DDL are hydrated and have a finite size, thereby preventing charge neutralization starting directly from the close-packed Me (hydr)oxide surface. The counter- and co-ions ions have a distance of closest approach to the surface. This has led to the formulation of a charge free layer, called the Stern layer (31). This double layer picture has been described as the Basic Stern (BS) model (32).

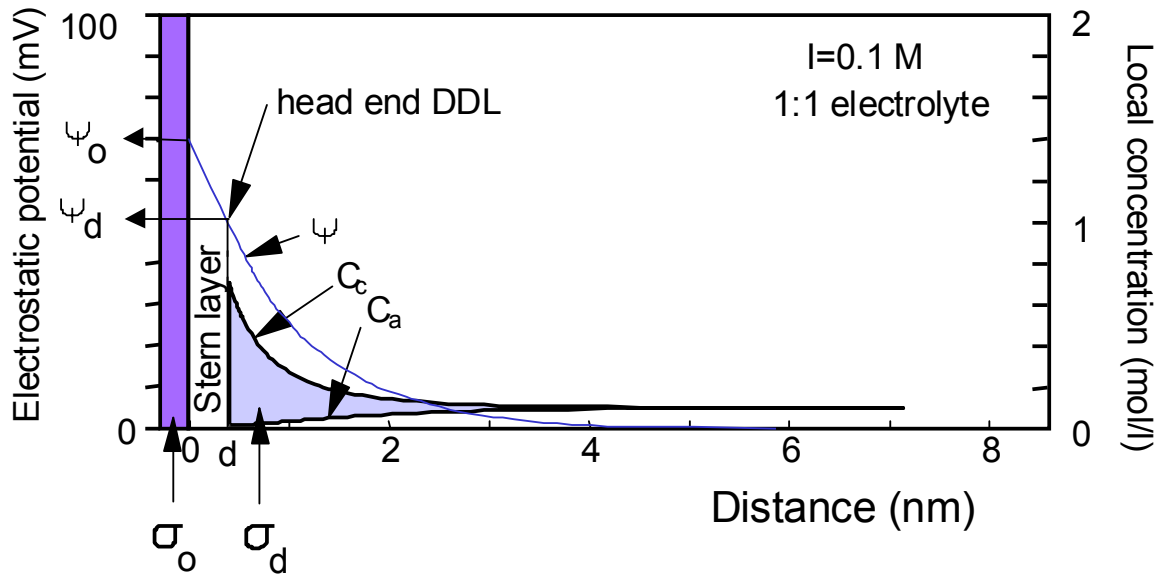

Fig.1 An example of the calculated charge distribution at the surface as given by the Basic Stern (BS) model. Surface charge (σ_0) is neutralized by charge in a double layer (σ_d). The double layer comprises an empty Stern layer, which may be treated as a plate capacitor, and a diffuse double layer in which the counter- and co-ions are located. The Stern layer is limited by two electrostatic planes. H ions are adsorbed in the surface plane (called 0-plane). The electrostatic plane at the head end of the diffuse double layer is called the d-plane. The electrostatic potential (ψ) and electrolyte ion concentration (C_c and C_a) are given as a function of distance from the surface. Although indicated as a rectangle with a given surface area, expressing an amount of charge, the surface charge σ_0 is theoretically located at a single position on the x- scale, i.e. located in a plane and not a layer.

As indicated in Fig.1, one may reach, even at low values of the surface potential, concentrations of 1 M or more at the head end of the DDL. From solution chemistry, it is known that electrolyte ions at high concentration may form ion pairs. A similar situation is present at the interface where the electrolyte ions may pair with surface groups (33). This

phenomenon of electrolyte ion / surface interaction has been confirmed by experiments (34,35). The adsorbed ions are considered as outer sphere complexes, involving ligand-ligand interactions, so the adsorbed ion remains separated from the surface group by an O or H_2O ligand. This implies that these ion pairs have a similar minimum distance of approach as the counter- and co-ions of the DDL. From this point of view, it is obvious that outer sphere complexes are adsorbed in an electrostatic plane positioned on the solution side of the Stern layer near the head end of the diffuse double layer. In the Gouy-Chapman concept of the DDL, ions are treated as point charges. We will also consider these charges as point charges.

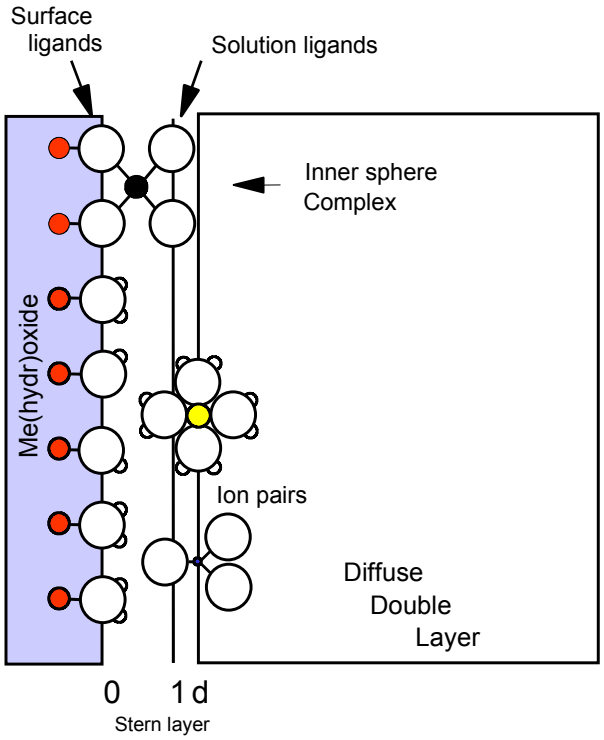

Fig.2 A schematic representation of the location of outer sphere complexes and inner sphere complexes at the interface. The outer sphere complexes are present at a position determined by the minimum distance of approach of (hydrated) ions to a closely packed Me (hydr)oxide surface and are treated, like the ions in the DDL, as point charges in the CD model. The inner sphere complexes are closer to the surface, penetrating the Stern layer. The surface complexes formed by ligand exchange, have common ligand(s) present at the same electrostatic position as the surface oxygens. The other ligands of the surface complex are thought to be located in a plane within the Stern layer region, called the 1-plane.

Let us now focus on the position of the central ion of surface complexes formed by the interaction of cations and anions (for example Cd^{2+}, Al^{3+}, $H_4SiO_4^o$, SeO_3^{2-}, and PO_4^{3-} etc.) with the solid through ligand exchange (Fig.2). These complexes are called inner sphere complexes (3). Due to ligand exchange, the inner sphere complexes are closer to the surface than the outer sphere complexes, leading to charge beyond the d-plane and within the Stern layer area. The inner sphere complexes are characterized by ligands, which are shared between Me ions of the solid and the central ion of the adsorbed complex. These common ligands are in the same position as the other (protonated) surface oxygens, OH(H) of the

MeOH and $MeOH_2$ surface species. The other - solution-oriented - ligands of the adsorbed complex are located within the Stern layer region in a hypothetical electrostatic plane, called the 1-plane. The double layer picture would remain simple if the position of the 1-plane and the d-plane coincided. As will be shown later, the experimental data do not allow this simplification to be made if adsorption is to be described over a wide range of indifferent salt concentrations. The above double layer picture, consisting of three electrostatic planes (0-, 1, and 2- or d- plane), will be called the Three Plane (TP) model.

Three Plane model

In the Three Plane model, three electrostatic planes are present, enclosing two empty layers in terms of charge, each with its own electrostatic capacitance. In the absence of specifically adsorbing ions, the TP model simplifies to the BS model because the mid plane does not contain any charge. The overall capacitance of the Stern layer region (C) in the BS and TP models, i.e. between the surface plane (0-plane) and the head end of the DDL (d-plane), can be found from classical acid-base titration data.

In the case of specific ion adsorption, the Stern layer region is divided into two layers separated by an electrostatic plane for the location of the solution-oriented ligands. The inner and outer layer capacitances, C_1 and C_2, respectively, are related to the overall Stern layer capacitance according to:

$$\frac{1}{C} = \frac{1}{C_1} + \frac{1}{C_2} \qquad [4]$$

The introduction of an additional electrostatic plane implies for the TP model that one of the capacitances of the two layers must be adjusted, while the other follows from Eq.[4], knowing the overall capacitance C from σ_0- pH data.

In the classical Triple Layer approach (33,36-38), here referred to as the TL model, the capacitance of the outer layer (C_2) is set to 0.2 F/m^2. As has been pointed out by Hiemstra & Van Riemsdijk (39), this assumption is based on a misinterpretation of the relation between the double layer properties of AgI and that of Me-(hydr)oxides. Analysis of the double layer properties of AgI and Me-(hydr)oxides has shown that the very low value for the capacitance of AgI ($C \equiv 0.2$ F/m^2) is due to the presence of strongly oriented water molecules in the first hydration shell of the Ag^+ and I^- ions of the solid. This strongly bound layer of hydration water is absent in the Me-hydroxide interface. It can be shown that for this reason, the overall capacitance of the Stern layer of Me (hydr)oxides is much greater than that of AgI. Our well-crystallized goethite preparation gives an overall experimental capacitance of about 0.9 F/m^2 (BS approach).

Locating charge

Once the location of complexes in the double layer has been defined, we can concentrate on the position of the charge. Part of the charge of an oxyanion complex, like adsorbed PO_4, is

present in ligands shared with the surface. The charge of the remaining ligands is placed at the physical position of these ligands, i.e. the 1-plane. As explained above (Eqs.[1]-[3]), the charge on surface oxygens can generally be found by taking into account the charge of the oxygen ion, a proton (if present) and the contribution of the Me ion(s) on the solid side of the surface (Fig.2). Extension of this concept to the Stern layer side of the surface implies that part of the neutralization of surface oxygens may be due to the presence of the central P^{5+} ion in the complex. A certain fraction *f* of the charge of the central cation in the complex will be attributed to the surface. The remaining part (1-*f*) is attributed to the other ligands of the complex, which are located in the 1-plane.

Several factors are responsible for the precise value of the charge distribution factor *f* of ions at the interface. A starting point is the Pauling bond valence concept (Eq.[2]). Let us apply this to an adsorbed silicic acid complex (Fig.3).

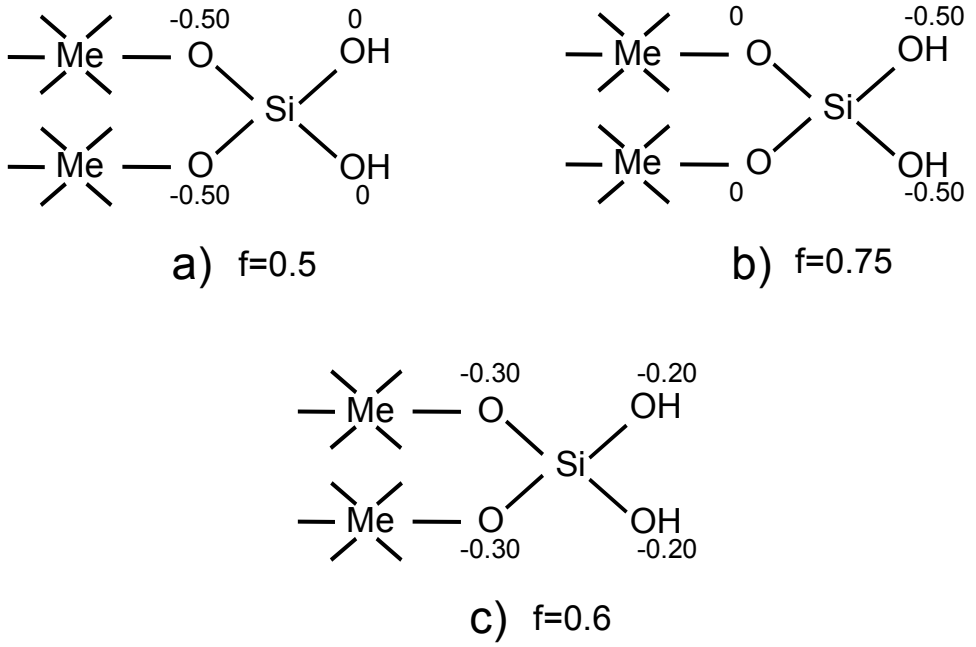

Fig.3 A schematic representation of a bidentate silicon oxo-complex bound to a Me hydroxide with trivalent Me ions in six fold coordination ($\nu = 3/6 = 0.5$). The charge of the various ligands is given for various choices of the value of the charge distribution factor *f*: (a) equal distribution of the charge of the central ion over the surrounding ligands; (b) an asymmetric distribution with neutral surface/solid oxygens; (c) the possible actual distribution with $f = 0.6$.

In Pauling's bond valence concept, ions tend to distribute charge equally over the coordinating ligands. The value of the charge distribution factor *f* of the Si ion is then defined as $f = n\ \nu_{Si}$, in which *n* is the number of common ligands ($n = 1$ for a monodentate, $n = 2$ for a bidentate) and ν_{Si} the bond valence. In the case of an equal distribution (i.e. one charge unit per bond), half ($f = 0.5$) of the charge of the Si ion is attributed to two surface oxygens and the remaining half to the solution-oriented ligands. As indicated in Fig.3 (Case a) for an adsorbed bidentate silicon surface complex, this gives neutral solution-oriented ligands ($z_{OH} = 0$) and negatively charged surface-oriented ligands ($z_O = -0.5$). An equal distribution of charge

may be in conflict with the Pauling concept of local neutralization of charge, which is related to the tendency of overall neutrality of the ligands in a solid. Because of adsorption, the former surface ligands become "buried" and therefore, will be more part of the solid. This implies that the surface ligands in the Me-ion surface complex may have a larger neutralization than the ligands on the solution side, leading to a larger value for *f*. If the common ligand in the solid/surface is fully neutralized, a situation as given in Fig.3b would result, equivalent to $f = 0.75$. Actually, for silicic acid adsorption on goethite, the data imply a value for *f* of about 0.6. This value can be considered as a trade-off between the two opposing tendencies described above. The corresponding charge on the ligands for this asymmetric distribution of the charge on the central ion is shown in Fig.3c. An additional complicating factor for a direct prediction of the value of *f* may be the presence of a covalent double bond in a surface configuration. Therefore, *f* is treated as an adjustable parameter in the CD model.

So far, we have not discussed the nature of the common ligands in a surface complex. If the common ligand is an oxygen ion, like the ones given in Fig.3, we might call the complex an oxo complex. If the ligand is a common OH group, found for instance in a Cu^{2+} or Cd^{2+} surface complex, it will be called a hydroxo complex. The distinction between oxo- and hydroxo complexes largely depends on the proton affinity of the common oxygen. The basic concepts of proton affinity are treated in our MUSIC model. The proton affinity is determined by the repulsive power(s) of the central ions surrounding the common O(H). Using the MUSIC model for estimating the log*K* values for protonation, it can be shown that the proton affinity of the common oxygen in an Fe-O-P or Fe-O-Si bond is too low to accept a proton in the normal pH range, while the proton affinity of an oxygen, bridging a Fe^{3+} and a divalent Cd ion, is high enough to give surface complexes with an OH as the common ligand, i.e. a Fe-OH-Cd linkage formed by the interaction of $\equiv FeOH^{-1/2}$ and Cd^{2+}. In the classical 2p*K* models, the formulated Me^{2+} surface complexes are quite different, since they are described as an Fe-O-Me linkage formed by FeO^- and Me^{2+} (37,41).

A combination of the CD factor *f* with a knowledge of the type of ligands around the Me centre (oxo- versus hydroxo-) can be used to calculate the changes in charge in the electrostatic planes during adsorption. This is required for the calculation of the electrostatic interaction energy of the adsorption reaction.

Adsorption energetics

The Gibbs free energy content, *G*, of a closed chemical system is composition dependent. At equilibrium, the system is in its minimum Gibbs free energy state and the change of *G* with the extent of the reaction is zero, written as $\Delta G_r \equiv 0$. This change of *G* can be written in terms of a standard Gibbs free energy ΔG_r^0 and a composition dependent Gibbs free energy change ΔG_c. The latter term (ΔG_c) can be defined as $RT \ln Q$, in which *Q* is the reaction quotient, related to the entropy of mixing of species. For adsorption reactions of charged species the first term is influenced by changes in electrostatic energy, ΔG_{el} (1,6,42,43). Formally, we may write for the equilibrium condition:

$$\Delta G_r \equiv \Delta G_r + \Delta G_c \equiv \Delta G_r + RT \ln Q \equiv \Delta G_r^{o} + \Delta G_{el} + RT \ln Q = 0 \quad [5]$$

The standard Gibbs Free energy change ΔG_r^0 can be connected by definition to the intrinsic reaction constant K_{in}, according to: $\log K_{in} \equiv - \Delta G_r^0 / 2.3RT$. The electrostatic energy change, ΔG_{el}, is variable due to the change in charge upon adsorption of ions and is determined by the electrostatic potential ψ according to $-z\mathrm{F}\psi$. The potential is generally calculated with an electrostatic model, in which the Charge Distribution of ions is involved. In Eq.[5], the value of the reaction quotient Q is also variable, depending on the composition of the system. From a thermodynamic-statistical point of view, the reaction quotient is generally expressed as:

$$RT \ln Q = RT \ln \Pi X_k^{r_k} \quad [6]$$

where generally one chooses for X_k of a species k, its mole fraction M_k. For gases, the mole fraction M_k is equivalent to the partial pressure P_k. For species in aqueous solution, the molar concentration C_k is normally chosen as the parameter for X_k. In dilute aqueous systems, C_k is directly proportional to the mole fraction M_k. The question is what should be chosen for X_k in the case of surface species?

Reaction quotients of mono- and bidentate adsorption reactions

Spectroscopic information about the binding of ions to surfaces has indicated that adsorbed ions may share one (monodentate) or two common ligands (bidentate) with the solid. In the literature, the reaction quotient for the bidentate surface reaction is often not clearly formulated in terms of the exponent for the surface component and the suggested exponent ranges from 1 to 2 (28,37,41,44). The definition of the reaction quotient, Q, should reflect (lattice) statistical effects as is done in the classical definitions of solution chemistry.

As an example, we will write the formulations for phosphate adsorption, which for the monodentate PO_4 adsorption can be written as:

$$\equiv \mathrm{FeOH}^{-1/2}(\mathrm{inf}) + \mathrm{H}^+(\mathrm{aq}) + \mathrm{PO}_4^{3-}(\mathrm{aq}) \Leftrightarrow \equiv \mathrm{FeO}^p\mathrm{PO}_3^q(\mathrm{inf}) + \mathrm{H}_2\mathrm{O}(\mathrm{l})\ ; K_1 \quad [7]$$

in which the index "inf" refers to the interface. The overall charge of the adsorption complex is attributed to the common oxygen in the surface (p) and three oxygens in the Stern layer (q). The sum of the charges p and q equals -2.5. The value of the overall reaction constant K_1 is a combination of the intrinsic constant K_{in1} and the (variable) electrostatic contribution, which depends on the location of the charge. One may write $K \equiv e^{-\Delta Gads/RT} \equiv e^{-(\Delta Gro + \Delta Gel) / RT}$. The definition of the reaction quotient Q for Eq.[7] in combination with the chemical equilibrium condition $\Delta G_r^0 = 0$ or $K = Q$, leads to:

$$K_1 = Q = \frac{\theta_{\mathrm{FeO}^p\mathrm{PO}_3^q}}{\theta_{\mathrm{FeOH}}} \frac{(\mathrm{H}_2\mathrm{O})}{[\mathrm{H}^+][\mathrm{PO}_4^{3-}]} \quad [8]$$

in which $[H^+]$ is the proton concentration and $[PO_4^{3-}]$ the concentration of PO_4^{3-} ions in solution and (H_2O) the activity of water (a mole fraction). Because of the statistical origin of the entropy contributions, the concentration of surface species in Eq.[8] has been defined on the basis of a mole fraction. This mole fraction θ for surface species i reacting with a type of surface group j can be defined generally as:

$$\theta_i = \frac{S_i}{N_{s,j}} \qquad [9]$$

in which S_i (mol/m^2) is the surface concentration of a species and $N_{s,j}$ the site density (mol/m^2) of surface group j.

In the case of monodentate adsorption, the definition based on mole fractions is equivalent to other definitions based on for instance mol/m^2, mol/g, or mol/L, because the units by which the surface species are represented cancel. This is not true for bidentate reactions.

The binding of phosphate in a bidentate complex can be written as:

$$2 \equiv \mathrm{FeOH}^{-1/2}(\mathrm{inf}) + 2\mathrm{H}^+(\mathrm{aq}) + \mathrm{PO}_4^{3-}(\mathrm{aq}) \Leftrightarrow \equiv (\mathrm{FeO})_2^p \mathrm{PO}_2^q(\mathrm{inf}) + 2\mathrm{H}_2\mathrm{O(l)}\ ; K_2 \qquad [10]$$

in which case two H^+ ions protonate the two surface OH groups forming chemically sorbed water which can be released in favor of two oxygens of PO_4. In this case, the sum of p and q equals -2. The reaction quotient Q in combination with the equilibrium condition can be defined as in Eq.[8]:

$$K_2 = Q = \frac{\theta_{(\mathrm{FeO})_2{}^p\mathrm{PO}_2{}^q}}{\theta_{\mathrm{FeOH}}^2} \frac{(\mathrm{H_2O})^2}{[\mathrm{H}^+]^2[\mathrm{PO}_4^{3-}]} \qquad [11]$$

in which the square term for ≡FeOH, resulting from the mass law, expresses the probability of finding two surface groups together in the same configuration in the lattice.

The thermodynamic constant should be independent of the experimental conditions such as the solid/solution ratio (g/L), surface area (m^2/L) etc. This is true if mole fractions are used in the definition of K rather than mol/L, mol/g, or mol/m^2. It is shown in the Appendix how this choice of unit may affect the calculations as formulated in the table of species.

Recent CIR-FTIR spectroscopic data have shown that one of the ligands of a phosphate bidentate complex may be protonated at low pH. The reaction defined in Eq.[10] can be extended by adding an extra proton which is needed to form the protonated ligand (OH):

$$2 \equiv \mathrm{FeOH}^{-1/2}(\mathrm{inf}) + 2\mathrm{H}^+(\mathrm{aq}) + \mathrm{PO}_4^{3-}(\mathrm{aq}) + \mathrm{H}^+(\mathrm{aq}) \Leftrightarrow \equiv (\mathrm{FeO})_2^p \mathrm{POOH}^q(\mathrm{inf}) + 2\mathrm{H}_2\mathrm{O(l)}\ ; K_3 \qquad [12]$$

This additional proton, written separately from the other protons in Eq.[12], will protonate one of the solution-oriented oxygens. It will give rise to a distinct electrostatic energy change (another Boltzmann accumulation factor) because it is not related to the 0-plane position as both other protons but in the 1-plane.

The corresponding reaction quotient and equilibrium condition for the above reaction is:

$$K_3 = Q = \frac{\theta_{(FeO)_2{}^{p}POOH^{q}}}{\theta^2_{FeOH}} \frac{(H_2O)^2}{[H^+]^3[PO_4^{3-}]} \qquad [13]$$

The difference between the log$K$ values for the protonated (logK_3) and non-protonated bidentate phosphate complex (logK_2) is related to the proton affinity constant for the protonation of the solution-oriented ligand (logK_{Hp}). One may write logK_{Hp} = logK_3-logK_2. This logK_{Hp} is related to the experimentally determinable (CIR-FTIR spectroscopy) ratio of ≡$(FeO)_2PO_2$ and ≡$(FeO)_2POOH$.

In summary, the changes in Gibbs Free energy are the sum of the contributions of the changes in standard Gibbs free energies $\Delta G_{ads}{}^{0}$ of adsorption (related to the intrinsic reaction constants K_{in}), changes in electrostatic energy ΔG_{el} (to be calculated) and changes related to the entropy of mixing RT ln$Q$. The concentrations of the surface components are best defined in terms of mole fractions (θ).

In the CD model, calculation of the electrostatic energy ΔG_{el} differs from the classical approach and this is discussed in the next paragraph.

Electrostatics

In the CD model, the electrostatic energy contribution (ΔG_{el}) is related to the electrostatic work done/released when the charge at position i with a certain potential (ψ) is changed by Δz_i according to:

$$\Delta G_{el} = \frac{\Delta z_i F}{RT} \psi_i \qquad [14]$$

In terms of the electrostatic contribution to the K value of the reaction this contribution equals $K_{el} = e^{-\Delta Gel / RT} = e^{-\Sigma \Delta z i F \psi i / RT}$ in which $e^{-F \psi i / RT}$ is the Boltzmann accumulation factor. In the cases where the adsorption contributes charge to different planes with different potentials, we have to know the individual charge attribution to each of these planes. This can be found by analyzing the change in charge resulting from surface complex formation. The net charge may change due to both adsorption and desorption reactions. The change of charge in the 0-plane (Δz_0) because of adsorption can be defined as:

$$\Delta z_0 = \Delta n_H z_H + f z_{Me} \qquad [15]$$

and for the 1-plane (Δz_1) as:

$$\Delta z_1 = (1 - f)\, z_{\mathrm{Me}} + \Sigma\, m_j\, z_j \qquad [16]$$

where Δn_{H} is the change in the number of protons on the surface ligand(s) involved in the surface reaction, z_{H} is the valence of the proton (+1) and f the charge distribution fraction. The change Δn_{H} depends on the number of common ligands (mono- or bidentate) and the change in the state of protonation of these ligands. The value of Δn_{H} may be positive, zero of negative. In Eq.[15] and Eq.[16], z_{Me} is the valence of the central ion in the surface complex. In Eq.[16], m_j is summed over the ligands positioned in the 1-plane and z_j is the charge on those ligands (z_j = 0, -1, or -2 respectively for an OH_2^o, OH^{1-}, or O^{2-} ligand).

As an example, we will derive the values of Δz_0 and Δz_1 for the bidentate phosphate adsorption reaction (Eq.[10]) in which two OH surface ligands are changed into two oxygens. This reaction implies a net release of two protons, i.e. Δn_{H} = -2. Knowing the value of the charge distribution fraction f of the central ion (f = 0.5 for P in $\equiv(FeO)_2PO_2$), the change in charge z_0 in the surface or 0-plane can be found by applying Eq.[15]: Δz_0 = [(-2).(+1)] + [(0.5).(+5)] = 0.5. The corresponding Boltzmann accumulation factor therefore equals $e^{-0.5\, F\, \psi 0\, /\, RT}$. Similarly, we may find the change in charge in the 1-plane (Δz_1). The charge is due to the ligands O^{2-} and/or OH^{1-} and their partial neutralization by the central ion (1-f) z_{Me}. In the case of $\equiv(FeO)_2PO_2$, Eq.[10] gives Δz_1 = [(1-0.50).(+5)] + [(2).(-2)] = -1.5 and a Boltzmann factor of $e^{-1.5\, F\, \psi 0\, /\, RT}$. The derived value of Δz_0 can also be found following the change of charge resulting from the different steps of the reaction, i.e. adsorption of protons resulting in the formation of two OH_2^o ligands (+2), release of both neutral OH_2^o ligands (-0), placement of two O^{-2} [(2).(-2)] ligands, and a partial neutralization by P [(0.5).(+5)], yielding Δz_0 = [+2] + [-0] + [(2).(-2)] + [(0.5).(+5)] = +0.5.

The calculated values Δz_0 and Δz_1 can be used to find the actual charges p and q on the ligands of the surface complex (Eq.[10]). The sum of both initial charges (-0.5) on the common O ligands before reaction and the change of charge Δz_0 (= 0.5) gives p = [(2).(-0.5)] + [0.5] = -0.5. The value of q equals Δz_1 resulting in $\equiv(FeO)_2^{-0.5}PO_2^{-1.5}$.

Besides surface species, species in solution also play a role in adsorption. Generally, ions in solution do not behave ideally due to mutual interactions, especially at higher ionic strengths (I). This interaction energy can be calculated by applying the Debye-Hückel theory for charged ionic species. It is introduced in the equilibrium condition by using activities, a_k, instead of concentrations, c_k, with $a_k = f_k\, c_k$ in which f_k is the activity coefficient of the ion species k. For I > 0.1 M, an additional empirical correction has to be introduced as is done in the Davies equation (45).

Adsorption on variable charge surfaces can be calculated with the CD model using the ECOSAT chemical speciation program, based on a modified approach of Westall and Hohl (32). The fractional charges of surface components are incorporated with a single minor change (see Appendix).

Sites and surface structure

The chemical reactivity of interfaces is determined by the type and number of surface groups present, which in turn is related to the type of crystal planes present. A number of experimental studies have determined the crystal morphology of goethite in some detail. Electron microscopy shows that goethite crystals are elongated in the c-axis direction giving a needle-like shape. Early work on goethite (46) suggested that the 100, 010, and 001 crystal faces were dominant. More recently, Electron Microscope (EM) studies of cross-sections of goethite needles perpendicular to the elongated c-direction have shown (47) that the dominant crystal plane is the 110 plane, which holds not only for synthetic but also for naturally formed crystals (48-54). EM studies of the goethite preparation used in this study confirmed the presence of predominantly 110 faces. At the end of the needles the 021 plane is found.

Knowing the dominant crystal face, one may assess the chemical composition of the surface by cutting an imaginary cross-section of the crystal in the appropriate direction. The composition may be identical (Fig.4) with the cut yielding the highest Fe density parallel to the 110 direction, as is done classically. On a unit cell basis, there are 3 rows of triply coordinated surface $\equiv Fe_3O(H)$ groups in the c-direction, one row with singly coordinated $\equiv FeOH(H)$ surface groups and one row with doubly coordinated surface $\equiv Fe_2OH$ groups.

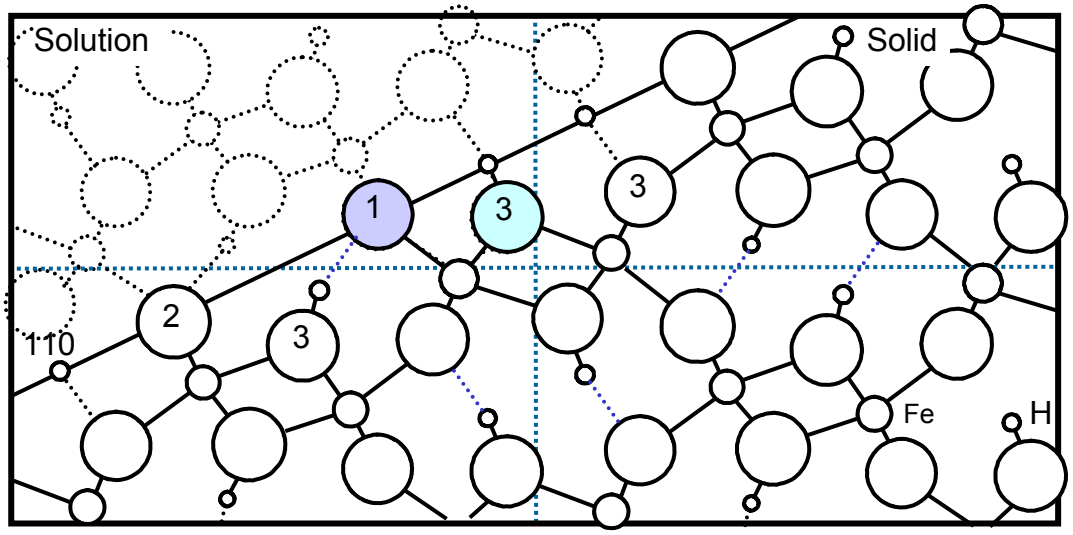

Fig.4 A schematic representation of the cross-section of goethite perpendicular to the c-axis showing the surface structure of the 110 face. The ions that have been removed from the structure in order to illustrate the composition of the interface are shown by fine dashed lines. In the solid, the oxygens (large circles) are triply coordinated with Fe^{3+} (only two Fe-O bonds are shown). The bold circles indicate a raised position in the lattice. Half of the oxygens have a proton attached (OH). At the interface, a lower coordination number (CN) is found. The CN is indicated by the numbers 1, 2, or 3, which identify the singly, doubly, or triply coordinated oxygens, respectively. The shaded surface oxygens are considered to be proton-reactive (see text).

As indicated in Fig.4, the 110 face will have one doubly coordinated $\equiv Fe_2OH^o$ surface group per unit cell length. It has been shown earlier (15), based on estimates of the proton binding constants of the doubly coordinated surface groups, that these doubly coordinated

surface groups are essentially inert and zero charged, i.e. over a very wide pH range the dominant doubly coordinated surface species is $\equiv Fe_2OH^o$.

The goethite surface is dominated by triply coordinated surface $\equiv Fe_3O(H)$ groups (Fig.4) and this will be reflected in the value of the PZC. The PZC of the goethites used in our study is high (9 ± 0.5) indicating a high value for the log*K* of the protonation reaction of triply coordinated surface groups. This contrasts with the low value for $\equiv Fe_3O$, predicted by the MUSIC model (15). It is reasonable to assume that the triply coordinated groups that have different positions in the surface structure may also differ in their proton affinity. In goethite, two types of triply coordinated groups are found, one protonated ($\equiv Fe_3OH$) and one non-protonated ($\equiv Fe_3O$). The proton-oxygen bond of the protonated $\equiv Fe_3OH^{1/2+}$ group is stronger than the proton-oxygen bond of the non-protonated $\equiv Fe_3O^{1/2-}$ group. This concept can be applied to the surface structure exposed by the imaginary cut in Fig.4 where one third of the triply coordinated surface groups has an H-bond with the singly (Fe) coordinated surface group. This configuration is very stable, i.e. the proton affinity is high, and the degree of protonation is hardly affected by pH. According to the structure, the two other types of triply coordinated surface groups are a hydroxyl and an oxygen ion, reflecting the difference in their proton affinities. The situation can be simplified if the difference in proton affinity between two types of triply coordinated groups is very large. It has been shown (16) that where there is large difference in proton affinity (large ΔpK) such types of surface species may become completely oppositely charged if present in a 1:1 ratio. For goethite this leads to $\equiv Fe_3O^{-1/2}$ species dominating the low affinity sites, and to $\equiv Fe_3OH^{+1/2}$ species dominating the high affinity sites. We consider the most inner-oriented triply coordinated surface groups as representative of this combination, i.e. the combination is zero charged over a large pH range. As a result, the charging behavior of goethite is probably determined by the remaining surface groups (shaded in Fig.4), namely the singly coordinated $\equiv FeOH(H)$ and a triply coordinated $\equiv Fe_3O(H)$. As mentioned above, in order to maintain reactivity, these two types of surface groups cannot have a large difference in proton affinity.

The above surface structural analysis is supported by our experience of PO_4 adsorption modeling for goethite. We have found that a complete description of PO_4 adsorption phenomena is only possible if the total site density of proton reactive groups is set to about 6 nm^{-2}, which is equivalent to two rows of reactive groups ($\equiv FeOH(H)$ and $\equiv Fe_3O(H)$) per unit cell length of the 110 face. In our simplifying approach, the proton affinity of the singly and triply coordinated surface group is set equal which means that the log*K* value equals the value of the Point of Zero Charge (18,55). Phosphate is thought to react only with the singly coordinated surface groups (9,19).

The 021 plane is exposed at the ends of the goethite needle. The length of the crystals will determine its relative abundance, which is often less than 10%. The 021 plane is characterized by alternating rows of singly and doubly coordinated surface groups. The site density of each type of group on this 021 face is about 7.4 nm^{-2}. The chemical composition of this plane is given in Fig.5.

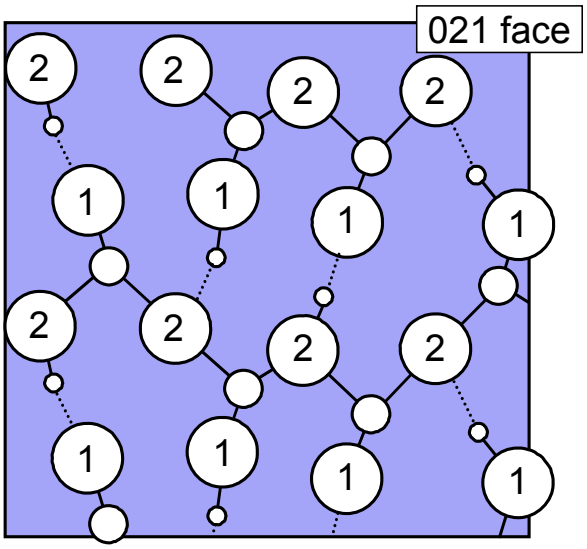

Fig.5 A schematic representation the surface structure of the 021 face of goethite in which singly and doubly coordinated oxygens (large circles) are present in rows. The numbers refer to the coordination number with Fe^{3+} ions (small circles). The singly coordinated surface groups are raised above the doubly coordinated surface groups. Hydrogen bonds are present between the singly and doubly coordinated surface groups.

Experimental

Three batches of pure crystalline goethite suspensions were made by slowly neutralizing freshly prepared 0.5 M Fe nitrate solution with 2.5 M NaOH, followed by aging at pH 12 for 90-110 h in an oven (60^{o}C) and dialysis for 2 weeks (16). All solutions were prepared with double-distilled water and contact with glassware was avoided. Each batch was characterized using Transmission Electron Microscopy (TEM), X-ray diffraction of a random powder specimen and Thermo Gravimetric Analysis (TGA). In addition, the BET surface area of the individual batches was determined by N_2 gas adsorption. This characterization indicated that the preparations contained pure non-porous goethite particles of mainly mono-domainic crystals, and were therefore identical with the preparation discussed previously (16). The charging curves of the individual batches were determined using the method described elsewhere (16). These experimental data showed that goethite crystals could be reproducibly prepared with only minor differences. For the adsorption experiments, a stock suspension was made by mixing three individual goethite suspensions. The electromobility of the stock suspension was measured in the pH range pH 8.5-10 in 0.01 M $NaNO_3$ without any attempt to exclude CO_2 using a Malvers Zetasizer III.

The type of crystal planes developed on the goethite crystals of our preparation was assessed from the shape of the crystals perpendicular to the c-axis as determined by TEM. Thin-sections were made for TEM examination by embedding the goethite in a synthetic organic polymer.

The PO_4 adsorption isotherms were measured at four different pH levels (pH = 4, 7, 9 and 11) in 0.01 M $NaNO_3$. CO_2-free NaOH solutions were made from a highly concentrated 1:1 $NaOH/H_2O$ mixture which had been centrifuged in order to remove any solid Na_2CO_3. The supernatant was pipetted into boiled double-distilled water and stored in a plastic bottle

placed in a CO_2-free desiccator equipped with a CO_2 absorbing column. About 60 mL of the diluted goethite suspension in 0.01 M $NaNO_3$ was placed in a thermostated vessel (20 ± 0.1 ^oC) and brought to pH 4 for 1 hour with 0.01 M HNO_3/0.01 M $NaNO_3$ to remove (bi)carbonate by purging purified moist N_2-gas. Next, the pH of the sample was raised with 0.01 M NaOH to the appropriate pH of the experiment. The sample was kept (pH-stat) at this pH for about 1 hour in order to reach equilibrium before a known volume of 0.005 M NaH_2PO_4/0.005 M $NaNO_3$ was added. After equilibration at the given pH for 20 hours (pH-stat) under continuous purging with N_2 gas, a sample was taken under N_2, and centrifuged at high speed without contact with air. The supernatant was filtered through a 0.025 μm filter to remove any fine particles. The P concentration was measured colorimetric by the molybdate blue method.

Based on a proper bookkeeping of the added volumes and concentrations of the chemicals NaH_2PO_4, HNO_3, and NaOH and the experimentally measured equilibrium P-concentration and pH, it is possible to calculate both the adsorption of PO_4 and the simultaneous adsorption of H^+ ions (or desorption of OH^-). The adsorption of H^+ is found from the net difference of the protons added (NaH_2PO_4, HNO_3, and NaOH) and the amount of remaining H left in solution after equilibration, according to:

$$H_{\text{ads}} = H_{\text{added}} - \Delta H_{\text{sol}}$$

with

$$H_{\text{added}} = 2\, V_1\, C_{\text{NaH}_2\text{PO}_4} + V_2\, C_{\text{HNO}_3} - V_3\, C_{\text{NaOH}}$$

and

$$\Delta H_{\text{sol}} = V_{\text{t}}\ (3[\text{H}_3\text{PO}_4] + 2[\text{H}_2\text{PO}_4^-] + 1[\text{H}_1\text{PO}_4^{2-}] + 1[\text{NaH}_1\text{PO}_4^-]) + \Delta V([\text{H}^+] - [\text{OH}^-])$$

in which V_t is the total volume of the system after addition of phosphate solution (V_1), acid (V_2) and/or base (V_3), and $\Delta V = V_1 + V_2 + V_3$. The concentration of the solution species [H^+], [OH^-], [H_3PO_4], [$H_2PO_4^-$], [HPO_4^{2-}] and [$NaHPO_4^-$] were calculated from the experimental pH and P-concentration. The intrinsic formation constants used for the calculation of the solution speciation are given in Table 1 and the activity coefficient f_k for a species k was calculated using the Davies equation (45,58,59):

$$\log f_k = -0.51 z_k^2 \left\{ \frac{\sqrt{I}}{1+\sqrt{I}} - 0.2I \right\} \qquad [17]$$

where I is the ionic strength and z_k is the valence of the species.

Table 1 Aqueous speciation reactions with equilibrium constants taken from Smith and Martell (57)

Species	Reaction		logK^o
HPO_4^{2-}	$PO_4^{3-} + H^+$	$\Leftrightarrow HPO_4^{2-}$	12.35
$H_2PO_4^-$	$PO_4^{3-} + 2H^+$	$\Leftrightarrow H_2PO_4^-$	19.55
$H_3PO_4^0$	$PO_4^{3-} + 3H^+$	$\Leftrightarrow H_3PO_4^0$	21.70
$NaHPO_4^-$	$PO_4^{3-} + H^+ + Na^+$	$\Leftrightarrow NaHPO_4^-$	13.4
H_2O	$H^+ + OH^-$	$\Leftrightarrow H_2O$	14.0

Basic charging behavior

Application and validation of the CD model starts with the description of the basic charging behavior of goethite.

Experimental results

The charging behavior of Me-(hydr)oxides is a basic property, from which the intrinsic double layer properties of the interface can be found, in particular the overall capacitance C of the Stern layer. The possibility of ion pair formation can also be evaluated and reaction constants for ion pair formation can be assessed.

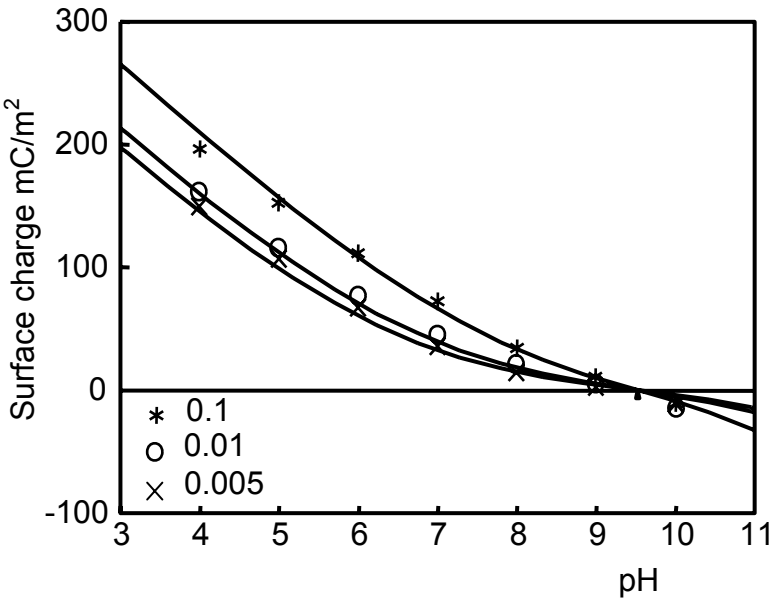

Fig.6 The experimental charging behavior of goethite at three different concentrations of $NaNO_3$ (interpolated points). The lines correspond to calculated charging curves using $N_s = N_{s,1}+N_{s,2} = 3.45 + 2.7 = 6.15$ nm^{-2}, $C = 0.9$ F/m^2, $\log K_{1,2} = \log K_{3,1} = 9.5$, and $\log K_c = \log K_a = -1$ (BS approach with ion pairs in the d-plane, see text for details and definitions).

The charging behavior of the goethite used in this study is shown at three electrolyte concentrations in Fig.6. The data points represent the weighted mean of the charging curves of the individual preparations with charge expressed per unit surface area using the weighted mean BET surface area (A = 105 ± 5 m^2/g). The PZC derived from the titration curves was

9.5 ± 0.1 which corresponds with the Iso Electric Point (IEP) for the bulked suspension in 0.01 M $NaNO_3$ (IEP = 9.4 ± 0.1).

Modeling the surface charge

The surface charge for goethite can be described within the CD concept by assuming that the charging of the 110 face of goethite is related to the presence of a row of singly coordinated ≡FeOH(H) surface groups and a row of $\equiv Fe_3O(H)$ surface groups per unit cell length. The singly coordinated surface groups may protonate in principle by two consecutive steps (Eq.[3]). However, the very high proton affinity of the $\equiv FeO^{-3/2}$ group, predicted by the MUSIC model (15), leads to the conclusion that the dominant singly coordinated species will be $\equiv FeOH^{-1/2}$ and $\equiv FeOH_2^{+1/2}$, i.e. the charging behavior will be determined by:

$$\equiv \mathrm{FeOH}^{-1/2} + \mathrm{H}^{+}(\mathrm{aq}) \Leftrightarrow \equiv \mathrm{FeOH}_2^{+1/2} \qquad [18]$$

Only one protonation step for triply coordinated surface groups can be defined:

$$\equiv \mathrm{Fe_3O}^{-1/2} + \mathrm{H}^{+}(\mathrm{aq}) \Leftrightarrow \equiv \mathrm{Fe_3OH}^{+1/2} \qquad [19]$$

A second protonation step is not possible because all four orbitals of the oxygen in the $\equiv Fe_3OH$ species are already occupied.

As discussed above, the log$K$ values of the two protonation reactions (Eqs.[18],[19]) cannot be too different. At present, the precise log$K$ values are unknown and we therefore set them to be equal. For a surface with only one protonation reaction, such as Eq.[18] or Eq.[19], the corresponding log$K$ value can be found directly from the PZC (18,55). This implies a value for the protonation constants $\log K_{1,2}$ and $\log K_{3,1}$ of 9.5 for our goethite preparation. A distinction between the two proton reactive groups is still important because only singly coordinated groups are active in oxyanion binding such as of PO_4 (9,19).

Assuming the presence of ion pairs, the corresponding reactions can be given as:

$$\equiv \mathrm{FeOH}^{-1/2} + \mathrm{Na}^{+}(\mathrm{aq}) \Leftrightarrow \equiv \mathrm{FeOH}^{-1/2} - \mathrm{Na}^{+} \qquad [20]$$

and

$$\equiv \mathrm{FeOH}_2^{+1/2} + \mathrm{NO}_3^{-}(\mathrm{aq}) \Leftrightarrow \equiv \mathrm{FeOH}_2^{+1/2} - \mathrm{NO}_3^{-} \qquad [21]$$

For the triply coordinated groups similar reactions can be defined:

$$\equiv \mathrm{Fe_3O}^{-1/2} + \mathrm{Na}^{+}(\mathrm{aq}) \Leftrightarrow \equiv \mathrm{Fe_3O}^{-1/2} - \mathrm{Na}^{+} \qquad [22]$$

and

$$\equiv Fe_3OH^{+1/2} + NO_3^-(aq) \Leftrightarrow \equiv Fe_3OH^{+1/2} - NO_3^- \quad [23]$$

In the CD model with the Three Plane (TP) approach, the ion pairs are assumed to be present in the plane at the head end of the DDL (2-or d-plane). We assume symmetrical ion pair formation, i.e. $K_{c(i)} = K_{a(i)}$.

In the calculation of the surface charge, a value for the site density N_s is required. This should be related to the chemical composition of the surfaces. TEM of thin-sections perpendicular to the c-direction showed wedge-shaped crystals characteristic of the presence of the 110 face and its equivalents. The goethite crystals in our preparation were very elongated which implies that the 110 face was dominant. Using the measured crystal dimensions, the surface area of the faces at the head end of the crystal (021 face) was estimated to be about 5% of the total surface area. An AFM study of goethite (53) has recently shown that the contribution of the 021 face may be significant due to the presence of numerous steps on the dominant faces. The 021 face has a reactive site density for singly coordinated groups of N_s = 7.4 nm^{-2}, being slightly higher than the total reactive site density (singly and triply coordinated groups) of the 110 face (N_s = 6 nm^{-2}). For reasons of simplicity, we consider the goethite interface as a single electrostatic face (See discussion). The charging behavior of goethite is not very sensitive to the precise value of the total site density. But the site density is critical for PO_4 modeling because the PO_4 affinity for singly coordinated surface groups is so high that site saturation may occur at low pH values. This implies that the value of N_s determines the P adsorption behavior and means that the site density of singly coordinated surface groups to be used in the modeling is somewhat greater than the value calculated for the 110 face alone (N_s = 3 nm^{-2}). The contribution of the 021 face, having a very high site density for singly coordinated groups, and the potential presence of defects must also be included. We have assumed site densities for the surface groups equivalent to a mixture of 10% 021 face and 90% 110 face, yielding a site density for singly ($N_{s,1}$) and triply ($N_{s,2}$) coordinated surface groups of 3.45 and 2.7 nm^{-2}, respectively.

A good description of the data can be found by assuming symmetric ion pair formation with $\log K_c = \log K_a = -1$ for both singly and triply coordinated surface groups. The charging curves, shown in Fig.6, have been calculated with a value for the overall Stern layer capacitance, C, of 0.9 F/m^2.

CD ion adsorption modeling

PO_4 adsorption

PO_4 adsorption on goethite is strongly related to the charging behavior of the Me (hydr)oxide. As shown by Hiemstra et al. (16), the experimental charging capacity for goethite may vary strongly depending on its method of preparation. Goethites with specific surface areas less than about 50 m^2/g are generally multi-domainic, having a large number of

imperfections (46). The charging behavior of these preparations is characterized by a large experimental capacitance (slope $\Delta C/m^2/\Delta pH$) (16, 39).

Our goethite preparation, made by the slow neutralization of Fe nitrate solution, has a high specific surface area (A = 105 m^2/g), and TEM observations showed well-developed mono-domainic crystals. The charge density of this goethite is considerably lower than that of multi-domainic goethite preparations. This can be illustrated by comparing the charge of this goethite with one made by the very rapid neutralization of Fe nitrate solution (A = 38 m^2/g). The experimental surface charge for these goethites at pH = 4 in a 0.1 M $NaNO_3$ solution was about 190 mC/m^2 and 300 mC/m^2, respectively.

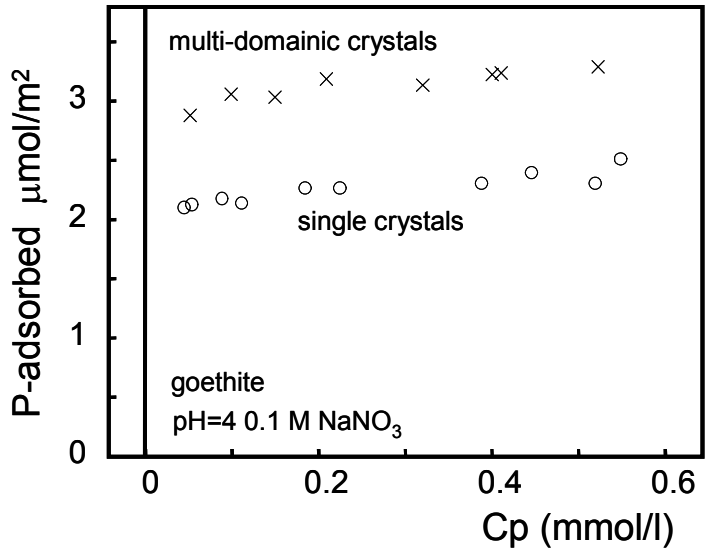

Fig.7 The adsorption of PO_4 by a mainly mono-domainic goethite with a low surface charge density (high surface area A) and a multi-domainic goethite with a high surface charge (low surface area A) at pH 4 in 0.1 M $NaNO_3$ as a function of the total orthophosphate concentration (C_p), illustrating the relation between surface charging and anion adsorption capacity.

The difference in proton reactivity may affect the adsorption behavior of PO_4. A higher positive surface charge at low pH induces a higher adsorption capacity for negative anions like PO_4, because more negative charge can be brought to the surface for a given change in electrostatic potential. Large adsorption densities are only possible if a sufficient number of sites is available. The enhanced anion adsorption for goethites with a high surface charge is shown in Fig.7. The combination of a low surface area, a very high surface charge and a high PO_4 adsorption capacity (measured on a surface area basis) can also be found in the literature. Sigg and Stumm (28) reported PO_4 adsorption values of more than 5 $\mu mol/m^2$ at pH 4 in a similar concentration range to that given in Fig.7. Only carefully chosen anion adsorption data sets should be compared directly.

The adsorption of PO_4 in 0.01 M $NaNO_3$ was determined at 4 pH values. Great care was taken to avoid contamination with Si and $(H)CO_3$. The data set is presented in Fig.8 together with the data set of Bowden (26), who studied the PO_4 adsorption under the same conditions

(pH, P-concentration, and electrolyte concentration). Both goethite preparations have a high surface area (A = 105 and 80 m^2/g, respectively), which makes it possible to compare the experimental results.

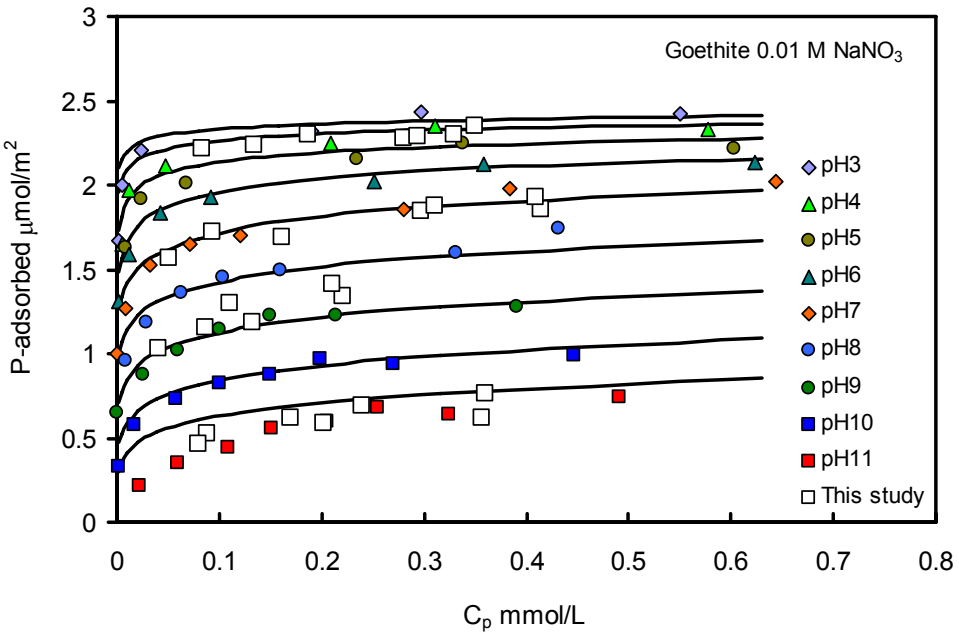

Fig.8 The adsorption of PO_4 by mono-domainic goethite used and that of Bowden et al.(26). The lines have been calculated with the CD model and are consistent with the surface species observed by CIR-FTIR spectroscopy.

The PO_4 adsorption data for a goethite, which was used to examine the surface PO_4 speciation (13) by CIR-FTIR spectroscopy, are also considered. In this case, the PO_4 adsorption isotherms were determined over a 10-fold higher PO_4 concentration range. The surface area of this goethite was also high (A = 81 m^2/g). The isotherms are presented in Fig.9, together with the calculated adsorption using the CD model with the same parameters as used in Fig.8.

The remarkable similarity in PO_4 adsorption behavior for the three data sets indicates that the charging of these goethites is essentially the same, which is confirmed by a comparison of the charging curves (Fig.10) in the 0.01 M electrolyte. Only a distinctive difference in charging is observed for the σ_0 -pH curve of Bowden et al. (26) above pH 9. The asymmetry of the curve could be an indication of carbonate contamination. The other two goethites have PZC values of 9.0 (60) and 9.5 ± 0.1 (this study). In the calculations, we have used a mean value for the PZC of 9.2, leading to $\log K_{1,2} = \log K_{3,1} = 9.2$. The capacitance C was set to 0.9 F/m^2 as used in the calculations in Fig.6. In all three cases, a good agreement exists between the PO_4 adsorption data and the CD model results.

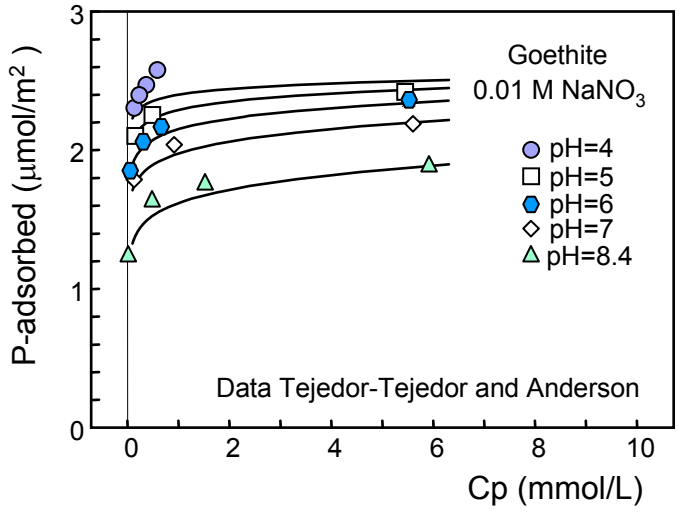

Fig.9 The adsorption of PO_4 by the goethite of Tejedor-Tejedor & Anderson (13) (A = 81m^2/g), over a tenfold higher phosphate concentration range compared with Fig.8. The lines have been calculated with the CD model using the same parameters as for Fig.8.

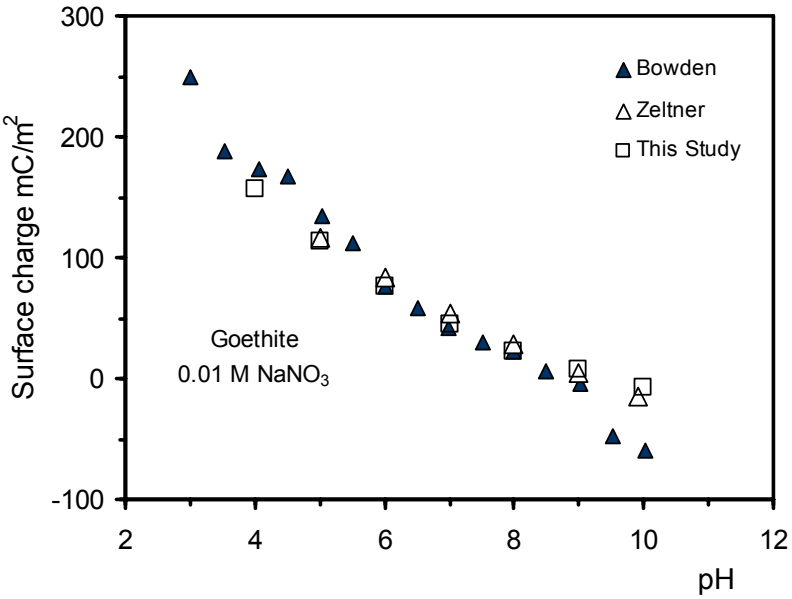

Fig.10 The surface charge in 0.01 M electrolyte for the goethites used in the PO_4 adsorption analyses. Data of Bowden et al. (26), Zeltner & Anderson (60), and this study.

Surface PO_4 speciation

The choices of species and parameters for the description of the PO_4 surface speciation are strongly constrained by the CIR-FTIR measurements. The IR data show that from pH 3.5-8 the dominant PO_4 surface species is a bidentate complex $\equiv(FeO)_2POO(H)$ (± 85%) which is protonated at low pH. The pH at which the protonation of the surface complex occurs is related to the total amount of PO_4 adsorbed. At high PO_4 loading the presence of the protonated $\equiv(FeO)_2POOH$ species becomes important because increased adsorption of PO_4 decreases the particle charge and may even cause charge reversal thereby enhancing protonation.

In Fig.11 (next page), the relative abundance of both bidentate surface species is shown for three different concentrations of added PO_4. The relative presence has been derived from the computed peak areas for the different adsorption bands given by Tejedor-Tejedor and Anderson (13) assuming that all complexes had a similar extinction coefficient. They assigned the 1123 ± 4 and 1006 ± 4 cm^{-1} bands to the protonated bidentate $\equiv(FeO)_2POOH$ species and the 1096 ± 6 and 1044 ± 6 cm^{-1} bands to the non-protonated $\equiv (FeO)_2PO_2$ species. We have assumed that each of the two peaks is representative for a particular phosphate surface complex and so have normalized the peak area of each species relative to the sum of the 4 above mentioned peaks. This yields a measure for the abundance of each species. This is plotted in Fig.11 as the relative intensity, IR. Note that the non-protonated bidentate surface species at pH 4 is only 20% at the lowest loading, whereas its abundance increases to more than 80 % at the same pH when the P loading is doubled.

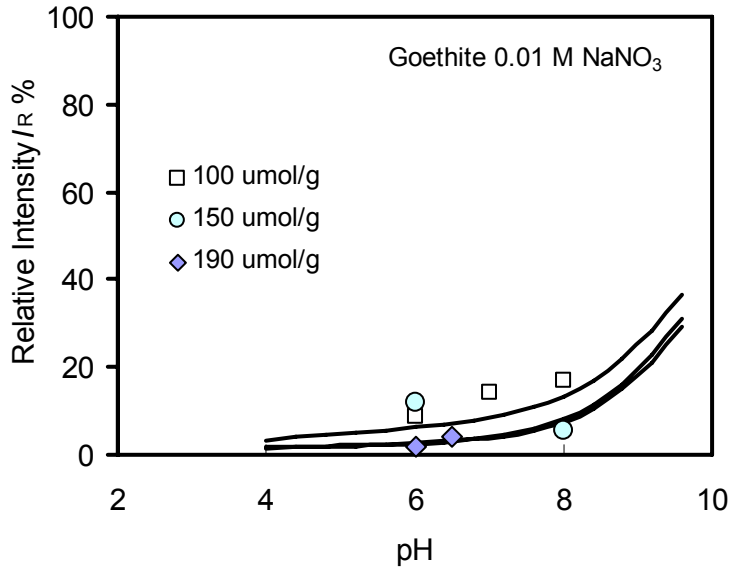

Fig.12 The increase in the relative intensity IR of the monodentate $\equiv FeOPO_3$ peak for three different PO_4 loadings. The data indicate a decrease in monodentate surface complexation with increasing PO_4 loading. The lines in the figure have been calculated using the CD model. Data: Tejedor-Tejedor & Anderson (13).

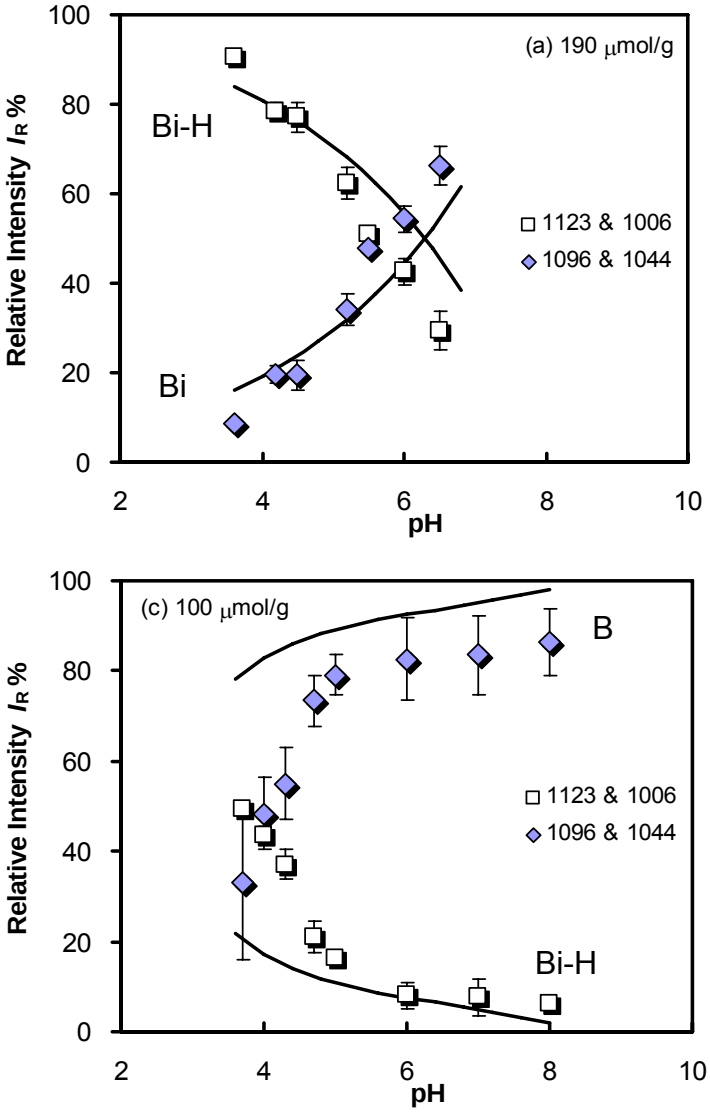

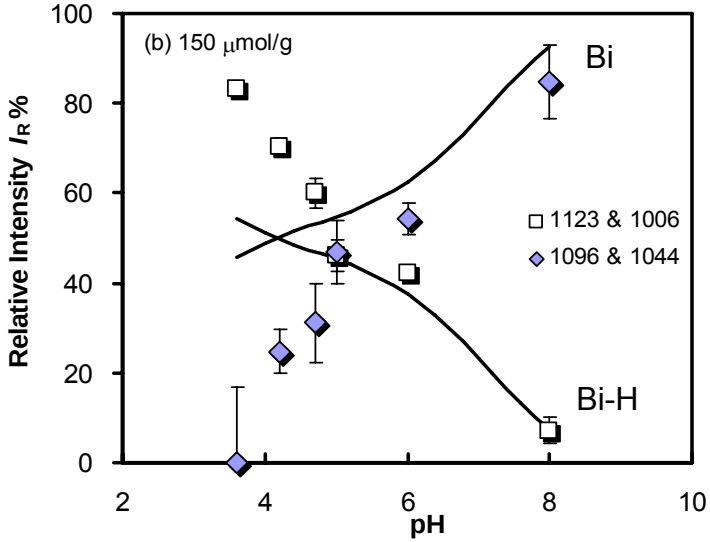

Fig.11 The increase of the relative intensities IR of the bidentate $\equiv(FeO)_2POOH$ peak (Bi-H) and corresponding decrease of the intensity of the $\equiv(FeO)_2POO$ peak (Bi) for three different PO_4 loadings: (a) 190 μmol/g, (b) 150 μmol/g, and (c) 100 μmol/g (A = 81m^2/g). The data indicate that protonation increases with PO_4 loading. The lines have been calculated using the CD model. Data: Tejedor-Tejedor & Anderson (13).

Besides the presence of bidentate complexes, the presence of monodentate complexes in the pH range 3.5-8 has also been reported. The possibilities for a quantitative interpretation are however rather limited due to low sensitivity at low species concentration observed. A semi-quantitative interpretation of the intensity of the 1025 ± 2 cm^{-1} band suggests an increased abundance of monodentate species with increasing pH and, interestingly, a relative decrease in abundance of monodentate species with increased PO_4 loading (Fig.12). This decrease arises from the presence of three highly negatively charged ligands in the 1-plane, which leads to an asymmetrical charge distribution in the monodentate species. With increasing PO_4 loading, the 1-plane becomes strongly negatively charged, favoring the presence of bidentate species, which introduce less charge into the 1-plane.

Detailed modeling

The adsorption reactions of PO_4 have been given for bidentate and monodentate surface complex formation earlier (Eqs.[7],[10],[12]). The precise value for the charge distribution factor, *f*, has to be adjusted. For simplicity, one could assume that *f* does not change for bidentate species because of protonation and that the monodentate complex has a value for *f* of half of the value found for the bidentate complex because the number of common surface ligands is half. However, the modeling only fitted the data well if we assigned a slightly larger value of *f* to the protonated bidentate species in comparison with the non-protonated species. This implies that two *f* factors have to be adjusted. For the non-protonated bidentate species the value of *f* of the central ion was found to be about $f = 0.5$, which is identical to the value that would be expected from Pauling's charge distribution concept using an equal distribution over all oxygen ligands. The monodentate complex has one bond with a surface group and the value of *f* is set to half the value of the bidentate complex, leading to $f = 0.25$. The value of *f* for the protonated bidentate complex was set higher at $f = 0.6$. This higher value is equivalent with an additional charge transfer towards the surface of half a unit charge due to protonation.

Initially, we explored the possibility of describing the data assuming the presence of only two electrostatic planes representing a Basic Stern approach, i.e. a 0-plane for the adsorption of H and common surface ligands and the 1- or d-plane for the adsorption of ion pairs and solution-oriented ligands. The parameters used assuming only two electrostatic planes are given as Case I in Table 2. All of the adsorption phenomena illustrated above, including the IR surface speciation (except monodentate surface species formation) and the particle charge could be described with this approach, except for the salt dependency. The observed salt dependency of PO_4 adsorption is small, while the predicted salt dependency based on the BS approach is large. Analysis of this discrepancy indicated that the interaction between ion pairs and the adsorbed PO_4 was too high. This implies that the solution-oriented ligands should not be placed in the same electrostatic plane as the ion pairs. For this reason, a separate plane was added, splitting the Stern layer region in two parts, yielding the Three Plane (TP) model.

Table 2 Surface parameters used in the modeling of the PO_4 data sets (13, 26, and this study) for 3 different options.

		Value		
Species	Eq.	Case I	Case II	Case III
C (F/m^2)	[4]	0.9	0.9	0.9
C_2 (F/m^2)	[4]	-	5	5
logK_{in1}	[7]	-	-	20.8
logK_{in2}	[10]	29.0	29.2	29.2
logK_{in3}	[12]	35.3	35.4	35.4
logK_H	[18],[19]	9.2	9.2	9.2

Case I: BS approach without monodentate surface species.
Case II: TP approach without monodentate surface species.
Case III: TP approach with mono- and bidentate surface species.

The TP approach enabled all adsorption phenomena, included the salt dependency, to be described very well (Case II and III). The modeling did not require the assumption of the presence of a monodentate complex. The corresponding parameters are given as case II in Table 2. However, the IR bands indicate the presence of the monodentate species at high pH and low PO_4 loading (Fig.12). For a complete description, we took into account the monodentate species (Case III in Table 2). Detailed information about the formulation of the model in terms of the table of species, which forms the basis of speciation calculations, is given in the Appendix. The CD model then predicts monodentate binding that is quantitatively in agreement with the observed increase in monodentate adsorption with increasing PO_4 loading. Monodentate complexes have been observed even at a very low P loading of 50 μmol/g $*$ 0.6 μmol/m^2 at pH 4 (13), as predicted by the CD model (~10%, Fig.12). The TP model requires a capacitance to be defined for both layers. They were derived from the salt dependency of specifically adsorbing ions.

Salt dependency

In the TP approach, an important factor influencing the salt dependency is the position of the mid plane (1-plane), i.e. the distance between the 1- and d-plane, which is reflected in the value of the capacitance C_2. The solution-oriented ligands of the adsorbed PO_4 molecule are placed in the 1-plane and the ion pairs in the 2- or d-plane. If the distance between these planes is increased (C_2 decreases), both planes with their adsorbed species will interact less, decreasing the salt dependency. Another factor is the distribution of the charge of the phosphate ion between the two adsorption planes (0, 1-plane). In the case of monodentate adsorption (high pH), a greater proportion of the negative charge is placed in the 1-plane, leading to a stronger salt dependency.

There is only one extended data set on PO_4 adsorption in the literature (Fig.13) that describes the salt dependency of the PO_4 adsorption on goethite as a function of pH and PO_4 concentration (27). The goethite of Barrow et al. (27) however has a relatively low PZC (PZC = 8.3). In the PO_4 modeling, we have used this PZC value to define the protonation constants log$K_{1,2}$ and log$K_{3,1}$. The value for the capacitance was set equal to that found for the other

goethites. Because of the different protonation behavior, the PO_4 adsorption constants ($\log K_{in1\text{-}3}$) had to be adjusted (Table 3). The charge distribution has not been changed. The modeling showed that the salt dependency could be described well if the value of the outer layer capacitance was set equal to about 4-5 F/m^2.

Table 3 Surface parameters (TP approach) used in the description of the PO_4 data set of Barrow et al. (27), shown in Fig.13.

Parameter	Value
C (F/m^2)	0.9
C_2 (F/m^2)	5
$\log K_{in1}$	19.5
$\log K_{in2}$	27.8
$\log K_{in3}$	33.8
$\log K_H$	8.3

The log$K$ values differ from the values given in Table 2 (Case III) because of the different logK_H used.

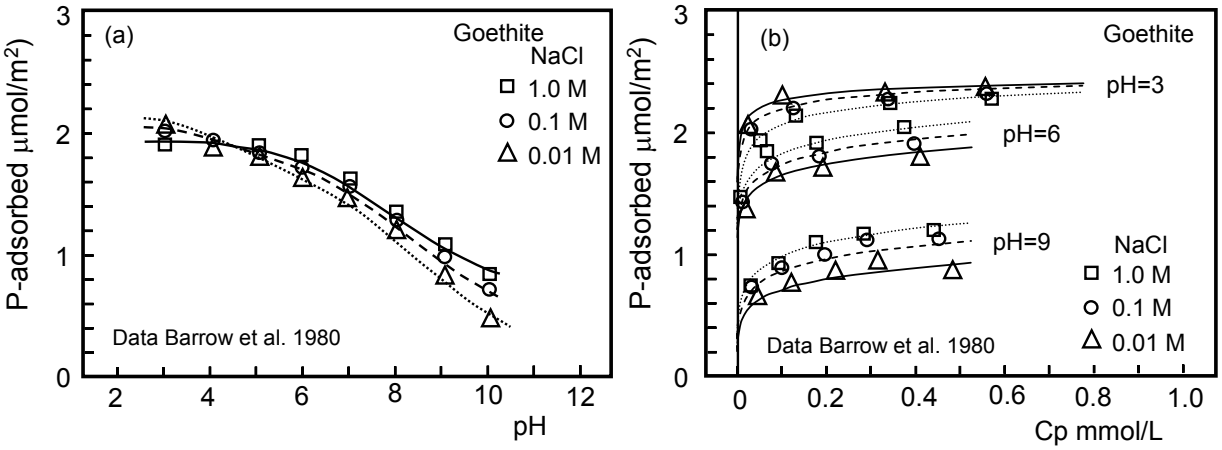

Fig.13 (a) pH dependent adsorption of PO_4 on goethite for three concentrations of background electrolyte; (b) adsorption isotherms for phosphate as a function of pH and salt concentration. The lines were calculated using the CD model. Data: Barrow et al. (27).

It is possible to interpret the capacitance value in terms of a distance, d, if the dielectric constant is known. Both are related according to:

$$C = \frac{\varepsilon_0 \varepsilon_r}{d} \qquad [24]$$

in which ε_0 and ε_r are the absolute and relative dielectric constants. At the interface the dielectric properties change from a high value at the solution side (ε_{water} = 80) to a low value

in the solid ($\varepsilon_{goethite}$ =11). If the dielectric properties of the outer layer are equal to that of water, the above given capacitance value C_2 is equivalent to a distance of about 0.13 nm between the 1- and d- plane. If the value of the dielectric constant is reduced in the vicinity of the goethite solid, for instance to about half the value of water, the distance doubles and will be in the order of the diameter of a water molecule. From this analysis, it can be concluded that the calculated distances are in reasonable agreement with the expected distances based on the molecular view of the interface presented above (Fig.2), i.e. the separation between the 0- and d-planes is equivalent to the size of a half or a whole water molecule.

Particle charge

An interesting aspect of the ion adsorption is the change of particle charge resulting from the adsorption. This change of particle charge is the net result of specific adsorption of cations and anions and the simultaneous adsorption or release of protons from the surface. The particle charge can be defined as the sum of the surface charge σ_0 (0-plane) and the charge of the 1-plane (σ_1). The adsorption of a cation generally leads to the release of protons and/or other competing cations, resulting in a pH decrease. In contrast, the adsorption of anions generally shows an increase of pH. This experimental behavior can be predicted when a mechanistic adsorption model is used.

The number of protons needed to keep the pH constant has been measured as a function of the amount of PO_4 adsorbed and the corresponding calculated H adsorption (Fig.14). The predicted H adsorption upon PO_4 adsorption using the CD model closely matches the observed stoichiometry, namely 2.5 to 1.

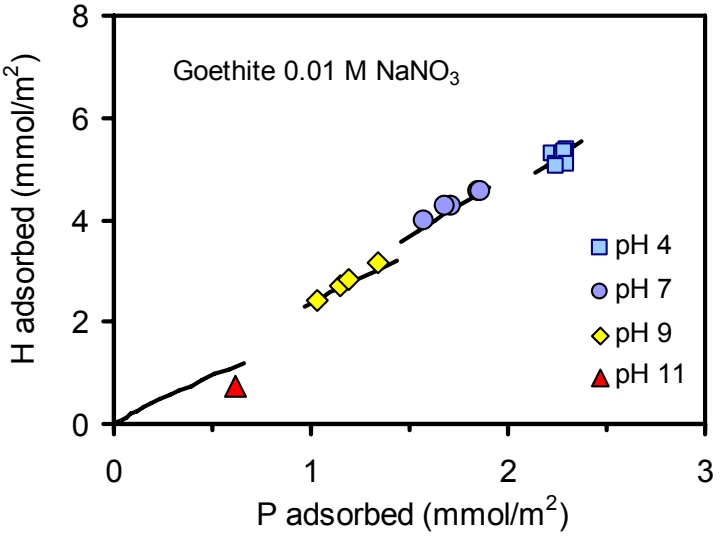

Fig.14 The simultaneous adsorption of protons as a function of phosphate adsorption at various constant pH values (this study). The lines are based on the CD model.

Another type of experimental data, which is related to particle charge, is the electromobility. This mobility may be interpreted, within limits, in terms of a potential at the imaginary plane of shear (2). This potential is called the ζ (zeta) potential. The measurement of the mobility as a function of pH leads to a pH at which the particle as a whole is apparently uncharged. This pH is called the Iso Electric Point (IEP). Tejedor-Tejedor and Anderson (13) have measured the electromobility of goethite as a function of pH and P loading for a system in which the adsorption and IR data were also collected (Fig.9,13). This mobility has been transformed into a zeta potential (Fig.15). It is possible to model the zeta potential if the position of the plane of shear is known. In earlier model approaches (37), it was assumed that this position is identical with the head end of the diffuse double layer (d-plane). In the CD model, hydrated ion pairs are bound in this plane, which supports the idea that the shear plane is somewhat further away from the surface. This is also sometimes assumed in the literature (5,61).

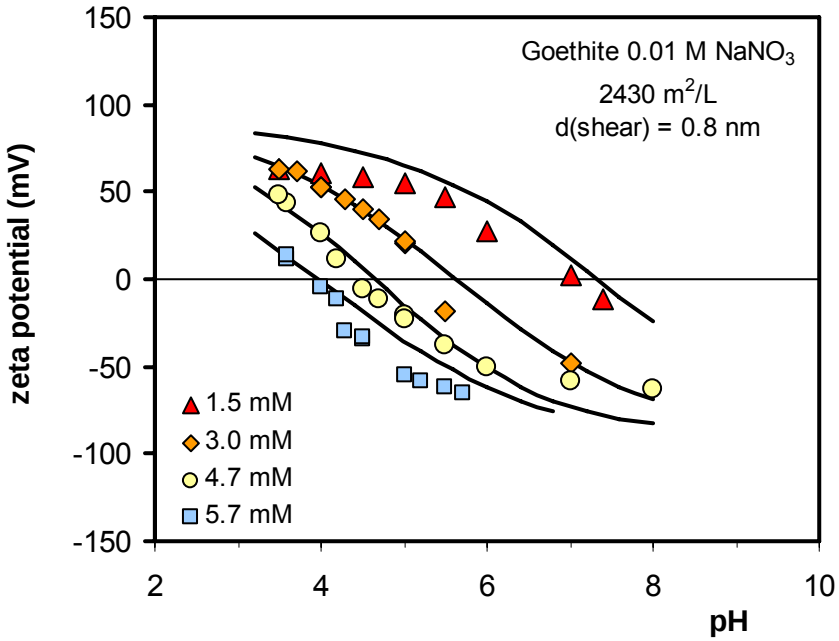

Fig.15 The (zeta) potential at the plane of shear, based on the measured electromobility of a goethite suspension with various initial concentrations of PO_4 as a function of pH in 0.01 M electrolyte (markers). The lines indicate the zeta potential calculated with the CD model assuming that the position of the plane of shear in solution is 0.8 nm from the head end of the DDL. Model parameters are given in Table 2 (Case III). Data: Tejedor-Tejedor & Anderson (13).

Modeling indicates that in a 0.01 M monovalent electrolyte the shear plane should be set about 0.5-1 nm from the 2- or d-plane, a distance equivalent to the thickness of 2 or 3 water molecules. Modeling two zeta potential data sets (35,36) of Me (hydr)oxides indicates that the distance d between the shear plane and the head end of the DDL can be related empirically to the electrolyte concentration c, according to $d = k\ c^{1/n}$. As indicated above, a quantitative interpretation of the zeta potential is accompanied by some uncertainty. The prediction of the IEP is more straightforward (6). In that case, it is assumed that the charge

within the plane of shear is zero. This occurs if the potential at the head end of the DDL is zero. Calculations with the CD model show that the IEP can be predicted fairly well (Fig.15).

Discussion

We have shown that a wide range of adsorption phenomena can be described well with the CD model. It should be kept in mind that the various phenomena were not measured for a single goethite preparation, which may reduce the possibility of finding accurately a single set of parameters for describing all the adsorption phenomena. Individual phenomena could have been described better if they had been optimized separately. With the CD model, it is relatively easy to describe the pH-dependent adsorption isotherms. Problems arise when the other observations must also be described with the same set of parameters. One of the major difficulties in the modeling was the attempt to describe the observed surface speciation (IR) in combination with the shift of the IEP with increasing PO_4 loading. A rather high value for the protonation constant was necessary to give a good description of the IR data over the whole range of PO_4 loading. However, this can give an excessively high positive charge for the particle at low pH resulting in a too small shift of the IEP upon PO_4 adsorption. This behavior may be related to the presence of surface site heterogeneity.

It has been shown recently (61,62) using Extended X-ray Absorption Fine Structure (EXAFS) analysis that oxyanions like SeO_3 and AsO_4 may form two types of bidentate inner sphere complexes. It is likely that this will also be the case for PO_4. The types of complexes formed are related to the exact location of the adsorbed species on a crystal surface. Distances measured with EXAFS indicate two distinct locations for bidentate adsorption on goethite. The difference is based on a difference in the number of Me ions in the solid (n_{Me}) binding both ligands of the bidentate surface complex, i.e. a mononuclear ($n_{Me} = 1$) and binuclear bidentate complex ($n_{Me} = 2$) can be distinguished (Fig.16).

The binuclear bidentate complex, which is bound to two surface groups connecting the corners of two octahedrons, is well known, i.e. it is called a double corner linkage (^{2}C). On goethite, this binuclear bidentate complex is dominant and can be found on the 110 face.

The two surface groups of the mononuclear bidentate complex are part of one Fe octahedron (Fig.16). The oxyanion is therefore bound in a so-called Edge linkage (^{2}E). Such edge linkages are possible for goethite on crystal faces cutting the c-axis, such as the 021 face. Based on IR studies (9), it has been assumed that oxyanions are reactive with only singly coordinated surface groups. This idea was supported by the finding that PO_4 adsorption is strongly reduced if crystal planes with doubly coordinated groups are dominant (17,22). However, one of the surface groups, which bind PO_4 in a mononuclear complex, is not a singly coordinated ≡FeOH surface group but a doubly coordinated ≡Fe_2OH group. Note that, although calling the PO_4 surface complex mononuclear (only one common Fe ion with the oxygens), the total number of Fe ions involved is three.

Similar types of mono- and bi-nuclear complexes have been established for adsorbed Cd by Spadini et al. (20), who found that the edge linkages could be identified as a high affinity site. If the edge bound bidentate complexes are relatively important for oxyanion binding at low loadings, the surface configuration can be characterized as being a high affinity complex. One may speculate about the reason for a high affinity character. A charge distribution factor of $f = 0.5$ in the $\equiv(FeO)_2{}^pPO_2{}^q$ and $\equiv Fe_1O_2{}^pPO_2{}^q$ bidentate complexes leads to a value of $p = -0.5$ and $p = 0$ respectively, i.e. in the case of an edge linkage, both surface ligands in combination can be neutralized and the charge is equally distributed over inner and outer ligands $f = 0.5$. Another reason could be the difference in the angle of the orbitals in the Fe-O-P linkage, being roughly in the order of 90^o and 130^o, respectively.

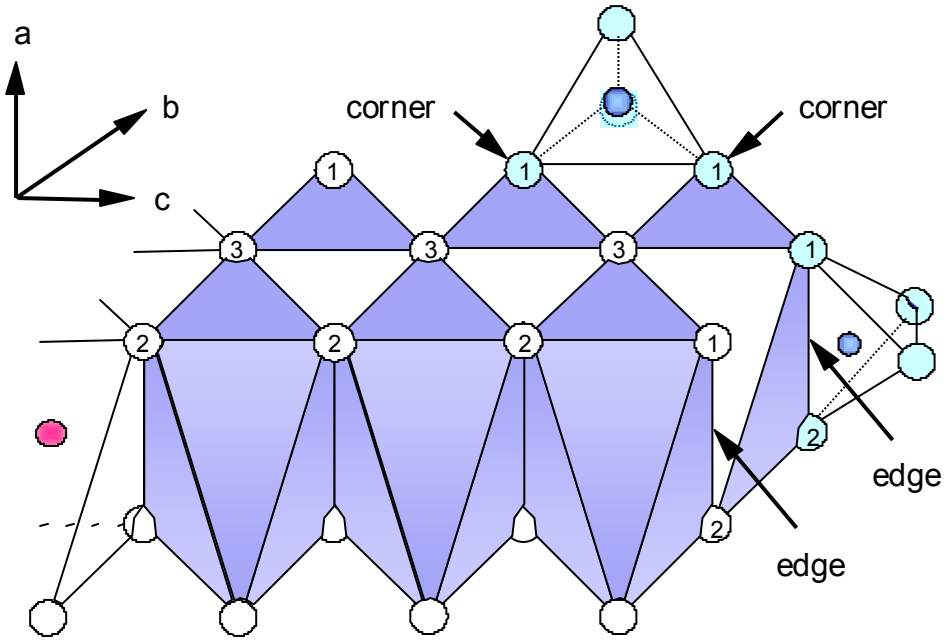

Fig.16 A schematic representation of two rows of FeO_6 octahedra present in the goethite crystal. The numbers 1, 2 or 3 on the oxygens refer to the number of coordinating Fe^{3+} ions. Two principle types of bidentate inner sphere complex are found: bonding to the edge of one octahedron (mononuclear bidentate, ^2E) or to two corners of two octahedrons (bidentate binuclear, ^2C).

We may apply this knowledge to the problem of matching the PO_4 IR data over the whole range of PO_4 loading and explain it based on the presence of high affinity sites. The high affinity edge (^2E) linkages are found on the 021 face, estimated to be for goethite roughly 10 % (22). At high PO_4, loading the majority of ^2C as well as ^2E sites is occupied with PO_4, so the PO_4 data are dominated by the dominant site with ^2C linkages (110 face). However, at a low loading the high affinity sites (^2E linkages) will contribute relatively more to the overall behavior than the low affinity sites, up to about 25 % of the PO_4 sites at a loading of 100 µmol/g in Fig.11c. A relatively high occupation at the 021 face will lead to a relatively greater presence of protonated bidentate surface complexes at this plane, because protonation is loading dependent (Fig.11). Under these conditions, the contribution to the high affinity sites

in the IR spectra may then be mainly in the form of the protonated $\equiv Fe_1O_2POOH$ species, while the 110 face is still dominated by the non-protonated $\equiv(FeO)_2PO_2$ species. This implies that the protonated form will be underestimated at low PO_4 loading if these sites are neglected. One can model this by distinguishing two separate electrostatic surfaces, a major surface for the low affinity sites, and a minor surface for the high affinity sites.

From the above analysis, one may conclude that the interpretation of the IR surface speciation at high loading is most reliable. Focusing on these data, we can model all of the other data with slightly different $\log K_{in2}$ (= 29.6) and $\log K_{in3}$ (= 35.6) values. The proton affinity constant of the bidentate surface complex $\log K_{Hp}$ ($\log K_{in3}$ - $\log K_{in2}$ = 6) found for our goethite in this case is equal to the $\log K_{Hp}$ (= 6) found for the goethite (Table 3) with the lower PZC (Fig.13).

A question arises as to whether the monodentate phosphate surface complex may become protonated. We have calculated the monodentate surface speciation assuming that the protonation constant $\log K_{Hp}$ found for bidentate complexes is also valid for the first protonation step for monodentate complexes. Using this value for monodentate complexes and assuming an equivalent shift of charge upon protonation (f = 0.35), indicates that at pH 4 very little protonation is likely to be observed.

It should be noted that our $\log K_{Hp}$ is considerably larger that the value that follows from the interpretation of Tejedor-Tejedor and Anderson (13). In our case, the protonation reaction involves a shift of charge from the 1-plane to the surface, which has a higher potential, whereas Tejedor-Tejedor & Anderson attributed the net charge of the proton fully to the 1-plane. In our approach, more energy is needed to overcome the positive potential barrier, yielding a higher $\log K_{Hp}$.

Conclusions

- The Charge Distribution (CD) model for cation and anion adsorption can be summarized as follows:
- On the scale of the compact part of the interface, adsorbed ions should not be treated as point charges.
- Inner sphere surface complexes of cations as well as oxyanions have a spatial distribution of charge, which can be attributed to two different electrostatic planes.
- The charge in the electrostatic planes results from the charge of the ligands present and of the central cation in the adsorption complex as well as any charge which may be derived from the metal ions in the solid.
- The CD model is a consistent extension of the MUSIC approach for deriving the charge of surface species.
- The charge distribution of the central ion in the surface complex can be estimated from the bond valence rule.
- Inner sphere complexes of cations are generally hydroxo complexes and of oxyanions are oxo complexes, i.e. the common ligand is a hydroxyl or oxygen, respectively.

- The mean electrostatic position of outer sphere ion pairs does not coincide with the solution-oriented ligands of inner sphere complexes. This leads to a Three Plane approach. The outer layer capacitance C_2 is relatively high (C_2 = 4-5 F/m^2), which is equivalent to the separation of the two adsorption planes by about a half to one water molecule.
- The surface activity of adsorbed binuclear bidentate complexes should be defined in terms of coverage (θ) rather than as a solution concentration (mol/L)
- The CD model enables the simultaneous description of the concentration, pH, and salt dependency of adsorption and the related charge phenomena: basic proton charging, proton exchange ratio, shift of IEP and zeta potentials, in combination with the surface speciation determined by spectroscopy (in situ CIR-FTIR) within the constraint of an intrinsic chemical surface composition.
- Both triply and singly coordinated surface groups contribute to the charging behavior of the goethite surface, whereas only the singly coordinated surface groups are active in binding PO_4. However, both types of groups affect phosphate adsorption via electrostatic interactions.
- Triply coordinated surface oxygen groups at the goethite interface exhibit a considerable variation in proton affinity, which can be related to structural differences.
- High affinity sites present on a separate electrostatic face may contribute significantly to the presence of protonated surface complexes at low phosphate loading.
- The relative decrease in monodentate oxyanion surface complexation with increasing loading and decreasing pH can be understood based on electrostatics and an asymmetric distribution of charge in the monodentate inner sphere surface complexes.
- Calculations involving broken charges in surface components can be made with only a minor change in standard algorithms for speciation calculations.

Acknowledgements

Mr.Th.A. Vens is gratefully acknowledged for his efforts in carefully carrying out the experimental work. Thanks are also due to Mr. A.J. Korteweg and Mr.A.J. Van der Linde (Dept. of Physical and Colloid Chemistry) for the BET analysis and the assistance in using the Zetasizer and due to Mr. J.D.J. Van Doesburg (Dept. of Soil Science & Geology) for the TGA and X-Ray diffraction analysis. Mr. H. Wijna, Mrs.E. Bou and Mr. F. Thiel are gratefully acknowledged for their contribution in the characterization of the goethite using TEM.

The authors express also their gratitude to Prof. U. Schwertmann and Dr. P.G. Weidler for their valuable contribution in the discussion about the crystal surfaces.

Part of this work was funded by a grant of the European Community, STEP CT90-0031.

References

1 Hingston, F.J., in "Adsorption of inorganics at Solid-Liquid interfaces" (M.A. Anderson and A.J. Rubin, Eds), Chap. 2,Ann. Arbor. Science Pub., Ann. Arbor., Michigan, 1981.

2 James, R.O., and Parks, G.A., in "Surfaces and Colloid Science". (ed.E. Matijevic) Vol.12 Chap.2. Plenum Press, 1982.

3 Sposito, G., "The Surface Chemistry of Soils". Oxford Univ.Press, New York, 1984.

4 Barrow, N.J., "Reactions with Variable Charge Soils." Martinus Nijhoff Publishers, Dordrecht, The Netherlands, 1987.

5 Dzombak, D.A., and Morel, F.M.M., "Surface complexation modelling: Hydrous Ferric Oxide", John Wiley, New York, 1990.

6 Davis, J.A., and Kent, D.B., in "Mineral-Water Interface Geochemistry" Reviews in Mineralogy (Hochella M.F., and White, A.F., Eds.), Vol.23, p.177., Miner.Soc.Am., Wasinghton D.C., 1990.

7 Goldberg, S., "Use of Surface Complexation Models in Soil Chemical Systems" in Advances in Agronomy (J.L. Sparks ed.) Academic press, Vol.47, p.233, 1992.

8 Stumm, W. "Chemistry of the Solid-water Interface". John Wiley Sons, New York, 1992.

9 Russell, J.D., Parfitt, L.R., Fraser, A.R., and Farmer, V.C., Nature 248, 220 (1974).

10 Parfitt, R.L., Atkinson, R.J., and Smart, R.S.C., Soil Sci.Soc.Am.Proc. 39, 837 (1975).

11 Parfitt, R.L., and Atkinson, R.J., Nature 264, 740 (1976).

12 Parfitt, R.L., Soil Sci.Soc.Am.Proc. 43, 623 (1979).

13 Tejedor-Tejedor, M.I., and Anderson, M.A., Langmuir 6, 602 (1990).

14 Van Riemsdijk, W.H., and Van der Zee, S.E.A.T.M., in "Interactions in the Soil Colloid - Soil Solution Interface" (Bolt, G.H., De Boodt, M.F., Hayes, M.H.B., and McBride, M.B., eds.), NATO ASI Series (E) Vol.190, Chap.8 Kluwer Academic Publishers, 1991.

15 Hiemstra, T., Van Riemsdijk, W.H., and Bolt, G.H., J. Colloid Interface Sci. 133, 91 (1989).

16 Hiemstra, T., De Wit, J.C.M., and Van Riemsdijk, W.H., J. Colloid Interface Sci. 133, 105 (1989).

17 Van Riemsdijk, W.H., and Lyklema, J., Colloids Surf. 1,33 (1980).

18 Hiemstra, T., Van Riemsdijk, W.H., and Bruggenwert, M.G.M., Neth.J.Agric.Sci. 35,281 (1987).

19 Torrent, J., Barron, V., and Schwertmann, U., Soil Sci.Soc.Am.J. 54, 1007 (1990).

20 Spadini, L., Manceau, A., Schindler, P.W., and Charlet, L., J. Colloid Interface Sci. 168, 73 (1994).

21 Manceau, A., and Charlet, L., J. Colloid Interface Sci. 168, 87 (1994).

22 Colombo, C., Barron, V., and Torrent, J., Geochim. Cosmochim.Acta 58, 1261. (1994).

23 Pauling, L., J.Am.Chem.Soc. 51, 1010 (1929).

24 Hingston, F.J., Posner, A.M., and Quirk, P.J., Disc. Farad. Soc., 52, 334 (1971).

25 Hingston, F.J., Posner, A.M., and Quirk, P.J., J.Soil Sci. 23, 177 (1972).

26 Bowden, J.W., Nagarajah, S., Barrow, N.J., Posner, A.M., and Quirk, P.J., Aust. J.Soil.Res. 18, 49-60 (1980).

27 Barrow, N.J., Bowden, J.W., Posner, A.M., and Quirk, P.J., Aust. J.Soil.Res. 18, 395 (1980).

28 Sigg, L. and Stumm, W., Colloid Surfaces 2, 101 (1981).

29 Bolt, G.H., in "Soil Chemistry B Physio-chemical Models" (G.H. Bolt,Ed.), 2nd ed., Chap.I.,Elsevier, Amsterdam,1982.
30 Sposito, G., "The Chemistry of Soils". Oxford Univ.Press, New York, 1989.
31 Stern, O., Z. Electrochem., 30, 508 (1924).
32 Westall, J. and Hohl, H., Adv.Colloid Interf.Sci., 12, 265 (1980).
33 Yates, D.E., Levine, S., and Healy, T.W., Chem. Soc. Faraday Trans.I, 70, 1807-1818 (1974).
34 Sprycha, R., J Colloid Interf. Sci., 102, 173 (1984).
35 Sprycha, R., J Colloid Interf. Sci., 127, 12 (1989).
36 Yates, D.E., The structure of the oxide/aqueous electrolyte interface. Ph.D.thesis, University of Melbourne, Melbourne,1975.
37 Davis, J.A., and Leckie, J.O., J. Colloid Interface Sci. 67, 90 (1978).
38 Davis, J.A., James, R.O., and J.O. Leckie., J. Colloid Interface Sci. 63, 480 (1978).
39 Hiemstra, T., and Van Riemsdijk, W.H., Colloids and Surf., 59, 7 (1991).
40 Shiao, S.-Y., and Meyer, R.E., J.Inorg.Nucl.Chem. 43, 3301 (1981).
41 Hohl, H., and Stumm, W., J.Colloid Interface Sci. 55, 281 (1976).
42 Schindler, P.W., and Stumm, W., in "Aquatic Surface Chemistry" (W. Stumm Ed.) Chap.4. John Wiley & Sons, New York. 1987.
43 Bolt, G.H., and Van Riemsdijk, W.H., in "Interactions in the Soil Colloid - Soil Solution Interface" (Bolt ,G.H., De Boodt, M.F., Hayes, M.H.B., and McBride, M.B., eds), NATO ASI Series (E) Vol.190, Chap.2 Kluwer Academic Publishers, 1991.
44 Davis, J.A., and Leckie, J.O., J. Colloid Interface Sci. 74, 32 (1980).
45 Davies, C.W., J.Chem.Soc., 2421 (1930).
46 Cornell, R.M., Posner, A.M., and Quirk, P.J., J.Inorg.Nucl.Chem., 36, 1937 (1974).
47 Schwertmann, U., and Cornell, R.M., "Iron Oxides in the Laboratory. Preparation and Characterization", Chap.5, VCH verlag, Weinheim, Germany, 1991.
48 Smith, K.L., and Eggleton, R.A., Clays Claymin. 31, 392 (1983).
49 Schwertmann, U., Claymin. 19, 9 (1984).
50 Mann, S., Cornell, R.M., and Schwertmann, U., Clay Mineral. 20, 255 (1985).
51 Van der Woude ,J.H.A., DeBruyn, P.J. and Pieters, J., Colloids Surfaces 9, 173 (1984).
52 Van der Woude, J.H.A., and DeBruyn, P.J., Colloids Surfaces 11, (1984).
53 Amouric, M., Baronnet, A., Nahon, D., and Didier, P., Clays and Clay minerals 34, 42 (1986).
54 Weidler P. G., Schwinn T., and Gaub H. E. (1996) *Clays Clay Minerals* 44, 437 (1996)
55 Van Riemsdijk, W.H., Bolt, G.H., Koopal, K.L., and Blaakmeer, J., J. Colloid Interface Sci. 109, 219 (1986).
56 Bolt, G.H., and Van Riemsdijk, W.H., in "Soil Chemistry B Physio-chemical Models" (G.H. Bolt, Ed.), 2nd ed., Chap.XIII. Elsevier, Amsterdam, 1982.
57 Smith, R.M., and Martell, A.E., "Critical Stability Constants" Vol.4, Plenum Press, New York, 1981.
58 Davies, C.W., "Ion Association", Butterworths London, 1962.
59 Morel, F.F.M., in "The Principles of Aquatic Chemistry" Wiley New York 1987.
60 Zeltner, W.A., and Anderson, M.A., Langmuir 4, 469 (1988).
61 Healy, T.W. and White, L.R., Adv. Colloid Interf. Sci. 9, 303 (1978).
62 Manceau, A., *Geochim. Cosmoschim. Acta* 59(17), 3647(1995)

Appendix

The formulation of the chemical equilibrium problem in terms of an ion speciation table is given in Table A for adsorption reactions. The ion speciation table relates species and components in reaction quotients and mass balances. The various components are given in the columns. In the CD model, 3 electrostatic components ($e^{-zF\psi i /RT}$) are defined for respectively the 0-, 1-, and 2- (or d-) plane. The chemical system of our example is built with 2 surface components (≡FeOH and $\equiv Fe_3O$) and 4 solution components (H, PO_4, Na, and NO_3). For the Na and NO_3 components, a known solution concentration is assumed, reducing the number of unknown solution components to H and PO_4. The surface and the solution species concentrations are all expressed in mol/L.

The species concentrations can be calculated by formulating the appropriate expressions with the help of the coefficients from the ion speciation table. Reading across the table, the general expression for the species concentration S (mol/L) is:

$$[S] = \Pi\ [C_k]^{n_k}\ \ 10^{log\,K} \qquad [A-1]$$

in which the term $\Pi\ [C_k]$ is the product of component concentrations, including electrostatic components, ($e^{-zF\psi i /RT}$), surface components (≡FeOH and $\equiv Fe_3O$) and solution components. The coefficients n_k are found in the rows. The log$K$ in Eq.[A-1] is the expression given in the last column of Table A. The expression for log$K$ can be an intrinsic equilibrium constant logK_{in} or the intrinsic equilibrium constant which includes concentration terms of the known components such as log[Na^+] or log[NO_3^-] in our example.

Two additional comments should be made about the table. The surface species in the table have to be expressed in mol/L which is not the same as the definitions given in the text, where relative surface concentrations or mole fractions (θ) have been used. In the case of monodentate adsorption, the value of the log$K$ is not affected by the use of mol/L instead of mole fractions. However, for bidentate surface species the value of the log$K_{in}(\theta)$ should be rewritten as an apparent log$K$ value, which can be used in the scheme. This leads to the derivation of a conversion factor, which converts the intrinsic adsorption constant K_{in} to an apparent constant, K_t, which can be used in the table:

$$K_{in} = \frac{\theta_{ads}}{\theta_{ref}^2 \Pi C_{n,sol}^{n_k}} = \frac{\dfrac{S_{ads}}{\rho\, AN_{s,j}}}{\left(\dfrac{S_{ref}}{\rho\, AN_{s,j}}\right)^2 \Pi C_{n,sol}^{n_k}} = \rho\, AN_{s,j}\left\{\frac{S_{ads}}{S_{ref}^2 \Pi C_{n,sol}^{n_k}}\right\} = \rho\, AN_{s,j} K_t \qquad [A-2]$$

in which S_{ads} is the species concentration of the adsorbed complex (mol/L), S_{ref} (mol/L) is the species concentration of the reference surface component (here the surface group ≡FeOH) and ρ the solid-solution ratio (kg/L), A the specific surface area (m^2/kg) and $N_{s,j}$ the site density (mol/m^2) of surface group j. In Eq.[A-2], $C_{k,sol}$ represents the various solution component concentrations. Based on Eq.[A-2], the logK_t for Table A equals logK_t = log$\underline{K}_{in}(\theta)$ - log(ρ

A$N_{s,j}$) in the case of bidentate surface complexation. In the table of species, calculations are based on concentrations, whereas equilibria are defined in terms of activities. The necessary activity corrections can be made by introducing the activity coefficients in the log$K$ value used in the calculations.

The table with coefficients can also be used to formulate the mass balances necessary for solving the chemical equilibrium problem. The mass balances related to the first three columns need some comments.

The mass balance formulated with coefficients from the first column expresses the change of charge (in mole unit charge = mole p^+) of the surface plane relative to the reference components chosen (≡FeOH and $\equiv Fe_3O$), expressed in mol/L. The mass balance expresses the difference in surface charge starting from a surface with only the two surface components (≡FeOH and $\equiv Fe_3O$ groups). The mass balance based on species concentrations (Σ) is therefore equal to:

$$\sum_1 = \frac{\rho A}{F}(\sigma_0 - \Sigma z_j F N_{s,j}) \qquad [A-3a]$$

in which σ_0 is the surface charge (C/m^2) and $\Sigma z_j F N_{s,j}$ is the charge of the surface when only the surface components j are present (z_j of both reference components $\equiv FeOH^{-1/2}$ and $\equiv Fe_3O^{-1/2}$ equals -0.5). The charge in C/m^2 is converted to mole p^+/m^2 using 1/F (F = 96485 C/mol p^+) and is recalculated to mol/L with the help of ρ (kg/L) and A (m^2/kg).

The expression [A-3a] is different from the expression used in the classical scheme due to the presence of the term $\Sigma z_j F N_{s,j}$. This term is not necessary if the charge of the reference surface component is zero, as is usually the case in calculations based on the classical 2pK approach in which SOH^o is used as the reference component. As shown in Table A and expression [A-3a], the standard computer code has only to be extended by the term and $\Sigma z_j F N_{s,j}$ in order to do all CD model calculations!

The value of the right hand side of Eq.[A-3a] can be found with help of electrostatics using the potential of the 0- and 1-plane according to:

$$\sigma_0 = C_1(\psi_0 - \psi_1) \qquad [A-3b]$$

in which C_1 is the capacitance of the first layer between the 0- and 1-plane.

For column 2, a similar approach is used. Here the mass balance based on surface speciation (Σ_2) is equal to:

$$\sum_2 = \frac{\rho A}{F}\sigma_1 \qquad [A-4a]$$

in which σ_1 is the charge of the 1-plane (C/m^2) based on electrostatic calculations, according to:

$$\sigma_0 + \sigma_1 = C_2(\psi_1 - \psi_2) \qquad [A-4b]$$

in which C_2 is the capacitance of the second layer between the 1- and 2- (or d-) plane.

For column 3, only a minor difference in approach is used. Here the mass balance based on surface speciation (Σ_3) is equal to:

$$\sum_3 = \frac{\rho A}{F}\sigma_2 \qquad [A-5]$$

where σ_2 is the charge of the 2- (or d-) plane (C/m^2). The charge in the 2- (or d-) plane can also be calculated from electrostatics. It should then be realized that the charge at the interface is present in four different locations. Charge is present at the surface in the 0 -plane (σ_0), in the 1-plane (σ_1), the 2- (or d-) plane (σ_2) and also in the DDL (σ_{ddl}). Because of overall electroneutrality, one may write:

$$\sigma_0 + \sigma_1 + \sigma_2 + \sigma_{ddl} = 0 \qquad [A-6]$$

The surface charge (σ_0) and the charge in the 1-plane (σ_1) can be found for a given set of potentials (ψ_0 , ψ_1 , ψ_2) using Eq.[A-3b] and [A-4b]. The charge in the DDL (σ_{ddl}) can be calculated, using ψ_d, according to:

$$\sigma_{ddl} = \pm\frac{1}{2}\sqrt{8000\varepsilon_0\varepsilon_r RT}\sqrt{\sum_i C_i(e^{-z_i F\psi_d RT} - 1)} \qquad [A-7]$$

in which ε_r and ε_0 are the relative and absolute dielectric constants. Combination of Eqs.[A-3b,A-4b,A-6,A-7] finally yields the charge in the 2- plane.

The calculation procedure starts with calculation of the speciation using estimates for the component concentrations. The mass balances, based on the calculated speciation, are compared with the expressions in the last row of the ion speciation table. If the difference is greater than the expected small value, i.e. an incorrect estimation of the component concentrations, an improvement of the estimates is calculated. The calculation procedure is repeated until a sufficiently accurate numerical solution is found, applying the commonly-used Newton-Raphson procedure.

TABLE A

An Example of the Table of Species for the CD–MUSIC Calculations for PO_4 Adsorption by Goethite

Components species (mol/liter)	$e^{-F\psi_0/RT}$	$e^{-F\psi_1/RT}$	$e^{-F\psi_2/RT}$	FeOH	Fe_3O	H	PO_4	log K
Na^+(aq)								0 + log[Na]
NO_3^-(aq)								0 + log[NO_3]
H^+(aq)						1		0
OH^-(aq)						−1		log K_w
PO_4^{-3}(aq)							1	0
HPO_4^{-2}(aq)						1	1	log K_{p1}
$H_2PO_4^{-1}$(aq)						2	1	log K_{p2}
$H_3PO_4^0$(aq)						3	1	log K_{p3}
$NaHPO_4^{-1}$(aq)						1	1	log K_{p4} + log[Na]
$FeOH^{-1/2}$				1				0
$FeOH_2^{+1/2}$	1			1		1		log K_{H1} = log $K_{1,2}$
$FeOH^{-1/2}$–Na^+			1	1				log K_c + log [Na]
$FeOH_2^{+1/2}$–NO_3^-	1		−1	1		1		log K_a + log K_{H1} + log[NO_3]
$FeO^pPO_3^q$	$-1 + 5f_1$	$5(1 - f_1) - 6$		1		1	1	log K_{in1}
$Fe_2O_2^gPO_2^q$	$-2 + 5f_2$	$5(1 - f_2) - 4$		2		2	1	log K_{in2} − log($\rho AN_{s,1}$)
$Fe_2O_2^gPOOH^q$	$-2 + 5f_3$	$5(1 - f_3) - 2 - 1$		2		3	1	log K_{in3} − log($\rho AN_{s,1}$)
$Fe_3O^{-1/2}$					1			0
$Fe_3OH^{+1/2}$	1				1	1		log K_{H2} = log $K_{3,1}$
$Fe_3O^{-1/2}$–Na^+			1		1			log K_c + log[Na]
$Fe_3OH^{+1/2}$–NO_3^-	1		−1		1	1		log K_a + log K_{H2} + log[NO_3]
Sum	$\frac{\rho A}{F}(\sigma_0 - \sum z_j F N_{s,j})$	$\frac{\rho A}{F}\sigma_1$	$\frac{\rho A}{F}\sigma_2$	$\rho AN_{s,1}$	$\rho AN_{s,2}$	H(t) − OH(t)	PO_4(t)	

Note. All log K values are based on intrinsic constants, adjusted for activity corrections in the case of $I \neq 0$.

Chapter 5

On the Relationship between Charge Distribution, Surface Hydration, and the Structure of the Interface of Metal (hydr)oxides

Tjisse Hiemstra and Willem H. Van Riemsdijk

On invitation published as Feature Article in Journal of Colloid and Interface Science. Volume 301, Issue 1, Page 1-18, September 1, 2006

Abstract

The double layer structure of metal (hydr) oxides is discussed. Charge separation may exist between the minimum distance of approach of electrolyte ions and the DDL domain. The corresponding capacitance value of the outer Stern layer is similar to the capacitance value of the inner Stern layer. The extended Stern model implicitly supports a hydration structure at the near-surface with some discrete layering of water and electrolyte ions. The significance of dipole orientation is analyzed theoretically. Dipole theory in combination with a calculated ion charge distribution is compared with the experimental overall charge distribution. Ion charge distribution for various oxyanions has been calculated applying the Brown bond valence concept to the geometry of surface complexes that have been optimized with MO/DFT calculations. The comparison is done in detail for silicic acid adsorption on goethite. In addition, results are discussed for arsenite, carbonate, sulphate, and phosphate, using the same approach. The dipole correction depends on the charge introduced in a neutral surface by ion adsorption, which differs for the various ions studied. The fractional correction factor ϕ derived for the experimental data agrees with the theoretical value $\phi_m = 0.17 \pm 0.02$. On an absolute scale, the dipole corrections are usually limited to the range of about 0-0.15 v.u. The CD values calculated with MO/DFT are not particularly sensitive (~ 0.03 v.u) to the precise Fe-octahedral geometry, which suggests that a calculated CD is a reasonable approximation in ion adsorption modeling for ill-defined Fe-oxides like HFO and natural Fe oxide materials of soils.

I Introduction

One of the most eye-catching properties of colloids is the existence of surface charge that is balanced by the charge of counter and co-ions. It results in a double layer, which was described as concept by Von Helmholtz in 1879 [1]. Counter and co-ions can be diffusely distributed with a respectively decreasing and increasing concentration towards the solution. In 1910 and 1913, Gouy [2] and Chapman [3] developed, separately from each other, a theory that is known as the diffuse double layer (DDL) theory. It describes the diffuse distribution of charged ions as a function of distance from a planar surface. Stern [4] extended the double layer theory to explain the relation between the charge of a mercury electrode and the interface potential between mercury and an electrolyte solution. He concluded that the charge in the diffuse double layer was separated from the surface charge of mercury by an empty layer, now known as a Stern layer. The physical explanation for it is the notion that the counter ions have a finite size with a corresponding minimum distance of approach to the surface, i.e. the structure of ions and interface is involved. Stern recognized that at the scale of the compact part of the double layer, ions should not be considered as point charges. Stern also recognized that electrolyte ions might specifically adsorb. This concept was later refined by Grahame [5].

Modern electrochemistry [6, 7] has largely contributed to the basic understanding of the behavior of metal (hydr)oxides. These theories have mainly focused on the double layer structure that is formed at the solution side of the surface. In particular, this part of the double layer is experienced and cherished by colloid chemists. However, interface behavior is not only determined by the properties of the double layer. Part of the behavior of the interface originates from the underlying materials, in particular the mineral structure. The surface is the borderline between both phases. The bond valence concept can be used to understand a mineral structure and its surface. In this concept, cation charge is distributed over the surrounding ligands and the sum of bond valences around a central anion should be equal to its charge. This idea originates from Pauling [8] and has been refined by Brown [9-11]. Although this approach is semi-empirical, many applications [12] show the high degree of accuracy. The bond valence concept has been applied to develop the MUlti SIte Complexation (MUSIC) model [13]. It allows differentiating various types of surface groups in terms of formal charge. A singly coordinated surface hydroxyl on silica has a formal charge of $\equiv SiOH^{0}$ while on a Fe oxide it is $\equiv FeOH^{-1/2}$. This difference leads for the corresponding oxides to a very different development of the pH dependent surface charge and surface potential [13]. At the solid-water interface of minerals, the surface oxygens may bind zero, one or two protons, depending on the pH in solution and the proton affinity of the surface group. The MUSIC model requires an estimation of the proton affinity of the various types of reactive groups on the surface of minerals [13, 14]. The proton affinity is linked to the *formal* charge of a surface group, using a set of formal rules that calculates the saturation of the oxygen valence. The model is calibrated on a selective set of solution species and applied assuming differences in hydration between species in solution and surface. This model is not meant to explain in detail the wide variety of the acid-base chemistry of solution monomers. Although the precise value of the affinity constants may be uncertain, the model is successful in understanding major differences in proton reactivity of surface groups and charging of

metal oxide surfaces. For instance, the model has highlighted that two successive protonation steps on one and the same ligand will lead a very different affinity constant for the reaction ($\Delta \log K_H \approx 10$), which implies that practically only the O/OH or the OH/OH_2 transition of a surface group can be observed in an experimental window [13], i.e. not both as in the 2 p*K*-model. Actually, a metal oxide has a multiple 1-p*K* behavior. Another prediction is the inertness of double coordinated surface groups on sesquioxides, which may result in non-charged crystal faces for gibbsite [15, 16] and hematite [17, 18] if perfectly crystallized. The model also predicts the difference in proton affinity for the two basic types of triply coordinated groups of α-FeOOH, which are present in the mineral structure as well as at the surface ($\equiv Fe_3O_I^{-1/2}$ and $\equiv Fe_3O_{II}H^{+1/2}$). In addition, the model describes successfully the variation in surface speciation of TiO_2 as observed with in-situ spectroscopy [18-20]. The MUSIC model may also account for changes in temperature as shown by the work of Machesky et al. [21].

Many ions can react with mineral surfaces via a ligand exchange mechanism, in which a part of the ligands of the adsorbed ion becomes common with the surface, while the other ligands remain in full contact with the interfacial water. Since the electrostatic gradients are often extremely large near the surface, the inner sphere complex formed experiences different double layer potentials. The Charge Distribution (CD) model [22] has been developed to account for this. The charge distribution depends on the structure of the inner sphere complex [22, 23]. The CD model can be combined with the MUSIC model to link information on the structure of the surface, the structure of the adsorbed surface species and the structure of the double layer to describe macroscopic adsorption phenomena [22, 24, 25].

In a number of cases, the CD value that is needed to describe the experimental data corresponds approximately to the CD value of the ion that can be derived from a simple Pauling bond valence analysis of the structure of the surface complex. At other occasions, the interfacial charge distribution has to be adjusted to obtain a good description. Ideally, the charge distribution can be linked to the geometry of the complexes, which can be assessed ideally by spectroscopy or by first principle calculations. The calculated distribution of ion charge might be used in surface complexation modeling to derive the electrostatic contribution of the ion charge to the Gibbs free energy change of the adsorption reaction. However, other processes may also contribute to the overall electrostatic energy, in particular the orientation of water molecules [7]. Bockris and Reddy [7] have argued that the picture of the double layer has often been “ionic centric” rather than “water centric”. Dipole orientation refers to the latter.

In this contribution, we will focus on the relation between hydration water and interfacial distribution of ion charge. We will derive a simplified model that estimates the electrostatic effect of the dipole orientation of water molecules as a feedback on the introduction of ion charge in the interface. We will show that the magnitude and sign of this correction factor is very much dependent on the nature of the surface species. We will use this model to explain the differences between the CD values obtained from modeling of macroscopic adsorption data and those obtained from a bond valence analysis of the geometry of surface complexes that we optimized with quantum chemical (QC) calculations. Although these computations are often very time consuming, the optimization of the geometries is done

in the presence of hydration water to obtain realistic results. This will be discussed for the species $Si(OH)_4$, $As(OH)_3$, CO_3^{2-}, SO_4^{2-}, and $H_xPO_4^{-3+x}$. The new theory enables to link the quantum chemically derived CD value to adsorption parameters in surface complexation modeling. In principle, the geometry of surface complexes can also be approached experimentally with spectroscopy. The new insight has been used to estimate for cations the range in magnitude of dipole corrections, using relevant EXAFS data.

II Material and methods

Material

Goethite (α-FeOOH) used in this study has been prepared as described in Hiemstra et al. [26]. The specific BET-surface area of this goethite, measured by N_2 gas adsorption, is 85 m^2/g.

Proton co-adsorption experiment

Proton co-adsorption upon the addition of silicic acid (H_4SiO_4) was measured, using the method described by Rietra et al. [23]. Accurate pH-stat titrations were carried out in a thermostatic Metrohm vessel (22.0 ± 0.1 ^oC) present in a constant temperature room. The vessel was continuously purged with moist, purified N_2 gas. A double junction reference electrode was used. The outer junction was filled with a 0.125 M $NaNO_3$ and 0.875 M KNO_3 solution to minimize the diffusion potential.

A mass of 10.00 (pH = 8) or 20.00 (pH = 6) gram of a stock suspension (46.87 g/kg, goethite) was diluted by pipetting ultra pure water and electrolyte solution to a calculated solution volume of approximately 40.0 mL, assuming a mass density of 4.37 g/cm^3 for goethite. The suspension was acidified to a pH of about 5 and purged with moist purified N_2 gas for 16 hours to remove adsorbed CO_2. The experiments were done at constant pH of 6.00 and 8.00 in 0.100 M $NaNO_3$. The electrodes were calibrated with commercial available pH buffer solutions. The drift of the electrodes during 24 hours was found to be restricted to less than about 0.02 pH unit. The suspensions were titrated in steps (1.00-2.50 mL) with a solution of 2.30 mM H_4SiO_4, made from $Na_2SiO_3.9\ H_2O$, acidified to pH 5.3 for removal of CO_2 (N_2 purging). In the experiments, the pH was kept constant at the chosen pH values using a 0.94 mM NaOH solution, placed in a CO_2 free desiccator. The reaction time per step was about 1 hour, leading to an apparent equilibrium. The total Na concentration (0.100 M) was kept constant by addition of 1.00 M $NaNO_3$ with another burette. The volume of the $NaNO_3$ solution to be added at each step was calculated based on a proper bookkeeping of added volumes and concentration of the chemicals. The Si concentration of the added solution was calibrated with ICP-MS using a commercial available stock solution.

Quantum chemical computations

The geometry of bidentate complexes of silicic acid bound to two Fe octahedrons was calculated using Spartan'04 software of Wavefunction [27]. The geometry optimizations were done using molecular orbital (MO) computations applying density functional theory (DFT). Pseudo potentials, defined in Spartan'04 as LACVP+** (Los Alamos Core Valence Potentials), were used. This set comprises the 6-31+G** basis set for main group elements H-Ar. The + and ** signs refer to the use of respectively diffuse and polarization functions. The geometries were optimized using the unrestricted Becke Perdew (BP86) model [28]. The calculated geometries have been interpreted with the Brown bond valence approach [11], in order to obtain the charge distribution value of the ≡ $(FeO)_2Si(OH)_2$ complexes. The various silicic acid complexes, optimized in this study, differ in the number of water molecules added to mimic hydration.

III Results and Discussion

A Double layer structure

Electrode surfaces

In Figure 1, the interface of a metal electrode has been given schematically. To quite some extent, the structure can also be representative for the interface of insoluble ionic substances like for instance AgI(s) [29, 30]. The metal surface can be charged. The charge is compensated by co- and counter-ions in solution that form, together with the charge of the surface, a double layer. A main characteristic of this interface is the presence of hydration water in direct contact with the electrode. It is known that this coordinative water is strongly bound to the surface and that the water layer is quite structured [31]. As a result, the value of the relative permittivity can be as low as $\varepsilon_r = 6$. Moreover, this water is not removed by low levels of hydrated, indifferent electrolyte ions. It implies that the charge in a metal electrode is separated from the indifferent ions by a layer with a thickness of about two water molecules. The water of the second layer is considered to be far less structured and is estimated to have a relative permittivity between electrical saturation ($\varepsilon_r = 6$) and free water ($\varepsilon_r = 78$). Because of the presence of the first layer of strongly and structurally bound water, one observes a quite low value for the electrostatic capacitance C ($F/m^2 = CV^{-1}/m^2$), which can have values of approximately $C \approx 0.2$ F/m^2.

The overall capacitance of the compact part of the double layer is the combination of the capacitances of two layers (Fig. 1). The capacitances are related in the interface structure according to the expressions:

$$\frac{1}{C} = \frac{1}{C_1} + \frac{1}{C_2} \qquad [1]$$

and

$$C_i = \frac{\varepsilon_{r,i}\varepsilon_o}{d_i} \qquad [2]$$

n which C is the overall capacitance, which is linked to the capacitances C_1 and C_2 of the two individual water layers. The relative and absolute permittivity are represented by respectively ε_r and ε_0 (8.85 10^{-12} F/m) and d is the distance between the two electrostatic planes involved.

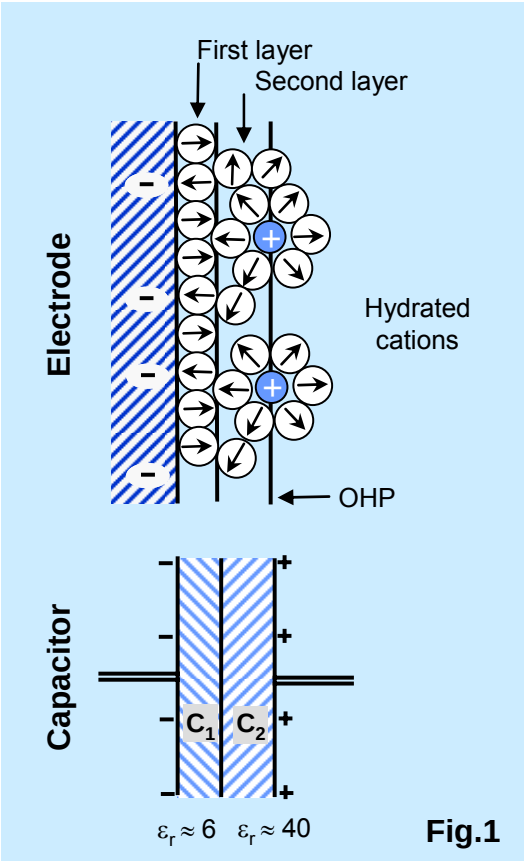

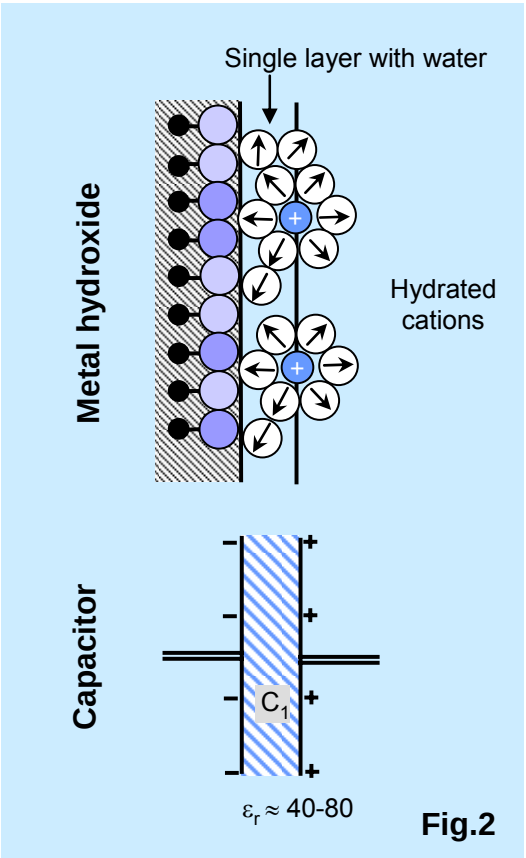

Fig.1 (left). The schematic structure of the oxygens at a metal electrode surface oxide (uppper) and the parallel plate capacitor (lower) with two different dielectrics, that in a series determines the overall capacitance of the layer of charge separation (Eq.[1]). It is thought that the 2-plane is the fence of the diffuse double layer region, resulting in a triple layer model with three electrostatic planes.

Figure 2 (right). The schematic structure of the oxygens at a metal hydroxide surface (upper) and the parallel plate capacitor (lower). The surface charge is located on surface groups that are coordinated with metal ions and a variable number of protons.

Based on the dielectric constants given (Fig. 1), the diameter of a water molecule ($d \approx$ 0.28 nm) and the radius of hydrated monovalent ions ($r \approx$ 0.35 ± 0.05 nm), the calculated

overall capacitance is 0.16 F/m^2, which is close to values observed [7]. Calculations show that the capacitance value is mainly due to the properties of the first layer of hydration water (chemisorbed). The properties of the second layer are less relevant, which may agree with the experimental observation that the overall capacitance is rather constant for ions that differ in hydration radius [7]. We note that the dominance of the primary layer on the double layer properties will make it more difficult to retrieve details of the double layer structure beyond the first layer. In this respect, interpretation of charging properties of metal (hydr) oxide interface may be of help.

Metal (hydr) oxide interface

The low experimental value for the capacitance of metal electrodes is quite different from the capacitance values found for metal (hydr) oxides. We have pointed out how this is related to the difference in structure of the double layer on metal oxides surfaces [32]. The main reason is that charge on metal (hydr) oxides is created by the relative amount of protons bound to the surface oxygens resulting in O, OH, or OH_2 surface ligands (Fig. 2). The corresponding electrostatic field can be described with the mean field theory [33]. The electrostatic field, radiating from the surface, becomes neutralized by hydrated cations and anions that can be present at a minimum distance of approach. This distance is expected to be equivalent to the primary hydration radius of those ions and comparable with the width of the second layer on the metal electrode surface (Fig. 1). Similar as for a metal electrode, this layer will have a relative permittivity that may be lower than that of free water, for instance having a value somewhere halfway between the above-mentioned extremes. In combination with a distance that is equivalent with the radius of a hydrated counter ion ($\approx 0.35 \pm 0.05$ nm), the capacitance of the layer of charge separation can be calculated (Eq.[2]), yielding $C \approx 1$ F/m^2. Such a value is typical for the interface of non-porous metal (hydr) oxides.

It might be argued that a metal hydroxide can be seen as a combination of a permanent excess charge on the metal ions and a variable neutralization at some distance by the surface ligands (Fig.2). If this idea is implemented as an extra capacitor, it can be shown that it is equivalent with the attribution of the metal ion charge to the surface ligands, as is done in the MUSIC model [13], apart from a potential difference between the metal ions of the mineral and surface ligands.

Terminology

On metal electrodes, hydrated counter and co-ions neutralize the surface charge. In electrochemistry, the electrostatic position of these ions at the minimum distance of approach is classically called the outer Helmholtz plane (OHP). The layer between the minimum distance of approach of hydrated ions and the charge at the electrode surface can be called a Stern layer. At metal electrodes, neutralization of charge may also result from ions that partially dehydrate and penetrate into the primary water layer. Bockris and Reddy [7] call

these ions contact-adsorbed ions. These ions are located at the so-called inner-Helmholtz plane (IHP). The full model has been called a triple layer model [7]. One may draw a comparison to the contact-adsorbed ions and ions that form inner sphere complexes on metal oxide surfaces. In both cases, water molecules are desorbed. Contact-adsorbed ions replace water molecules that are part of the Stern layer, whereas in case of inner sphere complexation on metal (hydr) oxides, ligands of the surface plane are involved. Since the structure of the double layer of an electrode and a metal oxide surface are fundamentally different in some aspects, the mentioned triple layer model has to be transformed into a picture valid for metal oxide surfaces. The most direct transformation of the triple layer model of metal electrodes is the removal of the first hydration layer from the model, which leads to the so-called Basic Stern model [34]. In the early days, it was used by Atkinson et al.[35], Stumm et al.[36], Bowden [37, 38], and others. However, the main stream has followed a different way for quite some while. The model of Yates [39], and later Davis and Leckie [40, 41] is also named Triple Layer (TL) model, but the model differs in some aspects from the triple layer model of Bockris and Reddy [7]. In the TL model, the electrostatic position of the IHP, where specifically adsorbed ions reside, coincides with the surface plane. A new layer of charge separation was introduced to disconnect the head end of the diffuse double layer (DDL) from the minimum distance of approach of hydrated ions. Apparently, it was supposed that the overall capacitance found for electrodes should also be valid for the double layer on metal hydroxide surfaces, i.e. the capacitance of the outer layer was set at $C_2 = 0.2$ F/m^2. However, as pointed out by Hiemstra and Van Riemsdijk [32], application of Eq.[2] with $\varepsilon_r = 40$ or 80 shows that this (charge free!) layer would have a width of about 2-3.5 nm, which is equivalent with too many water molecules to be physically realistic. Lately, this was also recognized by Sverjensky [42] who assumed that the capacitance of the inner and outer layer in the TL model are quite similar, i.e. he used a slightly arbitrary definition $C_1 \equiv C_2$.

Location of the head end of the DDL

Recently, the structure of the double layer has been discussed in terms of the position of individual types of electrolyte ions in the compact part of the double layer based on the analysis of experimental data [43]. Derivation of a correct physical-chemical picture from fitting data is not a trivial task [44, 45]. Coherent data are required. Rahnemaie et al. [43] used a large, internally consistent titration data set, collected for a wide range of types of electrolyte ions for one material in a well-defined reference state. The position of the individual types of electrolyte ions (Li^+, Na^+, K^+, Cs^+, Cl^-, and NO_3^-, ClO_4^-) in the double layer profile was traced with a CD approach. The charge of the various electrolyte ions was allowed to be located in the double layer between a minimum distance of approach and the head end of the diffuse double layer (DDL).

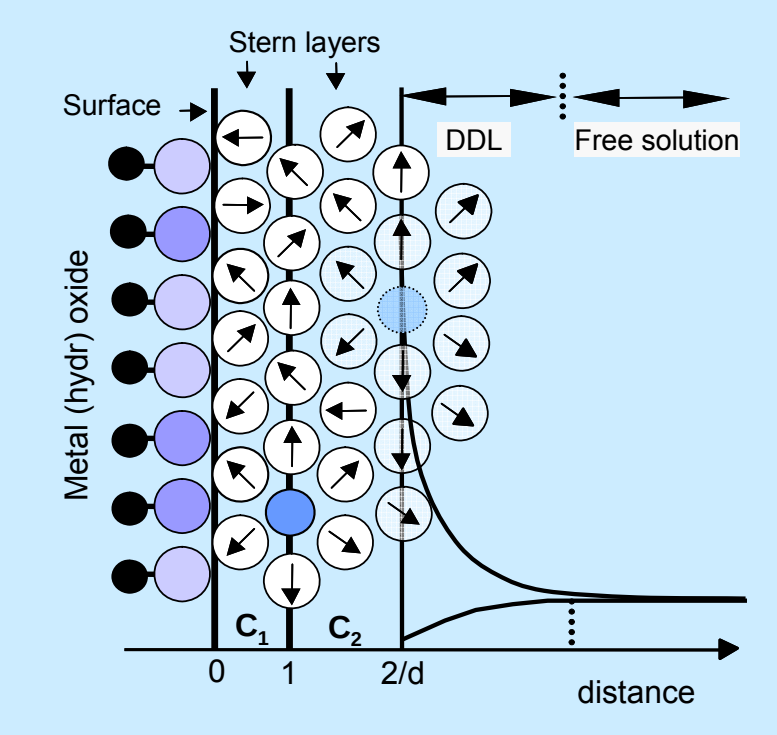

Figure 3. A schematic snapshot of the structure of the electric double layer on metal (hydr) oxides and the arrangement of ions. The surface water molecules tend to orientate on the charges present in the interface, but thermal motion tend to disturb this. The arrows represent schematically the orientation of the water dipoles. Hydrated ions can reach the minimum distance of approach and the corresponding charge is attributed to the 1-plane. The depicted ion in the second plane is conceptually part of the DDL charge. If charging of a metal (hydr) oxide is studied in a consistent manner for a series of electrolytes that strongly differ in strength of ion pair formation [43], the data analysis suggests that charge separation may exist between the diffuse double layer region and the minimum distance of approach at ion pair formation. Experimentally, the capacitances have found to be rather similar ($C_1 \approx C_2$). The relation between the capacitance of the layers and layer thickness depends of the relative permittivity ε_r. Therefore, a precise structural interpretation of the location of the head end of the DDL is difficult to obtain. Force measurements in case of a double layer overlap and X ray scattering data suggest a structuring of water in the double layer within about 0.9 nm (see text).

A free fit of those data showed that the position of the charge of the electrolyte ions Li^+, Na^+, NO_3^-, and ClO_4^- was approximately the same. The Cl^- was apparently somewhat closer to the surface. Outer sphere complexation for the largest cation studied, Cs^+, was negligible. The interaction of K^+ with the surface was found to be quite weak. At present, we recognize that the weakness of the interaction of this ion does not allow a conclusive judgment of its location. Moreover, the titrations in KNO_3 and $CsNO_3$ were done for only one salt level. A critical re-evaluation of the data shows, that without loss of quality in the description of the data, the charge of the K^+ ion can also be located at the same intermediate position as found for the other electrolyte ions, i.e. Li^+, Na^+, NO_3^-, and ClO_4^-. It implies that in a classical interpretation, all these ions can have the same electrostatic position. With only a small loss in quality of fit and with a strong reduction of the number of adjustable parameters, the description of the extended titration data set of Rahnemaie et al. (2006) can be simplified to a

double layer picture in which the charge of ion pairs is located in one electrostatic plane. The location of the Cl^- is uncertain. The Cl^- ion may coordinate with a surface ligand and be treated as an inner sphere complex with the surface OH_2 as common ligand, but it is also possible to locate the charge of the Cl^- in the same plane as the other ions. The model parameters describing the data for these two choices are given in respectively Table 1 and 2, assuming standard temperature (25 ^oC) in the calculations. Note that *by definition*, the position of the 1-plane differs from the position of that plane as allocated in the CD-electrolyte ion model of Rahnemaie et al. The adapted double layer picture for the electrolyte ions is given in Figure 3.

Recently, it has been shown [46] with X-ray standing wave spectroscopy (XRS) that a cation like Rb^+ is able to form inner sphere complexes at the 110 face of TiO_2 (rutile) when the surface is strongly negatively charged [47]. In such a case, the ion is partially dehydrated and directly coordinated to the surface groups. This process may also occur for other simple electrolyte cations and can be an important reason for the apparently high capacitance of many TiO_2 samples when analyzed with the classical approach [48]. This ion interaction is not depicted in Figure 3.

An important point that follows from the present analysis and additionally from the original work of Rahnemaie et al., is the difference in position of the head end of the DDL and the location of the electrolyte ions. Such a model can be classified as an Extended Stern (ES) model [34]. The extended Stern model differs from the Basic Stern (BS) model and also the Three Plane (TP) model [22] due to the presence a second layer that separates electrolyte ion pairs from the head end of the DDL. The ES model is conceptually comparable with the Triple Layer (TL) model but in the TL model an unrealistic low value for the capacitance of the outer layer ($C_2 \equiv 0.2$ F/m^2) is used *by definition*. For goethite, the double layer of the extended Stern approach, cannot be simplified to a basic Stern approach if the complete data set of Rahnemaie et al. [43] is to be described simultaneously. In other words, the use of a common double layer picture for all simple monovalent electrolyte ions requires charge separation between the minimum distance of approach of ion pairs and the head end of the DDL. The data in Table 1 show that the experimental capacitance of this second layer is found to be about 0.9 ± 0.1 F/m^2, if the Cl^- is considered as an inner sphere complex with the surface $\equiv OH_2$ as common ligand. If Cl^- treated as a single charge on the 1-plane, the fitted capacitance is slightly lower, i.e. 0.74 ± 0.1 F/m^2 (Table 2). In the analysis, it is assumed that the basic structure of the double layer is the same in different monovalent electrolyte solutions, independent of the type of ions present. This is not per se. Ion-water interactions may differ. Ions like Li^+ and Na^+ are called "structure making" since these ions contribute to the increase in viscosity of an aqueous solution in contrast to e.g. the Cs^+ ion which is called "structure breaking". Such a property might prohibit a common double layer picture for all simple electrolyte ions. However, if the data for Cs^+ or Cs^+ plus K^+ are removed from the data set, the data for Na^+ and Li^+ still point to the presence of a second Stern layer as illustrated in the capacitance value being respectively $C_2 = 1.5 \pm 0.9$ F/m^2 and $C_2 = 1.4 \pm 1.3$ F/m^2. Despite the uncertainty in the values of C_2 (0.7-1.5 F/m^2), the present data suggest that the capacitance value of the outer layer C_2 is rather similar that of the inner layer C_1. As mentioned above, Sverjensky [42] has recently increased the capacitance of the outer layer in

the TL model from 0.2 F/m^2 to a value that in his case is, *by definition*, equal to the inner capacitance ($C_1 \equiv C_2$). A higher capacitance value is more in line with a realistic physical chemical picture of the compact part of the double layer sketched above (Fig. 3). In this respect, double layer models for metal (hydr) oxides seem to converge.

Table 1. The charge allocation (Δz) and the affinity constants of interaction (log$K$) of monovalent cat- and anions interacting with oppositely charged surface groups of goethite as derived from modeling of the goethite titration data with the extended Stern model (Fig. 3). With the exception of Cl^-, all other electrolyte ions are placed at the 1-plane. The Cl^- ion is allowed to distribute the charge between the surface and 1-plane. The fitted capacitance of the first and second layer is respectively $C_1 = 0.86 \pm 0.01$ and $C_2 = 0.90 \pm 0.13$ F m^{-2}. The standard deviation is given for the fitted parameters. $R^2 = 0.998$ $N = 320$ data points

Ions*	Δz_0	Δz_1	Δz_2	log$K$
Li^+	0	+1	0	+0.19 ± 0.02
Na^+	0	+1	0	- 0.55 ± 0.03
K^+	0	+1	0	- 1.50 ± 0.11
NO_3^-	0	-1	0	- 0.53 ± 0.03
Cl^-	-0.08	-0.92	0	- 0.60 ± 0.03

* Cs^+ ions do not form significantly ions pairs on goethite

Table 2. As in Table 1, the allocation of charge (Δz) and the affinity constants of interaction (log$K$) if all electrolyte ions are placed at the 1-plane. The fitted capacitance for the first and second layer are respectively $C_1 = 0.93 \pm 0.01$ and $C_2 = 0.74 \pm 0.10$ F m^{-2}.

Ions*	Δz_0	Δz_1	Δz_2	log$K$
Li^+	0	+1	0	+0.10 ± 0.02
Na^+	0	+1	0	- 0.60 ± 0.03
K^+	0	+1	0	- 1.61 ± 0.13
NO_3^-	0	-1	0	- 0.68 ± 0.03
Cl^-	0	-1	0	- 0.45 ± 0.03

* Cs^+ ions do not form significantly ions pairs on goethite

Interpretation of the macroscopic capacitance in terms of a microscopic distance requires an assumption for the value of the relative permittivity (Eq.[2]) of the layer involved. A capacitance value for C_1 of about $C_1 \approx 0.9$ F/m^2 in combination with an effective $\varepsilon_r \approx 40$ is equivalent to the radius of about one hydrated cation (~0.35 ± 0.05 nm) while a capacitance value of $C_2 \approx 0.74$-0.93-1.5 F/m^2 might be roughly equivalent to a distance about ≥ 0.2-0.4-0.7 nm depending on the chosen $\varepsilon_r = 40$ or 60 (dielectric constant of a concentrated electrolyte solution). A clear charge separation between the minimum distance of approach and the head end of the DDL may indicate that water molecules are ordered and that the location of electrolyte ions can change only in discrete steps in the water structure near the surface. Such stepwise changes (≈ 0.25 nm or ½ √3 . d_{H2O}) have been observed experimentally for two (strongly) charged mica-surfaces that approach each other for distances smaller than about 1.8 nm [49-51]. Since two surfaces are involved, the suggested structuring of the water on the charged surfaces starts at half this value, i.e. ≤ ≈ 0.9 nm. Ordering of water in discrete layers has also been found experimentally for the charged surface of metallic Ag(s) using X-ray scattering [52]. Besides the presence of a primary layer of hydration layer on the metal surface (Fig.1), 2 to 3 additional discrete water layers, decaying in degree of ordering, have

been observed (≤ ≈ 0.7-0.8 nm). On the other hand, recently molecular dynamic results suggest the presence of only 1 or maybe 2 additional hydration layers at the 110 surface of TiO_2 [53]. A total layer thickness of ≤ ≈0.8 ± 0.1 nm may agree with the above given estimate of the total distance between surface and DDL region (≈0.35 ± 0.05 ≈ 0.4 ± 0.2 nm). We note that the degree of ordering and number of hydration layers may depend on the charge density, molecule structure of the mineral face involved and/or the presence of counter ions. The ordering of water not necessarily leads to a low dielectric constant. This can be exemplified by the value of the relative permittivity (ε_r = 99) of polycrystalline ice at 0 ^oC that is slightly higher than the value for water (ε_r = 89) at 0 ^oC [54]. The dipoles are able to switch in the ice structure via H bridging. This contrasts with the fixation of the dipole of water molecules of the primary hydration shell of electrolyte ions as illustrated by the decrease of the dielectric constant of electrolyte solutions with increase of the concentration, e.g. ε_r = 60 in 2 M NaCl [6]. It suggests that ion crowding in the compact part of the DDL may contribute to lowering of the dielectric constant.

So far, the permittivity and water structure have been considered as a constant for a particular location in the double layer. The permittivity depends on the medium which however can be influenced by the field [55]. The relation between field strength in an assumed homogeneous continuum of dipoles and the relative permittivity coefficient ε_r can be approximated [55] by

$$\varepsilon_r = \frac{\varepsilon_z - \varepsilon_s}{1 + b(-d\psi/dx)^2} + \varepsilon_s \qquad [3]$$

in which ε_z, and ε_s are respectively the relative dielectric constant at zero field and at saturation (ε_s = 6), and in which b is a constant (b = 1.2 10^{-17} mV^{-1}) and - $d\psi/dx$ is the field strength of a homogeneous field (Vm^{-1}). Application of the theory to ions like Na^+, Ca^{2+}, or Al^{3+} [32] shows the strong field radiated by ion leads to dielectric saturation of the water dipoles in the first hydration shell (ε_s = 6), i.e. the water dipoles will become fixed (see Fig.3). The mean field strength on charged surfaces is generally much weaker. For the average potential fall of 0, 100, or 200 mV over a Stern layer width of 0.35 ± 0.05 nm, one calculates for initially pure and free water, respectively ε_r = 78, ~42 ± 5 or ~21 ± 4. The calculation shows that adaptation of the permittivity is most relevant when the field is strong, i.e. most relevant for the inner Stern layer. It also shows that the average value can be in line with the mean relative permittivity derived above, but that a considerable variation may exist. We note that in general, for reasons of simplicity, such a possible variable field effect is not included in surface complexation models so far, i.e. the capacitances are kept constant as a simplifying approximation.

B Surface hydration in the interface

The above analysis suggests that water molecules become increasingly structured when approaching the surface. It may be assumed that this structuring is related to the presence of charge of various origins in the interface, as is conceptually illustrated in the double layer snapshot of Figure 3. The vectors in the figure represent the orientation of the water molecules. In a chemical picture, the structuring of water due to the presence of surface groups is based on the formation of hydrogen bonds, which will change because of protonation and de-protonation. The pattern is disturbed by thermal motion and the presence of counter charge ions.

In the past, we have attempted to reveal the influence of H bonding in the interface by using the F^- ion as a proxy to study the change in orientation of water molecules and corresponding H bonding when the F ion is adsorbed [56]. Fluoride is a special ion in the sense that it has approximately the same size as an OH group, which allows ligand exchange with the $\equiv FeOH^{-1/2}$ and $\equiv FeOH_2^{+1/2}$ groups of the surface. As discussed in ref. [56], the $\equiv FeF^{-1/2}$ groups formed on goethite (α-FeOOH) will hydrate differently compared to both other types of surface groups ($\equiv FeOH^{-1/2}$ and $\equiv FeOH_2^{+1/2}$). In a chemical picture, hydrogen bonds are formed between the F^- ion and water molecules in the Stern layer. This will change the average orientation of the water molecules in the interface. This change in orientation could semi-quantitatively explain the observed apparent charge transfer (Δz_0 = -0.67 v.u., Δz_1 = -0.33 v.u.) that occurs when the F^- ions are exchanged against surface OH or OH_2. That study made clear that changes in orientation of water molecules are important in understanding ion adsorption phenomena in the interface.

In a physical picture, water molecules can be treated as dipoles. The theory of the contribution of the orientation of water molecules to the Gibbs free energy of ion adsorption has been developed in electrochemistry [6, 7]. The theory describes the effects of dipoles in the interface and has been applied particularly to the highly oriented water molecules present in the first layer on metal-electrode surfaces, where the water molecules flip-flop between two main orientations (Fig. 1). The flip-flop theory for dipoles has recently been used in an attempt to describe the adsorption of anions on oxide surfaces [57]. We will discuss the dipole theory and show the do-and-don'ts of the application to the solid-solution interface of metal (hydr)oxides. We will show how the theory can be implemented in a MUlti SIte Complexation (MUSIC) approach [13] and how it is related to the interfacial charge distribution as described by the CD model [22].

Electrostatic dipole energy

Water molecules tend to orient due to the potential difference present in an electrostatic field. The flip-flop of water dipoles has been demonstrated experimentally for Al_2O_3 [58] when the pH of the aqueous solution crosses the PZC. Orientation of a dipole is related to electrostatic work. The presence of a potential difference will change the degree of orientation, which includes a change in energy. This molar free energy of dipole orientation ΔE_d can be expressed as [6]:

$$\Delta E_d = -\mu \cos\alpha \, N_{av} X \qquad [4]$$

where N_{av} is Avogadro's number (6.023 10^{+23} mol^{-1}), α is the angle between the direction of the field and the dipole, X is the field strength (V/m) and μ is dipole moment. The dipole moment is a measure for the amount of charge separation within a molecule, defined as charge q times distance p. Therefore, the corresponding unit is C.m or D (Debeye) where 1 D = 3.338 10^{-30} Cm. The minus sign in Eq.[4] indicates that energy is released when the negative site of the dipole can be directed towards the positive charge that radiates the field and *vice versa*.

The field strength X is defined as the potential change $d\psi$ over distance $d x$, i.e. $-d\psi/dx$. In case of application to water present in a Stern capacitor (Fig. 2) with a constant decrease of the potential with distance d between the 0- and 1-plane, we may write:

$$X = \frac{\psi_0 - \psi_1}{d} \qquad [5]$$

The combination of the equations [4] and [5] results in the expression for the molar energy of dipole orientation in the inner Stern layer, i.e.:

$$\Delta E_d = -\mu \cos\alpha \, N_{av} X = -\mu \cos\alpha N_{av} \frac{\psi_0 - \psi_1}{d} \qquad [6]$$

It is also possible to combine equation [6] with the expression that relates capacitance and distance (Eq.[2]) leading to:

$$\Delta E_d = -\mu \cos\alpha N_{av} X = -\mu \cos\alpha N_{av} C_1 \frac{\psi_0 - \psi_1}{\varepsilon_r \varepsilon_o} \qquad [7]$$

Equations [6] and [7] express the electrostatic energy release due to dipole orientation of one mole of water present in the inner Stern layer as a result of a field gradient. Recently, the concept has been applied to $\equiv OH_2$ molecules of the mineral surface that are coordinated to trivalent metal ions of a mineral lattice [57], forming a surface group. To use the field gradient of the inner Stern layer for such situation (chemisorbed $\equiv OH_2$) is questionable. It is more logical to suppose that the dipole energy of the water coordinated in the solid surface, is related to the local field radiated by the metal ion (e.g. Fe^{3+}, Al^{3+}, Ti^{4+} *etceteras*) to which the water group is bound chemically. As mentioned above, (Eq.[3]), this local ion-field is far stronger [32] and therefore dominant, fixing the dipole of the $\equiv OH_2$ group. The energy of dipole orientation of these surface $\equiv OH_2$ groups is likely to be independent of the potential fall present in the inner Stern layer. It implies that the energy of the water molecules that are part of the solid will be approximately constant. If a water molecule, fixed by metal

coordination, is exchanged in a ligand exchange reaction, the dipole energy change upon release of the coordinated water molecule is a constant term that is part of the intrinsic chemical Gibbs free energy change of the reaction involved.

The situation is different for the water molecules that are in the inner Stern region. Imagine a neutral surface that becomes charged due to ion adsorption. In the created field, dipoles will orient. The corresponding energy change ΔE_d (J per mole oriented-water) refers to the difference before and after charging. The shift in dipole orientation can be coupled to the charge Λ_0 that is introduced in the surface by the ion adsorption process. The assumption is that the relative number of oriented water molecules is proportional to the change of charge Λ_0 introduced on a neutral surface in an adsorption reaction. It leads to the definition of the relative amount of water r_w:

$$r_w \equiv n_w \Lambda_0 \qquad [8]$$

in which n_w is expressed as mol water / mol charge and Λ_0 as mol charge / mol ion. The value of r_w includes a sign, as will be illustrated later.

The dipole energy that represents the energy change per ion adsorbed on a neutral surface can be named the specific dipole energy change ΔE_{dip}, which is defined by combining eqs.[6] and [8], resulting in:

$$\Delta E_{dip} \equiv r_w \Delta E_d \equiv -n_w \Lambda_0 \, \mu \cos\alpha \, N_{av} \frac{(\psi_0 - \psi_1)}{d} \equiv -\phi \Lambda_0 F (\psi_0 - \psi_1) \qquad [9]$$

in which the factor ϕ is defined as:

$$\phi \equiv n_w \mu \cos\alpha \, N_{av} / (d F) \qquad [10]$$

The latter equation may also be written as $\phi \equiv n_w \, \mu \cos\alpha \, N_{av} \, C_1 / (\varepsilon_r \varepsilon_o F)$.

Expressing the specific energy release due to dipole orientation (ΔE_{dip}) in a specific affinity coefficient K_{dip}, we may write:

$$K_{dip} = e^{-\Delta E_{dip}/RT} \equiv e^{+\phi \Lambda_0 F(\psi_0 - \psi_1)/RT} = e^{+\phi \Lambda_0 F \psi_0/RT} \; e^{-\phi \Lambda_0 F \psi_1/RT} \qquad [11]$$

The above equation (Eq.[11]) comprises the electrostatic work that is related to the dipole energy change of interfacial water as a result of the introduction of charge in a neutral surface by ion adsorption. It can be combined with the electrostatic work that is related to locating the corresponding ion charge.

In case of inner sphere complexation, the ion charge is distributed over the 0- and 1-plane in the CD model. Generally, the change of charge in the 0- and 1- plane is the combination of the ion charge itself (n_0 and n_1) and additional proton charge (n_{H0} and n_{H1}).

The total ion charge introduced in the 0- or 1-plane equals respectively n_0+n_{H0} and n_1+n_{H1}. The corresponding electrostatic energy change is

$$K_{ion} = e^{-\Delta G_{ion}/RT} = e^{-(n_0+n_{H0})F\psi_0/RT}\ e^{-(n_1+n_{H1})F\psi_1/RT} \quad [12]$$

Both equations can be combined to give the overall electrostatic effect

$$K_{elec} = e^{-\Delta G_{elec}/RT} = e^{-(n_0+n_{H0}-\phi\Lambda_0)F\psi_0/RT}\ e^{-(n_1+n_{H1}+\phi\Lambda_0)F\psi_1/RT} \quad [13]$$

Equation [13] can be rewritten in terms of the overall charge distribution coefficients Δz_0 and Δz_1, according to:

$$K_{elec} \equiv e^{-\Delta z_0 F\psi_o/RT}\ e^{-\Delta z_1 F\psi_1/RT} \quad [14]$$

in which

$$\Delta z_0 = n_0 + n_{H0} - \phi\Lambda_0 \quad [15]$$

and

$$\Delta z_1 = n_1 + n_{H1} + \phi\Lambda_0 \quad [16]$$

Dipole energy is calculated using the neutral surface as reference. The reference state for the calculation of the value of Λ_0 can be represented by an on average neutral surface group. This reference state will be called the zero-charge reference state. Another reference state can be chosen, e.g. a charged surface group. If the reaction is written for another reference state, the number of protons in the reaction will be different. For a reaction written with surface groups having charge z_{ref}, we can link the corresponding ion and proton charge n_0+n_{H0} and n_1+n_{H1} to the change of charge Λ_0 and Λ_1 written for the zero charge reference state, according to:

$$\Lambda_0 = n_0 + n_{H0} + \Sigma n_{ref} z_{ref} \quad [17]$$

and

$$\Lambda_1 = n_1 + n_{H1} \quad [18]$$

The first expression shows that the charge added to a surface with overall neutral surface groups Λ_0 can be calculate from the ion charge (n_0) and proton charge (n_{H0}) that is attributed to the surface in an adsorption reaction with surface groups of charge $z_{ref.}$. The term $\Sigma\ n_{ref}\, z_{ref}$ represents the charge correction from any arbitrary reference state to the zero reference state.

The final overall affinity constant for ion adsorption is $K^o \equiv K_{dip}\, K_{ion}\, K_{chem} \equiv K_{elec}\, K_{chem}$ which results from the combination of electrostatic and chemical Gibbs free energy changes, i.e. $\Delta G^o \equiv \Delta G_{dip} + \Delta G_{ion} + \Delta G_{chem} \equiv \Delta G_{elec} + \Delta G_{chem}$. The conceptual physical-chemical picture, on which the above derivation is based, has been summarized in Figure 4.

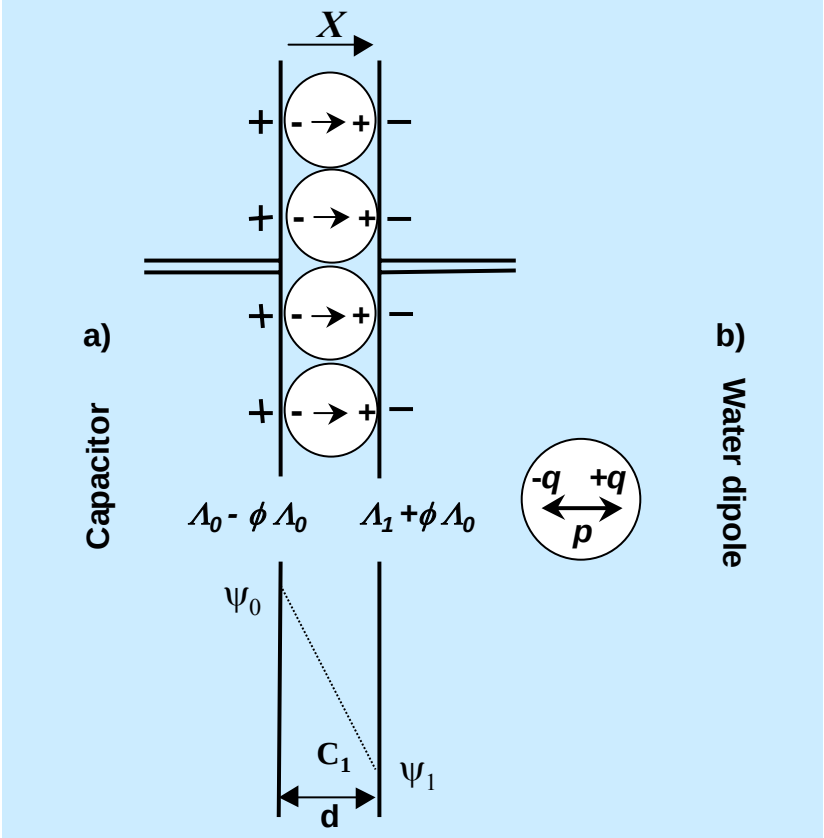

Figure 4. Ion charge separation (Λ_0, Λ_1) is a basic principle of ion adsorption in an interface, resulting in a double layer that in a simple picture can be represented by a capacitor with distance d (Fig. 4a). The ion charge separation is accompanied by increase in energy. Charge separation ($-q$, $+q$) is also present in a water molecule, which is known as a dipole (two poles) (Fig. 4b). The charge q is separated by a distance p which in combination is called a dipole moment μ ($\mu = q.p$). Water dipoles can be oriented in an electrostatic field. The dipole layer in itself forms a capacitor. If the distance of charge separation of the dipole capacitor (p) would correspond with the distance in ion charge separation (d), the intrinsic ion charge separation is reduced by an effective charge $\phi\,\Lambda_0$, resulting in $\Lambda_0 - \phi\,\Lambda_0$ and $\Lambda_1 + \phi\,\Lambda_0$. The orientation of the dipole leads to a release of energy, i.e. the electrostatic energy of dipole orientation is a negative quantity (Eq.[4]). Since the charge separation in a water dipole is relatively limited, it is obvious that the maximum value of ϕ will be much smaller than 1. The arrows indicate the direction of the field X and the dipole with $\cos\alpha = 1$. Note that $z_{ref} = 0$.

Application

The question that arises is "What is the direction (sign) and the magnitude of the dipole correction and how is it implemented?" The above expression for K_{elec} (Eq.[13]) comprises two Boltzmann factors. The electrostatic work can be seen as due to the introduction of ion

and proton charge n_{0+} n_{H0} with a feedback due to dipole effects, $\phi\Lambda_0$ (Eq.[15]). The dipole effect is calculated relatively to an uncharged surface, which we will exemplify.

A first example is for silica. The neutral surface can be represented by $\equiv SiOH^0$. Formation of $\equiv SiOH_2^+$, according to the reaction $\equiv SiOH^0 + 1\ H^+ \Leftrightarrow \equiv SiOH_2^{+1}$, leads to $\Lambda_0 = n_0 + n_{H0} + \Sigma\ n_{ref}\, z_{ref} = 0 + 1 + (1*0) = +1$ v.u. For the formation of $\equiv SiOH_2^{+1}$, we might also use $\equiv SiO^{-1}$ as reference group, according to the reaction $\equiv SiO^{-1} + 2\ H^+ \Leftrightarrow \equiv SiOH_2^{+1}$. The change of charge for the formation of $\equiv SiOH_2^{+1}$ relative to the zero reference state, expressed in Λ_0, equals $\Lambda_0 = n_0 + n_{H0} + \Sigma\ n_{ref}\, z_{ref} = 0 + 2 + (1*-1) = +1$ v.u., i.e. the same value as before. We might even use $\equiv SiOH_2^{+1}$ as reference group to form $\equiv SiOH_2^{+1}$ according to $\equiv SiOH_2^+ + 0\ H^+ \Leftrightarrow \equiv SiOH_2^{+1}$. We will find for the change of charge from the zero reference state $\Lambda_0 = n_0 + n_{H0} + \Sigma\ n_{ref}\, z_{ref} = 0 + 0 + (1*1) = +1$ v.u. The example shows that the value of Λ_0 is correctly calculated independent of the chosen reference states. Moreover, it shows that the number of protons in the reaction with corresponding charge does not indicate in a direct manner the magnitude of the correction term $\phi\,\Lambda_0$. The same can be demonstrated for proton desorption. Desorption of a proton from a neutral surface group, according to the reaction $\equiv SiOH^0 - 1\ H^+ \Leftrightarrow \equiv SiO^{-1}$, keeping $\equiv SiOH^0$ as reference group, gives $\Lambda_0 = n_0 + n_{H0} + \Sigma\ n_{ref}\, z_{ref} = 0 - 1 + (1*0) = -1$ v.u. In case of the use $\equiv SiOH_2^+$ as reference group, we have $\equiv SiOH_2^+ - 2\ H^+ \Leftrightarrow \equiv SiO^{-1}$ with $\Lambda_0 = n_0 + n_{H0} + \Sigma\ n_{ref}\, z_{ref} = 0 - 2 + (1*1) = -1$ v.u. and for $\equiv SiO^{-1}$ as reference group we also find $\Lambda_0 = -1$ v.u.

The formulated dipole theory can also be applied to a surface with only charged surface groups like $\equiv FeOH^{-1/2}$ and $\equiv FeOH_2^{1/2}$. At the corresponding neutral surface, the average number of protons per surface group is 1.5, i.e. the zero reference state can be represented by the hypothetical surface species $\equiv FeOH_{1.5}^0$. The formation reaction of $\equiv FeOH_2^{+0.5}$, including the dipole correction, can be represented as: $\equiv FeOH_{1.5}^0 + 0.5\ H^+ + H_2O \Leftrightarrow \equiv FeOH_2^{+0.5-x}\cdots H_2O^{+x}$ in which x abbreviates the absolute value $|\phi_m\,\Lambda_0|$. In a similar manner, we can formulate the formation of $\equiv FeOH^{-0.5}$, writing $\equiv FeOH_{1.5}^0 - 0.5\ H^+ + H_2O \Leftrightarrow \equiv FeOH^{-0.5+x}\cdots H_2O^{-x}$. The overall reaction is found in the combination of both reactions resulting in $\equiv FeOH^{-0.5+x} - H_2O^{-x} + H^+ \Leftrightarrow \equiv FeOH_2^{+0.5-x} - H_2O^{+x}$. This reaction can be used in SCM (see appendix).

The above cases can also be discussed in terms of dipole energy change. We consider the above-uncharged surface with $\equiv SiOH^0$ that binds one proton, which results in orientation of one corresponding dipole in the positive field. Simplifying for the moment to $\cos\alpha = +1$, the corresponding specific dipole energy change (Eq.[9]), expressed relative to the zero charge reference state, equals $\Delta E_{dip} = -\phi\,\Lambda_0\,F\,(\psi_0 - \psi_1)$. Since the potential difference $(\psi_0 - \psi_1)$ has a positive value, and also ϕ ($\phi \equiv n_w\ \mu\ N_{av} / (d\,F) > 0$) as well as Λ_0 (+1), the specific dipole energy change is negative ($\Delta E_{dip} < 0$), i.e. electrostatic energy is released. If the proton is desorbed again ($\Lambda_0 = -1$), the change in dipole energy is opposite. We may also compare protonation on a positive surface with deprotonation on a negative surface. The direction of the field is in both cases opposite, so is the direction of the dipole. It implies that in both cases $\cos\alpha$ will have the same sign ($\cos\alpha > 0$) and the value of ΔE_{dip} too ($\Delta E_{dip} < 0$). However, $(\psi_0 - \psi_1)$ is opposite in sign, which shows that $n_w\,\Lambda_0$ differs in sign too. Similarly as above, the

value of $n_w \Lambda_0$ is negative if negative charge is introduced and positive if positive charge is added to the surface plane.

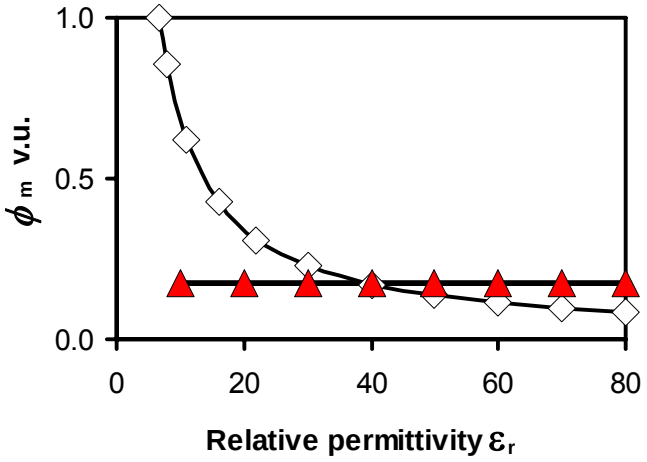

Figure 5. The equivalent molar shift ϕm of interfacial charge distribution value towards the surface as a function of the relative dielectric constant of the water layer in case of a constant capacitance (rhombuses) or a constant thickness (filled triangles) of the inner Stern layer (d = 0.35 ± 0.05 nm). The calculations refer to the formation of one mole of fully oriented water molecules per ion adsorbed (n_w = 1, α = 0). The dipole moment of liquid water is set at 2.9 D [59].

In the next step, we want to quantify the magnitude of the factor ϕ ($\equiv n_w \mu \cos \alpha N_{av}$ / (d F = $n_w \mu \cos \alpha N_{av} C_1$/ ($\varepsilon_r \varepsilon_0$ F)), if possible. One of the main obstructions is the unknown degree of orientation of the dipoles (α) and another problem is the unknown amount of dipole oriented water (n_w) that is involved. Moreover, the relative permittivity (ε_r) or thickness (d) of the inner Stern layer is uncertain, so is even the value of the dipole moment in liquid water to some extent [59]. Nevertheless, at present, calculations can be valuable to quantify the minimum and maximum values that may occur. We focus on the formation of 1 mole (n_w = 1) of fully oriented dipoles (α = 0 and cos α = 1), i.e. the maximum molar value ϕ_m. In Figure 5, we have calculated the value of ϕ_m as a function of the relative permittivity (ε_r) of the medium and express it per mole of water (n_w = 1) that will change to full orientation.

In the first calculation with this approach, the capacitance is set to a constant of 1 F/m^2 for the inner Stern layer capacitance of metal (hydr) oxides. The result of the calculation for a constant capacitance (rhombuses in Figure 5) suggests that the shift factor ϕ_m will be very significant for a low dielectric constant. However, in case of a structural interpretation of the double layer (Fig. 3), this changes. Accounting for the relation between the dielectric constant and the capacitance (Eq.[2]) in combination with $\phi_m = (\mu N_{av})/(d F)$ and a reasonable value of d = 0.35 ± 0.05 nm (Fig. 3), the calculation results in ϕ_m = +0.17 ± 0.02 for cos α = 1, irrespective of the interfacial dielectric constant (triangles in Figure 5). This value of ϕ_m should be considered as a maximum, since it assumes a complete change in orientation of the molecules involved (cos α = 1), whereas the actual average orientation might be less (cos $\alpha \leq$ 1), i.e. $\phi \leq 0.17 \pm 0.02$. Note that the lines in Fig.5 cross at ε_r = 40, which in combination with d = 0.35 nm is equal to the capacitance C_1 = 1 F/m^2.

Let's apply the value $\phi_m \approx 0.17 \pm 0.02$ to the protonation reaction on iron oxides. For the reaction $\equiv FeOH^{-0.5+x} \cdots\cdots H_2O^{-x} + H^+ \Leftrightarrow \equiv FeOH_2^{+0.5-x} \cdots\cdots H_2O^{+x}$ with $x = |\phi_m \Lambda_0|$, we may calculate Λ_0 with Eq.[17] giving $\Lambda_0 = +0.5$. The corresponding charge correction using $\phi_m \approx 0.17$ is rather limited, being $x = \phi_m \Lambda_0 \leq 0.09$ v.u. In principle, the dipole shift can be applied in proton adsorption modeling. However, it requires a full recalibration and parameterization of the adsorption model. For practical reasons and because of the uncertainties, this approach is not followed here at present.

We will analyze the effects of dipole orientation on ion adsorption further by comparing the theoretical and experimental value of the charge distribution for oxyanions.

C The charge distribution

The central theme of the CD model is the relation between the interfacial charge distribution and the structural interpretation of the interface [22]. Various factors may determine the precise value of the interfacial charge distribution. Starting point might be the Pauling bond valence concept. It has been shown that the major differences in the experimental charge distribution can be related to the *relative* number of ligands of an adsorbed ion that becomes common with the surface [23]. To improve the understanding and interpretation of the experimental CD value(s), quantum chemical (QC) calculations may be of help to quantify the CD value for inner sphere complexes and relate this to the overall interfacial charge distribution. In this study, we will illustrate this idea in detail for the adsorption of silicic acid $Si(OH)_4$. In addition, results for carbonate will be presented. We will also summarize the results of three other studies of which the details have or will be reported separately [60-62].

Structure of the Silicon Surface complex

The structure of surface complexes can be examined with spectroscopy. For Si, the interaction with iron oxides has been studied for solutions containing small Fe polymers [63, 64]. A study with FTIR [63] showed the presence of Fe-O-Si linkages at a low Fe/Si (<1) ratio, confirming the formation of inner sphere complexes. A recent EXAFS study showed that Si is present in the Fe coordination sphere at a distance of about 317 pm. It was argued that this distance is very close to the experimental distances found for bidentate surface complexes of PO_4, AsO_4, and SeO_3 [65-68]. The EXAFS study showed that Si would form double corner complexes upon interaction with singly coordinated surface groups.

Based on the results of EXAFS, the interaction of $H_4SiO_4^0(aq)$ with two $\equiv FeOH^{-1/2}$ surface groups can be formulated as:

$$2 \equiv FeOH^{-1/2} + H_4SiO_4^0(aq) \Leftrightarrow \equiv (FeO)_2^{-1+\Delta z_0} Si(OH)_2^{\Delta z_1} + 2H_2O(l) \qquad [19]$$

where Δz_o and Δz_1 represent respectively the overall change of charge in the 0- and 1-plane (Fig. 6) upon the adsorption of uncharged $H_4SiO_4^o$ with $\Delta z_o + \Delta z_1 = 0$.

As mentioned in the original paper on the CD model [22], the use of the Pauling concept to obtain the CD value of surface complexes, may in some cases be insufficiently

accurate, as was illustrated for the bidentate surface complex of silicic acid ≡ $(FeO)_2Si(OH)_2$ (Fig. 6). The charge on the ligands is given for two different choices (a,b) of the calculation of the charge distribution. In Figure 6a, the charge is calculated assuming a symmetrical Pauling distribution whereas in Figure 6b, asymmetrical distribution is used to fully neutralize the ligands common with the solid. The experimental CD found from analysis of adsorption data (to be described below) is given in Figure 6c. The actual value can be seen as a trade-off between the two opposing tendencies formulated in Figures 6a and 6b, but may also include a dipole contribution ($\phi\, \Lambda_0$).

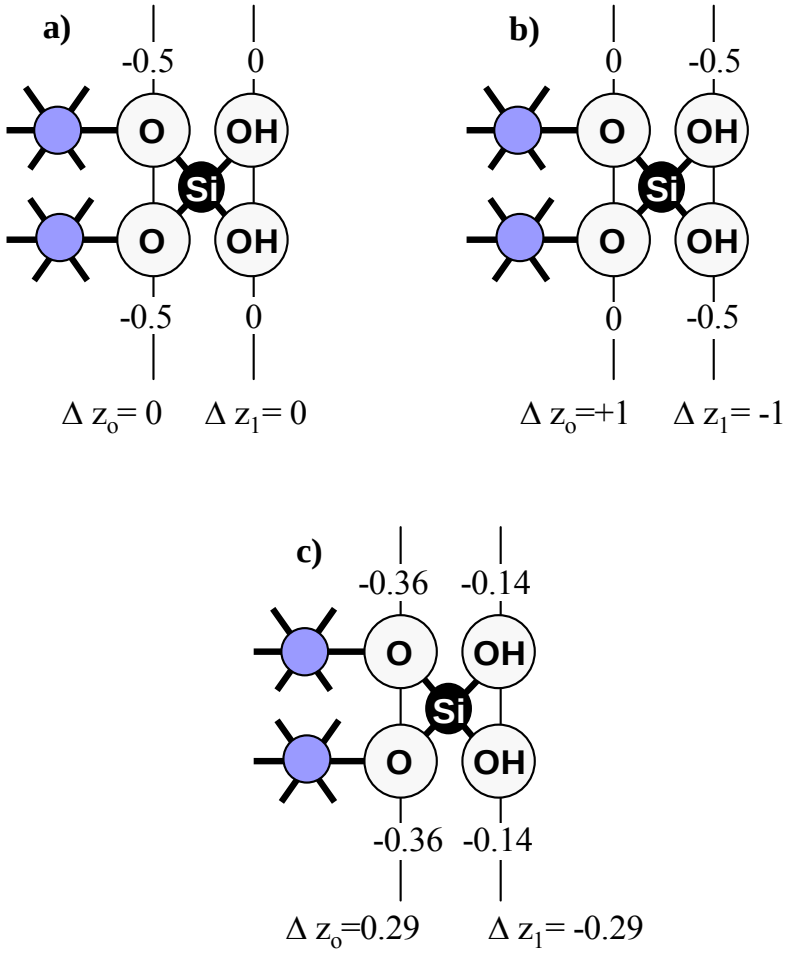

Figure 6. The schematic representation of a bidentate silicon complex bound to iron oxide The charge on the ligands is given for two different choices (a,b) of the charge distribution (Δz_0, Δz_1). In Figure 6a, the Si-charge is equally distributed based on the Pauling bond valence concept. In Figure 6b, an asymmetrical charge distribution exists, that fully neutralizes the ligands common with the solid. These values can be compared with the apparent charge distribution derived from adsorption experiments (c).

Experimental

The evaluation of the charge distribution can be done using proton co-adsorption data [23], if measured accurately under well defined conditions, like a constant pH, but also a constant ionic strength and further a constant temperature and the exclusion of CO_2. In our

experiment (Fig. 7), a high solid-solution ratio was used which results in an almost entire adsorption of the Si added. In such a case, the description of the data is only sensitive to the charge distribution, provided that only one type of surface species is formed [23]. The experimental co-adsorption at pH 6.00 and 8.00 differs (Fig. 7), but this variation can be described with one charge distribution value. For the data, using reaction (Eq.[19]), we find with modeling $\Delta z_0 = -\Delta z_1 = 0.29$ (Fig. 6c).

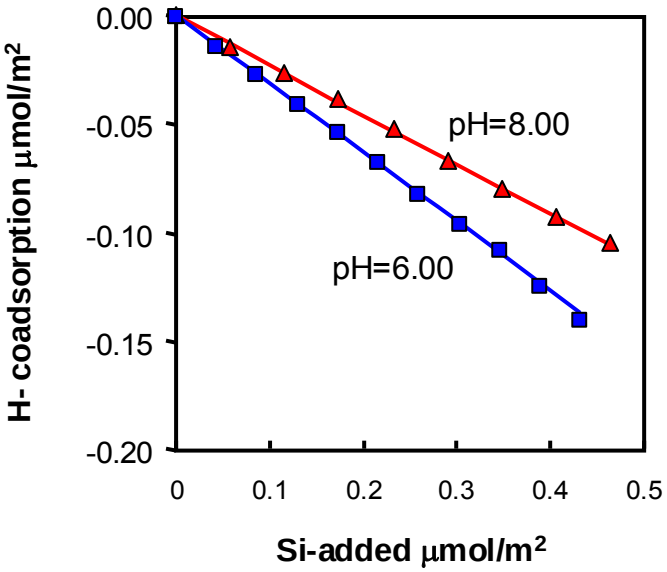

Figure 7. The co-adsorption of H on goethite for two pH values (I = 0.100 $NaNO_3$) upon addition of H_4SiO_4. Due to the chosen setup of the experiment with high solid solution ratios (800-1600 m^2/L), almost all added silicic acid (>99%) is adsorbed. The co-adsorption of H has a negative value, which implies that protons are released. The lines in the figure have been calculated with the CD model and MUSIC model, using the parameters of the extended Stern model of Table 2 in combination with a proton affinity constant of $\log K_H$ = 9.2 for the protonation of ≡ $FeOH^{-1/2}$ and ≡ $Fe_3O^{-1/2}$ groups having a site density N_s of respectively 3.45 and 2.7 nm^{-2} (see ref. [22]).

Quantum chemical computations

Quantum chemical computations have been carried out to derive the expected CD value from the geometry of the inner sphere complex. As a starting point, we defined a cluster with two Fe oxide octahedrons with the appropriate multiplicity (Fig. 8). The cluster serves as a template to mimic the goethite mineral. The initial geometry of the octahedrons is set equal to the geometry found for goethite [69]. Additional protons were added to obtain the zero-charged cluster, $Fe_2(OH)_6(OH_2)_4$ (z = 0). The defined O-H distances were set at 104 pm. In the zero-charge cluster, the Fe and OH ions form approximately a central plane. The OH_2 groups are located on-top on both sides of the octahedrons (Fig. 8).

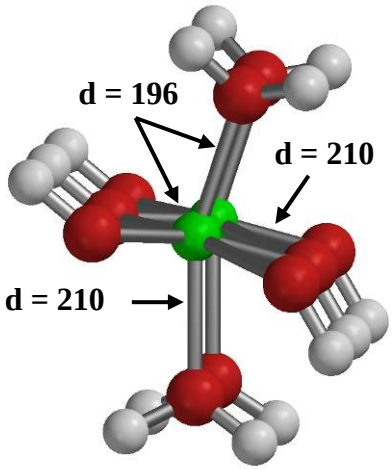

Figure 8. Two Fe (III)-O octahedrons with Fe-O distances (pm) and angles as found in goethite (α-FeOOH).

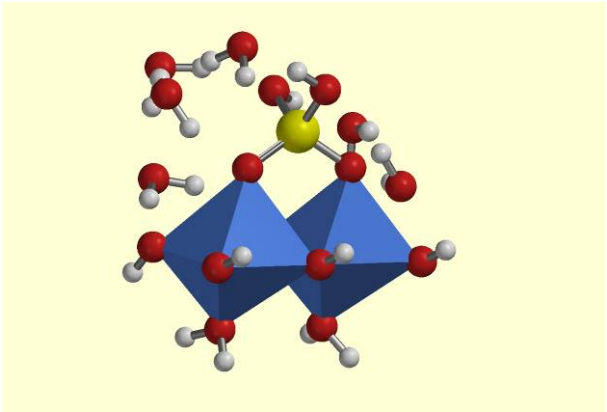

Figure 9. Two Fe(III)-O(H) octahedrons with a bidentate silicon complex on-top that is hydrated (structure III). The geometry is optimized with the BP86 model. The geometry of lower part of the octahedrons has been fixed (see text).

The basic bidentate complex of silicic acid without hydration water (structure I, see Table 3) was defined by exchanging both H_2O molecules on the top of the cluster against O ligands that are coordinated to the Si^{4+} ion. The exchanged OH_2 ligands on top of both octahedrons stand for protonated singly coordinated surface groups at the 110 face of goethite (Pbnm, Inorganic Crystal Structure Database). To mimic the influence of hydration, the free OH ligands in the coordination sphere of the adsorbed silicic acid were allowed to interact with two water molecules via H bridges (O-H···O) (structure II, see Table 3). In addition, we defined a hydrogen bond between each common O ligand in the Fe-O-Si bond and an additional water molecule (structure III). The geometry of this structure (III) with 6 water molecules for hydration is given in Figure 9. The ions in the lower half of both octahedrons (comprising 6 OH^-, 2 OH_2, and 2 Fe^{3+}) have a fixed position equivalent with the position in

the octahedrons of goethite. All other ions (H_4SiO_4) and the hydration water molecules were allowed to relax. The relevant geometric data of the structures I-III are given in Table 3. The experimental and calculated Fe-Si distances in the hydrated structures (II&III) agree within the uncertainty. The Fe-Si distance in the structure without hydration is slightly too small.

Table 3. The calculated distances (pm) in the geometry of bidentate silicon complexes (I, II, III) that differ in the number (n-H_2O) water molecules added for hydration, using the DFT-BP86 model.

Model	I	II	III	Exp
n-H_2O	0	4	4+2	
Si-OH	172.2	170.4	169.5	-
Si-OH	169.8	171.4	170.4	-
O-Si	164.4	163.4	165.6	-
O-Si	165.2	166.0	165.1	-
Fe-O	195.8 ± 0.1	197.0 ± 1.4	198.5 ± 1.5	196[*1]
Fe-Si	310.1 ± 0.1	320.5 ± 2.8	321.2 ± 1.8	317 ± 3[*2]
R_o	167.8	167.7	167.6	164[*3]
n_o[*4]	+0.17	+0.17	+0.12	
n_1[*4]	-0.17	-0.17	-0.12	

[*1] Distance present in the goethite structure without relaxation.
[*2] EXAFS study reports d (Fe-Si) = 317 ± 3 pm and a coordination number of CN = 2 ± 0.5 [64].
[*3] Average R_0 for Si in minerals [11]. Calculation of the geometry of the $Si(OH)_4.12H_2O$ moiety results in Si-O distances of 167.2, 167.3, 165.9 and 168.2 pm which is equivalent with R_o = 167.1 pm.
[*4] The charge of $H_4SiO_4^0$ attributed to the ligands of the 0- and 1-plane (n_0+n_1 = 0) based on application of the Brown bond valence concept to the calculated geometry (Eq.[20]).

Experiment versus Computation

The geometry's of Table 3 can be interpreted in terms of charge distribution using the Brown bond valence concept. According to Brown [11], the bond valence s is related to the distance R as:

$$s = e^{-(R-R_0)/B} \qquad [20]$$

in which B is a constant and R_0 is the element specific parameter. Brown and Altermatt [11] used the value B = 37 pm. The value of R_0 is chosen such that the sum of the bond valences around the Si ion corresponds to the formal valence (z = +4). The various R_0 values calculated for the optimized structures, including hydrated silicic acid $Si(OH)_4.12H_2O$ (Table 3), are systematically slightly larger than the R_0 value found for minerals. The bond valences can be evaluated in terms of interfacial charge distribution values. The quantum chemically obtained CD values differ from the CD value based on the Pauling Bond valence. Equal distribution of

the Si charge results in $\Delta z_0 = 0$ and $\Delta z_1 = 0$ (Fig. 6a). The calculations show that in the Si complexes the charge becomes asymmetrically distributed, but not as much as given in Figure 6b. The silicon-oxygen bond length is shortened for the bond with the common surface group while the bond length of the bond with the free ligand becomes relatively longer. It implies that more charge should be attributed to the surface (n_o). The calculated amount is in the range $n_0 = 0.12$ - 0.17 v.u. (Table 3). Note that $n_0 + n_1 = 0$ v.u. The difference in charge distribution (structure III versus II) is due to respectively the presence and absence of water that coordinates with the common O in the Fe-O-Si bond. The calculated charge distribution can be compared with the value found from modeling the proton co-adsorption data for Si binding. The experimental approach ($\Delta z_0 = 0.29$ v.u.) suggests that the charge on the 0-plane is about +0.14 ± 0.03 v.u. larger than derived from the QC calculated geometry ($n_0 = 0.15 \pm 0.03$ v.u.). For the 1- plane, the opposite is found. If this difference is related to the dipole effect, the value of $\phi \Lambda_0$ is -0.14 ± 0.03 v.u. The sign indicates that apparently negative charge is shifted to the 1-plane.

We will analyze the observed effect in detail based on the above presented theory for the electrostatic dipole orientation.

Dipole energy correction

In the adsorption reaction of silicic acid (Eq.[19]) no protons are explicitly formulated, i.e. no proton charge is explicitly introduced which means that n_{H0} and n_{H1} are zero. We note that nevertheless protons may be present on the surface species, but that these species are implicitly part of the charge of the other species in the reaction (≡ $FeOH^{-1/2}$ and $H_4SiO_4^0$). The ion charge distribution refers to $H_4SiO_4^0$ and therefore $n_0 + n_1 = 0$. As mentioned above, we found by QC calculation $n_0 = -n_1 = 0.14 \pm 0.03$ v.u. Based on this number and $n_{H0} = 0$, in combination with the reference state correction $\Sigma\, n_{ref}\, z_{ref} = 2* -1/2 = -1$, we may calculate the dipole correction term using $\phi_m = 0.17$. It yields a dipole correction term of $-\phi_m \Lambda_0 = -\phi_m (n_0+n_{H0} +\Sigma\, n_{ref.}\, z_{ref}) = -0.17\ (0.14\text{-}0\text{-}1) = +0.15$ v.u. Using Eq.[15] and Eq.[16], we find $\Delta z_0 = n_0+n_{H0}-\phi_m(n_0+n_{H0}+ \Sigma\, n_{ref}\, z_{ref}) = +0.14 +0.15 = +0.29 \pm 0.03$ v.u. and $\Delta z_1 = n_1 + n_{H1} +\phi_m(n_0 + n_{H0} + \Sigma\, n_{ref.}\, z_{ref}) = -0.29 \pm 0.03$ v.u. The calculated Δz_0 and Δz_1 values are equal to the values fitted to experimental data with the CD model. We note that silicic acid is a typical example of an ion that has a quite large dipole contribution in the CD values compared to the contribution of the ion itself. The dipole correction is relatively large and of the same magnitude as the shift of charge in the surface complex. Without dipole correction, the experimental data (Fig.7) cannot be understood, using the presented molecular picture.

Other oxyanions

We have carried out a series of other quantum chemical calculations to derive the expected charge distribution for various inner sphere complexes of $As(OH)_3$ ([61]), CO_3^{2-}, SO_4^{2-} ([60]), and PO_4^{3-} ([62]). In all cases, additional water molecules have been added to mimic hydration. The quantum chemically derived charge distributions of these ions are given in Table 4. For arsenite, we used a series of MO/DFT models, showing a variation of about ± 0.03 v.u. For the other ions, only the DFT-BP86 model was applied. For phosphate, our

results can be compared with two structures, reported by Kwon and Kubicki [70]. They used another MO/ DFT model and, moreover, in their calculations, the two iron octahedra were allowed to relax fully in contrast to our octahedra that have a geometry partially fixed to the structure of goethite. Nevertheless, the CD values calculated from both structures agree within a difference of only 0.02-0.03 v.u. (last note of Table 4). The results for arsenite as well as phosphate suggest that the CD values can be pinpointed relatively accurate. This is of great value since it allows an accurate calculation of the CD particularly in situations where derivation of the CD from experimental data is difficult.

Table 4. The Charge Distribution values (n_0, n_1) calculated from the DFT-optimized geometries of species hydrated with a number of water molecules (n_{hydr}), using the Brown bond valence concept. The sum of the charge distribution values n_0+n_1 corresponds to respectively the charge of $H_4SiO_4^0$, $As(OH)_3^0$, CO_3^{2-}, SO_4^{2-}, and PO_4^{3-}. The charge distribution coefficients Δz_0 and Δz_1 refer to the calculated change of charge as formulated in the reaction based on the above reference ion species and protons, in combination with the surface reference species ≡ $FeOH^{-1/2}$. These values have been calculated using the n_0, n_1 values derived from QC calculations and the location of the protons (n_{H0}, n_{H1}). Note $\phi_m \Lambda_0 = (n_0+n_{H0} + \Sigma\, n_{ref}.z_{ref})$.

Species	n_{hydr}	n_0	n_1	$\Delta z_0 = n_0 + n_{H0} - \phi_m\Lambda_0$	$\Delta z_1 = n_1 + n_{H1} + \phi_m\Lambda_0$
≡ $(FeO)_2Si(OH)_2$*[1]	4-6	0.15 ± 0.03	-0.15 ± 0.03	0.15+0+0.14 = 0.29	-0.15+0-0.14 = -0.29
≡ $(FeO)_2AsOH$*[2]	5	0.19 ± 0.03	-0.19 ± 0.03	0.19+0+0.14 = 0.33	-0.19+0-0.14 = -0.33
≡ $(FeO)_2CO$*[3]	5	-1.39	-0.61	-1.39+2+0.07 = 0.68	-0.61+0-0.07 = -0.68
≡ $FeOSO_3$*[4]	7	-0.51	-1.49	-0.51+1+0.00 = 0.49	-1.49+0-0.00 = -1.49
≡ $(FeO)_2PO_2$*[5]	8	-1.65	-1.35	-1.65+2+0.11 = 0.46	-1.35+0-0.11 = -1.46
≡ $(FeO)_2POOH$*[5]	8	-1.45	-1.55	-1.45+2+0.08 = 0.63	-1.55+1-0.08 = -0.63
≡ $FeOPO_2OH$*[5]	8	-0.76	-1.24	-0.76+1+0.04 = 0.28	-1.24+1-0.04 = -1.28

*[1] This study (DFT-BP86) The ± sign indicates the variation due to absence of presence of interaction of H_2O with common ligand in the Fe-O-Si bonds.
*[2] ref [61] (DFT- Local, EDF1, BP86, BLYP and B3LYP). The ± sign indicates variation depending on the QC model used.
*[3] This study (DFT-BP86)
*[4] ref [60] (DFT-BP86)
*[5] ref [62] (DFT- BP86). Interpretation of the hydrated fully-relaxed iron orthophosphate structures of ref. [70], yields n_0 = -1.67 and n_1 = -1.33 for ≡ $(FeO)_2PO_2$ and, n_0 = -0.73 and n_1 = -1.27 for ≡ $FeOPO_2OH$ (DFT-B3LYP).

Arsenite

Arsenite is a neutral molecule that forms inner sphere complexes by OH ligand exchange on goethite. EXAFS [71, 72] has shown that the dominant surface species is a bidentate complex. In addition, a monodentate complex is formed in a minor amount [73]. Application of this molecular picture in surface complexation modeling using the CD model showed that the bidentate complex attributed approximately Δz_0 = +0.28 ± 0.03 v.u. to the 0-plane and Δz_1 = -0.28 ± 0.03 v.u. to the 1-plane [61]. These numbers can be compared with the quantum chemical calculated charge distribution (Table 4). For the various QC models

applied, we found on average $n_0 = -n_1 = +0.19 \pm 0.03$ v.u. Note $n_0 + n_1 = 0$. Similar as in the case of silicon, positive charge is apparently moved from the 1-plane to the surface plane.

Interpretation for As (III) can be along the same lines as for the adsorption of Si. The adsorption of arsenite can be formulated as:

$$2 \equiv FeOH^{-1/2} + As(OH)_3^0\,(aq) \Leftrightarrow \equiv (FeO)_2^{-1+\Delta z_0} As(OH)^{\Delta z_1} + 2H_2O(l) \qquad [21]$$

with $\Delta z_0 + \Delta z_1 = 0$. Using Eq.[14] in combination with $\phi_m = 0.17$ v.u. results in a calculated dipole correction factor of $-\phi_m \Lambda_0 = -0.17\ (0.19+0-1) = +0.14$ v.u. The overall coefficients (Eqs.[15],16]) are $\Delta z_0 = 0.19 + 0 + 0.14 = +0.33 \pm 0.03$ v.u. and $\Delta z_1 = -0.19 + 0 - 0.14 = -0.33 \pm 0.03$ v.u. These values almost agree with the values observed ($\Delta z_0 = +0.28 \pm 0.03$, $\Delta z_1 = -0.28 \pm 0.03$).

For a moment, we return to the recent work of Sverjensky [42] who described the arsenite adsorption with the ligand exchange reaction given as $2\ SOH^0 + 2\ H^+ + AsO_2OH^{2-} \Leftrightarrow S_2^{2+}\text{---}(AsO_2OH)^{2-} + 2\ H_2O$ in which the charge of the protons is located in the 0-plane and the charge of the divalent arsenite ion in the β-plane, where also outer sphere complexes of the electrolyte ions reside. The created ionic charge distribution ($n_0 = +2$ and $n_1 = -2$) for the inner sphere complex is corrected by a supposed shift of charge (2 v.u.!) that is motivated as a result of a *variable* change in dipole energy due to release of 2 H_2O molecules from the surface plane, leading to $\Delta z_0 = 0$ and $\Delta z_1 = 0$. This interpretation is not in line with the spectroscopically observed inner sphere complex formation and difficult to understand in view of the above discussed origin of the variable dipole energy, which does not fit to the permanent dipole fixation of $\equiv OH_2$ coordinated to metal ions of the solid.

Carbonate

The effect of dipole energy correction can also be demonstrated for carbonate adsorption. The carbonate adsorption on goethite has been measured by Villalobos and Leckie [74]. The data can be interpreted with the CD model [75] in combination with the basic Stern approach, resulting in a charge distribution of CO_3^{2-} of $\Delta z_0 = -1.33 \pm 0.02$ v.u. and $\Delta z_1 = -0.67 \pm 0.02$ v.u. Reinterpretation of the data with the extended Stern model yields very similar values: $\Delta z_0 = -1.30 \pm 0.03$ v.u. and $\Delta z_1 = -0.70 \pm 0.03$ v.u. As has been argued by Hiemstra et al. [75], this charge distribution is typically for the formation of bidentate inner sphere complexes, whereas the dominance of monodentate complex formation was claimed [76, 77] based on the magnitude of infrared band splitting. A recent ATR-FTIR study [78] has confirmed that, as suggested, the main inner sphere complex is indeed a bidentate complex. The bidentate inner sphere complexation reaction can be given as:

$$2 \equiv FeOH^{-1/2} + 2H^+(aq) + CO_3^{-2}\,(aq) \Leftrightarrow \equiv (FeO)_2^{-1+\Delta z_0} CO^{-1+\Delta z_1} + 2\ H_2O(l) \qquad [22]$$

with $\Delta z_0 + \Delta z_1 = 0$. The QC calculated charge distribution coefficients of CO_3^{2-} in a hydrated bidentate complex is (DFT-BP86 model) is $n_0 = -1.39$ v.u and $n_1 = -0.61$ v.u. (Table 4). The

CD values, corrected for dipole effects are $\Delta z_0 = \Lambda_0 - \phi_m \Lambda_0 + \Sigma n_{ref}\, z_{ref} = n_0 + n_{H0} - \phi_m \Lambda_0 = n_0 + n_{H0} - \phi_m\, (n_0 + n_{H0} + \Sigma\, n_{ref}\, z_{ref}) = -1.32$ v.u. and $\Delta z_1 = \Lambda_1 - \phi_m \Lambda_0 = n_1 + n_{H1} + \phi_m \Lambda_0 = n_1 + n_{H1} + \phi_m (n_0 + n_{H0} + \Sigma\, n_{ref}\, z_{ref}) = -0.68$ v.u. Within the uncertainty, these values agree with the CD values derived from analysis of experimental data ($\Delta z_0 = -1.30 \pm 0.03$ v.u. and $\Delta z_1 = -0.70 \pm 0.03$ v.u).

Sulphate

Another oxyanion that we have studied is SO_4^{2-}. At a relatively high pH (pH>~6), sulphate forms outer sphere complexes, but at low pH also a monodentate inner sphere surface complex is formed [79-81]. The charge distribution of SO_4^{2-} in this complex has recently been calculated quantum-chemically [60], yielding $n_0 = -0.51$ v.u. and $n_1 = -1.49$ v.u. (Table 4). The corresponding reaction can be given as:

$$\equiv FeOH^{-1/2} + 1H^+(aq) + SO_4^{-2}(aq) \Leftrightarrow \equiv FeO^{-1/2+\Delta z_0}SO_3^{\Delta z_1} + 1H_2O(l) \qquad [23]$$

with $\Delta z_0 + \Delta z_1 = -1$. The overall derived CD values for this reaction are $\Delta z_0 = n_0 + n_{H0} - \phi_m \Lambda_0 = -0.51+1-0.17(-0.51+1-0.5) = +0.49$ v.u. and $\Delta z_1 = n_1 + n_{H1} + \phi_m \Lambda_0 = -1.49 + 0 + (0.17. -0.01) = -1.49$ v.u. The calculations show that no dipole effects are expected ($\phi_m \Lambda_0 = 0$). Due to the simultaneous presence of outer sphere complexes and monodentate inner sphere surface complexes, it is quite difficult to derive unequivocally the value of the CD for the inner sphere complex [60, 82, 83]. In the most recent attempt [60], the data could be described very satisfactory using for sulphate $\Delta z_0 \equiv -0.5$ and $\Delta z_1 \equiv -1.5$ which is in line with the concept presented here.

Phosphate

In another study [62], we have focused on the adsorption of phosphate (PO_4^{3-}). MO/DFT calculated CD values have been applied in the modeling of a new extensive data set of phosphate adsorption on goethite, suggesting the dominance of a bidentate and a protonated monodentate complex. The main features of the adsorption behavior could be described with this approach. However, we also experienced that fine-tuning was necessary in order to get a perfect description. It was found that the MO/DFT calculated CD values were attributing too little negative charge to the 1-plane in comparison to the values needed for a perfect description. For a best fit, it was necessary to shift the charge. In a free fit, the charge of the bidentate complex shifted with about +0.15 v.u. and for the protonated monodentate, the surface charge attribution was about +0.10 v.u. higher. These values should be interpreted with care since it is difficult to determine the precise CD values if more than one type of surface species is present in particular if in addition the types of surface species can be questioned [70, 84-86]. The observed trend agrees with what is expected. The adsorption of phosphate can be described with the reactions:

$$2 \equiv FeOH^{-1/2} + 2\, H^+ + PO_4^{-3}(aq) \Leftrightarrow \equiv (FeO)_2^{-1+\Delta z_0}PO_2^{\Delta z_1} + 2H_2O(l) \qquad [24]$$

$$\equiv FeOH^{-1/2} + 2\ H^{+} + PO_4^{-3}(aq) \Leftrightarrow \equiv FeO^{-1/2+\Delta z_0}PO_2OH^{\Delta z_1} + 1H_2O(l) \qquad [25]$$

with $\Delta z_0 + \Delta z_1 = -1$. For these surface species, the MO/DFT calculations result in respectively $n_0 + n_{H0} = 0.35$ v.u and $n_0 + n_{H0} = +0.24$ v.u. (Table 4). The estimation of the dipole correction factor can be found as $-\phi_m \Lambda_0 = +0.11$ v.u. and 0.04 v.u. which can be compared with the fitted values 0.15 v.u. and 0.10 v.u. The trend agrees but the calculated numbers are lower than revealed with the present interpretation of the experimental data.

The value of ϕ

The above data analysis can also be presented from the experimental point of view to derive the value of ϕ. We have seen that in several cases the calculated charge distribution obtained from geometry optimizations, Δz_0(QM), differs from the overall charge distribution that has been found from fitting experimental data, Δz_0(Exp). The difference might be due to dipole effects ($\phi \Lambda_0$), i.e. we assume:

$$\Delta z_0(QM) - \Delta z_0(Exp) \equiv \phi \Lambda_0 \qquad [26]$$

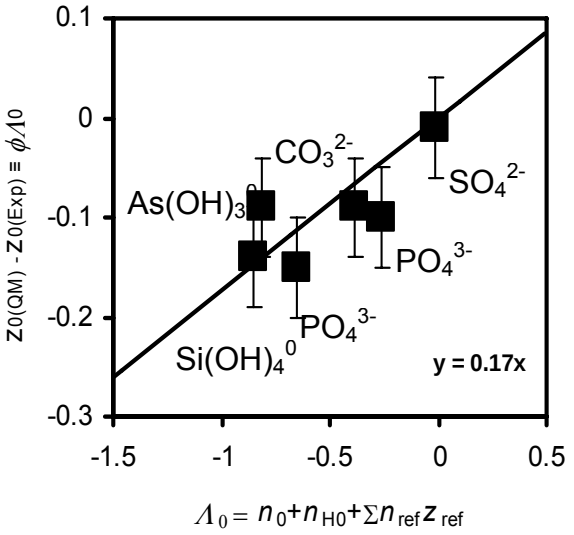

Figure 10. The relationship between the experimental and quantum-chemical determined charge attribution (Δz_0) which is supposed to be a dipole effect ($\phi \Lambda_0$), and the charge attribution Λ_0, based on introduced ion charge (n_0), protons (n_{H0}) with correction to the zero charge reference state of the surface ($\Sigma\ n_{ref}\ z_{ref}$). The slope of the line corresponds to the value ϕ, which is found to be 0.17. The error bar represents an error of 0.05 v.u., which can be considered as a minimum uncertainty.

As shown above, the charge attribution to the 0-plane is counted based on the attribution of the ion charge, the added proton charge and it is corrected to the zero charge reference state according to $\Lambda_0 = n_0 + n_{HO} + \Sigma\ n_{ref}\ z_{ref}$ (Eq.[17]). The value of Λ_0 has been plotted in Fig.10 against de above difference in Δz_0 (Eq.[26]). The error bar in the figure represents an error of

0.05 v.u. for the difference of Δz_0(Exp) and Δz_0(QM). As expected, a very good relationship exits between the amount of charge that is introduced in the 0-plane relative to the zero charge reference state (Λ_0) and the difference between the experimental and quantum chemically derived Δz_0, which is supposed to be due to dipole effects. The slope of the line through the origin represents the value of ϕ. Fitting the data in Fig. 10 leads to $\phi = 0.17 \pm 0.05$. The actual value ϕ is equal to the previously calculated value ϕ_m (Fig.5).

Cations

Finally, the question arises what might be the dipole effect in case of the inner sphere complexation of heavy metal ions? To preliminary answer this question, we choose as example two cations that behave extremely different, i.e. Cd(II) and Hg(II). Both species form bidentate inner sphere complexes. However, the two bidentate complexes exhibit a very different ion charge distribution, ranging from rather symmetrical (Cd^{2+}) to extremely asymmetrical (Hg^{2+}). The symmetrical charge distribution results in a rather small charge attribution of Cd^{2+} to the surface [24], since only two of a total of six ligands are common with the surface. As a result of the relatively small charge attribution, the common ligands in the Cd(II) complex are OH groups, in contrast to the common ligands in the complex of Hg(II) [87], which are proposed to be oxygens. It has been suggested that the Hg(II) ion will form two very strong bonds with the surface [87], leading to a strong charge attribution to the common ligands, removing the protons.

At the main crystal faces of goethite, 110 and 100 face [88] [89], the Cd^{2+} ions form double corner inner sphere complexes [90-92]. The reaction can be formulated as:

$$2 \equiv FeOH^{-1/2} + Cd(OH_2)_6^{2+}(aq) \Leftrightarrow \equiv (FeOH)_2^{-1+\Delta z_0} Cd(OH_2)_4^{\Delta z_1} + 2H_2O(l) \qquad [27]$$

with $\Delta z_0 + \Delta z_1 = 2$. If the Cd^{2+} charge is equally distributed over the ligands, we will have $n_0 = +0.67$ v.u. and $n_1 = +1.33$ v.u. In that case, application of the factor $\phi_m = 0.17$, results in a correction factor of $-\phi_m \Lambda_0 = -0.17\ (0.67 + 0 - 1) = +0.06$ v.u. It shows that the effects are expected to be relatively small in case of a symmetrical distribution of charge in a bidentate complex. Asymmetry in charge distribution is expected for cations like Cu^{2+} and Pb^{2+} [18, 93-96]. In such case, more charge (n_0) is introduced in the surface leading to even smaller correction factors for these heavy metal ions. However, if the asymmetry in a complex becomes too large, the situation may change drastically, as is the case for Hg(II).

For Hg(II) binding, the supposed reaction can be formulated as:

$$2 \equiv FeOH^{-1/2} + Hg(OH)_2^0(aq) + xH_2O(l) \Leftrightarrow \equiv (FeO)_2^{-1+\Delta z_0} Hg(OH_2)_x^{\Delta z_1} + 2H_2O(l) \qquad [28]$$

in which $\Delta z_0 + \Delta z_1 = 0$. If the $Hg(OH)_2^0$ charge is fully attributed to the surface ligands, we will have $n_0 = 0$ v.u. and $n_1 = +0$ v.u. In that case, a correction factor is $-\phi\Lambda_0 = -0.17*(0+0-1) = +0.17$ v.u., i.e. positive charge would flow from the 1- to the 0-plane. This picture is probably too extreme. Less surface charge attribution of Hg(II) may occur if Hg(II)

coordinates also with some water molecules of the Stern layer. In case of n_0 = -0.5 v.u. and n_1 = +0.5 v.u., one calculates $-\phi\Lambda_0$ = -0.17 * (-0.5+0-1) = +0.25 v.u.

When the value of Λ_0 (-1.5) for Hg(II) would be plotted in Fig.10, it will be in the lower end of the horizontal scale of Fig.10 in contrast to the expected position for Cd^{2+} and the other mentioned heavy metal ions, being closer to zero ($\Lambda_0 \geq$ -0.33). The main reason for this difference in behavior is the proposed release of protons from the common ligands [87]. In case of Hg(II), an oxo-complex is formed while Cd^{2+} ions form hydroxo-complexes. We conclude that the electrostatic correction factor for cations and anions is generally limited to a range of $\phi\Lambda_0$ values of about $\phi\Lambda_0 \approx$ - 0.2 v.u. to $\phi\Lambda_0 \approx$ 0 v.u. (Fig.10).

Additional hydration water

In principle, the introduction of charge in the 1-plane may lead to orientation of water molecules in the second Stern layer and beyond. This will result in additional dipole orientation energy. However, the potential gradient in the second Stern layer $(\psi_1-\psi_2) / d_2$ is expected to be far less. It implies that the electrostatic dipole energy will be much smaller, i.e. the model will be less sensitive for such a refinement and can be ignored for reasons of simplicity.

Outlook

In the above, we have shown how the macroscopic interfacial charge distribution is linked to the microscopic charge distribution and the electrostatic dipole correction. It is suggested that the microscopic charge distribution can be derived from the interpretation of the geometry of surface complexes, using the Brown bond valence approach. This requires information about the bond distances in the primary coordination sphere. For this degree of detail, quantum chemical calculations are probably most appropriate. The suggested approach has the advantage that it can account for changes in the coordination sphere that result from hydrolysis or protonation reactions. These effects are not easily extracted from adsorption data in a consistent manner. From a practical point of view, the suggested approach has the advantage that the CD value does not have to be an adjustable parameter, which is especially an advantage if several surface species are present simultaneously. In such a case, it is not an easy task to unravel individual charge distributions. Moreover, even if only one species is present, derivation of a CD value better than 0.05 v.u is not trivial while *approximation* of the CD with QC calculations probably may reach the same quality.

As mentioned, the CD values calculated from the iron ortho-phosphate geometries of ref. [62] and ref. [70] are very similar for structures without and with relaxation of the iron octahedrons. It suggests that the CD is rather insensitive to this constraint. Although the structures will differ in detail like the atomic distances, the resulting CD values are remarkably similar. The consequence might be that the calculated CD values of particular surface species are quite generally applicable to all Fe(III) oxides and hydroxides, i.e. quite universal at the level of accuracy of probably ~0.03 v.u. This might imply that a calculated CD for ion adsorption might be preferred for less well-defined Fe (hydr) oxide materials like 6-line ferrihydrite, hydrous ferric oxide (HFO) and particularly Fe oxides materials in natural

soils en sediments. In the latter case, the CD values are difficult or even impossible to derive from adsorption experiments.

Acknowledgement

Part of the work was funded by the TRIAS project 835.80.006 / Delft Cluster 5.17.

Conclusions

The above can be summarized in a series of conclusions:

- The double layer on metal hydroxides differs from that of metal electrodes and ionic solids like AgI(s) with the absence of strongly oriented water with a low permittivity, which results in very different electrostatic capacitance and a smaller distance of charge separation between surface charge and counter- and co-ion charge. The dominant influence of the primary water layer on metal electrodes may prevent the retrieval of detailed information of the double layer structure beyond this layer.
- The location of the head end of the DDL differs from the minimum distance of approach of electrolyte ions, which may result from some structuring of near surface water.
- The total width of the compact part of the double layer is probably slightly less than about ~1 nm, equivalent with a water-layer thickness of about 3 water molecules. The width of the inner part is equivalent with the radius of a hydrated ion (0.35 ± 0.05 nm).
- The capacitances of the inner and outer Stern layer are found to be similar in magnitude.
- Inner sphere complexation can be described with a distribution of charge over the inner Stern planes of the compact part of the double layer.
- The electrostatic effect of charge separation and distribution can be corrected for changes in dipole orientation of water molecules of the Stern layer.
- The overall charge distribution derived from adsorption data may differ from the CD value obtained from a Brown bond valence analysis of MO/DFT optimized geometries of surface complexes. The shift is related to the net amount of charge that is introduced in the surface relative to the situation of a surface speciation without charge.
- The dipole correction equals $\pm \phi_m \ (n_0 + n_{H0} + \Sigma\ n_{ref}\ z_{ref})$ in which n_0 and n_{H0} are respectively the charge attribution of the ion and proton(s) to the surface plane and $\Sigma\ n_{ref}\ z_{ref}$ represent the total charge present on the surface group(s) used in the adsorption reaction.
- The theoretical fractional molar correction factor ϕ_m is 0.17 ± 0.02. The experimental fractional correction factor ϕ agrees with the value of ϕ_m within the uncertainty.
- The electrostatic dipole correction is usually limited to a range of 0-0.15 v.u.
- The MO/DFT derived charge distribution is rather insensitive to the precise structure of the metal octahedra, suggesting a reasonable general applicability to Fe oxides, including ill-defined structures like HFO or soil iron oxides.
- Use of MO/DFT derived CD values leaves only the formation constant to be adjusted.

Appendix

Tableau formulating the protonation reaction of $\equiv FeOH^{-1/2}$ of a metal hydroxide surface and corresponding dipole correction. One may start with a fully deprotonated surface with $\equiv FeOH^{-1/2}$ as reference group. Dipoles will orient, leading to a correction of the surface charge of $+x$ v.u. At the formation of the protonated surface group, one unit charge is bound to the surface group (+1 v.u.), but corrected for a dipole effect $-x$ v.u. NB $x = |\phi_m \Lambda_0|$.

Species	$\exp(-zF\psi_0/RT)$	$\exp(-zF\psi_1/RT)$	$\exp(-zF\psi_2/RT)$	$FeOH^{-1/2}$	H^+	$\log K$
H^+	0	0	0	0	1	0
$\equiv FeOH^{-0.5+x}\,H_2O^{-x}$	$+x$	$-x$	0	1	0	0
$\equiv FeOH_2^{+0.5-x}\,H_2O^{+x}$	$1-x$	$+x$	0	1	1	$\log K_H$
Σ*	Σ_1	Σ_2	Σ_3	Σ_4	Σ_5	

* Σ = sum of all species concentrations multiplied by the coefficients representing mass balances.

The mass balances (Σ) are defined in mol/L and can be linked to the well-known electrostatic equations of the Extended Stern model (See ref. [22]).

References

1. H. Von Helmholtz, Ann. Physik. Chem. 7 (1879) 337.
2. G. Gouy, J. Phys. 9 (1910) 457.
3. D. L. Chapman, Philos. Mag. 6 (1913) 475.
4. O. Stern, Z. Electrochem. 30 (1924) 508.
5. D. C. Grahame, Chem. Rev. 41 (1947) 441.
6. J. O. M. Bockris, A. K. N. Reddy, Modern Electrochemistry 1. (2 nd ed.) Plenum: New York, 1976 Vol.1.
7. J. O. M. Bockris, A. K. N. Reddy, Modern Electrochemistry 2. (2 nd ed.) Plenum: New York, 1976 Vol.2.
8. L. Pauling, J. Am. Chem. Soc. 51 (1929) 1010.
9. I. D. Brown, Acta Cryst. B33 (1977) 1305.
10. I. D. Brown, Chem. Soc. Rev. 7 (1978) 359.
11. I. D. Brown, D. Altermatt, Acta Cryst. B41 (1985) 244.
12. I. D. Brown, The chemical bond in inorganic chemistry : the bond valence model. Oxford University Press: 2002 12.
13. T. Hiemstra, W. H. Van Riemsdijk, G. H. Bolt, J. Colloid Interf. Sci. 133 (1989) 91.
14. T. Hiemstra, P. Venema, W. H. Van Riemsdijk, J. Colloid Interf. Sci. 184 (1996) 680.
15. T. Hiemstra, W. H. Van Riemsdijk, M. G. M. Bruggenwert, Neth. J. Agric. Sci. 35 (1987) 281.
16. T. Hiemstra, Han Yong, W. H. Van Riemsdijk, Langmuir 15 (1999) 5942.
17. T. Hiemstra, W. H. Van Riemsdijk, Langmuir 15 (1999) 8045.
18. T. Hiemstra, W. H. Van Riemsdijk, in: Encyclopaedia of Surface and Colloid Science, 1 ed. Marcel Dekker, Inc.: New York, USA, 2002; pp 3773.

19. P. A. Connor, K. D. Dobson, A. J. McQuillan, Langmuir 15 (1999) 2402.
20. J. P. Fitts, M. L. Machesky, D. J. Wesolowski, X. M. Shang, J. D. Kubicki, G. W. Flynn, T. F. Heinz, K. B. Eisenthal, Chemical Physics Letters 411 (2005) 399.
21. M. L. Machesky, D. J. Wesolowski, D. A. Palmer, M. K. Ridley, J. Colloid Interf. Sci. 239 (2001) 314.
22. T. Hiemstra, W. H. Van Riemsdijk, J. Colloid Interf. Sci. 179 (1996) 488.
23. R. P. J. J. Rietra, T. Hiemstra, W. H. Van Riemsdijk, Geochim. Cosmochim. Acta 63 (1999) 3009.
24. P. Venema, T. Hiemstra, W. H. Van Riemsdijk, J. Colloid Interf. Sci. 183 (1996) 515.
25. T. Hiemstra, W. H. Van Riemsdijk, J. Colloid Interf. Sci. 210 (1999) 182.
26. T. Hiemstra, J. C. M. De Wit, W. H. Van Riemsdijk, J. Colloid Interf. Sci. 133 (1989) 105.
27. Anonymous Spartan '04 Wavefunction Inc.; Irvine CA USA, 2004.
28. J. Kong, C. A. White, A. I. Krylov, C. D. Sherrill, R. D. Adamson, T. R. Furlani, M. S. Lee, A. M. Lee, S. R. Gwaltney, T. R. Adams, C. Ochsenfeld, A. T. B. Gilbert, G. S. Kedziora, V. A. Rassolov, D. R. Maurice, N. Nair, Y. Shao, N. A. Besley, P. E. Maslen, J. P. Dombroski, H. Daschel, W. Zhang, P. P. Korambath, J. Baker, E. F. C. Byrd, T. Van Voorhis, M. Oumi, S. Hirata, C.-P. Hsu, N. Ishikawa, J. Florian, A. Warshel, B. G. Johnson, P. M. W. Gill, M. Head-Gordon, J. A. Pople, J. Computational Chem. 21 (2000) 1532.
29. J. T. G. Overbeek, in: Colloid Science I, H. R. Kruyt, (Ed.) Elsevier: Amsterdam, 1952; pp 115.
30. J. Lyklema, J. T. G. Overbeek, J. Colloid Interf. Sci. 16 (1961) 595.
31. M. A. Henderson, Surf. Sci. Reports 48 (2002) 5.
32. T. Hiemstra, W. H. Van Riemsdijk, Colloids Surfaces 59 (1991) 7.
33. M. Borkovec, Langmuir 13 (1997) 2608.
34. J. Westall, H. Hohl, Adv. Colloid Interf. Sci. 12 (1980) 265.
35. R. J. Atkinson, A. M. Posner, Q. J.P., J. Phys. Chem. 71 (1967) 550.
36. W. Stumm, C. P. Huang, S. R. Jenkins, Croat. Chem. Acta 42 (1970) 223.
37. J. W. Bowden. Models for Ion Adsorption on Mineral Surfaces. PhD, University of West Australia, 1973.
38. J. W. Bowden, A. M. Posner, P. J. Quirk, Aust. J. Soil Res. 15 (1977) 121.
39. D. E. m. Yates. The Structure of the Oxide/Aqueous Electrolyte Interface. Ph.D. thesis, University of Melbourne, Melbourne, 1975.
40. J. A. Davis, R. James, J. O. Leckie, J. Colloid Interf. Sci. 63 (1978) 480.
41. J. A. Davis, J. O. Leckie, J. Colloid Interf. Sci. 67 (1978) 90.
42. D. A. Sverjensky, Geochim. Cosmochim. Acta 69 (2005) 225.
43. R. Rahnemaie, T. Hiemstra, W. H. Van Riemsdijk, J. Colloid Interf. Sci. 293 (2006) 312.
44. J. Lützenkirchen, Environ. Sci. Technol. 32 (1998) 3149.
45. J. F. Boily, J. Lützenkirchen, O. Balmès, J. Beattie, S. Sjöberg, Colloids Surfaces A 179 (2001) 11
46. P. Fenter, L. Cheng, S. Rihs, M. Machesky, M. J. Bedzyk, N. C. Sturchio, J. Colloid Interf. Sci. 225 (2000) 154.
47. Z. Zhang, P. Fenter, L. Cheng, N. C. Sturchio, M. J. Bedzyk, M. Predota, A. Bandura, J. D. Kubicki, S. N. Lvov, P. T. Cummings, A. A. Chialvo, M. K. Ridley, P. Benezeth, L. Anovitz, D. A. Palmer, M. Machesky, D. J. Wesolowski, Langmuir 20 (2004) 4954.

48. K. Bourikas, T. Hiemstra, W. H. Van Riemsdijk, Langmuir 17 (2001) 749.
49. R. M. Pashley, J. N. Israelachvili, J. Colloid Interf. Sci. 101 (1984) 511.
50. J. N. Israelachvili, Intermolecular and Surface Forces. (2 nd ed.) Academic Press: London, 1991
51. J. N. Israelachvili, H. Wennerstrom, Nature 379 (1996) 219.
52. M. F. Toney, J. N. Howard, J. Richer, G. L. Borges, J. G. Gordon, O. R. Melroy, D. G. Wiesler, D. Yee, L. B. Sorensen, Surf. Sci. 335 (1995) 326.
53. M. Predota, A. V. Bandura, P. T. Cummings, J. D. Kubicki, D. J. Wesolowski, A. A. Chialvo, M. L. Machesky, J. Phys. Chem. B 108 (2004) 12049.
54. V. F. Petrenko, R. W. Whitworth, Physics of Ice. Oxford University Press: New York, 1999
55. B. E. Conway, Ionic Hydration in Chemistry and Biophysics. Elsevier: Amsterdam - Oxford - New York, 1981 12.
56. T. Hiemstra, W. H. Van Riemsdijk, Journal of Colloid and Interface Science 225 (2000) 94.
57. D. A. Sverjensky, K. Fukushi, Environ. Sci. Technol. 40 (2006) 263.
58. M. S. Yeganeh, S. M. Dougal, H. S. Pink, Phys. Rev. Letters 83 (1999) 1179.
59. A. V. Gubskaya, P. G. Kusalik, J. Chem. Phys. 117 (2002) 5290.
60. R. Rahnemaie, T. Hiemstra T., and W.H. Van Riemsdijk (2006) J. Colloid Interf. Sci. 297 (2006) 379.
61. M. Stachowicz, T. Hiemstra, W. H. Van Riemsdijk, J. Colloid Interf. Sci. J. Colloid Interf. Sci. 302 (2006) 62.
62. Rahnemaie R., Hiemstra T., and Van Riemsdijk W. H. Langmuir 23 (2007) 3680.
63. E. Doelsch, W. E. E. Stone, S. Petit, A. Masion, J. Rose, J. Bottero, D. Nahon, Langmuir 17 (2001).
64. G. S. Pokrovski, J. Schott, F. Farges, J.-L. Hazemann, Geochim. Cosmochim. Acta 67 (2003) 3559.
65. J. Rose, A. Flank, A. Masion, J. Bottero, P. Elmerich, Langmuir 13 (1997) 1827.
66. G. A. Waychunas, B. A. Rea, C. C. Fuller, J. A. Davids, Geochim. Cosmochim. Acta 57 (1993) 2251.
67. D. M. Sherman, S. R. Randall, Geochim. Cosmochim. Acta 67 (2003) 4223.
68. K. F. Hayes, A. L. Roe, G. E. Brown, Jr., K. Hodgson, J. O. Leckie, G. A. Parks, Science 238 (1987) 783.
69. J.-L. Hazemann, J. F. Berar, A. Manceau, Mat. Sci. Forum 79 (1991) 821.
70. K. D. Kwon, J. D. Kubicki, Langmuir 20 (2004) 9249.
71. B. A. Manning, S. E. Fendorf, S. Goldberg, Environ. Sci. Technol. 32 (1998) 2383.
72. M. L. Farquhar, J. M. Charnock, F. R. Livens, D. J. Vaughan, Environ. Sci. Technol. 36 (2002) 1757.
73. G. Ona-Nguema, G. Morin, F. Juillot, G. Calas, G. E. Brown, Jr., Environ. Sci. Technol. 39 (2005) 9147.
74. M. Villalobos, J. O. Leckie, Geochim. Cosmochim. Acta 64 (2000) 3787.
75. T. Hiemstra, R. Rahnemaie, W. H. Van Riemsdijk, J. Colloid Interf. Sci. 278 (2004) 282.
76. H. Wijnja, C. P. Schulthess, Soil Sci. Soc. Am. J. 65 (2000) 324.
77. M. Villalobos, J. O. Leckie, J. Colloid Interf. Sci. 235 (2001) 15.
78. J. R. Bargar, J. D. Kubicki, R. Reitmeyer, J. A. Davis, Geochim. Cosmochim. Acta 69 (2005) 1527.

79. S. J. Hug, J. Colloid Interf. Sci. 188 (1997) 415.
80. D. Peak, R. G. Ford, D. L. Sparks, J. Colloid Interf. Sci. 218 (1999) 289.
81. H. Wijnja, C. P. Schulthess, J. Colloid Interf. Sci. 229 (2000) 286.
82. R. Rietra, T. Hiemstra, W. H. van Riemsdijk, J. Colloid Interf. Sci. 218 (1999) 511.
83. R. P. J. J. Rietra, T. Hiemstra, W. H. Van Riemsdijk, J. Colloid Interf. Sci. 240 (2001) 384.
84. M. I. Tejedor-Tejedor, M. A. Anderson, Langmuir 6 (1990) 602.
85. P. Persson, N. Nilsson, S. Sjöberg, J. Colloid Interf. Sci. 177 (1995) 263.
86. Y. Arai, D. L. Sparks, J. Colloid Interf. Sci. 241 (2001) 317.
87. C. S. Kim, J. J. Rytuba, G. E. J. Brown, J. Colloid Interf. Sci. 271 (2004) 1.
88. P. G. Weidler, S. J. Hug, T. P. Wetche, T. Hiemstra, Geochim. Cosmochim. Acta 62 (1999) 3407.
89. F. Gaboriaud, J. Ehrhardt, Geochimica Et Cosmochimica Acta 67 (2003) 967.
90. L. Spadini, A. Manceau, P. W. Schindler, L. Charlet, J. Colloid Interf. Sci. 168 (1994) 73.
91. C. R. Collins, K. V. Ragnarsdottir, D. M. Sherman, Geochim. Cosmochim. Acta 63 (1999b) 2989.
92. J. F. Boily, S. Sjoberg, P. Persson, Geochimica Et Cosmochimica Acta 69 (2005) 3219.
93. C. L. Peacock, D. M. Sherman, Geochim. Cosmochim. Acta 68 (2004) 2623.
94. R. H. Parkman, J. M. Charnock, N. D. Bryan, D. J. Vaughan, Amer. Min. 84 (1999) 407.
95. J. R. Bargar, G. E. Brown, Jr., G. A. Parks, Geochim. Cosmochim. Acta 61 (1997) 2639.
96. J. D. Ostergren, T. P. Trainor, J. R. Bargar, G. E. Brown, Jr., G. A. Parks, J. Colloid Interf. Sci. 225 (2000) 466.

Chapter 6

Interaction of Silicic Acid with Goethite

Tjisse Hiemstra, Mark O. Barnett, and Willem H. van Riemsdijk

Published in Journal of Colloid and Interface Science
Volume 310, Issue 1, Pages 8-17, June 1, 2007

Abstract

The adsorption of Si on goethite (α-FeOOH) has been studied in batch experiments that cover the natural range of Si concentrations that are found in the environment. The results have been interpreted and quantified with the charge distribution (CD) and multi-site surface complexation (MUSIC) model in combination with an extended Stern (ES) layer model option. This new double layer approach (ES) accounts for ordering of interfacial water molecules leading to stepwise changes in the location of electrolyte ions near the surface (Hiemstra and Van Riemsdijk 2006).

The Si adsorption on goethite peaks at a pH of ~9 and decreases at lower and higher pH values. Thermodynamically, the pH-dependency of silicic acid adsorption is related to the value of the proton co-adsorption and can also be linked to the Si charge distribution in the interface as is discussed.

Based on published EXAFS data, the adsorption of Si on goethite was modeled as the formation of a bidentate surface complex. The charge distribution (CD) of this complex can be calculated from geometry, optimized with the Molecular Orbital / Density Functional Theory (MO/DFT), and combined with correction for water dipole orientation. The resulting CD value has been applied successfully in the description of the adsorption data. The use of a theoretical CD value has the practical advantage of a reduction of the number of adjustable parameters with a factor 2.

To describe the adsorption at a high Si loading, formation of a Si polymer, e.g. a tetramer, is proposed. Such a species is only contributing to the overall adsorption at solution concentrations above about 10^{-4} M, where super saturation with respect to quartz exists. The adsorbed silica polymer hydrolyzes at high pH. The reactive ligand of the polymer is quite acid ($\log K \approx 6.5$-7.1), which is typically for the $\equiv SiO^{-1}$ surface groups of polymerized Si, like amorphous SiO_2(s), and the $\equiv SiO^{-1}$ ligand of the aqueous dimer $Si_2O(OH)_5O^{-1}$(aq). The model used correctly predicts the change of particles charge and the shift in IEP due to proton release upon Si adsorption.

Introduction

After oxygen, silicon is the main element in the earth crust. It is released during weathering of Si-containing minerals and therefore it is a ubiquitous solute in surface- and ground-waters. In a natural solution, it is present as silicic acid, $H_4SiO_4^0$(aq) [1]. Silicic acid interacts with the surfaces of Al and Fe (hydr) oxides [2-9]. It forms innersphere complexes by exchanging ligands with surface groups [10]. This process is pH-dependent.

The overall pH dependency of an adsorption process is determined by two different characteristics. One factor is the pH dependency of the solution chemistry [2]. The other factor is the interaction of the adsorbing species with protons on the surface resulting in proton co-ad/desorption. The speciation of the silicate ion in a natural solution is usually very simple with only one dominant species, $H_4SiO_4^0$(aq). In such a case, the pH dependency is mainly determined by the interaction of silicic acid with protons on the surface as a result of the adsorption. It has been shown that the proton co-adsorption is strongly linked to the structure of the innersphere complex that is formed [11]. The structure results in an interfacial charge distribution that affects the electrostatic interaction with the protons at the surface. In principle, the interfacial charge distribution of an innersphere complex can be found from the analysis of adsorption data. Another approach would be to estimate the charge distribution based on a Pauling bond valence approach. It assumes an equal distribution of charge over the coordinating ligands [12]. The use of the Pauling concept to estimate the CD value of surface complexes, may be insufficiently accurate [13], since the actual CD value can be a trade off between two opposing tendencies, i.e. an equal distribution of charge over ligands versus a full neutralization of the ligands of the innersphere complexes that are common with the solid. It has been suggested [14] that the charge distribution can be derived from the geometry of surface complexes, using the Brown bond valence approach [15],[16],[17]. The geometry of innersphere complexes may be found with quantum chemical methods. Recently [18], it has been shown that the calculated charge distribution can be linked to the experimental CD value. To do so, one should include the effect of a change in dipole orientation of interfacial water because of the ion complexation.

The charge distribution not only regulates the pH dependency of the adsorption. It also affects the shape of the isotherm and the competition for adsorption sites with other ions [19]. When an ion adsorbs, it will interact with all the surface species that are already present in the interface. This interaction is predominantly of an electrostatic nature. The process of ion competition is particularly sensitive to the electrostatic potential acting on the charge of the ligands that are not common with the surface, since the surface potential of oxides is in general mainly dependent on the pH and only slightly affected by the presence of other adsorbed ions. Therefore, the charge distribution of the silicon over the ligands is essential for understanding the corresponding adsorption properties.

In this paper, we will study the pH and concentration dependency of the adsorption of silicic acid. The adsorption and competition will be interpreted with the Charge Distribution model [13] in combination with the MUSIC model [20], [21], using an Extended Stern layer (ES) model [18] to describe the double layer profile. In the data analysis, the charge distribution is used as constraint. The charge distribution is derived from geometries

optimized with Molecular Orbital calculations using Density Functional Theory (MO/DFT). It has the practical advantage that the number of adjustable parameters can be reduced. In the experiments, we will use a wide range of Si concentrations. At a high Si concentration and pH, aqueous Si-polymerization may be important [22-24]. It has been suggested that the oligomers may also be formed at the surface at a high Si-loading [8]. This issue will also be addressed in this study.

MUSIC model

In the lattice of goethite (α-FeOOH), two different types of triply coordinated oxygens exist, one protonated ($\equiv Fe_3\text{-}O_IH$) and one non-protonated ($\equiv Fe_3\text{-}O_{II}$) oxygen. Both types of oxygens (O_I & O_{II}) are also found at the surface of the dominant 110 face and in addition at the 100 face [21]. Oxygens with a lower Fe coordination are found at the surface too. These surface groups are doubly and singly coordinated with Fe ions. Doubly coordinated oxygens have a high affinity for protons, because the $\equiv Fe_2O_{II}^{-1}$ surface group is highly under saturated in terms of bond valence charge [21]. On the other hand, the uncharged surface species, $\equiv Fe_2O_{II}H^0$, is very stable and does not easily accept nor release a proton and is therefore essentially inert on the surface. Singly coordinated surface oxygens ($\equiv FeO_{II}^{-3/2}$) are highly unstable and are always transformed into at least $\equiv FeO_{II}H^{-1/2}$ in aqueous systems [21, 25]. Depending on the pH, the hydroxyl ($\equiv FeO_{II}H^{-1/2}$) may accept a second proton to form a charged surface water group ($\equiv FeO_{II}H_2^{+1/2}$).

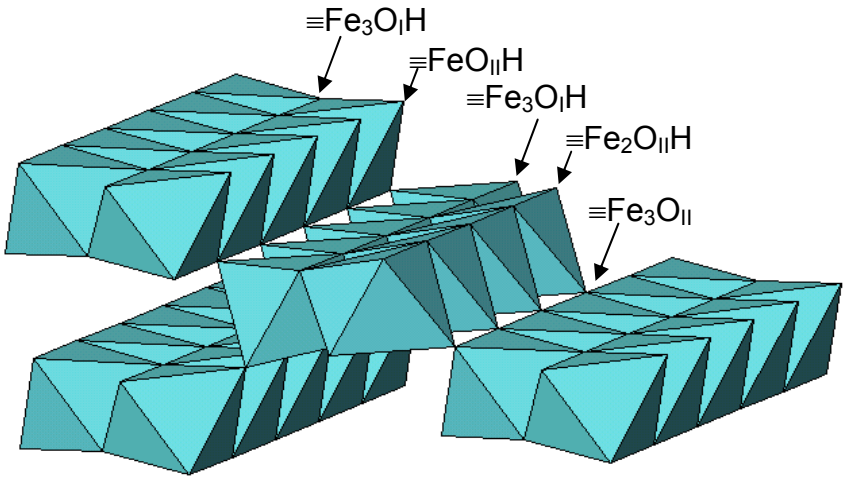

Fig.1. Stacking of the Fe-octahedrons of goethite showing the 110 face with singly, doubly and two types of triply coordinated surface groups.

The surface structure of the dominant 110 face of goethite is given in Fig.1. At this face, one row of singly coordinated surface groups is found on a unit cell basis, which is equivalent

with a site density N_s of 3 nm^{-2}. In addition, one row of doubly coordinated groups is present and, on a unit cell basis, also one row of triply coordinated groups (N_s = 3 nm^{-2}) with a low proton affinity (type II) and two rows (N_s = 6 nm^{-2}) with a high proton affinity (type I). The proton affinity of triply coordinated groups of type II ($\equiv Fe_3O^{-1/2}$) is very low. This group remains non-protonated, but contributes to the surface charge [21]. The affinity constant of the other type of triply coordinated surface group, type I, is estimated to be relatively high, more close to that of the singly coordinated group [21]. In the present approach, the affinity constants of these two proton reactive surface groups ($\equiv FeO_{II}H^{-1/2}$ and $\equiv Fe_3O_I^{-1/2}$) are set equal in the modeling [21]. Besides the presence of a 110 face, goethite may also have 100 faces [26, 27]. Its importance depends on the specific surface area [27]. The 100 face has in essence the same surface composition as the 110 face but the site density of the groups is slightly higher. Goethite crystals usually have a needle or lath shape. Faces like the 021 and 001 face terminate the goethite crystals at the top ends. These crystal faces have equal numbers of singly and doubly coordinated surface groups (N_s = 7-8 nm^{-2}). In the modeling, the protonation constant of these singly coordinated surface groups is taken equal to that of the 110 face.

Based on the above analysis, the surface charging can be calculated using two protonation reactions:

$$\equiv FeO_{II}H^{-1/2} + H^+(aq) \Leftrightarrow \equiv FeO_{II}H_2^{+1/2} \quad (1)$$

$$\equiv Fe_3O_I^{-1/2} + H^+(aq) \Leftrightarrow \equiv Fe_3O_IH^{+1/2} \quad (2)$$

The overall site density of goethite is calculated assuming 90% 110/100 face and 10 % 021/001 face, leading to approximately 2.7+0.75 = 3.45 nm^{-2} for the singly coordinated group [13]. The site density of the non-reactive triply coordinated surface group ($Fe_3O_{II}^{-1/2}$) is 2.7 nm^{-2}. The other type of triply coordinated group ($\equiv Fe_3O_I(H)$) has a site density of 5.4 nm^{-2}.

The above picture can be simplified, since the charge behavior of the three rows of triply coordinated groups is equivalent with that of one row of $\equiv Fe_3O_I(H)$ groups, which is due to internal compensation of charge of one row of $\equiv Fe_3O_IH^{+1/2}$ by one row of $\equiv Fe_3O_{II}^{-1/2}$ [21]. Hence, the overall apparent site density of triply coordinated surface groups ($\equiv Fe_3O_I(H)$) is set at 2.7 nm^{-2}.

Charge Distribution Model

In a double layer, the concept of point charges becomes problematic near the surface. Close to the surface, structural double layer details are needed if the aim is to use physically realistic species as observed with spectroscopy. In most surface complexation models, the charge of an innersphere surface complex is usually condensed to a point charge in the electrical double layer that is attributed to the surface, i.e., one electrostatic position is used for an innersphere surface complex. However, because adsorbed molecules and ions have a

physical size (i.e., they are not true point charges), the charge of an innersphere complex can be delocalized throughout the compact part of the double layer. Therefore, surface species experience a gradient of the electrostatic potential that strongly changes over very small distances in the compact part of the double layer. A surface complexation model has been proposed to account for this phenomenon [21]. The position of the ligands in the interface turned out to be crucial [11, 21], i.e. the structure of the surface complex is involved. In the case of the formation of surface complexes of silicic acid, only a part of the ligands of the Si surface complex will become common with the reactive surface groups. The remaining ligands are at some distance from the surface. In the charge distribution (CD) model, one part of the charge of the innersphere complex is attributed to the electrostatic surface plane (0-plane). The other part is located in an electrostatic plane (1-plane) at some distance from the surface (Fig.2).

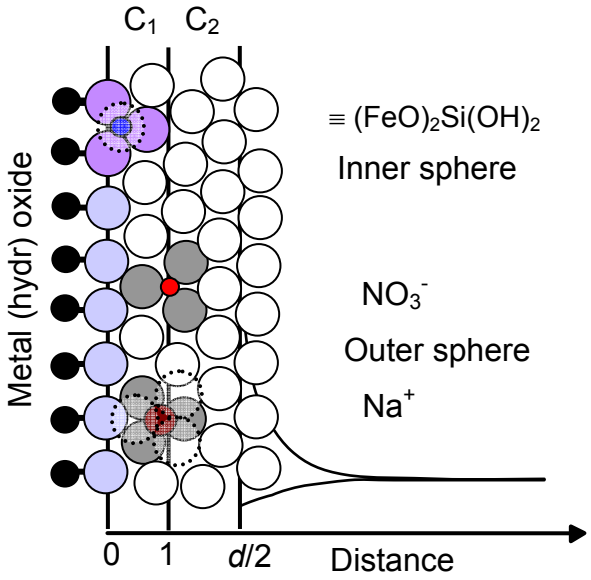

Fig. 2 A schematic picture of the double layer structure of the extended Stern layer model, showing a metal hydroxide surface with a silicate bidentate innersphere complex that distributes its charge between 0- and 1-plane and the outer sphere complexes of NO_3^- and Na^+ which charge is located in the 1 plane. The DDL is separated from the electrolyte ion pairs by an outer Stern layer.

Double layer Model

Surface groups of metal (hydr) oxides may interact with electrolyte ions, forming outer sphere complexes, known as ion pairs. These adsorbed cations and anions are located in the interface at a minimum distance of approach from the negatively- or positively-charged surface groups respectively [28]. Recently, the charging behavior of goethite has been measured for a series of electrolyte ions including Li^+, Na^+, K^+, Cs^+, NO_3^-, Cl^-, and ClO_4^- in a consistent manner [29]. Analysis of the data indicates that the head end of the diffuse double layer (DDL) is separated from the minimum distance of approach of electrolyte ions by a

second Stern layer. As discussed in [18], this observation can be related to the structuring of water molecules in the interface, probably allowing only stepwise changes of the location of these ions near the surface [18]. The result agrees with recent spectroscopic information. The structure of water near the surface can be measured with different approaches like force measurements [30, 31], X-ray reflectivity [32-34] and Sum Frequency Spectroscopy [35-38]. The force measurements for mica and X-ray reflectivity on Ag(s) and Al_2O_3(s) faces show ordering of water within a distance equivalent with about 3-4 and 2-3 layers of water respectively [18]. Sum Frequency Spectroscopy (SFS) on silica, quartz, Al_2O_3(s), and TiO_2(s) [38] points to the simultaneous presence of two types of water that differ in the degree of structuring. The SFS also shows that the number of polar-oriented water molecules increases if the interface becomes charged [37] and moreover, SFS points to a change in orientation of water dipoles on either side of the PZC [35]. As shown lately by Hiemstra and Van Riemsdijk [18], the latter aspect is implicitly part of the CD model. The first aspect is implemented in a new double layer model (Fig.2), which is derived from the analysis of titration. The double layer picture can be classified as an Extended Stern (ES) layer model [39]. In the model, the head end of the diffuse double layer (DDL) coincides with the 2-plane (Fig.2). The ions pairs are present in the 1-plane. In the present study, the ion pair formation constants for the electrolyte ions (Table 1) are taken from Rahnemaie et al. [40]. We note that electrolyte ions may also form innersphere complexes [41]. This is not shown in Fig.2.

Materials and methods

Materials

The goethite suspension used in this study was synthesized according to the method described in Hiemstra et al. [42]. In this procedure, a freshly prepared 0.5 M Fe(III) nitrate solution is slowly neutralized with 5 M NaOH with a rate of approximately 10 % per hour and brought to pH 12. It is followed by the conventional aging in the mother liquid for at least 48 hours at 60 ^oC [43]. Our goethite has been characterized previously by Hiemstra and van Riemsdijk [13, 21]. The needle-shaped particles have an average width and length of about respectively 10 and 100 nm. The material has a PZC of about 9.2. The BET surface area is 100 m^2/g.

Adsorption experiments

The adsorption of silicic acid to goethite was measured in five series of suspensions of 50 or 60 mL having a goethite concentration of 0.95, 2.65, or 3.20 g/L at a final ionic strength of 0.10 M $NaNO_3$. The initial Si concentrations were kept below the solubility of SiO_2(am) and were varied between ca. 10^{-4} and 10^{-3} M using a 49.9 ppm Si (1.78 mM) stock solution made from $Na_2SiO_3.9H_2O$. The Si concentration was standardized on the Na^+ concentration in the stock. The concentration also agreed with the expected concentration based on the mass of

$Na_2SiO_3.9H_2O$ added gravimetrically. The pH of the suspensions was varied between pH 3.5-11 by adding 0.010 M HNO_3 or NaOH. All chemicals were made in double distilled water and contact with glassware was avoided to prevent Si contamination. The suspensions were equilibrated for 20 hours, yielding equilibrium [44]. After measuring the pH, the suspension was centrifuged and the clear supernatant was stored after acidification to a concentration of 0.16 M HNO_3. The Si concentrations were determined colorimetrically using a molybdenum blue method. The Si stock solution was free of Si polymers according to the method of Beckwith and Reeve [45].

Table 1. Surface species, formation constants and charge allocation determining the primary charge of the goethite particles, using ≡ $FeOH^{-1/2}$, H^+ , Na^+, and NO_3^- as reference components. The capacitance of the Stern layers is set equal, i.e. $C_1 \equiv C_2 = 0.92$ F/m^2.

Species	log*K*	Δz_o	Δz_1	Δz_2
≡$FeOH^{-1/2}$	0	0	0	0
≡$FeOH_2^{+1/2}$	9.2	1	0	0
≡$FeOH^{-1/2}$-Na^+	-0.61	0	1	0
≡$FeOH_2^{+1/2}$-NO_3^{-1}	8.50	1	-1	0
≡$Fe_3O^{-1/2}$	0	0	0	0
≡$Fe_3OH^{+1/2}$	9.2	1	0	0
≡$Fe_3O^{-1/2}$-Na^+	-0.61	0	1	0
≡$Fe_3OH^{+1/2}$-NO_3^{-1}	8.50	1	-1	0

Calculations

The modeling and optimization of adsorption parameters have been done using the ECOSAT 4.8 program [46] in combination with the program FIT 2.5 of Kinniburgh [47]. Molecular orbital (MO) calculations have been carried out to derive the optimized geometry of silicic acid bound as a monodentate complex to Fe hydroxide octahedrons, using Spartan'04 software of Wavefunction [48]. The geometry optimizations were done using density functional theory (DFT). Pseudo potentials, defined in Spartan'04 as LACVP+** (Los Alamos Core Valence Potentials), were used. This set comprises the 6-31+G** basis set for main group elements H-Ar. The + and ** signs refer to the use of respectively diffuse and polarization functions, including H. The geometries were optimized using the Becke Perdew (BP86) model [49]. The calculated geometries have been interpreted with the Brown bond valence approach [50], in order to obtain the charge distribution value of the monodentate ≡ $FeOSi(OH)_3$ complex. The geometry of the bidentate complex ≡ $(FeO)_2Si(OH)_2$ has been given elsewhere [18].

Results and discussion

Si adsorption

The adsorption of Si (Fig.3a) was studied as a function of pH for five systems that vary in the solid-solution ratio. The corresponding equilibrium concentrations are given in Fig.3b.

The adsorption reaches a maximum around pH = 9, well-known from previous studies [2],[5],[9]. In the pH range below 9, the adsorption of Si decreases with decreasing pH. In this pH range, the solution speciation of silicic acid is pH independent, i.e. only the aqueous $Si(OH)_4^0$ species is present in significant concentrations. This implies that the observed pH dependency of the adsorption is due solely to the interaction of Si with the surface and is not due to a change in the aqueous speciation. From a thermodynamic point of view, the interaction of Si with a protonated *surface* ($\equiv SH_m$) can be formulated with the overall reaction:

$$\equiv SH_m + H_nSiO_4^{n-4} \Leftrightarrow \equiv SH_{m+n-p}SiO_4^{n-4-p} + p\,H^+ \qquad (3)$$

where $H_nSiO_4^{n-4}$ represent the average protonation status of the species in solution and $SH_{m+n-p}SiO_4^{n-4-p}$ represents the mean H status of the *surface* after adsorption. In the adsorption process, a net amount of protons (p) is released per mole of Si bound [18], i.e. the number p (eq.(3)) is positive. The formulated reaction predicts that in case of release of protons ($p > 0$), an increase in the proton concentration will lead to a decrease in the Si-adsorption (i.e., the equilibrium will shift to the left). This analysis illustrates that the relative amount (p) of protons released or co-adsorbed per ion adsorbed will determine the pH dependency of the adsorption process.

Thermodynamic consistency relationship

Proton co-ad(de)sorption and pH dependency are related by the important formalism of thermodynamic consistency [51]. To account for pH-dependent changes in aqueous speciation, the thermodynamic consistency relationship can also be written in a general form [14, 52]. For Si adsorption, we may write:

$$\left(\frac{\partial log\, C_{Si\text{-}tot}}{\partial pH}\right)_{\Gamma_{Si}} = \left(\frac{\partial \Gamma_H}{\partial \Gamma_{Si}} - n_H\right)_{pH} \equiv \left(\chi_H - n_H\right)_{pH} \qquad (4)$$

in which $\partial \log C_{Si\text{-}tot}/\partial pH$ is the change of the total concentration of aqueous Si ($C_{Si\text{-}tot}$) with a change of pH at a constant silicate loading, Γ_{Si}. The change of the proton adsorption ($\partial\Gamma_H$) at change of the silicate adsorption ($\partial\Gamma_{Si}$) is defined as the proton co-adsorption ratioχ. The expression says that the concentration change is equal to the change in H^+ adsorption (Γ_H) as a result of the adsorption of Si at the surface (Γ_{Si}) at a given constant pH after correction for the

mean relative number (n_H) of protons present on the species in solution at that pH. For calculating the proton balances in solution (n_H) and on the surface (Γ_H), a chosen reference species is required (e.g., see Hiemstra and Van Riemsdijk [14]). For silicic acid, the natural choice is $H_4SiO_4^0$. Below pH 9, the solution only contains significant concentrations of the Si reference species $H_4SiO_4^0$, which means $n_H = 0$ below pH ~9. At higher pH values (e.g., pH > ~11), we will have $n_H = -1$ if $H_3SiO_4^-$ is the only significant species.

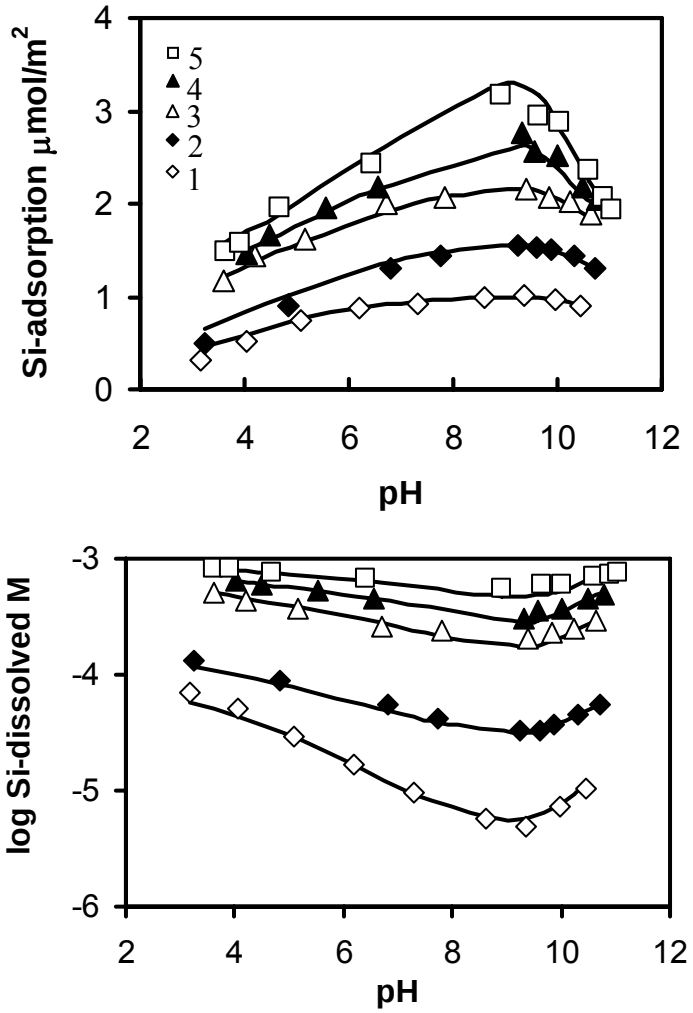

Fig. 3a. The adsorption of Si on goethite as a function of pH (I = 0.10 $NaNO_3$) in the five systems studied. The suspension concentrations for system 1 to 5 are respectively 0.95, 0.95 3.20, 2.65, 1.60 g/L. The initial Si concentrations for system 1 to 5 are respectively 0.100, 0.178, 0.89, 1.04, and 1.07 mM. In Fig. 3b, the logarithm of the corresponding equilibrium concentrations is given, which covers the range of natural concentrations. The lines in the figure have been calculated with the CD model using the recommend parameters of Table 3.

The thermodynamic consistency relationship (eq.(4)) can be applied to the Si adsorption curves of Fig.3. The value $\partial \log C_{Si\text{-}tot} / \partial pH$ can be read from the graph (Fig. 3b). The graph shows that the slope is not only a function of the pH, but also of the loading (Γ_{Si}). For the lowest loading level in Fig.3 at pH = 7 and I = 0.1 M ($\Gamma_{Si} \approx 0.8$ μmol/m^2), the slope is -0.25 ± 0.05. As described above, $n_H = 0$ for the species in solution at this pH. Introduction of these numbers in the thermodynamic consistency relationship (eq.(4)) results in a predicted H^+ co-adsorption $\partial\Gamma_H / \partial\Gamma_{Si}$ or χ of approximately $\chi \approx -0.20 \pm 0.05$ (at $\Gamma_{Si} \approx 0.8$ μmol/m^2). It implies that approximately 0.2 H^+ will be released per H_4SiO_4 adsorbed, i.e. $p \approx 0.2$ in eq.(3) at this pH and Si loading (Γ_{Si}). The proton release per H_4SiO_4 adsorbed to goethite at pH = 8 and pH = 6 has been measured in the loading range Γ_{Si} = 0 -0.5 μmol/m^2 [18]. The average experimental ratio $\partial\Gamma_H / \partial\Gamma_{Si}$ is about -0.25 v.u. (valence unit), which is in line with the above-derived estimate.

At high pH, the experimental slope is significantly different and has a positive value. This is mainly due to a change in the solution speciation. At pH = 10 the average number of protons per Si is considerably lower, e.g. n_H = -0.7 at pH = 10.2. This change in n_H results in a change of the slope $\partial \log C_{Si\text{-}tot} / \partial pH$ from a negative (pH = 7) to a positive value (pH = 10). The example illustrates that the pH dependency of adsorption is determined by two factors, i.e. a) the H^+ co-adsorption (the sole factor at low pH in case of silicic acid, and b) the solution speciation (responsible for the large decrease in adsorption at high pH in case of Si). The importance of changes in solution chemistry has been pointed out in the past by Hingston et al. [2] discussing their concept of the adsorption envelopes.

Particle charge

The value of p in eq. (3) can also be interpreted in terms of the change of the goethite particle charge upon adsorption of the neutral $H_4SiO_4^0$ species. According to the analysis of the data at a low Si loading, $p \sim 0.25$ at pH = 7, i.e. a net amount of protons is released (eq. (3)). This means that the surface will decrease in positive charge with an increase in the loading of Si, which also implies that the experimental point of zero charge will decrease in a set of titrations of goethite with an increase of silicic acid, as has been observed by Hingston et al. [2]. The net release of protons will also lead to a shift in the isoelectric point (IEP), as found by Garman et al. [53] and Luxton et al. [9] for Si adsorption on goethite (Fig.4) and by Davis et al. for Hydrous Ferric Oxide (HFO) [8]. This phenomenon results also from the CD model (Fig.4).

The particle charge and salt dependency of the adsorption are related. Increase of the electrolyte concentration will lead to a better screening of charge. Above the IEP, the adsorption will increase since a net negative charge is introduced with the Si adsorption leading to less repulsion at a higher salt level. The adsorption but will decrease below the IEP as a result of less attraction. This has been observed experimentally [54].

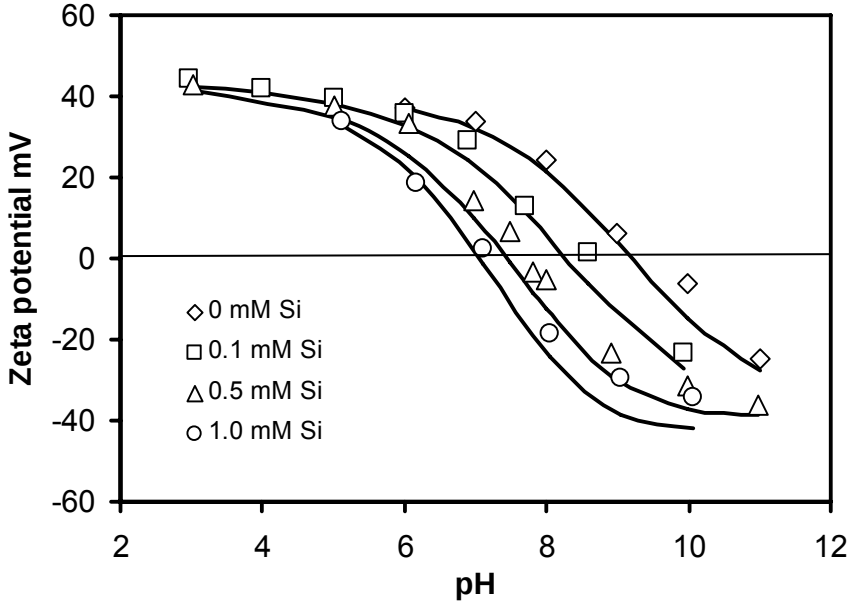

Fig. 4. The change of the IEP and zeta potential (mV) of goethite suspension (ρ =1.0 g/L, A = 72.3 m^2/g)) when loaded with silicic acid (initial concentration of Si = 0, 0.1, 0.5, and 1.0 mM). Data are from Luxton et al. [9]. The lines are predicted with the CD model in combination with the extended Stern layer model option, using the parameters of Tables 1 and 3. The plane of shear is placed at 1.8 nm from the head end of the DDL.

Solution and surface speciation

A correct modeling of the surface speciation first requires an accurate model of solution speciation. Classical studies of the solution speciation using acid-base titrations have suggested the formation of Si polymers at high Si concentration and high pH [55]. The solution speciation has also been followed with ^{29}Si NMR [22, 23]. Various complexes have been identified and the formation constants have been derived. At near-neutral pH and near the solubility limit of SiO_2(am), the dimer $Si_2O_2(OH)_5^{1-}$ was the only poly-Si species detected, and its concentration was at most 6% of the total Si in solution [22]. Felmy et al. [24] recently developed a comprehensive model of Si solution speciation applicable for a wide range of conditions. Below the solubility limit of SiO_2 (am) and pH<11 (the conditions of these experiments), oligomeric species were indeed less than 5% of total aqueous Si. Calculations, using the species and formation constants of Felmy et al. [24] show that in our experiments in aqueous solution only the dimer ($Si_2O_2(OH)_5^{1-}$) might be present at a minor concentration (< ~1%). We therefore utilized the following aqueous equilibria in modeling our data:

$$H_4SiO_4^0(aq) \Leftrightarrow H_3SiO_4^-(aq) + H^+(aq) \quad (5)$$

$$H_4SiO_4^0(aq) \Leftrightarrow H_2SiO_4^{2-}(aq) + 2H^+(aq) \quad (6)$$

$$2H_4SiO_4^0(aq) \Leftrightarrow Si_2O_2(OH)_5^-(aq) + H^+(aq) + H_2O(l) \quad (7)$$

with corresponding log$K$ values (I = 0 M, T = 298 K) of -9.82, -23.27, and -8.50 respectively. Recently, the formation constant of the neutral dimer $Si_2O(OH)_6^0$ has been estimated with quantum chemical methods [56], yielding approximately log$K \approx$ -1.5. Based on this estimate, the contribution of this species is expected to be low.

Before defining the adsorption reactions in detail, we will evaluate the surface speciation as found by in-situ spectroscopy. The interaction of Si with iron oxides has been studied for solutions containing small Fe polymers [10, 57]. A study with FTIR [57] showed the presence of a Fe-O-Si linkages at a low Fe/Si (<1) ratio, confirming the formation of innersphere complexes. A recent EXAFS study [10] showed that Si is present in the Fe coordination sphere at a distance of 317 ± 3 pm. It was argued that this distance is very close to the experimental distances found for bidentate surface complexes of PO_4, AsO_4, and SeO_3 [58-61]. The EXAFS study suggests that Si will form double corner complexes upon reaction with singly coordinated surface groups. The MO/DFT optimized structure [18] has a Fe-Si distance of 321 ± 0.5 pm, which is within the experimental value (317 ± 3 pm) considering the uncertainty in both numbers.

Based on the proposed mechanism [10], the interaction of $H_4SiO_4^0$ with two $\equiv FeOH^{-1/2}$ surface groups can be formulated as:

$$2 \equiv FeOH^{-1/2} + H_4SiO_4^0(aq) \Leftrightarrow \equiv (FeO)_2^{-1+\Delta z_0}Si(OH)_2^{\Delta z_1} + 2H_2O(l)\,;K_1 \quad (8)$$

with an equilibrium constant K_1 where Δz_o and Δz_1 represent the change of charge in the 0 and 1-plane (Fig.2) respectively upon the adsorption of uncharged $H_4SiO_4^o$ with $\Delta z_0+\Delta z_1 = 0$. With the above reaction, the experimental data at low loading could be described well. However, the Si adsorption Γ_{Si} at the two highest loadings was clearly underestimated. The main reason is the relative lack of reactive surface sites in relation to the amount of Si that was measured experimentally at the highest Γ_{Si}. The highest measured adsorption on our goethite is about 3.2 μmol/m^2, clearly higher that the theoretical maximum calculated from the site density of ≡FeOH(H) (2.86 μmol/m^2) assuming formation of bidentate surface complexes. Such a high loading for goethite has also been reported by Hingston [2],[54] and recently by Luxtor et al. [9]. If fitting is the sole aim, a practical solution might be to increase the number of sites. However, we consider the experimental observation as an indication of the presence of an additional adsorption mechanism.

The experimental data show that in the model more Si should be allowed to adsorb. Several options might explain the data. It is possible to formulate a monodentate reaction [9], which allows potentially twice as much binding. Another option is to assume that Si is interacting with another type of site. On the goethite surface, the $\equiv Fe_2OH^o$ site can be a candidate, forming $\equiv Fe_2OSi(OH)_3^o$. Both options improve the quality of the fit. A third model

option is related to the formation of Si oligomers at the surface. These oligomers, once formed, might represent a metastable situation in a process of surface precipitation. It should be noted that the solutions at high loading (Fig.3b) are oversaturated with respect to quartz ($C\text{-}Si_{max} = 10^{-4}$ M). Recently [62], it has been shown that the rate of polymerization (R) from super saturated solutions was related to the silicic acid concentration according to $R \propto [H_4SiO_4^0]^4$, which might suggest the formation of a tetramer. Modeling shows that our adsorption experiments are best explained assuming a contribution of adsorbed tetramers, although formation of a dimer cannot be excluded. The general reaction for the adsorption of tetramers is formulated as:

$$2 \equiv FeOH^{-1/2} + 4\,H_4SiO_4^0 \Leftrightarrow \equiv (FeO)_2^{-1+\Delta z_0} SiOHOSi_3O_{2+n}(OH)_{7-n}^{\Delta z_1 - n} + nH^+ + 5H_2O \qquad (9)$$

where n represents the number of protons released due to the deprotonation of OH ligands. The number of protons that are dissociated for the tetrameric surface species (n = 0, 1, 2, …) will be obtained by fitting the data. We assume that the Si-oligomer is also bound as a bidentate surface complex, which would be in line with the EXAFS experiments [10]. We assume at present that the charge attribution to the surface (Δz_0) is quite similar for both types of surface species, i.e. bidentate monomers (eq.(8)) and polymers (eq.(9)). As will be discussed, later the charge on the other ligands is located in the 1-plane (Δz_1).

Parameter evaluation

In the charge distribution model, the formation of an innersphere complex is described using two parameters, i.e. the charge distribution value (Δz) and the affinity for the surface ($\log K$). Usually, these parameters have been found by fitting data. However, such a procedure may be problematic if several surface species may be active simultaneously. It has been suggested that the charge distribution coefficients can be derived from the geometry of surface complexes [14], [18]. Molecular Orbital calculations using Density Functional Theory (MO/DFT) can be applied to obtain such geometries. The distances can be interpreted with the Brown bond valence approach resulting in ionic charge distribution coefficients (n_0, n_1). These values can be corrected for the effect of dipole orientation. This results in the overall charge distribution coefficients Δz_0 and Δz_1. The charge distribution value thus found for the bidentate complex is $\Delta z_0 = -\Delta z_1 = 0.29 \pm 0.03$ v.u. [18]. The given variation stems from the uncertainty in the number of water molecules that interact with the ligands of the Si complex. The charge distribution can also be evaluated from analysis of the proton co-adsorption data, provided that only one type of surface species is formed [11]. The charge distribution value found for these data at pH = 6 and pH = 8 using reaction (8) is $\Delta z_0 = -\Delta z_1 = 0.29$ v.u., which is equal to the theoretical value. In the parameters evaluation, the theoretical value has been used as known value. Only the affinity constant is fitted.

In the fitting process, the adsorption data can be used in very different ways to derive the parameters. In Table 2, we show the fitting results. The data were evaluated on different scales, i.e. on the absolute adsorption (Γ_{Si}) and concentration (C) scale, and in addition on the

relative adsorption scale (% adsorbed) and the logarithmic concentration scale (log C). In using the linear scale, the fitting will account most strongly for deviations at the highest concentration levels and the highest adsorption levels. With the relative adsorption and the logarithmic concentration scales, more weight is given to the lower adsorption levels and concentration range. The resulting log*K* values (Table 2) were generally consistent with one another (log*K* values generally differ ± <0.1). Based on the obtained parameter values, a set of average parameter values has been derived, which is given in Table 3.

Table 2. The formation constants (log*K*) of Si surface species using different scaling options. The quality of the fit is indicated with the root mean square error (RMSE) and the R^2 value. N = 46 data points.

Scale	$\log K_1$ *a	$\log K_2$ *b	$\log K_3$ *c	RMSE	R^2
$C_{Si\text{-}tot}$ (mol/L)	5.94 ±0.03	13.93 ± 0.09	7.49 ± 0.03	$1.4\ 10^{-5}$	0.998
Γ_{Si} (μmol/m^2)	5.85 ± 0.04	13.92 ± 0.08	7.36 ± 0.03	$7.4\ 10^{-2}$	0.989
Molar % Si-adsorbed	5.76 ±0.02	14.01 ± 0.12	7.38 ± 0.03	2.6	0.985
log $C_{Si\text{-}tot}$ (mol/L)	5.85 ± 0.01	14.04 ± 0.22	7.63 ± 0.03	$3.0\ 10^{-2}$	0.998

*a monomer eq.(8), *b,c oligomer eq.(9) with respectively $n = 0$ and $n = 1$

Table 3. Charge distribution values (Δz) and the averaged log*K* values found for the different surface species.

Species	Δz_0	Δz_1	Δz_2	log*K*
$\equiv(FeO)_2Si(OH)_2$	0.29*[1]	-0.29*[1]	0	5.85 ± 0.06
$\equiv(FeO)_2SiOHOSi_3O_2(OH)_7$	0.29	-0.29	0	13.98 ± 0.05
$\equiv(FeO)_2SiOHOSi_3O_{2+1}(OH)_{7\text{-}1}$	0.29	-0.29-1*[2]	0	7.47 ± 0.11

*[1] Value calculated applying the Brown bond valence concept to MO/DFT optimized geometries. The estimated uncertainty is about 0.03 v.u.

*[2] The value -1 v.u. refers to removal of a proton charge from one of the OH ligands.

Based on the log*K* values in Table 3, the proton affinity of the O ligand of the tetramer surface species can be calculated ($\log K_H = \log K_2 - \log K_3$). The proton affinity derived ($\log K_H = 6.51 \pm 0.12$) is clearly lower than the value for a monomer in solution (log*K* = 9.82). The $\log K_H$ value is relatively close to the log*K* value found for protonation of a singly coordinated oxygen at the surface of SiO_2, i.e., $\log K_H \approx 6.8$ to 7.5 [63] [64] [21, 65-67] [68]. The low $\log K_H$ value is probably characteristic for polymerized silicic acid. This is supported by the calculation of the protonation constant for the protonation reaction $Si_2O_2(OH)_5^{1-}(aq) + H^+(aq) \Leftrightarrow Si_2O(OH)_6$ (aq), i.e. log*K* = 7.0. This log*K* value is found from the combination of the above mentioned formation constants of the two dimer species being respectively log*K* = -8.5 [24] and log*K* = -1.5 [56].

In the above modeling, the negative charge created by deprotonation is set at the 1-plane. Actually, the structure of the Si-polymer at the surface is unknown and hydrolysable ligand could (also) be present at some larger distance from the surface. It might be argued that hydrolysis is suppressed in a negative electrostatic field. This suppression will be most strongly at the most negative potential. In case of a negative particle charge, the potential at the 1-plane will be lower than on the 2-plane. Ligands with the same proton affinity that experience a less negative potential will hydrolyze easier. The adsorption data can be

described equally well with locating the created negative charge at the 2-plane. The log$K$ values of Table 3 are in that case logK_1 = 5.84 ± 0.07, logK_1 = 14.10 ± 0.07, and logK_3 = 7.02 ± 0.09. In this interpretation, the affinity constant of the ligand is slightly larger, i.e. logK_H = logK_2 - logK_3 = 7.09 ± 0.10, which is due to the slightly lower electrostatic energy contribution which is compensated in a higher value of the intrinsic value. In conclusion, the logK_H of the ≡SiO^{-1} ligand on the Si polymer is in the order of log$K$ ≈ 6.5 to 7.1, which is close to the value for comparable groups at the surface of amorphous silica (SiO_2, s) and that of the aqueous dimer ($Si_2O_2(OH)_5^{1-}$, aq).

MO/DFT calculations

As discussed above, the adsorption of Si may exceed the estimated adsorption maximum based on the number of sites present at the surface to accommodate the bidentate monomer complexes. A higher adsorption may also be reached when a monodentate species is introduced. This option has recently been used by Luxton et al. [9], who applied the CD model. The CD values chosen were based on the Pauling charge distribution concept, although the authors recognized that the CD value might be different and might be obtained from quantum chemical calculations. Application of the Pauling bond valence approach results in $\Delta z_0 = 0$ and $\Delta z_1 = 0$ for bidentate as well as monodentate complexes. As shown by MO/DFT calculations [18], the charge in the Si bidentate complex is asymmetrically distributed. More charge of the Si^{4+} is to be attributed to the oxygen ligands that coordinate with Fe instead of a proton. In the case of a bidentate complex, there are two bonds with the surface whereas in the case of a monodentate complex, there is only one. Therefore, it may be expected that the formation of a bidentate complex results in more charge separation in the interface than the formation of the monodentate complex. Such a situation has recently also been found for the adsorption of $As(OH)_3$ [69]. This oxyanion may form mono- and bidentate innersphere complexes at the goethite surface [70]. Analysis of As(III) adsorption data showed that the bidentate complex attributes more positive charge to the surface than the monodentate complex. This also agreed with the calculation of the theoretical CD value of both As(III) complexes.

We have optimized the geometry of a Si-Fe monodentate complex ≡ $FeOSi(OH)_3$ (Fig.5) to derive the expected CD value which we may apply in a fitting procedure to test to what extent the presence of this species might explain the high Si loading of goethite. As a starting point, two iron octahedrons with Fe-O distances as found in goethite have been defined. The $Fe_2(OH)_4(OH_2)_4$ (z = 0) moiety is used to make a Fe-Si cluster by exchanging one water molecules against an oxygen of a $H_3SiO_4^-$ group. The exchanged OH_2 ligand is equivalent with a singly coordinated surface group of the 110 or 100 faces of goethite. The cluster formed represents the ≡ $FeOSi(OH)_3$ surface complex. It has three free Si-OH bonds and one common oxygen in the Fe-O-Si bond. The oxygen in the Fe-O-Si bond was allowed to interact with one water molecule via an H bridge (O-H···O). The free OH ligands in the coordination sphere of the Si were allowed to interact with three water molecules via H bridges, i.e. the total number water molecules is n_{H2O} = 9 + 1 = 10, (option A in Table 4).

However, during the optimization, two water molecules drifted away, resulting in two OH ligands that eventually interacted via H bonds with only two water molecules. In another optimization option (B in Table 4), no water molecule was defined to interact with the common oxygen ligand in the Fe-O-Si bond.

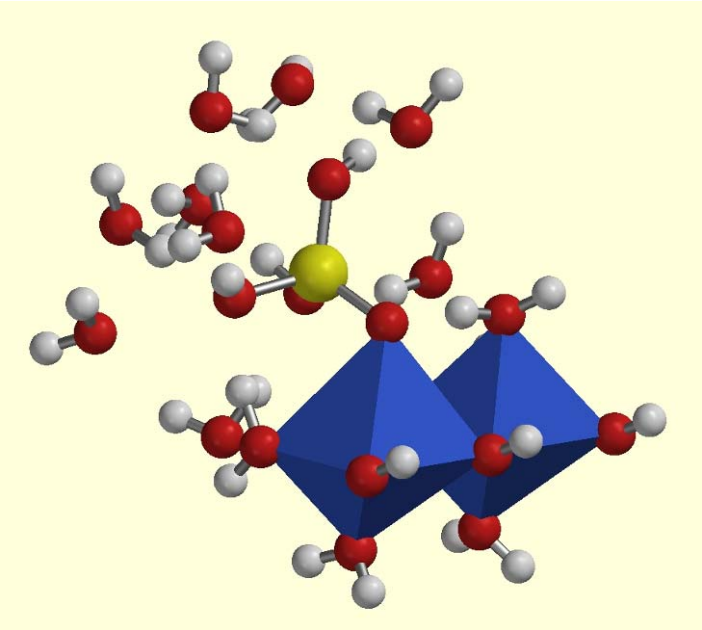

Fig.5. The MO-DFT (BP86) optimized geometry of a hydrated ($n_{H2O} = 9$) monodentate Si complex bound to a set of Fe octahedrons (option B of Table 4). The geometry of the Fe octahedra is fixed to the structure of goethite. The Fe-O-Si(OH)$_3$ unit and the water molecules are allowed to relax. See also Hiemstra and Van Riemsdijk [18].

The geometries of Table 4 can be interpreted in terms of charge distribution using the Brown bond valence concept. According to Brown [50], the bond valence s is related to the distance R as:

$$s = e^{-(R-R_0)/B} \qquad (10)$$

in which B is a constant (37 pm) and R_0 is the element specific parameter that is chosen such that the sum of the bond valences around the Si ion corresponds to the formal valence (z = +4). The quantum chemically obtained ionic CD values (n_0 and n_1) are given in Table 4. Based on the geometry, it is obvious that O-Si bond with the surface is stronger than the Si-OH bonds with the free ligands. It implies that more positive charge is to be attributed to the common oxygen, i.e. the 0-plane, resulting in positive numbers for n_0 and negative numbers for n_1 (Table 4), i.e. asymmetry in the charge distribution exists.

Table 4. The calculated distances (pm) in the geometry of a monodentate silicate complexes that differ in the number (n-H_2O) water molecules added for hydration, using the DFT-BP86 model.

	A	**B**
n-H_2O	9+1	9
Si-OH	163.8	164.2
Si-OH	165.9	167.0
Si-OH	169.9	168.5
O-Si	170.0	169.8
Fe-O*[1]	208.0	212.4
Fe-Si*[2]	325.0	329.4
R_o*[3]	167.3	167.3
n_0*[4]	+0.10	+0.08
n_1*[4]	-0.10	-0.08

*1 Distance present in the goethite structure without relaxation is 196 pm.

*2 EXAFS study reports d (Fe-Si) = 317 ± 3 pm and a coordination number of CN = 2 ± 0.5 [10]. The average value for Fe-So distance found with MO/DFT optimization of hydrated bidentate complexes is 321 ± 0.5 pm [18].

*3 Average R_0 for Si in minerals [50]. Calculation of the geometry of the $Si(OH)_4.12H_2O$ moiety results in Si-O distances of 167.2, 167.3, 165.9 and 168.2 pm which is equivalent with R_o = 167.1 pm.

*4 The charge of $H_4SiO_4^0$ attributed to the ligands of the 0- and 1-plane ($n_0 + n_1 = 0$) based on application of the Brown bond valence concept to the calculated geometry (Eq.(10)).

The calculated charge distribution values (n_0, n_1) can be combined with the required dipole correction to obtain the overall CD coefficients (Δz_0, Δz_1) that are active in the system. The relation is given by [18]:

$$\Delta z_0 = n_0 + n_{H0} - \phi(n_0 + n_{H0} + \Sigma n_{ref} z_{ref}) \quad (11)$$

and

$$\Delta z_1 = n_1 + n_{H1} + \phi(n_0 + n_{H0} + \Sigma n_{ref} z_{ref}) \quad (12)$$

in which n_{ref} and z_{ref} are respectively the number of reference groups and corresponding ion charge. In the above equations, n_{H0} and n_{H1} are the numbers of additional protons defined in the overall reaction and that are located at respectively in the 0- and 1-plane. In the formation reaction 1 $\equiv FeOH^{-1/2} + H_4SiO_4$ (aq) $\Leftrightarrow \equiv FeO^{-1/2}Si(OH)_3 + H_2O$ (l), no additional protons are present i.e. we have $n_{H0} = 0$ and $n_{H1} = 0$ and, $n_{ref} = 1$ and $z_{ref} = -1/2$. The charge distribution coefficients, Δz_0, Δz_1, calculated with eqs. (11, 12) are given in Table 5.

Table 5. The ionic Charge Distribution values (n_0, n_1) calculated from the MO/DFT (BP86) optimized geometries of Fe-Si species hydrated with a number of water molecules (n_{hydr}), using the Brown bond valence concept. The sum of the charge distribution values n_0+n_1 corresponds to the charge of $H_4SiO_4^0$. The charge distribution coefficients Δz_0 and Δz_1 refer to the calculated overall change of charge (eqs.11,12) as used in the appropriate reaction (eqs.(8, 9)).

Species	n_{hydr}	n_0	n_1	$\Delta z_{0\,(calc)}$	$\Delta z_{1(calc)}$	Δz_2
$\equiv (FeO)_2Si(OH)_2$*[1]	4-6	0.15 ± 0.03	-0.15 ± 0.03	0.29 ± 0.03	-0.29 ± 0.03	0
$\equiv FeOSi(OH)_3$ *[2]	9-10	0.09 ± 0.01	-0.09 ± 0.01	0.23 ± 0.03	-0.23 ± 0.03	0

*[1] Data from ref [18]
*[2] This study (MO/DFT-BP86)

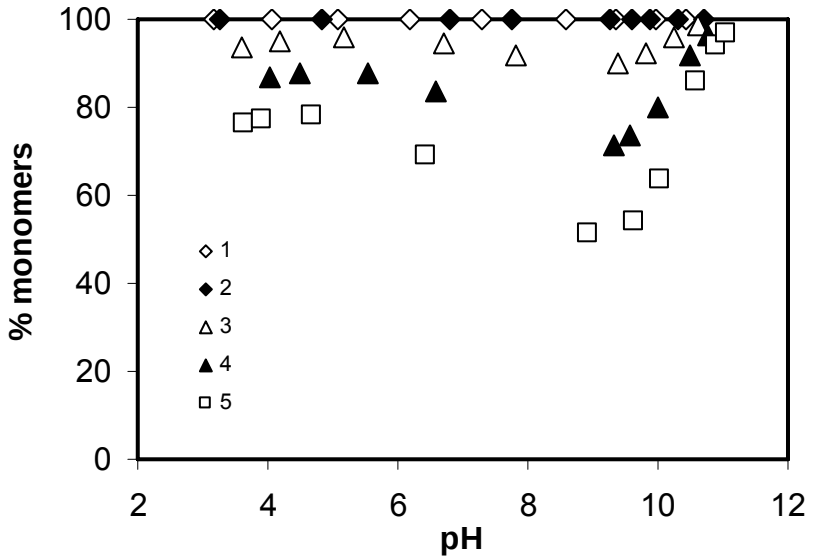

Fig. 6. The surface speciation as a function of pH and loading, expressed as the relative amount of Si present at the surface as monomers ($\equiv(FeO)_2Si(OH)_2$) for the five systems studied. Monomers are fully dominant in the systems 1 and 2. Formation of Si polymers at the surface is only found in the systems 3-5. In these systems, the equilibrium solution concentration is more than 10^{-4} M (see Fig.3b), a concentration at which supersaturation with respect to quartz exists.

Application

The charge distribution coefficients have been used as fixed parameters in fitting our adsorption data, omitting formation of oligomeric species. The adsorption cannot be described very well (R^2 = 0.95), in particular at the highest loading around pH = 8. Analysis of the adsorption behavior of the combination of a monodentate and a bidentate complex shows that the monodentate is particularly active at low pH. This is due to the difference in the CD value. As shown by Stachowicz et al. [69] for $As(OH)_3$, a species that attributes the largest amount of charge to the surface plane will have the largest interaction with the adsorbed protons in the surface plane, which will result in a larger proton co-desorption (largest value of p, eq.(3)).

Formation of such (bidentate) species is most suppressed at low pH. For this reason, a monodentate species will adsorb relatively stronger at low pH compared to the bidentate species. However, this is not the pH range where the highest adsorption is found.

Surface speciation

With the parameters derived (Table 3), we may calculate the magnitude of the contribution of the polymer species in our experiments. This is given in Fig.6. Comparison of the results of the calculation with the systems conditions show that polymers only contribute noticeably to the Si adsorption if the solution concentration is above about 10^{-4} M. At these solution conditions, super saturation with respect to quartz exists.

Conclusions

- Adsorption of Si on goethite can be successfully described with the CD model incorporating available structural information. The charge distribution values can be calculated with the Brown bond valence approach using the MO/DFT optimized geometries of surface complexes in combination with a correction for change in dipole ordination.
- CD modeling reveals that the main Si surface species is a bidentate complex at low loading ($\equiv(FeO)_2Si(OH)_2$). At high loading, a polymer is formed which might be a tetramer. This surface species only contributes to the Si adsorption in systems with a solution concentration above approximately the equilibrium concentration with quartz. A high Si loading on goethite due to the formation of a monodentate surface complex ($\equiv FeOSi(OH)_3$) is unlikely.
- The adsorbed Si polymer is rather easily hydrolyzed. The reactive ≡SiOH ligand of the polymer is quite acid compared to monomeric silicic acid. The proton affinity constant ($\log K_H \approx 6.5$-7.1) obtained for the $\equiv SiO^{-1}$ ligand of the adsorbed polymer is typical of polymerized silica as found for amorphous $SiO_2(s)$ and aqueous $Si_2O_2(OH)_5^{1-}(aq)$.
- The change in charge due to co-desorption of protons upon Si adsorption and the change of the IEP are predicted correctly with the CD-MUSIC distribution model
- The pH dependency of the adsorption of $\equiv(FeO)_2Si(OH)_2$ is related to the amount of charge added to the surface plane, which depends on the details of the structure of the surface complex, as resolved with MO/DFT calculations.

Acknowledgements

The authors want to thank Ivonne van Pelt for doing the Si adsorption experiments. The support of the Department of Civil Engineering at Auburn University and the Wageningen Institute for Environment and Climate Research (WIMEK) for a sabbatical that allowed Mark Barnett to participate in this research is gratefully acknowledged. Part of the work was also funded by the TRIAS project 835.80.006 / Delft Cluster 5.17 and FUNMIG project 516514, F16W-2004.

References

1. W. L. Lindsay, Chemical Equilibria in soils. Wiley-Interscience: New York, 1979
2. F. J. Hingston, A. M. Posner, J. P. Quirk, J. Soil Sci. 23 (1972) 177.
3. H. C. B. Hansen, T. P. Wetche, K. Raulundrasmussen, O. K. Borggaard, Clay Minerals 29 (1994) 341.
4. S. Glasauer, J. Friedl, U. Schwertmann, Journal of Colloid and Interface Science 216 (1999) 106.
5. J. P. Swedlund, J. G. Webster, Geochim. Cosmochim. Acta 33 (1999) 3413.
6. F. J. Doucet, C. Schneider, S. J. Bones, A. Kretchmer, I. Moss, P. Tekely, C. Exley, Geochimica Et Cosmochimica Acta 65 (2001) 2461.
7. J. P. Gustafsson, European Journal of Soil Science 52 (2001) 639.
8. C. C. Davis, H.-W. Chen, M. Edwards, Environ. Sci. Technol. 36 (2002) 582.
9. T. P. Luxton, C. J. Tadanier, M. J. Eick, Soil Sci. Soc. Am. J. 70 (2006) 204.
10. G. S. Pokrovski, J. Schott, F. Farges, J.-L. Hazemann, Geochim. Cosmochim. Acta 67 (2003) 3559.
11. R. P. J. J. Rietra, T. Hiemstra, W. H. Van Riemsdijk, Geochim. Cosmochim. Acta 63 (1999a) 3009.
12. L. Pauling, J. Am. Chem. Soc. 51 (1929) 1010.
13. T. Hiemstra, W. H. Van Riemsdijk, J. Colloid Interf. Sci. 179 (1996a) 488.
14. T. Hiemstra, W. H. Van Riemsdijk, in: Encyclopaedia of Surface and Colloid Science, 1 ed. Marcel Dekker, Inc.: New York, USA, 2002; pp 3773.
15. I. D. Brown, Acta Cryst. B33 (1977) 1305.
16. I. D. Brown, Chem. Soc. Rev. 7 (1978) 359.
17. I. D. Brown, The chemical bond in inorganic chemistry : the bond valence model. Oxford University Press: 2002 12.
18. T. Hiemstra, W. H. Van Riemsdijk, J. Colloid Interf. Sci. 301 (2006) 1.
19. T. Hiemstra, W. H. Van Riemsdijk, J. Colloid Interf. Sci. 210 (1999a) 182.
20. T. Hiemstra, W. H. Van Riemsdijk, G. H. Bolt, J. Colloid Interf. Sci. 133 (1989a) 91.
21. T. Hiemstra, P. Venema, W. H. Van Riemsdijk, J. Colloid Interf. Sci. 184 (1996b) 680.
22. L. W. Cary, B. H. W. S. de Jong, W. E. J. Dibble, Geochim. Cosmochim. Acta 46 (1982) 1317.
23. I. L. Svensson, S. Sjoberg, L.-O. Ohman, J. Chem. Soc. Faraday Trans. I 82 (1986) 3635.
24. A. Felmy, H. Cho, J. R. Rustad, M. J. Mason, J. Solution Chem. 30 (2001) 509.
25. J. R. Rustad, A. R. Felmy, B. P. Hay, Geochim. Cosmochim. Acta 60 (1996b) 1563.
26. P. G. Weidler, S. J. Hug, T. P. Wetche, T. Hiemstra, Geochim. Cosmochim. Acta 62 (1999) 3407.
27. F. Gaboriaud, J. Ehrhardt, Geochimica Et Cosmochimica Acta 67 (2003) 967.
28. O. Stern, Z. Electrochem. 30 (1924) 508.
29. R. Rahnemaie, T. Hiemstra, W. H. Van Riemsdijk, J. Colloid Interf. Sci. 293 (2006) 312.
30. R. M. Pashley, J. N. Israelachvili, J. Colloid Interf. Sci. 101 (1984) 511.
31. J. N. Israelachvili, H. Wennerstrom, Nature 379 (1996) 219.
32. M. F. Toney, J. N. Howard, J. Richer, G. L. Borges, J. G. Gordon, O. R. Melroy, D. G. Wiesler, D. Yee, L. B. Sorensen, Surf. Sci. 335 (1995) 326.
33. P. Fenter, N. C. Sturchio, Progress Surf. Sci. 77 (2004) 171.

34. J. G. Catalano, C. Park, Z. Zhang, P. Fenter, Langmuir 22 (2006) 4668.
35. M. S. Yeganeh, S. M. Dougal, H. S. Pink, Phys. Rev. Letters 83 (1999) 1179.
36. S. Kataoka, M. C. Gurau, F. Albertorio, M. A. Holden, S. M. Lim, R. D. Yang, P. S. Cremer, Langmuir 20 (2004) 1662.
37. V. Ostroverkhov, G. A. Waychunas, Y. R. Shen, Physical Review Letters 94 (2005).
38. Y. R. Shen, V. Ostroverkhov, Chemical Reviews 106 (2006) 1140.
39. J. Westall, H. Hohl, Adv. Colloid Interf. Sci. 12 (1980) 265.
40. Rahnemaie R., Hiemstra T., and Van Riemsdijk W. H. 23 (2007) 3680.
41. Z. Zhang, P. Fenter, L. Cheng, N. C. Sturchio, M. J. Bedzyk, M. Predota, A. Bandura, J. D. Kubicki, S. N. Lvov, P. T. Cummings, A. A. Chialvo, M. K. Ridley, P. Benezeth, L. Anovitz, D. A. Palmer, M. Machesky, D. J. Wesolowski, Langmuir 20 (2004) 4954.
42. T. Hiemstra, J. C. M. De Wit, W. H. Van Riemsdijk, J. Colloid Interf. Sci. 133 (1989b) 105.
43. R. J. Atkinson, A. M. Posner, Q. J.P., J. Phys. Chem. 71 (1967) 550.
44. C. Waltham, M. J. Eick, Soil Sci. Soc. Am. J. 66 (2002) 818.
45. R. S. Beckwith, R. Reeve, Aust. J. Soil Res. 1 (1963) 157.
46. M. G. Keizer, W. H. Van Riemsdijk ECOSAT, Technical Report Department Soil Science and Plant Nutrition; Wageningen Agricultural University: Wageningen, The Netherlands, 1998.
47. D. G. Kinniburgh Fit, Technical Report WD/93/23; British Geological Survey: Keyworth, Great Britain, 1993.
48. Anonymous Spartan '04 Wavefunction Inc.; Irvine CA USA, 2004.
49. J. Kong, C. A. White, A. I. Krylov, C. D. Sherrill, R. D. Adamson, T. R. Furlani, M. S. Lee, A. M. Lee, S. R. Gwaltney, T. R. Adams, C. Ochsenfeld, A. T. B. Gilbert, G. S. Kedziora, V. A. Rassolov, D. R. Maurice, N. Nair, Y. Shao, N. A. Besley, P. E. Maslen, J. P. Dombroski, H. Daschel, W. Zhang, P. P. Korambath, J. Baker, E. F. C. Byrd, T. Van Voorhis, M. Oumi, S. Hirata, C.-P. Hsu, N. Ishikawa, J. Florian, A. Warshel, B. G. Johnson, P. M. W. Gill, M. Head-Gordon, J. A. Pople, J. Computational Chem. 21 (2000) 1532.
50. I. D. Brown, D. Altermatt, Acta Cryst. B41 (1985) 244.
51. M. J. Perona, J. O. Leckie, J. Colloid Interf. Sci. 106 (1985) 65.
52. R. P. J. J. Rietra, T. Hiemstra, W. H. Van Riemsdijk, J. Colloid Interf. Sci. 229 (2000a) 199.
53. S. Garman, M. J. Eick, T. P. Luxton, J. Environ. Quality 33 (2004) 1703.
54. J. W. Bowden. Models for Ion Adsorption on Mineral Surfaces. PhD, University of West Australia, 1973.
55. C. F. J. Baes, R. E. Mesmer, The Hydrolysis of Cations. Robert E. Krieger Publishing Company: Florida, 1976
56. J. A. Tossell, Geochimica Et Cosmochimica Acta 69 (2005) 283.
57. E. Doelsch, W. E. E. Stone, S. Petit, A. Masion, J. Rose, J. Bottero, D. Nahon, Langmuir 17 (2001) 1399.
58. J. Rose, A. Flank, A. Masion, J. Bottero, P. Elmerich, Langmuir 13 (1997) 1827.
59. G. A. Waychunas, B. A. Rea, C. C. Fuller, J. A. Davids, Geochim. Cosmochim. Acta 57 (1993) 2251.
60. D. M. Sherman, S. R. Randall, Geochim. Cosmochim. Acta 67 (2003) 4223.
61. K. F. Hayes, A. L. Roe, G. E. Brown, Jr., K. Hodgson, J. O. Leckie, G. A. Parks, Science 238 (1987a) 783.

62. G. A. Icopini, S. L. Brantley, P. J. Heaney, Geochim. Cosmochim. Acta 69 (2005) 293.
63. P. W. Schindler, H. R. Kamber, Helv. Chim. Acta 15 (1968) 1781.
64. M. L. Hair, W. Hertl, J. Phys. Chem. 74 (1970) 91.
65. K. Marshall, G. L. Ridgewell, C. H. Rochester, J. Simpson, Chemistry and Industry 19 (1974) 775.
66. J. Sonnefeld, Colloid Polym. Science 275 (1995) 932.
67. N. Sahai, D. A. Sverjensky, Geochim. Cosmochim. Acta 61 (1997) 2801.
68. D. A. Sverjensky, Geochim. Cosmochim. Acta 69 (2005) 225.
69. M. Stachowicz, T. Hiemstra, W. H. Van Riemsdijk, J. Colloid Interf. Sci. 302 (2006) 62.
70. G. Ona-Nguema, G. Morin, F. Juillot, G. Calas, G. E. Brown, Jr., Environ. Sci. Technol. 39 (2005) 9147.

Chapter 7

Adsorption and Surface Oxidation of Fe(II) on Metal (hydr)oxides

Tjisse Hiemstra and Willem H. van Riemsdijk

Published in Geochimica et Cosmochimica Acta
Volume 71, Issue 24, Pages 5913-5933, December 15, 2007

Abstract

The Fe(II) adsorption by non-ferric and ferric (hydr)oxides has been analyzed with surface complexation modeling. The CD model has been used to derive the interfacial distribution of charge. The fitted CD coefficients have been linked to the mechanism of adsorption. The Fe(II) adsorption is discussed for TiO_2, γ-AlOOH (boehmite), γ-FeOOH (lepidocrocite), α-FeOOH (goethite) and HFO in relation to the surface structure and surface sites. One type of surface complex is formed at TiO_2 and γ-AlOOH, i.e. a surface coordinated Fe^{2+} ion. At the TiO_2 (Degussa) surface, the Fe^{2+} ion is probably bound as a quarto-dentate surface complex. The CD value of Fe^{2+} adsorbed to γ-AlOOH points to the formation of a tridentate complex, which might be a double edge surface complex. The adsorption of Fe(II) to ferric (hydr)oxides differs. The charge distribution points to the transfer of electron charge from the adsorbed Fe(II) to the solid and the subsequent hydrolysis of the ligands that coordinate to the adsorbed ion, formerly present as Fe(II). Analysis shows that the hydrolysis corresponds to the hydrolysis of adsorbed Al(III) for γ-FeOOH and α-FeOOH. In both cases, an adsorbed $M(III)(OH)_2^+$ is found in agreement with structural considerations. For lepidocrocite, the experimental data point to a process with a complete surface oxidation while for goethite and also HFO, the data can be explained assuming a combination of Fe(II) adsorption with and without electron transfer. Surface oxidation (electron transfer), leading to adsorbed ≡ $Fe(III)(OH)_2$, is favored at high pH (pH>~7.5) promoting the deprotonation of two Fe_{III}-OH_2 ligands. For goethite, the interaction of Fe(II) with As(III) and *vice versa* has been modeled too. To explain Fe(II)-As(III) dual-sorbate systems, formation of a ternary type of surface complex is included, which is supposed to be a monodentate As(III) surface complex that interacts with an Fe(II) ion, resulting in a binuclear bidentate As(III) surface complex.

1 Introduction

Iron is an element that is dynamically present on the boundary between the oxidized and reduced world. Only a tiny shell of the geosphere is oxidized due to photosynthesis. On the long-term geo-historic record, it is a relatively recent phenomenon. Reduced conditions are maintained in waterlogged soils and sediments due to back-consumption of oxygen and organic carbon by chemotrophic microorganisms. The rate of Fe(II) production by micro-organisms depends on the surface area of the ferric (hydr)oxide that is in contact with micro-organisms (BONNEVILLE et al., 2006). Under intermediate redox conditions ($10<pe<0$) and neutral pH values, iron can be present as aqueous Fe(II) in combination with Fe(III) (hydr)oxides. Under these conditions, dissolved Fe(II) may interact with these ferric oxides and also with other minerals as well as organic matter.

Adsorbed Fe(II) is known to be very reactive (STUMM and SULZBERGER, 1992), acting as a catalyst for the reduction of elements like Hg(II), As(V) (CHARLET et al., 2002), U(VI) (LIGER et al., 1999) or Cu(II) (MAITHREEPALA and DOONG, 2004) and for the transformation or natural attenuation of organic components (AMONETTE et al., 2000; KLAUSEN et al., 1995; LIGER et al., 1999; PECHER et al., 2002; STRATHMANN and STONE, 2003) (VIKESLAND and VALENTINE, 2002a) (KLUPINSKI et al., 2004; MAITHREEPALA and DOONG, 2004; VIKESLAND and VALENTINE, 2002b). In addition, adsorbed Fe(II) may strongly affect the Fe(III) dissolution rate of iron oxide minerals in the presence of organic anions (STUMM and SULZBERGER, 1992) (BALLESTEROS et al., 1998), may catalyze the transformation of Fe(III) minerals (ZHANG et al., 1992) (HANSEL et al., 2005; PEDERSEN et al., 2005).

Until recently, the interaction of Fe(II) with metal (hydr)oxides has only been studied sparingly under well-defined conditions. An important reason is the experimental challenge that is related to the work under reduced conditions, i.e. the oxidation rate of Fe(II) is very high in the experimental pH range of adsorption (EMMENEGGER et al., 1998; TAMURA et al., 1976) (KING, 1998). Traces of oxygen will immediately lead to transformation of Fe(II) into Fe(III).

Unfortunately, a number of Fe (II) adsorption data have been collected in systems that are difficult to interpret unequivocally. Sometimes, the data refer to multi-component systems in which sulphate is present due to the addition of Fe(II) as $Fe(II)SO_4$ (APPELO et al., 2002; CHARLET et al., 2002; LIGER et al., 1999), or the systems contain simultaneously Ca^{2+} (ZACHARA et al., 2000) or bicarbonate (CHOI et al., 2001). These ions may interfere. In other cases, thermodynamically instable combinations have been chosen, like Fe(II) in $NaClO_4$ (ZACHARA et al., 2000) (VIKESLAND and VALENTINE, 2002a) or in $NaNO_3$ (APPELO et al., 2002; JEON et al., 2003; LIGER et al., 1999). From this perspective, it may be better to rely on Fe(II) data measured in NaCl solutions, which has been used most extensively.

One of the most early adsorption data sets of Fe(II) is of Zhang et al. (ZHANG et al., 1992) who measured the Fe(II) adsorption on lepidocrocite (γ-FeOOH) in 0.6 M NaCl. Recently, Nano and Strathmann (NANO and STRATHMANN, 2006) have measured the Fe(II) binding to TiO_2 and boehmite (γ-AlOOH) in NaCl, and Dixit and Hering (DIXIT and HERING, 2006) measured it recently for goethite (α-FeOOH). As will be discussed in this paper, interpretation of these data suggests that the Fe(II) adsorption behavior does not only depend

on the types of surface sites that are involved in the binding, but that the Fe(II) binding may also depend on the presence of Fe(III) as component of the mineral structure. It has been suggested that in such a case an electron transfer between adsorbed Fe(II) and the mineral surface may occur (LARESE-CASANOVA and SCHERER, 2007; SILVESTER et al., 2005; WILLIAMS and SCHERER, 2004). Electron transfer will lead to changes in the interfacial charge distribution, which may be detected by analyzing the Fe(II) adsorption phenomena with the charge distribution (CD) model (HIEMSTRA and VAN RIEMSDIJK, 1996a).

The CD model is a surface complexation model, in which the charge of a surface complex is not considered as single unit, but is assumed to be spatially distributed in the compact part of the interface. In the present study, we will apply the CD model to analyze the Fe(II) adsorption behavior and determine to what extent the resulting charge distribution can be related to surface oxidation of adsorbed Fe(II), or not. First, the adsorption of Fe(II) on non-ferric metal (hydr)oxides will be analyzed, i.e. TiO_2 and γ-AlOOH (boehmite). It will be compared with the situation for iron (hydr)oxides, in particular goethite, lepidocrocite, and HFO. Before doing this, we will briefly discuss in the next section the factors that determine the interfacial charge distribution and we will introduce a recently suggested double layer picture (HIEMSTRA and VAN RIEMSDIJK, 2006) that has been used in the present data analysis.

2 Theory

2.1 Interfacial Charge Distribution

In a double layer, the concept of point charges becomes problematic near the surface. Close to the surface, structural double layer details are needed. More than 80 years ago, Stern (STERN, 1924) introduced the concept of charge separation between surface and counter ions to account for the minimum distance of approach of counter- and co-ions. Grahame (GRAHAME, 1947) extended the model, introducing electrolyte outer sphere complexation at the head end of the diffuse double layer, which was applied for the first time to metal oxide surfaces by Yates et al. (YATES et al., 1974) and Davis et al. (DAVIS et al., 1978a). In the first generation of surface complexation models, the charge of an innersphere surface complex has been condensed to a single unit that is located in the double layer profile. The location of ion charge in the electrostatic double layer is crucial in the modeling of the adsorption behavior of a component. This is due to the very large changes in the electrostatic potential in the inner compact part of the double layer (HIEMSTRA and VAN RIEMSDIJK, 2006). An innersphere complex experiences a gradient of electrostatic potentials. The corresponding electrostatic energy contribution cannot be calculated accurately with the simplified assumption of the presence of ion charge on one single electrostatic position in the interface. In the charge distribution model, one part of the charge of the innersphere complex is attributed to the surface. The remaining part is located at some distance from the surface.

A number of factors will determine the value of the interfacial charge distribution. First of all, the charge distribution will depend on the number of ligands that coordinate with the surface relative to the number of non-coordinating ligands. This has been demonstrated for a series of divalent oxyanions, comprising SO_4^{2-} & SeO_4^{2-}, MoO_4^{2-} & CrO_4^{2-}, and SeO_3^{2-} &

CO_3^{-2} (HIEMSTRA et al., 2004; RIETRA et al., 1999a). A refinement is necessary for ions that have a strongly asymmetrical coordination sphere. In that case, bond strength becomes an important parameter too. The bond strength is related to the relative bond length between the central ion of a complex and the coordinating ligands (BROWN, 2002; BROWN and ALTERMATT, 1985). In principle, the variation in bond length is experimentally accessible and can also be found with molecular orbital (MO) calculations (HIEMSTRA and VAN RIEMSDIJK, 2006), (STACHOWICZ et al., 2006), (HIEMSTRA et al., 2007), (RAHNEMAIE et al., 2007). The variation in bond strength, due to differences in the geometry of metal surface complexes, can rationalize the differences in the CD values found for a series of divalent metal cations like Hg(II), Pb(II), Cu(II), and Cd(II) (HIEMSTRA and VAN RIEMSDIJK, 2002). Recently, a third point has come into focus. It has been suggested that the overall CD value is also affected by changes in the orientation of the water dipoles in the compact part of the double layer due the introduction of surface charge (HIEMSTRA and VAN RIEMSDIJK, 2006). The dipole orientation of water can partly reduce the electrostatic effect of the interfacial accumulation of charge. The dipole contribution is generally relatively small (~ <0.15 valence units) but nevertheless often significant as has been shown for the adsorption of for instance uncharged $As(OH)_3$ (STACHOWICZ et al., 2006) and H_4SiO_4 (HIEMSTRA et al., 2007).

Finally, a new aspect is the possible change of the charge distribution in a surface complex due to electron transfer. If an adsorbed Fe(II) will release an electron that is taken up by an ion in the solid, the redistributed charge is a combination of the location of the electron in the surface and the adsorption of iron as Fe(III). Since Fe(III) is known for its strong hydrolysis, the electron transfer will also lead to release of protons from the water ligands that are bound to the adsorbed ion, formerly present as Fe(II).

2.2 Extended Stern layer model

Recently, the interfacial double layer model has been refined (HIEMSTRA and VAN RIEMSDIJK, 2006) based on the analysis of titration data. The data were collected for goethite in a variety of electrolyte solutions containing Li^+, Na^+, K^+, Cs^+, -chloride or -nitrate (RAHNEMAIE et al., 2006). The experimental curves were internally consistent because of the use of a common stock suspension. The data analysis indicated that the head end of the diffuse double layer (DDL) was separated from the minimum distance of approach of electrolyte ions (ions pairs) by a second Stern layer (HIEMSTRA and VAN RIEMSDIJK, 2006). The double layer picture can be classified as an Extended Stern (ES) layer model (WESTALL and HOHL, 1980). As discussed in Hiemstra and Van Riemsdijk (HIEMSTRA and VAN RIEMSDIJK, 2006), the double layer structure that emerges can be explained by the alignment of water molecules near the surface in several layers, in which the electrolyte ions can only change stepwise their position. This picture stems from recent experimental information obtained by different valuable approaches like force measurements (ISRAELACHVILI and WENNERSTROM, 1996; PASHLEY and ISRAELACHVILI, 1984), X-ray reflectivity (CATALANO et al., 2006; FENTER and STURCHIO, 2004; TONEY et al., 1995) and Sum Frequency Spectroscopy (KATAOKA et al., 2004; OSTROVERKHOV et al., 2005; SHEN and OSTROVERKHOV, 2006; YEGANEH et al., 1999). These measurements show increase in the

ordering of water within a distance of about 0.7-0.9 nm, which is equivalent to about 2-3 layers of water molecules (HIEMSTRA and VAN RIEMSDIJK, 2006).

Sum Frequency Spectroscopy for silica, quartz, Al_2O_3(s), and TiO_2(s) (SHEN and OSTROVERKHOV, 2006) shows that the number and orientation of polar water molecules changes with the interface charge (OSTROVERKHOV et al., 2005; YEGANEH et al., 1999). In case of the introduction of charge at the surface due to ion adsorption, water dipoles will orient in the electrostatic field. It results in a redistribution of charge in the compact part of the double layer, diminishing the induced field. As mentioned above, it has been shown that this dipole effect is implicitly part of the CD model (HIEMSTRA and VAN RIEMSDIJK, 2006). The dipole effect has been quantified for use in the CD model and the dipole correction can be combined with the ionic charge distribution. This will be illustrated later in the text.

2.3 Calculations

The modeling and objective optimization of the adsorption parameters has been done using the ECOSAT 4.8 program (KEIZER and VAN RIEMSDIJK, 1998) in combination with a recent version (2.581) of the program FIT of Kinniburgh (KINNIBURGH, 1993).

3 Results and Discussion

In the following sections, we will discuss the adsorption of Fe(II) for a series of materials. We will compare the adsorption of Fe(II) on ferric and non-ferric (hydr)oxides. For each mineral, first the structure of the surface will be analyzed, including a brief discussion on the development of the primary charge. Next, we will discuss the possible geometry of the Fe(II) surface complex based on EXAFS information measured for the adsorption of other metal ions as far as available. The interfacial CD will be derived by modeling the Fe(II) adsorption and a mechanistic interpretation of the CD will be given. In the approach, the extended Stern layer model has been simplified by using equal values for the inner and outer Stern layer capacitance. This simplification has also been proposed by Sverjensky (SVERJENSKY, 2005).

3.1 TiO_2

3.1.1 Surface structure

In the mineral structure of TiO_2, e.g. rutile and anatase, all oxygen ions are triply coordinated. At the surface, one or two Ti ions are lacking leading to the formation of respectively doubly (≡ $Ti_2O^{-2/3}$) and singly (≡ $TiOH^{-1/3}$) coordinated surface groups. The charge attribution to these surface groups can be done using the bond valence concept of Pauling (PAULING, 1929). The Ti^{4+} ion is hexa-coordinated and neutralizes on average +2/3 valence units (v.u.) per bond. In the interior, three bonds with +2/3 v.u. are required to

neutralize the negative oxygen charge (z = -2 v.u) leading to $\equiv Ti_3O^0$. A lower coordination of the oxygens at the surface will result in negative charge on these oxygens, which can be compensated by the adsorption of one or two additional protons per oxygen (HIEMSTRA et al., 1989a) (HIEMSTRA et al., 1996b). This leads to the definition of two proton adsorption reactions that can describe the surface charging behavior (BOURIKAS et al., 2001; FITTS et al., 2005; HIEMSTRA et al., 1989b; JING et al., 2005; MACHESKY et al., 1998; REGAZZONI et al., 1998; RIDLEY et al., 2004; RODRIGUEZ et al., 1996):

$$\equiv TiOH^{-1/3} + H^+(aq) \Leftrightarrow \equiv TiOH_2^{+2/3} \quad (1)$$

and

$$\equiv Ti_2O^{-2/3} + H^+(aq) \Leftrightarrow \equiv Ti_2OH^{+1/3} \quad (2)$$

The proton affinity ($\log K_H$) of both types of surface groups can be estimated by calculating the potential degree of saturation of the oxygens charge by applying the Brown bond valence concept (BROWN, 2002) in which the bond valence is linked to the Ti-O bond length. The estimated affinity constants explain the experimental PZC (HIEMSTRA et al., 1996b; MACHESKY et al., 2001) and also explain semi-quantitatively the in-situ IR absorption behavior observed by Conner et al. (CONNOR et al., 1999a) as discussed in reference (HIEMSTRA and VAN RIEMSDIJK, 2002).

3.1.2 Surface charge

The charging behavior of rutile and anatase has been evaluated by Bourikas et al. (BOURIKAS et al., 2001), resulting in a set of recommended ion pair formation constants (Table 1).

Table 1 The location of ion charge (Extended Stern layer model) and affinity constants used to describe the experimental charging behavior of TiO_2 (Degussa) and the adsorption of Fe(II) with the CD model. The capacitance of the inner Stern layer is set equal to the value of the outer layer $C_1 \equiv C_2$. For TiO_2 (Degussa), a value of 0.9 F/m^2 (BOURIKAS et al., 2001) has been used.

Surface group*[1]	Δz_0	Δz_1	Δz_2	$\log K_H$
$\equiv TiOH^{-1/3}$	0	0	0	0
$\equiv TiOH_2^{+2/3}$	1	0	0	6.3 *[2]
$\equiv TiOH^{-1/3}$-Na^+	0	1	0	-0.6*[3]
$\equiv TiOH_2^{+2/3}$-Cl^-	1	-1	0	6.3-1.2 = 5.1*[3]
$\equiv Ti_2O^{-2/3}$	0	0	0	0
$\equiv Ti_2OH^{+1/3}$	1	0	0	6.3*[2]
$\equiv Ti_2O^{-2/3}$-Na^+	0	1	0	-0.6*[3]
$\equiv Ti_2OH^{+1/3}$-Cl^-	1	-1	0	6.3-1.2 = 5.1*[3]
$\equiv(TiO)_2(TiOH)_2$-Fe(II)	1.43 ± 0.03	0.57 ± 0.03	0	3.39*[4] ± 0.03

*[1] Sites density is set at 6 nm^{-2} for each group (BOURIKAS et al., 2001) and (HIEMSTRA et al., 1996b)
*[2] Based on the PZC of TiO_2 of Degussa,
*[3] from (BOURIKAS et al., 2001),
*[4] fitted, this study.

For reasons of simplicity, the proton affinity constants ($\log K_H$) of the above protonation reactions were set equal to the value of the PZC in the approach. Bourikas et al. (BOURIKAS et al., 2001) reported that TiO_2 materials can be divided into two groups, i.e. those with a low Stern layer capacitance ($C \approx 0.9$ F/m^2), and those that have a higher capacitance ($C \approx 1.6$ F/m^2). The difference was attributed to the presence of a difference in hydration. However recently, it has been shown by spectroscopy that at the 110 face of rutile (ZHANG et al., 2004), cations may coordinate to surface groups forming quadro-dentate complexes. This is not only observed for a variety of divalent and trivalent ions, but it was also found for Rb^+ at very high pH and concentration. Additional innersphere complexation of such cations will strongly increase the proton desorption, which will apparently lead to a higher value for the Stern layer capacitance if formation of such complexes is not taken into account. It can be shown that if formation of innersphere complexes for simple monovalent electrolyte ions is allowed in the analysis of the charging behavior, the capacitance value decreases to values that can be considered as more representative for the capacitance of the inner layer Stern layer, found for many well-crystallized minerals like goethite, gibbsite, etcetera.

3.1.3 Fe(II) binding to TiO_2

The adsorption of Fe(II) by TiO_2 (Degussa P25) has been studied by Nano and Strathmann (NANO and STRATHMANN, 2006). The adsorption data are shown in Fig. 1 as a function of pH, electrolyte level, and mineral loading of the system. The data have been modeled using the parameter set given in Table 1. In a first approach, we assumed the formation of a bidentate complex for adsorbed Fe^{2+}. This model approach leads to a fitted CD with a very high charge attribution to the surface plane (Δz_0 ~1.4 v.u.). The fitted charge distribution cannot be understood by the combination of the formation of a bidentate complex and a Pauling distribution of charge of Fe^{2+} over the coordinating ligands. If Fe^{2+} is hexa-coordinated, a charge of only 0.33 v.u. is attributed per bond. In case of a bidentate complex, the expected ionic surface charge attribution is only 0.67 v.u. This number strongly differs from the above fitted result (Δz_0 ~1.4 v.u.).

As mentioned in 3.1.2, it has been shown recently (ZHANG et al., 2004) that a number of mono-, di- and trivalent metal ions may form quadro-dentate complexes at the 110 face of rutile (Fig.2). If this molecular picture is valid for Fe(II) bound by TiO_2 (Degussa), we may write:

$$2 \equiv Ti_2O^{-2/3} + 2 \equiv TiOH^{-1/3} + Fe^{2+}(aq) \Leftrightarrow \equiv (Ti_2O)_2(TiOH)_2^{-2+\Delta z_0} - Fe(II) -^{\Delta z_1} \qquad (3)$$

with $\Delta z_0 + \Delta z_1 = +2$ v.u. Application of this reaction in the modeling, results in a fitted interfacial CD value of $\Delta z_0 = 1.42 \pm 0.03$ v.u. and $\Delta z_1 = 0.58 \pm 0.03$ v.u. (Table 1). The calculated model lines are given in Fig.1.

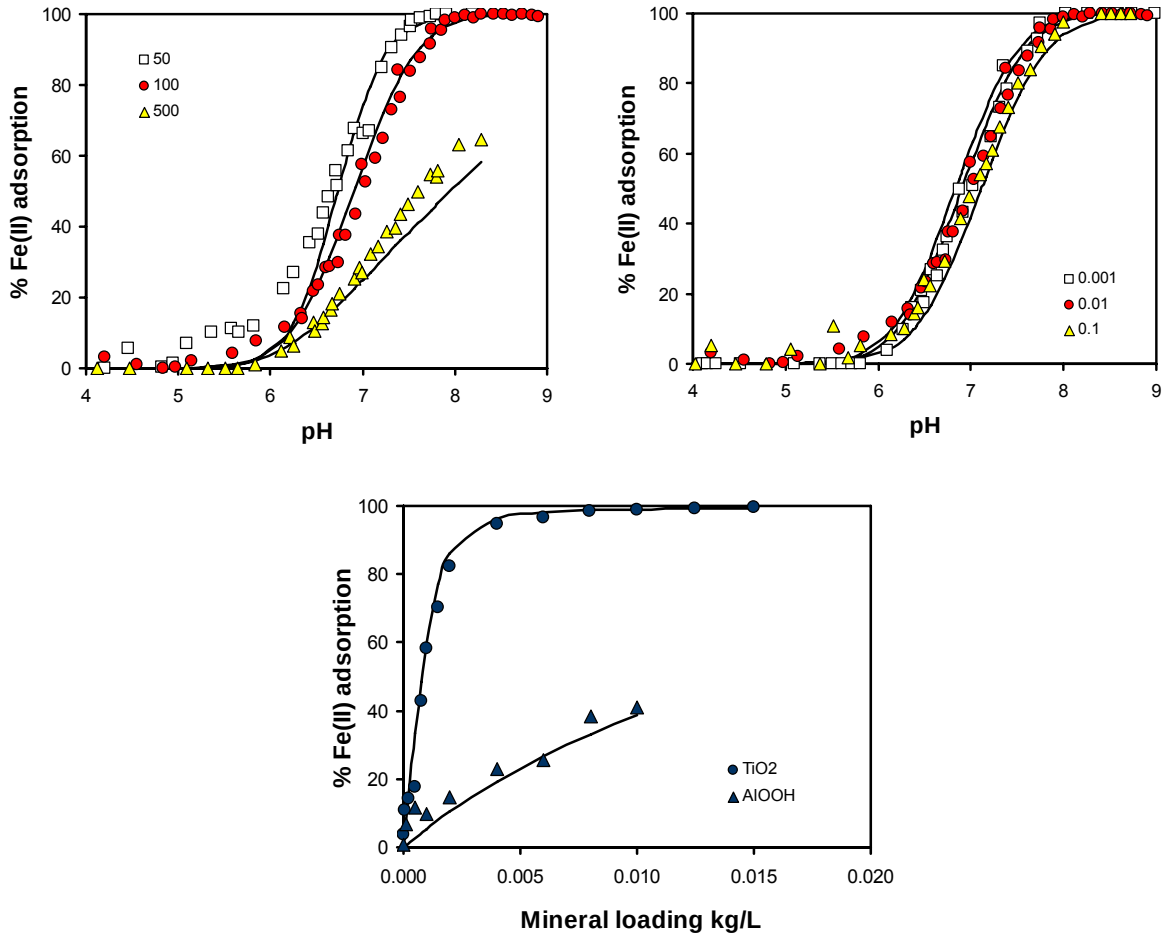

Fig.1a) The adsorption of Fe(II) on TiO_2-Degussa (2 g/L, 50 m^2/g) as a function of pH at three Fe(II) loadings (µmol/L) in 0.01 M NaCl.
Fig.1 b) The adsorption of Fe(II) (C-ini = 0.1 mM) on TiO_2-Degussa (2 g/L, 50 m^2/g) in NaCl as a function of the ionic strength.
Fig.1 c) The adsorption of Fe(II) (C-ini = 0.1 mM) on TiO_2-Degussa (50 m^2/g) and γ-AlOOH (85.8 m^2/g) at pH 7.5, I = 0.01 M NaCl as a function of mineral loading of the system.
All data points are of Nano and Strathmann (NANO and STRATHMANN, 2006). The lines have been calculated with the CD model using the parameter set of Table 1.

The fitted CD is now much more in agreement with a structural interpretation (Fig.2). In case of a coordination of Fe(II) with four surface groups, assuming hexa-coordination, 4/6 of the ion charge (n_0 = 1.33 v.u.) will contribute to the neutralization of the common ligands in the surface. The remaining part of the ion charge (n_1 = 0.67 v.u.), associated with the free ligands, is attributed to the first Stern plane.

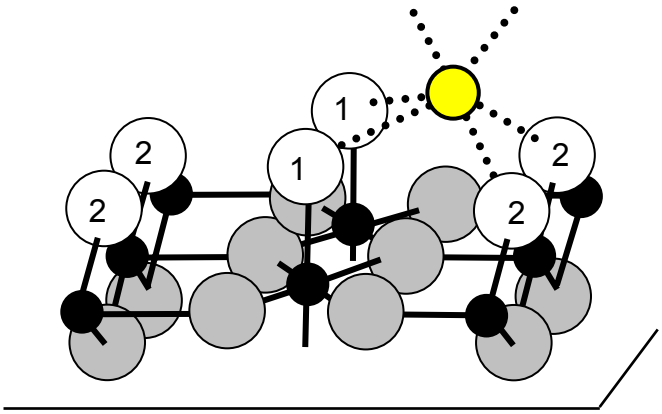

Fig.2. The structure of the 110 face of rutile with in its interior oxygens (dark gray spheres) that are triply coordinated by Ti ions (small black spheres). At the surface, doubly and singly coordinated surface groups are present in rows (white spheres). A metal ion (light small sphere) may coordinate to two ≡ $Ti_2O^{-2/3}$ and two ≡ $TiOH^{-1/3}$ surface groups, resulting in a quadro-dentate complex.

As mentioned above, it has been proposed that the introduction of ion charge in the surface will result in a small redistribution due to dipole orientation of water molecules in the compact part of the double layer. It has been found that the dipole orientation will redistribute a charge ϕ of about 0.17 v.u. per unit of charge created in the surface plane. Formally, the correction term ($\phi\Lambda_0$) can be defined generally as (HIEMSTRA and VAN RIEMSDIJK, 2006):

$$\phi\Lambda_0 = \phi(n_0 + n_{H0} + \Sigma n_{ref} z_{ref}) \qquad (4)$$

in which Λ_0 is the ionic charge introduced in the surface by the adsorption of metal ions (n_0) and any additional protons (n_{H0}), relative to the reference charge ($\Sigma\ n_{ref}\ z_{ref}$) that is found by the summation (Σ) of the charge on the reference groups (z_{ref}) over the number of reference groups (n_{ref}) as formulated in the reaction. Application of the equation to the Fe(II) adsorption on TiO_2 leads to $\phi\Lambda_0 = 0.17 * (1.33 + 0 + 2*\text{-}2/3 + 2 *\text{-}1/3) = -0.11$ v.u. This correction term ($\phi\Lambda_0$) can be combined with the ionic charge distribution (n_0+n_{H0}, n_1+n_{H1}) that includes the ion charge and any additional protons, which have been formulated in the reaction. The combination results in the overall charge distribution coefficients (Δz_0, Δz_1):

$$\Delta z_0 = n_0 + n_{H0} - \phi\Lambda_0 \qquad (5)$$

and

$$\Delta z_1 = n_1 + n_{H1} + \phi \Lambda_0 \quad (6)$$

In our case, application of these equations leads to the overall charge distribution coefficients $\Delta z_0 = n_0 - \phi \Lambda_0 = +1.33 + 0.11 = +1.44$ v.u. and $\Delta z_1 = n_1 + \phi \Lambda_0 = +0.67 - 0.11 = +0.56$ v.u. This number is, surprisingly or not, equal to the fitted value (Δz_1 = 1.43 v.u., Δz_1 = 0.57 v.u.) considering the uncertainty (± 0.03 v.u.). We note that the agreement is only firm provided that the assumption of an equal distribution of the charge of adsorbed Fe(II) over its coordinating ligands is sufficiently valid. One may turn the reasoning, stating that apparently Fe(II) distributes its charge reasonably equal over the coordinating ligands.

The high charge attribution of an ion to the surface is equivalent with a strong pH dependency of the ion adsorption. A pH dependency can also be high due to hydrolysis. Hydrolysis has been found for the adsorption of Zn^{2+} to rutile (ZHANG et al., 2006). This ion is bound in a monodentate fashion. Therefore, we have modeled the Fe^{2+} adsorption, assuming monodentate surface complex formation with in addition the possibility of hydrolysis. As constraint, we assumed the same charge attribution to the 0-surface plane for the binding of Fe^{2+} and $FeOH^+$, resulting in $\Delta z_0 = 0.34 \pm 0.02$ v.u. This number fully agrees with the CD value expected for a monodentate surface complex with hexa-coordination of Fe(II) ($\Delta z_0 = 0.33$ v.u.). However, we doubt the correctness of this picture because of the low value for the proton affinity constant of the adsorbed $FeOH^+$ species ($\log K_H = 6.7$) compared to the $\log K_H$ value for the hydrolysis in solution ($\log K_H = 9.5$). In case of Zn^{2+}, the enlarged hydrolysis is due to a decrease of the coordination number upon adsorption. A lower coordination number will increase the bond valence, which results in a lower proton affinity of the ligands. This process is less likely for Fe(II).

3.2 Boehmite (γ-AlOOH)

3.2.1 Surface structure

Boehmite (γ-AlOOH) is isostructural with lepidocrocite, the Fe analogue (γ-FeOOH) to be discussed later. In boehmite, two sheets of aluminum octahedra are linked together forming a bi-layer. In the interior of this layer, the oxygens are fourfold coordinated with respect to Al and at the exterior they are twofold coordinated. In the latter case, the oxygen is additionally neutralized by a proton forming the OH ion of γ -AlOOH. In the mineral, the layers are stacked in the b-axis direction and linked by hydrogen bonding.

Recently, the formation of γ -AlOOH has been studied in detail (BOKHIMI et al., 2002). Well-crystallized boehmite, prepared with a sol gel method, forms rhombus-shaped thin flat crystallites (Fig.3). It has been shown that the particles are bounded by the planar 010 face and at the edges by the 101 face and its equivalents. The size of the particles increases on aging, but the average shape is rather constant. Based on the average crystallite dimensions, one can calculate the ratio of the faces. The calculated surface area A of the both type of faces is $A_{face010} : A_{face101} \approx 2:1$

We have analyzed the surface structure of the 010 face and the 101 faces. The 010 face is made up by surface OH groups that are doubly coordinated to Al^{3+} i.e. $\equiv Al_2OH^0$ with in the deeper fourfold-coordinated oxygen ($\equiv Al_4O^0$). With respect to the $\equiv Al_2OH^0$ surface groups, the situation on the 010 face is partly comparable with the 001 face of gibbsite (HIEMSTRA et al., 1999b). At the 101 surface of boehmite, we have singly ($\equiv AlOH^{-1/2}$ or $\equiv AlOH_2^{+1/2}$) and doubly ($\equiv Al_2OH^0$) coordinated surface groups in a 1:1 ratio with a site density of N_s = 6.8 nm^{-2} for each type of surface group.

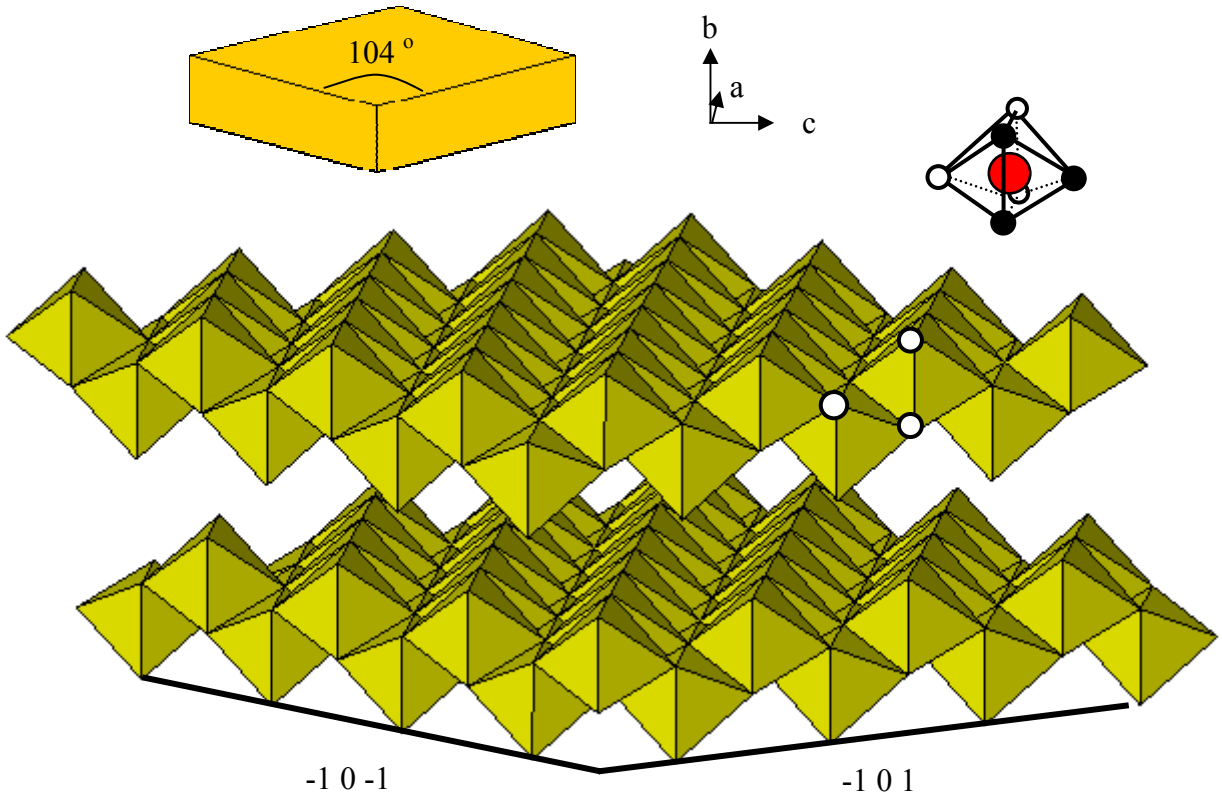

Fig.3. The idealized morphology of sol-gel prepared crystallites of boehmite forming flat thin rhombuses, with the 010 face on top and bottom and at the edges the 101 face and its equivalents. The crystal structure is made up by sheets of AlOOH octahedra. On the top and bottom of each sheet, doubly coordinated OH groups are present. In the interior, fourfold-coordinated oxygens are found. The white spheres indicate the surface ligands (one singly and two doubly coordinated surface groups) involved in ion binding, resulting in double edge sharing.

3.2.2 Surface charge

The proton speciation of the surface groups (Table 2) has been estimated on the basis of the MUSIC model approach (HIEMSTRA et al., 1996b). As mentioned previously, the chemical affinity of a surface oxygen is related to the formal charge that is calculated using a bond

valence approach. Part of the neutralization of the various surface oxygens is due to coordination with Al. Its contribution depends on the number of Al ions and the relative Al-O bond length. For boehmite, it has been found that the Al-O bond lengths in the Al coordination sphere depend on the crystallite size (BOKHIMI et al., 2001). In small, nano-sized particles, the octahedron is more distorted. We have calculated the affinity constant for the surface protonation reactions of singly and doubly coordinated surface groups, using the experimental bond lengths reported by Bokhimi et al. (BOKHIMI et al., 2001) for the very small (d_{020} ≈1-2 nm) and the large (d_{020} ≈ 10-20 nm) particles. These particle sizes are equivalent with a calculated specific surface area (flat rhombuses) of respectively about 800-500 and 80-50 m^2/g. The results are summarized in Table 2.

Table 2. The surface groups and corresponding calculated proton affinity constant affinity for the main crystal faces of boehmite. At the 010 face, the site density N_s is 9.75 nm^{-2} for the doubly coordinated surface groups. At the 101 face, the site density of the singly and doubly coordinated surface groups is both N_s = 6.8 nm^{-2}.

Face	Surface group	logK_H d ≈ 1-2 nm	logK_H d ≈ 10-20 nm
010	≡ Al_2O^{-1} *1	8.9	15.3
	≡ Al_2OH^0 *1	-3.0	3.5
101	≡ $AlO^{-3/2}$	18.3	21.7
	≡ $AlOH^{-1/2}$	6.4	9.9
	≡ Al_2O^{-1}	19.3	15.8
	≡ Al_2OH^0	7.4	3.9

*1 In case of defects on the 010 face, singly and triply coordinated surface groups are created having a log$K$ of respectively $\log K_{(\equiv AlOH)}$ = 9.7 and $\log K_{(\equiv Al3O)}$ = 5.3.

The proton affinities in Table 2 refer to the consecutive protonation reactions with respectively logK_{H1} and logK_{H2}, formulated as:

$$\equiv AlO^{-3/2} + 2H^+(aq) \Leftrightarrow \equiv AlOH^{-1/2} + H^+(aq) \Leftrightarrow \equiv AlOH_2^{+1/2} \quad (7)$$

and

$$\equiv Al_2O^{-1} + 2H^+(aq) \Leftrightarrow \equiv Al_2OH^0 + H^+(aq) \Leftrightarrow \equiv Al_2OH_2^{+1} \quad (8)$$

For large 10-20 nm particles, the logK_{H1} for the protonation of ≡ Al_2O^{-1} (Table 2) is very high. It implies that the doubly coordinated groups are very easily protonated to form ≡ Al_2OH^0. This surface species may accept a second proton but only at very low pH. It implies that a perfectly crystallized 010 face will usually have only ≡ Al_2OH^0 as surface group in the range of for instance pH = 4-10. For very small nano-particles ("pseudo-boehmite") a similar behavior is expected, but the formation of ≡ Al_2O^{-1} may occur more easily at high pH, if the mineral is perfectly crystallized.

The doubly coordinated surface OH groups at the 101 face of relatively large particles can also be considered as proton inactive in the given pH range. In contrast, the singly

coordinated surface group is proton active. The ≡OH/OH_2 groups will determine the surface charge and will suppress the reactivity of the doubly coordinated surface group as discussed in (HIEMSTRA et al., 1989b). It can be shown that the logK_{H2} value of the singly coordinated surface group represents the pristine point of zero charge (PPZC). Depending on the particle size, the estimated value may vary between PPZC ≈ 6.4 and 9.9.

The charging behavior of boehmite has been measured by Nordin et al. (NORDIN et al., 1997) and Klebanov et al. (KLEBANOV et al., 2001) for particles with a surface area of respectively 180 m^2/g and 124 m^2/g. The reported PZC values are respectively about 8.6 and 8.5-8.8 (KLEBANOV et al., 2001). Within the uncertainties, these values are in reasonable agreement with the estimation for 10-20 nm particles if the singly coordinated surface groups at the 101 face determine the charging behavior.

The most extensive titration work for boehmite has been reported by Klebanov et al. (KLEBANOV et al., 2001). According to the above analysis, a perfectly crystallized 010 face with only doubly coordinated surface groups is expected not to contribute significantly to the charging behavior in the normal pH range of titration. In the sol-gel preparation of Bokhimi et al. (BOKHIMI et al., 2002), the 010 face represents about 67 ± 5% of total the surface area. If the development of surface charge is restricted to the edge faces, attribution of the experimental charge to only the 101 face will result in an unrealistically high surface charge. Therefore, we assume that the 010 face also contributes and that this is due to the presence of defects. In case of Al vacancies in the lattice on the 010 face, singly and triply coordinated surface groups are formed with respectively a logK_H of 9.6 and 5.3, which will lead to a PZC of approximately 7.5 if present in a 1:1 ratio. We have arbitrarily chosen an apparent site density for the triply and singly coordinated surface groups at a defect 010 face, i.e. N_s(≡ AlOH) = N_s(≡ Al_3O) = 2 nm^{-2}. This assumption leads to an estimated overall site density of N_s(≡ AlOH) = 3.6 nm^{-2} and N_s(≡ Al_3O) = 1.3 nm^{-2} for boehmite with a 101 face and 010 face contribution of respectively 1/3 and 2/3.

Table 3. Location of ion charge and affinity constants used to describe the experimental charging behavior (KLEBANOV et al., 2001) and the Fe(II) adsorption (NANO and STRATHMANN, 2006) of boehmite applying C_1 = C_2 = 1.03 F/m^2.

Surface group	Δz_0	Δz_1	Δz_2	log$K$
≡ $AlOH^{-1/2}$	0	0	0	0
≡ $AlOH_2^{+1/2}$	1	0	0	8.79*[1] ± 0.12
≡ $AlOH^{-1/2}$-Na	0	1	0	+0.2*[2]
≡ $AlOH_2^{+1/2}$-Cl	1	-1	0	8.79-0.2*[2] = 8.59
≡ $Al_3O^{-1/2}$	0	0	0	0
≡ $Al_3OH^{+1/2}$	1	0	0	8.79*[1] ± 0.12
≡ $Al_3O^{-1/2}$-Na	0	1	0	+0.2*[2]
≡ $Al_3OH^{+1/2}$-Cl	1	-1	0	8.79-0.2*[2] = 8.59
≡ $(Al_2OH)_2$(AlOH) Fe_{II}*[3]	0.97 ± 0.05	1.03 ± 0.05	0	4.42*[1] ± 0.02

*[1] fitted, this study

*[2] from (HIEMSTRA et al., 1999b)

*[3] The surface complex refers to edge sharing of Fe(II) with two Al octahedra

To describe the proton titration data, we used the ion pair formation constants previously determined for gibbsite (HIEMSTRA et al., 1999b), i.e. $\log K_{Na} = 0.2$ and $\log K_{Cl} = -0.2$ (Table 3). As simplification, the proton affinity of singly and triply coordinated surface groups is set equal and the $\log K_H$ is derived by fitting the charging leading to $\log K_H = 8.79 \pm 0.12$. The $\log K_H$ value represents the PPZC. The fitted Stern layer capacitance is $C_1 \equiv C_2 = 1.03 \pm 0.02$ F/m^2. For the data of Nordin et al. (NORDIN et al., 1997) the capacitance was lower ($C_1 \equiv C_2 = 0.80$ F/m^2), which might point to a lower contribution of the 010 face to the overall charging behavior in that preparation.

3.2.3 Fe(II) adsorption to γ-AlOOH

So far, the formation of Fe(II) surface complexes on boehmite has not been studied spectroscopically. However, some information on ion complexation is available. Recently, the adsorption mode of another divalent metal ion, i.e. Ni^{2+}, has been measured with EXAFS (STRATHMANN and MYNENI, 2005). Both metal ions have approximately the same ion size, i.e. ionic radius of Ni(II) = 68pm and of Fe(II) = 73 pm (MARCUS, 1983). In the first shell of the adsorbed Ni ion, six oxygens are found with a Ni-O bond length of 205 ± 1 pm. Two Al ions are found in the second shell at a distance of 298 pm. A structural interpretation of these distances is most consistent with edge sharing (STRATHMANN and MYNENI, 2005). This finding can be used to identify for Ni(II) the adsorption site on the reactive surface of boehmite. According to the data, two Al ions are present in the second coordination sphere. This can be interpreted as edge sharing of the Ni ion with two Al octahedra. According to Bokhemi et al. (BOKHIMI et al., 2002), the morphology of well crystallized boehmite indicates that the 101 faces are chemically most reactive. Crystal growth at the 101 face can be seen as binding of Al ions at specific growth sites. The surface groups of this site are indicated in Fig. 3 with small white spheres. At crystal growth, edge sharing of the adsorbing ion with two Al octahedra of the solid will occur, resulting in an Al-Al distance of 287 pm. Based on the analogy sketched, we suggest that in case of Ni(II) and also Fe(II) adsorption, the same structural position is occupied.

An important question is the protonation status of the common ligands in case of the formation of a M(II) surface complex. If the common ligand would be an oxygen ion, it will become highly undersaturated with respect to charge. Using a bond valence approach, one calculates for the charge on the ligand in ≡ Al-O-Ni and ≡ Al_2-O-Ni bond respectively -1.13 v.u. and -0.67 v.u. if the Ni(II) ion contributes 0.33 v.u. and the Al ion(s) on average 0.5 v.u. (Pauling bond valences). The high degree of undersaturation suggests a high proton affinity, i.e. formation of an OH as common ligand is expected. In that case, the adsorption reaction of Fe(II) ions can be formulated as:

$$2 \equiv Al_2OH^0 + 1 \equiv AlOH^{-1/2} + Fe^{2+}(aq) \Leftrightarrow \equiv (Al_2OH)_2(AlOH)^{-1/2+\Delta z_0}\,Fe_{II}^{\Delta z_1} \qquad (9)$$

where $\Delta z_0 + \Delta z_1 = 2$. Application of this adsorption reaction in the modeling enables a good description ($R^2 = 0.96$) of the adsorption data (Fig. 1c and 4). Arbitrarily, the site density of the doubly coordinated surface groups has been set equal to that of the singly coordinated

surface groups (N_s = 3.6 nm^{-2}). The precise value has a minor influence (about 0.05 v.u.) on the fitted CD value. The fitted CD value and log$K$ value are given in Table 3.

The fitted CD value can be interpreted structurally. In this approach, we assume that the adsorbed Fe(II) will distribute the charge equally over its ligands, i.e. equal Fe-O distances. In case of coordination of a Fe(II) ion with three surface groups, assuming hexa-coordination, half of the ion charge will be attributed to the common ligands in the surface. The other half will be attributed to the free ligands in the Stern plane. It results in an ionic charge distribution coefficients of n_0 = +1.0 v.u. and n_1 = +1.0 v.u. Correcting for the dipole effect by applying eqs.(4-6) ($\phi\Lambda_0$ = 0.17 * (1 + 0 + 1 * -½) ≈ 0.09 v.u.) results in the overall charge distribution coefficients $\Delta z_0 = n_0 - \phi\Lambda_0$ = +0.91 v.u. and $\Delta z_1 = n_1 + \phi\Lambda_0$ = +1.09 v.u. The above fitted CD values are in agreement with the calculated ones, which supports the proposed adsorption mechanism of the formation of a tridentate Fe(II) complex at the surface.

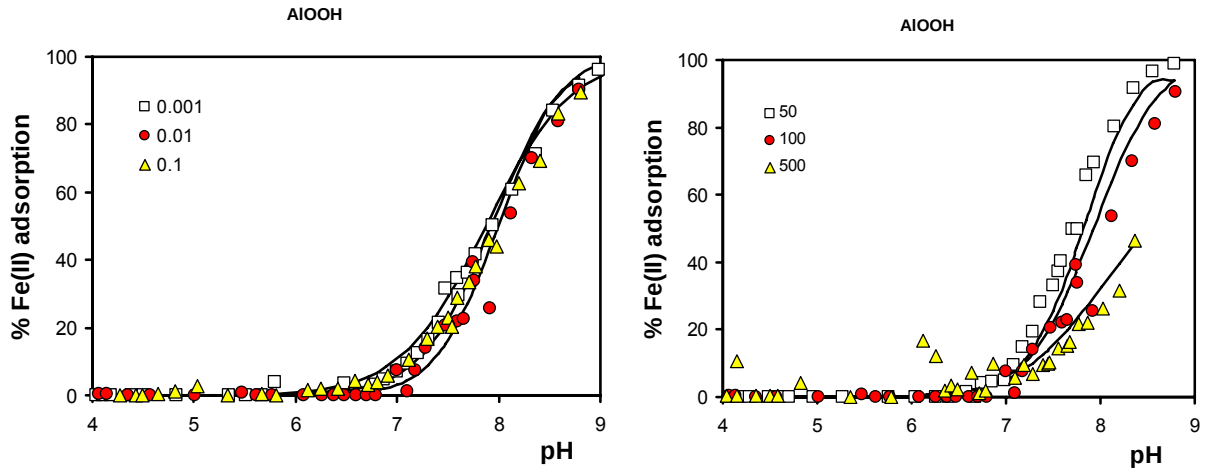

Fig.4a) The adsorption of Fe(II) on boehmite (5 g/L, 85.6 m^2/g) as a function of pH at three Fe(II) loadings (µmol/L) in 0.01 M NaCl.
Fig.4b) The adsorption of Fe(II) (C-ini = 0.1 mM) on boehmite (5 g/L, 85.6 m^2/g) in NaCl as a function of the ionic strength. The data points are of Nano and Strathmann (NANO and STRATHMANN, 2006). The lines have been calculated with the CD model using the parameter set of Table 3.

In summary, we conclude that the adsorption of the surface of TiO_2 and γ-AlOOH can be described as Fe(II) complexation without the assumption of any electron transfer. The differences in behavior of these two minerals phases can be linked satisfactory to a binding at particular sites.

3.3 Lepidocrocite γ-FeOOH

3.3.1 Surface structure

Lepidocrocite is isostructural with boehmite. Lepidocrocite (Fig.4) may have a rod or a plate-like morphology (LEWIS and FARMER, 1986) (MANCEAU et al., 2000) or a combination in which the elongated plates finger out in rods in the crystallographic c-direction (WEIDLER,

1996). Main mineral faces are supposed to be the 010 and 100 faces. Manceau et al. (MANCEAU et al., 2000) showed that 101 faces may develop too. These crystal faces can be formed at the c-axis termination of elongated crystals as sketched in Fig. 5. Atomic force measurements showed a relative contribution of the 010 face of about 70% (MANCEAU et al., 2000) for plate-like particles.

The surface composition of the various faces is given in Table 4. As for boehmite, the surface groups at the 010 face of lepidocrocite are all doubly coordinated (≡ Fe_2OH) if the 010 face is perfectly crystallized. The 100 face consists of three rows of singly (≡ FeOH) and one row of triply (≡ Fe_3O) coordinated surface groups (MANCEAU et al., 2000). At the 101 face and its equivalents, a combination of singly and doubly coordinated surface groups is found in a 1:1 ratio (Table 4).

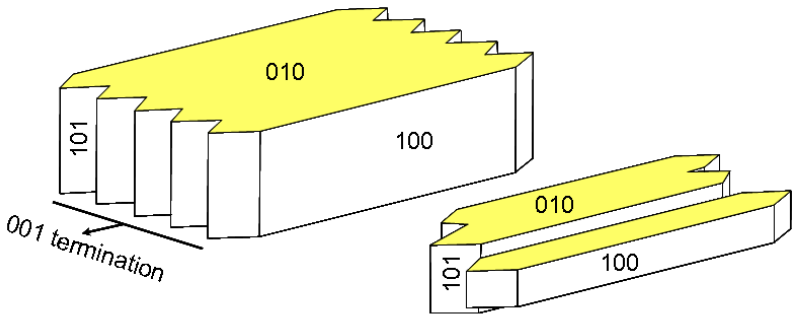

Fig.4. The idealized and simplified morphology of lepidocrocite crystals, with the 010 face on top and bottom and at the edges the 100 face and at the termination in the c direction 101 faces can be formed.

3.3.2 Surface charge

The proton affinity of the various surface groups has been estimated with the MUSIC approach in which the potential saturation of the surface oxygen is calculated on the basis of the neutralization by Fe, protons and H bonds. For Fe, the bond valence is calculated based on the bond lengths, being 198, 201, or 207 pm (ZHUKHLISTOV, 2001), giving a bond valence of respectively 0.55, 0.51 and 0.43 v.u. The proton is assumed to contribute 0.8 v.u. and a H-bond 0.2 v.u. The $\log K_H$ values for the consecutive protonation steps are given in Table 4. In case of a perfect crystal and perfect faces, the 101 and 100 can be considered as proton reactive with a PZC of respectively 9.7 and 7.3. As for boehmite, the main 010 face will not be reactive if it is perfectly crystallized. However, the experimental data for several materials (ZHANG et al., 1992) (MADRID and DIAZBARRIENTOS, 1988), (VENEMA et al., 1998) indicate that we have to assume that these faces contribute considerably to the overall surface charge, similar as for boehmite. The singly and triply coordinated surface groups that are supposedly present have a proton affinity of respectively $\log K_{H2} = 9.7$ and $\log K_{H1} = 5.3$ which will lead to a PZC of approximately 7.5 if present in equal numbers.

The PZC values reported for various lepidocrocite preparations are approximately PZC = 7.2 (DAVIES and MORGAN, 1989), PZC = 7.3 (ZHANG et al., 1992), PZC = 7.7 (PEACOCK and SHERMAN, 2004), PZC = 8.0 (VENEMA et al., 1998) (MADRID and DIAZBARRIENTOS, 1988).

Table 4. The surface groups and corresponding predicted proton affinity constants affinity for the main crystal faces of lepidocrocite.

Face	Reference surface group	N_s nm^{-2}	logK_{H1}	logK_{H2}
010*[1]	$\equiv Fe_2O_{II}^{-1}$ or $Fe_2O_{II}H^0$	8.4	11.5	-0.4
100	$\equiv FeO_I^{-3/2}$ or $\equiv FeOH_I^{-1/2}$	4.1	21.6	9.7
	$\equiv FeO_{II}^{-3/2}$ or $\equiv FeOH_{II}^{-1/2}$	8.2	23.1	11.3/**7.3**[*2]
	$\equiv Fe_3O_I^{-1/2}$	4.1	5.3	-
101	$\equiv FeO_I^{-3/2}$ or $\equiv FeO_IH^{-1/2}$	6.5	21.6	9.7*[3]
	$\equiv Fe_2O_{II}^{-1}$ or $\equiv Fe_2O_{II}H^0$	6.5	13.1	1.2

*1 In case of the presence of defects, singly and triply coordinated surface groups are found having a logK_H of respectively 9.7 and 5.3, resulting in a PZC of 7.5

*[2] The lower value is found if two H bonds are formed with this group resulting in a PZC = 7.3

*[3] The PZC of this face is expected to be high, i.e. PZC = 9.7.

Based on the above analysis, we make a simplification in order to make a representative description of the charging behavior. Assuming an apparent site density of 2 nm^{-2} for ≡ FeOH and ≡ Fe_3O at the defect 010 face and a relative contribution of the 010, 100 and 101 faces of respectively 2/3, 1/6, and 1/6, the apparent site density is about 4 sites per nm^2 for the singly coordinated and 2 nm^{-2} for the triply coordinated surface groups. We further simplify by setting the logK_H value for both types of surface groups equal to the value of the PZC as done for TiO_2 and γ-AlOOH. For the ion pair formation constants, we rely on the values found for goethite (RAHNEMAIE et al., 2007).

Table 5 Location of ion charge and affinity constants used to describe the experimental charging behavior and Fe(II) adsorption of lepidocrocite of Zhang et al. (ZHANG et al., 1992). The fitted capacitance value is $C_1 = C_2 = 1.24 \pm 0.05$ F/m^2 (Extended Stern layer model).

Surface group	Δz_0	Δz_1	Δz_2	logK_H
$\equiv FeOH^{-1/2}$	0	0	0	0
$\equiv FeOH_2^{+1/2}$	1	0	0	7.12 ± 0.1 *[1]
$\equiv FeOH^{-1/2}$-Na	0	1	0	-0.60*[2]
$\equiv FeOH_2^{+1/2}$-Cl*[3]	1	-1	0	7.12 -0.45*[2]
$\equiv FeOH_2^{+1/2}$-NO_3 *[3]	1	-1	0	7.12 -0.70*[2]
$\equiv (FeOH)_2$-$Al(OH)_2$ *[4]	+0.86 ± 0.05	+0.14 ± 0.05	0	-0.47 ± 0.09
$\equiv (FeOH)_2$-$Fe_{III}(OH)_2$ *[5]	+0.24 ± 0.10	-0.24 ± 0.05	0	-6.96 ± 0.09

*[1] fitted

*[2] from (RAHNEMAIE et al., 2007)

*[3] Cl in case of (ZHANG et al., 1992) and NO_3 in case of (SILVESTER et al., 2005).

*[4] Defined in eq.(10)

*[5] Defined in eq.(11) as Fe^{2+} adsorption with interfacial electron transfer

Using this approach, we have modeled the surface charge behavior of Madrid et al. (MADRID and DIAZBARRIENTOS, 1988), Zhang et al. (ZHANG et al., 1992) and Venema et al. (VENEMA et al., 1998), resulting in a set of Stern layer capacitances ($C_1 = C_2$) of respectively 0.79, 1.24, and 0.98 F/m^2. The value of Zhang et al. (ZHANG et al., 1992) is rather high. Their material has a rather low surface area (A_{BET} = 17.1 m^2/g), in contrast to both other materials which have respectively A_{BET} = 116 m^2/g and 73 m^2/g. Increase of the apparent capacitance with decreasing surface area has previously also been noticed for goethite (BOILY et al., 2001; GABORIAUD and EHRHARDT, 2003; HIEMSTRA et al., 1989b; SVERJENSKY, 2005). The

parameters for the description of the proton adsorption data of Zhang et al. (ZHANG et al., 1992) are given in Table 5. The proton titration curve in 0.6 M NaCl is shown in Fig. 6.

3.3.3 Al^{3+} adsorption to γ-FeOOH

The adsorption of Fe(II) might be accompanied by the transfer of an electron, changing adsorbed Fe^{2+} into adsorbed Fe^{3+} (LARESE-CASANOVA and SCHERER, 2007; WILLIAMS and SCHERER, 2004). To better understand the adsorption behavior of a trivalent cation, we will analyze first the adsorption behavior of Al^{3+} which has been measured by Zhang et al. (ZHANG et al., 1992) for the same lepidocrocite material that has been used for the adsorption study of Fe(II).

A first exploration of the modeling of the Al(III) adsorption indicated that for a good fit, the charge attribution to the 1-plane should be low (~ 0.1 v.u.). This low charge attribution is probably due to hydrolysis of the water ligands that are coordinated to the adsorbed Al(III). Hydrolysis is expected since Al^{3+} hydrolyzes also easily in solution. Moreover, the protons on the ligands of adsorbed Al(III) will experience a repulsive field that will stimulate the hydrolysis. We found that the data are best explained if two water ligands are hydrolyzed, i.e. formation of adsorbed $Al(OH)_2^+$. Furthermore, the fitted surface charge attribution related to the adsorption option of $Al(OH)_2^+$ ($\Delta z_0 \approx 1$ v.u.) points to the formation of a bidentate complex because in that case approximately 1/3 of the Al^{3+} charge (1 v.u.) is to be found at the surface. In case of a bidentate complex, two ligands are common with the surface and the other four ligands are free (Fig.6). The suggestion of the formation of an adsorbed $Al(III)(OH)_2^+$ complex, implies that half of the ligands in the Stern plane is hydrolyzed and the other half is not (Fig.6). This is approximately equal to the situation that is found for the singly coordinated surface groups at the surface of for instance gibbsite. In the PPZC, half of the groups is $\equiv AlOH^{-1/2}$, while the other half is $\equiv AlOH_2^{+1/2}$. It can be shown that even in case of charging of the surface, the ratio $\equiv AlOH : \equiv AlOH_2$ remains relatively close to the 1:1 ratio, even at low pH, which follows from the relatively low experimental excess amount of protons in relation to the number of reactive groups. The relatively low reactivity is caused by the suppressing effect of the electrostatic field. In case of a bidentate mechanism, the adsorption reaction of Al(III) on lepidocrocite can be formulated as:

$$2 \equiv FeOH^{-1/2} + Al^{3+}(aq) + 2H_2O \Leftrightarrow \equiv (FeOH)_2^{-1+\Delta z_0} Al_{III}(OH)_2^{\Delta z_1} + 2H^+(aq) \qquad (10)$$

with $\Delta z_0 + \Delta z_1 = 1$ v.u.

To be more precise, we have calculated the expected CD in case of a Pauling bond valence distribution in this bidentate complex. The expected ion charge distribution is $n_0 + n_{H0} = 1 + 0 = 1$ v.u. and $n_1 + n_{H1} = 2 - 2 = 0$ v.u. Including the dipole effect (eqs.(4-6)) with $\phi\Lambda_0 = 0$ gives $\Delta z_0 = 1.0$ v.u. and $\Delta z_1 = +0.0$ v.u. It should be noted that the same result will be found in case of the formation of a bidentate complex as a result of the reaction of Al(III) with one $\equiv Fe_3O^{-1/2}$ and one $\equiv FeOH^{-1/2}$.

Using the above adsorption reaction (eq.(10)), the final fitting was done leading to a good description of the data (Fig.6). The fitted CD parameters are $\Delta z_0 = 0.86 \pm 0.05$ v.u. and

$\Delta z_1 = +0.14 \pm 0.05$ v.u. (Table 5). In case we assume the formation of bidentate complex formed from $\equiv Fe_3O^{-1/2}$ and $\equiv FeOH^{-1/2}$, the fitted CD values are $\Delta z_0 = 0.81 \pm 0.07$ v.u. and $\Delta z_1 = +0.19 \pm 0.07$ v.u. Both results point to the formation of a hydrolyzed bidentate surface complex, but the charge in the 1-plane is slightly larger than expected ($\Delta z_1 = 0$). This may be due to the formation of some additional adsorbed $AlOH^{2+}$, but its contribution could not be resolved from the data.

Bidentate complex formation can be due to the formation of a double corner or a single edge surface complex. Complex formation of Al(III) on lepidocrocite has not been studied with spectroscopy. For Cd(II), the binding mode on lepidocrocite has been studied by several authors using EXAFS (MANCEAU et al., 2000; PARKMAN et al., 1999; RANDALL et al., 1999). At high loading, only one type of complex was found. It has a relatively short Fe-Cd distance, which is characteristic for the formation of edge-linked complexes. At a lower loading, also a double corner complex is found (MANCEAU et al., 2000). For Cd^{2+}, formation of double edge complexes (tridentate surface complexation) has been suggested for the 001 face (MANCEAU et al., 2000). At the 001 and 100 faces, double corner complex formation (bidentate surface complexes) is also possible for cations. The formation of double corner complexes (bidentate surface complexes) has been reported for oxyanions, like $As(III)(OH)_3$ (ONA-NGUEMA et al., 2005) and $As(V)O_4$ (RANDALL et al., 2001) on lepidocrocite.

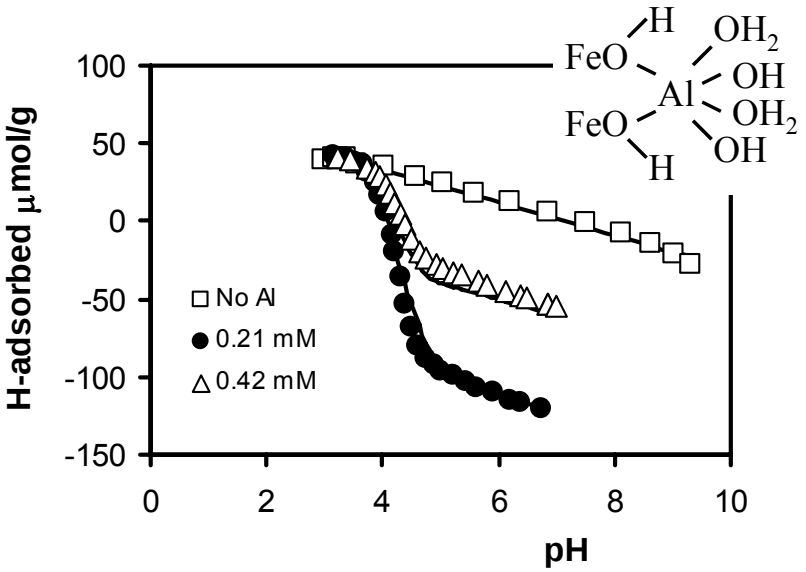

Fig.6. The variation in the proton adsorption of lepidocrocite (10 g/ L, 17.1 m^2/g) in the absence and presence of Al(III) as a function of the ph (I = 0.6 M NaCl). The data are from (Zhang et al., 1992). The lines have been calculated using eq.(10) and Table 5.

3.3.4 Fe(II) adsorption to γ-FeOOH

The adsorption behavior of Fe(II) on lepidocrocite (Fig. 7) has also been characterized with proton titrations (ZHANG et al., 1992). As mentioned above, the Fe(II) adsorption can be affected by electron transfer. Such an electron transfer will lead to a significant change of the expected CD value. To assess the CD values that can be accepted as possibly due to electron transfer, we have calculated the expected Δz_0 and Δz_1 values in case of adsorption with and without electron transfer. The results are summarized in Table 6 and the details of the calculations are explained in the footnotes. Bidentate and tridentate complexes with and without electron transfer have been chosen. In case of the formation a Fe(III) surface complex, hydrolysis will occur. As argued above for Al(III), the formation of adsorbed $Fe(III)(OH)_2$ is most likely.

The calculations (Table 6) show that the surface charge attribution for the adsorption of Fe(II) as bidentate surface complex without electron transfer is almost equal to the value expected for tridentate complexes with electron transfer. A major difference is that in case of the presence of Fe(III) as central ion, the complex will hydrolyze, leading to a negative charge in the 1-plane ($\Delta z_1 < 0$). In case of bidentate complexes with and without electron transfer, the CD values for both electrostatic planes will differ.

Table 6. Calculated location of ion charge for Bidentate (B) and Tridentate (T) complexes with and without electron transfer having $\equiv FeOH^{-/12}$ and/or $\equiv Fe_3O^{-1/2}$ as reference groups and a Pauling distribution of the central ion.

Surface complex	Δz_0 *1	Δz_1 *1
$\equiv B^{*2}$-Fe(II)	0+0.67+0+0.06 = +0.73	1.33+0-0.06 = +1.27
$\equiv T^{*2}$-Fe(II)	0+1.0 +0 +0.09 = +1.09	1.0+0-0.09 = +0.91
$\equiv B^{*3}$-Fe(III)$(OH)_2$	-1+1.0+0+0.17 = +0.17	2.0-2-0.17 = -0.17
$\equiv T^{*3}$-Fe(III)$(OH)_2$	-1+1.5+0+0.17 = + 0.67	1.5-2-0.17 = -0.67

*1 $\Delta z_0 \equiv n_e + n_0 + n_{H0} - \phi\lambda_0$ and $\Delta z_1 \equiv n_1 + n_{H1} + \phi\lambda_0$ (eq.(4-6))

*2 Surface complexes without electron transfer, using $n_0 + n_1 = +2$ v.u.

*3 Surface complexes with electron transfer, using $n_0 + n_1 = +3$ v.u. Note $n_e + n_0 + n_1 = 2$ v.u.

In a first approach to model the data, we have assumed bidentate Fe(II) binding without electron transfer (B-Fe(II)). The data can be described reasonably well in case of bidentate complex formation if we allow a free fit of the log*K* and the CD value. However, the fitted charge distribution, $\Delta z_0 = 2.54 \pm 0.21$ v.u. and $\Delta z_1 = -0.54 \pm 0.21$ v.u., is certainly in conflict with the assumed mechanism. This changes if we assume the formation of a bidentate surface complex with electron transfer and subsequent hydrolysis (B-Fe(III)$(OH)_2$), using the reaction:

$$2 \equiv FeOH^{-1/2} + Fe^{2+}(aq) + 2H_2O \Leftrightarrow \equiv (FeOH)_2^{-1+\Delta z_0} Fe_{III}(OH)_2^{\Delta z_1} + 2\,H^+(aq) \qquad (11)$$

with $\Delta z_0 + \Delta z_1 = 0$ v.u. The fitted CD is $\Delta z_0 = 0.24 \pm 0.10$ v.u. and $\Delta z_1 = -0.24 \pm 0.10$ v.u. A similar CD is found, if the above reaction is written with one $\equiv FeOH^{-1/2}$ and one $\equiv Fe_3O^{-1/2}$ surface group, i.e. $\Delta z_0 = 0.20 \pm 0.09$ v.u. and $\Delta z_1 = -0.20 \pm 0.09$ v.u. The fitted CD values are within the uncertainty equal to the expected value for bidentate complex formation with electron transfer and subsequent hydrolysis, i.e. $\Delta z_0 = +0.17$ v.u., $\Delta z_1 = -0.17$ v.u. (Table 6). Apparently, the adsorbed Fe(II) seems to react as a Fe(III) ion. A noticeable difference that remains is the affinity. Comparing the data (Figs. 6 and 7) or the log*K* values (Table 5) shows that the Al(III) ion is far more strongly bound than "Fe(III)".

In conclusion, we have seen so far that variation in Fe(II) binding on TiO_2 and γ-AlOOH can be linked to the local structure of the surface complexes. For Fe(II) binding to γ-FeOOH this is only possible if electron transfer is accepted, i.e. surface oxidation of adsorbed Fe(II) takes place at this ferric oxo-hydroxide surface resulting in a hydrolyzed $Fe(III)(OH)_2$ complex with an electron in the surface.

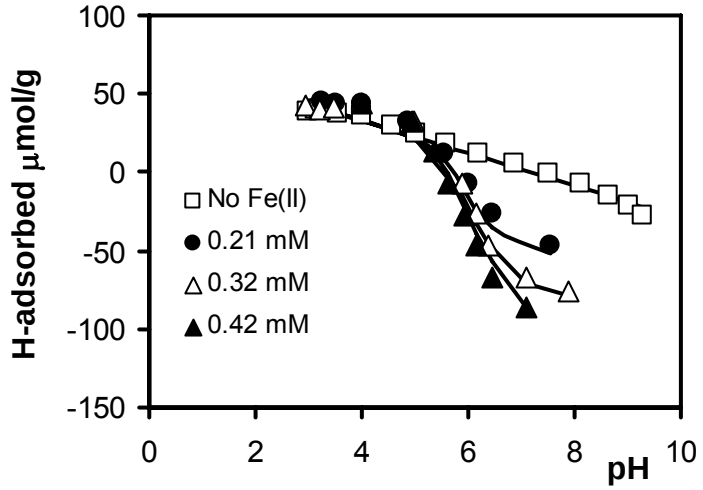

Fig.7. The variation in the proton adsorption of lepidocrocite (10 g/ L, 17.1 m^2/g) in the absence and presence of Fe(II) as a function of the ph (*I* = 0.6 M NaCl). The data are from (ZHANG et al., 1992). The lines have been calculated using eq. (11) and Table 5.

3.4 Goethite (α- FeOOH)

3.4.1 Reactive groups

Another Fe(III) oxo-hydroxide is goethite. In the lattice of goethite (α-FeOOH), two different types of triply coordinated oxygens exists, one non-protonated ($\equiv Fe_3\text{-}O_I$) and one protonated ($\equiv Fe_3\text{-}O_{II}H$) oxygen. The difference in proton affinity of both triply coordinated oxygens can be linked to a difference in the distances between the oxygen and the coordinating Fe-ions (HIEMSTRA et al., 1996b). The Fe-O distances are respectively of 196

and 210 pm, which results in bond valences of respectively 0.6 and 0.4 v.u. Both types of oxygens (O_I & O_{II}) are also found as surface groups ($\equiv Fe_3O_I^{-1/2}$ and $\equiv Fe_3O_{II}H^{-1/2}$) at the surface of the dominant 110 face and also the 100 face (HIEMSTRA et al., 1996b), (WEIDLER et al., 1999), (GABORIAUD and EHRHARDT, 2003). The site density of $\equiv Fe_3O_{II}H^{+1/2}$ is twice that of $\equiv Fe_3O_I^{-1/2}$ (respectively N_s = 6 and 3 nm^{-2}). In case of a large difference in proton affinity for both types of triply coordinated surface groups, it can be shown that the overall charging behavior is equivalent with the use of a site density of only N_s = 3 nm^{-2} (HIEMSTRA et al., 1996b) for the triply coordinated surface groups.

Goethite has also surface groups with lower Fe coordination, i.e. doubly and singly coordinated oxygens. The doubly coordinated ≡ Fe_2OH groups are probably not proton reactive. Singly coordinated surface oxygens ($\equiv FeO_I^{-3/2}$) are highly instable and are always transformed into $\equiv FeO_IH^{-1/2}$ in aqueous systems (HIEMSTRA et al., 1989a), (RUSTAD et al., 1996b). Depending on the pH, the hydroxyl ($\equiv FeO_IH^{-1/2}$) may accept a second proton forming a charged surface water group ($\equiv FeO_IH_2^{+1/2}$). The site density is 3 nm^{-2} at the 110 face.
In the present approach, the affinity constants of both proton reactive surface groups ($\equiv FeOH^{-1/2}$ and $\equiv Fe_3O_{II}^{-1/2}$) are set equal in the modeling (HIEMSTRA and VAN RIEMSDIJK, 1996a), (HIEMSTRA et al., 1996b).

Table 7 Location of ion charge and affinity constants used to describe the charging behavior, the Fe(II) (DIXIT and HERING, 2006) and the Al(III) (LÖVGREN et al., 1990) adsorption of goethite.

Surface group	Δz_0	Δz_1	Δz_2	logK_H
$\equiv FeOH^{-1/2}$	0	0	0	0
$\equiv FeOH_2^{+1/2}$	1	0	0	9.2
$\equiv FeOH^{-1/2}$-Na*[1]	0	1	0	-0.60
$\equiv FeOH_2^{+1/2}$-Cl*[1]	1	-1	0	9.2-0.45 = 8.75
$\equiv FeOH_2^{+1/2}$-NO_3*[1]	1	-1	0	9.2-0.7 = 8.5
$\equiv FeOH_2^{+1/2}$-ClO_4*[2]	1	-1	0	9.2-1.4 = 7.8
$\equiv (FeOH)_2$-$Al(OH)_2$ *[3]	0.95 ± 0.03	0.05 ± 0.03	0	1.51 ± 0.08
$\equiv (FeOH)_2$-Fe_{II} *[4]	≡ 0.73*[5]	≡ 1.27	0	8.47 ± 0.05
$\equiv (FeOH)_2$-$Fe_{III}(OH)_2$*[4]	≡ 0.17*[5]	≡ -0.17	0	-9.31 ± 0.08
$\equiv (FeO)_2As_{III}OH$*[7]	≡ 0.34*[6]	≡ -0.34*[6]	0	7.26 to 6.58
$\equiv FeOAs_{III}(OH)_2$*[7]	≡ 0.16*[6]	≡ -0.16*[6]	0	4.91 to 4.62
$\equiv FeOAs_{III}(OH)_3Fe_{II}$ *[8]	0.08 ± 0.05	+0.92 ± 0.05	0	3.38 ± 0.10

*[1] log$K$ from (RAHNEMAIE et al., 2007)
*[2] log$K$ fitted on the data of Rietra et al. (RIETRA et al., 2000a))
*[3] Defined in eq.(14)
*[4] Defined in eqs.(16&17) as Fe^{2+} adsorption without and with electron transfer
*[5] Taken by definition from Table 6
*[6] Taken from (STACHOWICZ et al., 2006)
*[7] log$K$ values vary for the bidentate complex between the various goethite preparations. See text.
*[8] Defined in eq.(18)

Faces like the 021 and 001 face terminate the goethite needles at the top ends of the crystals (SPADINI et al., 2003). These crystal faces have equal numbers of singly and doubly coordinated surface groups (N_s = 7-8 nm^{-2}). In the modeling, the protonation constant of these

singly coordinated surface groups is taken equal to that of the 110 face. The overall site density of the singly coordinated surface groups of goethite is calculated assuming 90% 110/100 face and 10 % 021/001 face, leading to 2.7+0.75 = 3.45 nm^{-2} for the singly coordinated group (HIEMSTRA and VAN RIEMSDIJK, 1996a). The overall net site density of the reactive triply coordinated surface group is 2.7 nm^{-2}.

3.4.2 Surface charge

Based on the above analysis, the surface charging can be calculated using two protonation reactions:

$$\equiv FeO_IH^{-1/2} + H^+(aq) \Leftrightarrow \equiv FeO_IH_2^{-1/2+\Delta z_0} \quad (12)$$

and

$$\equiv Fe_3O_{II}^{\ -1/2} + H^+(aq) \Leftrightarrow \equiv Fe_3O_{II}H^{-1/2+\Delta z_0} \quad (13)$$

In the Fe(II) adsorption modeling, we have used the proton affinity constant of $\log K_H = 9.2$ for both groups (HIEMSTRA and VAN RIEMSDIJK, 1996a). The ion pair formation constants, given in Table 7, are from Rahnemaie et al. (RAHNEMAIE et al., 2007). In the modeling, a capacitance value of 0.93 F/m^2 (well-structured goethite) is used.

3.4.3 Al^{3+} adsorption on goethite

Before analyzing the behavior for Fe(II), we will first focus on the Al(III) adsorption, similar as we have done for lepidocrocite. The data are from Lövgren et al. (LÖVGREN et al., 1990), who titrated goethite in the presence of different initial concentrations of Al(III) in 0.1 M $NaNO_3$ (Fig.8). As will be discussed below, the charge distribution is most closely explained by the formation of a bidentate complex. Similar as for lepidocrocite, we also find in this case a strong hydrolysis, i.e. binding as $Al(OH)_2^+$. The proposed complex can be formed at the 110 face, most likely as a double corner complex. The reaction can be formulated as:

$$2 \equiv FeOH^{-1/2} + Al^{3+}(aq) + 2H_2O \Leftrightarrow \equiv (FeOH)_2^{-1+\Delta z_0}\, Al_{III}(OH)_2^{+\Delta z_1} + 2\,H^+(aq) \quad (14)$$

with $\Delta z_0+\Delta z_1 = 1$ v.u. As for lepidocrocite, the expected overall charge distribution for the formation of this complex is $\Delta z_0 = 1.0$ v.u. and $\Delta z_1 = +0.0$ v.u. if a Pauling bond valence attribution is valid. We have calculated the geometry of this surface complex using MO/DFT computations applying various DFT models

The calculation approach is described in (HIEMSTRA and VAN RIEMSDIJK, 2006). The bond lengths of the Al with the surface groups are given in Table 8. The bond lengths vary with the type of ligands involved (common OH, free OH, and OH_2). Application of the

Brown's bond valence principle results in $n_0 + n_{H0} = 1.03 \pm 0.05$ v.u. and $n_1 + n_{H1} = -0.03 \pm 0.05$ v.u. The uncertainty (± 0.05) is estimated based on our previous experience that the precise value depends on the model used, the hydration and the defined FeOOH cluster (HIEMSTRA et al., 2007; HIEMSTRA and VAN RIEMSDIJK, 2006; RAHNEMAIE et al., 2007; STACHOWICZ et al., 2006). The dipole correction term is negligible, leading to a set of CD coefficients of $\Delta z_0 = 1.03$ v.u. and $\Delta z_1 = -0.03$ v.u. Although the individual bond length and valences are quite different, the calculated CD is almost equal to the Pauling estimate within the uncertainty.

Table 8. The calculated distances (pm) in the geometry of bidentate $Al(OH)_2$ complex using various DFT models.

Bond	B3LYP	EDF1	EDF2	Exp
FeOH-Al	192.4	193.1	191.3	
FeOH-Al	192.6	192.9	191.2	-
Al-OH	180.8	182.3	183.9	-
Al-OH	183.7	182.5	180.5	-
$Al-OH_2$	204.7	208.1	202.6	-
$Al-OH_2$	219.7	225.6	216.4	
Fe-OH	195.5 ± 0.2	198.3 ± 0.3	193.8 ± 0.2	196[*1]
Fe-Al	360 ± 1	363 ± 1	356 ± 1	355 ± 3[*2]
R_o	167.8	169.0	166.9	165.1[*3]
n_o[*4]	+1.03	+1.05	+1.03	
n_1[*4]	-0.03	-0.05	-0.03	

[*1] Distance present in the goethite structure without relaxation.
*2 The Fe-Ga distance characteristic for double corner complexation is d(Fe-Ga) = 355 ± 3 pm (PERSSON et al., 2006).
[*3] Average R_0 for Al in minerals.
[*4] The charge of $Al(OH)_2^+$ attributed to the ligands of the 0- and 1-plane application of the Brown bond valence concept to the calculated geometry, using $s = \exp((R_0-R)/37)$ in which s is the bond valence, R the bond length and R_0 the Al specific constant.

In the modeling, the primary proton adsorption data were fitted first. It results in $\log K_H = 9.09 \pm 0.07$ and the capacitance $C_1 \equiv C_2 = 1.06 \pm 0.02$ F/m^2 for the data of Fig.8. Next, the titration data with added Al(III) were fitted resulting in a set of charge distribution values $\Delta z_0 = +0.95 \pm 0.03$ v.u. and $\Delta z_1 = +0.05 \pm 0.03$ v.u.. The CD value agrees with the above-calculated value within the range of uncertainties, i.e. the dominant binding mechanism is probably a bidentate complex with the hydrolysis of two outer ligands. We note that the formation of bidentate complexes on goethite has frequently been reported in EXAFS studies for metal ions like for Cd(II) (MANCEAU et al., 2000), Cu(II) (PEACOCK and SHERMAN, 2004), Zn(II) (WAYCHUNAS et al., 2002) and Hg(II) (KIM et al., 2004).

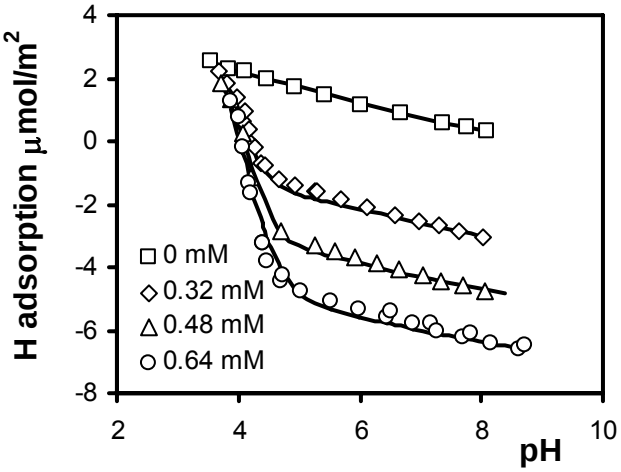

Fig.8. The variation in the proton adsorption of goethite (7.16 g/ L, 39.9 m^2/g) in the absence and presence of Al(III) as a function of the ph (I = 0.1 M $NaNO_3$). The data are from (LÖVGREN et al., 1990). The lines have been calculated using eq.(14) and Table 7. The capacitance and logK_H have been adjusted to the values given in the text.

3.4.4 Fe(II) on goethite

The Fe(II) adsorption of goethite has recently been measured extensively by Dixit and Hering (DIXIT and HERING, 2006). The binding of Fe(II) was found to be reversible. The data are given in Fig.9. The modeling of the data has been done in several steps. A primary modeling indicates that in case of binding as Fe(II) ion without electron transfer, the charge attribution is relatively high, i.e. $\Delta z_0 \approx 1.2$ v.u.. Such a value is more representative for the formation of a tridentate surface complex than for the formation of a bidentate surface complex. Tridentate surface complexes can be formed at the 021 face, as has been found for Cd(II) (MANCEAU et al., 2000; SPADINI et al., 1994), but the total Fe(II) loading in the experiments of Dixit and Hering (DIXIT and HERING, 2006) is relatively high which implies that the 110 face has to accommodate a considerable part of the ferrous ions. In principle, tridentate complexes can be formed at the 110 face at interaction with two ≡ FeOH and one ≡ Fe_3O (double edge sharing), according to.

$$2 \equiv \mathrm{FeOH}^{-1/2} + 1 \equiv \mathrm{Fe_3O}^{-1/2} + \mathrm{Fe}^{2+}(\mathrm{aq}) \Leftrightarrow \equiv (\mathrm{FeOH})_2(\mathrm{Fe_3O})^{-1.5+\Delta z_0}\,\mathrm{Fe_{II}}^{\Delta z_1} \qquad (15)$$

with Δz_0+$\Delta z_1 = 2$. Using this reaction, the CD values, obtained in a very good fit ($R^2 = 0.986$), are $\Delta z_0 = 1.26 \pm 0.03$ v.u. and $\Delta z_1 = 0.74 \pm 0.03$ v.u. The fitted Δz_0 value is larger than the expected value of $\Delta z_0 = 1.09$ (Table 6), but the formation of a tridentate complex cannot be excluded definitively. However, as noted above, divalent ions usually form double corner bidentate surface complexes at the 110 face. Tridentate complex formation has only been suggested for the Pb(II)ion (BARGAR et al., 1997b). The Pb(II) ion is probably exceptionable

since this ion is able to change its coordination and bond valence drastically upon adsorption (CN = 3). From this perspective, one may consider bidentate complex formation for Fe(II) at the 110 face as more likely. If this is the case, the Fe(II) adsorption is maybe a combination of an adsorption process with and without electron transfer. Unfortunately, the fitting procedure is unable to generate for this data a set of reliable CD and log*K* values if two reactions are assumed to occur simultaneously (4 parameter fit). To reduce the number of parameters, we have fixed the CD values to calculated values for bidentate (B) and tridentate (T) complexation as given in Table 6. Several options were explored.

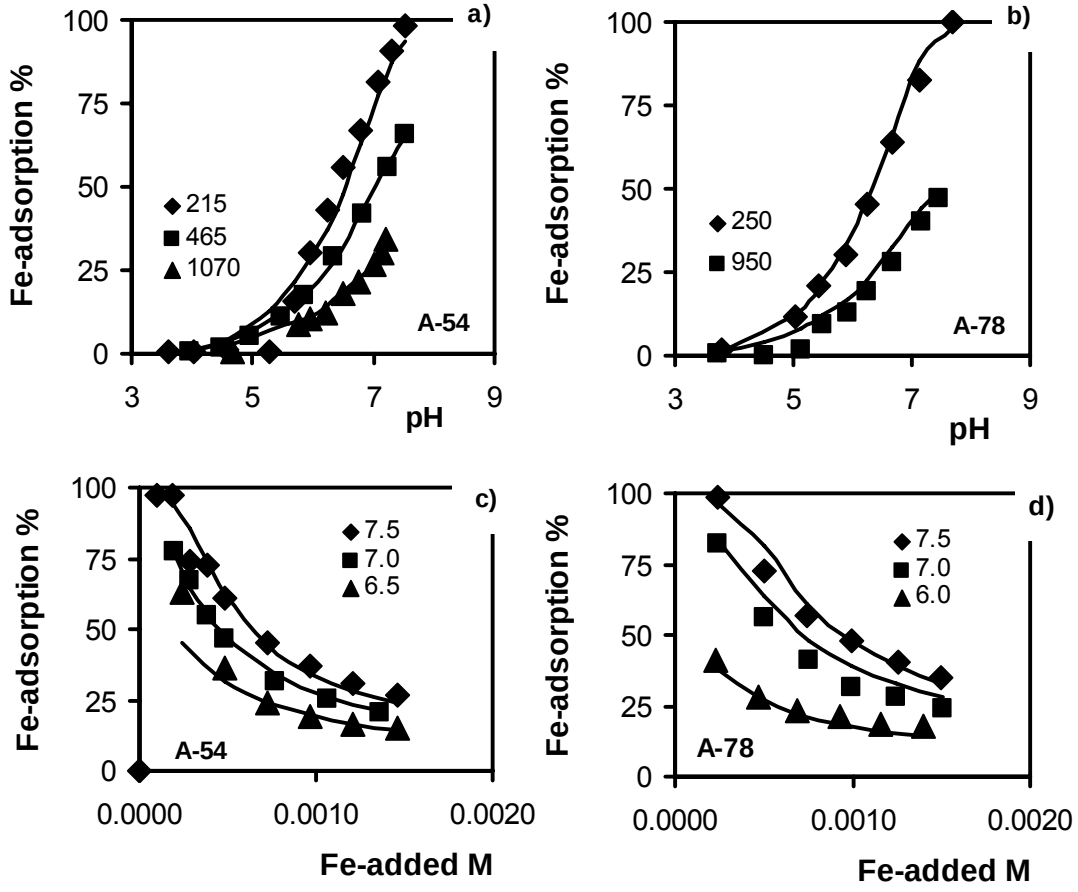

Fig.9. Adsorption edges of Fe(II) on two goethites (2.5 g/L) as a function of pH and loading in 0.01 M NaCl. Fig.8a,b Surface area = 54 m^2/g and Fig. 8c,d Surface area = 78 m^2/g. Data are from Dixit and Hering (DIXIT and HERING, 2006). The lines have been calculated with the parameters of Table 7.

In case of bidentate complexation, the fit for the combination B-Fe(II) & B-Fe(III)$(OH)_2$ surface complex gives the best result ($R^2 = 0.980$): The reactions are:

$$2 \equiv FeOH^{-1/2} + Fe^{2+}(aq) \Leftrightarrow \equiv (FeOH)_2^{-1+\Delta z_0} Fe_{II}^{\Delta z_1} \qquad (16)$$

with $\Delta z_0 + \Delta z_1 = 2$ and

$$2 \equiv FeOH^{-1/2} + Fe^{2+}(aq) + 2H_2O \Leftrightarrow \equiv (FeOH)_2^{-1+\Delta z_0} Fe_{III}(OH)_2^{\Delta z_1} + 2\,H^+(aq) \qquad (17)$$

with $\Delta z_0+\Delta z_1 = 0$. The fitted log*K* values have been given in Table 7. The model lines are in Fig.9. We note that other combinations like B-Fe(II) & T-Fe(III)$(OH)_2$ cannot be excluded on the basis of the quality of the fit ($R^2 = 0.978$). It shows that the model is flexible enough to describe the data, i.e. in this case the precise mechanism can only be proposed based on additional considerations.

Finally, we note that recently Scherer et al. (SCHERER et al., 2005) have indicated in an abstract that preliminary Mössbauer spectroscopy data for the adsorption of Fe(II) on hematite point to surface oxidation but also the presence of some adsorbed Fe(II). This would be in line with the above model (eqs.(16-17)).

To understand the conditions that favor electron transfer, we have calculated the relative contribution of adsorbed Fe^{2+} and adsorbed "Fe(III)$(OH)_2$" as a function of pH and loading (Fig.10). The adsorption of $Fe(OH)_2$ is more pH dependent than the adsorption of Fe(II) species. It implies that the surface oxidation becomes relatively more important at high pH. At pH<~7, adsorbed ferrous iron is present as adsorbed Fe^{2+} while above pH>~7.5, it is adsorbed as a Fe(III)$(OH)_2$ ion with electron transfer to the solid. This agrees with a recent Mössbauer study, showing that the ratio of Fe(II)/Fe(III) adsorbed to montmorillonite is reversible and decreases at high pH (GEHIN et al., 2007).

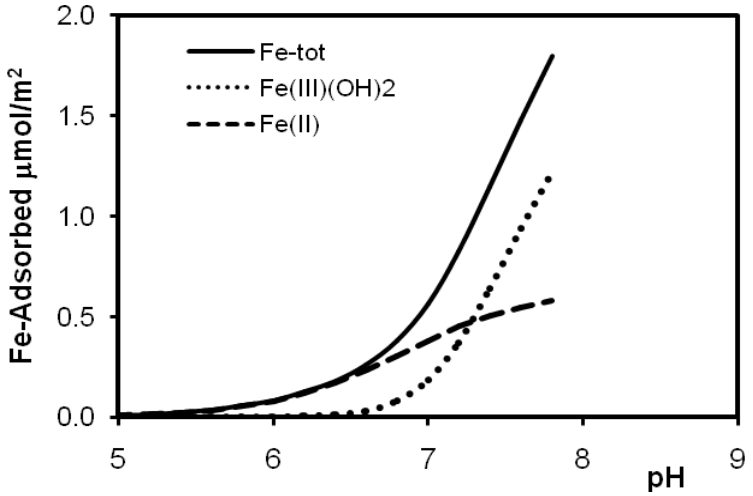

Fig.10. The total Fe(II) adsorption (full line) on goethite as a function of pH, made up by a contribution of the Fe(II) species (dashed line) and $Fe(OH)_2$ species (dotted line) as a function of pH in 0.01 M NaCl at an equilibrium concentration of 0.5 mM Fe(II).

3.4.5 Fe(II)- As(III) interaction

Dixit and Hering (DIXIT and HERING, 2006) have also measured the influence of As(III) on the Fe(II) adsorption and *vice versa* for one of their goethite preparations (A78). To predict

the effect of the presence of As(IIII) on the adsorption Fe(II) on goethite, first the adsorption behavior of As(III) will be parameterized.

The main surface species of As(III) on goethite is a bidentate complex (ONA-NGUEMA et al., 2005). It is formed by interaction of $As(III)(OH)_3$ with singly coordinated surface groups on the main crystal face of goethite (SUN and DONER, 1996). In addition, a monodentate complex may be present in a minor amount. This species contributes at high loading (STACHOWICZ et al., 2006). The reactions can be formulated as:

$$2 \equiv FeOH^{-1/2} + As(OH)_3^0(aq) \Leftrightarrow \equiv (FeO)_2^{-1+\Delta z_0} As(OH)^{\Delta z_1} + 2\,H_2O(l) \quad . \tag{18}$$

and

$$1 \equiv FeOH^{-1/2} + As(OH)_3^0(aq) \Leftrightarrow \equiv FeO^{-1/2+\Delta z_0} As(OH)_2^{\Delta z_1} + 1\,H_2O(l) \tag{19}$$

with $\Delta z_0+\Delta z_1 = 0$.

Dixit and Hering (DIXIT and HERING, 2003) have measured the As(III) adsorption for one of the goethites (A54) extensively. Unfortunately, for the goethite on which Fe(II)-As(III) interaction has been measured (A78) only a few data points are available at zero addition of Fe(II) (Fig.11b). To model the data, we used the CD values for As(III) surface complexes that have been calculated by Stachowicz et al. (STACHOWICZ et al., 2006). These charge distribution coefficients (Table 7) have been derived from the geometries of the As(III) surface complexes, found by molecular orbital (MO) optimization using Density Functional Theory (DFT). The data for A54 could be described well with $\log K(\equiv (FeO)_2\text{-}AsOH) = 6.86 \pm 0.04$ and $\log K(\equiv FeO\text{-}As(OH)_2) = 4.86 \pm 0.05$ ($R^2 = 0.987$). Application to the sparingly available data for the A78 goethite systems without added Fe(II) leads to a too high prediction of the As(III) adsorption. We have further adapted the $\log K$ values by fitting the $\log K$ values for the small data set of A78, leading to respectively $\log K(\equiv (FeO)_2\text{-}AsOH) = 6.56 \pm 0.47$ and $\log K(\equiv FeO\text{-}As(OH)_2) = 4.62 \pm 0.13$, which have been used in the final fitting of the Fe(II) adsorption.

Application of these parameters to the Fe(II)-As(II) system leads to the prediction of a strong reduction of the As(III) adsorption (Dotted line in Fig.11b). The main reason is site competition, which is most prevalent at high pH, where both ions have the highest adsorption in the mono-sorbate systems. The amounts of As(III) and Fe(II) added in the dual-sorbate systems are both high, equivalent with a loading of 2-3 umol/m^2 for each element. It implies that the large majority of singly coordinated surface groups is used to accommodate all these ions. The experimental data show even an increase of As(III) loading with increase of the Fe(II) loading. The strong increase may point to the formation of a ternary complex or for instance surface precipitation. Modeling shows that any ternary complex has to be a monodentate surface complex, due to the lack of free sites at the surface. The data could be described well assuming that the monodentate As(III) surface complex (eq.(19)) may interact with a Fe(II) ion. The relevant formation reaction that can describe the data well can be formulated as:

$$\equiv FeOH^{-1/2} + As(OH)_3^0(aq) + Fe^{2+}(aq) \Leftrightarrow \equiv FeO^{-1/2+\Delta z_0}As(OH)_2Fe_{II}OH^{\Delta z_1} + H^+(aq) \quad (20)$$

with $\Delta z_0+\Delta z_1 = +1$. Our modeling suggests the release of one proton at the formation of a Fe(II)-As(III) surface complex (eq.(20)). Proton release may for instance be due to the formation of an OH ligand in the Fe(II) coordination sphere or the change in the coordination number of the As(III) from CN = 3 to 4 ($As(OH)_3^0$ to $As(OH)_4^-$) or the formation of an As-O-Fe bond. These details are difficult to resolve here. We have fitted the CD value and the log*K* on the Fe(II) adsorption data (Fig.11a) and tested the results by looking to the predicted corresponding As(III) binding (Fig.11b). The fit on the Fe(II) data leads to $\Delta z_0 = 0.08 \pm 0.05$ $\Delta z_1 = 0.92 \pm 0.05$ v.u. and log$K = 3.50 \pm 0.12$. The fitted CD value is in agreement with what is expected for the formation of a As(III) monodentate surface complex. The CD of a hydrated monodentate $\equiv FeOAs(OH)_2$ complex is $\Delta z_0 = 0.09$ and $\Delta z_1 = -0.09$ v.u.(STACHOWICZ et al., 2006), when calculated with the MO/DFT geometry approach (HIEMSTRA and VAN RIEMSDIJK, 2006). It is interesting to note the $\equiv FeO\text{-}As(OH)_2Fe_{II}OH$ can be considered as a binuclear-bidentate complex. At the surface of goethite, binuclear-bidentate surface complexes are found to be dominant (ONA-NGUEMA et al., 2005). The fitted Fe(II) adsorption is given in Fig.11a as lines. The corresponding prediction of the As(III) binding is given in Fig.11b.

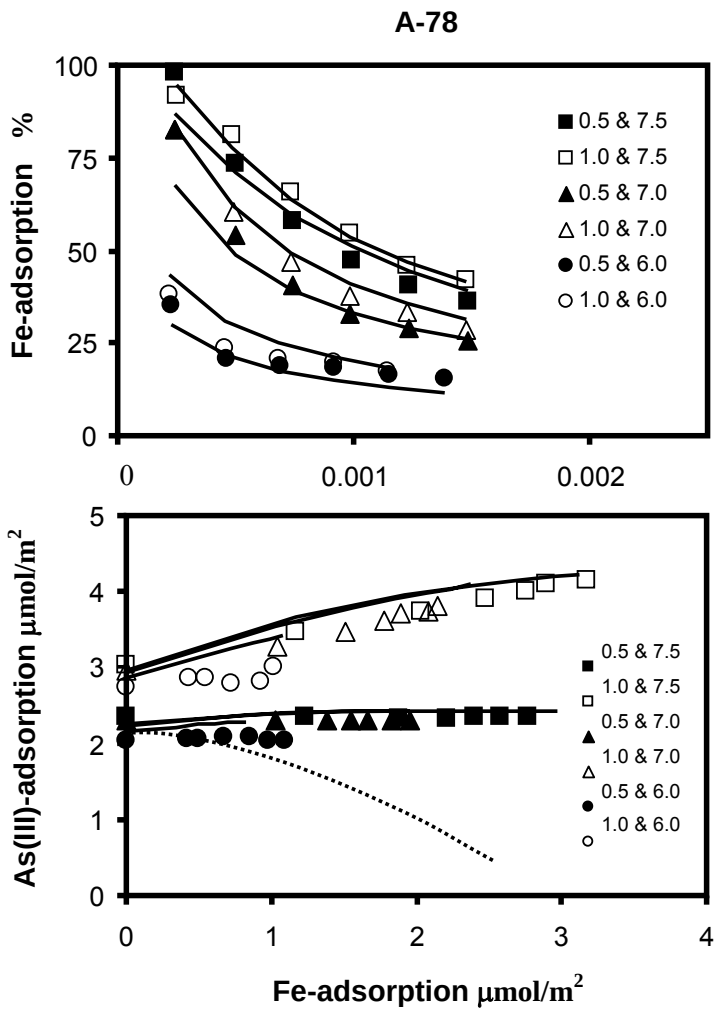

Fig.11a. Adsorption edges of Fe(II) for As(III)-Fe(II) goethite systems (2.5 g/L) in 0.01 M NaCl for pH = 6, 7, and 7.5 and an initial As(III) concentration of 0.5 or 1 mM As. Fig.11b. The adsorption of As(III) as a function of the adsorption of Fe(II), corresponding to the data of Fig.11a. Data are from Dixit and Hering (DIXIT and HERING, 2006). The full lines have been calculated with the parameters of Table 7. The dotted line refers to the As(III) adsorption at pH = 6 without formation of the ternary Fe(II) As(III) surface complex.

3.5 HFO

The experimental information with respect to the Fe(II) binding by (2-line) ferrihydrite is very sparse (APPELO et al., 2002; LIGER et al., 1999). In the reported experiments, sulphate is present since Fe(II) has been added as $Fe(II)SO_4$. Moreover, the Fe(II) binding has been measured in $NaNO_3$ and both data sets are, according to Appelo et al., not fully consistent. For these reasons, our modeling will be a first-order approach.

The structure of 2-line ferrihydrite or hydrous ferric oxide (HFO) has been discussed recently by Spadini et al. (SPADINI et al., 2005). The structure of HFO and goethite is related. Two characteristic Fe-O bond lengths are found (COMBES et al., 1989; WAYCHUNAS et al., 1993), i.e. d-FeO ≈ 195 ± 1 pm and d-FeOH = 209 ± 1 pm, which are close to the two Fe-O distances found in goethite. The fundamental unit of a synthetic 2-line ferrihydrite is the $Fe(O,OH)_6$ octahedron present in double chains which are cross-linked. The inter-chain linkage is probably disordered which may result in smaller Fe-Fe distances (WAYCHUNAS et al., 1993). Similar as for goethite, the structure of HFO gives rise to the presence of singly, doubly, and triply coordinated surface groups. The relative short chain length of the crystals will enhance the number of singly coordinated surface groups at the expense of triply coordinated surface groups. In case of an equal fraction of "110- and 021-like" faces, three-quarters of the apparent reactive surface sites might be singly coordinated surface groups. In the modeling, the site density of both groups is set at respectively N_s (≡ FeOH) = 6 nm^{-2} and N_s (≡ Fe_3O) = 2 nm^{-2}. In addition, the site density of the doubly coordinated group is arbitrarily set equal to the density of the singly coordinated groups N_s (≡ Fe_2OH) = 6 nm^{-2}. For modeling the particle charge, we have used the capacitance values and the ion pair formation constants as found for goethite (Table 7) and the proton affinity constants of the proton reactive surface groups are set equal to the PZC (PZC = 8.2). An effective surface area A_{eff} of 600 m^2/g has been used (DAVIS and LECKIE, 1978b). As discussed later, this number may be doubted in Fe(II)-HFO systems.

The adsorption behavior is probably dominated by the crystal faces that terminate the chains (021/001 like faces). At the 021 face, ions may form tridentate complexes, as shown for Cd(II) (SPADINI et al., 2003). The Cd^{2+} ion interacts with one doubly and two singly coordinated surface groups. If Fe(II) adsorbs at the same position, the reaction is:

$$2 \equiv FeOH^{-1/2} + 1 \equiv Fe_2OH^0 + Fe^{2+} \Leftrightarrow \equiv (FeOH)_2(Fe_2OH)^{-1+\Delta z_0}Fe(II)^{\Delta z_1} \qquad (21)$$

with $\Delta z_0 + \Delta z_1 = 2$. In case of a Pauling distribution, we have an equal ion charge distribution over both electrostatic planes. The calculated overall CD values are $\Delta z_0 = 1.0$ v.u. and $\Delta z_1 = 1.0$ v.u.

In the modeling, we have applied the above reaction and fitted the CD values of $\Delta z_0 = 1.30 \pm 0.16$ v.u. and $\Delta z_1 = 0.70 \pm 0.16$ v.u. The value of Δz_0 is too high compared to the above expected value, which may indicate that also surface oxidation may occur via electron transfer

to the solid and a subsequent hydrolysis of the ligands. This is supported by recent Mössbauer spectroscopy (SILVESTER et al., 2005). The reaction can be formulated as:

$$2 \equiv FeOH^{-1/2} + \equiv Fe_2OH^0 + Fe^{2+} + 2H_2O \Leftrightarrow \equiv (FeOH)_2(Fe_2OH)^{-1+\Delta z_0}Fe_{III}(OH)_2^{\Delta z_1} + 2H^+ \quad (22)$$

with $\Delta z_0 + \Delta z_1 = 0$. The CD coefficients for this tridentate reaction are expected to be $\Delta z_0 = +0.59$ v.u. and $\Delta z_1 = -0.59$ v.u. Following the same approach as done for goethite, i.e. fixing the CD values to the above expected values, we have fitted the adsorption edge using both reactions resulting in a good fit with $\log K(Fe_{II}) = 4.59 \pm 0.12$ and $\log K(Fe_{III}(OH)_2) = -13.07 \pm 0.38$ ($R^2 = 0.98$) as shown in Fig.12a.

More recently, Appelo et al. (APPELO et al., 2002), have measured the Fe(II) adsorption using the same experimental approach as Liger et al. (LIGER et al., 1999), but using a higher solid:solution ratio. The result, a measured adsorption isotherm at pH ~7, is given in Fig.12b with black squares. For comparison, also the Fe(II) adsorption found by Liger et al. is given (black sphere), showing that both data sets are not completely consistent. The adsorption isotherm can be described well if the above log*K* values, fitted to the adsorption edge of Fig.12a, are both increased by about 0.8 log*K* units, resulting in the lower line in Fig.12b through the HFO data points.

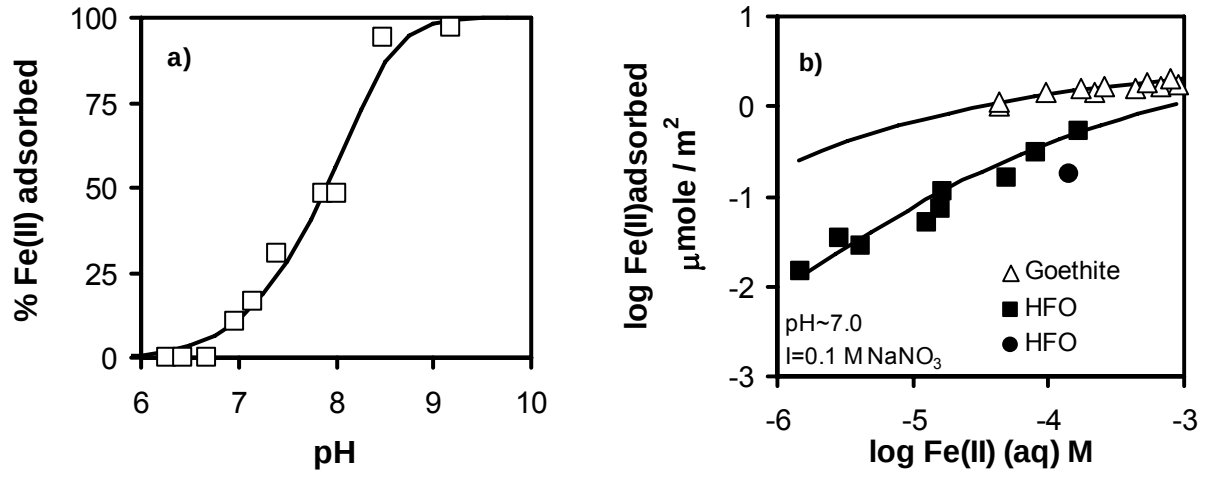

Fig.12a. Adsorption edge of Fe(II) (0.16 mM) on 2-line ferrihydrite, HFO (0.21 g/L) as a function of pH in 0.1 M $NaNO_3$. Data are from (LIGER et al., 1999). Fig.12b. Adsorption isotherms of Fe(II) for goethite (open symbols) and HFO (closed symbols) at pH~7 in 0.1 M $NaNO_3$. For HFO, the black squares are from (APPELO et al., 2002) and the black sphere is from (LIGER et al., 1999). The lines have been calculated. See text in section 3.5 and 3.6.

3.6 General discussion

The Fe(II) interaction with non-ferric minerals differs from ferric-minerals. In the modeling of the Fe(III) minerals, we have found indications of interfacial electron transfer upon Fe^{2+} adsorption, that may change the overall CD value. For lepidocrocite, the surface oxidation is apparently complete, whereas for goethite and HFO, two types of surface species might be present. The formation reaction for both types of surface species can be combined and written as a chemical equilibrium between $\equiv S_{III}\text{-}Fe_{II}$ and $\equiv S_{II}\text{-}Fe_{III}(OH)_2$. The resulting internal redox reaction reads:

$$\equiv S_{III} - Fe_{II} + 2H_2O \Leftrightarrow \equiv S_{II} - Fe_{III}(OH)_2 + 2H^+ \qquad (23)$$

The log$K$ value follows from the difference in log$K$ values of the formation reactions of both surface species. For goethite, we find $\Delta\log K$ = -9.31 + -8.47 ≈ -17.8 ± 0.1. For HFO, $\Delta\log K$ = = -13.07 + -4.59 ≈ -17.7 ± 0.5. The calculation shows that, despite large differences in the constituting log$K$ values for both minerals, the log$K$ for the equilibrium between adsorbed Fe(II), with and without electron transfer (eq.23), is equal within the uncertainties.

The intrinsic log$K$ value of eq. (23) can be interpreted as a combination of an electron transfer reaction (logK_E) and a deprotonation of two OH_2 ligands (-logK_H), producing ≡ Fe(III)-OH. The latter one is contributing most to the standard Gibbs free energy change of the reaction given. If the protonation constant of a Fe(III)OH ligand is about logK_H = 8 ± 1, the intrinsic logK_E value for the electron transfer will be log$K_E \leq \approx 2 \pm 2$. It is important to note that the log$K$ found for the above redox reaction (eq.23) cannot be applied to lepidocrocite. The formation of S(II)-Fe(III)$(OH)_2$ is relatively stronger, which might point to a higher electron transfer affinity (logK_E) for this mineral. At present, an explanation is speculative. Maybe, it is related to the difference in mineral structure (MANCEAU et al., 2000). The location of the electron in the mineral is also unknown, i.e. "Is it at the surface as part of a defined complex, or is it present at certain defects in the mineral bulk?" In the latter case, a mineral with a low surface area and a high defect density is favored in the surface oxidation reaction.

For goethite, reversibility of the adsorption has been claimed (DIXIT and HERING, 2006). In other cases, adsorbed Fe(II) could not be extracted and this was attributed to instability of the lattice leading to transformation to a Fe(III)/Fe(II) mineral (JEON et al., 2003). If both processes occur simultaneously, the final outcome will be time, pH, and material dependent.

Our speciation calculation (Fig.10) has shown that the above reaction is favored by a high pH value. For HFO, we calculate that at pH = 7 (Fig.12b), the adsorption isotherm is fully dominated by the adsorption of Fe(II), i.e. no surface oxidation yet. This is also found for goethite. A noticeable difference between goethite and HFO is the apparently much higher affinity of the Fe^{2+} ions for goethite than for HFO, as is illustrated in Fig.12b with the experimental (triangles) and calculated adsorption isotherm of Fe(II) on goethite (upper line). The reason is unknown. A noticeable difference in the experiments is the use of an organic pH buffer (PIPES) and the use of NaCl in case of goethite, while for HFO $NaNO_3$ is used without a pH buffer. However, another possible explanation might be an incorrect use of a

high surface area for HFO. According to (HANSEL et al., 2005) and (PEDERSEN et al., 2005), the presence of Fe^{2+} strongly catalyzes the transformation of HFO to other minerals like goethite and lepidocrocite. The transformation may be already significant within hours. It might imply that surface area used is too high leading to a too low experimental loading if expressed per unit surface area.

Above pH ~7.5, surface oxidation with electron transfer to the solid is expected to dominate. The overall reaction is driven by the deprotonation of the $-OH_2$ ligands, as also follows from the mass action law of eq.(23), i.e. the release of two protons. In contrast, one expects that the electron transfer itself will be favored by a low pH, because of the positive surface charge for these conditions. The positive surface potential attracts the electron that can be released by the adsorbed Fe(II), leading to interfacial redistribution of charge.

5 Conclusions

- At the surface of non-ferric (hydr)oxides, divalent iron is bound without electron transfer. At ferric (hydr)oxides, adsorbed Fe(II) may transfer an electron to the solid, creating a trivalent ion that will hydrolyze. The complex formed is equivalent with adsorbed $Fe(OH)_2$.
- The charge distribution of Fe(II), adsorbed on the surface of TiO_2 without hydrolysis, is characteristic for the formation of a quarto-dentate surface complex. Such complexes have recently been found for a series of mono-, di- and trivalent cations with spectroscopy.
- The charge distribution of Fe(II), adsorbed on the surface of γ-AlOOH (boehmite), points to the formation of a tridentate surface complex. Such type of surface complexes have also been found for Ni(II) using EXAFS.
- The titration data of Fe(II)-lepidocrocite can be explained as due to a complete surface oxidation of adsorbed divalent iron via electron transfer to the solid. The experimental Fe(II) adsorption data of goethite and HFO can be explained by Fe(II) binding with and without electron transfer.
- Goethite and HFO react quite similar with respect to electron exchange between an adsorbed ferrous ion and a ferric ion of the mineral lattice. However, the affinity of Fe(II) for goethite is significantly larger than for HFO.
- Surface oxidation is favored by a high pH value, since it is dominantly driven by the deprotonation of Fe_{III}-OH_2 ligands. Surface oxidation dominates above pH~7.5, while Fe(II) is present below pH ~7 as an adsorbed Fe^{2+} ion.
- At the goethite surface, Fe(II) and As(III) may form a ternary surface complex in which As(III) is present as a binuclear bidentate complex.

Acknowledgements Part of this work was funded by the TRIAS project 835.80.006 / Delft Cluster 5.17, and by the EU project, FUNMIG (516514, F16W-2004)

6 References

Amonette J. E., Workman D. J., Kennedy D. W., Fruchter J. S., and Gorby Y. A. (2000) Dechlorination of carbon tetrachloride by Fe(II) associated with goethite. *Environ. Sci. Tech.* 34(21), 4606-4613.

Appelo C. A. J., Van der Weiden M. J. J., Tournassat C., and Charlet L. (2002) Surface complexation of ferrous iron and carbonate on ferrihydrite and the mobilization of arsenic. *Environ. Sci. Tech.* 36(14), 3096-3103.

Ballesteros M. C., Rueda E. H., and Blesa M. A. (1998) The influence of iron (II) and (III) on the kinetics of goethite dissolution by EDTA. *J. Colloid Interface Sci.* 201(1), 13-19.

Bargar J. R., Brown G. E., Jr., and Parks G. A. (1997b) Surface Complexation of Pb(II) at Oxide-Water interfaces: II XAFS and Bond-valence Determination of Mononuclear Pb(II) Sorption Products and Surface Functional Groups on Iron Oxides. *Geochim. Cosmochim. Acta* 61, 2639-2652.

Boily J. F., Lützenkirchen J., Balmès O., Beattie J., and Sjöberg S. (2001) Modeling proton binding at the goethite (a-FeOOH)-water interface. *Colloids Surfaces A* 179(1), 11 - 27.

Bokhimi X., Sanchez-Valente J., and Pedraza F. (2002) Crystallization of sol-gel boehmite via hydrothermal annealing. *Journal of Solid State Chemistry* 166(1), 182-190.

Bokhimi X., Toledo-Antonio J. A., Guzman-Castillo M. L., and Hernandez-Beltran F. (2001) Relationship between crystallite size and bond lengths in boehmite. *Journal of Solid State Chemistry* 159(1), 32-40.

Bonneville S., Behrends T., Van Cappellen P., Hyacinthe C., and Roling W. F. M. (2006) Reduction of Fe(III) colloids by Shewanella putrefaciens: A kinetic model. *Geochim. Cosmochim. Acta* 70(23), 5842-5854.

Bourikas K., Hiemstra T., and Van Riemsdijk W. H. (2001) Ion Pair Formation and Primary Charging behaviour of Titanium Oxide (Anatase and Rutile). *Langmuir* 17(3), 749-756.

Brown I. D. (2002) *The chemical bond in inorganic chemistry : the bond valence model*. Oxford University Press.

Brown I. D. and Altermatt D. (1985) Bond-Valence Parameters Obtained from a Systematic Analysis of the Inorganic Crystal Structure Database. *Acta Cryst.* B41, 244-247.

Catalano J. G., Park C., Zhang Z., and Fenter P. (2006) Termination and water adsorption at the alpha-Al_2O_3 (012) - Aqueous solution interface. *Langmuir* 22(10), 4668-4673.

Charlet L., Bosbach D., and Peretyashko T. (2002) Natural attenuation of TCE, As, Hg linked to the heterogeneous oxidation of Fe(II): an AFM study. *Chemical Geology* 190(1-4), 303-319.

Choi S., Hong S., Ahn K., and Baumann E. R. (2001) Adsorption of ferrous iron on the lepidocrocite surface. *Environmental Technology* 22(3), 355-365.

Combes J. M., Manceau A., Calas G., and Bottero J. Y. (1989) Formation of Ferric Oxides from Aqueous-Solutions - a Polyhedral Approach by X-Ray Absorption-Spectroscopy .1. Hydrolysis and Formation of Ferric Gels. *Geochim. Cosmochim. Acta* 53(3), 583-594.

Connor P. A., Dobson K. D., and McQuillan A. J. (1999a) Infrared Spectroscopy of the TiO_2/Aqueous Solution Interface. *Langmuir* 15, 2402-2408.

Davies S. H. R. and Morgan J. J. (1989) Manganese(II) Oxidation-Kinetics on Metal-Oxide Surfaces. *J. Colloid Interface Sci.* 129(1), 63-7Davis J. A., James R., and Leckie J. O. (1978a) Surface

Ionization and Complexation at the Oxide/Water Interface. I Computation of Electrical Double Layer Properties in Simple Electrolytes. *J. Colloid Interf. Sci.* 63, 480-499.

Davis J. A. and Leckie J. O. (1978b) Surface ionization and complexation at the oxide/water interface. II Surface properties of amorphous iron oxyhydroxide and adsorption of metal ions. *J. Colloid Interf. Sci.* 67, 90-105.

Dixit S. and Hering J. G. (2003) Comparison of arsenic(V) and arsenic(III) sorption onto iron oxide minerals: Implications for arsenic mobility. *Environ. Sci. Tech.* 37(18), 4182-4189.

Dixit S. and Hering J. G. (2006) Sorption of Fe(II) and As(III) on goethite in single- and dual-sorbate systems. *Chemical Geology* 228(1-3), 6-15.

Emmenegger L., King D. W., Sigg L., and Sulzberger B. (1998) Oxidation kinetics of Fe(II) in a eutrophic Swiss lake. *Environ. Sci. Tech.* 32(19), 2990-2996.

Fenter P. and Sturchio N. C. (2004) Mineral-water interfacial structures revealed by synchrotron X-ray scattering. *Progress Surf. Sci.* 77, 171-258.

Fitts J. P., Machesky M. L., Wesolowski D. J., Shang X. M., Kubicki J. D., Flynn G. W., Heinz T. F., and Eisenthal K. B. (2005) Second-harmonic generation and theoretical studies of protonation at the water/alpha-TiO_2 (110) interface. *Chemical Physics Letters* 411(4-6), 399-403.

Gaboriaud F. and Ehrhardt J. (2003) Effects of different crystal faces on the surface charge of colloidal goethite (alpha-FeOOH) particles: An experimental and modeling study. *Geochim. Cosmochim. Acta* 67(5), 967-983.

Gehin A., Greneche J. M., Tournassat C., Brendle J., Rancourt D. G., and Charlet L. (2007) Reversible surface-sorption-induced electron-transfer oxidation of Fe(II) at reactive sites on a synthetic clay mineral. *Geochim. Cosmochim. Acta* 71(4), 863-876.

Grahame D. C. (1947) The Electrical Double Layer and the Theory of Electrocapillarity. *Chem. Rev.* 41, 441-501.

Hansel C. M., Benner S. G., and Fendorf S. (2005) Competing Fe(II)-induced mineralization pathways of ferrihydrite. *Environ. Sci. Tech.* 39(18), 7147-7153.

Hiemstra T., Barnett M. O., and Van Riemsdijk W. H. (2007) Interaction of Silicic Acid with Goethite. *J. Colloid Interf. Sci.* 310, 8-17.

Hiemstra T., De Wit J. C. M., and Van Riemsdijk W. H. (1989b) Multisite proton adsorption modeling at the solid/solution interface of (hydr)oxides: A new approach. II. Application to various important (hydr)oxides. *J. Colloid Interf. Sci.* 133, 105-117.

Hiemstra T., Han Yong, and Van Riemsdijk W. H. (1999b) Interfacial Charging Phenomena of Aluminum (Hydr)oxides. *Langmuir* 15, 5942-5955.

Hiemstra T., Rahnemaie R., and Van Riemsdijk W. H. (2004) Surface Complexation of Carbonate on Goethite: IR spectroscopy, Structure and Charge Distribution. *J. Colloid Interf. Sci.* 278, 282-290.

Hiemstra T. and Van Riemsdijk W. H. (1996a) A surface Structural Approach to Ion Adsorption: The Charge Distribution (CD) Model. *J. Colloid Interf. Sci.* 179, 488-508.

Hiemstra T. and Van Riemsdijk W. H. (2002) On the Relationship between Surface Structure and Ion Complexation of Oxide-Solution Interfaces. In *Encyclopaedia of Surface and Colloid Science*, pp. 3773-3799. Marcel Dekker, Inc.

Hiemstra T. and Van Riemsdijk W. H. (2006) On the relationship between charge distribution, surface hydration and the structure of the interface of metal hydroxides. *J. Colloid Interf. Sci.* 301, 1-18.

Hiemstra T., Van Riemsdijk W. H., and Bolt G. H. (1989a) Multisite Proton Adsorption Modeling at the Solid/Solution Interface of (Hydr)oxides: A New Approach. I. Model Description and Evaluation of Intrinsic Reaction Constants. *J. Colloid Interf. Sci.* 133, 91-104.

Hiemstra T., Venema P., and Van Riemsdijk W. H. (1996b) Intrinsic proton affinity of reactive surface groups of metal (hydr)oxides: The bond valence principle. *J. Colloid Interf. Sci.* 184, 680-692.

Israelachvili J. N. and Wennerstrom H. (1996) Role of hydration and water structure in biological and colloidal interactions. *Nature* 379(6562), 219-225.

Jeon B. H., Dempsey B. A., and Burgos W. D. (2003) Kinetics and mechanisms for reactions of Fe(II) with iron(III) oxides. *Environ. Sci. Tech.* 37(15), 3309-3315.

Jing C. Y., Meng X. G., Liu S. Q., Baidas S., Patraju R., Christodoulatos C., and Korfiatis G. P. (2005) Surface complexation of organic arsenic on nanocrystalline titanium oxide. *J. Colloid Interface Sci.* 290(1), 14-21.

Kataoka S., Gurau M. C., Albertorio F., Holden M. A., Lim S. M., Yang R. D., and Cremer P. S. (2004) Investigation of water structure at the TiO_2/aqueous interface. *Langmuir* 20(5), 1662-1666.

Keizer M. G. and Van Riemsdijk W. H. (1998) ECOSAT, Technical Report Department Soil Science and Plant Nutrition. Wageningen Agricultural University.

Kim C. S., Rytuba J. J., and Brown G. E. J. (2004) EXAFS study of mercury(II) sorption to Fe- and Al-(hydr)oxides I effect of pH. *J. Colloid Interf. Sci.* 271, 1-15.

King D. W. (1998) Role of carbonate speciation on the oxidation rate of Fe(II) in aquatic systems. *Environ. Sci. Tech.* 32(19), 2997-3003.

Kinniburgh D. G. (1993) Fit, Technical Report WD/93/23. British Geological Survey.

Klausen J., Trober S. P., Haderlein S. B., and Schwarzenbach R. P. (1995) Reduction of Substituted Nitrobenzenes by Fe(Ii) in Aqueous Mineral Suspensions. *Environ. Sci. Tech.* 29(9), 2396-2404.

Klebanov A. V., Bogdanova N. F., Ermakova L. E., Sidorova M. P., and Osmolovskii M. G. (2001) Electrosurface properties of hydr(oxides) and oxide nanostructures in 1 : 1 electrolyte solutions: 1. Adsorption characteristics of boehmite, goethite, and silicon dioxide. *Colloid Journal* 63(5), 562-567.

Klupinski T. P., Chin Y. P., and Traina S. J. (2004) Abiotic degradation of pentachloronitrobenzene by Fe(II): Reactions on goethite and iron oxide nanoparticles. *Environ. Sci. Tech.* 38(16), 4353-4360.

Larese-Casanova P. and Scherer M. M. (2007) Fe(II) sorption on hematite: New insights based on spectroscopic measurements. *Environ. Sci. Tech.* 41(2), 471-477.

Lewis D. G. and Farmer V. C. (1986) Infrared Absorption of surface hydroxyl groups and lattice vibrations in Lepidocrocite (g-FeOOH) and Boehmite (g-AlOOH). *Clay Minerals* 21, 93-100.

Liger E., Charlet L., and Van Cappellen P. (1999) Surface catalysis of uranium(VI) reduction by iron(II). *Geochim. Cosmochim. Acta* 63(19-20), 2939-2955.

Lövgren L., Sjöberg S., and Schindler P. W. (1990) Acid/base reactions and aluminium (III) complexation at the surface of goethite. *Geochim. Cosmochim. Acta* 54, 1301-1306.

Machesky M. L., Wesolowski D. J., Palmer D. A., and Ichiro-Hayashi K. (1998) Potentiometric Titrations of Rutile Suspensions to 250 ^{o}C. *J. Colloid Interf. Sci.* 200, 298-309.

Machesky M. L., Wesolowski D. J., Palmer D. A., and Ridley M. K. (2001) On the temperature dependence of intrinsic surface protonation equilibrium constants: An extension of the revised MUSIC model. *J. Colloid Interf. Sci.* 239(2), 314-327.

Madrid L. and Diazbarrientos E. (1988) Description of Titration Curves of Mixed Materials with Variable and Permanent Surface-Charge by a Mathematical-Model .1. Theory .2. Application to Mixtures of Lepidocrocite and Montmorillonite. *Journal of Soil Science* 39(2), 215-225.

Maithreepala R. A. and Doong R. A. (2004) Synergistic effect of copper ion on the reductive dechlorination of carbon tetrachloride by surface-bound Fe(II) associated with goethite. *Environ. Sci. Tech.* 38(1), 260-268.

Manceau A., Nagy K. L., Spadini L., and Ragnarsdottir K. V. (2000) Influence of Anionic structure of Fe-Oxyhydroxides on the structure of Cd surface complexes. *J. Colloid Interf. Sci.* 228, 306-316.

Marcus Y. (1983) Ionic-Radii in Aqueous-Solutions. *Journal of Solution Chemistry* 12(4), 271-275.

Nano G. V. and Strathmann T. J. (2006) Ferrous iron sorption by hydrous metal oxides. *J. Colloid Interface Sci.* 297(2), 443-454.

Nordin J., Persson P., Laiti E., and Sjoberg S. (1997) Adsorption of o-phthalate at the water-boehmite (gamma-AlOOH) interface: Evidence for two coordination modes. *Langmuir* 13(15), 4085-4093.

Ona-Nguema G., Morin G., Juillot F., Calas G., and Brown G. E., Jr. (2005) EXAFS analysis of arsenite adsorption onto two-line ferrihydrite, hematite, goethite, and lepidocrocite. *Environ. Sci. Technol.* 39(23), 9147-9155.

Ostroverkhov V., Waychunas G. A., and Shen Y. R. (2005) New information on water interfacial structure revealed by phase-sensitive surface spectroscopy. *Physical Review Letters* 94(4).

Parkman R. H., Charnock J. M., Bryan N. D., and Vaughan D. J. (1999) Reactions of copper and cadmium ions in aqueous solution with goethite, lepidocrocite, mackinawite, and pyrite. *Amer. Min.* 84, 407-419.

Pashley R. M. and Israelachvili J. N. (1984) Molecular layering of water in thin films between mica surfaces and its relation to hydration forces. *J. Colloid Interf. Sci.* 101(2), 511-523.

Pauling L. (1929) The Principles Determining the Structure of Complex Ionic Crystals. *J. Am. Chem. Soc.* 51, 1010-1026.

Peacock C. L. and Sherman D. M. (2004) Copper(II) sorption onto goethite, hematite and lepidocrocite: A surface complexation model based on ab initio molecular geometries and EXAFS. *Geochim. Cosmochim. Acta* 68(12), 2623-2637.

Pecher K., Haderlein S. B., and Schwarzenbach R. P. (2002) Reduction of polyhalogenated methanes by surface-bound Fe(II) in aqueous suspensions of iron oxides. *Environ. Sci. Tech.* 36(8), 1734-1741.

Pedersen H. D., Postma D., Jakobsen R., and Larsen O. (2005) Fast transformation of iron oxyhydroxides by the catalytic action of aqueous Fe(II). *Geochim. Cosmochim. Acta* 69(16), 3967-3977.

Persson P., Zivkovic K., and Sjoberg S. (2006) Quantitative adsorption and local structures of Gallium(III) at the water-alpha-FeOOH interface. *Langmuir* 22(5), 2096-2104.

Rahnemaie R., Hiemstra T., and Van Riemsdijk W. H. (2006) A new structural approach for outersphere complexation, tracing the location of electrolyte ions. *J. Colloid Interf. Sci.* 293, 312-321.

Rahnemaie R., Hiemstra T., and Van Riemsdijk W. H. (2007) Geometry, Charge Distribution and Surface Speciation of Phosphate on Goethite. *Langmuir* 23, 3680-3689.

Randall S. R., Sherman D. M., and Ragnarsdottir K. V. (1999) The mechanism of cadmium surface complexation on iron oxyhydroxide minerals. *Geochim. Cosmochim. Acta* 63, 2971-2987.

Randall S. R., Sherman D. M., and Ragnarsdottir K. V. (2001) Sorption of As(V) on green rust ($Fe_4(II)Fe_2(III)(OH)_{12}SO_4.3H_2O$) and lepidocrocite (gamma-FeOOH): Surface complexes from EXAFS spectroscopy. *Geochim. Cosmochim. Acta* 65(7), 1015-1023.

Regazzoni A. E., Mandelbaum P., Matsuyoshi M., Schiller S., Bilmes S. A., and Blesa M. A. (1998) Adsorption and photooxidation of salicylic acid on titanium dioxide: A surface complexation description. *Langmuir* 14(4), 868-874.

Ridley M. K., Machesky M. L., Wesolowski D. J., and Palmer D. A. (2004) Modeling the surface complexation of calcium at the rutile-water interface to 250 degrees C. *Geochim. Cosmochim. Acta* 68(2), 239-251.

Rietra R. P. J. J., Hiemstra T., and Van Riemsdijk W. H. (1999a) The Relationship between Molecular Structure and Ion Adsorption on Variable Charge Minerals. *Geochim. Cosmochim. Acta* 63(19/20), 3009-3015.

Rietra R. P. J. J., Hiemstra T., and Van Riemsdijk W. H. (2000a) Electrolyte Anion Affinity and its Effect on Oxyanion Adsorption on Goethite. *J. Colloid Interf. Sci.* 229, 199-206.

Rodriguez R., Blesa M. A., and Regazzoni A. E. (1996) Surface complexation at the TiO_2 (anatase) aqueous solution interface: Chemisorption of catechol. *J. Colloid Interface Sci.* 177(1), 122-131.

Rustad J. R., Felmy A. R., and Hay B. P. (1996b) Molecular Statics Calculations of Proton Binding to Goethite Surfaces: A New Approach to Estimation of Stability Constants for Multisite Surface Complexation Models. *Geochim. Cosmochim. Acta* 60, 1563-1576.

Scherer M. M., Larese-Casanova P., and Williams A. G. B. (2005) Fe(II) adsorption at the oxide-water interface: From macrosopic observations to spectroscopic measurements. *Geochim. Cosmochim. Acta* 69(10), A359-A359.

Shen Y. R. and Ostroverkhov V. (2006) Sum-frequency vibrational spectroscopy on water interfaces: Polar orientation of water molecules at interfaces. *Chemical Reviews* 106(4), 1140-1154.

Silvester E., Charlet L., Tournassat C., Gehin A., Greneche J. M., and Liger E. (2005) Redox potential measurements and Mossbauer spectrometry of Fe-II adsorbed onto Fe-III (oxyhydr)oxides. *Geochim. Cosmochim. Acta* 69(20), 4801-4815.

Spadini L., Manceau A., Schindler P. W., and Charlet L. (1994) Structure and Stability of Cd^{2+} Surface Complexes on Ferric Oxides. 1 Results from EXAFS spectroscopy. *J. Colloid Interf. Sci.* 168, 73-86.

Spadini L., Schindler P. W., Charlet L., Manceau A., and Ragnarsdottir K. V. (2003) Hydrous ferric oxide: evaluation of CD-HFO surface complexation models combining Cdk EXAFS data, potentiometric titration results and surface site structures identified from mineralogical knowledge. *J. Colloid Interf. Sci.* 266, 1-18.

Spadini L., Schindler P. W., and Sjoberg S. (2005) On the stability of the $AlOSi(OH)_3^{2+}$ complex in aqueous solution. *Aquatic Geochemistry* 11(1), 21-31.

Stachowicz M., Hiemstra T., and Van Riemsdijk W. H. (2006) Surface speciation of As(III) and As(V) adsorption in relation to charge distribution. *J. Colloid Interf. Sci.* 302, 62-75.

Stern O. (1924) Zur theory der electrolytischen doppelschicht. *Z. Electrochem.* 30, 508-516.

Strathmann T. J. and Myneni S. C. B. (2005) Effect of soil fulvic acid on nickel(II) sorption and bonding at the aqueous-boehmite (gamma-AIOOH) interface. *Environ. Sci. Tech.* 39(11), 4027-4034.

Strathmann T. J. and Stone A. T. (2003) Mineral surface catalysis of reactions between Fe-II and oxime carbamate pesticides. *Geochim. Cosmochim. Acta* 67(15), 2775-2791.

Stumm W. and Sulzberger B. (1992) The Cycling of Iron in Natural Environments - Considerations Based on Laboratory Studies of Heterogeneous Redox Processes. *Geochim. Cosmochim. Acta* 56(8), 3233-3257.

Sun X. and Doner H. (1996) An Investigation of Arsenate and Arsenite Bonding Structures on Goethite by FTIR. *Soil Sci.* 161, 865-872.

Sverjensky D. A. (2005) Prediction of surface charge on oxides in salt solutions: Revisions for 1:1 (M+L-) electrolytes. *Geochim. Cosmochim. Acta* 69(2), 225-257.

Tamura H., Goto K., and Nagayama M. (1976) Effect of Ferric Hydroxide on Oxygenation of Ferrous-Ions in Neutral Solutions. *Corrosion Science* 16(4), 197-207.

Toney M. F., Howard J. N., Richer J., Borges G. L., Gordon J. G., Melroy O. R., Wiesler D. G., Yee D., and Sorensen L. B. (1995) Distribution of water molecules at Ag(111)/electrolyte interface as studied with surface X-ray scattering *Surf. Sci.* 335 (1-3), 326-332

Venema P., Hiemstra T., and Van Riemsdijk W. H. (1998) Intrinsic Proton Affinity of Reactive Surface Groups of Metal (Hydr)oxides: Application to Iron (Hydr) oxides. *J. Colloid Interf. Sci.* 198, 282-295.

Vikesland P. J. and Valentine R. L. (2002a) Iron oxide surface-catalyzed oxidation of ferrous iron by monochloramine: Implications of oxide type and carbonate on reactivity. *Environ. Sci. Tech.* 36(3), 512-519.

Vikesland P. J. and Valentine R. L. (2002b) Modeling the kinetics of ferrous iron oxidation by monochloramine. *Environ. Sci. Tech.* 36(4), 662-668.

Waychunas G. A., Fuller C. C., and Davids J. A. (2002) Surface Complexation and Precipitate Geometry for Aqueous Zn(II) Sorption on Ferrihydrite I: X-ray absorption extended fine structure spectroscopic analysis. *Geochim. Cosmochim. Acta* 66(7), 1119-1137.

Waychunas G. A., Rea B. A., Fuller C. C., and Davids J. A. (1993) Surface chemistry of ferrihydrite. 1. EXAFS studies of the geometry of coprecipitated and adsorbed arsenate. *Geochim. Cosmochim. Acta* 57, 2251-2269.

Weidler P. G. (1996) Oberflächen und porositäten synthetischer Eisenoxide, Technische Universität München.

Weidler P. G., Hug S. J., Wetche T. P., and Hiemstra T. (1999) Determination of Growth Rates of 100 and 110 faces of Synthetic Goethite by Scanning Force Microscopy. *Geochim. Cosmochim. Acta* 62, 3407-3412.

Westall J. and Hohl H. (1980) A Comparison of Electrostatic Models for the Oxide/solution Interface. *Adv. Colloid Interf. Sci.* 12, 265-294.

Williams A. G. B. and Scherer M. M. (2004) Spectroscopic evidence for Fe(II)-Fe(III) electron transfer at the iron oxide-water interface. *Environ. Sci. Tech.* 38(18), 4782-4790.

Yates D. E., Levine S., and Healy T. W. (1974) Site-binding Model of the Electrical Double Layer at the Oxide/Water Interface. *J. Chem. Soc. Faraday Trans. I* 70, 1807-1818.

Yeganeh M. S., Dougal S. M., and Pink H. S. (1999) Vibrational spectroscopy of water at liquid / solid interfaces: Crossing the isoelectric point of a solid surface *Phys. Rev. Letters* 83(6), 1179-1182

Zachara J. M., Smith S. C., and Fredrickson J. K. (2000) The effect of biogenic Fe(II) on the stability and sorption of Co(II)EDTA^{2-} to goethite and subsurface sediment. *Geochim. Cosmochim. Acta* 64(8), 1345-1362.

Zhang Y., Charlet L., and Schindler P. W. (1992) Adsorption of Protons, Fe(II) and Al(III) on Lepidocrocite (Gamma-FeOOH). *Colloids and Surfaces* 63(3-4), 259-268.

Zhang Z., Fenter P., Cheng L., Sturchio N. C., Bedzyk M. J., Predota M., Bandura A., Kubicki J. D., Lvov S. N., Cummings P. T., Chialvo A. A., Ridley M. K., Benezeth P., Anovitz L., Palmer D. A., Machesky M., and Wesolowski D. J. (2004) Ion adsorption at the rutile-water interface: linking molecular and macroscopic properties. *Langmuir* 20(12), 4954-4969.

Zhang Z., Fenter P., Kelly S. D., Catalano J. G., Bandura A. V., Kubicki J. D., Sofo J. O., Wesolowski D. J., Machesky M. L., Sturchio N. C., and Bedzyk M. J. (2006) Structure of hydrated Zn^{2+} at the rutile TiO_2 (110)-aqueous solution interface: Comparison of X-ray standing wave, X-ray absorption spectroscopy, and density functional theory results. *Geochim. Cosmochim. Acta* 70(16), 4039-4056.

Zhukhlistov A. P. (2001) Crystal structure of lepidocrocite Fe O (O H) from electron diffraction data. *Kristallografiya* 46(5), 805-808.

Chapter 8

Nanoparticles in Natural systems I: The Effective Reactive Surface Area of the Natural Oxide Fraction in Field Samples

Tjisse Hiemstra, Juan Antelo, Rasoul Rahnemaie, and Willem H. van Riemsdijk

Published in Geochimica et Cosmochimica Acta
Volume 74, Issue 1, Pages 41-58, January 1, 2010

Abstract

Information on the particle size and reactive surface area of natural samples is essential for the application of surface complexation models (SCM) to predict bioavailability, toxicity, and transport of elements in the natural environment. In addition, this information will be of great help to enlighten views on the formation, stability, and structure of nanoparticle associations of natural organic matter (NOM) and natural oxide particles.

Phosphate is proposed as a natively present probe ion to derive the effective reactive surface area of natural samples. In the suggested method, natural samples are equilibrated (≥ 10 days) with 0.5 M $NaHCO_3$ (pH = 8.5) at various solid-solution ratios. This matrix fixes the pH and ionic strength, suppresses the influence of Ca^{2+} and Mg^{2+} ions by precipitation these in solid carbonates, and removes NOM due to the addition of activated carbon in excess, collectively leading to the dominance of the PO_4-CO_3 interaction in the system. The data have been interpreted with the Charge Distribution (CD) model, calibrated for goethite, and the analysis results in an effective reactive surface area (SA) and a reversibly bound phosphate loading Γ for a series of top soils.

The oxidic SA varies between about 3-30 m^2/g sample for a large series of representative agricultural top soils. Scaling of our data to the total iron and aluminum oxide content (dithionite-citrate-bicarbonate extractable), results in the specific surface area between about 200-1200 m^2/g oxide for most soils, i.e. the oxide particles are nano-sized with an equivalent diameter in the order of ~1-10 nm if considered as nonporous spheres. For the top soils, the effective surface area and the soil organic carbon fraction are strongly correlated. The oxide particles are embedded in a matrix of organic carbon (OC), equivalent to ~1.4 ± 0.2 mg OC/m^2 oxide for many soils of the collection, forming a NOM-mineral nanoparticle association with an average NOM volume fraction of ~80%. The average mass density of such a NOM-mineral association is ~1700 ± 100 kg/m^3 (i.e. high-density NOM). The amount of reversibly bound phosphate is rather close to the amount of phosphate that is extractable with oxalate. The phosphate loading varies remarkably ($\Gamma \approx$ 1-3 μmol/m^2 oxide) in the samples. As discussed in part II of this paper series (HIEMSTRA et al., 2010), the phosphate loading (Γ) of field samples is suppressed by surface complexation of NOM, where hydrophilic, fulvic, and humic acids act as a competitor for (an)ions via site competition and electrostatic interaction.

1 Introduction

The bioavailability as well as mobility of ions largely depends on the interaction with organic matter and mineral particles. The interaction is a complex process, often involving much more than a simple adsorption reaction or ion exchange. Factors such as pH, ionic strength, the presence of competing or promoting ions as well as the nature and the amount of substrate, all affect the distribution of cat- and anions over the solid and solution phase.

Our understanding of the binding of ions to well-defined mineral particles has increased in the last decade because of the development of in-situ surface spectroscopy and surface complexation models (SCM). Ideally, SCM may predict changes in situations where experimental data are not available or difficult to collect. Surface complexation models have widely been used to estimate the distribution of metal- and oxyanions between solution and mineral surfaces (ALI and DZOMBAK, 1996a; ANTELO et al., 2005; BOILY, 1999; CHRISTL and KRETZSCHMAR, 1999; CRISCENTI and SVERJENSKY, 1999; DAVIS and LECKIE, 1978b; DZOMBAK and MOREL, 1990; HIEMSTRA and VAN RIEMSDIJK, 1996a; LUTZENKIRCHEN, 2004; PONTHIEU et al., 2006; TADANIER and EICK, 2002).

In general, the application of SCM to natural systems like soils, sediments, and other aquatic media is quite complicated. Natural systems are usually complex, containing many different elements that may interact with a number of mineral particles. Two important complications related to the application of SCM to field samples are "how to derive the reactive surface area of the oxide fraction?" and "how to deal with the interaction of natural organic matter with oxide particles?" Both aspects need our attention at priority. In part I of this paper series, we discuss the determination of the effective surface area of the natural oxide fraction in field samples. In part II (HIEMSTRA et al., 2010), the effective NOM loading of the natural oxide fraction will be assessed. Both are required to apply surface complexation modeling to field samples. These are also of great interest to enlighten views on the formation, stability, and structure of nanoparticle associations of natural organic matter (NOM) and natural oxide particles.

Any application of electrostatic SCM's to natural systems requires in the first place information about the reactive surface area of the material involved in the adsorption process. Most SCM use an electrostatic module with a diffuse double layer (DDL) to calculate the interaction energy between ions that are adsorbed at the charged surface. The corresponding theory uses the electric field strength that represents the charge per unit surface area (C/m^2). Various approaches can be followed to incorporate a reactive surface area in a SCM.

A) The classical method of gas adsorption, i.e. BET method, has been used to measure the reactive surface area of natural sands (LOGUE et al., 2004; ROSENTRETER et al., 1998). A disadvantage is that natural materials are often heterogeneous, in which part of the measured surface area (A in m^2/kg material) may be not reactive in the adsorption process that is considered. For instance, clay minerals may be present, while the focus is on the oxide fraction. It is also possible that adsorbed natural organic matter (NOM) may mask part of the mineral surface area (KAISER and GUGGENBERGER, 2000; KAISER and GUGGENBERGER, 2003). The BET surface of natural ferrihydrites (SCHWERTMANN and FISCHER, 1973) as well as synthetic oxides (EUSTERHUES et al., 2003; KAISER and GUGGENBERGER, 2000; MÖDL et

al., 2007) are negatively correlated with the NOM content. To reduce this effect, one may try to remove the organic matter (KAISER and GUGGENBERGER, 2003; MAYER, 1994; WAGAI et al., 2009). In addition, one may remove the oxide fraction(s) and estimate from the difference the contribution(s) (EUSTERHUES et al., 2005). In the latter procedure, the surface area with oxidic properties present at the edges of clay particles may not be included and measuring a surface area with a method-by-difference may lead to large uncertainties. Moreover, the oxidation of organic matter may change the remaining mineral particles (MAYER, 1994). Another point is the strong dehydration that is part of the BET measurement. This may decrease irreversibly the surface area because small particles in the dry state may have a high area of contact, as found for the nano-colloids of synthetic ferrihydrite (DAVIS and LECKIE, 1978b; DZOMBAK and MOREL, 1990). An alternative approach is the use of ethylene glycol monoethyl ether (EGME) as probe molecule (CIHACEK and BREMNER, 1979) but this conventional method typically measures the surface area of clay mineral fraction (KENNEDY et al., 2002) which includes in particular the surface area of the basal planes. From this perspective, the use of an EGME surface area is problematic if the surface complexation of anions is to be evaluated. Nevertheless, it has been used for scaling MoO_4^{2-} adsorption of soils (GOLDBERG et al., 2002), illustrating the urge for development of better methods.

B) Focusing on iron and aluminum (hydr)oxides in a natural sample, another approach is to measure the amount of reactive solid phase(s) by selective dissolution, and attribute an assumed specific surface area (SSA in m^2/g oxide) to the constituent dissolved (CANCES et al., 2003; DIJKSTRA et al., 2004; EUSTERHUES et al., 2005; GUSTAFSSON, 2001; LOFTS and TIPPING, 1998; LUMSDON, 2004; SCHRODER et al., 2005; WENG et al., 2001). The first step in the procedure is the determination of the iron and aluminum (hydr)oxide content of a soil or aquifer material. Extraction with Dithionite-Citrate-Bicarbonate (DCB) (MEHRA and JACKSON, 1960) is considered to represent the total iron (hydr)oxide content. The most reactive part of the natural (hydr)oxide fraction is usually characterized by the extraction of Fe and Al with acid ammonium-oxalate (RODEN and ZACHARA, 1996; SCHWERTMANN, 1973) or a bicarbonate-citrate-ascorbate (pH = 8) mixture (KOSTKA and LUTHER, 1994; MEIMA and COMANS, 1998). The oxalate extraction is catalyzed by Fe(II) ions and therefore may include Fe(II)/Fe(III) minerals like magnetite (Fe_3O_4) if present (KOSTKA and LUTHER, 1994), whereas this is suppressed or avoided when using ascorbate. The next step in the procedure is transforming the extracted amount of Fe and Al into a corresponding surface area. The specific surface area of the most reactive Fe oxide fraction is usually set equal to the specific surface area of 2-line ferrihydrite (DAVIS et al., 1978a; DZOMBAK and MOREL, 1990) but may also refer to particles with less surface area such as nanogoethite (THOMPSON et al., 2006; VAN DER ZEE et al., 2003). For the Al fraction, a very high surface area has been assumed (DIJKSTRA et al., 2004; GUSTAFSSON, 2001). Assumed is the presence of gibbsite but this Al fraction can also be due to the presence of phyllosilicates (WISEMAN and PUTTMANN, 2006) and other silicates like allophane (GUSTAFSSON, 2001). The Fe-DCB extraction will include the crystalline Fe oxide fraction of natural materials, which may have a considerably smaller surface area than ferrihydrite, for instance a difference of a factor 10. Nevertheless, its contribution may be important because the DCB fraction can be relatively large in certain samples. In top soils, the difference between the Fe fraction extracted with oxalate and total

iron (DCB) may be not very large, while in sub soils the difference may be a factor of about 3 to even 10 (WENG et al., 2001).

C) A third approach to derive the surface area uses SCM with a set of adsorption constants derived for a reference material (representative metal oxide). The method derives the reactive surface area that is needed to explain the experimental adsorption of a natural material with the chosen set of parameters. If adsorption data of heavy metals are used, the major disadvantage is that the metal ion binding in the soil material can easily be dominated by the organic fraction and ion exchange (VOEGELIN et al., 2001; WENG et al., 2001). To assess a realistic reactive surface area for metal oxides, we consider the use of an anion as a probe molecule as the most adequate choice.

In the present paper, a method is discussed that uses a well-chosen probe anion to estimate the effective reactive oxide surface area of natural samples. The distribution of the anion over the solid and solution phase is determined and interpreted using separately determined binding properties of the probe anion for a representative oxide mineral, yielding an effective reactive surface area. The term "effective" is used since it is assumed that the behavior of the natural (hydr)oxide fraction can be represented by a model oxide. A rational is that the collective behavior is strongly dominated by electrostatic properties, which are, -in a first order approach-, rather similar for the various oxides of iron and aluminum. For the model oxide, we have chosen goethite because it is an important iron (hydr)oxide identified in many natural systems (CORNELL and SCHWERTMANN, 1996; THOMPSON et al., 2006; VAN DER ZEE et al., 2003), and an extensive database is available for ion adsorption on goethite derived for the charge distribution (CD) model (HIEMSTRA and VAN RIEMSDIJK, 1996a). Ferrihydrite can be considered as a good or even better alternative. However, a corresponding database for ferrihydrite is not available yet, although a first step in this direction has recently been made (HIEMSTRA and VAN RIEMSDIJK, 2009a). The chosen probe ion is phosphate, since it binds predominantly to metal oxide surfaces. Moreover, phosphate is omnipresent in natural systems in relevant amounts, even if the solution concentration is very low, and its behavior has been studied extensively in literature. To approach the effective reactive surface area successfully, it is essential that the surface complexation model can predict the phosphate adsorption behavior in natural systems. This requires well-defined conditions.

Natural systems are multi-component systems. It implies that many interactions can influence the distribution of an ion over the solid and solution phase. The adsorption of phosphate is influenced by the major cations (Na^+, K^+, Ca^{2+}, Mg^{2+}, Al^{3+}) and major inorganic anions (HCO_3^-, Cl^-, NO_3^-, SO_4^{2-}) of the natural aqueous solution. Ideally, the complicated solution matrix is replaced by a simpler set of solution conditions that minimizes the number of relevant interactions.

In many phosphate extraction methods, ions are added in high concentrations to compete with the phosphate ions adsorbed to natural particles. Electrolytic, acidic, or basic solutions are added to desorb the readily extractable phosphate fraction from soil samples. An inspiring method is based on the carbonate ion as competitor (OLSEN et al., 1954). A solution with a high concentration of $NaHCO_3$ (0.5 M), adjusted to pH 8.5, is used. The added solution will buffer the pH and fix the ionic strength. The created conditions stimulate the phosphate desorption process due to (a) the relatively high pH value of the extraction solution and (b)

the competitive binding of carbonate ions (RAHNEMAIE et al., 2007a). In addition (c), the added (bi)carbonate will reduce the concentration of Ca^{2+} and Mg^{2+} due to precipitation of these ions in solid carbonates. Ca^{2+} and Mg^{2+} ions act cooperative in the phosphate binding when adsorbed (RIETRA et al., 2001a; STACHOWICZ et al., 2008). For the conditions of the extraction, a large part of the natural organic matter (NOM) fraction will dissolve and is removed in the procedure by adding a large excess of activated carbon. Overall, the triple action (a-c) of the 0.5 M $NaHCO_3$ solution in combination with the presence of activated carbon creates conditions that enable a more accurate calculation of the phosphate-oxide interaction.

The aim of this study is to determine the effective reactive surface area of the metal oxide fraction of natural materials and this is the beginning rather than the end of a journey. A series of equilibrations of a soil with $NaHCO_3$ solutions will be carried out for a set of different samples. The competitive phosphate-carbonate ad/desorption process in the samples will be interpreted with the Charge Distribution model (HIEMSTRA and VAN RIEMSDIJK, 1996a), yielding an effective surface area.

With the above approach, for the first time, a procedure is developed that determines for natural samples the effective reactive oxide surface area. This information will be applied in part II (HIEMSTRA et al., 2010) to analyze the effect of the presence of NOM at the surface of natural oxide particles under standardized field conditions, for fertilized top soils simulated by a 0.01 M $CaCl_2$ background electrolyte solution (VAN ERP et al., 1998). This will result in the calculation of an effective NOM density. The combination of determining an effective surface area of oxide particles and an effective NOM density will enable a consistent scaling of SCM to field samples conditions.

2. Materials and Methods

2.1 Soils Samples

From a large collection of representative agricultural top soils of the Netherlands, known as the Copernicus Series (VAN ERP et al., 1998), a subset was chosen. A number of general characteristics of this selection are shown in Table 1. As follows from Table 1, the soil samples cover a wide range of organic carbon contents (~1-15 % OC), clay contents (~3-30 %), pH values (~4-7), DOC (~5-70 mg/L), and aqueous soluble orthophosphate concentrations (~1-30 μM).

2.2 Natural Oxide Fraction

The general set of soil characteristics (Table 1) has been extended with ammonium oxalate extractions to determine the Fe and Al oxide fraction that is strongly related to the smallest particles (RODEN and ZACHARA, 1996; SCHWERTMANN, 1973). The soils were extracted with 0.2 M oxalate of pH = 3.00, i.e. 16.2 g $(COONH_4)_2.H_2O$ with 10.9 g $(COOH)_2.2H_2O$ per liter, for 2 hours in the dark at 22 ± 1 ^oC using a solid-solution ratio (SSR) of 0.05 kg soil/L. The selected soils differ by a factor 10 in the measured Fe and Al contents (Table 1). In almost all soils, oxalate extractable Fe is somewhat higher than the extractable Al. In addition, dithionite-citrate-bicarbonate (DCB) extractions were done to determine the total Fe oxide fraction. Aluminum was also measured in these extracts. Comparing Fe extracted with oxalate and DCB shows that on average the Fe-DCB fraction is about 1.4 times larger, which has previously also been found for other Dutch top soils (WENG et al., 2001). According to Wada (1989), the DCB treatment is thought to extract the same components as the oxalate extraction with the exception of allophane and imogolite, but it extracts in addition crystalline oxy-hydroxides of Fe. Sodium dithionite is a strong reducing agent that solubilizes secondary iron (hydr)oxides, including goethite, hematite, and maghemite. Normally, the reductant-ligand-buffer behavior of the DCB extraction is increased by heating the solution to 70-80 ºC, but also dithionite is capable dissolving the crystalline Fe oxides at room temperature in overnight extractions employing a higher citrate concentration (HOLMGREN, 1967). In the present study, we carried out the dithionite extraction with the bicarbonate buffer solution using the following procedure: a volume of 30 mL of a solution of 0.66 M citrate and 0.11 M sodium bicarbonate was added to polyethylene tubes containing 0.30 g of soil sample. Sodium dithionite (0.64 g) was added to each tube, and the suspensions were shaken overnight (~ 16 h). Next, the samples were centrifuged and the supernatants were removed and stored for Fe and Al analysis. Dissolved Fe, Al, and/or P concentrations in the different extracts were measured by inductively coupled plasma atomic emission spectroscopy (ICP-AES). Blanks with the buffer solution were prepared and the analyses were duplicated in all cases. All extraction experiments were carried out in polyethylene labware to avoid silica contamination, and the temperature was maintained at 22 ± 1 ºC in a constant temperature room.

Table 1. Soil characteristics of the Copernicus series

Soil[*)]	OC[a)]	< 2µm	Fe-ox[b)]	Al-ox[b)]	P-ox[b)]	Fe-DCB[c)]	Al-DCB[c)]	pH[d)]	DOC[d)]	Na^{+}[d)]	K^{+}[d)]	Mg^{2+}[d)]	Ca^{2+}[d)]	$P\text{-}PO_4$[d)]	R_{ev}[e)]	A[e)]	FeNOM[f)]
	%	%	mmol/kg						mgC/L	mM	mM	mM	mM	µM	mmol/kg	m^2/g soil	µmol m^{-2}
1	1.8	5	32.4	34.4	19.6	48	41	4.3	11.6	0.0	0.3	0.3	9.6	30.0	23.0± 0.4	11.3 ± 0.3	1.07 ± 0.04
2	2.2	7	48.5	32.6	22.7	119	39	5.2	19.6	1.2	9.1	0.6	9.3	17.7	27.3± 4.6	14.9 ± 3.0	1.46 ± 0.17
3	3.7	8	342.2	18.6	38.2	852	27	5.6	16.2	0.7	4.1	1.2	8.9	1.6	50.4± 6.0	32.7 ± 4.7	1.27 ± 0.11
4	3.3	11	92.7	32.7	31.5	125	34	5.6	13.7	1.4	7.2	0.8	9.3	6.8	55.4± 3.4	34.0 ± 2.3	1.54 ± 0.00
5	1.3	15	75.7	20.2	14.9	168	30	4.9	19.5	0.5	1.2	0.5	9.5	2.3	9.3± 0.2	5.0 ± 0.1	0.72 ± 0.04
6	1.5	9	42.9	16.4	8.6	68	25	5.0	12.6	0.2	1.8	0.4	9.7	1.9	5.3 ± 0.5	3.1 ± 0.4	0.96 ± 0.19
7	0.9	11	50.3	19.1	14.9	135	27	5.7	8.7	0.5	2.1	0.3	10.0	17.1	14.3± 2.2	6.6 ± 1.4	1.12 ± 0.40
8	3.0	14	95.9	31.1	18.8	101	32	5.0	26.6	0.7	3.3	0.7	9.4	1.6	15.7± 1.2	10.8 ± 0.9	0.83 ± 0.04
9	4.9	21	211.3	27.5	34.9	242	36	4.6	37	2.4	5.3	1.0	8.8	2.6	41.2± 0.6	27.3 ± 0.5	1.23 ± 0.00
10	8.3	25	252.2	46.2	25.7	318	59	4.9	32	1.0	2.2	0.7	9.4	0.6	21.9± 1.7	18.9 ± 1.5	1.48 ± 0.01
11	14.0	28	131.7	57.7	20.3	146	n.d.	5.5	71.7	2.1	5.5	2.3	8.2	2.9	19.4± 1.5	15.2 ± 1.3	1.94 ± 0.03
12	3.3	13	114.4	20.9	30.2	233	29	4.5	23.9	1.3	11.2	0.9	9.0	27.1	42.1± 1.5	23.3 ± 1.0	1.37 ± 0.02
13	1.8	26	64.8	32.2	14.0	178	32	7.2	13.8	1.2	1.4	0.4	10.1	2.3	9.1 ± 0.8	4.5 ± 0.6	0.62 ± 0.27
14	0.6	3	10.5	3.0	7.8	16	6	6.8	4.9	0.3	2.4	0.2	10.1	17.1	9.5 ± 0.6	3.4 ± 0.4	0.41 ± 0.44
15	4.1	28	117.1	38.9	24.0	200	30	6.4	17.7	1.1	3.6	0.8	9.5	5.8	18.7± 1.5	9.8 ± 1.0	1.29 ± 0.13
16	1.0	6	31.4	23.7	15.6	84	34	6.0	6	0.1	3.2	0.2	10.1	9.4	11.3± 0.5	5.2 ± 0.3	1.01 ± 0.13
17	2.9	12	115.7	29.4	40.2	277	32	7.1	12.5	0.5	3.9	0.5	10.0	23.9	47.0± 6.2	23.0 ± 3.7	1.41 ± 0.15
18	2.1	12	67.8	28.8	19.3	116	36	5.6	17.5	1.2	3.1	0.5	10.4	4.2	21.9± 1.4	13.6 ± 1.0	1.53 ± 0.04
19	1.6	17	42.4	29.9	11.2	153	59	6.3	12	0.4	0.7	0.3	10.3	4.2	8.3 ± 0.7	4.4 ± 0.5	1.22 ± 0.21

[*)] Soils with numbers in bold were selected to study of the rate of equilibration

[a)] Organic carbon according to Kurmies.

[b)] 2 hours extraction (solid solution ratio SSR = 0.05 g/L) with 0.2 M oxalate (pH = 3.0), see text.

[c)] Based on Holmgren (1967), see text. n.d. = not determined. The average amount of Al^{3+} bound by the CEC is about 4 ± 3 mmol/kg, which is ~10% of the amount of Al extracted with oxalate or DCB. At precipitation, this amount of Al^{3+} will probably not contribute much to the formation of new surface area.

[d)] Measured in a 0.01 M $CaCl_2$ extract (Solid Solution Ratio SSR = 0.1 kg/L, time = 2 hours, van Erp et al. (1998)).

[e)] Fitted using the 0.5 M $NaHCO_3$ equilibrium data.

[f)] Calculated in order to explain the PO_4 concentration in 0.01 M $CaCl_2$ based on the R_{ev} and A derived from 0.5 M HCO_3 equilibration (HIEMSTRA et al., 2010)

Table 2. Tableau defining the formation reactions of surface species in the CD model using the extended stern layer option with $C_1 = 0.93$ and $C_2 = 0.75$ F/m^2.

Surface species	≡ $FeOH^{-1/2}$	≡ $Fe_3O^{-1/2}$	≡ $HNOM^{-1}$	Δz_0	Δz_1	Δz_2	H^+	Na^+	K^+	Ca^{2+}	Mg^{2+}	Cl^-	PO_4^{3-}	CO_3^{2-}	log$K$
≡ $FeOH^{-1/2}$	1	0	0	0	0	0	0	0	0	0	0	0	0	0	0
≡ $FeOH_2^{+1/2}$	1	0	0	+1	0	0	1	0	0	0	0	0	0	0	9.0
≡ $FeOH^{-1/2}\cdots Na^+$	1	0	0	0	+1	0	0	1	0	0	0	0	0	0	-0.60±0.03
≡ $FeOH^{-1/2}\cdots K^+$	1	0	0	0	+1	0	0	0	1	0	0	0	0	0	-1.61±0.13
≡ $FeOH_2^{+1/2}\cdots Cl^-$	1	0	0	+1	-1	0	1	0	0	0	0	1	0	0	8.55±0.03
≡ $Fe_3O^{-1/2}$	0	1	0	0	0	0	0	0	0	0	0	0	0	0	0
≡ $Fe_3OH^{+1/2}$	0	1	0	+1	0	0	1	0	0	0	0	0	0	0	9.0
≡ $Fe_3O^{-1/2}\cdots Na^+$	0	1	0	0	+1	0	0	1	0	0	0	0	0	0	-0.60±0.03
≡ $Fe_3O^{-1/2}\cdots K^+$	0	1	0	0	+1	0	0	0	1	0	0	0	0	0	-1.61±0.13
≡ $Fe_3OH^{+1/2}\cdots Cl^-$	0	1	0	+1	-1	0	1	0	0	0	0	0	0	0	8.55±0.03
≡ $(FeO)_2PO_2$	2	0	0	0.46	-1.46	0	2	0	0	0	0	0	1	0	29.72±0.01
≡ $FeOPO_2OH$	1	0	0	0.28	-1.28	0	2	0	0	0	0	0	1	0	27.63±0.01
≡ $(FeO)_2CO$	2	0	0	0.62	-0.62	0	2	0	0	0	0	0	0	1	22.01±0.02
≡ $(FeO)_2CO\cdots Na^+$	2	0	0	0.62	0.38	0	2	1	0	0	0	0	0	1	22.03±0.05
≡ $FeOH_2^{+1/2}\cdots CO_3^{2-}$	1	0	0	+1	-2	0	1	0	0	0	0	0	0	1	10.22±0.20
≡ $Fe_3OH^{+1/2}\cdots CO_3^{2-}$	0	1	0	+1	-2	0	1	0	0	0	0	0	0	1	10.22±0.20
≡ $FeOH^{-1/2}Ca^{2+}$	1	0	0	0.31	1.69	0	0	0	0	1	0	0	0	0	3.23±0.05
≡ $FeOH^{-1/2}CaOH^+$	1	0	0	0.31	0.69	0	-1	0	0	1	0	0	0	0	-6.42±0.08
≡ $FeOH^{-1/2}\cdots Ca^{2+}$	1	0	0	0	+2	0	0	0	0	1	0	0	0	0	1.8±0.95
≡ $Fe_3O^{-1/2}\cdots Ca^{2+}$	0	1	0	0	+2	0	0	0	0	1	0	0	0	0	1.8±0.95
≡ $(FeOH)_2^{-1}Mg^{2+}$	2	0	0	0.72	1.28	0	0	0	0	0	1	0	0	0	4.52±0.02
≡ $(FeOH)_2^{-1}MgOH^+$	2	0	0	0.72	0.28	0	-1	0	0	0	1	0	0	0	-6.78±0.07
≡ $FeNOM^{0\text{-}0.5\text{-}1}$ *	1	0	1	1.5	-1	-0.5	0	0	0	0	0	0	0	0	0
$CaCO_3$ (soil) #	0	0	0	0	0	0	0	0	0	1	0	0	0	1	logK_{so} = -8.4

*Not used for the speciation calculations in the $NaHCO_3$ extracts, because of the assumed absence of interaction of NOM. The site density N_{HNOM} (Table 1) of the hypothetical species ≡ FeNOM has been calculated using eq.(1) in part II (HIEMSTRA et al., 2010), interpreting the PO_4 concentration in 0.01 M $CaCl_2$ solution. The charge at the 0-, 1- and 2-plane after formation of FeNOM is respectively 0, -1, and -0.5 v.u. which is created by redistribution of the total reference charge of -1.5 v.u., see text in part II (HIEMSTRA et al., 2010).

For the Bakers Hill soil, logK_{so} = -7.3 has been used.

2.3 Phosphate Desorption

The competitive desorption method for phosphate that was used in this study is based on the phosphate extraction method with bicarbonate used by Barrow and Shaw (1976a; 1976b). The phosphate desorption has been carried out by adding a freshly prepared 0.50 M $Na(H)CO_3$ solution (pH 8.5) to soils creating different solid/solution ratios (SSR). The 0.50 M $Na(H)CO_3$ solution was freshly prepared by dissolving 42.4 g $NaHCO_3$ (Merck PA) per liter. The pH of this solution has been adjusted to pH 8.50 by pipetting about 8-10 mL/L of a 2 M NaOH solution (8 g NaOH / 100 mL). A set of commercial buffers of pH 7 and pH 9 or 10 was used to calibrate the pH meter used. Note that the extraction solution is supersaturated with respect to atmospheric CO_2 and significant escape of CO_2 should be prevented.

For each soil, a series with a solid-solution ratio (SSR) of 1/5, 1/20, 1/50, 1/100, 1/200, and 1/300 kg/L was prepared by adding *x* g air-dry soil to *y* mL 0.50 M $Na(H)CO_3$ solution in low-density polyethylene bottles according to *x* g / *y* mL = 2.0 g soil /10 mL (50 mL bottle), 1.0 g /20 mL (50 mL bottle), 1.0 g /50 mL (100 mL bottle), 1.0 g /100 mL (100 mL bottle), 1.0 g /200 mL (250 mL bottle), and 0.5g /150 mL (250 mL bottle). To suppress or remove the competitive interaction of NOM, 0.40 g of activated carbon (Merck PA) per gram of soil sample was added to the suspensions. It turned out that this activated carbon contained unfortunately some phosphate soluble in 0.5 M $Na(H)CO_3$. Therefore, the calculated phosphate loading was later corrected (< 2-5 %) for this. For a subset of six soils, the reaction kinetics has been studied separately by extracting the samples for 4, 24, 48, 100, and 360 hours.

The suspensions were shaken very gently to avoid abrasion that could change the amount of extracted PO_4, if new surface area would be created. A reciprocal shaker with a mild motion (~30 cycles /min) was used for the gentle mixing of the soil suspensions. The final reaction time was fixed at 10 or 15 days (~240 or 360 hours), based on the above-mentioned study of the kinetics of the phosphate desorption. After equilibration, the soil suspensions were centrifuged to separate supernatant and solid. The sampled supernatant was carefully acidified to pH 2.0 by pipetting a calibrated volume of 1 M HCl and additionally diluted with 0.01 M HCl if necessary. The acidified (diluted) supernatant was analyzed spectrophotometrically for orthophosphate applying a molybdenum-blue method using a Segmented Flow Analysis (SFA) device.

For a number of samples, the pH values of the soil suspensions have been checked after completion of the experiment to ensure that the conditions of the soil suspensions were not changing throughout the experiment. Since Ca, Mg, and Si potentially may interfere in the phosphate-adsorption process, these concentrations have also been measured in the extracts of a limited number of samples using ICP-AES.

2.4 Surface Complexation Modeling

Surface complexation models are based on thermodynamic principles that do not require an exclusive molecular picture. It implies that a good model description can be found using surface species that have no link to the microscopic state. If the challenge is to use

realistic surface species, as observed with spectroscopic methods, many of these SCM cannot be used, because the framework to define such realistic species is not suitable enough. For instance, in the generalized two layer (GTL) model (DZOMBAK and MOREL, 1990), the interface is simplified to a surface plane and a diffuse double layer (DDL) that neutralizes the surface charge. This conceptual structure does not allow distinguishing inner- and outer-sphere complexation. The same can be said with respect to the constant capacitance (CC) model in which the double layer is simplified to an electrical capacitor. More realistic is the use of a DDL with at least one Stern layer (STERN, 1924), resulting in a basic or an extended Stern layer model (WESTALL and HOHL, 1980). Many SCM's use a generic reactive site, SOH^0, that can be traced back to the work of Parks and DeBruyn (1962). For Fe and Al (hydr)oxides, the generic site (SOH^0) is actually a combination of two surface groups ($SOH^{-1/2}$ and $SOH_2^{+1/2}$) as pointed out by Hingston et al. (1968). The use of a generic SOH^0 site will lead by definition to an incorrect formulation of ion complexation reactions such as mono-, bi-, and tetra-dentate complex formation (HIEMSTRA and VAN RIEMSDIJK, 1999a).

A specific problem in the use of realistic surface species has been the reduction of the charge of surface complexes to a single point charge. This simplification strongly affects the computation of the electrostatic interaction energy and ignores that a surface species experiences the gradient of the electrostatic potential in the compact part of the double layer. The charge distribution (CD) concept can be used to account for this phenomenon (HIEMSTRA and VAN RIEMSDIJK, 1996a). In this model approach, part of the formal charge of an inner sphere complex is attributed to the surface and the remaining part is present at some distance from the surface. It has been shown that the interfacial charge distribution is strongly linked to the molecular structure of inner sphere surface complexes (HIEMSTRA et al., 2004; HIEMSTRA and VAN RIEMSDIJK, 2006; HIEMSTRA and VAN RIEMSDIJK, 2007; RIETRA et al., 1999a).

In the present evaluation of the reactive surface area, the CD model (HIEMSTRA and VAN RIEMSDIJK, 1996a) will be used. As pointed out, it has the advantage that one may use realistic surface species as observed with spectroscopy and the model is able to describe successfully ion interactions in multi-component systems as recently demonstrated in the work of Stachowicz et al. (2008). Another advantage is that the model has been extensively parameterized in a consistent manner for a large number of ions that may bind to a high-surface area goethite. The parameter set covers at present the major cations (Na^+, K^+, Ca^{2+}, Mg^{2+}, Al^{3+}, Fe^{2+}), major anions (Cl^-, HCO_3^-, NO_3^-, SO_4^{2-}), and neutral species ($H_4SiO_4^0$) that are present in the natural aqueous phase and may interact with additionally present ions such as phosphate and many others minors.

The primary surface charge of goethite can be described by proton binding to two types of surface groups, which are singly ($\equiv FeOH^{-1/2}$) or triply ($\equiv Fe_3O^{-1/2}$) coordinated to Fe in the solid (Table 2). The effective site density is set at respectively N_s = 3.45 nm^{-2} and N_s = 2.7 nm^{-2} (HIEMSTRA et al., 1996b). The charged surface groups may interact with electrolyte ions forming ion pairs and in addition, they may form innersphere complexes with other ions. Both types of surface complexes are located differently in the electrostatic double layer (EDL).

As mentioned, the simplest but realistic EDL approach comprises a diffuse double layer (DDL) that is separated from the surface by a Stern layer. At the surface, the primary protons reside, and the charge of electrolyte ion pairs can be attributed to the other electrostatic plane

(1-plane). This plane represents the minimum distance of approach of electrolyte ions (ion pairs). According to the CD model (HIEMSTRA and VAN RIEMSDIJK, 1996a), the charge of the innersphere complexes can be distributed between the planes at either side of the Stern layer. Recently, it has been suggested for goethite that the head end of the DDL is separated from the minimum distance of approach of indifferent electrolyte ions by a second Stern layer (HIEMSTRA and VAN RIEMSDIJK, 2006; RAHNEMAIE et al., 2006). The physical explanation is the increasing ordering of water molecules in one or several layers near the surface, which only allows a stepwise penetration of electrolyte ions into the compact part of the EDL (HIEMSTRA and VAN RIEMSDIJK, 2006). The resulting double layer representation has three planes (0-, 1-, 2-plane) and two Stern layers with a capacitance of C_1 = 0.93 F/m^2 and C_2 = 0.74 F/m^2 (Table 2). The model can be called an Extended Stern layer model (WESTALL and HOHL, 1980) and is very similar to the recently adapted Triple Layer (TL) model (SVERJENSKY, 2005).

For goethite, the pH dependent adsorption behavior of phosphate has been studied extensively (RAHNEMAIE et al., 2007b). The goethite-phosphate interaction can be described using two surface species (Table 2). In-situ FTIR spectroscopy (TEJEDOR-TEJEDOR and ANDERSON, 1990) suggests the dominant presence of a bidentate double corner complex ≡ $(FeO)_2PO_2$. According to Rahnemaie et al. (2007b), a protonated monodentate complex (≡ $FeOPO_2OH$) may additionally form at high loading and low pH. The monodentate species explains the CD value that emerges from the data analysis of the phosphate adsorption (RAHNEMAIE et al., 2007b). The reactions can be expressed in terms of reference components, leading to:

$$2 \equiv FeOH^{-1/2} + PO_4^{3-}(aq) + 2H^+(aq) \Leftrightarrow \equiv (FeO)_2^{-1+\Delta z_0} PO_2^{\Delta z_1} + 2\,H_2O(l) \quad K_{(FeO)_2PO_2} \qquad (1a)$$

and

$$1 \equiv FeOH^{-1/2} + PO_4^{3-}(aq) + 2H^+(aq) \Leftrightarrow \equiv FeO^{-1/2+\Delta z_0} PO_2OH^{\Delta z_1} + 1\,H_2O(l) \quad K_{FeOPO_2OH} \qquad (1b)$$

The charge distribution of these surface complexes (Δz_0, Δz_1) has been derived from the geometry of the surface complexes that has been obtained by molecular orbital calculations (MO) using Density Functional Theory (DFT).

The phosphate-bicarbonate interaction has been studied for goethite in the concentration range 0-0.5 M (H)CO_3 (RAHNEMAIE et al., 2007a). The main carbonate surface species is a bidentate double corner complex (BARGAR et al., 2005; HIEMSTRA et al., 2004). Its formation can be written as:

$$2 \equiv FeOH^{-1/2} + CO_3^{2-}(aq) + 2H^+(aq) \Leftrightarrow \equiv (FeO)_2^{-1+\Delta z_o} CO^{\Delta z_1} + 2\,H_2O(l) K_{(FeO)_2CO} \quad (2a)$$

For this complex, the charge distribution has also been derived from the MO-DFT optimized geometry (RAHNEMAIE et al., 2007a).

CD modeling (RAHNEMAIE et al., 2007a) suggests that the carbonate complex (eq. (2a)) may interact at a high electrolyte concentration with a Na^+ ion leading to:

$$2 \equiv FeOH^{-1/2} + CO_3^{2-}(aq) + 2H^+(aq) + Na^+(aq) \Leftrightarrow \equiv (FeO)_2^{-1+\Delta z_o} CO\text{-}Na^{\Delta z_1} + 2\,H_2O(l) \quad K_{(FeO)_2CO\text{-}Na} \quad (2b)$$

In addition, the protonated surface groups may interact with CO_3^{2-} forming outersphere complexes (BARGAR et al., 2005), i.e. $\equiv FeOH_2^{+1/2}$ - CO_3^{2-} and $\equiv Fe_3OH^{+1/2}$ - CO_3^{2-} (Table 2). The adsorption of phosphate and also carbonate may be influenced by the presence of Ca^{2+} (RIETRA et al., 2001a; STACHOWICZ et al., 2008). In a 0.5 M $NaHCO_3$ solution, the Ca^{2+} activity is rather limited by the formation of solid $CaCO_3$ (s). In soil, part of the Ca^{2+} ions are initially adsorbed by organic matter and clay and will be released by ion exchange when $NaHCO_3$ is added in a high concentration. CD modeling suggests that calcium ions may bind as inner- and outer-sphere complexes at the goethite surface (RIETRA et al., 2001a; STACHOWICZ et al., 2008). For Mg^{2+}, only the formation of a bidentate innersphere surface complex can be resolved (STACHOWICZ et al., 2008). For the divalent cations, the model has been calibrated on proton titration data (RAHNEMAIE et al., 2006) in the presence of Ca^{2+} and Mg^{2+} and has been tested on a collection of Ca^{2+} and Mg^{2+} adsorption data given in Stachowicz et al. (2008). The present parameter set for Ca^{2+} and Mg^{2+} slightly differs from the set of Stachowicz et al. (2008) to be consistent with the other parameters that refer to a goethite with a slightly lower PZC (RAHNEMAIE et al., 2007a; RAHNEMAIE et al., 2007b). The parameters are given in Table 2.

The surface complexation modeling was done with the ECOSAT software (KEIZER and VAN RIEMSDIJK, 1998) in combination with FIT (KINNIBURGH, 1993). The aqueous speciation reactions used are given in the Appendix.

3. Results and Discussion

3.1 Desorption Kinetics

Barrow and Shaw (1976b) studied extensively a number of factors that can affect the phosphate extraction by bicarbonate, such as the time dependency of desorption. Initially, the phosphate desorption rate was quite high, slowed down in some hours, but the desorption starts to reverse at prolonged extraction times (~ 10-200 hours). This effect was stronger at high solid-solution ratios. This remarkable behavior may be due to the pretreatment of the samples. These samples originated from a virgin soil but were loaded artificially with phosphate in the lab. Although these samples were incubated for two years, the artificial P-loading may have led to a relatively high saturation of particularly the external surfaces leaving the core of the (micro) aggregates relatively unaffected. At prolonged times of extraction, the soil particles may progressively disintegrate, leading to the exposure of pristine surfaces, previously not sufficiently loaded with phosphate. The gradually uncovered surfaces may adsorb some phosphate that has been released in the extraction from the higher loaded parts. The increased exposure of a soil due to abrasion is supported by an additional observation (BARROW and SHAW, 1975) showing that vigorous shaking of these preloaded soil samples led to more phosphate binding to probably previously internal surface area.

In the present work, the soil samples have been loaded with phosphate in nature during long-term agricultural practices. We expect that this will lead to a more even distribution over external and internal surfaces. Six samples for our collection were selected randomly to study the desorption kinetics. The time dependency of the bicarbonate extraction was studied for different solid/solution ratios. The effect of varying the SSR is shown in Fig.1a for soil sample S2 in detail, and in Fig.1b, it is shown for all six soils that were selected to study the kinetics.

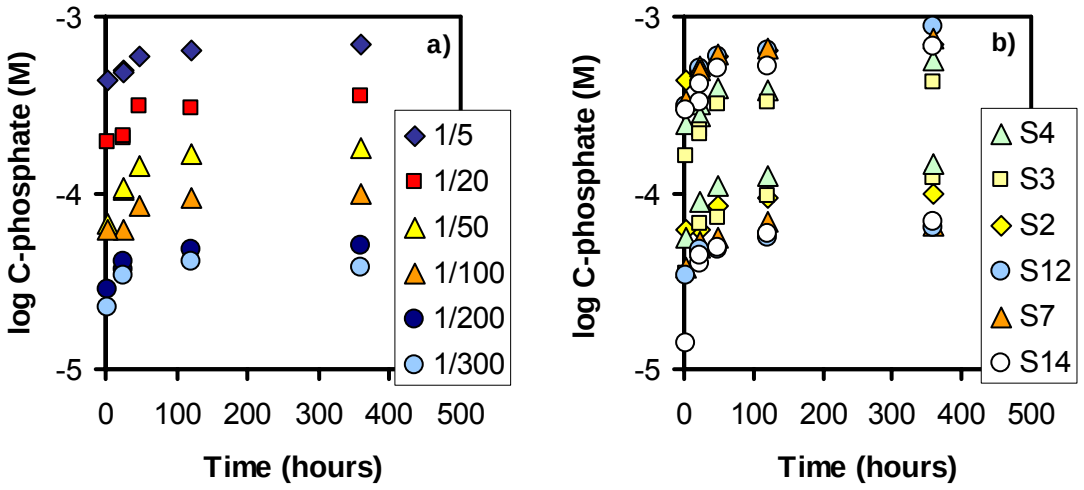

Fig.1 a) Time dependency of the release of phosphate from a soil sample (S2) extracted with 0.5 M bicarbonate (pH = 8.5) at various solid-solution ratios (SSR) and b) the desorption kinetics for a selected set of samples for SSR = 1/5 (highest set of concentrations) and 1/100 kg/L (lowest set of concentrations).

Fig.1a shows an instant release of phosphate when the bicarbonate solution is added. It is followed by an additional increase of the concentration to an apparent equilibrium state that is approached at longer time scales. In Fig.1b, the desorption kinetics are shown for six samples using a SSR of 1/5 and 1/100 kg/L. In contrast to the results shown by Barrow and Shaw (1976b), no re-adsorption of phosphate and corresponding decrease of the phosphate concentration is observed at prolonged periods of shaking. This may point to more homogeneity in the P distribution over the soil matrix and less abrasion of the soil material. Based on the measurements, further experiments were done using for most samples 360 hours (15 days) of equilibration. Some samples were equilibrated for 10 days.

3.2 Mechanism

A remarkable characteristic of the desorption process is the fast initial release that depends on the SSR. This fraction of phosphate can be interpreted as bound at external surfaces of soil oxides. The further release of phosphate may come from interior parts of the metal oxide aggregates. Slow release of phosphate is generally observed in soils that are extracted with a low or very low solid-solution ratio, forcing phosphate to diffuse out of the porous matrix to meet ultimately an equilibrium criterion at a low PO_4 concentration. In case of extraction of soils with a low-solid solution ratio using water or a simple electrolyte solution such as 0.01 M $CaCl_2$, the phosphate desorption is usually very slow (KOOPMANS et al., 2004). If explained in terms of diffusion, it is due to the small gradient of the phosphate concentration within the aggregates. As described later, embedding of oxide particles in a condensed matrix of natural organic matter molecules may also contribute to the kinetic behavior. A low SSR will ultimately lead to a large release of phosphate, but the rate of desorption is quickly reduced because a little decrease of the loading already leads to a strong decrease of the equilibrium concentration. This follows from the high-affinity character of the phosphate adsorption isotherm. The low phosphate concentrations created in the interior of the aggregates will make the diffusion gradient and corresponding rate (very) low.

To improve the efficiency of desorption, one may add a competitive ion. In our case, bicarbonate ions are used. If added in a high concentration, these ions will quickly diffuse into the porous matrix and desorb phosphate locally, resulting in a relatively high PO_4 concentration in the interior and a corresponding relatively large concentration gradient and rate of diffusion. Moreover, the competition between carbonate and phosphate will change the shape of the adsorption isotherm. It will get a less high-affinity character, which will maintain for a longer time a high gradient and corresponding rate of diffusion. The presence of the competitor in the interior may also lead to redistribution of PO_4 inside the porous micro-aggregates that are internally not in equilibrium state. This process may also contribute to the observed decrease of the phosphate concentration in $NaHCO_3$ extracts of a rapidly P-loaded soil sample at prolonged times of equilibration as used by Barrow and Shaw (1976b).

A kinetic process with two-steps has also been found in some studies of the adsorption of phosphate by synthetic mineral oxides (LUENGO et al., 2006; TORRENT et al., 1990). The data presented by Strauss et al. (1997) revealed that many iron oxides have a fast initial adsorption process, followed by a slower process that may last for several days or even weeks. There is still some controversy about the mechanisms involved in the slow process,

but Torrent et al. (1992) suggested that this slow step is a slow diffusion of phosphate to the surface of pores located between domains of contiguous crystals or between aggregated particles. The ATR-IR results found by Luengo et al. (2006) are compatible with this mechanism for the slow adsorption process, which allow them to conclude that the surface complexes formed after the first minutes of reaction migrate rather slowly into the pores of the mineral surface without changing appreciably their identity.

3.3 Phosphate Loading and Buffering

Fig.2 illustrates the change of the phosphate concentration (*c*) in the $NaHCO_3$ solution at near-equilibrium conditions upon varying the SSR for 5 representative soils. The highest phosphate concentrations are found at the highest SSR. These concentrations differ by a factor 20 for the samples in our data set. It illustrates that the chosen soils will clearly differ in phosphate loading per unit surface area. As will be shown later, the PO_4 loading is between about 1-3 μmol/m^2 in our soils.

As follows from the graph, the concentrations decrease when the solid/solution ratio decreases. If the solid would not release any phosphate, a linear curve is expected because then only dilution of the free soil solution takes place. In the log-log plot of Fig.2, the slope of a linear dilution curve is 1, equal to the slope of the dotted line. The trend in the data deviates from such a linear curve, most strongly at the highest solid-solution ratios. This is due to a non-linear release of PO_4 from the soil matrix at dilution of the sample (lower SSR). It may be expected that soils with the lowest variation in the phosphate concentration, i.e. the highest buffering, will have a relatively high reactive surface area. This is discussed next.

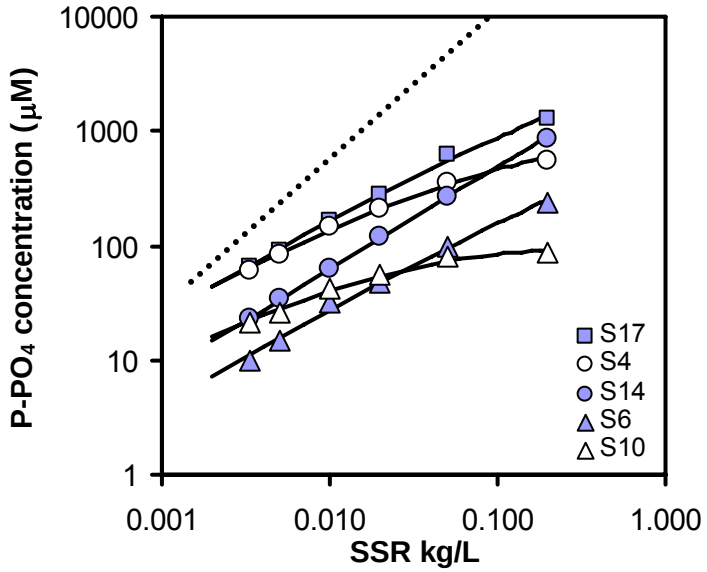

Fig.2 The change of the phosphate concentration as a function of the solid-solution ratio in 0.5 M $NaHCO_3$ at pH 8.5 for soils that differ in non-linear phosphate buffering because of differences in reactive surface area. The full lines are fitted to the CD model using Table 2. Saturation of the solution with calcite was assumed. The dotted line represents a linear dilution curve.

3.4 Solid-solution Distribution

For a given adsorption behavior, the deviation from the linear dilution curve is related to the amount of effective reactive surface area A (m^2/kg soil) available in the sample. In the probe-ion extraction, the total amount of phosphate per unit mass that can be bound reversibly (R_{ev} in mole per kg soil) is a constant, given by the field conditions in the soil when sampled. The total amount of reversible phosphate is distributed over solid and solution during equilibration, which leads to the following mass balance:

$$R_{ev} = A\,\Gamma + \rho^{-1} c \tag{3}$$

in which Γ is the phosphate adsorption per unit effective reactive surface area (mol/m^2), and ρ is the solid solution ratio SSR (kg/L). When the SSR (ρ) is lowered, the experimental phosphate concentration (c) in solution will decrease (Fig.2). This will lead to a lower phosphate adsorption (Γ). If the adsorption isotherm (i.e. the relation $\Gamma \leftrightarrow c$), expressed per unit surface area is known, we may calculate the effective reactive surface area A (m^2/kg soil) from:

$$A = \frac{\Delta(\rho_i^{-1} c_i)}{\Delta\Gamma_i} \tag{4}$$

in which Δ indicates the change of the indicated parameter values with index i = 1, 2. Once A is calculated, we may also find the total amount of phosphate that is reversibly adsorbed by the sample (R_{ev}). Interestingly, the total amount of reversibly adsorbed phosphate (R_{ev}) can be found even though only a small fraction of the total amount is extracted and redistributed over the solid and solution phase in the equilibrium state. To find R_{ev}, a total extraction is not at all required. Only correct numbers for A and R_{ev} will be found if the actual phosphate adsorption isotherm of the material (i.e. the equilibrium relation $\Gamma \leftrightarrow c$) is sufficiently accurately approached for the conditions applied. In our approach, Γ is calculated with the CD model for every experimental value of c. In principle, a minimum of two concentrations is sufficient to calculate the effective reactive surface area (eq.(4)), but in the present approach, we have used six different solid-solution ratios (ρ). The reason is that the fitted parameters are sensitive to small variations in the experimental concentration.

Before applying the probe-ion method to our samples, we tested the ability of the CD model to describe the competitive phosphate adsorption behavior for a soil at pH 8.5 as a function of the $NaHCO_3$ solution concentration. Such experimental data are available in literature for an Australian soil from Bakers Hill (BARROW and SHAW, 1976b) as given in Fig.3. The pristine soil has been incubated in advance with phosphate and aged at 70 °C. The experiments have been carried out at different solid-solution ratios. The ionic strength has been kept constant at 1 M by adding additional NaCl. Unfortunately, the extraction time has been only 16 hours.

The data show a strong influence of the HCO_3^- concentration, which is most significant in the concentration range below about 0.5 M. However, the highest PO_4 desorption (per unit mass of soil material) is for the lowest solid-solution ratio, where the low concentration nevertheless represents a large amount of phosphate because of the relatively large solution volume per unit mass. As shown by Barrow and Shaw (BARROW and SHAW, 1976b), the maximum desorption is about 30 % of the initially added P when extracted at a SSR of 1:300. In case of a SSR of 1:6, the maximum desorption is only about 15 % in 0.5 M $NaHCO_3$. In other words, most of the phosphate (>70 to >85 %) remains bound.

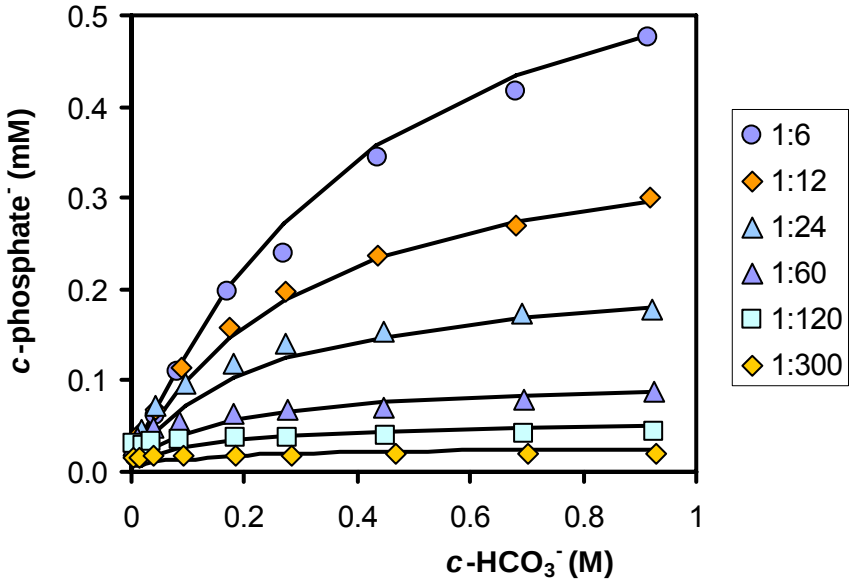

Fig.3 Effect of bicarbonate concentration and soil-solution ratio on the phosphate concentration equilibrated for 16 hours with soil of Bakers Hill (BARROW and SHAW, 1976a; BARROW and SHAW, 1976b). The lines show the simulated phosphate concentrations in the extraction solutions (a mixture of NaCl and $NaHCO_3$, I = 1 M) using the CD model and the parameters of Table 2. Saturation of the solution with $CaCO_3.H_2O$ (s) was assumed (see text).

3.5 Modeling

The adsorption of carbonate by the soil of Bakers Hill (Fig.3) has been modeled with the CD model using the parameters of Table 2. The effective reactive surface area (A m^2/kg soil) was the only adjustable parameter in eq. (3) in combination with the amount of reversibly bound phosphate (R_{ev} mol/kg). It may be assumed that the Ca^{2+} activity in the $(H)CO_3$ solutions (pH = 8.5) is controlled by a $CaCO_3$ phase. The lowest calcium carbonate solubility is for calcite (log K_{so} = -8.4). However, well-crystallized calcite may not be instantaneously formed at precipitation. A more soluble meta-stable $CaCO_3$ .x H_2O phase may form first. Amorphous calcium carbonate as well as mono- (x = 1), and hexa-hydrated (x = 6) calcium carbonate are more soluble. The reported solubility products are respectively log K_{so} = -6.4, -7.2, and -7.6 (BRECEVIC and KRALJ, 2007). To asses the solubility product that may be appropriate for the calcium carbonate freshly formed in the $NaHCO_3$ extraction solution of the Bakers Hill soil (Fig.3), we have fitted simultaneously also the calcium carbonate solubility, leading to logK_{so} = -7.4 ± 0.1. This number is close to the solubility of $CaCO_3.H_2O$

(s). This mineral can be found in dynamic lake sediments and is relatively stable if ions such as Mg^{2+} are present (BRECEVIC and KRALJ, 2007). The effective reactive surface area of the Baker Hill soil that has been fitted equals $A = 5.5 \pm 0.1$ m^2/g soil. The quality of the fit (Fig.3) shows that the CD model is able to describe the competition of phosphate and carbonate in a soil in $NaHCO_3$/NaCl solutions at pH 8.5. We note that the further modeling indicated that the influence of Ca^{2+} is limited to those systems of Fig.3 that have the lowest $(H)CO_3$ concentrations but correspondingly the highest Ca^{2+} activities. The Ca^{2+} ions, when adsorbed, promote the adsorption of PO_4 (RIETRA et al., 2001a) and suppress the phosphate concentration.

As mentioned above, the fitted surface area should be considered as an effective reactive surface area. The behavior of the soil oxide fraction is effectively represented by the behavior of the goethite mineral for which the model has been calibrated. The effective surface area (A) of the soil (m^2 / g soil) can be transformed into an effective specific surface area (SSA) for the metal oxide fraction of the soil (m^2 /g oxide). The free Fe and Al content, extractable with the method of Coffin (COFFIN, 1963) is 2 mg Fe/g and 1.8 mg Al/g soil (BARROW and SHAW, 1975), equivalent with approximately 8 mg oxide / g soil. This results in a SSA of about 700 m^2/g sesquioxides. It suggests that the reactive metal oxide fraction in this soil consists of very small oxide particles with a SSA, which is typically for ferrihydrite (HIEMSTRA and VAN RIEMSDIJK, 2009a).

The amount of reversibly bound phosphate equals $R_{ev} = 11.1 \pm 0.1$ mmol/kg, when fitted simultaneously with A. This number is slightly lower than the amount of PO_4 added to the pristine soil, i.e. 400 μg P/g soil or ~13 mmol/kg. It suggests that more than ¾ of the added PO_4 can be recovered. A lower recovery might be due to non-equilibrium or some of the phosphate has been transformed into an insoluble mineral fraction.

3.6 Data Copernicus Soil Series

For some of our own soil samples, we have measured the Ca^{2+} concentration in the (bi)carbonate extract after equilibration for 10-15 days, revealing an apparent $CaCO_3$ solubility product of $\log K_{so} = -8.5 \pm 0.3$. Within the error, this number is equal to the solubility product of calcite. It deviates from the above apparent $\log K$ value for freshly precipitated $CaCO_3$ which may be due to difference in aging (16 hours versus 10-15 days). In the further calculations, we have used for our soils the solubility of calcite, but we note that the effect of Ca^{2+} is minor for soils in 0.5 M $NaHCO_3$.

In the extracts, the Si concentrations were in general between ~ 0.2 - 2 mg Si/L and about 2-10 times lower than the phosphate concentrations. Based on modeling (HIEMSTRA et al., 2007), it is expected that in our soils the relatively low Si level will have no important influence of the phosphate loading.

The total amount of reversibly bound phosphate (R_{ev}) and the effective surface area (A) have been fitted for each sample. The quality of the fit (n = 6 data points) was usually high (R^2>0.98-0.99). As illustration, the model descriptions are shown as lines for the selected soils in Fig. 2. We have evaluated our data using for the phosphate concentration the linear and the logarithmic scale. The fitted average values of A and R_{ev} are presented in Table 1. The

given deviation (±) is related to the chosen scaling of the concentration. For our set of soils, the effective reactive surface area varies by a factor of about 10 and is between about 3 and 30 m^2/g soil. The total amount of reversibly bound phosphate R_{ev} also varied strongly amongst the samples. When expressed per m^2 oxide surface, the phosphate loading in the soils differs by about a factor 2-3, covering the range $R_{ev}/A = \Gamma \approx$ 1-3 μmol/m^2. Considering the high affinity character of the phosphate adsorption isotherms ($\Gamma \leftrightarrow c$) in a $CaCl_2$ solution (BARROW et al., 1980), this variation in Γ is remarkably high compared to the relatively small variation in the equilibrium concentration (c) of phosphate in 0.01 M $CaCl_2$ (c ≈ 1-30 μM) and pH (4-7). The larger variation in phosphate loading is due to the interaction with NOM, as is further discussed in more detail in Part II of this series (HIEMSTRA et al., 2010).

3.7 Reversibly Adsorbed Phosphate

The reversibly bound phosphate content R_{ev} (mmol/kg) can be compared with the phosphate fraction that is found by other approaches such as an extraction with ammonium oxalate. This comparison is shown in Fig.4. The data in the lower range are often slightly above the 1:1 relationship (dotted line), i.e. more PO_4 is extracted with oxalate. If an enhanced extraction of PO_4 with oxalate is realistic for these soils, it may point to a contribution of phosphate from another source. Oxalate dissolves simultaneously Fe and Al ions and this dissolution may release some additional phosphate that is otherwise present in the soil matrix as for instance occluded phosphate (WALKER and SYERS, 1976) or as phosphate being part of a mineral phase or a co-precipitate. The latter has been proposed for highly fertilized soils (VANDERZEE and VANRIEMSDIJK, 1988), marine sediments (HYACINTHE and VAN CAPPELLEN, 2004), and lake and ground waters (GRIFFIOEN, 2006; LIENEMANN et al., 1999; WOLTHOORN et al., 2004).

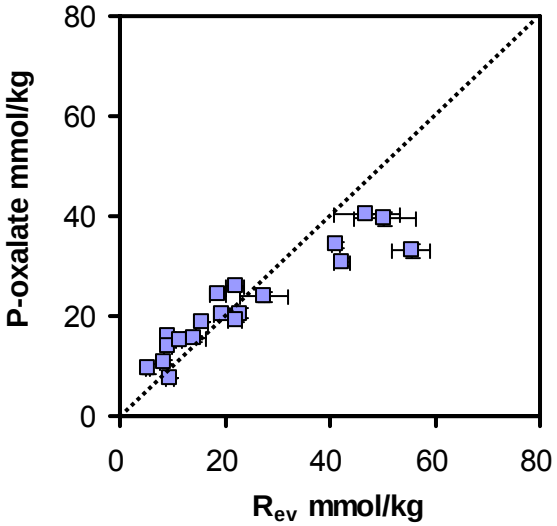

Fig.4. The amount of phosphate extracted with ammonium oxalate (P_{ox}) in relation to the calculated amount of reversibly adsorbed phosphate (R_{ev}). The dotted line represents the 1:1 relationship. In case of high phosphate contents, a higher amount of reversibly bound P is calculated than found with oxalate.

At high phosphate contents, the predicted total amount of reversibly bound PO_4 (R_{ev}) is in some cases significantly larger than the amount found in the oxalate extract, in particular if the data are evaluated on a linear concentration scale for phosphate in the $NaHCO_3$ experiments. For a given P-loading per unit surface area (μmol/m^2), a slightly higher amount of calculated PO_4 (R_{ev}) will also imply the calculation of a slightly too high surface area. It is possible that the assumed phosphate adsorption behavior (model) is not entirely reflecting the actual adsorption properties of the natural oxide fraction and this can be due to many factors, including an incomplete removal of adsorbed NOM. This problem cannot be solved yet but needs future attention.

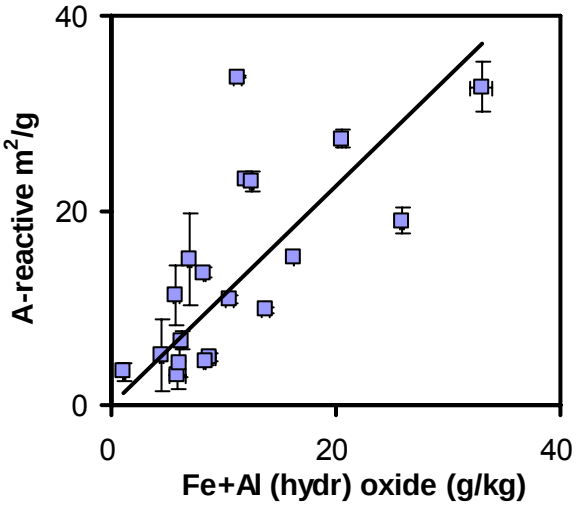

Fig.5. The effective reactive surface area *A* as a function of the amount of Fe and Al (hydr)oxide (g/kg) extractable with ammonium oxalate, assuming a molar mass of 89 and 78 g/mol for respectively Fe and Al (hydr)oxide. The slope of the full line represents the mean specific surface area.

3.8 Surface Area and Specific Surface Area

The effective reactive surface areas calculated for our soils are only weakly correlated ($R^2 = 0.45$ for $n = 19$) with the oxalate extractable fraction of Fe and Al (Fig.5, full line). A similar result is found when using the DCB extractable Fe and Al fraction (not shown). A low correlation is expected if variation exists in the size of the oxide particles and its corresponding effective specific surface area (SSA). The mean effective SSA is represented by the slope of the line in Fig.5. Between the samples, the effective SSA differs by about a factor 5.

As mentioned in the Introduction, the surface area of soil oxides is often calculated based on a Fe and Al (hydr) oxide extraction and an assumed SSA. If the surface areas are scaled to the amount of Fe and Al (hydr) oxides extractable with oxalate, the average SSA is about 1000 ± 790 m^2/g. If scaled on the amount of (hydr) oxides extractable with DCB, the average SSA equals 720 ± 540 m^2/g. The high value of the SSA suggests the presence of very small (hydr)oxide particles and the very large variation indicates that no single SSA can be used for the natural oxide fraction to asses the reactive surface area based on Fe and Al extraction methods.

The above-calculated SSA is based on an assumed molar mass of M = 89 g/mol Fe (goethite) and M = 78 g/mol Al (gibbsite). However, it has been shown very recently (HIEMSTRA and VAN RIEMSDIJK, 2009a) that nanoparticles have an enhanced molar mass. This effect is about 15% for nanoparticles of this small size and corresponding large SSA. Therefore, the average SSA will actually be slightly smaller, i.e. about ~ 630 ± 470 m^2/g (DCB). The thus-scaled SSA values are shown on the y-axis of Fig.6.

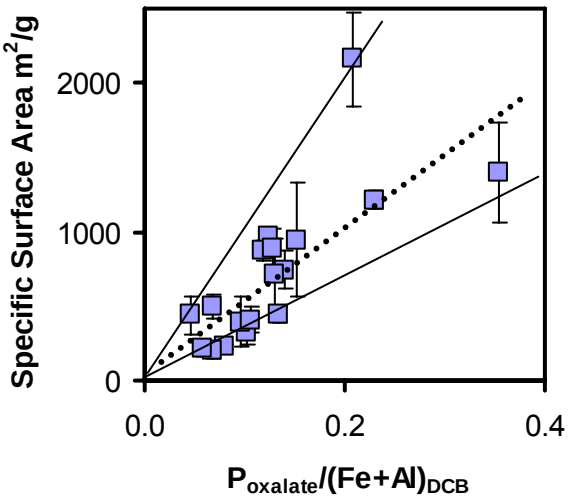

Fig.6. The calculated effective specific surface area of natural metal oxide particles in agricultural top soils as a function of the phosphate loading, defined as the ratio of oxalate extractable phosphate (mmol/kg) and amount of iron and aluminum extractable with DCB (mmol/kg). The dotted line refers to a phosphate loading of 2 μmol/m^2 at the surface of an oxide with a molar mass of 100 g/mole in the case that all phosphate is reversibly bound. The upper and lower full lines are for a loading of 1 and 3 μmol/m^2 respectively.

If expressed in an equivalent diameter (d) for non-porous spherical particles with a typical mass density ρ of 3.5 g/cm^3 (HIEMSTRA and VAN RIEMSDIJK, 2009a), the effective diameter varies between d ~ 1-10 nm when calculated with $d = 6 / (\rho\ SSA)$. Most samples in our study have an effective particle size that is typical for synthetic ferrihydrites. For instance, the particle size of freshly-prepared two-line ferrihydrite varies between about 1.5 and 3.0 nm (MURPHY et al., 1976), while for 6-line ferrihydrite the numbers are about 5-7 nm (JANNEY et al., 2000). Some of our samples have a very high effective SSA and the corresponding effective particle size is extremely low (about 1 nm). This may be partly due to an overestimation of the P content (R_{ev}) and corresponding surface area (A), see discussion at Fig.2. The use of goethite as representative mineral may also contribute to this. If the natural oxide particles have a higher site density and a higher phosphate adsorption density, a lower effective surface area and a larger effective particle size will be found. Nevertheless, the formation of extremely small particles can also not be excluded yet. Recently, an interesting observation was reported by Eusterhues et al. (2008) showing that synthetic ferrihydrite will form considerably smaller particles when prepared in the presence of organic matter.

In Fig.6, the SSA derived by the probe ion method is given as a function of the relative phosphate loading. For scaling of the x-axis in the figure, we used for phosphate the amount extractable with oxalate and for Fe and Al the amount extractable with DCB, i.e. scaling on experimental data. The dotted line represents the theoretical relationship assuming for phosphate, extractable with oxalate, a reversible binding of 2 μmol/m^2. The upper and lower lines in Fig.6 are for respectively 1 and 3 μmol/m^2 of oxalate extractable phosphate. This chosen range of phosphate loadings (1-3 μmol/m^2) is representative for the range in our soils found by modeling the equilibration of phosphate in 0.5 M Na(H)CO_3. As shown in Part II (HIEMSTRA et al., 2010), the phosphate loading of field samples is not only imposed by the average concentration of phosphate in the field, but is also strongly affected by the adsorption of organic matter and the presence of DOC in solution.

In principle, a small particle size will result in a higher solubility of the oxide particles, depending on the surface energy. Surface energy is related to a different ensemble of bonds in the interface compared to the bulk and therefore, it can be affected by ion adsorption (WENG et al., 2006). Recently, it has been suggested that the adsorption of oxyanions will lead to a reduction of the solubility of ferrihydrite particles (FUKUSHI and SATO, 2005). In particular, phosphate has a large effect in lowering the solubility of ferrihydrite making the particles relatively more stable. Increase of the loading will allow the presence of smaller particles at the same overall chemical stability. In other words, the presence of adsorbed phosphate can compensate an enhanced solubility due to a smaller particle size.

4 Mineral-NOM association

4.1 NOM-loading

The information about the effective surface area *A* of soils and specific surface area *SSA* of natural soil oxide particles can be very useful to sharpen our view on the nature of natural oxide fraction in relation to organic matter. In soils, natural organic matter is often associated with the finest mineral fractions (EUSTERHUES et al., 2003; SCHULTEN and LEINWEBER, 2000). Radiocarbon dating shows that organic matter, bound by the mineral fraction, is relatively old (EUSTERHUES et al., 2003; TORN et al., 1997). This suggests that it is relatively stable which is in agreement with the work of Keil et al. (1994), and others (TORN et al., 1997; WAGAI and MAYER, 2007).

In our study, a clear relationship is found between the effective reactive surface area *A* of the soils and the organic carbon content (Fig.7a), with the exception of some soils with relatively very high organic carbon contents. For the selected set of soils with 5% organic carbon (OC) or less (dark data points, $n = 17$), linear regression results in A (m^2/g) = 6.0 %OC ($R^2 = 0.92$). If only sandy soils (clay fraction < 8%) or sandy and loamy soils (clay fraction ≤ 12%) are considered, one finds in both cases A (m^2/g) = 8.0 %OC ($R^2 = 0.97$ for $n = 10$). The average relationship is given as full line in Fig.7a and the dotted line represents a four times higher carbon content per unit surface area. The observed correlation (full line) suggests the presence of an association of NOM with oxidic surfaces formed by Fe and Al (hydr)oxides

and probably the edges of clay minerals. However, soils can also have quite some additional carbon (dotted line). This may be present at the planar faces of clay minerals, bound by intercalation (EUSTERHUES et al., 2003), but may also be present due to multi-layer adsorption, leading to a higher carbon content per unit surface area in an oxide-NOM association. In addition, organic matter may be present as low density organic matter (WAGAI et al., 2008), which does not have a significant association with mineral particles and may be present in a coagulated / precipitated form.

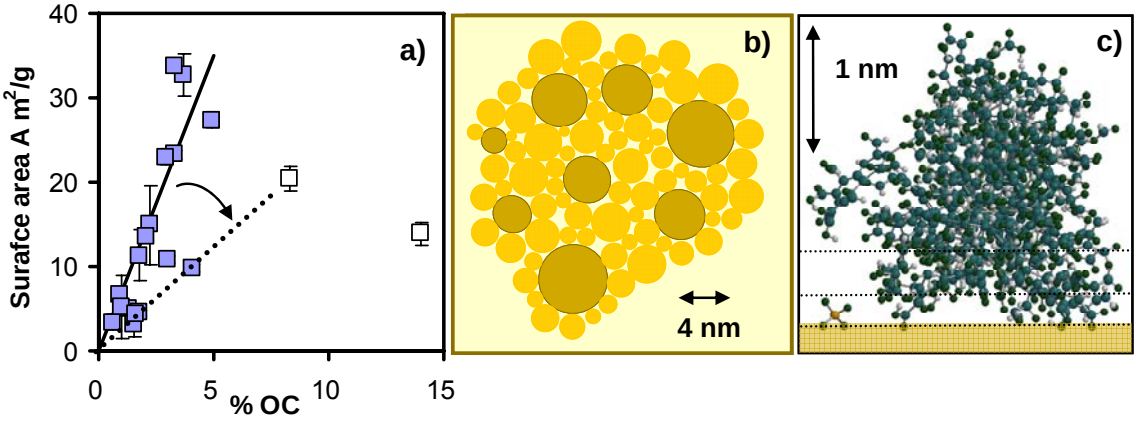

Fig.7a) The effective reactive surface area as a function of the organic carbon content of the Copernicus soil series. At a relatively low % OC, the effective surface areas increase with the OC fraction (closed symbols). The full line refers to 1.4 mg OC/m^2, which is equivalent with NOM layer thickness of 2.0 nm. The dotted line refers to the presence more carbon (5 mg OC/m^2).
Fig.7b) A schematic 2D model for an organo-mineral association. The (micro) aggregate has oxide particles as darker spheres (~ 4.0 ± 2.6 nm) surrounded by a layer (~2.0 ± 0.3 nm) of attached organic matter molecules (~1.4 ± 0.2 mg OC/m^2) that have an average NOM volume fraction of about 80% and an average mass density of ~1.7 g/cm^3. The NOM molecules have a variable degree of chemical interaction with the mineral surface groups depending on factors like pH and phosphate loading.
Fig.7c) NOM molecule (M~10000 Dalton) attached to a mineral surface in comparison to a phosphate ion (left side in 7c). The horizontal dotted lines represent the electrostatic Stern planes of the ES model. NOM and PO_4 dominantly interact via the ligand distribution in the inner Stern layer space.

For a further interpretation, we may express the amount of natural organic matter (NOM) in our samples per unit effective surface area. Using the average slope *s* of the above relationship (*s* = 7.0 ± 1), the mean organic carbon content is ~1.4 ± 0.2 mg OC/m^2. This is equivalent with ~2.5 ± 0.4 mg NOM/m^2 in case of a carbon content of 58 %. These results can be compared with literature data, but note that in literature the BET surface area has generally been used whereas our data refer to an oxidic surface area. The BET surface area should be measured after carbon removal, because organic matter may mask the actual mineral surface area (KAISER and GUGGENBERGER, 2003). For marine sediments, the carbon loading (KEIL et al., 1994; MAYER, 1994) measured in this way, is in the order about 0.8 ± 0.1 mgC/m^2 BET surface area. This loading is lower and this might be due to the different scale used for surface area, but it may also be related to a difference in the environmental conditions present in both systems (marine sediment versus agricultural top soils).

We may compare the apparent organic carbon loading with the adsorption maximum of natural organic acids at iron (hydr) oxide surfaces. The above OC loading (~1.4 ± 0.2 mg OC/m^2) is between the maximum loading of oxide surfaces with purified FA, ~0.6 mg OC/m^2 (FILIUS et al., 2000; GU et al., 1996; GU et al., 1994; ZHOU et al., 2001), and HA, ~2.5 mgC/m^2 (ANTELO et al., 2007; WENG et al., 2007). This comparison shows that potentially a considerable part of the organic matter in the agricultural soils can be stored directly at the surface of the nano-oxide particles.

4.2 Structural Model

To develop a structural picture of an oxide-NOM association (Fig.7b), we may calculate the equivalent thickness of a hypothetical NOM layer at the particle surface based on the data of Fig.7a. Assuming a mass density of 1250 kg NOM/m^3, the above NOM loading of 2.5 ± 0.4 mg NOM/m^2 has an equivalent thickness of ~ 2.0 ± 0.3 nm. This number falls in the range of the size of natural organic acids like purified FA and HA molecules, which are about 1 and 3 nm respectively (WENG et al., 2007). In Fig.7c, adsorbed HA is shown as an example. Only a small part of the NOM is present in the Stern layers. The compact part of the ES double layer is in total approximately 0.7 ± 0.2 nm (HIEMSTRA and VAN RIEMSDIJK, 2006). The average equivalent thickness of NOM (2.0 ± 0.3 nm) is about half the average particle size of the natural oxides (~ 4.0 ± 2.6 nm) in the soils studied. In combination, the average equivalent particle size of humic acid coated oxide particle will be ~ 8 ± 3 nm. Field flow fractionation (FFF) of the colloidal fraction (<0.2 μm) of a forest soil, shows nanosized particles of a similar (hydrodynamic) diameter (HASSELLOV and VON DER KAMMER, 2008) as we have established.

The surface loading with carbon can be brought into further perspective by expressing the presence of both, organic matter and mineral particles, as a volume. In the calculation, the mass density of ferrihydrite (Fh) and NOM is set at respectively 3500 kg/m^3 (HIEMSTRA and VAN RIEMSDIJK, 2009a) and 1250 ± 150 kg/m^3. The calculated volume ratio NOM/Fh for oxide particles with an average specific surface area of ~630 m^2/g equals approximately 4.4 m^3 NOM / m^3 Fh. This calculation shows that the relative volume of NOM is considerable. The calculated volume ratio can be transformed into an average mass density (ρ) of the NOM-oxide association being close to ρ ~1700 ± 100 kg/m^3 particles. The calculated mass density refers to oxide particles in our soils with the average specific surface area. However, at a given NOM loading per unit surface area (mg NOM/m^2), a variation in the particle size will lead to a range of mass densities of the NOM-oxide association. Increase of the oxide particle size will lead to an increase of the mass density of the NOM-oxide association. For instance, in case of a specific surface area of 300 m^2/g for the natural (hydr)oxide particles, the calculated mass density of the mineral-NOM association will be ρ ~ 2000 kg/m^3 particles. A comparable number is calculated for synthetic ferrihydrite (Fh) with a maximum loading of organic carbon of 320 mg OC / g Fh or 720 mg NOM/ g Fh (KAISER et al., 2007), having a volume ratio NOM/Fh of ~ 2 m^3 NOM /m^3 Fh. On the other hand, the presence of larger molecules like humin (M~ 100000 Dalton, d ~ 10 nm) will decrease the mass density of the

micro-aggregates if present. In addition, the mass density will be lowered due to the presence of Al as a light element in the natural oxide fraction compared to Fe. The above-calculated mass densities are typical numbers for the heavy density fractions of natural organic matter in soils (CHRISTENSEN, 1992; WAGAI et al., 2008). These fractions are generally considered as more refractorily in terms of microbial decomposition and can be very dominant (>80-90%) in soils (WAGAI et al., 2008).

In Fig.7b, the oxide-NOM association is schematically depicted as a combination of attached but rather separate particles. Actually, the ensemble of individual organic molecules (FA, HA, and humin) may interact with each other partly forming intertwined structures, enforced by hydrophobic effects, metal-ion- and H-bridging. These binding mechanisms may support the incorporation of additional organic matter in the NOM mineral nano-particles of the micro-aggregates, depending on the soil conditions regulating the input and output of organic matter at the system level. The presence of organic matter above a monolayer coverage of ~1-2 mg OC/m^2 is found for a number of our soils (Fig.7a) and in literature. The incorporation of additional carbon in the oxide-NOM nanoparticle association is effectively similar to a multilayer adsorption of variety of NOM molecules in the NOM-oxide association. This will decrease the mass density of the NOM-oxide association. Of course, formation of coagulated organic matter will also lead to a carbon loading above a monolayer level. This coagulated fraction is considered as true light-density organic matter. The light-density fraction either true or mineral-associated is often quite limited in extent (WAGAI et al., 2008). The high-density fraction usually dominates and may have a significantly lower higher C/N ratio, which may point to microbial-processed organic matter (WAGAI et al., 2008) in the mineral-NOM association.

It is remarkable that a large number of the agricultural soils has a surprisingly low loading when scaled per unit effective surface area. We may speculate that this is due to the rather intense use of these soils with favorable conditions for microbial degradation of organic matter, such as the quality of the organic matter, the availability of nutrients in particular nitrogen, and pH. In addition, temperature, the physical accessibility, the soil moisture content, and the presence of sufficient oxygen are important factors. The present methodology to derive an effective surface area, allowing new scaling of NOM, may contribute to an improvement of the understanding of these factors as regulators of the dynamics of natural organic matter in soil. In addition, the present methodology to derive the effective surface area may improve our understanding of soil formation.

The embedding of oxide particles in a matrix of NOM (Fig.7b) may (partly) explain the slow adsorption kinetics of PO_4 that is often observed in experiments with soil. For adsorption, the phosphate ions have to penetrate into a negatively charged gel-like matrix (Fig.7b) from which these ions are excluded electrostatically. Moreover, the final adsorption of PO_4 may require desorption of NOM which may also be a rather slow process.

At a given adsorption of NOM, its chemical interaction with the surface groups of the (hydr)oxide by ligand exchange (Fig.7c) can be variable. The surface interaction depends on the profile of the electrostatic potential in the inner Stern layer, which is determined by the collective presence of e.g. protons, phosphate, and NOM ligands. This mutual interaction can be handled with the LCD model (WENG et al., 2008). In part II (HIEMSTRA et al., 2010), we

will discuss a straightforward strategy to implement in simplified manner the effect of interfacial NOM in the CD model.

5 Conclusions

- The equilibration of natural samples using 0.5 M sodium bicarbonate (pH = 8.5) solution and an excess amount of activated carbon reduces the complexity of these systems in terms of modeling compared to natural multi-component conditions. The high concentration of the added competitor (HCO_3^- ions) enables a fast penetration in natural porous oxides, desorption of phosphate, and equilibration at internal and external surfaces, reaching a (semi) -equilibrium in about 10 -15 days.
- The competitive phosphate-carbonate behavior is determined by the interfacial charge distribution (CD) of the various surface species. This behavior enables the description of the HCO_3^- concentration dependency of the phosphate adsorption and the effect of a changing solid-solution ratio in natural samples by choosing only an effective reactive surface area and a fraction of reversibly adsorbed phosphate.
- The effective reactive surface area (A) on our top soils ranges between A ~3 and ~30 m^2/g sample and is not very well correlated with the amount of Fe and Al oxide extracted with oxalate or DCB. The effective specific surface area (SSA) of the natural oxide fraction, scaled on the total iron and aluminum (hydr)oxide (DCB) content, is mostly between SSA ~200 and ~1200 m^2/g oxide and the corresponding spherical particle size is between ~1-10 nm.
- In the set of mineral soils studied, a strong correlation exists between the natural oxide fraction and natural organic matter. For many non-clay soils, the NOM loading is about 1.4 ± 0.2 mgC/m^2, equivalent with a monolayer thickness of about 2.0 ± 0.3 nm. The observed relationship suggests the formation of a NOM-oxide nanoparticle association. The calculated average NOM volume in such micro-aggregates is ~80% and the mass density is about 1700 kg/m^3, a typical value for the high-density organic matter fraction. Only a fraction of the total amount of organic matter associated with the oxide particles is active in the competition with phosphate that mainly takes place in the inner Stern layer near the surface.
- For the top soils studied, the variation in the reversible phosphate loading is unusually large (Γ = ~ 1 - 3 μmol/m^2) considering the limited variation in the phosphate concentrations and pH and the shape of the high-affinity isotherm. The large natural variation is supposed to be due to the interaction of NOM as will be discussed in part II of this series.

Acknowledgment

We greatly appreciate the comments and questions of our reviewers. We also like to thank the Associate Editor. We highly appreciate the financial support of the EU, funding project FUNMIG (516514, F16W-2004).

Appendix

Table A. Aqueous speciation reactions and their equilibrium constants ($I = 0$).

Species	Reaction	log K
HPO_4^{2-}	$PO_4^{3-} + 1H^+ \Leftrightarrow HPO_4^{2-}$	12.35 [a]
$H_2PO_4^-$	$PO_3^{3-} + 2H^+ \Leftrightarrow H_2PO_4^-$	19.55 [a]
$H_3PO_4^0$	$PO_4^{3-} + 3H^+ \Leftrightarrow H_3PO_4^0$	21.70 [a]
$NaPO_4^{2-}$	$PO_4^{3-} + 1Na^+ \Leftrightarrow NaPO_4^{2-}$	2.05 [b]
$NaHPO_4^-$	$PO_4^{3-} + 1H^+ + 1Na^+ \Leftrightarrow NaHPO_4^-$	13.4 [a,b]
$CaPO_4^-$	$PO_4^{3-} + 1Ca^{2+} \Leftrightarrow CaPO_4^-$	6.46 [a]
$CaHPO_4^0$	$PO_4^{3-} + 1H^+ + 1Ca^{2+} \Leftrightarrow CaHPO_4^0$	15.09 [a]
$CaH_2PO_4^+$	$PO_4^{3-} + 2H^+ + 1Ca^{2+} \Leftrightarrow CaH_2PO_4^+$	20.95 [a]
HCO_3^-	$CO_3^{2-} + 1H^+ \Leftrightarrow HCO_3^-$	10.33 [a]
$H_2CO_3^*$	$CO_3^{2-} + 2H^+ \Leftrightarrow H_2CO_3^*$	16.69 [a]
$CO_2(g)$	$CO_3^{2-} + 2H^+ \Leftrightarrow H_2O(l) + CO_2(g)$	18.15 [a]
$NaHCO_3^0$	$CO_3^{2-} + 1Na^+ + 1H^+ \Leftrightarrow NaHCO_3^0$	10.14 [c]
$NaCO_3^-$	$CO_3^{2-} + 1Na^+ \Leftrightarrow NaCO_3^-$	1.02 [c]
$Na_2CO_3^0$	$CO_3^{2-} + 2Na^+ \Leftrightarrow Na_2CO_3^0$	0.01 [a]
$CaHCO_3^+$	$CO_3^{2-} + 1H^+ + 1Ca^{2+} \Leftrightarrow CaHCO_3^+$	11.45 [a]
$CaCO_3^0$	$CO_3^{2-} + 1Ca^{2+} \Leftrightarrow CaCO_3^0$	3.14 [a]
$CaCl^+$	$Ca^{2+} + 1Cl^- \Leftrightarrow CaCl^+$	-1.0 [a]
$CaCl_2^0$	$Ca^{2+} + 2Cl^- \Leftrightarrow CaCl_2^0$	0.0 [a]
$NaCl^0$	$Na^+ + Cl^- \Leftrightarrow NaCl^0$	-0.80 [d]
$NaNO_3^0$	$Na^+ + NO_3^- \Leftrightarrow NaNO_3^0$	-0.60 [e]
$H_2O(l)$	$H^+ + OH^- \Leftrightarrow H_2O(l)$	14.00 [e]

[a] From Lindsay (1979),
[b] From Rahnemaie et al. (2007b),
[c] From Millero and Scheiber (1982),
[d] From Sverjensky et al.(1997),
[e] From Smith and Martell (1981)

References

Ali M. A. and Dzombak D. A. (1996a) Competitive sorption of simple organic acids and sulfate on goethite. *Environ. Sci. Technol.* 30, 1061-1071.

Antelo J., Arce F., Avena M., Fiol S., López R., and Macías F. (2007) Adsorption of a soil humic acid at the surface of goethite and its competitive interaction with phosphate. *Geoderma* 138(1-2), 12-19.

Antelo J., Avena M., Fiol S., Lopez R., and Arce F. (2005) Effects of pH and ionic strength on the adsorption of phosphate and arsenate at the goethite-water interface. *J. Colloid Interf. Sci.* 285(2), 476-486.

Bargar J. R., Kubicki J. D., Reitmeyer R., and Davis J. A. (2005) ATR-FTIR spectroscopic characterization of coexisting carbonate surface complexes on hematite *Geochim. Cosmochim. Acta* 69(6), 1527-1542.

Barrow N. J., Bowden J. W., Posner A. M., and Quirk J. P. (1980) Describing the effects of electrolyte on adsorption of phosphate by a variable charge surface. *Aust. J. Soil Res.* 18(4), 395 - 404

Barrow N. J. and Shaw T. C. (1975) Slow Reactions between Soil and Anions .5. Effects of Period of Prior Contact on Desorption of Phosphate from Soils. *Soil Sci.* 119(4), 311-320.

Barrow N. J. and Shaw T. C. (1976a) Sodium bicarbonate as an extractant for soil phosphate, I. Separation of the factors affecting the amount of phosphate displaced from soil from those affecting secondary adsorption. *Geoderma* 16(2), 91-107.

Barrow N. J. and Shaw T. C. (1976b) Sodium bicarbonate as an extractant for soil phosphate, II. Effect of varying the conditions of extraction on the amount of phosphate initially displaced and on the secondary adsorption. *Geoderma* 16(2), 109-123.

Boily J.-F. (1999) The Surface Complexation of Ions at the Goethite (a-FeOOH)/ Water Interface: a Multisite Complexation Approach, Umeå University.

Brecevic L. and Kralj D. (2007) On calcium carbonates: from fundamental research to application. *Croatica Chemica Acta* 80(3-4), 467-484.

Cances B., Ponthieu M., Castrec-Rouelle M., Aubry E., and Benedetti M. F. (2003) Metal ions speciation in a soil and its solution: experimental data and model results. *Geoderma* 113(3-4), 341-355.

Christensen B. T. (1992) Physical fractionation of soil and organic matter in primary particle size and density separates. *Adv. Soil Sci.* 20, 1-90.

Christl I. and Kretzschmar R. (1999) Competitive sorption of copper and lead at the oxide-water interface: Implications for surface site density. *Geochim. Cosmoschim. Acta* 63(19-20), 2929-2938.

Cihacek L. J. and Bremner J. M. (1979) Simplified Ethylene-Glycol Monoethyl Ether Procedure for Assessment of Soil Surface-Area. *Soil Sci. Soc. Am. J.* 43(4), 821-822.

Coffin D. E. (1963) A method for the determination of free iron in soils and clays. *Can. J. Soil Sci.* 43, 7-17.

Cornell R. M. and Schwertmann U. (1996) The iron oxides : structures, properties, reactions, occurrence and uses VCH.

Criscenti L. J. and Sverjensky D. A. (1999) The Role of Electrolyte Anions (ClO_4^-, NO_3^-, and Cl^-) in Divalent Metal (M^{2+}) Adsorption on Oxide and Hydroxide Surfaces in Salt Solution. *Am. J. Sci.* 299, 828-899.

Davis J. A., James R., and Leckie J. O. (1978a) Surface Ionization and Complexation at the Oxide/Water Interface. I Computation of Electrical Double Layer Properties in Simple Electrolytes. *J. Colloid Interf. Sci.* 63, 480-499.

Davis J. A. and Leckie J. O. (1978b) Surface ionization and complexation at the oxide/water interface. II Surface properties of amorphous iron oxyhydroxide and adsorption of metal ions. *J. Colloid Interf. Sci.* 67, 90-105.

Dijkstra J. J., Meeussen J. C. L., and Comans R. N. J. (2004) Leaching of heavy metals from contaminated soils: An experimental and modeling study. *Environ. Sci. Technol.* 38(16), 4390-4395.

Dzombak D. A. and Morel F. M. M. (1990) Surface Complexation Modeling: Hydrous Ferric Oxide. *John Wiley & Sons: New York*, 393.

Eusterhues K., Rumpel C., Kleber M., and Kogel-Knabner I. (2003) Stabilisation of soil organic matter by interactions with minerals as revealed by mineral dissolution and oxidative degradation. *Org. Geochem.* 34(12), 1591-1600.

Eusterhues K., Rumpel C., and Kogel-Knabner I. (2005) Organo-mineral associations in sandy acid forest soils: importance of specific surface area, iron oxides and micropores. *Eur. J. Soil Sci.* 56(6), 753-763.

Eusterhues K., Wagner F. E., Hausler W., Hanzlik M., Knicker H., Totsche K. U., Kogel-Knabner I., and Schwertmann U. (2008) Characterization of Ferrihydrite-Soil Organic Matter Coprecipitates by X-ray Diffraction and Mossbauer Spectroscopy. *Environ. Sci. Technol.* 42(21), 7891-7897.

Filius J. D., Hiemstra T., and Van Riemsdijk W. H. (2000) Adsorption of Fulvic Acid on Goethite. *Geochim. Cosmochim. Acta* 64(1), 51-60.

Fukushi K. and Sato T. (2005) Using a surface complexation model to predict the mature and stability of nanoparticles. *Environ. Sci. Technol.* 39(5), 1250-1256.

Goldberg S., Lesch S. M., and Suarez D. L. (2002) Predicting molybdenum adsorption by soils using soil chemical. parameters in the constant capacitance model. *Soil Sci. Soc. Am. J.* 66(6), 1836-1842.

Griffioen J. (2006) Extent of immobilisation of phosphate during aeration of nutrient-rich, anoxic groundwater. *Journal of Hydrology* 320(3-4), 359-369.

Gu B. H., Mehlhorn T. L., Liang L. Y., and McCarthy J. F. (1996) Competitive adsorption, displacement, and transport of organic matter on iron oxide .1. Competitive adsorption. *Geochim. Cosmoschim. Acta* 60(11), 1943-1950.

Gu B. H., Schmitt J., Chen Z. H., Liang L. Y., and McCarthy J. F. (1994) Adsorption and Desorption of Natural Organic-Matter on Iron-Oxide - Mechanisms and Models. *Environ. Sci. Technol.* 28(1), 38-46.

Gustafsson J. P. (2001) Modelling competitive anion adsorption on oxide minerals and an allophane-containing soil. *Eur. J. Soil Sci.* 52(4), 639-653.

Hassellov M. and Von der Kammer F. (2008) Iron oxide as Geochemical Nanovectors for Metal Transport in Soil-River systems. *Elements* 4, 401-406.

Hiemstra T., Antelo J., van Rotterdam A. M. D., and van Riemsdijk W. H. (2010) Nanoparticles in natural systems II: The natural oxide fraction at interaction with natural organic matter and phosphate. *Geochim. Cosmoschim. Acta* 74(1), 59-69.

Hiemstra T., Barnett M. O., and Van Riemsdijk W. H. (2007) Interaction of Silicic Acid with Goethite. *J. Colloid Interf. Sci.* 310, 8-17.

Hiemstra T., Rahnemaie R., and Van Riemsdijk W. H. (2004) Surface Complexation of Carbonate on Goethite: IR spectroscopy, Structure and Charge Distribution. *J. Colloid Interf. Sci.* 278, 282-290.

Hiemstra T. and Van Riemsdijk W. H. (1996a) A surface Structural Approach to Ion Adsorption: The Charge Distribution (CD) Model. *J. Colloid Interf. Sci.* 179, 488-508.

Hiemstra T. and Van Riemsdijk W. H. (1999a) Surface structural ion adsorption modeling of competitive binding of oxyanions by metal (hydr)oxides. *J. Colloid Interf. Sci.* 210, 182-193.

Hiemstra T. and Van Riemsdijk W. H. (2006) On the relationship between charge distribution, surface hydration and the structure of the interface of metal hydroxides. *J. Colloid Interf. Sci.* 301, 1-18.

Hiemstra T. and Van Riemsdijk W. H. (2007) Surface complexation of selenite on goethite: MO/DFT geometry and charge distribution. *Croatica Chemica Acta* 80(3-4), 313-324.

Hiemstra T. and Van Riemsdijk W. H. (2009a) A Surface Structural Model for Ferrihydrite I: Sites related to Primary charge, Molar Mass, and Mass Density. *Geochim. Cosmochim. Acta* 73, 4423-4436.

Hiemstra T., Venema P., and Van Riemsdijk W. H. (1996b) Intrinsic proton affinity of reactive surface groups of metal (hydr)oxides: The bond valence principle. *J. Colloid Interf. Sci.* 184, 680-692.

Hingston F. J., Posner A. M., and Quirk J. P. (1968) Adsorption of Selenite by Goethite. In *Symposium on adsorption from aqueous solution Advances in Chemical Series*, Vol. 70, pp. 82-90.

Holmgren G. G. (1967) A Rapid Citrate-Dithionite Extractable Iron Procedure. *Soil Sci. Soc. Am. Proc.* 31(2), 210-&.

Hyacinthe C. and Van Cappellen P. (2004) An authigenic iron phosphate phase in estuarine sediments: composition, formation and chemical reactivity. *Mar. Chem.* 91(1-4), 227-251.

Janney D. E., Cowley J. M., and Buseck P. R. (2000) Transmission electron microscopy of synthetic 2-and 6-line ferrihydrite. *Clays Clay Miner.* 48(1), 111-119.

Kaiser K. and Guggenberger G. (2000) The role of DOM sorption to mineral surfaces in the preservation of organic matter in soils. *Org. Geochem.* 31(7-8), 711-725.

Kaiser K. and Guggenberger G. (2003) Mineral surfaces and soil organic matter. *Eur. J. Soil Sci.* 54(2), 219-236.

Kaiser K., Mikutta R., and Guggenberger G. (2007) Increased stability of organic matter sorbed to ferrihydrite and goethite on aging. *Soil Sci. Soc. Am. J.* 71(3), 711-719.

Keil R. G., Montlucon D. B., Prahl F. G., and Hedges J. I. (1994) Sorptive Preservation of Labile Organic-Matter in Marine-Sediments. *Nature* 370(6490), 549-552.

Keizer M. G. and Van Riemsdijk W. H. (1998) ECOSAT, Equilibrium Calculation of Speciation and Transport. Technical Report Department Soil Quality. Wageningen University.

Kennedy M. J., Pevear D. R., and Hill R. J. (2002) Mineral surface control of organic carbon in black shale. *Science* 295(5555), 657-660.

Kinniburgh D. G. (1993) Fit, Technical Report WD/93/23. British Geological Survey.

Koopmans G. F., Chardon W. J., de Willigen P., and van Riemsdijk W. H. (2004) Phosphorus desorption dynamics in soil and the link to a dynamic concept of bioavailability. *J. Environ. Qual.* 33(4), 1393-1402.

Kostka J. E. and Luther G. W. (1994) Partitioning and Speciation of Solid-Phase Iron in Salt-Marsh Sediments. *Geochim. Cosmoschim. Acta* 58(7), 1701-1710.

Lienemann C. P., Monnerat M., Dominik J., and Perret D. (1999) Identification of stoichiometric iron-phosphorus colloids produced in a eutrophic lake. *Aquatic Sciences* 61(2), 133-149.

Lindsay W. L. (1979) *Chemical Equilibria in soils*. Wiley-Interscience.

Lofts S. and Tipping E. (1998) An assemblage model for cation binding by natural particulate matter. *Geochim. Cosmoschim. Acta* 62(15), 2609-2625.

Logue B. A., Smith R. W., and Westall J. C. (2004) U(VI) adsorption on natural iron-coated sands: comparison of approaches for modeling adsorption on heterogeneous environmental materials. *Appl. Geochem.* 19(12), 1937-1951.

Luengo C., Brigante M., Antelo J., and Avena M. (2006) Kinetics of phosphate adsorption on goethite: Comparing batch adsorption and ATR-IR measurements. *J. Colloid Interf. Sci.* 300(2), 511-518.

Lumsdon D. G. (2004) Partitioning of organic carbon, aluminium and cadmium between solid and solution in soils: application of a mineral-humic particle additivity model. *Eur. J. Soil Sci.* 55(2), 271-285.

Lutzenkirchen J. (2004) Modelling uranyl adsorption to quartz - application of the CD-MUSIC concept. *Geochim. Cosmoschim. Acta* 68(11), A502-A502.

Mayer L. M. (1994) Surface-Area Control of Organic-Carbon Accumulation in Continental-Shelf Sediments. *Geochim. Cosmoschim. Acta* 58(4), 1271-1284.

Mehra O. P. and Jackson M. L. (1960) Iron oxide removal from the soils and clays by dithionite-citrate system buffered with sodium bicarbonate. *Clay Clays Miner.* 7, 317-327.

Meima J. A. and Comans R. N. J. (1998) Application of surface complexation precipitation modeling to contaminant leaching from weathered municipal solid waste incinerator bottom ash. *Environ. Sci. Technol.* 32(5), 688-693.

Millero F. J. and Schreiber D. R. (1982) Activity Coefficients of the Ionic Components of natural water. *Am. J. Sci.* 282, 1508-1540.

Mödl C., Wörmann H., and Amelung W. (2007) Contrasting effects of different types of organic material on surface area and microaggregation of goethite. *Geoderma* 141(3-4), 167-173.

Murphy P. J., Posner A. M., and Quirk J. P. (1976) Characterization of Partially Neutralized Ferric Nitrate Solutions. *J. Colloid Interf. Sci.* 56(2), 270-283.

Olsen S. R., Cole C. V., Watanabe F. S., and Dean L. A. (1954) Estimation of available phosphorous in soils by extraction with sodium bicarbonate, Vol. 939, pp. 1-19. US Department of Agriculture Circular.

Parks G. A. and De Bruyn P. L. (1962) The Zero Point of Charge of Oxides. *J. Phys. Chem.* 66, 967-973.

Ponthieu M., Juillot F., Hiemstra T., van Riemsdijk W. H., and Benedetti M. F. (2006) Metal ion binding to iron oxides. *Geochim. Cosmoschim. Acta* 70(11), 2679-2698.

Rahnemaie R., Hiemstra T., and Van Riemsdijk W. H. (2006) A new structural approach for outersphere complexation, tracing the location of electrolyte ions. *J. Colloid Interf. Sci.* 293, 312-321.

Rahnemaie R., Hiemstra T., and Van Riemsdijk W. H. (2007a) Carbonate adsorption on goethite in competition with phosphate. *J. Colloid Interf. Sci.* 315(2), 415-425.

Rahnemaie R., Hiemstra T., and Van Riemsdijk W. H. (2007b) Geometry, Charge Distribution and Surface Speciation of Phosphate on Goethite. *Langmuir* 23, 3680-3689.

Rietra R. P. J. J., Hiemstra T., and Van Riemsdijk W. H. (1999a) The Relationship between Molecular Structure and Ion Adsorption on Variable Charge Minerals. *Geochim. Cosmochim. Acta* 63(19/20), 3009-3015.

Rietra R. P. J. J., Hiemstra T., and Van Riemsdijk W. H. (2001a) Interaction of Calcium and Phosphate Adsorption on Goethite. *Environ. Sci. Technol.* 35, 3369-3374.

Roden E. E. and Zachara J. M. (1996) Microbial reduction of crystalline iron(III) oxides: Influence of oxide surface area and potential for cell growth. *Environ. Sci. Technol.* 30(5), 1618-1628.

Rosentreter J. J., Swantje Quarder H., Smith R. W., and McLing T. (1998) Uranium Sorption onto Natural Sands as a function of Sediment Characteristics and Solution pH. In *Adsorption of Metals by Geomedia* (ed. E. A. Jenne). Academic Press.

Schroder T. J., Hiemstra T., Vink J. P. M., and van der Zee S. (2005) Modeling of the solid-solution partitioning of heavy metals and arsenic in embanked flood plain soils of the rivers Rhine and Meuse. *Environ. Sci. Technol.* 39(18), 7176-7184.

Schulten H. R. and Leinweber P. (2000) New insights into organic-mineral particles: composition, properties and models of molecular structure. *Biol. Fert. Soils* 30(5-6), 399-432.

Schwertmann U. (1973) Use of Oxalate for Fe Extraction from Soils. *Can. J. Soil Sci.* 53(2), 244-246.

Schwertmann U. and Fischer W. R. (1973) Natural Amorphous Ferric Hydroxide. *Geoderma* 10(3), 237-247.

Smith R. M. and Martell A. E. (1981) *Critical Stability Constants*. Plenum.

Stachowicz M., Hiemstra T., and van Riemsdijk W. H. (2008) Multi-competitive interaction of As(III) and As(V) oxyanions with Ca^{2+}, Mg^{2+}, PO_4^{3-}, and CO_3^{2-} ions on goethite. *J. Colloid Interf. Sci.* 320(2), 400-414.

Stern O. (1924) Zur theory der electrolytischen doppelschicht. *Z. Electrochem.* 30, 508-516.

Strauss R., Brummer G. W., and Barrow N. J. (1997) Effects of crystallinity of goethite .2. Rates of sorption and desorption of phosphate. *Eur. J. Soil Sci.* 48(1), 101-114.

Sverjensky D. A. (2005) Prediction of surface charge on oxides in salt solutions: Revisions for 1:1 (M+L-) electrolytes. *Geochim. Cosmochim. Acta* 69(2), 225-257.

Sverjensky D. A., Shock E. L., and Helgeson H. C. (1997) Prediction of the thermodynamic properties of aqueous metal complexes to 1000 degrees C and 5 kb. *Geochim. Cosmoschim. Acta* 61(7), 1359-1412.

Tadanier C. J. and Eick M. J. (2002) Formulating the charge-distribution multisite surface complexation model using FITEQL. *Soil Sci. Soc. Am. J.* 66(5), 1505-1517.

Tejedor-Tejedor M. I. and Anderson M. A. (1990) Protonation of Phosphate on the Surface of Goethite as Studied by CIR-FTIR and Electrophoretic Mobility. *Langmuir* 6, 602-611.

Thompson A., Chadwick O. A., Rancourt D. G., and Chorover J. (2006) Iron-oxide crystallinity increases during soil redox oscillations. *Geochim. Cosmoschim. Acta* 70(7), 1710-1727.

Torn M. S., Trumbore S. E., Chadwick O. A., Vitousek P. M., and Hendricks D. M. (1997) Mineral control of soil organic carbon storage and turnover. *Nature* 389(6647), 170-173.

Torrent J., Barron V., and Schwertmann U. (1990) Phosphate adsorption and desorption by goethites differing in crystal morphology. *Soil Sci. Soc. Am. J.* 54, 1007-1012.

Torrent J., Schwertmann U., and Barron V. (1992) Fast and Slow Phosphate Sorption by Goethite-Rich Natural Materials. *Clays Clay Miner.* 40(1), 14-21.

van der Zee C., Roberts D. R., Rancourt D. G., and Slomp C. P. (2003) Nanogoethite is the dominant reactive oxyhydroxide phase in lake and marine sediments. *Geology* 31(11), 993-996.

van Erp P. J., Houba V. J. G., and Van Beusichem M. L. (1998) One hundredth molar calcium chloride extraction procedure. Part I: A review of soil chemical, analytical, and plant nutritional aspects. *Commun. Soil Sci. Plan.* 29(11-14), 1603-1623.

Vanderzee S. and Vanriemsdijk W. H. (1988) Model for Long-Term Phosphate Reaction-Kinetics in Soil. *J. Environ. Qual.* 17(1), 35-41.

Voegelin A., Vulava V. M., and Kretzschmar R. (2001) Reaction-based model describing competitive sorption and transport of Cd, Zn, and Ni in an acidic soil. *Environ. Sci. Technol.* 35(8), 1651-1657.

Wada K. (1989) Allophane and imogolite. In *Minerals in Soil environment* (ed. J. B. Dixon, and Weed, S.B.), pp. 1051-1087. Soil Science Society of America.

Wagai R. and Mayer L. M. (2007) Sorptive stabilization of organic matter in soils by hydrous iron oxides. *Geochim. Cosmoschim. Acta* 71(1), 25-35.

Wagai R., Mayer L. M., and Kitayama K. (2009) Extent and nature of organic coverage of soil mineral surfaces assessed by a gas sorption approach. *Geoderma* 149(1-2), 152-160.

Wagai R., Mayer L. M., Kitayama K., and Knicker H. (2008) Climate and parent material controls on organic matter storage in surface soils: A three-pool, density-separation approach. *Geoderma* 147(1-2), 23-33.

Walker T. W. and Syers J. K. (1976) Fate of Phosphorus During Pedogenesis. *Geoderma* 15(1), 1-19.

Weng L. P., Temminghoff E. J. M., and van Riemsdijk W. H. (2001) Contribution of individual sorbents to the control of heavy metal activity in sandy soil. *Environ. Sci. Technol.* 35(22), 4436-4443.

Weng L. P., Van Riemsdijk W. H., and Hiemstra T. (2006) Adsorption free energy of variable-charge nanoparticles to a charged surface in relation to the change of the average chemical state of the particles. *Langmuir* 22(1), 389-397.

Weng L. P., Van Riemsdijk W. H., and Hiemstra T. (2007) Adsorption of humic acids onto goethite: Effects of molar mass, pH and ionic strength. *J. Colloid Interf. Sci.* 314(1), 107-118.

Weng L. P., Van Riemsdijk W. H., and Hiemstra T. (2008) Humic Nano-Particles at the Oxide-Water Interface: Interaction with Phosphate Ion Adsorption. *Environ. Sci. Technol.* 42(23), 8747-8752.

Westall J. and Hohl H. (1980) A Comparison of Electrostatic Models for the Oxide/solution Interface. *Adv. Colloid Interf. Sci.* 12, 265-294.

Wiseman C. L. S. and Puttmann W. (2006) Interactions between mineral phases in the preservation of soil organic matter. *Geoderma* 134(1-2), 109-118.

Wolthoorn A., Temminghoff E. J. M., Weng L. P., and van Riemsdijk W. H. (2004) Colloid formation in groundwater: effect of phosphate, manganese, silicate and dissolved organic matter on the dynamic heterogeneous oxidation of ferrous iron. *Appl. Geochem.* 19(4), 611-622.

Zhou Q. H., Maurice P. A., and Cabaniss S. E. (2001) Size fractionation upon adsorption of fulvic acid on goethite: Equilibrium and kinetic studies. *Geochim. Cosmoschim. Acta* 65(5), 803-812.

Chapter 9

Nanoparticles in Natural Systems II: The Natural Oxide Fraction at Interaction with Natural Organic Matter and Phosphate

Tjisse Hiemstra, Juan Antelo, A.M.D. (Debby) van Rotterdam, and Willem H. van Riemsdijk

Published in Geochimica et Cosmochimica Acta
Volume 74, Issue 1, Pages 59-69, January 1, 2010

Abstract

Information on the particle size and reactive surface area of natural samples and its interaction with natural organic matter (NOM) is essential for the understanding bioavailability, toxicity, and transport of elements in the natural environment. In part I of this series (HIEMSTRA et al., 2010), a method is presented that allows the determination of the effective reactive surface area (A, m^2/g soil) of the oxide particles of natural samples which uses a native probe ion (phosphate) and a model oxide (goethite) as proxy. In soils, the natural oxide particles are generally embedded in a matrix of natural organic matter (NOM) and this will affect the ion binding properties of the oxide fraction. A remarkably high variation in the natural phosphate loading of the oxide surfaces (Γ, μmol/m^2) is observed in our soils and the present paper shows that it is due to surface complexation of NOM, acting as a competitor via site competition and electrostatic interaction. The competitive interaction of NOM can be described with the charge distribution (CD) model by defining a ≡NOM surface species. The interfacial charge distribution of this ≡NOM surface species can be rationalized based on calculations done with an evolved surface complexation model, known as the ligand and charge distribution (LCD) model. An adequate choice is the presence of a charge of -1 v.u. at the 1-plane and -0.5 v.u. at the 2-plane of the electrical double layer used (Extended Stern layer model).

The effective interfacial NOM adsorption can be quantified by comparing the experimental phosphate concentration, measured under standardized field conditions (0.01 M $CaCl_2$), with a prediction that uses the experimentally derived surface area (A) and the reversibly bound phosphate loading (Γ, μmol/m^2) of the sample (Part I) as input in the CD model. Ignoring the competitive action of adsorbed NOM leads to a severe under- prediction of the phosphate concentration by a factor ~10-1000. The calculated effective loading of NOM is low at a high phosphate loading (Γ) and vice versa, showing the mutual competition of both constituents. Both constituents in combination usually dominate the surface loading of natural oxide fraction of samples and form the backbone in modeling the fate of other (minor) ions in the natural environment.

Empirically, the effective NOM adsorption is found to correlate well to the organic carbon content (OC) of the samples. The effective NOM adsorption can also be linked to DOC. For this, a Non-Ideal Competitive adsorption (NICA) model is used. DOC is found to be a major explaining factor for the interfacial loading of NOM as well as phosphate. The empirical NOM-OC relation or the parameterized NICA model can be used as an alternative for estimating the effective NOM adsorption to be implemented in the CD model for calculation of the surface complexation of field samples. The biogeochemical impact of the NOM-PO_4 interaction is discussed.

1. Introduction

The bioavailability, toxicity, and mobility of ions in the environment are largely determined by the interaction with organic matter and mineral particles. The interaction is a complex process, involving factors such as the pH, ionic strength, the presence of competing or promoting ions as well as the nature and the amount of substrates, all affecting the distribution of cat- and anions over the solid and solution phase.

Development of in-situ surface spectroscopy and surface complexation models (SCM) have largely increased our insight in the adsorption processes of ions, in particular for well-defined systems. Surface complexation models have been widely applied to these systems. Ideally, SCM may predict changes in situations where experimental data are not available or difficult to collect. This is highly relevant for understanding the fate of elements at the field scale.

The application of SCM to natural systems like soils, sediments, and other aquatic media is quite complicated. Natural systems usually contain many different elements that may interact with a range of particles. In Part I of this series (HIEMSTRA et al., 2010), we have discussed how to derive the effective reactive surface area of the oxide particles. We proposed to use a naturally present probe ion and a model oxide with known binding properties as proxy to derive the effective reactive oxide surface area of natural samples. In this way, the adsorption behavior of the natural oxide fraction is represented by the behavior of the model oxide with a database of adsorption parameters. The rational is that in a first order approach the collective mutual behavior is strongly regulated by general electrostatic properties of a charged interface. In the method to determine the effective reactive surface area (A), a field sample is equilibrated with 0.5 M $NaHCO_3$ solutions at different solid solution rations (SSR) and the phosphate concentration is measured. The competitive phosphate-carbonate ad/desorption process in the sample is interpreted with the Charge Distribution model (HIEMSTRA and VAN RIEMSDIJK, 1996a). The CD model has been calibrated for the model oxide, i.e. goethite (RAHNEMAIE et al., 2007). Application of the CD model yields an effective surface area (A) and the amount of reversibly bound phosphate (R_{ev}). The particles of the natural oxide fraction are nano-sized (HIEMSTRA et al., 2010).

Even if an effective surface area is known and a database with parameters for ion binding to the model oxide is available, a remaining complication for applying SCM to natural systems is the presence of natural organic matter (NOM). It has been shown that the surfaces of the natural oxide particles are loaded with humic materials (HIEMSTRA et al., 2010; KAISER and GUGGENBERGER, 2000). This will strongly affect the binding of inorganic anions (BAUER and BLODAU, 2006; GERKE, 1993; GRAFE et al., 2002; GUSTAFSSON, 2006; KARLTUN, 1998; WENG et al., 2008). Therefore, this organo-mineral interaction requires attention if the aim is to apply SCM to natural samples under field conditions.

The interaction of NOM and metal oxide particles has been studied by many authors (DAVIS, 1982; EVANKO and DZOMBAK, 1999; FILIUS et al., 2000; GU et al., 1996; GU et al., 1994; TIPPING, 1981; WENG et al., 2007). The interaction is complicated, even without the presence of other adsorbing ions that may interact, such as phosphate and calcium. At present, a mechanistic framework is in development to describe such interactions in model systems (FILIUS et al., 2003; WENG et al., 2006; WENG et al., 2007). In the model, the NOM

adsorption is calculated based on a Ligand and Charge Distribution (LCD) approach. In a recent contribution (WENG et al., 2008), the competition between phosphate and humic & fulvic acids (HA & FA) has been studied for goethite. HA binds stronger than FA to goethite, but remarkably the study also showed that FA is a much stronger competitor for phosphate. This difference can be explained by a difference in the size of the molecules. HA molecules are more strongly bound than the FA molecules because the charge per molecule is much higher for large-sized molecules (WENG et al., 2007). On the other hand, the FA molecules are smaller and can approach the surface more closely. Adsorbed FA is mainly present in the compact part of the double layer, where it acts as a good competitor for phosphate. The LCD model (WENG et al., 2008) is potentially a powerful approach to model these interactions. However, for application to natural systems, it requires detailed information with respect to the mass distribution of natural organic acids in these systems. Therefore, we will formulate in the present paper a combined experimental and theoretical methodology that enables the incorporation of the interfacial NOM in the standard CD model.

In the new approach, the impact of adsorbed natural organic matter (NOM) on the binding of anions will be evaluated leading to an effective NOM density that is apparently active in the natural samples under standardized field conditions represented by 0.01 M $CaCl_2$ (VAN ERP et al., 1998). Phosphate is used as naturally present probe anion in the $CaCl_2$ solution and information of the phosphate loading, obtained with the 0.5 M HCO_3 equilibration (HIEMSTRA et al., 2010) will be included in the methodology. The phosphate loading is used as input in the CD model to evaluate the experimental phosphate concentration measured in the $CaCl_2$ systems. This leads to the calculation of the effective amount of NOM that is apparently active in the interface.

For a large set of samples, the variation of the NOM density will be studied, identifying factors that explain the calculated effective NOM density, such as the solution concentrations of PO_4 and DOC. This part of the data analysis will be done with a non-electrostatic version of the Non-Ideal Competitive adsorption (NICA) model (KINNIBURGH et al., 1999). Empirically, the relative NOM adsorption will be evaluated by considering general soil characteristics. If other information is absent, empirical relationships can be used to estimate the effective NOM adsorption to be implemented in the CD model for modeling the surface complexation of field samples.

The development of a consistent methodology to determine for natural samples the effective reactive oxide surface area as well as the effective NOM density enables, for the first time, a realistic scaling of SCM to field conditions.

2. Materials and Methods

2.1 Soils Samples

Representative agricultural top soils of the Netherlands (VAN ERP et al., 1998) have been used. The soil samples of the Copernicus soil series cover a wide range of organic carbon contents (~1-15 % OC) and clay contents (~3-30 %). The amount of reactive oxides has been characterized by extracting the soil with ammonium oxalate (pH = 3) and Dithionite Citrate

Bicarbonate (DCB). The effective surface area and reversibly bound fraction of phosphate have been determined with equilibration of the soils in 0.5 M $NaHCO_3$ (pH = 8.5) at a variable solid-solution ratios (HIEMSTRA et al., 2010). The details of the methods and main relevant soil characteristics have been presented in Hiemstra et al. (2010).

2.2 Equilibration at Standardized Field Conditions

A 10 mM $CaCl_2$ solution has been used to standardize the conditions at equilibration. This background electrolyte solution approximately simulates the relevant average field conditions of fertilized top soils. Native soils may have a lower ionic strength and for these, the use of 2.5 mM $CaCl_2$ has been suggested (SCHRODER et al., 2005). Our samples have been equilibrated using a high solid-solution ratio (SSR = 0.1 kg/L). The equilibrium state is reached relatively fast (2 hours) since not much desorption is needed in this procedure (VAN ERP et al., 1998). The pH has been measured in the 0.01 M $CaCl_2$ suspension and after phase separation by centrifugation (20 min 6000 rpm), the filtered supernatant has been analyzed for the major cations. In the extract, orthophosphate has also been measured. A molybdenum-blue method is used that has been adapted to measure relatively low PO_4 concentrations with a Segmented Flow Analysis (SFA) device. These data are given in Part I (HIEMSTRA et al., 2010).

For a limited number of samples, the speciation of DOC in the 0.01 M $CaCl_2$ solution has been measured. Hydrophilic acids (Hy), Fulvic acids (FA), and Humic acids (HA) have been separated using the method of Van Zomeren and Comans (2007). The concentration of dissolved C was measured with a TOC analyzer.

2.3 Surface Complexation Modeling

Surface complexation modeling will be done using the CD model (HIEMSTRA and VAN RIEMSDIJK, 1996a). The surface reactions, corresponding charge distribution, and affinity constants have been given in Hiemstra et al. (2010). The surface complexation modeling has been done with the ECOSAT software (KEIZER and VAN RIEMSDIJK, 1998) in combination with FIT (KINNIBURGH, 1993).

3 Results And Discussion

For clarity, the next sections treat two main issues. The first three Sections (3.1-3.3) discuss the application of the probe ion method to soils at standardized field conditions (0.01 M $CaCl_2$). It shows that the PO_4 equilibrium concentration is strongly under predicted if the presence of NOM is ignored (3.1). Therefore, an interfacial NOM loading is theoretically defined (3.2) and application in SCM shows that the phosphate loading in natural soils is suppressed by competition of adsorbed NOM that correlates with DOC (3.3). In the next two Sections, a thermodynamic model is formulated (3.4) and applied (3.5) to gain insight in the overall relationships between adsorbed and dissolved orthophosphate and NOM/DOC of natural soils. Finally (3.6), a road map is added that describes the procedure to apply the effective NOM loading in surface complexation models.

3.1 P-loading and Solution Composition

The probe ion procedure to determine the reactive surface area of natural materials (HIEMSTRA et al., 2010) has been developed for the application to natural systems where ion adsorption is to be predicted. Its applicability can be tested for the soil samples under standardized field conditions (0.01 M $CaCl_2$). Starting point is the phosphate loading Γ (μmol PO_4 /m^2) in the samples resulting from the 0.5 M $NaHCO_3$ equilibration extraction and subsequent modeling.

The variation in the phosphate loading, derived with the probe ion method (HIEMSTRA et al., 2010), is relatively high (Γ ~1-3 μmol/m^2). For natural soils, the observed loading is imposed by the average conditions experienced by the oxide fraction in the field, such as the pH and phosphate concentration (c_{PO4}). Surprisingly, the relationship between logΓ and logc_{PO4} measured in the 0.01 M $CaCl_2$ solution (n = 19 data points) shows a large scattering (R^2 = 0.31), whereas the correlation between logΓ and log DOC is much better (R^2 = 0.66). It is important to notice that without a scaling to surface area no relationship between the phosphate loading and the dissolved phosphate concentration is found (R^2 = 0.06). On a mass basis, one is blind in this respect.

This statistical result suggests that DOC is a major explaining factor for the variation in the adsorption of PO_4. The observed correlation might be due to a DOC-PO_4 competition at the oxide surface. According to the typical shape of a high-affinity adsorption isotherm, the adsorption of phosphate will only slightly change in the high concentration range, where the loading becomes increasingly independent of phosphate concentration (Fig.1). If adsorbed NOM determines the phosphate surface saturation, one may observe a correlation with DOC that can be stronger than the contribution of the phosphate concentration.

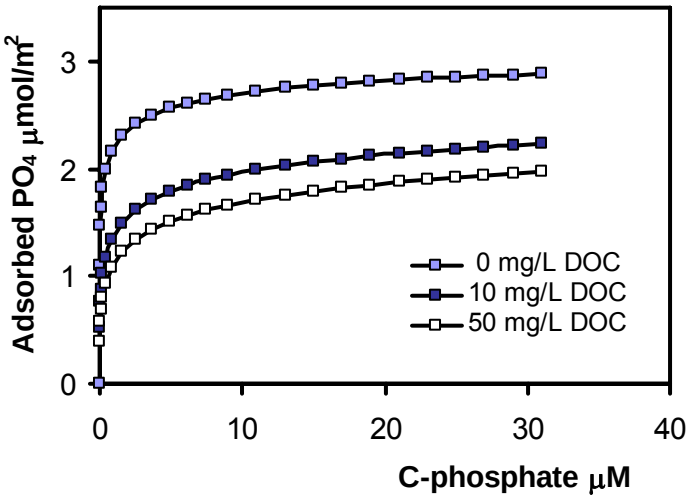

Fig.1. Conceptual picture of the phosphate adsorption isotherms in 0.01 M $CaCl_2$ (pH = 5.5) at a DOC concentration of 0, 10, and 50 mg/L. The variation in the DOC concentration has a large effect on the PO_4 adsorption. The lines have been calculated using the NICA model, which was fitted to the experimental data (see text).

The experimental phosphate concentration in 0.01 M $CaCl_2$ can be evaluated using the reversible phosphate loading Γ as input in the CD model. The loading can be derived with the 0.5 M $NaHCO_3$ equilibration procedure (HIEMSTRA et al., 2010). In case of the presence of adsorbed NOM, it may be expected that the model will predict a lower phosphate concentration in 0.01 M $CaCl_2$ if the competition of adsorbed NOM is not included in the modeling. In the bicarbonate equilibrium extraction, adsorbed NOM is probably largely removed by the combination of a high pH, a very low Ca concentration, and the addition of active carbon in excess that all stimulate the removal of carbon from the soil matrix. In contrast, one may expect that the soil material in a 0.01 M $CaCl_2$ solution will have a nanoparticle association of NOM and oxides such as depicted in Part I (HIEMSTRA et al., 2010).

The orthophosphate equilibrium concentrations in the 0.01 M $CaCl_2$ solutions, predicted with the above approach, are indeed much too low (10-1000 times) when compared to the experimental data. The deviations are very large and variable. The average concentration differs by $\Delta\log c = 1.6 \pm 0.7$.

The effective NOM density present in the interface can be quantified by comparing the predicted and the experimental phosphate concentration in the 0.01 M $CaCl_2$ solution. The possible influence of adsorbed NOM on the anion competition can be calculated by defining a NOM surface species that can be used in the standard CD approach. The NOM adsorption involves competition for surface sites as well as an electrostatic competition due to the introduction of negative charge in the EDL. This is discussed next.

3.2 NOM Surface Species

To implement the effect of the adsorption of NOM in the CD model, we may define a NOM surface species, ≡ FeNOM, that is formed from a surface component $\equiv HNOM^z$. The sole use of surface components is mathematically elegant. Others (GUSTAFSSON, 2006) have used a solution component in combination with a hypothetical affinity constant ($\log K$) to create interfacial NOM. In the traditional calculation scheme of columns and rows as presented in Table 2 of Part I (HIEMSTRA et al., 2010), adsorbed NOM can be created by combining the surface components $\equiv FeOH^{-1/2}$ and $\equiv HNOM^z$, visualized schematically as:

$$\equiv FeOH^{-1/2} + \equiv HNOM^z \Leftrightarrow \equiv FeNOM^{-1/2+z+\Delta z_0,\ \Delta z_1,\ \Delta z_2} + H_2O \qquad K \equiv 1 \qquad (1)$$

In the calculation scheme (Table 2, Part I, (HIEMSTRA et al., 2010)), $\equiv HNOM^z$ is a virtual component. NOM is only present as ≡FeNOM species. The total surface charge of the created ≡FeNOM species ($-1/2+z$) is redistributed as defined by the three charge distribution coefficients Δz_i shown in eq.(1). This charge can be redistributed over three electrostatic planes ($i = 0,1,2$). The sum of the charge distribution coefficients is zero, i.e. $\Delta z_0+\Delta z_1+\Delta z_2 = 0$, since no additional charge from any solution component is entering the interface.

3.2.1 Classical Use of CD

As suggested above, the interaction of adsorbed NOM with adsorbed PO_4 can be due to site competition as well as an electrostatic competition. Therefore, the charge (z) per reacted surface group and its location (Δz_i) are relevant. These have been chosen based on the results of surface speciation calculations done for fulvic acid that is adsorbed by goethite (FILIUS et al., 2000; FILIUS et al., 2003; WENG et al., 2005; WENG et al., 2008).

A typical small FA molecule may have on average about 4 -COOH groups and 1 -COH group (FILIUS et al., 2000). The works of Filius et al. (2000; 2003) suggest that upon adsorption one of the carboxylate groups ($RCOO^-$) will form an innersphere complex according to the ligand exchange reaction:

$$\equiv FeOH^{-1/2} + H^+(aq) + RCOO^{-1}(aq) \Leftrightarrow \equiv FeO^0 - CO^{-0.5} - R + H_2O(l) \qquad (2)$$

In this classical formulation, the charge of the proton is added to the surface plane and as a result of ligand exchange releasing a H_2O. The charge of $RCOO^-$ is distributed equally over the 0- and 1-plane. The corresponding CD is $\Delta z_0 = +1-0.5 = +0.5$ valence units (v.u.) and $\Delta z_1 = -0.5$ v.u. (FILIUS et al., 1997). Overall, the reaction will neutralize the surface oxygen charge (changing from -1/2 to 0 v.u.) and adds a charge of -0.5 v.u. to the 1-plane.

The other functional groups of the adsorbed FA molecule are present outside the surface in the Stern layer. Surface complexation modeling suggests that this ensemble of functional groups attributes on average a net charge of about $\Delta z_1 = -1$ v.u. per $\equiv FeOH^{-1/2}$ to the 1-plane (FILIUS et al., 2000; 2003) in the relevant pH range. Therefore, the combination of inner- and outersphere complexation results in a total charge attribution to the 1-plane of $\Delta z_1 = -0.5+-1 = -1.5$ v.u. In the presence of Ca^{2+}, the surface speciation suggested by the LCD model (WENG et al., 2005) is similar.

The above modeling results have been obtained with a SCM model that uses the Basic Stern approach. FA molecules are relatively large compared to inorganic anions and an Extended Stern layer model can be considered as more suitable. In that approach, the outer sphere ligands can be present in the 1- and 2-plane. If the corresponding charge of the outer sphere ligands (-1 v.u.) is equally distributed over both planes, the overall charge distribution, including innersphere complexation, results in $\Delta z_0 = +0.5$ v.u., $\Delta z_1 = -1.0$ v.u., and $\Delta z_2 = -0.5$ v.u. The FA surface species can be represented as $\equiv FeO^0\text{-}CO^{-1}\text{-}R^{-0.5}$.

3.2.2 Effective CD using Surface Components Only

The proposed coefficients in Section *3.2.1* are valid if the adsorption of FA is modeled using the combination of a solution component (FA, aq) and a surface component ($\equiv FeOH^{-1/2}$). However, in the reaction scheme (HIEMSTRA et al., 2010), the ≡FeNOM species is formed directly from surface components only, i.e. from the combination of 1 $\equiv FeOH^{-1/2}$ and 1 $\equiv HNOM^z$ (eq.(1)) with $z = -1$ v.u.. The total charge of these two surface components in the reference state is -1.5 v.u. When defined, the surface component charge is conventionally attributed to the surface plane but will be neutralized upon formation of the surface species

≡FeNOM (eq.(1)). This is done by redistribution of the charge in the interface. A charge of +1.5 v.u. charge is transformed from the Stern planes to the surface plane, i.e. $\Delta z_0 = +1.5$ v.u., $\Delta z_1 + \Delta z_2 = -1.5$ v.u., and $\Delta z_0 + \Delta z_1 + \Delta z_2 = 0$ v.u. The charge in the Stern layers is distributed such that one gets the above suggested values for adsorbed FA, i.e. $\Delta z_1 = -1.0$ v.u. and $\Delta z_2 = -0.5$ v.u. In summary, the charge distribution coefficients in the present model for the formation of $\equiv FeNOM^{0\ -1\ -0.5}$ from 1 $\equiv FeOH^{-1/2}$ and 1 $\equiv HNOM^{-1}$ (eq.(1)) will be $\Delta z_0 = +1.5$ v.u., $\Delta z_1 = -1.0$ v.u., and $\Delta z_2 = -0.5$ v.u. (Table 2 in part I).

Recently, the ligand and charge distribution (LCD) approach has been adapted (WENG et al., 2006; 2008). In the newest approach, half of the functional groups of FA is attributed to the 2-plane, while the other half is present in the 0- or 1-plane. The distribution of the ligands between the 0- and 1-plane depends on the degree of innersphere complexation, which is obtained by modeling. The new LCD approach confirms that on average approximately one ligand per adsorbed FA molecule will interact with the surface by ligand exchange forming an innersphere complex leading to $\Delta z_0 = +0.5$ v.u. and $\Delta z_1 = -0.5$ v.u. However, according to the new model approach, the other -COOH groups will dissociate protons more strongly than previously suggested, i.e. -2 v.u. instead of -1 v.u. per FA. This is found for simple oxide systems with only FA, but the situation changes if phosphate is present too. In that case, the interface becomes more negatively charged and this will suppress the dissociation of the -COOH groups. As a result, the charge present on the functional groups in the 1-plane is on average more close to -1 v.u. and therefore, the above chosen coefficients (Table 2 in Part I) are consistent with this recent picture (WENG et al., 2008), if adsorbed phosphate is present.

It should be noted that the present approach (eq.(1)) is a strong simplification. Actually, the charge and ligand distribution is variable and depends on factors such as pH, phosphate, and NOM loading. Moreover, large NOM molecules like HA may attribute charge to the DDL (WENG et al., 2007). Calculation of these effects requires an adequate theoretical framework such as the recent LCD model (WENG et al., 2007; WENG et al., 2008). In principle, such an approach allows quantification of the relationship between dissolved and adsorbed NOM, which is absent in the above model formulation (eq.(1)).

3.3 Effective NOM Adsorption Density

3.3.1 Phosphate NOM Competition

By defining a NOM surface species (eq.(1)), the CD model can calculate an effective NOM adsorption density (≡FeNOM). In the calculation, we search for the apparently required NOM adsorption density that explains the 10-1000 times higher phosphate concentration in 0.01 M $CaCl_2$ in the various samples using as constraint the phosphate loading and surface area that we derived with equilibration in 0.5 M $NaHCO_3$ (Part I, probe ion method). For the calculation of ≡FeNOM, we used the experimental pH value in 0.01 M $CaCl_2$ as well as the measured Na^+, K^+, Ca^{2+}, and Mg^{2+} concentrations as given in Hiemstra et al. (2010). We note that it turned out that the latter is not essential. The use of only 0.01 M Ca^{2+} and 0.02 M Cl^- as ion concentrations is sufficient.

The phosphate loading Γ (μmol/m^2) of a soil is an essential factor in the calculation of ≡FeNOM. The loading Γ is the combination of the amount of reversibly adsorbed phosphate content R_{ev} and the effective reactive surface area A, which are both used as input parameters in the CD model. It is important to notice that the uncertainty in the determination of the absolute value of A as well as R_{ev} is usually relatively high, on average about 10% (HIEMSTRA et al., 2010). However, the uncertainty in the phosphate loading Γ is generally much smaller, i.e. about 2 %, even though Γ is a combination of the surface area A and the content R_{ev} ($\Gamma = R_{ev} / A$), The reason is that the values of A and R_{ev} are strongly correlated. A small uncertainty in the phosphate loading Γ is important because a small variation in Γ will already lead to a rather large variation in the phosphate concentration in solution, as follows from the shape of the isotherm in Fig.1. Correspondingly, this leads to a relatively large uncertainty in the calculated effective NOM adsorption. Practically, it implies that the calculation of the effective NOM adsorption density should only be based on that combination of A and R_{ev} that correctly represents the value of Γ found at evaluation of the $NaHCO_3$ equilibration data with the probe ion method.

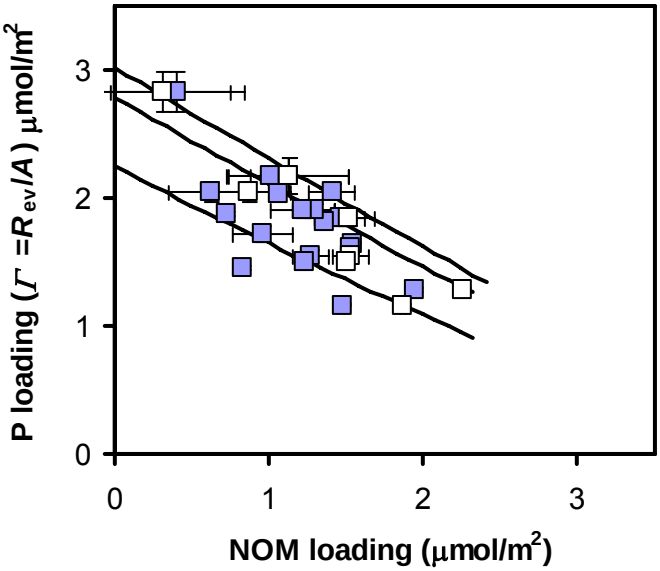

Fig.2. The PO_4 loading (Γ) derived from the interpretation of the $NaHCO_3$ equilibrium extraction data as a function of the effective NOM adsorption (≡FeNOM in μmol/m^2) to explain the PO_4 concentration in the $CaCl_2$ extracts. The closed symbols refer to the soils presented in Table 1 of Part I (HIEMSTRA et al., 2010). The open symbols are from additional measurements of the PO_4 concentration and pH in 0.01 M $CaCl_2$ after sample storage for 10 years (see text). The lines have been calculated with the CD model described for an average of pH = 5.5 and from bottom-up for respectively c-PO_4 = 1, 10, and 30 μM. The parameters are given in Table 2 of Part I (HIEMSTRA et al., 2010).

In Fig.2, the error bar for the phosphate loading Γ refers to the difference in loading at evaluation of the $NaHCO_3$ extract using the linear or the logarithmic scale for the phosphate concentration, as described in part I. The uncertainty in Γ leads to a variation in the predicted

equilibrium concentration of phosphate in the 0.01 $CaCl_2$ solution, which is rather high due to the high-affinity shape of the adsorption isotherm (Fig.1), and correspondingly, this leads to an uncertainty in the calculated effective NOM adsorption.

As follows from Fig.2, the calculated effective NOM adsorption density (≡FeNOM) clearly varies amongst the soils studied. Our analysis shows that soils with a high PO_4 loading (Γ in μmol/m^2) have a low effective NOM adsorption density (≡FeNOM μmol/m^2) and vice versa (Fig.2). The behavior observed is typical for a competitive adsorption process.

Our calculations immediately make clear why the selected soils have a relatively large variation in the P-loading (Γ ~1-3 μmol/m^2) while this is not expected from the variation of the experimental PO_4 concentration in the $CaCl_2$ extract if the PO_4 adsorption is based on only PO_4, H^+, and Ca^{2+} interaction (Fig.1, upper curve). What causes this difference? It is most likely the presence of DOC that leads to adsorbed NOM.

Table 1. The pH and phosphate concentration in 0.01 M $CaCl_2$ solution, and the corresponding speciation of DOC with Hydrophilic acids (Hy), Fulvic acids (FA), and Humic acids (HA) using the method of Van Zomeren and Comans (2007). The data were collected 10 years after sampling of the Copernicus soil series. For comparison to the original data, see Table 1 part I

Soil	pH	P-PO_4	DOC (mgC/L)			
		μM	Total	Hy	FA	HA
2	5.16	24.6	29	23	6	0
3	5.64	3.5	32	24	8	0
7	5.77	16.3	14	11	3	0
9	4.45	7.7	112	89	20	2
10	5.02	1.9	83	65	18	0
11	5.45	10.4	144	107	37	0
13	7.24	4.5	24	19	5	0
14	6.75	20.9	8	4	4	0

3.3.2 Interfacial NOM and DOC

The $CaCl_2$ data set used (HIEMSTRA et al., 2010) refers to the original measurements done shortly after sampling. Ten years later, a number of samples have been reanalyzed and these $CaCl_2$ data are in Table 1 as part of this study. Meanwhile, the PO_4 concentrations in the 0.01 M $CaCl_2$ extract have increased. The DOC concentrations have increased too, probably due to some slow NOM disintegration. The simultaneous increase of the phosphate as well as the DOC concentration is consistent with the concept of a NOM-PO_4 competition. The increase of the amount of relatively small DOC molecules will lead to some more adsorption of NOM in the compact part of the EDL, resulting in more competition with PO_4. The corresponding amount of adsorbed NOM has been calculated and is given in Fig.2 and 3 as open symbols.

In Fig.3, the calculated NOM adsorption of the soils is given as a function of the DOC concentration (mg/L) measured in a 0.01 M $CaCl_2$. Soils with a low effective NOM

adsorption also have a low DOC concentration in solution. As illustrated in Fig.3, increase of the DOC concentration leads to an increase of the NOM adsorption, and according to Fig.2, to a decrease of the PO_4 loading. At high DOC concentrations, the loading of NOM apparently approaches a maximum.

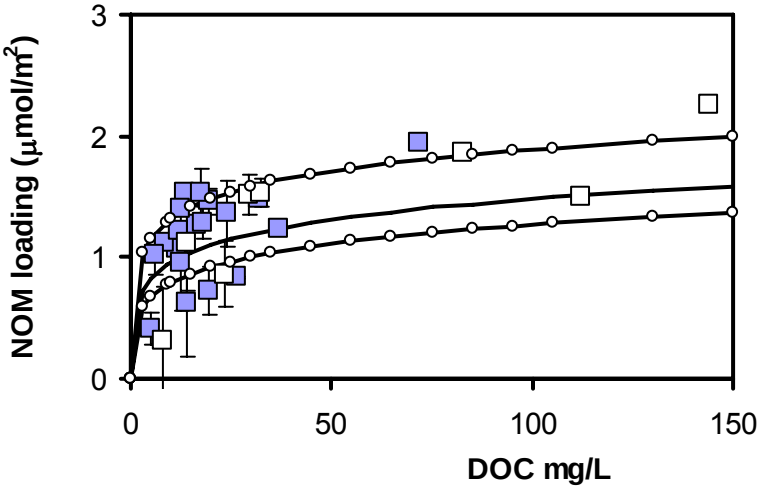

Fig.3. The effective NOM adsorption density (µmol/m^2) acting as competitor for phosphate plotted versus the DOC concentration present in 0.01 M $CaCl_2$ extract of the Copernicus soil series. The data points (symbols defined in Fig.2) have been found by analyzing the experimental phosphate concentrations of the 0.01 M $CaCl_2$ solutions using the PO_4 loading Γ derived from the $NaHCO_3$ equilibrium extractions. The lines in Fig.3 have been calculated with the NICA model (Table 2) for three phosphate concentrations that cover the experimental range (top-down for respectively 1, 10, and 30 µM) using the average pH (pH = 5.5).

3.3.3 Interfacial Carbon Loading

With the present approach, it is impossible to link the calculated effective NOM adsorption (Fig.2) directly to an actual carbon density. This can be seen as a limitation. The effective NOM adsorption density has been derived by fit, evaluating the competition of NOM with PO_4. The same level of competition, i.e. the same effective NOM adsorption, can be due to a very different amount of adsorbed carbon because the competition of NOM with PO_4 depends largely on the molecular size of the NOM molecules involved. This distribution is difficult to quantify. From a practical perspective of surface complexation modeling, the use of an effective loading may be seen as an advantage. Our approach does not require particular knowledge about the amount of interfacial carbon bound and its detailed speciation.

Despite the above, quantifying the carbon density that might be involved in the effective NOM adsorption may gain insight in the amount of carbon that is active in the Stern layer region near the oxide surface. To calculate the apparent amount of carbon that is involved in the effective NOM adsorption, an arbitrary choice is used for the molar mass of 750 g/mol. Such a molar mass leads to a particle size that fits to the total Stern layer.

This molar mass can be combined with the range of observed effective NOM adsorption, being 0-1.5 µmol/m^2 (Fig.3), leading to 0-0.5 mg OC/m^2 or 0-0.8 mg NOM/m^2.

These numbers are substantially lower than the total carbon and NOM adsorption on natural oxide surfaces, which is ~1.4 mg OC/m^2 or ~2.5 mg NOM/m^2 as shown in Part I (HIEMSTRA et al., 2010). The apparent amount of carbon in the interface is only about 30%. Nevertheless, the estimated effective carbon loading may agree conceptually with the structure of an association of NOM and oxide nanoparticles as depicted in Part I. Only a part of the total amount of adsorbed organic matter is directly involved in the competition with phosphate in the compact part of the double layer. A large fraction of the adsorbed organic matter is further away from the surface. Based on the total thickness of the Stern layer of 0.7 nm (HIEMSTRA and VAN RIEMSDIJK, 2006) and the corresponding volume, the maximum NOM adsorption in the inner Stern layer can be calculated at a given a mass density of 1250 kg/m^3, leading to about 0.8 mg NOM/m^2. This maximum loading is rather close to the highest effective loading in our soils in case of a molar mass of 750 g/mole.

3.4 NICA Model: Linking DOC and ≡NOM

Thermodynamics are the basis of surface complexation modeling. A thermodynamic approach implies that it may not reflect necessarily the processes at the molecular level. We will discuss here a simplified non-electrostatic version of the non-ideal competitive adsorption (NICA) model to describe the interaction between DOC and phosphate in relation to adsorbed NOM and phosphate. It will be used to gain insight in overall relationships between adsorbed and dissolved phosphate and NOM/DOC.

The NICA model has been developed to describe the adsorption of the ions by organic matter (KINNIBURGH et al., 1999). The model combines chemical heterogeneity with a local non-ideal adsorption isotherm. In case of a homogeneous surface, the NICA equation for the adsorption of ion i with a binding constant K_i reduces to:

$$\Gamma_i = \Gamma_{\max} \frac{n_i}{n_{\mathrm{REF}}} \frac{(K_i C_i)^{n_i}}{1+\sum (K_j C_j)^{n_j}} \tag{3}$$

in which $\Gamma_{\max}$ (μmol/m^2) is the maximum adsorption density and n_i represents the non-ideality parameter of ion with index i. The index j in the denominator refers to the various types of ions that may adsorb. In our case, this may be protons, phosphate, and DOM molecules. Thermodynamic consistency requires that the adsorption is scaled to a chosen reference ion (KINNIBURGH et al., 1999). In the modeling, the non-ideal coefficients of DOC and PO_4 were set equal and therefore, both can be used as reference. Implicitly, this choice means that both species can reach the same adsorption maximum if all sites are occupied and both species have the same reaction stoichiometry with respect to the surface sites used. We note that the NICA model has been used previously to model the binding of phosphate (ABOU NOHRA et al., 2007; JIAO et al., 2008). A major difference is that we use a scaling per unit surface area, which reveals the influence of DOC/NOM, which has not been considered previously. We note that the NICA equation will reduce to the competitive Langmuir equation for $n_i = 1$.

The challenge is to describe simultaneously the PO_4 adsorption with and without the presence of DOC as a function of phosphate concentration and pH. Therefore, we have generated with the CD model 36 data points for the PO_4 adsorption in 0.01 M $CaCl_2$ in the absence of DOC for a wide range of phosphate concentrations (0.1-30 μM) and covering the range pH = 4-7. These synthetic adsorption data could be described very well ($R^2 = 0.97$) with the fitted parameters of Table 2. In the approach, the site density was set at Γ_{max} = 3.5 μmol/m^2. With this chosen number, a reasonable description can be obtained for the adsorption density of phosphate as well as NOM in soil without further scaling. The binding constant for DOC was derived by trial and error, evaluating simultaneously the phosphate and NOM adsorption for the soils studied. The standard deviation for the description of the phosphate adsorption of the soils (27 data points) is 0.25 μmol/m^2 and $R^2 = 0.66$. For NOM, the standard deviation is 0.25 μmol/m^2 and $R^2 = 0.32$.

Table 2. The parameters of the non-ideal competitive adsorption model describing which is used to construct the lines of Figs.1, 3, and 4

Parameter	value
$n_{REF} \equiv n_{PO4} \equiv n_{DOM}$ *1	0.29 ± 0.01
log$K$PO$_4$	8.5 ± 0.1
logK_{DOM}*2	6.9 ± 0.1
n_H*3	0.09 ± 0.01
logK_H	≡ 9
Γ_{max}*3 μmol/m^2	≡ 3.5

*1 Equal numbers implies that PO_4 and DOC can reach the same adsorption maximum. Both n values can serve as reference in eq.(3) (n_{REF}). Note ≡ chosen

*2 The value of logK_{DOM} is valid assuming a molar mass of M = 750 g / mole for DOM (= $CH_2O)_x$, x = 25)

*3 The low value of n_H illustrates the weak pH dependency of the overall adsorption of PO_4 in the multi-component systems. The value of n_H is low compared to the value found for humics (Milne et al., 2003), and might be related to the much stronger feedback of electrostatics on the change of the relative proton loading of sites θ_H on oxide surfaces. For H^+, the highest adsorption will be much lower, i.e. $\Gamma_H = \Gamma_{max}\ n_H/n_{ref} \sim 1.1$ μmol/m^2 which is ~ 100 mC/m^2. This number can be considered in a first order approach as representative for sesquioxides in the pH range considered.

In this thermodynamic model, total dissolved orthophosphate (c_{PO4}) was used. Moreover, the DOC is represented by one type of molecule whereas it has been shown that natural DOC fraction is a mixture of different types of organic molecules such as fulvic (FA), humic (HA), and hydrophilic acids (Hy), which all have variable charge. For a limited set of eight samples, we have fractionated the DOC in the three above-mentioned fractions using the method of Van Zomeren and Comans (2007). As follows from Table 1, most carbon in the solution was present as hydrophilic acids, 76 ± 8 %. A small fraction was present as FA and very little or no humic acid was found in the 0.01 M $CaCl_2$ extracts. The data show that the DOC has a low molecular mass and for these organic molecules in particular, it may be expected that they have a relatively strong interaction with phosphate (WENG et al., 2008). Moreover, small natural organic acids are more weakly bound by (hydr)oxide surfaces compared to molecules with a high molecular mass and corresponding charge such as HA

(WENG et al., 2007). Therefore, DOC can be considered as labile and reactive for oxyanion competition.

For modeling, the DOC (mg/L) concentration is to be expressed as a DOM particle concentration (C_{DOM} in mol/L). An arbitrary assumption was made for the molar mass and carbon content. We assume that DOM can be represented by $(CH_2O)_x$ with a molar mass of M = 750 g/mol (i.e. x = 25 mol C/ mol DOM). The resulting molar DOM concentration (mol/L) has been used to parameterize the NICA model in combination with the total molar orthophosphate concentration of the solution (c_{PO4}) and the H^+ activity. It is important to note that any other choice of a value for the molar mass *M* will lead in the fitting to the same description of the data, but another fitted value of K_{DOM}. In the fitting, the product $K_{DOM}.c_{DOM}$ is independent of the choice of the molar mass *M*. A higher *M* leads to a lower c_{DOM} and *vice versa* but a correspondingly higher K_{DOM}.

3.5 NICA application

The parameter set of Table 2 has been used to construct the phosphate isotherms for a number of DOC concentrations, as given in Fig.1. The results of the thermodynamic model (Fig.1), as well as the previous multi-linear regression of the data (Section 3.2), show the relative significance of the variation in DOC for the phosphate loading. In nature, many biogeochemical factors may influence the actual DOC concentration in ecosystems. DOC can be produced as a byproduct of microbial degradation of organic matter but can also be released from oxide surfaces due to changes in the phosphate status of a soil. DOC itself can also be decomposed or absorbed in NOM supra-molecules. The complex nature of these interactions and processes makes it very difficult to do predictions of the DOC concentrations in the field. Therefore, like pH, the DOC concentration is most effectively used as input in, rather than as output from, modeling.

The undemanding non-electrostatic NICA approach has been used to relate the NOM adsorption to the DOC concentration in solution. The lines in Fig.3 have been calculated for three phosphate concentrations that cover the experimental range (1, 10, and 30 μM) using the average pH value (pH = 5.5). As clear from Fig.3, the quality of prediction of the density of ≡FeNOM is only reasonable. The standard error is 0.25 μmol/m^2. As discussed above, the amount of adsorbed NOM is based on the interaction with PO_4, and therefore it will refer particularly to small organic acids, because these are most effective in the competition as discussed above.

The NICA model can be used to generate the expected relationship between dissolved phosphate and the DOC concentration at a given pH and P loading (Fig.4). The range of conditions corresponds to those previously used to calibrate the NICA model, i.e. pH~4-7, c-PO_4 ~0.1-30 μmol/L, and DOC ~ 0-100 mg/L, all in 0.01 M $CaCl_2$ solution. The calculations have been done for a SSR, representative for soils in the field (10 kg/L) and refer to an average effective surface area of A = 15 m^2/g soil. Fig.4 shows that one may expect for a given phosphate loading a rather strong increase of phosphate concentration in case of an increase of the DOC concentration. The large variation in the c-PO_4 and DOC relationship (Fig.4) implies that if a series of soils with a variable PO_4 loading is considered, no simple

relationship between dissolve phosphate and DOC will be found. A third point is that the calculated phosphate concentration decreases with an increase of the pH from 5 to 7 in a 0.01 M $CaCl_2$ extract. Calcium ions will promote the adsorption of phosphate at high pH (RIETRA et al., 2001a) and this effect is large in 0.01 M $CaCl_2$. In nature, the situation may be different. The pH dependency can be smaller, absent, or even opposite depending on the Ca^{2+} and Mg^{2+} concentrations in the pore water under field conditions. Moreover, the solubility of DOC may change with pH, which will effect the competition with phosphate at the oxide surfaces and the corresponding phosphate concentration in solution.

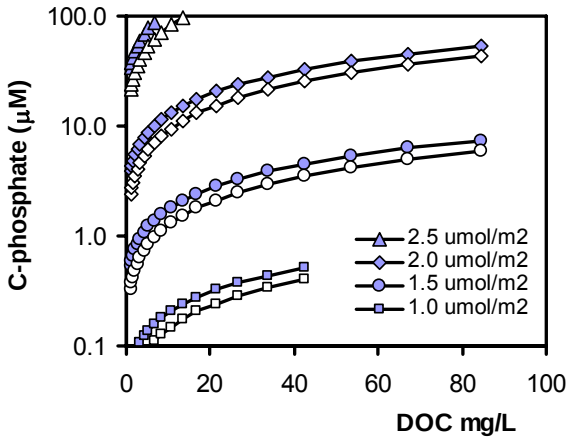

Fig.4. The effect of DOC on the phosphate concentration (note the logarithmic scale) in 0.01 M $CaCl_2$ for a soil with a P loading of 1.0, 1.5, 2.0, and 2.5 µmol/m^2 at pH = 5 & 7 (closed and open symbols respectively), SSR = 10 kg/L, and an average A = 15 m^2/g soil. The lines have been calculated with the NICA model (Table 2).

3.6 Epilogue

Above, we have shown how CD modeling can be implemented when it comes to application in field samples. It can be summarized as follows.

A) The $NaHCO_3$ equilibrium extraction method (HIEMSTRA et al., 2010) will provide a straightforward measure for the oxidic surface area of a sample. The surface area is to be considered as an effective surface area that has the advantage that it is able to mimic the observed adsorption behavior using the most important oxyanion bound by natural oxide surfaces as calibrating ion (PO_4).

B) The $NaHCO_3$ equilibrium extraction method will also reveal the fraction of reversibly bound ions (PO_4). The combination of this fraction and the effective surface area can be introduced in the CD model for an environmental application, if one accounts for the impact of the presence of adsorbed humic material. The impact of organic matter can be incorporated in the CD model in a first order approach by defining with only surface components a hypothetical surface species (≡FeNOM) that mimics the site and electrostatic competition. The effective NOM density (≡FeNOM) can only be applied in the CD model as long as the effective NOM adsorption is not significantly changed by the competition with other ions.

C) There are several approaches to derive or estimate the effective adsorption density of NOM (≡FeNOM). Above, we have described how one may derive the effective adsorption density of NOM using as input the pH and phosphate concentration determined in a 0.01 M $CaCl_2$ extract for a given amount of reversibly bound phosphate (R_{ev}) and a known effective surface area A.

If a change of DOC is to be considered for a prediction, we suggest to estimate the effective adsorption density of NOM using the parameterized NICA model (Table 2). For this approach, data have to be available for the PO_4 and DOC concentrations and the pH value, preferably measured in a 0.01 M $CaCl_2$ extract at SSR of 0.1 kg/L. The actual calculation of ≡FeNOM is straightforward, simply introducing the experimental concentrations in the NICA model (eq.(3)), yielding Γ_{DOC} (mol/m^2), which can be recalculated to ≡FeNOM in nm^{-2} (1 nm^{-2} = 1.66 μmole/m^2).

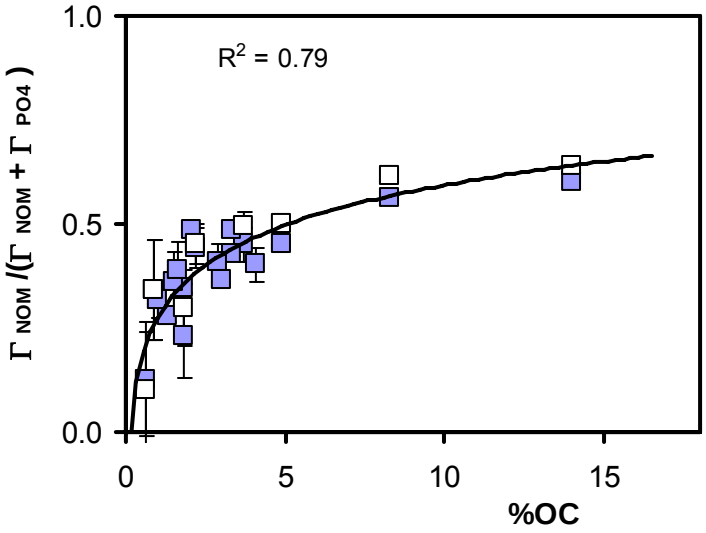

Fig.5. The relative adsorption of effective NOM ≡ Γ_{NOM} / (Γ_{NOM}+Γ_{PO4}) can be correlated (line) with the logarithm of organic carbon percentage in the agricultural soil samples studied, i.e. y = 0.32 log x +0.27. Symbols as defined in Fig.2.

A third approach to estimate the effective NOM site density is based on an empirical relationship and can be deployed if other data are not available. We have found for our agricultural top soils (27 data points) that the relative NOM densities, defined as Γ_{NOM} / (Γ_{NOM}+Γ_{PO4}), are strongly related (R^2 = 0.79) by the total organic carbon content of the sampled material (Fig.5). The advantage of the use of this relationship is that the organic carbon percentage is often measured as a general characteristic of samples. The measured carbon content in combination with the phosphate loading Γ_{PO4} determined experimentally with the probe ion method leads to an estimation of the Γ_{NOM}, which then can be applied in the CD model for application to field samples. This increase of surface coverage of NOM with the organic carbon content is in line with recent results found by studying the energetics of N_2 gas adsorption in soils (WAGAI et al., 2009).

D) Once the effective adsorption density of NOM (≡FeNOM) has been derived or estimated, it can be implemented in the SCM calculation scheme given in part I (HIEMSTRA et al., 2010).

In natural systems, the interfacial properties of the oxides will be determined by the dominant binding of only a few inorganic ions and additionally interfacial ≡NOM. The proton is generally the potential determining ion of the surface and this ion will indirectly also determine the pristine Stern potentials (ψ_1 and ψ_2). However, the Stern potentials are strongly changed by electrostatic charge entering the interface via adsorption of other species (Δz_1 and Δz_2). Modeling shows that in non-acid soils, NOM, PO_4^{3-}, and Ca^{2+} are generally the most important components in determining these electrostatic potentials. For this reason, these components (H^+, Ca^{2+}, PO_4^{3-}, and NOM) cannot be ignored in any realistic study or description of the adsorption of these ions and those present in minor amounts in the interface, in particular oxyanions such as $As(OH)_3$, AsO_4^{3-}, CrO_4^{2-}, SeO_3^{2-}, *etceteras*. Some species may have an intermediate position, being present in higher concentrations, such as SO_4^{2-} and H_4SiO_4. The latter one can be important at neutral and alkaline pH conditions (ground and surface waters) and the first one is bound in acid soils (e.g. forest soils), together with Al^{3+}. Our calculations suggest that these ions may adsorb, but the amounts are often relatively low in comparison to PO_4 and NOM. In such case, these species are not primary potential determining ions strongly affecting the adsorption of the major species of the interface.

4 Conclusions

- For the agricultural top soils studied, the variation in the reversible phosphate loading is unusually large (Γ = ~ 1 - 3 μmol/m^2). This natural variation is strongly related to the amount of adsorbed NOM and vice versa. The effective amount of adsorbed NOM (0~2 μmol/m^2) is found by interpreting the phosphate concentration in 0.01 M $CaCl_2$ using the phosphate loading derived in the 0.5 M $NaHCO_3$ equilibration experiment as input in CD model. The competition is based on a defined ≡FeNOM surface species that competes with phosphate. This interaction is due to site and electrostatic competition. The charge attribution to the 1-plane of the EDL is important for the electrostatic competition. The attribution of -1 v.u. per reacted group to the 1-plane is adequate to describe the competition and this choice can be rationalized by the surface speciation calculated with the various LCD model approaches. At a given pH and phosphate concentration in solution, the calculated PO_4-NOM competition shows an approximately 1:1 exchange.
- At a given P loading, the PO_4 concentration in natural aqueous solutions is largely driven by the presence of DOC and adsorbed NOM. The actual PO_4 loading in field samples, measured with $NaHCO_3$ equilibration, is generally much lower than predicted from the phosphate concentration in the natural aqueous solutes or 0.01 M $CaCl_2$. Conversely, the PO_4 concentration predicted with the CD model without considering the presence of adsorbed ≡NOM is about 10-1000 (or more) times too low.

- The effective NOM density (0 ~ 2 μmol/m^2) as well as phosphate density (1 ~ 3 μmol/m^2) are correlated to the experimental phosphate and DOC concentration. The effective NOM adsorption can be linked to these solution parameters using a simplified NICA model that is parameterized on the available data. The model calculations show how DOC may affect the apparent phosphate loading and its relation with the phosphate concentration. The model also shows that the NOM adsorption density is predominantly determined by the DOC concentration with only a minor effect of the phosphate concentration.
- The DOC fraction of agricultural soils in 0.01 M $CaCl_2$ extracts consists of small organic acids with a prominent fraction of hydrophilic acids. These small and labile organic acids are expected to be most competitive for anion binding.
- The parameterized NICA model can be used to estimate the change in effective NOM adsorption if a change of DOC is to be considered.
- The effective NOM adsorption of agricultural top soils can be estimated using an empirical correlation between the relative NOM adsorption and the logarithm of the total organic carbon content of the samples. This approach is useful if other relevant information is lacking.

Acknowledgments

Meindert Keizer is gratefully acknowledged for his readiness to maintain and adapt the ECOSAT software. We also highly appreciate the comments and questions of our reviewers and like thank the Associate Editor for this effort. The financial support of the EU funding project FUNMIG (516514, F16W-2004) is gratefully acknowledged.

References

Abou Nohra J. S., Madramootoo C. A., and Hendershot W. H. (2007) Modelling phosphate adsorption to the soil: Application of the non-ideal competitive adsorption model. *Environ. Polut.* 149(1), 1-9.

Bauer M. and Blodau C. (2006) Mobilization of arsenic by dissolved organic matter from iron oxides, soils and sediments. *Sci Tot Environ* 354(2-3), 179-190.

Davis J. A. (1982) Adsorption of Natural Dissolved Organic-Matter at the Oxide Water Interface. *Geochim. Cosmoschim. Acta* 46(11), 2381-2393.

Evanko C. R. and Dzombak D. A. (1999) Surface complexation modeling of organic acid sorption to goethite. *J. Colloid Interf. Sci.* 214(2), 189-206.

Filius J. D., Hiemstra T., and Van Riemsdijk W. H. (1997) Adsorption of small weak organic acids on goethite: Modeling of mechanisms. *J. Colloid Interf. Sci.* 195(2), 368-380.

Filius J. D., Hiemstra T., and Van Riemsdijk W. H. (2000) Adsorption of Fulvic Acid on Goethite. *Geochim. Cosmochim. Acta* 64(1), 51-60.

Filius J. D., Meeussen J. C. L., Lumsdon D. G., Hiemstra T., and Van Riemsdijk W. H. (2003) Modeling the binding of fulvic acid by goethite: The speciation of adsorbed FA molecules. *Geochim. Cosmochim. Acta* 67(8), 1463-1474.

Gerke J. (1993) Phosphate Adsorption by Humic/Fe-Oxide Mixtures Aged at pH-4 and pH-7 and by Poorly Ordered Fe-Oxide. *Geoderma* 59(1-4), 279-288.

Grafe M., Eick M. J., Grossl P. R., and Saunders A. M. (2002) Adsorption of arsenate and arsenite on ferrihydrite in the presence and absence of dissolved organic carbon. *J. Environ. Qual.* 31(4), 1115-1123.

Gu B. H., Mehlhorn T. L., Liang L. Y., and McCarthy J. F. (1996) Competitive adsorption, displacement, and transport of organic matter on iron oxide .1. Competitive adsorption. *Geochim. Cosmoschim. Acta* 60(11), 1943-1950.

Gu B. H., Schmitt J., Chen Z. H., Liang L. Y., and McCarthy J. F. (1994) Adsorption and Desorption of Natural Organic-Matter on Iron-Oxide - Mechanisms and Models. *Environ. Sci. Technol.* 28(1), 38-46.

Gustafsson J. P. (2006) Arsenate adsorption to soils: Modelling the competition from humic substances. *Geoderma* 136(1-2), 320-330.

Hiemstra T., Antelo J., Rahnemaie R., and van Riemsdijk W. H. (2010) Nanoparticles in natural systems I: The effective reactive surface area of the natural oxide fraction in field samples. *Geochim. Cosmoschim. Acta* 74(1), 41-58.

Hiemstra T. and Van Riemsdijk W. H. (1996a) A surface Structural Approach to Ion Adsorption: The Charge Distribution (CD) Model. *J. Colloid Interf. Sci.* 179, 488-508.

Hiemstra T. and Van Riemsdijk W. H. (2006) On the relationship between charge distribution, surface hydration and the structure of the interface of metal hydroxides. *J. Colloid Interf. Sci.* 301, 1-18.

Jiao Y., Hendershot W. H., and Whalen J. K. (2008) Modeling phosphate adsorption by agricultural and natural soils. *Soil Sci. Soc. Am. J.* 72(4), 1078-1084.

Kaiser K. and Guggenberger G. (2000) The role of DOM sorption to mineral surfaces in the preservation of organic matter in soils. *Org. Geochem.* 31(7-8), 711-725.

Karltun E. (1998) Modelling SO_4^{2-} surface complexation on variable charge minerals. II. Competition between SO_4^{2-}, oxalate and fulvate. *Eur. J. Soil Sci.* 49(1), 113-120.

Keizer M. G. and Van Riemsdijk W. H. (1998) ECOSAT, Equilibrium Calculation of Speciation and Transport. Technical Report Department Soil Quality. Wageningen University.

Kinniburgh D. G. (1993) Fit, Technical Report WD/93/23. British Geological Survey.

Kinniburgh D. G., van Riemsdijk W. H., Koopal L. K., Borkovec M., Benedetti M. F., and Avena M. J. (1999) Ion binding to natural organic matter: competition, heterogeneity, stoichiometry and thermodynamic consistency. *Colloid Surf. A* 151(1-2), 147-166.

Milne C. J., Kinniburgh D. G., Van Riemsdijk W. H., and Tipping E. (2003) Generic NICA-Donnan model parameters for metal-ion binding by humic substances. *Environ. Sci. Technol.* 37(5), 958-971.

Rahnemaie R., Hiemstra T., and Van Riemsdijk W. H. (2007) Carbonate adsorption on goethite in competition with phosphate. *J. Colloid Interf. Sci.* 315(2), 415-425.

Rietra R. P. J. J., Hiemstra T., and Van Riemsdijk W. H. (2001a) Interaction of Calcium and Phosphate Adsorption on Goethite. *Environ. Sci. Technol.* 35, 3369-3374.

Schroder T. J., Hiemstra T., Vink J. P. M., and van der Zee S. (2005) Modeling of the solid-solution partitioning of heavy metals and arsenic in embanked flood plain soils of the rivers Rhine and Meuse. *Environ. Sci. Technol.* 39(18), 7176-7184.

Tipping E. (1981) The Adsorption of Aquatic Humic Substances by Iron-Oxides. *Geochim. Cosmoschim. Acta* 45(2), 191-199.

van Erp P. J., Houba V. J. G., and Van Beusichem M. L. (1998) One hundredth molar calcium chloride extraction procedure. Part I: A review of soil chemical, analytical, and plant nutritional aspects. *Commun. Soil Sci. Plan.* 29(11-14), 1603-1623.

van Zomeren A. and Comans R. N. J. (2007) Measurement of humic and fulvic acid concentrations and dissolution properties by a rapid batch procedure. *Environ. Sci. Technol.* 41(19), 6755-6761.

Wagai R., Mayer L. M., and Kitayama K. (2009) Extent and nature of organic coverage of soil mineral surfaces assessed by a gas sorption approach. *Geoderma* 149(1-2), 152-160.

Weng L. P., Koopal L. K., Hiemstra T., Meeussen J. C. L., and Van Riemsdijk W. H. (2005) Interactions of calcium and fulvic acid at the goethite-water interface. *Geochim. Cosmoschim. Acta* 69(2), 325-339.

Weng L. P., Van Riemsdijk W. H., and Hiemstra T. (2006) Adsorption free energy of variable-charge nanoparticles to a charged surface in relation to the change of the average chemical state of the particles. *Langmuir* 22(1), 389-397.

Weng L. P., Van Riemsdijk W. H., and Hiemstra T. (2007) Adsorption of humic acids onto goethite: Effects of molar mass, pH and ionic strength. *J. Colloid Interf. Sci.* 314(1), 107-118.

Weng L. P., Van Riemsdijk W. H., and Hiemstra T. (2008) Humic Nano-Particles at the Oxide-Water Interface: Interaction with Phosphate Ion Adsorption. *Environ. Sci. Technol.* 42(23), 8747-8752.

Summary

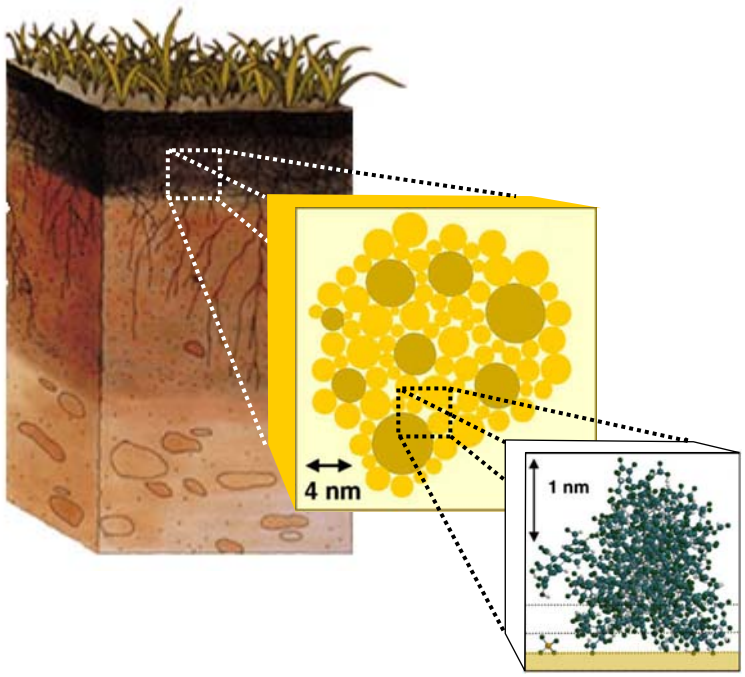

Fig.1 A soil profile with a matrix of organic matter in which oxide particles are embedded where organic molecules interact with the mineral surface.

Soil formation

Live on earth exists in a thin layer of air, water, and soil. Soils have been formed from rocks by weathering. In this process, the original minerals gradually dissolve and residues may accumulate. Some chemical elements are rather soluble and easily leached from the soil profile, while other elements are very insoluble and therefore may accumulate in soil. Insoluble elements may form new minerals. Iron (Fe) and aluminum (Al) are examples of relatively insoluble elements. At weathering, these elements are released, but may form new minerals in soil such as Fe and Al oxides and hydroxides. Iron (hydr)oxides minerals will color soils with yellow, orange, or red tints. In addition, soil organic matter is formed, giving the soil a black or brown color (Fig.1)

Small particles

Freshly formed minerals are often present as very small particles (Fig.1), nanoparticles. Tiny particles have a large surface area compared to their mass. Even a little amount of small particles may represent a large surface area. Just one gram may have a surface area of 600 m^2!, maybe larger than the size of your backyard ☺. A high surface area is very important, because surfaces are crucial in regulating the geochemical behavior of many elements. Surfaces of minerals in contact with water form a so-called solid / solution interface. The interface will have properties that partly originate from the underlying mineral. Therefore, in this thesis the focus is on the structure of surfaces in relation to the mineral bulk.

Mineral structure: Pauling bond valence

The backbone of minerals, like silicates and oxides, is oxygen (O). Oxygen may occupy almost 90% of the volume of such minerals. Between the oxygen atoms, small atoms are situated of various elements, such as Calcium (Ca), Sodium (Na), Iron (Fe), Aluminum (Al) and Silicon (Si). The oxygen (O) is negatively charged and called an anion and the other elements in these minerals are positively charged, called cations.

Cations and anions are regularly ordered in a mineral. The structure of minerals can be understood using some simple ruling factors described by Linus Pauling (1901-1994). One of the Pauling rules is that in stable structures, cations are located in the mineral lattice in such a way that the charge of the oxygen is locally neutralized. For calculating this, the charge of each cation is divided over the surrounding oxygens, resulting in the charge per bond. This charge per bond is called the Pauling Bond valence and the sum of the bond valences around an oxygen ion will balance the charge of the oxygen. In this way, the charge is neutralized. With this and other rules, the structure of minerals can be understood. This thesis shows how the Pauling bond valence concept can be applied to surfaces.

At the mineral-water interface

In minerals, the bonds between cations and anions are strong and for this reason, minerals are solids. Liquid water is also a collection of oxygen ions (O^{2-}). In water, oxygen ions are bridged together by hydrogen ions, also known as protons (H^+). The hydrogen bonds are relatively weak and this makes that water (H_2O) is usually not a solid, but a liquid, except at low temperature where it may become ice. In the interface between solid and solution, water and minerals meet. Both, water and minerals have the same backbone, i.e. oxygen ion, bound together by hydrogen ions and/or other cations.

Surface charge

A very important aspect of mineral surfaces is that they may carry charge. If a surface is positively charged, the surface has more cations (+) than anions (-). For oxides, the positive charge is due to the binding of extra hydrogen ions (H^+). These hydrogen ions or protons bind to the oxygens present at the mineral surface. The amount of extra hydrogen ions (H^+) bound depends on the concentration of the H^+ in solution. The pH of the solution is a measure for the hydrogen ion (H^+) concentration. At low pH, many H^+ ions are available in solution and the hydrogen ion binding by the surface is relatively large. At a high pH with a lower H^+ concentration, fewer hydrogen ions (H^+) will be bound by the surface oxygens and at a sufficiently high pH, the surface may become negatively charged, because too many protons (hydrogen ions) have left the surface. In that case, the negative charge of the oxygen ions is not sufficiently compensated. At a certain pH, i.e. proton (H^+) concentration in solution, the surface will be uncharged. This pH is called the point of zero charge (PZC).

Point of zero charge

Mineral surfaces differ in PZC. Some mineral surfaces have a low PZC. An example is quartz (SiO_2), popular known as “sand”. The reactive surface groups are $\equiv SiOH^0$. The surface oxygens carry a proton because at the formation of the surface, Si-O-Si bonds have been

broken and replaced by a Si-O-H bond. The PZC of quartz is about 2. At a pH of 2, a relatively high concentration of hydrogen ions is in solution. The concentration of hydrogen ions in the soil solution is less, and for this reason, the quartz surface will release protons and becomes negatively charged in the normal pH range of soils (pH = 4-8).

Other minerals have a high PZC, for instance goethite, the most important Fe (hydr)oxide of soils. The PZC of goethite is about 9. A very low concentration of protons (H^+) is needed to keep the surface uncharged. The H^+ concentration in the soil solution is usually higher. Therefore, the surface of goethite (FeOOH) will bind extra hydrogen ions and will usually be positively charged in soils.

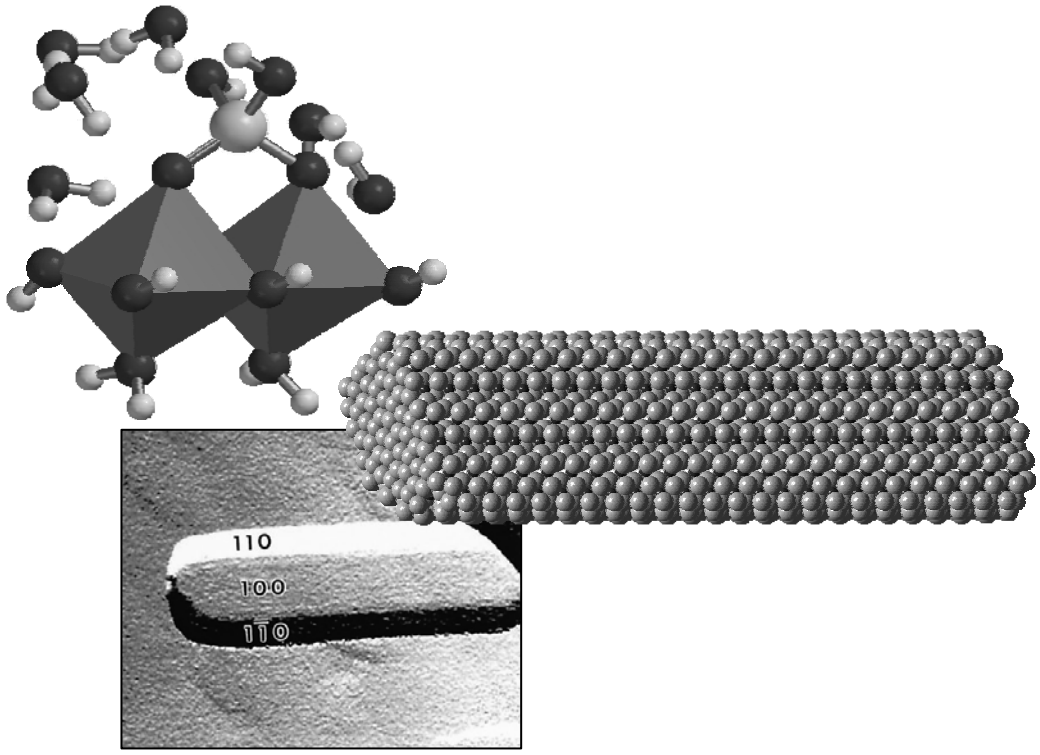

Fig.2 At the bottom left, a microscope picture of a mineral (goethite), consisting of atoms arranged in a mineral lattice shown in the middle. On top, left, a hydrated surface complex, calculated with quantum chemistry that consists of two Fe octahedra representing a mineral surface that binds an oxyanion, surrounded by water molecules.

MUSIC model

Why do minerals have a different PZC and therefore a different charge? This is one of the questions answered in this thesis. To explain this, we need a better picture of the surface. We will use goethite as example, a needle-shaped particle (Fig.2). In the interior of goethite (FeOOH), the oxygens are bound by three Fe^{3+} ions. It is said that the oxygen is triply coordinated. At the surface, some of the oxygen ions have the same number of Fe-O bonds as in the solid. However, formation of the goethite surface is also accompanied by breaking some Fe-O bonds. As a result, the corresponding oxygen ions will miss one or two bonds with Fe ions. These oxygens have a so-called lower coordination number (CN). If one Fe-O bond

exists, the oxygen is said to be singly coordinated, and in case of the presence of two Fe-O bonds, it is doubly coordinated. If one or two Fe ions are absent in the coordination sphere, the neutralization of the oxygen charge is less. The charge deficit of this surface oxygen can be compensated by taking up one or two hydrogen ions. How much and how easily hydrogen ions are bound will depend on how much charge is missing because of breaking bonds. It has been shown in this thesis that the degree of undersaturation of the charge of the surface oxygens is a good measure for the affinity of the oxygens for protons (H^+). The charge of surface oxygens is calculated with the above mentioned bond valence analysis. The proton affinity of surface oxygens represents a binding energy. The theory described in the thesis enables the prediction of the proton affinity of the various types of surface oxygens of particular minerals. The combination of different proton affinities can explain the various PZC values found for minerals. The theory is known as the MUlti SIte Complexation (MUSIC) model. With the model, the surface charge of particles can be calculated. It is of great practical and fundamental interest.

Binding of ions

Surface groups and their charge are important because surface groups will not only react with protons (H^+) but also with other cations (+) and anions (-) that are present in the soil solution. The reaction of ions is surface-group-specific, as can be illustrated for goethite reacting with phosphate ions from the soil solution. This reaction is highly relevant because phosphate is an important nutrient for plants. The phosphate ion has a high affinity for one particular type of surface group, i.e. the singly coordinated ≡FeOH group. Phosphate will not react with the doubly ($\equiv Fe_2OH$) or triply coordinated ($\equiv Fe_3O(H)$ groups at the goethite surface. The high affinity of phosphate (PO_4^{3-}) for the ≡FeOH surface group leads to a high phosphate loading of the goethite surface and correspondingly, a low concentration in the soil solution.

For ecosystems, a strong binding has the advantage that phosphate, as important nutrient, is not easily leached from the soil profile. However, the disadvantage for plants is that it is more difficult to extract a sufficiently large amount of phosphate via the soil solution. A good model that describes the relation between the concentration in solution and the amount bound by the surface at various conditions will be of great help to understand soil-plant relationships. Therefore, development of an ion adsorption model is highly relevant and a new and powerful model has been described in this thesis. The resulting model is known as the Charge Distribution (CD) model. The background of the CD model is explained in the next paragraphs.

CD model

When a proton (H^+) adsorbs at a surface, an increasing amount of positive charge will accumulate at the surface. The accumulating charge acts repulsive on further adsorption of H^+. The H^+ ions create themselves a so-called electrostatic field that will progressively decrease the bond strength. Therefore, the proton affinity (adsorption energy) is not a constant. It is strongly (!) changed by the electrostatic field. This is not only true for H^+ ions, but also for other cations, such as calcium (Ca^{2+}) or heavy metals ions like zinc (Zn^{2+}), copper

(Cu^{2+}), lead (Pb^{2+}), etcetera. For instance, binding of copper ions at low pH is more difficult, because the surface is already positively charged by adsorbed protons (H^+). The H^+-binding has created a repulsive field for the copper cations. At high pH, fewer protons are bound and the repulsion is less. Therefore, more copper can bind. For anions, like PO_4^{3-} or SO_4^{2-}, the opposite is true. At low pH, these negative ions are initially attracted by the positive field. With more adsorption, the particle will become less positively charged, due to the neutralization of the positive field by the negative charge of the phosphate ions that adsorb. One of the challenges and difficulties is to calculate the effect of the electrostatic field on the adsorption of ions. This effect is generally huge, but more important it is highly variable. The question is "How much electrostatic energy (attraction/ repulsion) is involved in the adsorption of ions"? This is answered in this thesis with the CD model

Charge distribution and Electrostatic attraction and repulsion

The electrostatic energy is strongly related to the position of the charged ion in the electrostatic field. If the ion is at a large distance, the interaction is weak and not much energy is involved. Close to the surface, the interaction becomes much stronger. How much? That will depend on the type of complex that is formed. A difficulty is that ions can be relatively large. An example is phosphate. Phosphate consists of four oxygen ions bound together by a phosphorous (P) in the center, forming PO_4^{3-}. The oxygens are also called ligands. When the phosphate ion reacts with the surface, the oxygen of the surface group (≡FeOH) is replaced by an oxygen ion / ligand of PO_4^{3-}. This process is called ligand exchange. Phosphate may react with two ≡FeOH groups of the surface, forming $\equiv(FeO)_2PO_2$. In the surface complex, half of the phosphate ion is common with the surface and the other half not. Where is the corresponding charge of PO_4^{3-}? The answer of the CD model is that the charge is partly in the surface where the field can be strong and the other part is at some distance where the field is often weaker. The CD model suggests that the phosphate charge (-3) is distributed in the interface. It has been shown that the charge distribution mainly depends on the distribution of the ligands in the interface. Where are the oxygens, i.e. the ligands? For $\equiv(FeO)_2$-P-O_2, half of the ligands of PO_4^{3-} is common with the surface, i.e. the relative charge distribution (CD) is 50% -50%. For $\equiv(FeO)_2$-Se-O, two third of the ligands of SeO_3^{2-} (selenite) is common with the surface, i.e. the relative CD is 67% -33%, and for ≡FeO-S-O_3, a quarter of the ligands of sulphate (SO_4^{2-}) is common with the surface, i.e. CD = 25% -75%. The same principle can also be applied to cadmium (Cd^{2+}) adsorption, forming e.g. $\equiv(FeOH)_2$-Cd-$(OH_2)_4$. In this complex, one third of the ligands is common with the surface, i.e. CD = 33% - 67%. Summarizing, charge distribution is linked to ligand distribution.

Asymmetrical charge distribution

In the soil solution, one may find also neutral complexes. A typical example is silicic acid ($Si(OH)_4^0$) that enters the solution by dissolution of sand (quartz). This neutral complex may also bind to the goethite surface, forming $\equiv(FeO)_2$-Si-$(OH)_2$. Since silicic acid does not carry charge, the expectation can be that there is no influence of the electrostatic field. However, interpretation of silicon (Si) adsorption data with the CD model suggests the

presence of some positive charge at the surface, mirrored by the same amount of negative charge at both other ligands that are outside the surface. How come?

To answer this question, one may do some quantum chemical calculations that reveal the detailed geometry of $\equiv(FeO)_2$-Si-$(OH)_2$. It shows that the Si-O bonds are not equally strong in the surface complex. The Si-O bonds with the surface are stronger. For this reason, more positive charge of the central Si^{4+} is to be attributed to the surface ligands (O) and less to the free ligands (OH). It suggests that the charge distribution will also depend on the bond length distribution. The relation between the bond length and the distribution of charge can be calculated with an empirical, but very powerful, relationship that originates from mineralogy, leading to the Brown bond valence.

The role of water

Actually, the most important neutral species of the soil solution is water, i.e. H_2O. Overall, the water molecule is neutral. However, the protons (H^+) are bound at one side. That part of the molecule is locally more positively charged and the other side is more negatively charged. One may say that there is charge distribution within the water molecule. The water molecules, present in a layer near the surface, may change their orientation when the surface changes in charge due to ion adsorption. If the surface becomes more positively charged, the negative side of water may orient on the positive surface charge, locally slightly neutralizing some of the charge created by the adsorbed ion. This feedback process leads to a correction on the ionic charge distribution. In this thesis, the corresponding theory has been formulated.

Lack of oxygen

Only a tiny shell of the geosphere is oxidized due to photosynthesis, producing oxygen. If soil is isolated from the atmosphere, there will be a lack of oxygen due to consumption by microorganisms for respiration. In stead of oxygen gas (O_2), micro-organisms can also use Fe (hydr)oxides to respire. This leads to the formation of Fe^{2+}. This ion is less positively charged than Fe^{3+} found in Fe (hydr)oxides, because it has got a negatively charged electron from the microbes. The Fe^{2+} ion is very soluble in contrast to Fe^{3+}.

CD value and electron transfer

Similar as other cations, Fe^{2+} may adsorb to mineral surfaces, including the surface of goethite (FeOOH). With the CD model, it has been discovered that the adsorbed Fe^{2+} may change into Fe^{3+}, by transferring the electron to the surface. It leads to the formation of adsorbed Fe^{3+}. However, the hydrated Fe^{3+} complex is not very stable. As in solution, the water molecules bound by Fe^{3+} will easily release protons (H^+). It is said that the ion hydrolyzes. Application of the CD model shows that two protons will be released from the water molecules of adsorbed Fe^{3+}, leading to $\equiv(Fe_{II}OH)_2Fe_{III}(OH)_2(OH_2)_2$. Due to the release of two protons, the process of electron transfer will be strongly pH dependent, and for goethite, the CD model shows that electron transfer from adsorbed Fe^{2+} to goethite is only relevant above neutral pH.

Charge distribution summarized

In summary, the CD model shows that a) ionic charge distribution is due to a distribution of ligands with b) corresponding bond lengths, and in some cases also c) electron transfer. The interfacial charge distribution includes also some correction for reorientation of water molecules.

Application to a classical colloid

The ion adsorption framework developed can be applied in science, technology, and the environment. Before discussing the latter, a brief word is said on a long-standing scientific issue, i.e. the charging of solid silver iodide, AgI(s), a classical model colloid. The charge behavior has been measured extensively. Varying the silver (Ag^+) or corresponding iodide (I^-) concentration will change the particle charge, from negative to positive or *vice versa*. This is due to binding of Ag^+ and I^- ions. In the classical interpretation, the ions bind at the same electrostatic position. Application of the CD model shows that negative charge is created in the surface. This charge is separated from positive charge present outside the surface, which is due to the binding of Ag^+. Iodide ions do not adsorb there. Binding of the constituting ions at different electrostatic positions in the interface, implies charge distribution. The charge distribution can be understood from the structure of the surface and the surface complexes. This analysis, described in the introductory chapter of this thesis, illustrates the great power of the present framework that is based on a structural approach.

Application to soils

In the last part of the thesis, attention is paid to how the CD-MUSIC framework can be applied in soil and geochemistry. Two important questions have been addressed.

A first question is "How do we get information about the amount of surface area of the soil oxide fraction?" This is a very difficult and challenging question, and in the thesis, the onset of an answer is given. Suggested is to measure the reaction of soil phosphate after adding a solution with a high concentration of sodium bicarbonate ($NaHCO_3$). The added CO_3^{2-} (carbonate) ion is a competitor for phosphate (PO_4^{3-}) and will also remove calcium (Ca^{2+}) by precipitation, forming solid calcium carbonate, $CaCO_3$(s). The $NaHCO_3$ solution will buffer the pH at ~8.5. In addition, active carbon is added to remove organic molecules that dissolve from soil organic matter at high pH in a $NaHCO_3$ solution. If we dilute a soil with a $NaHCO_3$ solution, some phosphate is released from the iron (Fe) and aluminum (Al) (hydr)oxide surfaces. If the phosphate concentration strongly decreases upon dilution, less surface area with adsorbed phosphate will be present in the soil than in a soil where the concentration decrease is rather limited due to buffering. The response of the soil is compared with predictions made by the CD model. The reaction of the soil is compared with the reaction of goethite, the main Fe (hydr)oxide of soils and answers the question: "Which surface area best explains the data?" The analysis shows that soil oxide particles are often very small, only a few nanometer. A nanometer (nm) is one million times smaller than a millimeter (mm), very small. The surface area found for representative Dutch top soils have been compared with a range of soil characteristics. A strong relation is found between the soil

surface area and soil organic carbon. It is postulated that the soil (hydr)oxide particles are embedded in natural organic matter, as illustrated in Figure 1.

In soil, organic molecules may bind to oxide particles. This may influence ion adsorption, in particular the anion adsorption. Both will compete for the same sites and additionally they interact via electrostatics. The influence of organic matter is noticeable when the phosphate loading is scaled to the reactive surface area, showing that the loading is statistically best explained by DOC and phosphate concentration in solution.

If the surface loading measured in the $NaHCO_3$ dilution experiments is used to predict the phosphate binding at standardized soil conditions, the predicted PO_4^{3-} concentration is considerably lower (10-1000 times) than measured in 0.01 M $CaCl_2$, most likely due to competition with adsorbed natural organic matter. By defining a hypothetical surface species, the behavior of adsorbed natural organic matter (≡NOM) has been mimicked. This species is used to estimate the amount needed to explain the data. The apparent surface loading of ≡NOM is inversely related to the experimental phosphate (PO_4^{3-}) loading, indeed pointing to competition. The surface loading of ≡NOM increases with the concentration of dissolved organic carbon (DOC) in the $CaCl_2$ extract and correlates with soil organic matter.

Since the concentration of DOC in the soil solution is the integrated result of many processes, the use of DOC as input rather than as output of a model is at present a simple way to be practical and describe (an)ion adsorption behavior in soil and geochemical applications. This thesis provides the framework for it.

Samenvatting

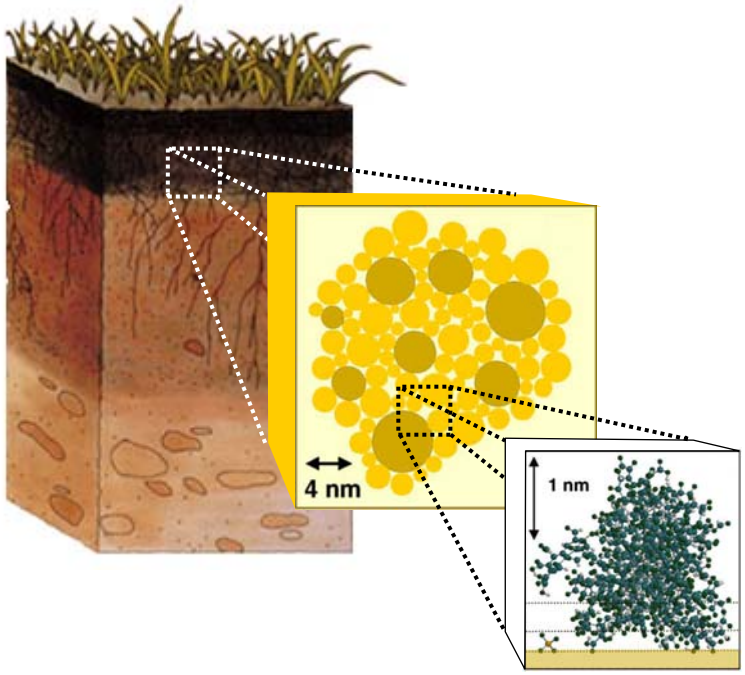

Fig.1. Een bodemprofiel met een matrix van organische stof waarin ijzer en aluminium oxidedeeltjes zijn ingebed. Daarbij reageren de organische moleculen met het minerale oppervlak

. *Bodemvorming*

Leven op aarde bestaat in een dunne laag met lucht, water, en bodem. Bodems zijn gevormd door verwering van rots. In dit proces worden de oorspronkelijke mineralen geleidelijk opgelost en residuen blijven achter.

Sommige chemische elementen zijn vrij goed oplosbaar en spoelen uit, terwijl andere elementen zeer slecht oplosbaar zijn en deze kunnen zich daarom ophopen in de bodem. Onoplosbare elementen kunnen nieuwe mineralen vormen. IJzer (Fe) en aluminium (Al) zijn voorbeelden van relatief onoplosbare elementen. Bij verwering komen deze elementen vrij, en vormen dan in de bodem vrij onoplosbare oxiden en hydroxiden. IJzer(hydr)oxiden geven bodems kleur met gele, oranje of rode tinten. Bij bodemvorming wordt er ook humus / organische stof gevormd, waardoor de bodem een zwarte of bruine kleur krijgt (Fig.1).

Kleine deeltjes

Vers gevormde mineralen zijn vaak aanwezig als zeer kleine deeltjes (Fig.1), nanodeeltjes. Kleine deeltjes hebben een groot oppervlak in vergelijking met hun massa. Zelfs een kleine hoeveelheid van zulke deeltjes kan een groot oppervlak vertegenwoordigen. Eén gram kan een oppervlak hebben van wel 600 m^2!, wellicht groter dan uw achtertuin ☺. Een groot oppervlak is erg belangrijk, omdat oppervlakken van cruciaal belang zijn bij het reguleren van het gedrag van veel elementen. Minerale oppervlakken in contact met water vormen een zogenaamd vaste stof - vloeistof grensvlak. Het grensvlak heeft eigenschappen

die deels afkomstig zijn van het onderliggende mineraal. Daarom wordt in dit proefschrift de nadruk gelegd op de structuur van oppervlakken in relatie tot de onderliggende minerale structuur.

Minerale opbouw: Pauling bindingsvalentie

Het structuurvormende element van mineralen zoals silicaten en oxiden is zuurstof (O). Zuurstof kan bijna 90% van het volume innemen bij deze mineralen. Tussen de zuurstofatomen bevinden zich kleine atomen van andere elementen, zoals calcium (Ca), natrium (Na), ijzer (Fe), aluminium (Al) en silicium (Si). Zuurstof (O) is negatief geladen. We noemen zo'n negatief geladen deeltje een anion. In de meeste mineralen zijn de andere elementen positief geladen. Positieve deeltjes worden kationen genoemd.

Kationen en anionen zijn in een mineraal systematisch geordend. De structuur van mineralen kan worden begrepen met behulp van enkele eenvoudige regels, geformuleerd door Linus Pauling (1901-1994). Eén van de Paulingregels is dat in stabiele structuren kationen in het mineraalrooster aanwezig zijn op een zodanige plaats dat steeds de lading van de zuurstofionen lokaal wordt geneutraliseerd in het rooster. Voor de berekening hiervan, wordt de lading van elk kation verdeeld over de omliggende zuurstofatomen, wat resulteert in een lading per binding. Deze lading per binding wordt de Pauling bindingsvalentie genoemd en de som van de bindingsvalenties rond een zuurstof ion komt overeen met de lading van dat zuurstofion. Daarmee is de lading geneutraliseerd. Met deze en andere regels kan de structuur van mineralen worden begrepen. Dit proefschrift laat zien hoe het Paulingconcept met bindingsvalenties kan worden toegepast op oppervlakken.

Op het grensvlak tussen mineraal en water

In mineralen zijn de bindingen tussen de kationen en anionen sterk en om deze reden zijn mineralen vaste stoffen. Vloeibaar water is ook een verzameling van zuurstofionen (O^{2-}), maar die worden geneutraliseerd met H^+-ionen, ook wel waterstofionen genoemd. In water zijn zuurstofionen met elkaar verbonden door middel van waterstofbruggen. De waterstofbruggen zijn relatief zwak en dit maakt dat water (H_2O) meestal geen vaste stof is, maar een vloeistof, behalve bij lage temperatuur, dan wordt het ijs. In een mineraal / water grensvlak ontmoeten de vaste stof (het mineraal) en oplossing (water) elkaar. Water en mineralen hebben hetzelfde structuurvormende element, namelijk zuurstof. Onze natuurlijke omgeving is in feite vooral een stapeling van zuurstof. De negatief geladen zuurstofionen worden bij elkaar gehouden door waterstofionen en/of andere kationen.

Oppervlaktelading

Een zeer belangrijk aspect van minerale oppervlakken is dat ze lading kunnen bezitten. Als een oppervlak positief geladen is, zijn er meer kationen (+) dan anionen (-). Voor oxiden is de positieve lading het gevolg van binding van extra H^+ ionen. Deze H^+ ionen binden aan de zuurstofionen, die aanwezig zijn in het minerale oppervlak. De overmaat aan gebonden waterstofionen (H^+) is afhankelijk van de concentratie van H^+ in oplossing. De pH van de oplossing is een maat voor de zuurgraad en geeft de concentratie van waterstofionen (H^+) aan. Bij een lage pH zijn er veel H^+-ionen beschikbaar in oplossing. Aan het oppervlak kan er dan een overmaat aan H^+ gebonden worden. Het oppervlak is dan positief geladen. Bij een hoge pH is de H^+ concentratie laag en worden er minder H^+ ionen gebonden aan het oppervlak. Het

oppervlak kan zelfs negatief geladen worden bij een heel lage H^+ concentratie. Teveel H^+ ionen hebben dan het oppervlak verlaten. In dat geval wordt de negatieve lading van de zuurstofionen niet voldoende gecompenseerd en is het oppervlak negatief geladen. Bij een bepaalde pH, dat wil zeggen een bepaalde H^+ concentratie in oplossing, is het oppervlak ongeladen. Deze pH_0 wordt het ladingsnulpunt genoemd. Een oxide oppervlak kan dus positief, neutraal, of negatief geladen zijn door te veel, precies genoeg, of te weinig gebonden H^+ om de lading van de zuurstof (O^{2-}) aan het oppervlak te compenseren.

Ladingsnulpunt of Pont of Zero charge (PZC)

Minerale oppervlakken verschillen in ladingsnulpunt. Sommige mineralen hebben een laag ladingsnulpunt. Een voorbeeld is kwarts (SiO_2), populair gezegd "zand". De reactieve oppervlaktegroepen $\equiv SiOH^0$ ontstaan door het breken van een Si-O-Si binding en vervanging door een Si-O-H binding. Het ladingsnulpunt (PZC) van kwartszand is ongeveer $pH_0 = 2$. Om het kwarts oppervlak neutraal te houden is er een relatief hoge concentratie van H^+ ionen in de oplossing nodig. De feitelijke concentratie van H^+ in de bodemoplossing is meestal veel lager, en om deze reden, is het kwartsoppervlak meestal negatief geladen in de bodem bij een normale pH (~4-8). Een deel van de H^+ ionen zijn vertrokken van het oppervlak en het oppervlak is negatief en heeft $\equiv SiO^{-1}$ groepen.

Een aantal belangrijke bodemmineralen hebben een hoog ladingsnulpunt. Een voorbeeld is goethiet (FeOOH), het belangrijkste Fe (hydr)oxide van de bodem met een ladingsnulpunt van PZC~9. De bijgehorende H^+ concentratie is heel laag. In de bodemoplossing is concentratie meestal hoger. Er is daardoor meer H^+ gebonden dan nodig is voor neutralisatie van de zuurstof. Daarom is goethiet meestal positief geladen in de bodem.

MUSIC model

Waarom hebben mineralen eigenlijk een verschillend ladingsnulpunt en waarom een andere lading? Dit is één van de vragen die in dit proefschrift beantwoord worden. Om dit te verklaren moeten we een beter beeld van het oppervlak hebben. We zullen gebruik maken goethiet (FeOOH) als voorbeeld. Het is naaldvormig (Fig.2). In het binnenste van goethiet zijn de zuurstofatomen omringd door drie Fe^{3+}-ionen. Er wordt gezegd dat de zuurstof drievoudig gecoördineerd is. Aan het oppervlak heeft een deel van de zuurstofionen hetzelfde aantal Fe-O bindingen dan in de vaste stof. Echter, bij de vorming van het goethiet-oppervlak zijn er ook Fe-O bindingen verbroken. Als gevolg hiervan zullen de desbetreffende zuurstofionen één of twee bindingen met Fe-ionen missen. Deze zuurstofionen hebben dan een lager coördinatiegetal (CN). Als zuurstof slechts één Fe-O binding heeft, wordt gezegd dat het enkelvoudig gecoördineerd is. Een O met twee Fe-O bindingen is het dubbel gecoördineerd. Als één of twee Fe ionen ontbreken in de coördinatie (omringing), wordt zuurstof minder geneutraliseerd. Het ladingstekort van de zuurstofionen aan het oppervlak kan worden gecompenseerd door de binding van één of twee H^+. Hoeveel precies en hoe gemakkelijk H^+ ionen worden gebonden zal afhangen van de hoeveelheid lading die ontbreekt als gevolg van het breken van bindingen. Dit proefschrift laat zien dat de mate van onderverzadiging van de zuurstoflading van de oppervlaktegroep een goede maat voor zijn affiniteit om H^+ te binden. De theorie beschreven in dit proefschrift maakt een voorspelling mogelijk van de H^+ affiniteit / bindingssterkte / bindingsenergie van de verschillende soorten

van minerale oppervlaktegroepen. De combinatie van verschillende H^+ affiniteiten leidt tot het verklaren van de variatie in ladingsnulpunt, gevonden voor verschillende oxiden. Het model staat bekend als het Multi-Site Complexation (MUSIC) model en kan de oppervlaktelading van mineralen berekenen.

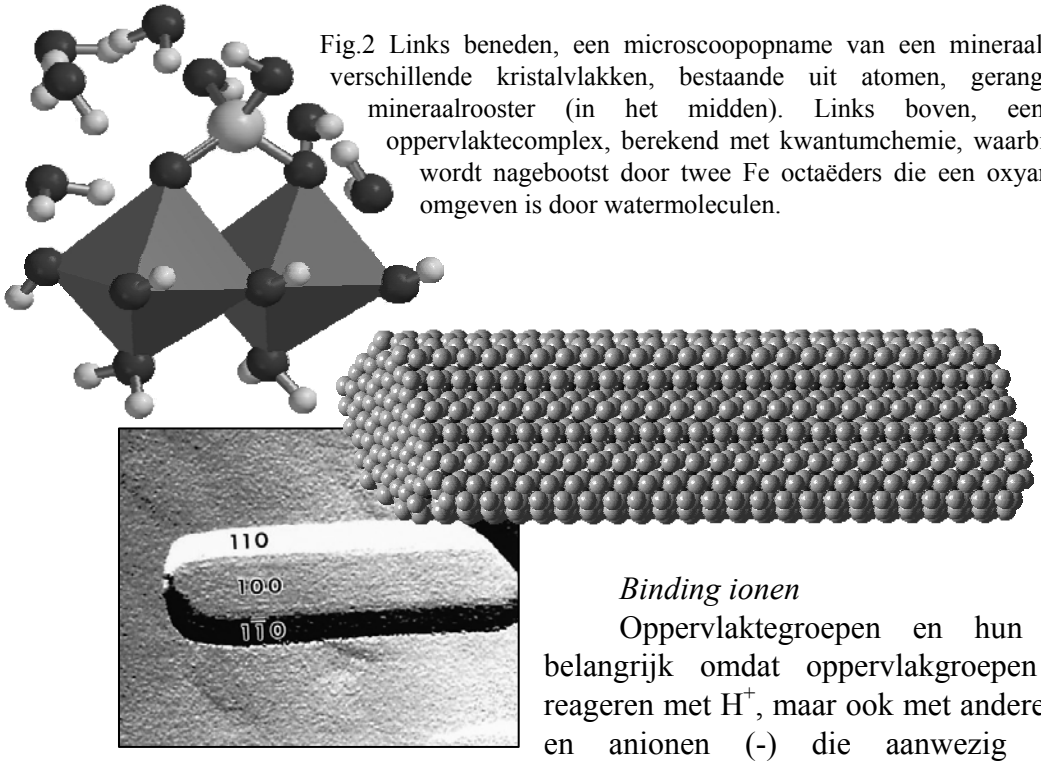

Fig.2 Links beneden, een microscoopopname van een mineraal (goethiet) met verschillende kristalvlakken, bestaande uit atomen, gerangschikt in een mineraalrooster (in het midden). Links boven, een gehydrateerd oppervlaktecomplex, berekend met kwantumchemie, waarbij het oppervlak wordt nagebootst door twee Fe octaëders die een oxyanion binden dat omgeven is door watermoleculen.

Binding ionen

Oppervlaktegroepen en hun lading zijn belangrijk omdat oppervlakgroepen niet alleen reageren met H^+, maar ook met andere kationen (+) en anionen (-) die aanwezig zijn in de bodemoplossing. De reactie van deze ionen is specifiek voor een bepaald type oppervlaktegroepen, zoals kan worden geïllustreerd voor het belangrijkste ijzer(hydr)oxide in de bodem, namelijk goethiet. Dit mineraal kan reageren met fosfaationen (PO_4^{3-}) uit de bodemoplossing. Deze reactie is van groot belang omdat fosfaat voor planten een belangrijke voedingsstof is. Het fosfaation heeft een hoge affiniteit voor de enkelvoudig gecoördineerde oppervlaktegroep ≡FeOH. Fosfaat zal niet reageren met de dubbel gecoördineerde ($\equiv Fe_2OH$) of drievoudig gecoördineerde ($\equiv Fe_3O$) groepen van het goethiet-oppervlak. De hoge affiniteit van fosfaat voor de ≡FeOH oppervlakgroep leidt tot een hoge oplading van het goethiet oppervlak met PO_4^{3-} en daardoor een lage concentratie in de bodemoplossing.

Voor een ecosysteem heeft een sterke binding het voordeel dat fosfaat, als belangrijke voedingsstof, niet gemakkelijk wordt uitgespoeld uit de bodem. Echter, het nadeel voor de planten is dat het moeilijker wordt om voldoende fosfaat op te nemen via de bodemoplossing. Een goed model dat de relatie beschrijft tussen de concentratie in de bodemoplossing en de hoeveelheid fosfaat gebonden aan het oppervlak draagt bij aan een beter begrip van bodem-plant relaties. Daarom is de ontwikkeling van een goed adsorptiemodel voor ionen zeer relevant en in dit proefschrift is een nieuw en krachtig model beschreven. Het model staat bekend als het ladingsdistributie model, in het Engels het Charge Distribution (CD) model. De achtergrond van de CD-model wordt uiteengezet in de volgende paragrafen.

CD model

Wanneer een oppervlak H^+ ionen bindt, zal zich in een toenemende mate positieve lading ophopen aan het oppervlak. De accumulerende lading zal verdere adsorptie van H^+ sterk afremmen. Door ophoping creëren de H^+-ionen zelf een afstotend elektrisch veld waardoor de bindingsterkte afneemt. Daarom is de H^+ affiniteit (adsorptie-energie) geen constante. De bindingssterkte / H^+ affiniteit / adsorptie-energie wordt heel sterk (!) veranderd door het zelf opgewekte elektrische veld. Dit geldt niet alleen voor H^+, maar ook voor andere kationen, zoals calcium (Ca^{2+}) en magnesium (Mg^{2+}), en zware metaalionen zoals zink (Zn^{2+}), koper (Cu^{2+}), lood (Pb^{2+}), cadmium (Cd^{2+}) enzovoort. De binding van koperionen is bijvoorbeeld bij lage pH moeilijker, omdat het oppervlak al positief geladen is door geadsorbeerde H^+. De gebonden H^+ ionen hebben een positief elektrisch veld gemaakt dat afstotend werkt op de positief geladen koperionen (Cu^{2+}). Bij hoge pH zijn er minder H^+ ionen gebonden en daardoor is de afstoting minder en kan er meer koper binden. Voor anionen, zoals fosfaat PO_4^{3-} of sulfaat SO_4^{2-} is het tegendeel waar. Bij een lage pH worden deze negatieve ionen in eerste instantie sterk aangetrokken door het positieve veld. Bij meer adsorptie zal het oppervlak minder positief geladen zijn als gevolg van de neutralisering van de positieve lading door de negatieve lading van de gebonden fosfaat- of sulfaat- ionen. Ook hier is de bindingsterkte niet constant, maar neemt af. Eén van de uitdagingen en moeilijkheden is om het effect te berekenen van het elektrostatische veld op de adsorptie van ionen. Dit effect is over het algemeen groot maar meer belangrijk, het is heel variabel. De vraag is "Hoeveel elektrostatische energie (aantrekking / afstoting) is betrokken bij de binding van ionen"? Deze vraag wordt beantwoord in dit proefschrift met de CD-model.

Ladingsverdeling en Elektrostatische aantrekking of repulsie

De elektrostatische energie is sterk gerelateerd aan de positie van het geladen ion in het elektrostatische veld. Als het ion op grote afstand is, zal de interactie zwak zijn en er is niet veel energie bij betrokken. Dichtbij en aan het oppervlak is de interactie veel sterker. Hoeveel? Dat hangt af van het type complex dat wordt gevormd. Een probleem is dat de ionen relatief groot kunnen zijn. Een voorbeeld is fosfaat. Fosfaat bestaat uit vier zuurstofionen bijeengehouden door een fosfor (P) in het centrum, leidend tot PO_4^{3-}. De zuurstofionen worden ook wel liganden genoemd. Wanneer het fosfaat ion reageert met ≡FeOH van het oppervlak, wordt de zuurstof van de oppervlaktegroep vervangen door een zuurstofion / ligand van PO_4^{3-}. Dit proces heet liganduitwisseling. Fosfaat kan reageren met twee ≡FeOH groepen van het oppervlak en het vormt $\equiv(FeO)_2$-P-O_2. In deze structuur is de helft van de fosfaat-ion gemeenschappelijk met het oppervlak en de andere helft niet. Waar is de overeenkomstige lading van PO_4^{3-}? Het antwoord van de CD-model is dat de lading deels in het oppervlak aanwezig is, waar het veld sterk kan zijn, en het andere deel is op enige afstand van het oppervlak, waar het veld vaak zwakker is. Het CD model suggereert dat de fosfaatlading (3-) in het grensvlak verdeeld is. Het proefschrift laat zien dat de ladingsverdeling vooral afhankelijk is van de verdeling van de liganden in het grensvlak. Waar bevinden zich de zuurstofionen, dat wil zeggen de liganden? Voor $\equiv(FeO)_2PO_2$ is de helft van de liganden van PO_4^{3-} gemeenschappelijk met het oppervlak, dat wil zeggen de relatieve ladingsverdeling (CD) is 50% -50%. Voor ≡ $(FeO)_2$-Se-O is tweederde van de liganden van SeO_3^{2-} (seleniet) gemeenschappelijk met het oppervlak, dat wil zeggen de relatieve CD is 67% -33%. En voor ≡FeO-S-O_3 is een kwart van de liganden van SO_4^{2-}

gemeenschappelijk met het oppervlak, dat wil zeggen de CD is 25% -75%. Hetzelfde principe kan ook worden toegepast op de adsorptie van cadmium ionen (Cd^{2+}) met de vorming van $\equiv(FeOH)_2$-Cd-$(OH_2)_4$. In dit complex is een derde van de liganden gemeenschappelijk met het oppervlak, dat wil zeggen de CD is 33% - 67%. Samenvattend, de ladingsdistributie is gekoppeld aan de distributie van liganden.

Asymmetrische ladingsverdeling

In de bodemoplossing kan men ook complexen zonder lading aantreffen. Een typisch voorbeeld is kiezelzuur ($Si(OH)_4^0$), dat door het oplossen van zand (kwarts) in het bodemwater komt. Dit neutrale complex kan ook binden aan het oppervlak van goethiet en $\equiv(FeO)_2$-Si-$(OH)_2$ vormen. Omdat kiezelzuur ongeladen is, kan men de verwachting hebben dat er geen invloed van het elektrostatische veld zal zijn. Interpretatie van silicium (Si) adsorptiegegevens met het CD-model suggereert echter de aanwezigheid van positieve lading aan het oppervlak en eenzelfde hoeveelheid negatieve lading op de andere liganden buiten het oppervlak. Hoe kan je dat verklaren?

Om deze vraag te beantwoorden kan men zogenaamde kwantumchemische berekeningen doen die de details van de geometrie van $\equiv (FeO)_2$-Si-$(OH)_2$ geven. Hieruit blijkt dat de Si-O bindingen in het oppervlaktecomplex niet allemaal even sterk zijn. De Si-O bindingen met het oppervlak zijn sterker. Om deze reden moet er meer positieve lading van het centrale Si^{4+} ion aan de oppervlakte-liganden (O) worden toegekend en minder aan de vrije liganden (OH) van het complex. Het suggereert dat de ladingsverdeling eveneens zal afhangen van de verdeling van de bindingslengten. De relatie tussen de bindingslengte en de verdeling van de lading kan worden berekend met een empirische, maar zeer krachtige relatie die afkomstig is uit de mineralogie en die leidt tot de bindingsvalentie.

De rol van water

Eigenlijk is het belangrijkste neutrale deeltje van de bodemoplossing het water (H_2O) molecuul. Over het geheel genomen is het watermolecuul neutraal. Echter, de H^+ ionen zijn slechts aan één zijde gebonden. Dat deel van het molecuul is lokaal meer positief geladen en de andere kant is meer negatief geladen. Men kan zeggen dat er sprake is van ladingsverdeling binnen het watermolecuul. De watermoleculen, aanwezig in een waterlaag aan het oppervlak, kunnen hun oriëntatie veranderen afhankelijk van de lading aan het oppervlak. Als het oppervlak meer positief geladen wordt, kan de negatieve kant van het watermolecuul zich oriënteren op de positieve lading waardoor lokaal de oppervlaktelading, ontstaan door ionadsorptie, iets geneutraliseerd wordt. Dit proces van terugkoppeling leidt tot een correctie op de ladingsverdeling behorende bij het oppervlakte complex. In dit proefschrift is de bijgehorende theorie geformuleerd.

Gebrek aan zuurstof

Slechts een kleine schil van de aardse geosfeer is geoxideerd als gevolg van het fotosynthese proces dat zuurstof maakt. Als de bodem afgesloten is van de atmosfeer, zal er een gebrek aan zuurstof ontstaan als gevolg van het zuurstofverbruik door micro-organismen ten behoeve van hun ademhaling. In plaats van zuurstof (O_2) kunnen micro-organismen ook ijzer (Fe) (hydr)oxiden gebruiken om te ademen. Dit leidt tot de vorming van tweewaardige ijzer ionen (Fe^{2+}). Dit ion is minder positief geladen dan de Fe^{3+} ionen die in Fe (hydr)oxiden

aanwezig is. Dit komt doordat het Fe^{3+} een negatief geladen elektron heeft overgenomen van de microben en een Fe^{2+} is geworden. Het Fe^{2+}-ion is goed oplosbaar in tegenstelling tot Fe^{3+}.

CD waarde en elektronoverdracht

Evenals andere kationen kan Fe^{2+} adsorberen aan minerale oppervlakken, met inbegrip van het goethite oppervlak (FeOOH). Met de CD model werd ontdekt dat de geadsorbeerde Fe^{2+} kan veranderen in Fe^{3+}, door de overdracht van een elektron aan het oppervlak. Het leidt tot de vorming van geadsorbeerd Fe^{3+}. Echter, een gehydrateerd Fe^{3+} is niet erg stabiel. Evenals in oplossing laat een watermolecuul (H_2O) gebonden aan Fe^{3+} gemakkelijk H^+ionen los. Er wordt gezegd dat het Fe^{3+} ion hydrolyseert. Toepassing van het CD model laat zien dat twee H^+ ionen worden vrijgemaakt uit gebonden watermoleculen en dit leidt tot het $\equiv (Fe_{II}OH)_2Fe_{III}(OH)_2(OH_2)_2$ oppervlaktecomplex. Door de betrokkenheid van H^+ ionen bij de elektronoverdracht wordt het proces sterk pH-afhankelijk, en voor goethiet laat het CD model zien dat de elektronenoverdracht van Fe^{2+} naar goethiet alleen relevant is boven neutrale pH.

Ladingsverdeling samengevat

Samengevat, het onderzoek laat zien dat (a) de ion-ladingsverdeling in het grensvlak gekoppeld is aan een verdeling van de liganden en (b) de bijbehorende bindingslengten, (c) ook een mogelijke elektronenoverdracht. De ladingsverdeling in het grensvlak bevat daarnaast (d) een correctie door heroriëntatie van de watermoleculen in het grensvlak.

Toepassing op een klassiek colloïde

Het in dit proefschrift ontwikkelde algemene raamwerk voor oppervlaktelading en ion adsorptie kan worden toegepast in wetenschap, technologie, en milieu. Vóórafgaande aan de bespreking van dit laatste, een kort woord over een andere, lang aanwezige, wetenschappelijke kwestie, namelijk de lading van zilverjodide, AgI (s), een klassiek modelcolloïde. Het ladingsgedrag is uitgebreid gemeten. Bij variëren van de zilver- (Ag^+) of jodide- (I^-) concentratie zal de lading van het deeltje veranderen van negatief naar positief en *vice versa*. Het is het gevolg van de binding van de Ag^+ en/of I^- aan het oppervlak. In de klassieke interpretatie binden beide ionen op dezelfde positie in het elektrische veld. Toepassing van de ladingsdistributie (CD) model laat echter zien dat er in het oppervlak negatieve lading ontstaat die gescheiden is van positieve lading aanwezig buiten het oppervlak en die ontstaat door de binding van Ag^+ ionen. Jodide (I^-) bindt daar niet. De binding van deze ionen op een verschillende plaats in het elektrische veld betekent in feite ladingsdistributie. Deze ladingsdistributie kan begrepen worden uit de structuur van de kristaloppervlakken en de structuur van de oppervlaktecomplexen, een prachtig resultaat beschreven in het inleidende hoofdstuk van dit proefschrift. Het illustreert de grote kracht van het huidige ion adsorptie-raamwerk dat is gebaseerd op een structuurbenadering.

Toepassing in de bodem

In het laatste deel van het proefschrift wordt aandacht besteed aan de toepassing van het CD-MUSIC model in de bodem- en geochemie. Twee belangrijke vragen zijn opgeworpen.

Een eerste vraag is "Hoe krijgen we informatie over de grootte van het reactief oppervlak van de oxide fractie van de grond?" Dit is een zeer moeilijke en uitdagende vraag, en in het proefschrift, is het begin van een mogelijk antwoord gegeven. Aanbevolen wordt om

de reactie van bodemfosfaat te meten na het toevoegen van een hoge concentratie van natriumbicarbonaat ($NaHCO_3$). Het toegevoegde carbonaat (CO_3^{2-}) ion is een concurrent voor fosfaat (PO_4^{3-}), en door het carbonaat ion wordt aanwezig calcium (Ca^{2+}) verwijderd in de vorm van een neerslag als vast calciumcarbonaat, $CaCO_3$ (s). De $NaHCO_3$ oplossing zal de pH bufferen op pH ~ 8.5. Daarnaast is er actieve kool toegevoegd om organische moleculen te verwijderen die uit de organische stof vrijkomen bij hoge pH. Na toevoeging van $NaHCO_3$ zal er fosfaat vrijkomen. Nu gaan we de bodemsuspensie verdunnen met een $NaHCO_3$ oplossing. Hierdoor daalt de fosfaatconcentratie. Er kan echter ook nog extra fosfaat vrijkomen van de ijzer en aluminium (hydr)oxide oppervlakken. Dan daalt het fosfaatgehalte van de oplossing bij verdunning minder sterk. De mate van daling hangt dus af van hoeveel oxide oppervlak aanwezig is. Daalt de concentratie sterk, dan is er minder oppervlak beschikbaar om de concentratie aan fosfaat in de oplossing te bufferen. De gemeten reactie van de bodem wordt vergeleken met voorspellingen die gemaakt worden met de CD model. De reactie van de bodem wordt vergeleken met de reactie van goethiet, het belangrijkste Fe (hydr)oxide van de bodem en geeft antwoord op de vraag: "Welke grootte van het oppervlak verklaart de gegevens het beste?"

Uit de analyse blijkt dat de bodemoxide-deeltjes vaak erg klein zijn, slechts een paar nanometer. Eén nanometer (nm) is één miljoen keer kleiner dan een millimeter (mm). De grootte van het oppervlak gevonden voor representatieve Nederlandse bodems is vergeleken met een reeks van bodemeigenschappen. Een sterke relatie wordt gevonden tussen het reactief oppervlak en het organisch koolstofgehalte van de bodem. Er wordt gepostuleerd dat de bodem (hydr)oxide deeltjes zijn ingebed in een matrix van natuurlijke organische stof zoals weergegeven in de figuur 1.

Een tweede vraag is “Hoe gaan we om met organische moleculen die binden aan oxidedeeltjes (Fig.1)? Deze binding kan van invloed zijn op de ion-adsorptie, in het bijzonder op de adsorptie van anionen. Beide zullen concurreren om dezelfde plaatsen en bovendien hebben beide onderling een sterke repulsieve interactie via hun lading. De invloed van organische stof is zichtbaar als de fosfaatbelading per eenheid reactieve oppervlak wordt uitgedrukt. Deze fosfaatbelading kan statistisch gezien het best verklaard door de concentratie van opgelost organisch koolstof (DOC) en opgelost fosfaat.

Als het reactieve oppervlak en de fosfaatbelading, gemeten met de $NaHCO_3$ verdunningsmethode, worden gebruikt om de fosfaatconcentratie in een bodem te voorspellen voor gestandaardiseerde condities, blijkt de voorspelde waarde aanzienlijk lager te zijn (10 tot 1000 keer) dan gemeten in 0,01 M $CaCl_2$ oplossing. Waarschijnlijk is dit het gevolg van concurrentie met geadsorbeerde natuurlijke organische stof (NOM). Door het definiëren van een hypothetisch oppervlaktemolecuul, ≡ NOM, kan het effect van gebonden organische stof worden nagebootst. Dit hypothetisch oppervlaktemolecuul wordt gebruikt in de schatting van de hoeveelheid ≡ NOM die er nodig is om de gegevens te verklaren. De schijnbare belading met ≡ NOM is omgekeerd evenredig aan experimentele belading met fosfaat (PO_4^{3-}), een beeld dat past bij concurrentie. De belading met ≡ NOM neemt toe met de concentratie van opgeloste organische koolstof (DOC) in de $CaCl_2$-extract en correleert met de hoeveelheid organische stof in de bodem.

Omdat de concentratie van DOC in de bodem het geïntegreerde resultaat is van vele processen, is het gebruik van DOC als input in plaats van als output van een model op dit moment een eenvoudige en praktische manier om het effect van DOC en NOM op het ion

adsorptie gedrag te modelleren in de bodem- en geochemische toepassingen. Dit proefschrift levert daarvoor het raamwerk

Dankwoord

Het dankwoord van een proefschrift is voor de velen, niet in de laatste plaats ook voor mijzelf, het onderdeel dat je graag leest dan wel schrijft.

Als je, zoals ik, zo'n lange tijd onderdeel van een vakgroep bent geweest, heb je een groot aantal mensen zien zijn, komen, blijven, en/of gaan. Veel meer dan menigeen beseft, hebben velen bijgedragen aan dit proefschrift, vaak zonder zich daar misschien bewust van te zijn. Anderen leverden een waardevolle directe bijdrage. In alle gevallen, mijn uiterst hartelijke dank hiervoor.

Mijn liefde voor mijn vakgebied begon op de Dreijen, waar ik als student een klein afstudeervak deed. Het bleek een heerlijke proeftuin te zijn. Het was mijn latere collega Theo Bruggenwert die als studiecoördinator mij overtuigde van het belang van het opdoen van voldoende fundamentele kennis in je studie. "Dat gaat nooit meer verloren" was zijn stelling. "Het andere leer je later nog wel bij". Het betekende voor mij een zekere inhaalrace. Ik deed in mijn doctoraal nog een heel aantal kandidaatsvakken, zoals Thermodynamica bij Willem Norde, Lyklema's Grensvlakscheikunde met het erg interessant bijgehorende (groot) practicum verzorgd door Arie de Keizer en anderen, Chemische Evenwichten II bij Willem van Riemsdijk en Hans Beek, Optische mineralogie, en het uiterst interessante vak Theoretische Teeltkunde bij de Wit, Goudriaan, en Rabbinge.

Voor ik naar de Dreijen kwam, deed ik eerst mijn hoofdvak op Duivendaal in combinatie met een afstudeervak Kleimineralogie bij Prof. Van der Plas. De vrijheid was enorm. Zelf je eigen weg vinden was het adagium bij hem. Voor mij was het een geweldig leermoment. Ik ontdekte toen pas waar mijn hart lag. Veel heb ik daar ook geleerd van Jan van Doesburg, waarvoor mijn dank. In diezelfde tijd, haalde Theo Bruggenwert me over om ook bij hem een klein afstudeervak te doen. Ook daar kreeg ik alle ruimte om vrij te experimenteren en die nam ik ook. Opstellingen bouwen en proeven doen die ik zelf interessant of leerzaam vond. Op zaterdag of dinsdagnacht een "essentieel" monster nemen, of ontdekken dat glaswerk, vervuild met hematiet, wel schoon werd in zuurbak Nr 1 maar niet in Nr 2, en nu weten waarom. Ik zou wensen dat alle tegenwoordige studenten die dat kunnen en willen zo'n zelfde vrijheid zouden hebben en kunnen nemen. Mijn laatste bijvak was Colloïdchemie bij Prof. Lyklema. De sfeer op die vakgroep was er één van betrokkenheid. Menige "wildvreemde" die het studentenlab passeerde op weg naar de koffie kwam nieuwsgierig vragen wat je aan het doen was. Dat gold ook voor de kenmerkende colloquia waar velen zich stevig roerden in de discussies. Mijn feitelijke medebegeleider was Willem van Riemsdijk die zijn proefschrift bij Lyklema aan het afronden was. Alle genoemde en niet-genoemde mensen die aan mijn vorming bijdroegen, dank ik daarvoor.

Het was de tijd van bezuiniging ("Bestek 81"), maar toch wist ik na een overbruggend studentenassistentschap bij Fysische en Colloïd Chemie, een eerste tijdelijke baan te krijgen bij de Universiteit van Utrecht. Ik was er nog maar net begonnen toen Theo Bruggenwert bij me langs kwam met het verzoek van Prof. Bolt om Hans Beek, die ziek was, te vervangen. Na de nodige aarzeling nam ik mijn besluit "Terug naar Wageningen". Maar daarvoor, was er nog een sollicitatiegesprek in de avonduren in de tuin van Gerard Bolt die me omstandig de natuurkunde achter de orgelpijp uitlegde en bij de demonstratie bijna een zojuist aangekochte

pijp uit zijn handen liet glijden en toen guitig opmerkte: “Oeps, ik mag er ook niet aanzitten van mijn vrouw”. Buitengewone dank ben ik verschuldigd aan Gerard Bolt en Theo Bruggenwert voor het grote vertrouwen dat ze in me hebben gesteld.

Bij mijn komst op de vakgroep ging ik eerst verder werken aan het klei-aluminium project (Kalho) waarvoor ik als student voorbereidende proeven had gedaan. Eén van de eerste dingen die ik ging doen was het maken van gibbsiet ($Al(OH)_3$), een mooi modelmineraal. “Ga daar maar de zinkadsorptie aan meten. Is nuttig en móet interessant zijn”, zei Gerard Bolt. Het gibbsiet is gemaakt, maar de adsorptie van zink is er nooit aan gemeten. Voor productieproces van een ambitieuze hoeveelheid gibbsiet van 300 gram, sprokkelde ik dagelijks gedurende heel veel weken meer dan 100-200 liter dubbelgedistilleerd water bijeen uit alle destillatieapparaten die men op het Dreijen complex en omgeving maar kon vinden. Het uiteindelijke gibbsiet werd voor mijn latere onderzoek een heel belangrijk materiaal, dat anders dan oorspronkelijk bedoeld, is ingezet bij het onderzoek naar de oplossnelheid van mineralen. Dit was een hot-topic in de beginjaren ‘80 toen sterke verzuring van het milieu duidelijk werd. Theo Vens heeft in die jaren geholpen bij de metingen aan gibbsiet. Unieke data zijn verzameld die nog steeds actueel zijn en tot discussies leiden. Theo, heel hartelijk bedankt voor je toegewijde inzet.

Met de verzamelde gegevens en mijn ideeën over de rol van H^+ binding aan de zogenoemde dubbel gecoördineerde OH groepen van gibbsiet ben ik naar Willem Van Riemsdijk gegaan omdat hij ook met dit materiaal had gewerkt. Willem zag onmiddellijk de grote waarde van mijn titratiewerk. Het werd het begin van een zeer intensieve en succesvolle samenwerking. Ons eerste gezamenlijke artikel over de lading op gibbsiet is verschenen ter gelegenheid van het afscheid van Gerard Bolt in 1987. De ambitie om de H^+ reactiviteit van de oppervlaktegroepen van alle (hydr)oxiden te begrijpen monde uit in het MUSIC model dat in 1989 werd gepubliceerd. Het was één van de meest fascinerende perioden van ons onderzoek. Brainstormen en testen, op grafiekenpapier met de hand een relatie plotten en de euforie die het gaf toen gaandeweg de ligging van het volgende punt te voorspellen was. Met Willem op kerstavond met de benen omhoog, berekeningen doen met Han de Wit op zijn kamer, onbereikbaar voor iedereen, ook het thuisfront die dat niet waardeerde. Het is daarna ook niet meer voorgekomen.

Met het MUSIC model was de basis gelegd voor een algemeen ionadsorptiemodel. De eerste student die hieraan heeft gewerkt was Mario Villalobos. Zijn opdracht was de adsorptie van fosfaat aan goethiet te beschrijven. Het was weinig succesvol. Sorry Mario. Het concept was in orde maar we begrepen nog weinig van goethiet. Dat veranderde door de samenwerking met Prof. Udo Schwertmann in een project waaraan ook Peter Venema als AIO meewerkte. Met Peter was het prettig samenwerken. Peter implementeerde de eerste gecomputeriseerde titratieopstelling. Het onderzoek verliep vlot. Samen hebben we ook de postdoctorale cursus in katalyse gedaan in 1993. Elke week op vrijdag naar Utrecht en hard studeren. Erg Leuk. En ander hoogtepunt voor elk van ons was het geven van een voordracht op de Geo-8 bijeenkomst in Straatsburg (1995). Het was een succes. Uitgenodigd door Alain Manceau voor een select diner, maakten we kennis met belangrijke vakgenoten. Bovendien nodigde Alain ons ook direct uit om enkele weken later één van de voordrachten nogmaals te geven, nu in Parijs op het congres *Biogeochemistry of Trace Elements*. Alain, thanks for the

inspiring discussions that we have and have had. Peter, je kijk op zaken was altijd nuchter en je beschouwde je bijdrage soms als niet zo veel betekenend. Toch heb je sterk bijgedragen aan o.a. het opnieuw formuleren van het MUSIC model dat in 1996 verscheen. Ook daarvoor mijn dank.

Citraat is een uitscheidingsproduct van plantenwortels. Het leek me daarom verstandig om de adsorptie van citraat te meten. Aanvankelijk werd dit door studenten gedaan. Daarbij kon ik rekenen op de analytische expertise van Jaap Nelemans, waarvoor mijn dank. Citraat was een gelukkige keuze omdat enige tijd later Jeanine Geelhoed als AIO de fosfaatopname ging meten in model systemen met goethiet-zand en planten. Het gaf mij en haar de mogelijkheid om de citraat en fosfaat interactie te bestuderen. Daar Jeanine ook sulfaat in haar systemen gebruikte, is ook de deze interactie bestudeerd. Deze samenwerking heeft tot twee succesvolle artikelen geleid. Jeanine heel hartelijk dank voor je efficiëntie, watervlugge, en zeer accurate experimenten. Jij en ik hebben er veel van geleerd.

In vrijwel dezelfde periode startte René Rietra zijn werkzaamheden. René, je bent een buitengewoon bekwame experimentator en je werd en wordt voortdurend gedreven door nieuwsgierigheid en denkt daar zelfstandig over na. Je hebt veel eigen ideeën en experimenten ontwikkeld. Jouw methode van iontitraties is heel eenvoudig maar intelligent van opzet en geeft uniek inzicht in de relatie tussen binding en complexstructuur. Het heeft tot een heel mooi en klassiek artikel geleid. Het is één van mijn favorieten. Je bent daarnaast een zeer aimabel mens zonder veel uiterlijk vertoon en samenwerken met je is eenvoudig. Heel hartelijk dank, dat weet je.

De adsorptie van kleine organische zuren aan goethiet is voortgezet door Jeroen Filius en uitgebreid naar de binding van fulvozuur. Jeroen, samenwerken met jou was altijd prettig. Je hebt zelf heel goede ideeën ontwikkeld en mijn inbreng was dan ook mijns inziens redelijk beperkt tot het kritisch je bevragen en je manuscripten rood en blauw te kleuren. Ik vond het heerlijk om samen met je in de koffiekamer op het aanrecht te zitten en te praten over van alles en nog wat. Jeroen, bedankt!

Terugkijkend, was de periode rond 2000 heel bijzonder. Er waren veel AIO's en de wetenschappelijk groepsbesprekingen in de kelder op de Dreijen waren heel bijzonder. Ik beschouw het als één van de grootste hoogtepunten in mijn loopbaan waaruit een groot gevoel van saamhorigheid sprak. Het was inspirerend en stimulerend en gaf mij van tijd tot tijd het gevoel van vleugels. Ik denk dat die inspiratie door iedereen die aan de discussiebijeenkomsten deelnam, zo werd gevoeld.

Na deze periode, werd het een beetje rustiger. Ik stak veel tijd in onderwijs. Rasoul Rahnemaie came as a PhD student. Your start was initially difficult, but after it was decided that I would be your supervisor, you grew in your role. As many of the PhD students that I have supervised, you were a great experimentalist and I also admire that you could keep calm when checking all kinds of non-successful model calculations before getting a consistent picture. You have studied carefully the adsorption of phosphate at interaction with carbonate. The interesting thing is that measuring only the phosphate adsorption at high pH in carbonate systems, resulted in a correct prediction of the binding of CO_2, as measured by Mario Villalobos of Stanford University over a large range of pH and loading conditions in open and close systems. Whauw. Accidentally, Mario was my first MSc student that worked in the

early days on the phosphate adsorption using for the first time the CD model. Rasoul, it was a pleasure to meet you as person. I thank you for the pleasant cooperation that we had and still have.

Monika Stachowicz is de laatste PhD student die aan ion-adsorptie en goethite heeft gewerkt. Monika, je hebt heel wat problemen moeten oplossen voordat je met plezier aan het meten kon gaan. Ik moet je zeker danken voor je doorzettingsvermogen en je bereidheid om van je onderzoek een groot succes te maken. Het is een heel mooi eindresultaat geworden, ook nu ik er vanaf deze plaatst weer naar kijk. Ik ben er trost op. Jij vast ook.

Last but not least wil ik Debby Los bedanken voor de prettige samenwerking en je bereidwilligheid gegevens met me te delen. Daarnaast natuurlijk, dank ik je voor jouw altijd vrolijke gezicht dat zo aanstekelijk op mij en anderen werkt.

De meest gelukkige tijd heb ik doorgebracht op de Dreijen. De manier van huisvesting was er één waardoor als van nature je een deel van een groter geheel kon voelen. Met de verhuizing naar de nieuwe setting is alles sterk veranderd en ik kan er maar moeilijk aan wennen dat we nu wonen in een steriel en sfeerloos gebouw dat nog het meeste weg heeft van een ..... Wat een vooruitgang.

Sinds de verhuizing heb ik voor het eerst een kamergenoot (afgezien van een korte tijd tijdens de verbouwing van de Dreyen, toen Marc Benedetti en ik uiterst plezierig een kamer deelden). Gelukkig heb ik ook nu een kamergenoot getroffen “waarmee ik goed uit de voeten kan”. Liping, dit is een zegswijze ☺. Het is aangenaam je als kamergenoot te hebben en dat je me opport koffie te drinken. Ook onze tussentijdse gesprekjes op de kamer bevallen me zeer. Natuurlijk is het ook fijn om met je samen te werken en dat ik een zekere bijdrage hebt mogen leveren aan een groot aantal publicaties van jou over de adsorptie van humus en fulvozuren met oxiden. Het heeft me veel geleerd en ik dank je voor jouw vertrouwen.

Een heel speciaal woord van dank heb ik voor Meindert Keizer. Je kunt nog zoveel mooie data hebben, nog zulke goede ideeën en weet ik niet wat meer, voor een goede interpretatie is goede software nodig. Meindert, je staat daar altijd garant voor. Als er speciale wensen mijnerzijds zijn en waren, ben je altijd bereid er snel (!) en effectief (!) aan te werken. Heel veel dank daarvoor. Het is en was een heel erg belangrijke bijdrage aan mijn onderzoek.

Over time, I got the opportunity to cooperate and publish papers with a number of postdocs, visitors, and others. In almost all cases, Willem has made this possible and stimulated me. The first postdoc to mention is Han Yong from the University of Nanjing. He came to Wageningen to become trained in surface chemistry. Han Yong has extensively measured the proton binding by various Al hydroxides. I would like to thank him for his efforts, resulting in one of the papers of this thesis. Peter Weidler was part of the research project with Peter Venema in cooperation with Prof. Schwertmann. Peter thanks for your help and willingness to answer at irregular moments my questions. I would also like to thank David Kinniburgh who has been so very kind to help me to improve my English texts at several occasions and for lending me his nice thesis. Moreover, his program FIT was and is of great help. I am also grateful to Johannes Lützenkirchen for our irregular but stimulating email discussions. Thanks for your critical remarks and questions. Kyriakos Bourikas has worked on titanium oxides that are used in catalysis. We can be proud that in the short period that you were in our lab in 1999, you have been able to make two successful papers. I have

enjoyed your enthusiasm to work. Many thanks. In 2005, Mark Barnett has visited our department during his sabbatical leave. He has contributed to the paper on the adsorption of silicic acid that is part of the present thesis. Mark, thanks. Rather recently, Juan Antelo Martinez has been in our lab and together with him, we have further developed a method to estimate the reactive surface area of the soil oxides fraction and the interaction of this fraction with organic matter and phosphate. Juan, I hope you have enjoyed it as much as I did. Thanks for your contributions resulting in the last two papers of this thesis.

A very special word is for Moira Ridley. We met a number of years ago at an ACS conference in the USA where you gave a solid and impressive presentation, as you always do. During your sabbatical in Wageningen, we have analyzed your extensive date sets on rutile. I have tremendously enjoyed the work we did together. It was exciting to model your data, revealing systemically that simple electrolyte cations may form innersphere complexes and how this can be extracted from your high-quality data with the CD model. It is a large step forward. Moira, you have done a great job. When you left Wageningen, I was enthusiastic about the results, but I know that you are not easily satisfied. At home, you have critically improved it far above any of my expectations. Almost “too good to be true”. I am proud that I have been part of the work and I look forward to cooperate with you in the future. Many thanks.

On a conference in München, I have met André Rossberg. He asked me for cooperation to understand the surface complexation of uranium. The match with you was good and your uncomplicated attitude I enjoy most. We have worked together in your project and made two nice papers. Thank you very much for the pleasant and humorous email contacts we have. Aé, I hope we can continue our work in one way or another.

Hoewel mijn directe activiteiten op het laboratorium door de jaren heen relatief beperkt zijn geweest, betekent dit niet dat de bijdragen van de talloze medewerkers van het laboratorium minder belangrijk zouden zijn. Allereerst is er de goede kwaliteit van meten. Betrouwbare en nauwkeurige gegevens zijn de hoeksteen. Ook was er de bereidwilligheid me te helpen met allerlei hand- en spandiensten en om mijn vragen te beantwoorden. Hiervoor allen dank, in het bijzonder Peter Nobels, Gerlinde Vink en Monique Driessen, Jaap Nelemans en Willeke van Tintelen, Arie van de Berg, en heel veel anderen onder wie Kees Koenders.

De aanwezigheid van een secretariaat en administratie maakt het werken aangenaam en gemakkelijk. "Tjisse, let je hier of daar even op? Heb je dat al gedaan?" En altijd wel een praatje of een lolletje. Riette, Caroline, Minke, Esther, and Winnie en vele anderen, heel veel dank voor deze zorgzaamheid en vooral jullie geduld met mij.

Ook een woord van dank aan alle studenten die bij mij een afstudeervak deden. Ze hebben experimenten gedaan en gegevens verzameld die in een aantal gevallen deel werden van een publicatie. Maar minstens zo belangrijk, ze stelden de juiste en “onjuiste” vragen en waren dan een gewillig oor bij een antwoord dat gestructureerd zou moeten zijn maar dat daarbij kon blootleggen wat nog niet helder werd begrepen.

Ook wil ik mijn collega’s bedanken waarmee in het onderwijs heb samengewerkt. Door hun andere manier van kijken kan je veel leren over de betekenis van de bodem in landbouw, ecologie, milieu, en system Earth. Hartelijk dank.

Na al die vele woorden zou je kunnen denken waar blijft het bijzondere woord van dank voor de promotor? Beste Willem, waar zou het onderzoek zijn uitgekomen zonder jouw inbreng? Zeker is, een heel andere en veel bescheidener uitkomst. Je heldere manier van denken en je aanwijzingen zijn altijd van groot belang geweest. Je bent optimistisch en bent niet bang voor uitdagingen, mogelijke en schijnbaar onmogelijke én onmogelijke. Het is uiterst inspirerend. Door de jaren heen heb je steeds weer voor mij kansen gecreëerd en stimulerende initiatieven genomen. Daarbij ben je plezierig en gemakkelijk in omgang. Het is altijd fijn om met je te "pingpongen". Dit is het goede woord. Je doet het samen. In dat spel, houd je de bal op de tafel maar je speelt scherp. Je daagt uit en corrigeert. Ik heb heel veel aan je te danken. Je bent een uitstekend klankbord. Je hebt een fijne neus voor wat wel of niet een goede weg kan zijn. Daarmee bof ik en al de anderen van onze groep. Als er in de kantlijn van het manuscript "hmm~~" staat dan ben ik gewaarschuwd. Mogelijk is hier iets niet in orde, wat ik serieus neem vanwege je bewuste en onbewuste gevoel voor potentiële "nattigheid". Maar gelukkig duld je tegenspraak. Dat maakt het voor me bijzonder. Eigenwijsheid mág en móet.

Ook dank ik jou en Trudy voor al die andere zaken buiten het directe werk. De plezierige reis(z)en die we hebben gemaakt, het lenen van een viool, het aanbod om jullie gárage (je uitspraak ☺) ter beschikking te stellen voor het restaureren van een bootje, je zeillessen, jullie uitnodiging voor een etentje, en het delen van allerlei ervaringen in goede en soms mindere tijden. Heel fijn.

Tot slot is er een bijzonder woord van dank voor het thuisfront. Nelly, jij en ik verstaan elkaar vaak al met een half woord. Een man als onderzoeker is wel eens een crime. Nooit klaar met het werk. Vaak te laat. Waar zit je toch met je gedachten? Mijn oprechte excuses. Je geduld met mij en mijn onderzoek is te groot om onder woorden te brengen. Met veel liefs bedank ik je voor jouw vaak onvoorwaardelijke steun die mij en ons hier heeft gebracht. En kids, jullie zijn groot en je vader is trots op zijn dochters. Het is fijn te zien dat jullie allemaal jullie gegeven talenten hebben kunnen én willen benutten. Dat maakt het leven nog extra aangenaam.

Niet onvermeld mag blijven mijn dank voor de dierbare zorg en toewijding van mijn ouders.

Jullie aller,

Tjisse

☺

About the author

Tjisse Hiemstra was born as son of Thomas Hiemstra and Neeltje Meidertsma in Zwolle, The Netherlands, at December 3rd, 1954. He did his secondary school ("HBS-B") at the "Meander College" in Zwolle. He studied Soil Sciences ("Bodemkunde en Bemestingsleer") at Wageningen University (formerly "Landbouw Hogeschool, LH"), The Netherlands and graduated with honors in 1980. Soil Formation and Field Soil Sciences ("Regionale Bodemkunde") was his major and he did additionally three minors, i.e. in Clay mineralogy, Soil Chemistry, and Colloid Sciences. This combination of disciplines reflects his profound interest in natural processes based on a fundamental and mechanistic understanding.

He started his career at the department Petrology, Mineralogy, Crystallography, Geochemistry, and Soil science of Utrecht University, The Netherlands in May 1980, but returned a short time later to Wageningen where he became staff member in the group "Soil Physics and Chemistry" of Prof. Dr. Ir. Gerard Bolt and his successor in "Soil Chemistry" Prof. Dr. Willem van Riemsdijk, at the former Department Soil Science and Plant Nutrition, presently known as Soil Quality. He obtained the Certificate of Proficiency of the Netherlands Institute for Catalysis Research after following the post-graduated course in Catalysis in 1994.

Tjisse Hiemstra is married with Nelly Vrolijk and they have three daughters, Hannah Eleonore, Anna Louise, and Johanna Maria.

List of publications

Bourikas K., Hiemstra T., and Van Riemsdijk W. H. (2001) Adsorption of molybdate monomers and polymers on titania with a multisite approach. *J. Phys. Chem. B* 105(12), 2393-2403.

Bourikas K., Hiemstra T., and Van Riemsdijk W. H. (2001) Ion Pair Formation and Primary Charging behaviour of Titanium Oxide (Anatase and Rutile). *Langmuir* 17(3), 749-756.

Filius J. D., Hiemstra T., and Van Riemsdijk W. H. (1997) Adsorption of small weak organic acids on goethite: Modeling of mechanisms. *J. Colloid Interf. Sci.* 195(2), 368-380.

Filius J. D., Hiemstra T., and Van Riemsdijk W. H. (2000) Adsorption of Fulvic Acid on Goethite. *Geochim. Cosmochim. Acta* 64(1), 51-60.

Filius J. D., Meeussen J. C. L., Hiemstra T., and van Riemsdijk W. H. (2001) Modeling the binding of benzenecarboxylates by goethite: The ligand and charge distribution model. *J. Colloid Interf. Sci.* 244(1), 31-42.

Filius J. D., Meeussen J. C. L., Lumsdon D. G., Hiemstra T., and Van Riemsdijk W. H. (2003) Modeling the binding of fulvic acid by goethite: The speciation of adsorbed FA molecules. *Geochim. Cosmochim. Acta* 67(8), 1463-1474.

Geelhoed J. S., Hiemstra T., and Van Riemsdijk W. H. (1997) Phosphate and sulfate adsorption on goethite: Single anion and competitive adsorption. *Geochim. Cosmochim. Acta* 61, 2389.

Geelhoed J. S., Hiemstra T., and Van Riemsdijk W. H. (1998) Competitive Interaction between Phosphate and Citrate on Goethite. *Environ. Sci. Technol.* 32, 2119-2123.

Hiemstra T., Antelo J., Rahnemaie R., and van Riemsdijk W. H. (2010) Nanoparticles in natural systems I: The effective reactive surface area of the natural oxide fraction in field samples. *Geochim. Cosmoschim. Acta* 74(1), 41-58.

Hiemstra T., Antelo J., van Rotterdam A. M. D., and van Riemsdijk W. H. (2010) Nanoparticles in natural systems II: The natural oxide fraction at interaction with natural organic matter and phosphate. *Geochim. Cosmoschim. Acta* 74(1), 59-69.

Hiemstra T., Barnett M. O., and Van Riemsdijk W. H. (2007) Interaction of Silicic Acid with Goethite. *J. Colloid Interf. Sci.* 310, 8-17.

Hiemstra T., De Wit J. C. M., and Van Riemsdijk W. H. (1989b) Multisite proton adsorption modeling at the solid/solution interface of (hydr)oxides: A new approach. II. Application to various important (hydr)oxides. *J. Colloid Interf. Sci.* 133, 105-117.

Hiemstra T., Han Yong, and Van Riemsdijk W. H. (1999b) Interfacial Charging Phenomena of Aluminum (Hydr)oxides. *Langmuir* 15, 5942-5955.

Hiemstra T., Rahnemaie R., and Van Riemsdijk W. H. (2004) Surface Complexation of Carbonate on Goethite: IR spectroscopy, Structure and Charge Distribution. *J. Colloid Interf. Sci.* 278, 282-290.

Hiemstra T. and Van Riemsdijk W. H. (1990) The kinetics of dissolution reactions of Al(hydr)oxides: role of surface structure and multisite surface speciation. *Trans. 14th Int. Congr. Soil Sci. Kyoto* Vol. 2, 28-33.

Hiemstra T. and Van Riemsdijk W. H. (1990) Multiple Activated Complex Dissolution of Metal (Hydr)Oxides: A Thermodynamic Approach Applied to Quartz. *J. Colloid Interf. Sci.* 136(1), 132-150.

Hiemstra T. and Van Riemsdijk W. H. (1991) Physical chemical interpretation of primary charging behaviour of metal (hydr)oxides. *Colloids Surfaces* 59, 7-25.

Hiemstra T. and Van Riemsdijk W. H. (1996a) A surface Structural Approach to Ion Adsorption: The Charge Distribution (CD) Model. *J. Colloid Interf. Sci.* 179, 488-508.

Hiemstra T. and Van Riemsdijk W. H. (1999a) Surface structural ion adsorption modeling of competitive binding of oxyanions by metal (hydr)oxides. *J. Colloid Interf. Sci.* 210, 182-193.

Hiemstra T. and Van Riemsdijk W. H. (1999c) Effect of Different Crystal Faces on the Experimental Interaction Force and Aggregation of Hematite. *Langmuir* 15(23), 8045-8051.

Hiemstra T. and Van Riemsdijk W. H. (2000) Fluoride adsorption on goethite in relation to different types of surface sites. *J. Colloid Interf. Sci.* 225(1), 94-104.

Hiemstra T. and Van Riemsdijk W. H. (2002) On the Relationship between Surface Structure and Ion Complexation of Oxide-Solution Interfaces. In *Encyclopaedia of Surface and Colloid Science*, pp. 3773-3799. Marcel Dekker, Inc.

Hiemstra T. and Van Riemsdijk W. H. (2006) Biogeochemical speciation of Fe in ocean water. *Mar. Chem.* 102(3-4), 181-197.

Hiemstra T. and Van Riemsdijk W. H. (2006) On the relationship between charge distribution, surface hydration and the structure of the interface of metal hydroxides. *J. Colloid Interf. Sci.* 301, 1-18.

Hiemstra T. and Van Riemsdijk W. H. (2007) Adsorption and surface oxidation of Fe(II) on metal (hydr)oxides. *Geochim. Cosmochim. Acta* 71(24), 5913-5933.

Hiemstra T. and Van Riemsdijk W. H. (2007) Surface complexation of selenite on goethite: MO/DFT geometry and charge distribution. *Croatica Chemica Acta* 80(3-4), 313-324.

Hiemstra T. and Van Riemsdijk W. H. (2009a) A Surface Structural Model for Ferrihydrite I: Sites related to Primary charge, Molar Mass, and Mass Density. *Geochim. Cosmochim. Acta* 73, 4423-4436.

Hiemstra T., Van Riemsdijk W. H., and Bolt G. H. (1989a) Multisite Proton Adsorption Modeling at the Solid/Solution Interface of (Hydr)oxides: A New Approach. I. Model Description and Evaluation of Intrinsic Reaction Constants. *J. Colloid Interf. Sci.* 133, 91-104.

Hiemstra T., Van Riemsdijk W. H., and Bruggenwert M. G. M. (1987) Proton adsorption mechanism at the Gibbsite and aluminum oxide solid/solution interface. *Neth. J. Agric. Sci.* 35, 281-293.

Hiemstra T., Van Riemsdijk W. H., Rossberg A., and Ulrich K. U. (2009b) A Surface Structural Model for Ferrihydrite II: Adsorption of Uranyl and Carbonate. *Geochim. Cosmochim. Acta* 73(4437-4451).

Hiemstra T., Venema P., and Van Riemsdijk W. H. (1996b) Intrinsic proton affinity of reactive surface groups of metal (hydr)oxides: The bond valence principle. *J. Colloid Interf. Sci.* 184, 680-692.

Meeussen J. C. L., Scheidegger A., Hiemstra T., Van Riemsdijk W. H., and Borkovec M. (1996) Predicting Multicomponent Adsorption and Transport of Fluoride at Variable pH in a Goethite-Silica Sand System. *Environ. Sci. Technol.* 30, 481-488.

Ponthieu M., Juillot F., Hiemstra T., Van Riemsdijk W. H., and Benedetti M. F. (2006) Metal ion binding to iron oxides. *Geochim. Cosmoschim. Acta* 70(11), 2679-2698.

Rahnemaie R., Hiemstra T., and Van Riemsdijk W. H. (2006) Inner- and Outersphere Complexation of Ions at the Goethite-Solution Interface. *J. Colloid Interf. Sci.* 297, 379-388.

Rahnemaie R., Hiemstra T., and Van Riemsdijk W. H. (2006) A new structural approach for outersphere complexation, tracing the location of electrolyte ions. *J. Colloid Interf. Sci.* 293, 312-321.

Rahnemaie R., Hiemstra T., and Van Riemsdijk W. H. (2007) Carbonate adsorption on goethite in competition with phosphate. *J. Colloid Interf. Sci.* 315(2), 415-425.

Rahnemaie R., Hiemstra T., and Van Riemsdijk W. H. (2007) Geometry, Charge Distribution and Surface Speciation of Phosphate on Goethite. *Langmuir* 23, 3680-3689.

Ridley M. K., Hiemstra T., Van Riemsdijk W. H., and Machesky M. L. (2009) Inner-sphere complexation of cations at the rutile-water interface: A concise surface structural interpretation with the CD and MUSIC model. *Geochim. Cosmoschim. Acta* 73(7), 1841-1856.

Rietra R. P. J. J., Hiemstra T., and van Riemsdijk W. H. (1999) Sulfate adsorption on goethite. *J. Colloid Interf. Sci.* 218(2), 511-521.

Rietra R. P. J. J., Hiemstra T., and Van Riemsdijk W. H. (1999a) The Relationship between Molecular Structure and Ion Adsorption on Variable Charge Minerals. *Geochim. Cosmochim. Acta* 63(19/20), 3009-3015.

Rietra R. P. J. J., Hiemstra T., and Van Riemsdijk W. H. (1999b) Sulfate Adsorption on Goethite. *J. Colloid Interf. Sci.* 218, 511-521.

Rietra R. P. J. J., Hiemstra T., and Van Riemsdijk W. H. (2000a) Electrolyte Anion Affinity and its Effect on Oxyanion Adsorption on Goethite. *J. Colloid Interf. Sci.* 229, 199-206.

Rietra R. P. J. J., Hiemstra T., and Van Riemsdijk W. H. (2001a) Interaction of Calcium and Phosphate Adsorption on Goethite. *Environ. Sci. Technol.* 35, 3369-3374.

Rietra R. P. J. J., Hiemstra T., and Van Riemsdijk W. H. (2001b) Comparison of Selenate and Sulfate Adsorption on Goethite. *J. Colloid Interf. Sci.* 240, 384-390.

Rossberg A., Ulrich K. U., Weiss S., Tsushima S., Hiemstra T., and Scheinost A. C. (2009) Identification of uranyl surface complexes on ferrihydrite: Advanced EXAFS data analysis and CD-MUSIC modelling. *Environ. Sci. Technol.* 43(5), 1400-1406.

Schroder T. J., Hiemstra T., Vink J. P. M., and van der Zee S. (2005) Modeling of the solid-solution partitioning of heavy metals and arsenic in embanked flood plain soils of the rivers Rhine and Meuse. *Environ. Sci. Technol.* 39(18), 7176-7184.

Stachowicz M., Hiemstra T., and Van Riemsdijk W. H. (2006) Surface speciation of As(III) and As(V) adsorption in relation to charge distribution. *J. Colloid Interf. Sci.* 302, 62-75.

Stachowicz M., Hiemstra T., and Van Riemsdijk W. H. (2007) The arsenic-bicarbonate interaction on goethite particles. *Environ. Sci. Technol.* 41(16), 5620-5625.

Stachowicz M., Hiemstra T., and Van Riemsdijk W. H. (2008) Multi-competitive interaction of As(III) and As(V) oxyanions with Ca^{2+}, Mg^{2+}, PO_4^{3-}, and CO_3^{2-} ions on goethite. *J. Colloid Interf. Sci.* 320(2), 400-414.

Van Riemsdijk W. H. and Hiemstra T. (1999) From Molecular Structure to Ion Adsorption Modelling. In *Mineral-Water Interfacial Reactions, Kinetics and Mechanisms*, Vol. 715 (ed. D. L. a. G. Sparks, T.J.), pp. 68-86. American Chemical Society.

Van Rotterdam A. M. D., Temminghoff E. J. M., Schenkeveld W. D. L., Hiemstra T., and van Riemsdijk W. H. (2009) Phosphorus removal from soil using Fe oxide-impregnated paper: Processes and applications. *Geoderma* 151(3-4), 282-289.

Venema P., Hiemstra T., and Van Riemsdijk W. H. (1996a) Comparison of different site binding models for cation sorption: Description of pH dependency, salt dependency, and cation-proton exchange. *J. Colloid Interf. Sci.* 181, 45-59.

Venema P., Hiemstra T., and Van Riemsdijk W. H. (1996b) Multisite Adsorption of Cadmium on goethite. *J. Colloid Interf. Sci.* 183, 515-527.

Venema P., Hiemstra T., and Van Riemsdijk W. H. (1997) Interaction of Cadmium with Phosphate on Goethite. *J. Colloid Interf. Sci.* 192, 94-103.

Venema P., Hiemstra T., and Van Riemsdijk W. H. (1998) Intrinsic Proton Affinity of Reactive Surface Groups of Metal (Hydr)oxides: Application to Iron (Hydr) oxides. *J. Colloid Interf. Sci.* 198, 282-295.

Venema P., Hiemstra T., and Van Riemsdijk W. H. (1996) Multisite adsorption of cadmium on goethite. *J. Colloid Interf. Sci.* 183(2), 515-527.

Venema P., Hiemstra T., and Van Riemsdijk W. H. (1997) Interaction of cadmium with phosphate on goethite. *J. Colloid Interf. Sci.* 192(1), 94-103.

Weidler P. G., Hug S. J., Wetche T. P., and Hiemstra T. (1999) Determination of Growth Rates of 100 and 110 faces of Synthetic Goethite by Scanning Force Microscopy. *Geochim. Cosmochim. Acta* 62, 3407-3412.

Weng L. P., Koopal L. K., Hiemstra T., Meeussen J. C. L., and Van Riemsdijk W. H. (2005) Interactions of calcium and fulvic acid at the goethite-water interface. *Geochim. Cosmoschim. Acta* 69(2), 325-339.

Weng L. P., Van Riemsdijk W. H., and Hiemstra T. (2006) Adsorption free energy of variable-charge nanoparticles to a charged surface in relation to the change of the average chemical state of the particles. *Langmuir* 22(1), 389-397.

Weng L. P., Van Riemsdijk W. H., and Hiemstra T. (2007) Adsorption of humic acids onto goethite: Effects of molar mass, pH and ionic strength. *J. Colloid Interf. Sci.* 314(1), 107-118.

Weng L. P., Van Riemsdijk W. H., and Hiemstra T. (2008) Cu^{2+} and Ca^{2+} adsorption to goethite in the presence of fulvic acids. *Geochim. Cosmoschim. Acta* 72(24), 5857-5870.

Weng L. P., Van Riemsdijk W. H., and Hiemstra T. (2008) Humic Nano-Particles at the Oxide-Water Interface: Interaction with Phosphate Ion Adsorption. *Environ. Sci. Technol.* 42(23), 8747-8752.

Weng L. P., Van Riemsdijk W. H., and Hiemstra T. (2009) Effects of Fulvic and Humic Acids on Arsenate Adsorption to Goethite: Experiments and Modeling. *Environ. Sci. Technol.* 43(19), 7198-7204.

Weng L. P., Van Riemsdijk W. H., Koopal L. K., and Hiemstra T. (2006) Adsorption of humic substances on goethite: Comparison between humic acids and fulvic acids. *Environ. Sci. Technol.* 40(24), 7494-7500.

Weng L. P., Van Riemsdijk W. H., Koopal L. K., and Hiemstra T. (2006) Ligand and Charge Distribution (LCD) model for the description of fulvic acid adsorption to goethite. *J. Colloid Interf. Sci.* 302(2), 442-457.